



**Electrochemical Advanced Oxidation Processes:
Application to the Degradation of Synthetic and Real Wastewaters**

*Thesis submitted in partial fulfillment of the requirements for the degree of
Doctor of Philosophy in Environmental Engineering
at the Faculty of Engineering, University of Porto*

Maria Francisca da Costa Moreira

Supervisor: Vítor Jorge Pais Vilar, Ph.D.
Co-Supervisors: Enric Brillas Coso, Ph.D. (University of Barcelona)
Rui Alfredo da Rocha Boaventura, Ph.D.

Laboratory of Separation and Reaction Engineering – Laboratory of Catalysis and Materials (LSRE-LCM)
Department of Chemical Engineering
Faculty of Engineering
University of Porto
April, 2016

Acknowledgments

My sincere gratitude goes to my supervisors: Dr. Vítor Vilar, for encouraging me to pursue the Ph.D. course, giving me the opportunity to go abroad to learn and all inexhaustible support, patience, trust and friendship; Dr. Enric Brillas, for receiving me so well in his laboratory and always being so supportive and tremendously helpful; and Dr. Rui Boaventura, for providing me the necessary resources for carrying out the work and all support. Without your assistance and valuable knowledge would not have been possible to meet all the objectives.

I am also very grateful to Dr. Sergi Garcia-Segura for all the guidance, help and encouragement and Dr. Juan Soler for all the help and partnership. Thank you, Dr. Fátima Alpendurada, for helping me with some analyses, and Dr. Cheng, for providing some space in your office during my first Ph.D. times and always being so kind. My thanks go also to Jose Luis Almart, Dr. Tânia Silva and Dr. Petrick Soares for contributing somehow for the accomplishment of some tasks.

A mention must be made to *Fundação para a Ciência e a Tecnologia* (FCT) for the Ph.D. grant (reference SFRH/BD/80361/2011) and to the following host laboratories: Laboratory of Separation and Reaction Engineering – Laboratory of Catalysis and Materials (LSRE-LCM) of Faculty of Engineering, University of Porto and Laboratory for Materials Electrochemistry and the Environment (LMEE) of Faculty of Chemistry, University of Barcelona. Financial support was mainly provided by: PEst-C/EQB/LA0020/2011 and PEst-C/EQB/LA0020/2013 projects, co-financed by FCT and FEDER under COMPETE; UID/EQU/50020/2013 project, co-financed by FCT/MEC and FEDER under Program PT2020; NORTE-07-0124-FEDER-0000008 project, co-financed by QREN, ON2 program and FEDER; and AdvancedLFT project (reference FCOMP-01-0202-FEDER-033960), financed by FEDER under COMPETE program of QREN within the I&DT system.

An extended greeting goes to my esteemed colleagues from LSRE and LMEE (so many!) for all the good and funny moments spent together. I wish you the best of luck.

Finally, I would like to express my genuine acknowledgment to my family, especially to my beloved parents, and also to my dear João and my close friends for all unconditional support and love and inexhaustible patience and tolerance. Thank you so much!

With love to my parents

*Start by doing what is necessary;
then do what is possible;
and suddenly you are doing the impossible.*

San Francesco d'Assisi

Abstract

Water pollution by organic compounds arising from human activities is a major global environmental problem that requires a rapid and effective answer. In the last years, electrochemical advanced oxidation processes (EAOPs) have been acquiring high relevance for water treatment. These processes are able to degrade recalcitrant organic compounds, mainly via the electrochemical generation of strong oxidants such as hydroxyl radicals ($\bullet\text{OH}$).

The current thesis focuses on the assessment of the technical feasibility of using some EAOPs for the degradation of recalcitrant organic compounds of five solutions: (i) a 290 mg L⁻¹ Sunset Yellow FCF (SY) azo dye aqueous solution in 7.0 g Na₂SO₄ L⁻¹, (ii) a 20.0 mg L⁻¹ trimethoprim (TMP) antibiotic aqueous solution in 7.0 g Na₂SO₄ L⁻¹, (iii) a wastewater collected after secondary treatment of a municipal wastewater treatment plant (MWWTP) spiked with TMP at mg L⁻¹ levels or 19 pharmaceutical compounds at µg L⁻¹ levels, (iv) a winery wastewater, and (v) a municipal sanitary landfill leachate. EAOPs were directly applied to the both pure solutions, hereinafter also referred to synthetic wastewaters, and also to the secondary MWWTP effluent. For the winery wastewater and the landfill leachate, these processes were combined with other technologies. The winery wastewater was subjected to biological oxidation before EAOPs to remove the biodegradable organic fraction. For the sanitary landfill leachate treatment, the following multistage strategy was applied: (i) initial biological treatment for ammonium oxidation, removal of alkalinity and biodegradation of organics, (ii) coagulation for removal of humic acids and suspended solids, (iii) EAOP for degradation of recalcitrant organic compounds and biodegradability enhancement, and (iv) final biological treatment. The following five EAOPs were under focus: anodic oxidation (AO), anodic oxidation with electrogenerated hydrogen peroxide (AO-H₂O₂), electro-Fenton (EF), photoelectro-Fenton (PEF) and solar photoelectro-Fenton (SPEF). EAOPs were performed in four lab- and pilot-scale experimental units, all equipped with a boron-doped diamond (BDD) or a platinum (Pt) anode and a carbon-PTFE air-diffusion cathode. Two of these units were designed and constructed within this thesis.

The efficiency of the various EAOPs for recalcitrant organic compound degradation was assessed mainly in terms of mineralization and pollutants concentration decay. The mineralization ability of EAOPs increased in the following order: AO-H₂O₂ < AO < EF < PEF with UVA radiation (PEF-UVA) < SPEF. The low efficiency of AO-H₂O₂ can be mainly related to the low oxidation power of either $\bullet\text{OH}$ weakly physisorbed at the anode surface or H₂O₂ electrogenerated at the

cathode. The AO process was applied to wastewaters showing chloride ions in their composition and then the superiority of AO over AO-H₂O₂ can be mainly attributed to the absence of active chlorine species in the latter process due to their reaction with the electrogenerated H₂O₂. The mineralization was enhanced in EF by virtue of the attack of •OH produced from Fenton's reaction. The additional •OH generation from the FeOH²⁺ photoreduction and the possible direct photolysis of Fe(III)-carboxylate complexes were responsible for the higher efficiency of PEF-UVA process. In SPEF, the mineralization was highlighted due to the ability of natural sunlight to emit in the visible region and its slightly higher UV intensity compared to the employed UVA lamp. However, the SPEF process presented only a slightly superiority over PEF-UVA for the degradation of the winery wastewater and the landfill leachate, diverging from the synthetic solutions. These results indicate the suitability of using UVA lamps, even with low energy power, for the PEF treatment of some wastewaters. Under the best experimental conditions, high degradation rates were attained for all wastewaters when using PEF-UVA and SPEF processes, although with distinct consumptions of electrical energy and UV radiation. To reach a mineralization of 50% by SPEF process, around 2.8 kWh m⁻³ and 3.9 kJ L⁻¹ were consumed both for the synthetic SY wastewater and the winery effluent; 0.26 and 0.89 kWh m⁻³ and 3.6 and 9.9 kJ L⁻¹ were spent for the synthetic TMP wastewater and the secondary MWWTP effluent, respectively, both spiked with a TMP content of 20.0 mg L⁻¹; and 30 kWh m⁻³ and 4.9 kJ L⁻¹ were consumed for the landfill leachate. The relative ability of EAOPs to degrade TMP was the same as for mineralization, contrary to what was found for SY removal, for which EF, PEF-UVA and SPEF processes showed quite similar efficiency. This means that the azo dye was mainly destroyed by •OH produced from Fenton's reaction. In the degradation of the secondary MWWTP effluent, the presence of additional dissolved organic matter induced lower degradation rates than in its absence, likely due to the scavenging of •OH and/or filtration of photochemically active light.

The influence of operational variables on EAOPs efficiency was extensively studied. The effect of the anode nature proved to be dependent on the wastewater composition since the BDD anode achieved only slightly superiority over the Pt one for the treatment of the TMP solution, but its superiority was pronounced for the landfill leachate remediation. In general, the use of higher current densities (*j*) led to increasing degradation rates. However, this improvement came along with higher energy consumptions and, for the winery wastewater and the landfill leachate, almost null/slightly mineralization enhancement was achieved for the highest *j*, likely due to the raise of parasitic reactions. Distinct *j* values were selected as the best ones for the various solutions: 33, 5.0, 25 and 200 mA cm⁻² for the pure SY solution, the pure TMP solution, the winery wastewater

and the landfill leachate, respectively. The increase of the initial total dissolved iron concentration ($[TDI]_0$) improved the efficiency of PEF-UVA up to a value for which this enhancement was decelerated/ceased, suggesting an equilibrium between positive effects coming from the enhancement of Fenton's reaction and negative effects arising from the increase of parasitic reactions and attenuation of light-induced mechanisms. Best $[TDI]_0$ values of 35 and 60 mg L⁻¹ were obtained for the treatment of the winery effluent and the landfill leachate, respectively. Typically, a pH value close to 2.8 leads to maximum degradation efficiencies for EAOPs based on Fenton's reaction, mostly due to the presence of higher concentrations of photoactive iron species and absence of iron precipitation. This was observed for the landfill leachate, but the fastest TMP removals occurred at pH of 3.5 and 4.0. This suggests the influence of the wastewater composition on the best pH value. The addition of Fe(III)-carboxylate complexes to the pure TMP solution and to the landfill leachate in 1:1 to 1:9 Fe(III)-to-carboxylate molar ratios allowed working at higher pH values (3.5 to 5.0), with even higher degradation rates. Oxalate, citrate and tartrate ligands revealed to be efficient, contrary to malate. Higher pollutants removal rates were achieved when using greater pollutants contents. The influence of temperature on the efficiency of EAOPs based on Fenton's reaction proved to be dependent on pH and effluent composition since the amount of iron precipitate and photoactive species varies with these parameters. Depending on the wastewater composition, the UVC radiation proved to be able to lead to superior or quite similar degradations to those achieved when using UVA radiation. The employment of artificial UVA-Vis light provided lower mineralization.

EAOPs were compared with the analogous chemical processes, showing higher mineralization efficiency. However, the chemical processes induced faster removal of some pollutants at the reaction beginning due to a higher initial availability of H₂O₂. Additionally, the viability of SPEF process at large scale was demonstrated and the by-products generated during pollutants degradation were comprehensively studied.

Resumo

A poluição da água por compostos orgânicos provenientes de atividades humanas constitui um dos principais problemas ambientais a nível global que necessita de uma resposta rápida e eficaz. Nos últimos anos, os processos eletroquímicos de oxidação avançados (PEOAs) têm adquirido elevada relevância no tratamento de águas. Estes processos são capazes de degradar os compostos orgânicos recalcitrantes, maioritariamente por intermédio da geração eletroquímica de oxidantes fortes, tais como os radicais hidroxilo ($\bullet\text{OH}$).

A presente tese foca-se na avaliação da viabilidade técnica do uso de alguns PEOAs na degradação de compostos orgânicos recalcitrantes em cinco soluções: (i) uma solução aquosa com 290 mg L⁻¹ de corante azóico Sunset Yellow FCF (SY) em 7,0 g Na₂SO₄ L⁻¹; (ii) uma solução aquosa com 20,0 mg L⁻¹ de antibiótico trimetoprima (TMP) em 7,0 g Na₂SO₄ L⁻¹; (iii) uma água residual recolhida após tratamento secundário numa estação de tratamento de águas residuais (ETAR) municipal, fortificada com TMP na ordem dos mg L⁻¹ ou 19 compostos farmacêuticos na ordem dos µg L⁻¹; (iv) um efluente vinícola; e (v) um lixiviado de aterro sanitário municipal. Os PEOAs foram diretamente aplicados a ambas as soluções puras, doravante também designadas por águas residuais sintéticas, e também ao efluente secundário da ETAR. No efluente vinícola e no lixiviado, procedeu-se à combinação destes processos com outras tecnologias. O efluente vinícola foi sujeito a uma oxidação biológica antes dos PEOAs com o intuito de se remover a fração orgânica biodegradável. No caso do lixiviado, foi aplicada uma estratégia compreendendo as seguintes etapas: (i) tratamento biológico inicial para oxidação do azoto amoniacal, remoção da alcalinidade e biodegradação dos compostos orgânicos; (ii) coagulação para a remoção dos ácidos húmicos e dos sólidos suspensos; (iii) PEOA para a degradação dos compostos orgânicos recalcitrantes e aumento da biodegradabilidade; e (iv) tratamento biológico final. Consideraram-se os seguintes cinco PEOAs: oxidação anódica (OA), oxidação anódica com eletrogeração de peróxido de hidrogénio (OA-H₂O₂), eletro-Fenton (EF), fotoeletro-Fenton (FEF) e fotoeletro-Fenton solar (FEFS). Os PEOAs foram realizados em quatro unidades experimentais à escala laboratorial e piloto, todas elas equipadas com um ânodo de diamante dopado com boro (DDB) ou de platina (Pt) e um cátodo de difusão de ar de carbono-PTFE. Duas destas unidades foram projetadas e construídas no âmbito desta tese.

A eficiência dos vários PEOAs na degradação de compostos orgânicos recalcitrantes foi avaliada principalmente em termos de mineralização e de decaimento da concentração dos poluentes. A

capacidade de mineralização dos PEOAs aumentou na seguinte ordem: OA-H₂O₂ < OA < EF < FEF com radiação UVA (FEF-UVA) < FEFS. A baixa eficiência do processo OA-H₂O₂ deve-se maioritariamente ao baixo poder oxidante quer dos •OH fracamente adsorvidos na superfície do ânodo quer do H₂O₂ electrogerado no cátodo. O processo OA foi aplicado a águas residuais com íões cloreto na sua composição e, sendo assim, a superioridade da OA sobre a OA-H₂O₂ pode ser principalmente atribuída à ausência de espécies ativas de cloro no último processo devido à sua reação com o H₂O₂ electrogerado. A mineralização foi melhorada no EF em consequência do ataque dos •OH produzidos através da reação de Fenton. A geração adicional de •OH a partir da fotorredução de FeOH²⁺ e a possível fotólise direta de complexos Fe(III)-carboxilato foram responsáveis pela maior eficiência do processo FEF-UVA. No FEFS, a mineralização aumentou devido à capacidade da luz solar natural em emitir na região do visível e à sua intensidade de radiação UV ligeiramente superior comparativamente com a da lâmpada UVA utilizada. No entanto, o processo FEFS foi apenas ligeiramente superior ao FEF-UVA na degradação do efluente vinícola e do lixiviado, divergindo das águas residuais sintéticas. Estes resultados remetem para a adequabilidade do uso de lâmpadas UVA, mesmo com baixo poder energético, no tratamento de algumas águas residuais por FEF. Nas condições experimentais ótimas, foram alcançadas elevadas taxas de degradação para todas as águas residuais aquando do uso dos processos FEF-UVA e FEFS, embora com consumos distintos de energia elétrica e de radiação UV. Para atingir uma mineralização de 50% através da aplicação do processo FEFS, foram consumidos cerca de 2,8 kWh m⁻³ e 3,9 kJ L⁻¹ quer na água residual sintética com SY quer no efluente vinícola; 0,26 e 0,89 kWh m⁻³ e 3,6 e 9,9 kJ L⁻¹ na água residual sintética com TMP e no efluente secundário da ETAR, respetivamente, ambos fortificados com uma concentração de TMP de 20,0 mg L⁻¹; e 30 kWh m⁻³ e 4,9 kJ L⁻¹ no lixiviado. A capacidade relativa dos PEOAs no que se refere à degradação da TMP foi igual à obtida em termos de mineralização, em contraste com o que foi observado na remoção do SY, para o qual os processos EF, FEF-UVA e FEFS apresentaram uma eficiência semelhante. Isto significa que o corante azóico foi maioritariamente destruído por •OH produzidos na reação de Fenton. Na degradação do efluente secundário da ETAR, a presença de matéria orgânica adicional induziu menores taxas de degradação do que as obtidas na sua ausência, possivelmente devido à captura de •OH e/ou filtração da luz fotoquimicamente ativa.

A influência de variáveis operacionais na eficiência de degradação dos PEOAs foi amplamente estudada. O efeito da natureza do ânodo provou ser dependente da composição da água residual, uma vez que o ânodo de DDB foi apenas ligeiramente superior ao ânodo de Pt no tratamento da solução pura de TMP, mas a sua superioridade foi elevada no tratamento do lixiviado. Em geral,

o uso de densidades de corrente (j) superiores levou à obtenção de taxas de degradação crescentes. No entanto, esta melhoria envolveu simultaneamente consumos energéticos mais elevados e, no efluente vinícola e no lixiviado, o incremento da mineralização foi nulo/praticamente nulo para os valores de j mais elevados, possivelmente devido ao aumento de reações parasitas. Foram selecionados valores de j distintos como sendo os melhores para as diferentes soluções: 33; 5,0; 25 e 200 mA cm⁻² para a solução pura de SY, a solução pura de TMP, o efluente vinícola e o lixiviado, respetivamente. O aumento da concentração inicial de ferro dissolvido total ([FDT]₀) melhorou a eficiência do processo FEF-UVA até um valor para o qual esta melhoria diminuiu/cessou, sugerindo um equilíbrio entre os efeitos positivos provenientes do aumento da reação de Fenton e os efeitos negativos resultantes do crescimento de reações parasitas e da atenuação dos mecanismos induzidos pela luz. Foram obtidos valores ótimos de [FDT]₀ de 35 e 60 mg L⁻¹ para o tratamento do efluente vinícola e do lixiviado, respetivamente. Tipicamente, um valor de pH de aproximadamente 2,8 leva a eficiências de degradação máximas para os PEOAs baseados na reação de Fenton, sobretudo devido à presença de concentrações superiores de espécies fotoativas de ferro e ausência de precipitação de ferro. Este comportamento foi observado para o lixiviado, no entanto, as remoções de TMP mais rápidas ocorreram a pH de 3,5 e 4,0. Estes resultados sugerem a influência da composição da água residual no melhor valor de pH. A adição de complexos de Fe(III)-carboxilato à solução pura de TMP e ao lixiviado, em razões molares de Fe(III)/carboxilato de 1:1 a 1:9, possibilitou o uso de valores de pH mais elevados (de 3,5 a 5,0), com taxas de degradação inclusivamente superiores. Os ligantes de oxalato, citrato e tartarato revelaram ser eficientes, contrariamente ao malato. Foram obtidas taxas de remoção de poluentes mais elevadas aquando da aplicação de concentrações de poluentes superiores. A influência da temperatura na eficiência dos PEOAs baseados na reação de Fenton provou ser dependente do pH e da composição do efluente, visto que o teor de ferro precipitado e de espécies fotoativas varia com estes parâmetros. Dependendo da composição da água residual, a radiação UVC mostrou poder originar degradações superiores ou praticamente iguais às obtidas com o uso de radiação UVA. O emprego de luz artificial UVA-Vis proporcionou uma mineralização inferior.

Os PEOAs foram comparados com os processos químicos análogos, verificando-se que permitem alcançar eficiências superiores de mineralização. No entanto, os processos químicos conduziram a remoções mais rápidas de alguns poluentes no início da reação devido a uma disponibilidade superior de H₂O₂. Complementarmente, a viabilidade do processo FEFS a grande escala foi demonstrada e os subprodutos gerados no decorrer da degradação dos poluentes foram exaustivamente estudados.

Resumen

La contaminación del agua mediante compuestos orgánicos procedentes de actividades humanas es un gran problema medioambiental global que precisa de una rápida y efectiva respuesta. En los últimos años, los procesos electroquímicos de oxidación avanzada (PEOAs) han ido adquiriendo una gran relevancia para el tratamiento de aguas. Estos procesos son capaces de degradar compuestos orgánicos recalcitrantes, primordialmente vía la generación electroquímica de oxidantes fuertes como el radical hidroxilo ($\bullet\text{OH}$).

La presente tesis está enfocada en evaluar la viabilidad técnica de la aplicación de algunos PEOAs para degradar compuestos orgánicos recalcitrantes de cinco soluciones: (i) una solución acuosa de 290 mg L⁻¹ del colorante azoico Sunset Yellow FCF (SY) en 7,0 g Na₂SO₄ L⁻¹; (ii) una solución acuosa de 20,0 mg L⁻¹ del antibiótico trimetoprima (TMP) en 7,0 g Na₂SO₄ L⁻¹; (iii) un agua residual después del tratamiento secundario de una estación depuradora de aguas residuales (EDAR) municipal con adición de la TMP a niveles de mg L⁻¹ o de 19 compuestos farmacéuticos a niveles de µg L⁻¹; (iv) un agua residual vinícola; y (v) un lixiviado de un vertedero sanitario municipal. Los PEOAs se aplicaron directamente a ambas soluciones puras, referidas como aguas residuales sintéticas, y también al efluente secundario de la EDAR. Para el agua residual vinícola y el lixiviado, estos procesos se combinaron con otras tecnologías. Las aguas residuales vinícolas fueron oxidadas biológicamente antes de los PEOAs para eliminar la fracción orgánica biodegradable. En el tratamiento del lixiviado se aplicó una estrategia con las siguientes etapas: (i) un tratamiento inicial biológico para la oxidación del amonio, la eliminación de la alcalinidad y la biodegradación de contaminantes orgánicos; (ii) una coagulación para eliminar ácidos húmicos y sólidos en suspensión; (iii) un PEOA para degradar los compuestos orgánicos recalcitrantes y mejorar la biodegradabilidad; y (iv) un tratamiento biológico final. Se consideraron los cinco PEOAs siguientes: oxidación anódica (OA), oxidación anódica con peróxido de hidrógeno electrogenerado (OA-H₂O₂), electro-Fenton (EF), fotoelectro Fenton (FEF) y fotoelectro-Fenton solar (FEFS). Los PEOAs se efectuaron en cuatro unidades experimentales a escala de laboratorio y piloto, todas ellas equipadas con un ánodo de diamante dopado con boro (DDB) o de platino (Pt) y un cátodo de difusión de aire de carbón-PTFE. Dos de estas unidades fueron diseñadas y construidas en esta tesis.

La eficiencia de los diferentes PEOAs para degradar los compuestos orgánicos recalcitrantes se evaluó principalmente en términos de su mineralización y del descenso de la concentración de los

contaminantes. Su capacidad de mineralización aumentó en el orden siguiente: OA-H₂O₂ < OA < EF < FEF con radiación UVA (FEF-UVA) < FEFS. La baja eficiencia del método de OA-H₂O₂ puede relacionarse primordialmente al bajo poder oxidante del radical •OH débilmente fisisorbido en la superficie del ánodo o bien del H₂O₂ electrogenerado en el cátodo. El proceso de OA se aplicó a aguas residuales conteniendo iones cloruro en su composición, por lo que la superioridad de la OA con respecto a la OA-H₂O₂ puede atribuirse a la ausencia de especies activas cloradas en el último proceso debido a su reacción con el H₂O₂ electrogenerado. La mineralización se mejoró en EF gracias al ataque del radical •OH producido en la reacción de Fenton. La generación adicional de radical •OH a partir de la fotorreducción del FeOH²⁺ y la posible fotólisis directa de los complejos de Fe(III)-carboxilato eran los responsables de la mayor eficiencia del proceso de FEF-UVA. En el FEFS, la mineralización aumentaba debido a la capacidad de la luz natural solar de emitir en la región visible y de su ligeramente superior intensidad UV comparada a la aplicada por la lámpara UVA. Sin embargo, el proceso de FEFS sólo resultó ser ligeramente superior al de FEF-UVA en la degradación de las aguas residuales vinícolas y del lixiviado, divergiendo de las soluciones sintéticas. Estos resultados ponen de manifiesto el uso adecuado de lámparas UVA, incluso de baja potencia energética, para el tratamiento de algunas aguas residuales mediante el FEF. En las mejores condiciones experimentales, se alcanzaron elevadas velocidades de degradación en todos los casos utilizando los procesos de FEF-UVA y FEFS, aunque con distintos consumos de energía eléctrica y de radiación UV. Para lograr un 50% de mineralización por el proceso de FEFS, se consumieron unos 2,8 kWh m⁻³ y 3,9 kJ L⁻¹ tanto para la solución sintética de SY como el efluente vinícola; 0,26 y 0,89 kWh m⁻³ y 3,6 y 9,9 kJ L⁻¹ para la solución sintética de TMP y el efluente secundario de la EDAR, respectivamente, ambos conteniendo 20,0 mg L⁻¹ de TMP; y 30 kWh m⁻³ y 4,9 kJ L⁻¹ para el lixiviado. La capacidad relativa de los PEOAs para degradar la TMP fue la misma que para la mineralización, contrariamente a la eliminación del SY, para el que los procesos de EF, FEF-UVA y FEFS mostraban una eficiencia similar. Esto significa que el colorante azoico era principalmente destruido por el radical •OH producido por la reacción de Fenton. En la degradación del efluente secundario de la EDAR, la presencia adicional de materia orgánica disuelta inducía menores velocidades de degradación que en su ausencia por la captura de radicales •OH y/o la filtración de luz activa fotoquímicamente.

La influencia de las variables operacionales sobre la eficiencia de los PEOAs se estudió extensivamente. Se encontró que la naturaleza del ánodo dependía de la composición del agua residual dado que el ánodo de DDB no sólo era ligeramente superior sobre el de Pt para el tratamiento de la solución de TMP, sino que su superioridad era más pronunciada para la

descontaminación del lixiviado. En general, el uso de una mayor densidad de corriente (j) dio lugar a velocidades de degradación crecientes. Sin embargo, esta mejora daba lugar a mayores consumos de energía y, para el agua residual vinícola y el lixiviado, se logró una casi nula o ligera mejora de la mineralización para la mayor j , debido al aumento de las reacciones parásitas. Se seleccionaron distintos valores de j para las diversas soluciones: 33, 5,0, 25 y 200 mA cm⁻² para la solución pura de SY, la solución pura de TMP, el agua residual vinícola y el lixiviado de vertedero, respectivamente. El aumento de la concentración inicial de hierro disuelto total ($[HDT]_0$) mejoró la eficiencia del proceso de FEF UVA hasta un valor para el cual se deceleró o cesó esta mejora, sugiriendo un equilibrio entre los efectos positivos provenientes del incremento de la reacción de Fenton y los efectos negativos procedentes de la aceleración de las reacciones parásitas y la atenuación de los mecanismos de luz inducida. Se obtuvieron los mejores valores de la $[HDT]_0$ de 35 y 60 mg L⁻¹ para el tratamiento del efluente vinícola y del lixiviado, respectivamente. Típicamente, un valor del pH próximo a pH 2,8 da lugar a las máximas eficiencias de degradación para los PEOAs basados en la reacción de Fenton, primordialmente debido a la presencia de mayores concentraciones de especies de hierro fotoactivas y a la ausencia de la precipitación de hierro. Esto se observó para el lixiviado, pero las velocidades de eliminación de la TMP ocurrían a pH de 3,5 y 4,0. Esto sugiere la influencia de la composición del agua residual sobre el mejor valor del pH. La adición de complejos de Fe(III) carboxilato a la solución pura de TMP y a la del lixiviado de vertedero en relaciones molares de 1:1 a 1:9 de Fe(III)-a-carboxilato permitió trabajar a mayores valores del pH (de 3,5 a 5,0), incluso con mayores velocidades de degradación. Los ligandos de oxalato, citrato y tartrato revelaron ser eficientes, contrariamente al malato. Se alcanzaron mayores velocidades de eliminación de los contaminantes al operar con contenidos superiores de ellos. La influencia de la temperatura sobre la eficiencia de los PEOAs basados en la reacción de Fenton dependía del pH y de la composición del efluente puesto que la cantidad de hierro precipitado y de las especies fotoactivas variaban con estos parámetros. Dependiendo de la composición del agua residual, se encontró que la radiación UVC daba lugar a degradaciones superiores o muy similares a las alcanzadas con la radiación UVA. El empleo de luz artificial de UVA-Vis condujo a una menor mineralización.

Se compararon los PEOAs con los procesos químicos análogos, mostrando una mayor eficiencia. No obstante, los procesos químicos eran más rápidos en eliminar algunos contaminantes y en el inicio de la reacción debido a la mayor disponibilidad de H₂O₂. Además, se demostró la viabilidad del proceso de FEFS a gran escala y se estudiaron exhaustivamente los productos generados durante la degradación de los contaminantes.

Table of Contents

1	Introduction	1
1.1	Water pollution by persistent organic compounds.....	3
1.2	Wastewater treatment.....	5
1.3	Fundamentals of EAOPs.....	7
1.3.1	Anodic oxidation.....	7
1.3.2	Electro-Fenton.....	12
1.3.3	Photoelectro-Fenton and solar photoelectro-Fenton.....	14
1.4	Influence of operational parameters on EAOPs.....	17
1.4.1	Initial organics concentration.....	17
1.4.2	Background electrolyte composition.....	18
1.4.3	Current density or applied current or potential.....	20
1.4.4	Stirring rate or liquid flow rate.....	21
1.4.5	Temperature.....	22
1.4.6	pH.....	22
1.4.7	Oxygen or air feeding flow rate.....	23
1.4.8	Initial total dissolved iron concentration.....	24
1.5	Degradation of synthetic wastewaters by EAOPs.....	27
1.5.1	Wastewaters containing dyes.....	27
1.5.1.1	Dye content.....	27
1.5.1.2	Background electrolyte.....	32
1.5.1.3	Process.....	33
1.5.1.4	Electrochemical reactor.....	35
1.5.1.5	Operational parameters.....	38
1.5.2	Wastewaters containing pesticides.....	41
1.5.2.1	Pesticide content.....	41
1.5.2.2	Background electrolyte.....	45
1.5.2.3	Process.....	45
1.5.2.4	Electrochemical reactor.....	47
1.5.2.5	Operational parameters.....	48
1.5.3	Wastewaters containing pharmaceuticals.....	49
1.5.3.1	Pharmaceutical content.....	50
1.5.3.2	Background electrolyte.....	53
1.5.3.3	Process.....	53
1.5.3.4	Electrochemical reactor.....	55
1.5.3.5	Operational parameters.....	57
1.5.4	Other synthetic wastewaters.....	58

1.6	Degradation of real wastewaters by EAOPs.....	63
1.6.1	Textile wastewaters	63
1.6.2	Pharmaceutical wastewaters and urban wastewaters after secondary treatment	65
1.6.3	Landfill leachates.....	68
1.6.3.1	Landfill leachate characteristics and pre-treatments.....	71
1.6.3.2	Process.....	71
1.6.3.3	Electrochemical reactor	72
1.6.3.4	Operational parameters.....	73
1.6.4	Other real wastewaters.....	73
1.7	Objectives and outline of the thesis	77
1.8	References	81
2	Materials and methods.....	97
2.1	Chemicals	99
2.2	Analytical determinations.....	101
2.2.1	Miscellaneous	101
2.2.2	Biodegradability assessment.....	106
2.2.2.1	Respirometry	106
2.2.2.2	Zahn-Wellens test	107
2.2.3	Actinometry measurements	108
2.2.3.1	2-Nitrobenzaldehyde concentration actinometry	108
2.2.3.2	Hydrogen peroxide actinometry	108
2.2.3.3	Ferrioxalate actinometry.....	109
2.2.3.4	Calculations	109
2.3	Modeling of degradation kinetics	111
2.4	Experimental units and procedures.....	113
2.4.1	Lab-scale undivided reactor with 150 mL capacity.....	113
2.4.1.1	Description.....	113
2.4.1.2	Hydrogen peroxide accumulation.....	115
2.4.1.3	Experimental procedure.....	115
2.4.2	Pilot-scale flow plant with 10 L capacity	120
2.4.2.1	Description.....	120
2.4.2.2	Experimental procedure.....	122
2.4.3	Lab-scale flow plant with 2.2 L capacity.....	122
2.4.3.1	Description.....	122
2.4.3.2	Radiation sources and photonic flux.....	125
2.4.3.3	Hydrogen peroxide accumulation	128
2.4.3.4	Experimental procedure.....	129
2.4.4	Pilot-scale flow plant with 35 L capacity	132
2.4.4.1	Description.....	132
2.4.4.2	Photonic flux.....	135

2.4.4.3	Hydrogen peroxide accumulation.....	135
2.4.4.4	Experimental procedure.....	136
2.4.5	Biological system I.....	137
2.4.5.1	Description	137
2.4.5.2	Experimental procedure.....	137
2.4.6	Biological system II.....	138
2.4.6.1	Description	138
2.4.6.2	Experimental procedure.....	139
2.4.7	Coagulation/aeration process.....	139
2.5	References	141
3	Degradation of Sunset Yellow FCF azo dye by electrochemical advanced oxidation processes	143
3.1	Introduction	145
3.2	Materials and methods.....	146
3.3	Results and discussion.....	147
3.3.1	Comparative decolorization and mineralization of SY by EAOPs at lab-scale	147
3.3.2	Comparative SY concentration decay by EAOPs at lab-scale	152
3.3.3	Identification and evolution of oxidation products at lab-scale.....	154
3.3.4	Degradation of SY by SPEF at pilot-scale	159
3.3.5	Proposed reaction pathway for SY mineralization	163
3.4	Conclusions	167
3.5	References	169
4	Degradation of trimethoprim antibiotic by electrochemical advanced oxidation processes ...	171
4.1	Introduction	173
4.2	Materials and methods.....	174
4.3	Results and discussion.....	177
4.3.1	Characteristics of the pure TMP solution	177
4.3.2	Effect of operational parameters on the PEF-UVA-BDD process	179
4.3.2.1	Initial total dissolved iron concentration	179
4.3.2.2	Current density	184
4.3.2.3	pH.....	186
4.3.3	Comparison of AO-H ₂ O ₂ , EF, PEF-UVA, SPEF, Fenton and PF-UVA processes.....	188
4.3.4	BDD vs. Pt anodes in PEF-UVA and SPEF processes.....	191
4.3.5	TMP degradation at pilot-scale	194
4.3.6	Nitrogen mass balance.....	195
4.3.7	Generated aromatic products	196
4.3.8	Efficiency of EAOPs using a real wastewater matrix	199
4.3.8.1	Comparison of synthetic and real wastewaters.....	199
4.3.8.2	Comparison of AO, AO-H ₂ O ₂ , PEF-UVA and PEF-UVC processes for the degradation of TMP in a real wastewater matrix	201

4.3.8.3	Degradation of pharmaceutical compounds in a real wastewater matrix at mg L ⁻¹ and µg L ⁻¹ levels	202
4.4	Conclusions	205
4.5	References	207
5	Degradation of trimethoprim antibiotic by UVA photoelectro-Fenton process assisted by Fe(III)-carboxylate complexes	211
5.1	Introduction	213
5.2	Materials and methods	214
5.3	Results and discussion	215
5.3.1	UV-Vis spectra of different solutions	215
5.3.2	Preliminary results for TMP degradation	215
5.3.3	PEF-UVA-BDD degradation in the presence of various Fe(III)-carboxylate complexes	219
5.3.4	Effect of pH and initial Fe(III)-to-carboxylate molar ratio on PEF-UVA-BDD process	226
5.3.5	Effect of initial TMP concentration on PEF-UVA-BDD process	229
5.3.6	Effect of temperature on PEF-UVA-BDD process	231
5.3.7	Role of different oxidizing species	234
5.3.8	Costs on carboxylate ligands	235
5.4	Conclusions	237
5.5	References	239
6	Remediation of a winery wastewater combining aerobic biological oxidation and electrochemical advanced oxidation processes	243
6.1	Introduction	245
6.2	Materials and methods	246
6.3	Results and discussion	247
6.3.1	Characteristics of the raw winery wastewater	247
6.3.2	Aerobic biological oxidation	247
6.3.3	EAOPs	250
6.3.3.1	General	250
6.3.3.2	Influence of initial total dissolved iron concentration on PEF-UVA-BDD process	251
6.3.3.3	Influence of current density on PEF-UVA-BDD process	253
6.3.3.4	Comparison of AO-H ₂ O ₂ , EF, PEF-UVA and SPEF processes	256
6.3.3.5	Evolution of generated carboxylic acids and inorganic ions during EAOPs	259
6.3.4	Biodegradability during SPEF-BDD process	260
6.4	Conclusions	263
6.5	References	265
7	Incorporation of electrochemical advanced oxidation processes in a multistage strategy for sanitary landfill leachate remediation	269
7.1	Introduction	271
7.2	Materials and methods	272
7.3	Results and discussion	275
7.3.1	Characteristics of the raw sanitary landfill leachate	275

7.3.2	Biological treatment	275
7.3.3	Coagulation/aeration process.....	278
7.3.4	EAOPs.....	280
7.3.4.1	General	280
7.3.4.2	Influence of current density on PEF-UVA-BDD process	281
7.3.4.3	Comparison of EF, PEF-UVA, SPEF, Fenton, PF-UVA and SPF processes	283
7.3.5	Biodegradability enhancement during SPEF process.....	286
7.4	Conclusions	289
7.5	References	291
8	Electrochemical advanced oxidation processes for sanitary landfill leachate remediation: Evaluation of operational variables	295
8.1	Introduction	297
8.2	Materials and methods.....	297
8.3	Results and discussion.....	299
8.3.1	Influence of anode material on EF, PEF-UVA and SPEF processes	299
8.3.2	Influence of initial total dissolved iron concentration on PEF-UVA-BDD process.....	302
8.3.3	Influence of pH on PEF-UVA-BDD process and use of Fe(III)-oxalate complexes	303
8.3.4	Influence of temperature on PEF-UVA-BDD process	307
8.3.5	Influence of radiation source on PEF-BDD and SPEF-BDD processes.....	310
8.4	Conclusions	313
8.5	References	315
9	Conclusions and future work	319
9.1	Conclusions	321
9.1.1	Efficiency of EAOPs	322
9.1.1.1	Efficiency of EAOPs in terms of mineralization.....	322
9.1.1.2	Efficiency of EAOPs in terms of target pollutants decay.....	324
9.1.1.3	Efficiency of EAOPs in terms of decolorization.....	325
9.1.2	Influence of operational variables on EAOPs efficiency	325
9.1.2.1	Nature of the anode	325
9.1.2.2	Current density	326
9.1.2.3	Initial total dissolved iron concentration	326
9.1.2.4	pH.....	327
9.1.2.5	Use of Fe(III)-carboxylate complexes.....	327
9.1.2.6	Initial pollutants concentration	327
9.1.2.7	Temperature.....	328
9.1.2.8	Radiation source	328
9.1.3	Comparison between EAOPs and the analogous AOPs.....	328
9.1.4	Scale-up from lab- to pilot-scale	329
9.1.5	By-products generated during the degradation of pollutants.....	329
9.2	Suggestions for future work	330

List of Figures

- Figure 1.1.** EAOPs covered in this thesis and their main reactions..... 7
- Figure 1.2.** Sketch of a thermostated undivided cell of around 100 mL capacity equipped with a carbon-PTFE O₂-diffusion cathode. Reprinted (adapted) from Brillas et al. [55], Copyright © (1995), with permission from The Electrochemical Society..... 35
- Figure 1.3.** Sketch of a simple reactor equipped with an electrochemical cell, a pump and a reservoir. Reprinted (adapted) from Nava et al. [166], Copyright © (2014), with permission from Springer-Verlag Berlin Heidelberg 36
- Figure 1.4.** Sketch of a 2.5 L pre-pilot-scale flow plant equipped with a filter-press electrochemical cell, a planar photoreactor with a mirror at the bottom, a reservoir, a pump and heat exchangers. Reprinted (adapted) from Salazar et al. [88], Copyright © (2011), with permission from Elsevier..... 37
- Figure 1.5.** Sketch of a 10 L pilot-scale flow plant equipped with a filter-press electrochemical cell, a photoreactor with borosilicate tubes and an aluminum reflector, a reservoir, a pump and heat exchangers. Reprinted (adapted) from Garcia-Segura et al. [146], Copyright © (2011), with permission from Elsevier. 37
- Figure 1.6.** Effect of current density on (a) DOC removal, (b) mineralization current efficiency and (c) energy consumption per unit DOC mass as a function of time for the treatment of 127 mg Acid Yellow 9 L⁻¹ in 14 g Na₂SO₄ L⁻¹ by SPEF using the 2.5 L flow plant with a filter-press cell and a planar photoreactor of Figure 1.4 equipped with a BDD anode and a carbon-PTFE air-diffusion cathode, pH of 3.0, 35 °C and [TDI]₀ of 28 mg L⁻¹. Current density: (●) 25, (■) 50, (▲) 100 and (◆) 150 mA cm⁻². Reprinted (adapted) from Ruiz et al. [163], Copyright © (2011), with permission from Elsevier..... 39
- Figure 1.7.** DOC removal as a function of time for the treatment of 194 mg 4-CPA L⁻¹ in 7.0 g Na₂SO₄ L⁻¹ by various EAOPs using a 100 mL undivided cell equipped with a Pt anode and a carbon-PTFE air-diffusion cathode, pH of 3.0, 35 °C, [TDI]₀ of 56 mg L⁻¹ for EF, PEF-UVA and SPEF and *j*_{cat} of 32 mA cm⁻². EAOP: (a-○) AO, (b-□) AO-H₂O₂, (c-△) EF and (d-◇) PEF-UVA. Reprinted (adapted) from Boye et al. [127], Copyright © (2002), with permission from American Chemical Society..... 46
- Figure 1.8.** DOC removal as a function of consumed specific charge for the treatment of 164 mg salicylic acid L⁻¹ in 7.0 g Na₂SO₄ L⁻¹ by various EAOPs using a 100 mL undivided cell equipped with a (a) Pt or (b) BDD anode and a carbon-PTFE air-diffusion cathode, using pH of 3.0, 35 °C, [TDI]₀ of 28 mg L⁻¹ for EF, PEF-UVA and SPEF and *j*_{cat} of 33 mA cm⁻². EAOP: (○,●) AO, (□,■) AO-H₂O₂, (△,▲) EF, (▽,▼) PEF-UVA and (◇,◆) SPEF. Reprinted (adapted) from Guinea et al. [149], Copyright © (2008), with permission from Elsevier..... 54
- Figure 1.9.** Mineralization current efficiency as a function of consumed specific charge for experiments reported in Figure 1.8b. Reprinted from Guinea et al. [149], Copyright © (2008), with permission from Elsevier..... 55
- Figure 2.1.** Sketch of the lab-scale undivided reactor with 150 mL capacity. 114
- Figure 2.2.** Variation of accumulated H₂O₂ concentration with time during the electrolysis of 100 mL of a 7.0 g Na₂SO₄ L⁻¹ solution at pH of 3.0 and 35 °C in the 150 mL capacity lab-scale undivided reactor equipped with a BDD anode and a carbon-PTFE air-diffusion cathode. Current density: (■) 16.7, (●) 33.3 and (▲) 100 mA cm⁻²..... 115
- Figure 2.3.** Sketches of (a) the pilot-scale flow plant with 10 L capacity and (b) the respective one-compartment filter-press reactor. 121
- Figure 2.4.** Sketches of (a) the lab-scale flow plant with 2.2 L capacity and (b) the one-compartment filter-press MicroFlowCell reactor. 124

- Figure 2.5.** Pictures of the lab-scale flow plant with 2.2 L capacity under (a) PEF operation using an UVA artificial lamp and (b) SPEF operation. 125
- Figure 2.6.** Spectral irradiance of UVA, UVA-Vis and UVC lamps and natural sunlight (UVA lamp: measured with the spectro-radiometer and confirmed by Philips; UVA-Vis lamp: measured with the spectro-radiometer – not calibrated – qualitative information; UVC lamp: supplied by Philips; natural sunlight: AM1.5G reference spectrum [17]). 126
- Figure 2.7.** Variation of accumulated H_2O_2 concentration with time during the electrolysis of 1250 mL of a 7.0 g $\text{Na}_2\text{SO}_4 \text{ L}^{-1}$ solution at pH of 3.0 and 20 °C in the 2.2 L capacity lab-scale flow plant equipped with a BDD anode and a carbon-PTFE air-diffusion cathode. Current density: (a) (■) 2.5, (●) 5 and (▲) 10 mA cm^{-2} and (b) (◆) 50, (▼) 100 and (★) 150 mA cm^{-2} . Plot (a) also presents the change of H_2O_2 concentration under (⊗) EF, (⦿) PEF and (⊕) SPEF conditions with $[\text{TDI}]_0 = 2.0 \text{ mg L}^{-1}$ at 5 mA cm^{-2} and (○) using a Pt anode instead of BDD. 129
- Figure 2.8.** Sketches of (a) the pilot-scale flow plant with 35 L capacity and (b) the one-compartment filter-press ElectroMPCell reactor. 133
- Figure 2.9.** Pictures of the pilot-scale flow plant with 35 L capacity. (a) Front view and (b) back view. 134
- Figure 2.10.** Variation of accumulated H_2O_2 concentration with time during the electrolysis of 25 L of a 7.0 g $\text{Na}_2\text{SO}_4 \text{ L}^{-1}$ solution at pH of 3.0 and 20 °C in the 35 L capacity pilot-scale flow plant equipped with a Pt anode and a carbon-PTFE air-diffusion cathode. Current density: (■) 50, (●) 100 and (▲) 200 mA cm^{-2} 136
- Figure 2.11.** Sketch of the biological system I (IBR + conditioner tank). 138
- Figure 2.12.** Sketch of the biological system II (reactor vessel). 139
- Figure 3.1.** Evaluation of color removal as a function of time for the treatment of 290 mg SY L^{-1} in 7.0 g $\text{Na}_2\text{SO}_4 \text{ L}^{-1}$ by various EAOPs using pH of 3.0, 35 °C, $[\text{TDI}]_0$ of 28 mg L^{-1} for EF-BDD, PEF-UVA-BDD and SPEF-BDD and j of 33.3 mA cm^{-2} . EAOP: (■) AO- H_2O_2 -BDD, (●) EF-BDD, (▲) PEF-UVA-BDD and (◆) SPEF-BDD. The inset panel of Figure 3.1a shows the UV-Vis absorption spectrum of the initial SY solution diluted 1:5. 149
- Figure 3.2.** Evolution of normalized DOC removal as a function of time for the treatment of 290 mg SY L^{-1} in 7.0 g $\text{Na}_2\text{SO}_4 \text{ L}^{-1}$ by various EAOPs using pH of 3.0, 35 °C, $[\text{TDI}]_0$ of 28 mg L^{-1} for EF-BDD, PEF-UVA-BDD and SPEF-BDD and j of 33.3 mA cm^{-2} . EAOP: (■) AO- H_2O_2 -BDD, (●) EF-BDD, (▲) PEF-UVA-BDD and (◆) SPEF-BDD. 150
- Figure 3.3.** Effect of current density on normalized DOC removal as a function of consumed specific charge for the treatment of 290 mg SY L^{-1} in 7.0 g $\text{Na}_2\text{SO}_4 \text{ L}^{-1}$ by (a) AO- H_2O_2 -BDD, (b) EF-BDD, (c) PEF-UVA-BDD and (d) SPEF-BDD using pH of 3.0, 35 °C and $[\text{TDI}]_0$ of 28 mg L^{-1} for EF-BDD, PEF-UVA-BDD and SPEF-BDD. Current density: (■) 16.7, (●) 33.3 and (▲) 100 mA cm^{-2} 152
- Figure 3.4.** Evolution of normalized SY concentration decay as a function of time for the treatment of 290 mg SY L^{-1} in 7.0 g $\text{Na}_2\text{SO}_4 \text{ L}^{-1}$ by various EAOPs using pH of 3.0, 35 °C, $[\text{TDI}]_0$ of 28 mg L^{-1} for EF-BDD, PEF-UVA-BDD and SPEF-BDD and j of 33.3 mA cm^{-2} . EAOP: (■) AO- H_2O_2 -BDD, (●) EF-BDD, (▲) PEF-UVA-BDD and (◆) SPEF-BDD. 153
- Figure 3.5.** Evolution of the concentration of (a) tartronic, (b) oxalic, (c) formic and (d) oxamic acids during the treatment of 290 mg SY L^{-1} in 7.0 g $\text{Na}_2\text{SO}_4 \text{ L}^{-1}$ by (■) AO- H_2O_2 -BDD, (●) EF-BDD, (▲) PEF-UVA-BDD and (◆) SPEF-BDD using pH of 3.0, 35 °C and $[\text{TDI}]_0$ of 28 mg L^{-1} 158
- Figure 3.6.** Effect of current density on (a) color removal, (b) normalized DOC removal and (c) energy consumption per unit DOC mass as a function of time for the treatment of 290 mg SY L^{-1} in 7.0 g $\text{Na}_2\text{SO}_4 \text{ L}^{-1}$ by SPEF-Pt at the 10 L pilot-scale flow plant using pH of 3.0, 35 °C and $[\text{TDI}]_0$ of 28 mg L^{-1} . Current density: (■) 33.2, (●) 55.4 and (▲) 77.6 mA cm^{-2} 160
- Figure 3.7.** (a) Evolution of normalized SY concentration decay as a function of time for the treatment of 290 mg SY L^{-1} in 7.0 g $\text{Na}_2\text{SO}_4 \text{ L}^{-1}$ by SPEF-Pt at the 10 L pilot-scale flow plant using pH of 3.0, 35 °C, $[\text{TDI}]_0$ of 28 mg L^{-1} and j of 77.6 mA cm^{-2} . (b) Evolution of the concentration of (■) tartronic, (●) oxalic, (▲) formic and (◆) oxamic acids during the abovementioned treatment. 163

- Figure 3.8.** Proposed reaction sequence for the mineralization of Sunset Yellow FCF in acidic medium by EAOPs. $M(\cdot\text{OH})$ denotes the reactive $\cdot\text{OH}$ generated either at a Pt or BDD anode surface, whereas BDD($\cdot\text{OH}$) represents this radical on a BDD anode surface. 164
- Figure 4.1.** Absorption spectra of different solutions at pH = 3.5 (without dilution). $[\text{TMP}] = 20.0 \text{ mg L}^{-1}$, $[\text{Na}_2\text{SO}_4] = 7.0 \text{ g L}^{-1}$, $[\text{Fe}^{2+}] = 2.0 \text{ mg L}^{-1}$ and $[\text{Fe}^{3+}] = 2.0 \text{ mg L}^{-1}$. The spectral irradiances of UVA lamp and natural sunlight are also shown (UVA lamp: measured with the spectro-radiometer and confirmed by Philips; natural sunlight: AM1.5G reference spectrum [14]). 178
- Figure 4.2.** Fe^{3+} speciation diagrams as a function of solution pH in a calculated system containing: (a, b) $3.58 \times 10^{-5} \text{ M}$ of Fe^{3+} ($2.0 \text{ mg Fe}^{3+} \text{ L}^{-1}$), $4.93 \times 10^{-2} \text{ M}$ of SO_4^{2-} and $9.86 \times 10^{-2} \text{ M}$ of Na^+ ($7.0 \text{ g Na}_2\text{SO}_4 \text{ L}^{-1}$) (ionic strength = 0.148 M) or (c, d) $3.58 \times 10^{-5} \text{ M}$ of Fe^{3+} ($2.0 \text{ mg Fe}^{3+} \text{ L}^{-1}$) in absence of Na_2SO_4 (ionic strength $\sim 0 \text{ M}$). Data were calculated by the chemical equilibrium modeling system MINEQL+ [15] using the equilibrium constants of Table 4.2. The formation of the solid iron phase $\text{Fe}(\text{OH})_3$ was (a, c) excluded and (b, d) included in the calculation. 179
- Figure 4.3.** Effect of initial total dissolved iron concentration on (solid symbols) normalized TMP concentration decay and (open symbols) normalized DOC removal as a function of time for PEF-UVA-BDD treatment of a $20.0 \text{ mg TMP L}^{-1}$ solution in $7.0 \text{ g Na}_2\text{SO}_4 \text{ L}^{-1}$ using pH of 3.0, 20°C and j of 10 mA cm^{-2} . $[\text{TDI}]_0$: (■, □) 2.0, (●, ○) 3.0, (▲, △) 4.0 and (◆, ◇) 8.0 mg L^{-1} 180
- Figure 4.4.** Evaluation of PF process in terms of: (a) (solid symbols) normalized TMP concentration decay and (open symbols) normalized DOC removal and (b) (solid symbols) total dissolved iron concentration and (open symbols) H_2O_2 consumption as a function of time for treatment of a $20.0 \text{ mg TMP L}^{-1}$ solution using pH of 3.5, 20°C and $[\text{TDI}]_0$ of 2.0 mg L^{-1} . Conditions: (■, □) $7.0 \text{ g Na}_2\text{SO}_4 \text{ L}^{-1}$ and total addition of stoichiometric H_2O_2 at $t = 0 \text{ min}$, (●, ○) absence of Na_2SO_4 and gradual H_2O_2 addition and (▲, △) $7.0 \text{ g Na}_2\text{SO}_4 \text{ L}^{-1}$ and gradual H_2O_2 addition. 184
- Figure 4.5.** Effect of current density on (a) normalized TMP concentration decay, (b) energy consumption per unit TMP mass, (c) (open symbols) normalized DOC removal and (dot profile) H_2O_2 concentration and (d) mineralization current efficiency as a function of time for PEF-UVA-BDD treatment of a $20.0 \text{ mg TMP L}^{-1}$ solution in $7.0 \text{ g Na}_2\text{SO}_4 \text{ L}^{-1}$ using pH of 3.0, 20°C and $[\text{TDI}]_0$ of 2.0 mg L^{-1} . Current density: (■, □) 2.5, (●, ○) 5, (▲, △) 10, (◆, ◇) 50, (▼, ▽) 100 and (★, ☆) 150 mA cm^{-2} 186
- Figure 4.6.** Effect of pH on (a) (solid symbols) normalized TMP concentration decay and (open symbols) normalized DOC removal and (b) total dissolved iron concentration as a function of time for PEF-UVA-BDD treatment of a $20.0 \text{ mg TMP L}^{-1}$ solution in $7.0 \text{ g Na}_2\text{SO}_4 \text{ L}^{-1}$ using 20°C , $[\text{TDI}]_0$ of 2.0 mg L^{-1} and j of 5.0 mA cm^{-2} . Initial pH: (■, □) 3.0, (●, ○) 3.5, (▲, △) 4.0 and (◆, ◇) 4.5. 187
- Figure 4.7.** Evaluation of (a) normalized TMP concentration decay, (b) normalized DOC removal and (c) H_2O_2 concentration (for EAOPs) or H_2O_2 consumption (for AOPs) as a function of time for treatment of $20.0 \text{ mg TMP L}^{-1}$ solution in $7.0 \text{ g Na}_2\text{SO}_4 \text{ L}^{-1}$ by various processes using pH of 3.5, 20°C , $[\text{TDI}]_0$ of 2.0 mg L^{-1} for Fenton's reaction based processes, j of 5.0 mA cm^{-2} for EAOPs and initial H_2O_2 addition of 103 mg L^{-1} for AOPs. Process: (■) AO- H_2O_2 -BDD (●) EF-BDD, (▲) PEF-UVA-BDD, (◆) SPEF-BDD, (▼) Fenton and (★) PF-UVA. 189
- Figure 4.8.** (a,b) Effect of (■, □) BDD and (●, ○) Pt anodes on treatment by (solid symbols) PEF-UVA and (open symbols) SPEF processes of a $20.0 \text{ mg TMP L}^{-1}$ solution in $7.0 \text{ g Na}_2\text{SO}_4 \text{ L}^{-1}$ using pH of 3.5, 20°C , $[\text{TDI}]_0$ of 2.0 mg L^{-1} and j of 5.0 mA cm^{-2} . (a) (Solid profile) normalized TMP concentration decay and (dot profile) normalized DOC removal for PEF-UVA and (b) normalized DOC removal for SPEF as a function of accumulated UV energy per L of solution. In plot (c), evolution of the concentration of (■, □) oxalic and (●, ○) formic acids during (solid symbols) SPEF-BDD and (open symbols) SPEF-Pt. 193
- Figure 4.9.** (a) Normalized TMP concentration decay and (b) normalized DOC removal as a function of accumulated UV energy per L of solution for SPEF-Pt treatment of a $20.0 \text{ mg TMP L}^{-1}$ solution in $7.0 \text{ g Na}_2\text{SO}_4 \text{ L}^{-1}$ using pH of 3.5, 20°C , $[\text{TDI}]_0$ of 2.0 mg L^{-1} and j of 5.0 mA cm^{-2} at (■, □) lab-scale, i.e. using the 2.2 L lab-scale flow plant, and at (●, ○) pilot-scale, i.e. using the 35 L pilot-scale flow plant. 195

- Figure 4.10.** Evolution of (■) nitrate ion, (●) ammonium ion, (▲) total organic nitrogen and (★) total dissolved nitrogen as a function of time during SPEF-Pt process using pH of 3.5, 20 °C, $[TDI]_0$ of 2.0 mg L⁻¹ and j of 5.0 mA cm⁻². 196
- Figure 4.11.** (Solid symbols) Normalized TMP concentration decay and (open symbols) normalized DOC removal as a function of accumulated UV energy per L of solution for SPEF-Pt treatment at pH of 3.5, 20 °C, $[TDI]_0$ of 2.0 mg L⁻¹ and j of 5.0 mA cm⁻² of two distinct matrices spiked with 20.0 mg TMP L⁻¹: (■, □) ultrapure water with 7.0 g Na₂SO₄ L⁻¹ and (●, ○) real wastewater collected after secondary treatment of a MWWTP. 200
- Figure 4.12.** Evaluation of (a) normalized TMP concentration decay and (b) normalized DOC removal as a function of time for treatment of the real wastewater spiked with 5.0 mg TMP L⁻¹ by various EAOPs using the pH of the effluent (6.8) for AO and AO-H₂O₂ and pH of 3.5 for PEF, 20 °C, $[TDI]_0$ of 2.0 mg L⁻¹ for PEF and j of 5.0 mA cm⁻². EAOP: (★, ☆) AO-BDD, (■, □) AO-H₂O₂-BDD, (▲, △) PEF-UVA-BDD and (▼, ▽) PEF-UVC-BDD. 202
- Figure 4.13.** Normalized TMP concentration decay as a function of time for AO-BDD treatment of the real wastewater spiked with (★) 5.0 mg TMP L⁻¹ and (☆) mixture of 19 pharmaceutical compounds in 16-34 µg L⁻¹ levels using the pH of the effluent (6.8), 20 °C and j of 5.0 mA cm⁻². 203
- Figure 4.14.** Decay profiles of 19 pharmaceutical compounds in 16-34 µg L⁻¹ levels as a function of time for AO-BDD treatment of Figure 4.13. 204
- Figure 5.1.** Absorption spectra of different solutions at pH = 3.5 (without dilution). $[TMP] = 20.0$ mg L⁻¹, $[Na_2SO_4] = 7.0$ g L⁻¹, $[Fe^{2+}] = 2.0$ mg L⁻¹, $[Fe^{3+}] = 2.0$ mg L⁻¹, 1:3 Fe(III)-to-oxalate molar ratio, 1:1 Fe(III)-to-citrate molar ratio, 1:1 Fe(III)-to-tartrate molar ratio and 1:1 Fe(III)-to-malate molar ratio. The spectral irradiance of UVA lamp is also shown, measured with the spectro-radiometer and confirmed by Philips. 216
- Figure 5.2.** Fe³⁺ speciation diagrams as a function of solution pH in a calculated system containing: (a) 1.07×10^{-4} M of oxalate ion (1:3 Fe(III)-to-oxalate molar ratio), (b) 3.58×10^{-5} M of citrate ion (1:1 Fe(III)-to-citrate molar ratio), (c) 3.58×10^{-5} M of tartrate ion (1:1 Fe(III)-to-tartrate molar ratio) or (d) 3.58×10^{-5} M of malate ion (1:1 Fe(III)-to-malate molar ratio), with 3.58×10^{-5} M of Fe³⁺ (2.0 mg L⁻¹), 1.07×10^{-4} M of Cl⁻ (9.7 mg FeCl₃·6H₂O L⁻¹), 4.93×10^{-2} M of SO₄²⁻ and 9.86×10^{-2} M of Na⁺ (7.0 g Na₂SO₄ L⁻¹) (ionic strength = 0.148 M). Data were calculated from the chemical equilibrium modeling system MINEQL+ [14] using the equilibrium constants of Table 5.1. The formation of the solid iron phase Fe(OH)₃ was included in the calculation despite the slow formation of solid phases on the time scale of the experiments. 217
- Figure 5.3.** Effect of Fe(III)-carboxylate complexes on (a) normalized TMP concentration decay, (b) normalized DOC removal and (c) total dissolved iron concentration as a function of time for PEF-UVA-BDD treatment of a 20.0 mg TMP L⁻¹ solution in 7.0 g Na₂SO₄ L⁻¹ using pH of 4.5, $[TDI]_0$ of 2.0 mg L⁻¹, 20 °C and j of 5.0 mA cm⁻². Fe(III)-carboxylate complex (Fe(III)-to-carboxylate molar ratio): (■) Fe(III)-oxalate (1:3), (●) Fe(III)-citrate (1:1), (▲) Fe(III)-tartrate (1:1) and (◆) Fe(III)-malate (1:1). (☆) Classical PEF-UVA-BDD process (without carboxylic acids addition) at pH of 3.5. 220
- Figure 5.4.** Fe³⁺ speciation diagrams as a function of solution pH in a calculated system containing: (a) 1.07×10^{-4} M of oxalate ion (1:3 Fe(III)-to-oxalate molar ratio), (b) 3.58×10^{-5} M of citrate ion (1:1 Fe(III)-to-citrate molar ratio), (c) 3.58×10^{-5} M of tartrate ion (1:1 Fe(III)-to-tartrate molar ratio) or (d) 3.58×10^{-5} M of malate ion (1:1 Fe(III)-to-malate molar ratio), with 3.58×10^{-5} M of Fe³⁺ (2.0 mg L⁻¹) and 1.07×10^{-4} M of Cl⁻ (9.7 mg FeCl₃·6H₂O L⁻¹) in the absence of Na₂SO₄ (ionic strength ~ 0 M). Data were calculated from the chemical equilibrium modeling system MINEQL+ [14] using the equilibrium constants of Table 5.1. The formation of the solid iron phase Fe(OH)₃ was included in the calculation despite the slow formation of solid phases on the time scale of the experiments. 222
- Figure 5.5.** Evolution of the concentration of (■) oxalic, (●) formic, (◆) citric, (▼) tartaric and (★) malic acids during PEF-UVA-BDD treatment under conditions of Figure 5.3. System: (a) Fe(III)-oxalate, (b) Fe(III)-citrate, (c) Fe(III)-tartrate and (d) Fe(III)-malate. 224

Figure 5.6. Effect of pH and initial Fe(III)-to-carboxylate molar ratio on (a) normalized TMP concentration decay, (b) total dissolved iron concentration and (c) normalized DOC removal as a function of time for PEF-UVA-BDD treatment of a 20.0 mg TMP L⁻¹ solution in 7.0 g Na₂SO₄ L⁻¹ using [TDI]₀ of 2.0 mg L⁻¹, 20 °C and *j* of 5.0 mA cm⁻². Conditions: (■) pH of 4.5 and 1:3 Fe(III)-to-oxalate molar ratio, (●) pH of 5.0 and 1:3 Fe(III)-to-oxalate molar ratio, (▲) pH of 5.0 and 1:6 Fe(III)-to-oxalate molar ratio, (◆) pH of 5.0 and 1:9 Fe(III)-to-oxalate molar ratio, (▼) pH of 5.5 and 1:9 Fe(III)-to-oxalate molar ratio, (□) pH of 4.5 and 1:1 Fe(III)-to-citrate molar ratio and (○) pH of 5.0 and 1:1 Fe(III)-to-citrate molar ratio. 227

Figure 5.7. Fe³⁺ speciation diagrams as a function of solution pH in a calculated system containing: (a) 2.15 × 10⁻⁴ M of oxalate ion (1:6 Fe(III)-to-oxalate molar ratio) or (b) 3.22 × 10⁻⁴ M of oxalate ion (1:9 Fe(III)-to-oxalate molar ratio), with 3.58 × 10⁻⁵ M of Fe³⁺ (2.0 mg L⁻¹), 1.07 × 10⁻⁴ M of Cl⁻ (9.7 mg FeCl₃·6H₂O L⁻¹), 4.93 × 10⁻² M of SO₄²⁻ and 9.86 × 10⁻² M of Na⁺ (7.0 g Na₂SO₄ L⁻¹) (ionic strength = 0.148 M). Data were calculated from the chemical equilibrium modeling system MINEQL+ [14] using the equilibrium constants of Table 5.1. The formation of the solid iron phase Fe(OH)₃ was included in the calculation despite the slow formation of solid phases on the time scale of the experiments..... 229

Figure 5.8. Effect of initial TMP concentration on (a) normalized TMP concentration decay and (b) normalized DOC removal for PEF-UVA-BDD treatment of a TMP solution in 7.0 g Na₂SO₄ L⁻¹ using pH of 4.5, [TDI]₀ of 2.0 mg L⁻¹, 1:1 Fe(III)-to-citrate molar ratio, 20 °C and *j* of 5.0 mA cm⁻². Initial TMP concentration: (■) 2.0, (●) 5.0, (▲) 10.0 and (◆) 20.0 mg L⁻¹. The inset panels depict the corresponding decays in mg L⁻¹. 230

Figure 5.9. Effect of temperature on (a) normalized TMP concentration decay and (b) normalized DOC removal for PEF-UVA-BDD treatment of a 20.0 mg TMP L⁻¹ solution in 7.0 g Na₂SO₄ L⁻¹ using pH of 4.5, [TDI]₀ of 2.0 mg L⁻¹, 1:3 Fe(III)-to-oxalate molar ratio, 20 °C and *j* of 5.0 mA cm⁻². Temperature: (■) 10, (●) 20 and (▲) 40 °C. 232

Figure 5.10. Theoretical molar fraction of (a) Fe(ox)₂⁻ and Fe(ox)₃³⁻ and (b, c) FeOH²⁺ species, regarding the total Fe³⁺ concentration, as a function of the solution pH at: (solid profile) 10 °C, (dash profile) 20 °C and (dash dot profile) 40 °C. Systems: (a) 1.07 × 10⁻⁴ M of oxalate ion (1:3 Fe(III)-to-oxalate molar ratio), 3.58 × 10⁻⁵ M of Fe³⁺ (2.0 mg L⁻¹), 1.07 × 10⁻⁴ M of Cl⁻ (9.7 mg FeCl₃·6H₂O L⁻¹), 4.93 × 10⁻² M of SO₄²⁻ and 9.86 × 10⁻² M of Na⁺ (7.0 g Na₂SO₄ L⁻¹), (b) absence of oxalate ion and (c) absence of oxalate ion and Na₂SO₄. Ionic strength of 0.148 or ~ 0 M in the presence and absence of Na₂SO₄, respectively. Data were calculated from the chemical equilibrium modeling system MINEQL+ [14] using the equilibrium constants of Table 5.1. The formation of the solid iron phase Fe(OH)₃ was included in the calculation despite the slow formation of solid phases on the time scale of the experiments. 233

Figure 5.11. Effect of (●) D-mannitol and (▲) sodium azide on normalized TMP concentration decay for PEF-UVA-BDD treatment of a 20.0 mg TMP L⁻¹ solution in 7.0 g Na₂SO₄ L⁻¹ using pH of 4.5, [TDI]₀ of 2.0 mg L⁻¹, 1:1 Fe(III)-to-citrate molar ratio, 20 °C and *j* of 5.0 mA cm⁻². (■) Absence of scavenging agents. 235

Figure 6.1. Assessment of the efficiency of biological oxidation in the treatment of the raw winery wastewater in terms of (■) DOC removal, (●) total dissolved polyphenols concentration decay and (▲) pH. 249

Figure 6.2. Influence of initial total dissolved iron concentration on (a) normalized DOC removal and (b) total dissolved iron concentration as a function of time for PEF-UVA-BDD treatment of the winery wastewater after biological oxidation using pH of 2.8, 25 °C and *j* of 100 mA cm⁻². [TDI]₀: (■) 20, (●) 35 and (▲) 70 mg L⁻¹. 252

Figure 6.3. Effect of current density on (a) normalized DOC removal, (b) energy consumption per unit DOC mass, (c) H₂O₂ concentration and (d) total dissolved polyphenols concentration decay as a function of time for PEF-UVA-BDD treatment of the winery wastewater after biological oxidation using pH of 2.8, 25 °C and [TDI]₀ of 35 mg L⁻¹. Current density: (■) 10, (●) 25 and (▲) 100 mA cm⁻². 254

- Figure 6.4.** Evaluation of (a) normalized DOC removal, (b) H_2O_2 concentration and (c) total dissolved polyphenols concentration decay as a function of time for treatment of the winery wastewater after biological oxidation by various EAOPs using pH of 2.8, 25 °C, $[\text{TDI}]_0$ of 35 mg L^{-1} in EF-BDD, PEF-UVA-BDD and SPEF-BDD, and j of 25 mA cm^{-2} . EAOP: (■) AO- H_2O_2 -BDD, (●) EF-BDD, (▲) PEF-UVA-BDD and (◆) SPEF-BDD. The inset panel of Figure 6.4a depicts the normalized DOC removal in PEF-UVA-BDD and SPEF-BDD systems as a function of accumulated UV energy per L of solution. (d) SPEF-BDD process assessment in terms of (◆) normalized DOC removal and (◇) normalized COD removal..... 258
- Figure 6.5.** Time course of (a) percentage of $[\text{LMCA}]/[\text{DOC}]$ ratio and concentration of (b) oxalic and (c) malic acids during the (■) AO- H_2O_2 -BDD, (●) EF-BDD, (▲) PEF-UVA-BDD and (◆) SPEF-BDD processes of Figure 6.4..... 260
- Figure 6.6.** Biodegradability of samples collected at different times of a SPEF-BDD treatment under conditions of Figure 6.4 assessed by respirometry. The inset panel depicts the biodegradable character of a sample according to its $\text{bCOD}/[\text{COD}]$ ratio. A.B.O.: Winery wastewater after biological oxidation..... 261
- Figure 7.1.** Change of (■) DOC, (Δ) ammonium (N-NH_4^+), (◇) nitrite (N-NO_2^-) and (☆) nitrate (N-NO_3^-) concentrations in a biological process batch of the raw landfill leachate and after coagulation and aeration steps. 277
- Figure 7.2.** Fe^{3+} speciation diagrams as a function of solution pH in a calculated system containing the average amounts of NO_3^- , SO_4^{2-} , Cl^- , Ca^{2+} , Mg^{2+} , K^+ and Na^+ ions of the landfill leachate after aeration (Table 7.1) and 60 mg L^{-1} of Fe^{3+} (ionic strength = 0.390 M). Data were calculated from the chemical equilibrium modeling system MINEQL+ [35] using the equilibrium constants of Table 5.1. The formation of the solid iron phase $\text{Fe}(\text{OH})_3$ was included in the calculation despite the slow formation of solid phases on the time scale of the experiments. 281
- Figure 7.3.** Effect of current density on (a) normalized DOC removal, (b) total dissolved iron concentration, (c) specific energy consumption per unit DOC mass and (d) H_2O_2 concentration as a function of time for PEF-UVA-BDD treatment of the pre-treated landfill leachate using pH of 2.8, 20 °C and $[\text{TDI}]_0$ of 60 mg L^{-1} . Current density: (■) 25, (●) 100, (▲) 200 and (◆) 300 mA cm^{-2} 282
- Figure 7.4.** Evolution of normalized DOC removal (a1, b1) as a function of time and (a1.1 and a1.2) as a function of accumulated UV energy per L of solution; (a2, b2) time-course of H_2O_2 concentration (for EAOPs) or H_2O_2 consumption (for AOPs) during the treatment of the pre-treated landfill leachate by various processes using pH of 2.8, 20 °C, j of 200 mA cm^{-2} for EAOPs and $[\text{H}_2\text{O}_2]$ of 200-400 mg L^{-1} for AOPs. EAOPs: (■) EF-BDD- $[\text{TDI}]_0$ of 12 mg L^{-1} , (●) EF-BDD- $[\text{TDI}]_0$ of 60 mg L^{-1} , (▲) PEF-UVA-BDD- $[\text{TDI}]_0$ of 60 mg L^{-1} and (◆) SPEF-BDD- $[\text{TDI}]_0$ of 60 mg L^{-1} . AOPs: (○) Fenton, (Δ) PF-UVA and (◇) SPF, all using $[\text{TDI}]_0$ of 60 mg L^{-1} . Extra processes: (☆) UVA photolysis with initial H_2O_2 addition of 700 mg L^{-1} and (▲) (dot profile) PEF-UVA-BDD- $[\text{TDI}]_0$ of 60 mg L^{-1} with initial H_2O_2 addition of 700 mg L^{-1} 284
- Figure 7.5.** Zahn-Wellens test for samples collected during SPEF-Pt process at pilot-scale using pH of 2.8, 20 °C, $[\text{TDI}]_0$ of 60 mg L^{-1} and j of 200 mA cm^{-2} . Samples were characterized in Table 7.3. (■) - S_0 , (□) - S_1 , (●) - S_2 , (○) - S_3 , (▲) - S_4 , (Δ) - S_5 , (◆) - S_6 , (◇) - S_7 , (★) - S_8 , (☆) - S_9 and (×) - Reference (DOC at day 0 = 218 mg L^{-1}). 287
- Figure 8.1.** Influence of anode material, (solid symbols) BDD and (open symbols) Pt, on normalized DOC removal as a function of time for treatment of the pre-treated landfill leachate by (■, □) EF- $[\text{TDI}]_0$ of 12 mg L^{-1} , (●, ○) EF- $[\text{TDI}]_0$ of 60 mg L^{-1} , (▲, Δ) PEF-UVA- $[\text{TDI}]_0$ of 60 mg L^{-1} and (◆, ◇) SPEF- $[\text{TDI}]_0$ of 60 mg L^{-1} using pH of 2.8, 20 °C and j of 200 mA cm^{-2} . The inset panel depicts the normalized DOC removal in SPEF systems as a function of accumulated UV energy per L of solution. Extra process: (★) AO- $[\text{TDI}]_0$ of 12 mg L^{-1} using a BDD anode, a Pt cathode, pH of 2.8, 20 °C and j of 200 mA cm^{-2} 300
- Figure 8.2.** Effect of initial total dissolved iron concentration on (a) normalized DOC removal and (b) total dissolved iron concentration as a function of time for PEF-UVA-BDD treatment of the pre-treated landfill leachate using pH of 2.8, 20 °C and j of 200 mA cm^{-2} . $[\text{TDI}]_0$: (■) 20, (●) 40, (▲) 60 and (◆) 80 mg L^{-1} 303

Figure 8.3. Effect of pH and initial addition of 1:3 Fe(III)-to-oxalate molar ratio on (a) normalized DOC removal and (b) total dissolved iron concentration as a function of time for PEF-UVA-BDD treatment of the pre-treated landfill leachate using 20 °C, $[TDI]_0$ of 60 mg L⁻¹ and j of 200 mA cm⁻². pH values for trials without oxalic acid addition: (■) 2.8, (●) 3.5 and (▲) 4.0. pH values for trials with oxalic acid addition: (□) 2.8, (○) 3.5, (△) 4.0 and (◇) 5.0..... 305

Figure 8.4. Fe³⁺ speciation diagrams as a function of the solution pH in a calculated system containing the average amounts of NO₃⁻, SO₄²⁻, Cl⁻, Ca²⁺, Mg²⁺, K⁺ and Na⁺ of the landfill leachate after aeration (Table 7.1), 60 mg L⁻¹ of Fe³⁺ and 1:3 Fe(III)-to-oxalate molar ratio (ionic strength = 0.396 M). Data were calculated by the chemical equilibrium modeling system MINEQL+ [32] using the equilibrium constants of Table 5.1. The formation of the solid iron phase Fe(OH)₃ was included in the calculation despite the slow formation of solid phases on the time scale of the experiments. 306

Figure 8.5. (a) Absorption spectra of the pre-treated sanitary landfill leachate at various pH values, without and with $[Fe^{3+}] = 60$ mg L⁻¹ and 1:3 Fe(III)-to-oxalate molar ratio (diluted 1:25). (b) Absorption spectrum of FeOH²⁺ at pH of 2.9 [33]; absorption spectra of the pre-treated sanitary landfill leachate at pH of 2.8 (diluted 1:25 and without dilution); and spectral irradiances of UVA, UVA-Vis and UVC lamps and natural sunlight (UVA lamp: measured with the spectro-radiometer and confirmed by Philips; UVA-Vis lamp: measured with the spectro-radiometer; UVC lamp: supplied by Philips; natural sunlight: AM1.5G reference spectrum [34]). 307

Figure 8.6. Effect of temperature on (a) normalized DOC removal, (b) total dissolved iron concentration and (c) H₂O₂ concentration (for PEF-UVA-BDD) or H₂O₂ consumption (for PF-UVA) as a function of time for (solid symbols) PEF-UVA-BDD and (open symbols) PF-UVA treatment of the pre-treated landfill leachate using pH of 2.8, $[TDI]_0$ of 60 mg L⁻¹, j of 200 mA cm⁻² for PEF-UVA-BDD and $[H_2O_2]$ of 200-400 mg L⁻¹ for PF-UVA. Temperature: (■) 15, (●, ○) 20, (▲, △) 30 and (◆, ◇) 40 °C..... 309

Figure 8.7. Effect of radiation source on normalized DOC removal as a function of time for PEF-BDD and SPEF-BDD treatment of the pre-treated landfill leachate using pH of 2.8, 20 °C, $[TDI]_0$ of 60 mg L⁻¹ and j of 200 mA cm⁻². Radiation: (■) UVA, (●) UVA-Vis and (▲) UVC artificial light and (◆) natural sunlight with $\overline{UV}_{G,n} = 46$ W m⁻². (△) PEF-BDD-UVC process using $[TDI]_0$ of 12 mg L⁻¹ (effluent content), pH of 2.8, 20 °C and j of 200 mA cm⁻². 312

List of Tables

Table 1.1. Potential for O ₂ evolution of various anodes materials used in AO [22, 38].....	9
Table 1.2. Main EAOPs operational parameters and influence on degradation effectiveness.	25
Table 1.3. Examples on the treatment of synthetic wastewaters contaminated with dyes by EAOPs.....	27
Table 1.4. Examples on the treatment of synthetic wastewaters contaminated with pesticides by EAOPs.	42
Table 1.5. Examples on the treatment of synthetic wastewaters contaminated with pharmaceuticals by EAOPs.....	50
Table 1.6. Examples on treatment of synthetic wastewaters polluted with other contaminants by EAOPs.	58
Table 1.7. Examples on the treatment of real textile wastewaters by EAOPs.....	64
Table 1.8. Examples on the treatment of real pharmaceutical and secondary WWTPs effluents by AO..	67
Table 1.9. Examples on the treatment of real landfill leachates by AO.	69
Table 1.10. Examples on the treatment of other real wastewaters by EAOPs.....	76
Table 2.1. Physico-chemical properties of Sunset Yellow FCF azo dye and trimethoprim antibiotic.	99
Table 2.2. Physico-chemical properties of chemicals employed in EAOPs, AOPs, biological treatments and coagulation.	100
Table 2.3. Analytical determinations.	101
Table 2.4. Use of experimental units within the thesis.	113
Table 2.5. Operational characterization of EAOPs performed in the various plants.....	117
Table 2.6. Characteristics of UVA, UVA-Vis and UVC lamps and natural sunlight.....	127
Table 3.1. Pseudo-first-order kinetic constants for SY decolorization (k_{dec}) and SY concentration decay (k_{SY}) along with the corresponding R^2 and S^2_R , obtained for the treatment of solutions of 290 mg SY L ⁻¹ in 7.0 g Na ₂ SO ₄ L ⁻¹ under conditions of Figures 3.1, 3.4, 3.6a and 3.7a	149
Table 3.2. Pseudo-first-order kinetic constants for DOC removal (k_{DOC}) along with the corresponding R^2 and S^2_R , obtained for the treatment of solutions of 290 mg SY L ⁻¹ in 7.0 g Na ₂ SO ₄ L ⁻¹ under conditions of Figures 3.2, 3.3 and 3.6b.	151
Table 3.3. Aromatic products and hydroxylated derivatives identified by LC-MS in negative mode during the EF-BDD treatment of 290 mg SY L ⁻¹ in 7.0 g Na ₂ SO ₄ L ⁻¹	155
Table 4.1. Physicochemical characterization of the real wastewater collected after secondary treatment of a MWWTP.	175
Table 4.2. Equilibrium reactions and respective equilibrium constants (log K) provided by the chemical equilibrium modeling system MINEQL+ [15] and used in the speciation diagrams calculation (T = 25 °C and ionic strength = 0 M).	178
Table 4.3. Pseudo-first-order kinetic constants for TMP concentration decay (k_{TMP}) along with the corresponding R^2 and S^2_R , obtained for the treatment of 20.0 mg TMP L ⁻¹ in 7.0 g Na ₂ SO ₄ L ⁻¹ and real wastewater collected after secondary treatment of a MWWTP spiked with some pollutants under conditions of Figures 4.3, 4.4a, 4.5a, 4.6a, 4.7a, 4.8a, 4.9a, 4.11, 4.12a and 4.13.....	181
Table 4.4. Pseudo-first-order kinetic constants for DOC removal (k_{DOC}) along with the corresponding R^2 and S^2_R , obtained for the treatment of 20.0 mg TMP L ⁻¹ in 7.0 g Na ₂ SO ₄ L ⁻¹ and real wastewater collected after secondary treatment of a MWWTP spiked with 20.0 mg TMP L ⁻¹ under conditions of Figures 4.3, 4.4a, 4.5c, 4.6a, 4.7b, 4.8a,b, 4.9b and 4.11.	182

Table 4.5. Aromatic products and hydroxylated derivatives identified by LC-MS in positive and negative mode during the PEF-UVA-Pt treatment of 20.0 mg TMP L ⁻¹ in 7.0 g Na ₂ SO ₄ L ⁻¹	197
Table 5.1. Equilibrium reactions and respective equilibrium constants (log K^a) and enthalpies (ΔH) used in the chemical equilibrium modeling system MINEQL+ [14] for speciation diagrams calculation (T = 25 °C and ionic strength = 0 M ^a).	218
Table 5.2. Pseudo-first-order kinetic constants for TMP concentration decay (k_{TMP}) and initial TMP removal rates ($r_{0(\text{TMP})}$) along with the corresponding R^2 and S^2_R , obtained for the PEF-UVA-BDD treatment of TMP solutions in 7.0 g Na ₂ SO ₄ L ⁻¹ under conditions of Figures 5.3a, 5.6a, 5.8a, 5.9a and 5.11.....	221
Table 5.3. Pseudo-first-order kinetic constants for DOC removal (k_{DOC}) and initial DOC removal rates ($r_{0(\text{DOC})}$) along with the corresponding R^2 and S^2_R , obtained for the PEF-UVA-BDD treatment of TMP solutions in 7.0 g Na ₂ SO ₄ L ⁻¹ under conditions of Figures 5.3b, 5.6c, 5.8b and 5.9b.	221
Table 6.1. Physicochemical characterization of winery wastewater along the various stages of treatment: raw, after 10 days of biological oxidation and after 240 min of SPEF-BDD process. The discharge limits for WWTPs final effluents according to Portuguese legislation (Decree-Law no. 236/98) and European Directive no. 91/271/CEE are also displayed.	248
Table 6.2. Concentration of FeOH ²⁺ and Fe(OH) _{3(s)} in various systems containing 46 or 1600 mg L ⁻¹ of SO ₄ ²⁻ and 20, 35 or 70 mg L ⁻¹ of Fe ³⁺ (ionic strength = 1.84-5.49 × 10 ⁻² M). Data were calculated by the chemical equilibrium modeling system MINEQL+ [21] using its equilibrium constants and considering the amounts of NH ₄ ⁺ , Cl ⁻ , Ca ²⁺ , Mg ²⁺ , K ⁺ and Na ⁺ determined by ion chromatography after biological oxidation (Table 6.1).	251
Table 6.3. Pseudo-first-order kinetic constants for DOC removal (k_{DOC}) along with the corresponding R^2 and S^2_R , obtained for the treatment of the winery wastewater after biological oxidation under conditions of Figures 6.2a, 6.3a and 6.4a.	253
Table 7.1. Physicochemical characterization of sanitary landfill leachate along the various stages of treatment: raw, after 6-7 days of biological process, after coagulation, after aeration, after SPEF-BDD/neutralization/clarification and after 28 days of Zahn-Wellens test. The discharge limits for WWTPs final effluents according to Portuguese legislation (Decree-Law no. 236/98) and European Directive no. 91/271/CEE are also displayed.	273
Table 7.2. Pseudo-first-order kinetic constants for DOC removal (k_{DOC}) along with the corresponding R^2 and S^2_R , obtained for the treatment of the pre-treated landfill leachate under conditions of Figures 7.3a and 7.4a1,b1.	282
Table 7.3. Characterization of Zahn-Wellens test samples in terms of DOC and COD at day 0 and day 28, BOD ₅ at day 0 and D_t at day 28.	287
Table 8.1. Pseudo-first-order kinetic constants for DOC removal (k_{DOC}) along with the corresponding R^2 and S^2_R , obtained for the treatment of the pre-treated landfill leachate under conditions of Figures 8.1, 8.2a, 8.3a, 8.6a and 8.7.	301
Table 8.2. Concentration of FeOH ²⁺ and Fe(OH) _{3(s)} at temperatures of 15, 20, 30 and 40 °C in a system containing the average amounts of NO ₃ ⁻ , SO ₄ ²⁻ , Cl ⁻ , Ca ²⁺ , Mg ²⁺ , K ⁺ and Na ⁺ of the landfill leachate after aeration (Table 7.1) and 60 mg L ⁻¹ of Fe ³⁺ (ionic strength = 0.390 M). Data were calculated by the chemical equilibrium modeling system MINEQL+ [32] using the equilibrium constants of Table 5.1.....	310
Table 9.1. Main results on the efficiency of the EAOPs for the mineralization of the solutions under study.	323

Notation

Acronyms

[TDI] ₀	Initial total dissolved iron concentration (mg L ⁻¹)
[TDI]	Total dissolved iron (mg L ⁻¹)
2-NB	2-Nitrobenzaldehyde
AC	Activated carbon
ACF	Activated carbon fiber
AO	Anodic oxidation
AOP	Advanced oxidation process
BDD	Boron-doped diamond
BOD ₅	5-day biochemical oxygen demand (mg O ₂ L ⁻¹)
CF	Carbon felt
CFD	Computational fluid dynamics
CNT	Carbon nanotube
COD	Chemical oxygen demand (mg O ₂ L ⁻¹)
CPC	Compound parabolic collector
DAD	Diode array detector
DIC	Dissolved inorganic carbon (mg L ⁻¹)
DOC	Dissolved organic carbon (mg L ⁻¹)
DSA	Dimensionally stable anode
EAOP	Electrochemical advanced oxidation process
EC	Electrocoagulation
EF	Electro-Fenton
EPDM	Ethylene propylene diene monomer
F/M	Food to microorganism ratio
GDE	Gas-diffusion electrode
HPLC	High performance liquid chromatography
IBR	Immobilized biomass reactor
LC	Liquid chromatograph
LC-MS	Liquid chromatography-mass spectrometry
LMCA	Low-molecular-weight carboxylic acids
LMCT	Ligand-to-metal charge transfer
LOD	Limit of detection
LOQ	Limit of quantification
MCE	Mineralization current efficiency (%)
MF	Microfiltration
MS	Mass spectrometry
MWWTP	Municipal wastewater treatment plant
NDIR	Nondispersive infrared detector
NF	Nanofiltration
PAD	Photodiode array detector
PAN	Polyacrylonitrile
PC	Peroxi-coagulation
PEF	Photoelectro-Fenton
PF	Photo-Fenton
PP	Polypropylene

PTFE	Polytetrafluoroethylene
PVC	Polyvinyl chloride
RO	Reverse osmosis
ROS	Reactive oxygen species
RSM	Response surface methodology
RVC	Reticulated vitreous carbon
SPC	Solar heterogeneous photocatalysis
SPE	Solid phase extraction
SPEF	Solar photoelectro-Fenton
SPF	Solar photo-Fenton
SS	Stainless steel
SUVA _{A254}	Specific ultraviolet absorbance at 254 nm ($\text{mg}^{-1} \text{m}^{-1}$)
SVI	Sludge volume index (mL g^{-1})
SY	Sunset Yellow FCF
TDC	Total dissolved carbon (mg L^{-1})
TMP	Trimethoprim
TOC	Total organic carbon (mg L^{-1})
TSS	Total suspended solids (mg L^{-1})
UF	Ultrafiltration
UPLC-MS/MS	Ultra performance liquid chromatography-tandem mass spectrometer
UV	Ultraviolet
UVA	Ultraviolet A
UVB	Ultraviolet B
UVC	Ultraviolet C
UV-Vis	Ultraviolet-Visible
VSS	Volatile suspended solids (mg L^{-1})
WWTP	Wastewater treatment plant

Symbols

bCOD	Biodegradable fraction of COD ($\text{mg O}_2 \text{L}^{-1}$)
COD _{acetate}	COD of acetate solution ($\text{mg O}_2 \text{L}^{-1}$)
CO_T	Total consumed oxygen ($\text{mg O}_2 \text{L}^{-1}$)
E	Electrode potential (V)
EC _V	Energy consumption per unit volume (kWh m^{-3})
EC _{DOC}	Energy consumption per unit DOC mass (kWh (kg DOC)^{-1})
E_{cell}	Average cell potential (V)
EC _{TMP}	Energy consumption per unit TMP mass (kWh (kg TMP)^{-1})
E°	Standard redox potential (V/SHE)
F_0	Photonic flux (Einstein s^{-1} or J s^{-1})
I	Current intensity (mA)
j	Current density (mA cm^{-2})
j_{cat}	Cathodic current density (mA cm^{-2})
k_{dec}	Pseudo-first-order kinetic constant for SY decolorization (dimensionless)
k_{DOC}	Pseudo-first-order kinetic constant for DOC removal (min^{-1} or L kJ^{-1})
k_{SY}	Pseudo-first-order kinetic constant for SY removal (min^{-1})
k_{TMP}	Pseudo-first-order kinetic constant for TMP removal (min^{-1} or L kJ^{-1})
Q	Consumed specific charge (Ah L^{-1})
Q_{UV}	Accumulated UV energy (kJ L^{-1})

R^2	Coefficient of determination (dimensionless)
S^2_R	Residual variance (dimensionless, min^{-1} or L kJ^{-1})
T	Temperature ($^{\circ}\text{C}$)
t_r	Retention time (min)
V	Volume (L)
Y_H	Heterotrophic biomass yield coefficient (dimensionless)
λ	Wavelength (nm)

Chemical names

$\bullet\text{OH}$	Hydroxyl radical
$^1\text{O}_2$	Singlet oxygen
$\text{Cl}\bullet$	Chlorine radical
Cl_2	Chlorine
ClO^-	Hypochlorite ion
ClO_3^-	Chlorate ion
ClO_4^-	Perchlorate ion
H_2O_2	Hydrogen peroxide
HCl	Hydrochloric acid
HClO	Hypochlorous acid
HClO_4	Perchloric acid
$\text{HO}_2\bullet$	Hydroperoxyl radical
IrO_2	Iridium dioxide
KCl	Potassium chloride
Na_2SO_4	Sodium sulfate
NaCl	Sodium chloride
NaClO_4	Sodium perchlorate
NaNO_3	Sodium nitrate
Nb	Niobium
O_3	Ozone
PbO_2	Lead dioxide
Pt	Platinum
Ru	Ruthenium
RuO_2	Ruthenium dioxide
Sb_2O_4	Antimony tetroxide
Sb_2O_5	Antimony pentoxide
Si	Silicon
SnO_2	Tin dioxide
$\text{SO}_4\bullet^-$	Sulfate radical
Ta_2O_5	Tantalum pentoxide
Ti	Titanium
TiO_2	Titanium dioxide
Zr	Zirconium

1 Introduction

The problematic of water pollution by recalcitrant organic compounds and the need for proper treatment of these effluents is firstly given. Electrochemical advanced oxidation processes (EAOPs) are presented as a powerful treatment technology. Fundamentals of the main five EAOPs, i.e. anodic oxidation (AO), anodic oxidation with electrogenerated hydrogen peroxide (AO-H₂O₂), electro-Fenton (EF), photoelectro-Fenton (PEF) and solar photoelectro-Fenton (SPEF), are described to better analyze their characteristics, oxidative properties and the influence of various operational parameters on their performance. An exhaustive review on the treatment of various synthetic and real wastewaters by these EAOPs, alone and in combination with other methods, is then given. Lastly, objectives and thesis outline are provided.

1.1 Water pollution by persistent organic compounds

One of the main current worldwide concerns is the growth of water pollution by organic compounds arising from many industrial, agricultural and urban human activities. The vast majority of these compounds are persistent organic pollutants, owing to their resistance to conventional chemical, biological and photolytic processes. As a result, they have been detected in rivers, lakes, oceans and even drinking water all over the world. This constitutes a serious environmental health problem mainly due to their toxicity and potential hazardous health effects (carcinogenicity, mutagenicity and bactericidal) on living organisms, including human beings [1-4].

Dyes, pesticides and pharmaceuticals are some of the most common recalcitrant organic pollutants. The water contamination with dyes mainly arises from the industrial production of textiles, leather, paper, food, drinks, cosmetics and inks [1]. The more well-known environmental problem related to the water contamination by dyes encompasses wastewater color. This is not only an aesthetic problem, but also a health problem on aquatic ecosystems because of light penetration reduction affecting photosynthesis and animal life. However, more hazardous problems can arise from potential toxicity, carcinogenicity and mutagenicity of these compounds to living organisms [1, 2, 5]. Among the various organic dyes, azo dyes are the more commercialized (around 70% of world total production) and recalcitrant ones [6]. Agriculture activities and pesticide manufacturing plants are the main sources of water pollution with pesticides [4]. Pharmaceuticals and their bioactive metabolites are continuously introduced into the aquatic systems by emission from production sites, direct disposal of overplus drugs in households and hospitals, excretion after drug administration to humans and animals and water treatments in fish farms [7]. Both pesticides and pharmaceuticals were developed to have an efficient pharmacological or biological activity at small levels of ng L^{-1} or $\mu\text{g L}^{-1}$ levels, which further strengthens their hazardousness [4, 7].

Also the deposition of urban and industrial solid wastes into landfills leads to the production of a highly contaminated wastewater called leachate by means of percolation of rainfall in combination with the decomposition of the solid wastes [8].

1.2 Wastewater treatment

Conventional methods for the remediation of wastewaters include biological, physical and chemical treatments.

Biological treatments are the most widely applied class of treatments to the remediation of wastewaters because of their low cost. However, non-biodegradable and toxic compounds cannot be treated by them and, furthermore, they require long treatment times (up to some months), large implementation areas and microorganisms are very sensitive to environmental conditions, which can cause some operational problems [6, 9-11].

Physical methods are based on contaminants separation from aqueous solution. They include sedimentation, filtration, adsorption, membrane processes, among others [10]. Coagulation and flocculation treatments are physico-chemical treatments. The main drawback of all these processes is related to their inability to degrade the organic contaminants, only promoting their transference from a liquid phase to a solid one, with the need for further proper treatment of the solid phase. Furthermore, some treatments like adsorption and membrane separation processes can be very expensive since materials need to be cleaned and disposed of.

Conventional chemical processes use oxidative agents to remove contaminants or modify their structure. Chlorine dioxide (ClO_2^-) and hydrogen peroxide (H_2O_2) are well-known oxidative agents [12, 13]. Nevertheless, in most cases the oxidation power of such agents is not enough to provide high recalcitrant organic contaminants removal. Furthermore, the application of chlorine species can lead to the generation of organochlorinated intermediates that have carcinogenic potential [14].

Since conventional treatments can only promote partial elimination of persistent organic compounds, over around the past three decades research efforts have been made at developing more effective technologies. In this context, advanced oxidation processes (AOPs) acquired high relevance [15]. AOPs are based on the in situ production of highly reactive hydroxyl radicals ($\bullet\text{OH}$) that non-selectively react with most organics, being able to degrade even highly recalcitrant compounds [16]. This radical is the second strongest oxidant known after fluorine, displaying a high standard redox potential of $E^\circ(\bullet\text{OH}/\text{H}_2\text{O}) = 2.80 \text{ V/SHE}$ [17] and rate constants for reaction with several contaminants in the order of 10^6 to $10^{10} \text{ M}^{-1} \text{ s}^{-1}$ [18]. Moreover, $\bullet\text{OH}$ have a short

lifetime, estimated as only a few nanoseconds in water [19], and so they can be self-eliminated from the treatment system. The most common AOPs are H_2O_2 with UVC radiation ($\text{H}_2\text{O}_2/\text{UVC}$), ozone and ozone based processes (O_3 , O_3/UVC , $\text{O}_3/\text{H}_2\text{O}_2$ and $\text{O}_3/\text{H}_2\text{O}_2/\text{UVC}$), titanium dioxide based processes (TiO_2/UV and $\text{TiO}_2/\text{H}_2\text{O}_2/\text{UV}$) and Fenton's reaction based methods (Fenton – $\text{Fe}^{2+}/\text{H}_2\text{O}_2$ and photo-Fenton (PF) – $\text{Fe}^{2+}/\text{H}_2\text{O}_2/\text{UV}$) [20, 21].

Over the last two decades, electrochemical advanced oxidation processes (EAOPs) have gained increasing attention as a promising class of AOPs [22-25]. The former, simplest and most popular EAOP is anodic oxidation (AO), where organics can be directly oxidized at the anode surface by electron transfer and/or indirectly oxidized by $\bullet\text{OH}$ weakly physisorbed at the anode surface and/or agents at the bulk solution such as active chlorine species, O_3 , persulfates and H_2O_2 [26, 27]. When AO is performed along with cathodic electrogeneration of H_2O_2 , the process is called anodic oxidation with electrogenerated H_2O_2 (AO- H_2O_2) [28]. The electrochemical production of H_2O_2 in simultaneous with the addition of Fe^{2+} to the bulk originates the common and widely studied electro-Fenton (EF) process, in which additional $\bullet\text{OH}$ are produced in the bulk from Fenton's reaction. Furthermore, Brillas' group has proposed and extensively studied photoelectro-Fenton (PEF) and solar photoelectro-Fenton (SPEF) processes, which combine the EF technique with irradiation provided by artificial light or natural sunlight, respectively [23]. Other EAOPs like peroxi-coagulation (PC), Fered-Fenton, electrochemical peroxidation and sonoelectro-Fenton have also been applied to the remediation of various wastewaters [29-31]. Due to the high capital and operating costs of EAOPs, the development of combined treatment strategies including biological processes, chemical coagulation, electrocoagulation (EC) and membrane processes have also been proposed to optimize the wastewater treatment [29, 32, 33].

1.3 Fundamentals of EAOPs

Five main EAOPs, including AO, AO-H₂O₂, EF, PEF and SPEF processes, are in the focus of the current thesis and, consequently, their theoretical aspects will be comprehensively discussed below. Figure 1.1 summarizes the main reactions occurring in these EAOPs.

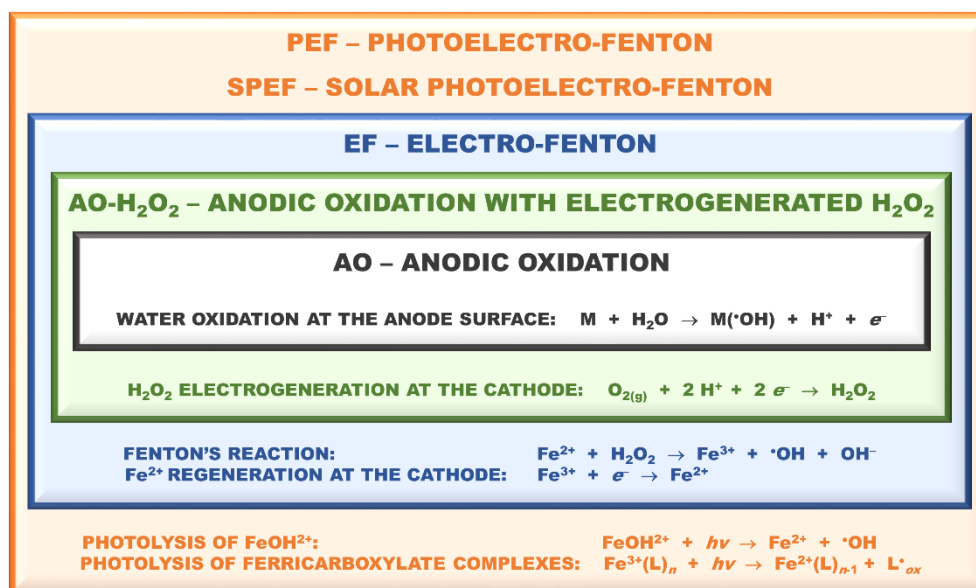


Figure 1.1. EAOPs covered in this thesis and their main reactions.

1.3.1 Anodic oxidation

AO involves the pollutants oxidation by: (i) direct electron transfer to the anode surface M, (ii) heterogeneous reactive oxygen species (ROS) produced as intermediates of oxidation of water to oxygen, including the powerful physisorbed $\bullet OH$ at the anode surface, denoted $M(\bullet OH)$, generated via Eq. (1), and weaker oxidants like H₂O₂ produced from $M(\bullet OH)$ dimerization by Eq. (2) and O₃ formed from water discharge at the anode surface by Eq. (3), and/or (iii) other oxidant agents electrochemically produced from ions existing in the bulk [27].



The efficiency of AO is highly dependent on the mass transfer of pollutants from the bulk to the anode surface or its vicinity [27]. Furthermore, studies performed during the last twenty years have shown strong influence of the anode material nature on both efficiency and selectivity of AO. Two very distinct behaviors of organic pollutants degradation depending on the anode material have been reported: (i) partial organics degradation, along with the formation of many refractory species as final products, and (ii) large or total organics mineralization, i.e., conversion into CO₂, water and inorganic ions, together with the production of few or null amounts of refractory intermediates. The more accepted explanation for this behavior was proposed by Comninellis [34], slightly being modified afterwards by Marselli et al. [35]. The model considers the interaction of M([•]OH) with the anode surface as the responsible for the existence of two types of anode materials: (i) the so-called active anodes, with low O₂-overpotentials, in which the M([•]OH) is transformed into a higher state oxide or superoxide MO via Eq. (4) that in combination with the anode surface M (redox couple MO/M) acts as selective mediator in the oxidation of organics, and (ii) the so-called non-active anodes, with high O₂-overpotentials, in which M([•]OH) are so weakly physisorbed at the anode surface that can react with organics, providing their mineralization.



As a general rule, the higher potential for O₂ evolution of the anode material, the weaker is the interaction of M([•]OH) with the anode surface and the higher is the chemical reactivity towards organics oxidation [27]. Ruthenium dioxide (RuO₂), iridium dioxide (IrO₂), platinum (Pt), graphite and other sp² carbon based electrodes are typical examples of active anodes and exhibit potentials for O₂ evolution in general lower than 1.8 V/SHE, as can be seen in Table 1.1. Carbon-based materials cannot be robust enough against incineration, sometimes even when low *j* is applied [36]. On the other hand, lead dioxide (PbO₂), tin dioxide (SnO₂) and boron-doped diamond (BDD) electrodes can be considered as non-active electrodes, presenting potentials of O₂ evolution from 1.8 to 2.6 V/SHE (see Table 1.1). The BDD anode is the most potent non-active anode known, thereby being considered the most suitable anode for AO [27, 35]. The characteristics of BDD electrodes, including the substrate nature, e.g. silicon (Si), titanium (Ti), niobium (Nb), the boron content, the sp³/sp² ratio and the BDD layer thickness, can strongly influence the organics oxidation [37].

Table 1.1. Potential for O₂ evolution of various anodes materials used in AO [22, 38].

Anode material	Potential for O ₂ evolution (V/SHE)
RuO ₂	1.4-1.7
IrO ₂	1.5-1.8
Pt	1.6-1.9
Graphite	1.7
PbO ₂	1.8-2.0
SnO ₂	1.9-2.2
BDD	2.2-2.6

The AO process can be improved by the action of oxidants like active chlorine species, persulfate, perphosphate, percarbonate and H₂O₂ that are electrochemically generated from agents existing in the bulk solution such as chloride, sulfate (or hydrogen sulfate), phosphate, carbonate (or hydrogen carbonate) and oxygen, respectively [27]. While active chlorine, persulfate, perphosphate and percarbonate are produced from anodic oxidation, the H₂O₂ is generated from cathodic reduction. Salts can already compose the wastewater matrix or, alternatively, they can be externally added. In the presence of these indirect oxidation processes, the AO is often called electrochemical oxidation.

Active chlorine species are the main indirect oxidation agents employed in wastewater treatment. The electrochemical oxidation with active chlorine is based on the direct oxidation of chloride ions at the anode to yield chlorine (Cl₂) through Eq. (5), which diffuses away from the anode to be disproportionated to hypochlorous acid (HClO) and chloride via Eq. (6) [27].

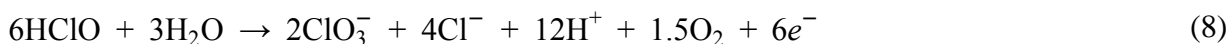


In the solution bulk, the HClO is in equilibrium with hypochlorite ion (ClO⁻) with pK_a of 7.5, as shown in Eq. (7) [39].

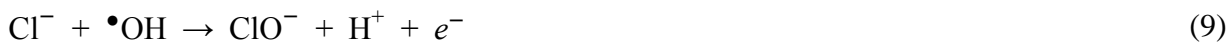


Up to pH of 3 the predominant active chlorine species is Cl₂, from pH of 3 to 8 the dominant species is HClO and for pH above 8 the ClO⁻ prevails [40]. Since HClO ($E^\circ = 1.49$ V/SHE) and Cl₂ ($E^\circ = 1.36$ V/SHE) exhibit higher redox potentials than ClO⁻ ($E^\circ = 0.89$ V/SHE), the oxidation of organics should be faster in acidic than in alkaline media [41]. HClO content can be decreased due to their electrochemically conversion to chlorate ion (ClO₃⁻) according to Eq. (8), with

consequent attenuation of organics degradation since ClO_3^- is not a good oxidant for organics at room temperature [42].



For some electrodes, such as BDD, the perchlorate ion (ClO_4^-) is also formed during AO because of the action of $\text{M}(\bullet\text{OH})$ via Eqs. (9)-(12) [42].



ClO_4^- is the least reactive oxidant of the chloro-oxoanions and it is known for its hazardousness for human health [43]. The rates of electrode reactions (5) and (8)-(12) are a function of the electrocatalytic activity of the anode, chloride content, salt cation, stirring or liquid flow rate, temperature and applied current [44, 45].

In addition, the formation of organochlorinated species, including chloramines, trihalomethanes, haloacetonitriles and haloketones, has been detected during AO due to reaction of active chlorine species with different functional groups of organic matter [46-48]. This is a major drawback of AO in the presence of active chlorine, because organochlorinated products are very toxic and usually more recalcitrant than parent molecules.

The strong persulfate, perphosphate and percarbonate oxidants can be efficiently produced by Eqs. (13), (14) and (15), respectively [27], only using non-active anodes such as BDD and PbO_2 [49, 50].



H_2O_2 can be generated in the bulk from the two-electron reduction of oxygen (directly injected as pure gas or bubbled air) at the cathode surface in acidic/neutral media, according to Eq. (16) with $E^\circ = 0.68 \text{ V/SHE}$ [51].



Reaction (16) is easier than the four-electron reduction of oxygen to water ($E^\circ = 1.23$ V/SHE). In alkaline solutions, oxygen is reduced to hydroperoxide ion (HO_2^-), the conjugate base of H_2O_2 ($\text{p}K_a = 11.64$) [52]. The electrogeneration of H_2O_2 sometimes is called electroperoxidation [53] and the AO process carried out with electrochemical production of this oxidant is named anodic oxidation with electrogenerated H_2O_2 (AO- H_2O_2) [28].

H_2O_2 production and stability depend on factors such as cell configuration, cathode properties and operational conditions. Parasitic reactions such as H_2O_2 electrochemical reduction at the cathode surface via Eq. (17) and, in much lesser extent, H_2O_2 disproportion in the bulk from Eq. (18) can occur using both undivided and divided electrochemical cells, diminishing the H_2O_2 accumulation in the system [54].



Furthermore, when an undivided cell is used, H_2O_2 can also be oxidized to oxygen at the anode according to Eqs. (19) and (20), producing the weak oxidant hydroperoxyl radical (HO_2^\bullet) as intermediate [55].



To attain high H_2O_2 electrogeneration efficiency, the contact between cathode, oxygen and water must be maximized. For this reason, porous cathodes like gas-diffusion electrodes (GDEs) and three-dimensional electrodes of high specific surface area are preferred for H_2O_2 electrogeneration. Since carbon is non-toxic and exhibits a high overpotential for H_2 evolution and low catalytic activity for H_2O_2 decomposition, along with relative good stability, conductivity and chemical resistance, carbonaceous cathodes have been widely employed for H_2O_2 electrogeneration with high efficiency [23]. Good examples of these cathodes are carbon-polytetrafluoroethylene (PTFE) gas (O_2 or air) diffusion electrodes [56, 57], carbon or graphite felts [58, 59], carbon sponge [60, 61], activated carbon fiber (ACF) [62, 63], carbon nanotube (CNT) [64, 65], reticulated vitreous carbon (RVC) [66, 67] and BDD [68, 69].

H₂O₂ itself is only a moderately strong oxidant, exhibiting $E^\circ(\text{H}_2\text{O}_2/\text{H}_2\text{O}) = 1.77 \text{ V/SHE}$ in acidic medium and $E^\circ(\text{H}_2\text{O}_2/\text{OH}^-) = 0.88 \text{ V/SHE}$ in alkaline medium [70]. It is able to only attack reduced sulfur compounds, cyanides and some organics such as aldehydes, formic acid and some nitro-organic and sulfo-organic compounds [71]. For this reason, electrochemical processes with H₂O₂ electrogeneration are usually performed in the presence of Fe²⁺ ion to yield the Fenton's reagent, whose chemistry is explained in the section below.

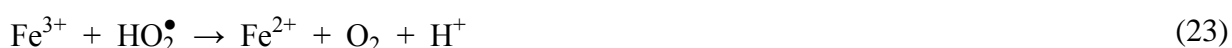
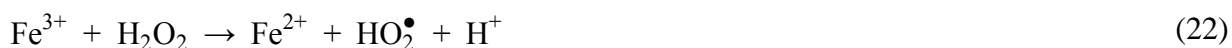
1.3.2 Electro-Fenton

The Fenton's reagent is a mixture of H₂O₂ and Fe²⁺, discovered by Fenton [72] and later clarified by Haber and Weiss [73]. It leads to the formation of the powerful •OH by the so-called Fenton's reaction (21) [73].



Sun and Pignatello [74] showed that Fenton's reaction can be efficiently applied in acidic pH of 2.8-3.0. For most of the aqueous solutions, precipitation does not take place yet.

In excess of H₂O₂, Fe³⁺ can be reduced to Fe²⁺ via Eqs. (22) and (23) [73].



Both Eqs. (22) and (23) are much slower than Fenton's reaction (21). Furthermore, Eq. (22) scavenges H₂O₂ to generate HO₂•, which exhibits a much lower oxidation power than •OH, and so it can be regarded as a parasitic reaction competing with Fenton's reaction (21) [23]. Also other parasitic reactions (24) and (25) can occur in the presence of H₂O₂ and Fe²⁺ in excess, respectively, and, as a consequence, the ratio [H₂O₂]/[Fe²⁺] must be optimized for each specific case [75].



Some of the major drawbacks of classical Fenton process, in which chemical Fenton's reagent is added to solution, are related to (i) the cost and risks associated with the provision, storage and transport of H₂O₂, (ii) the use of high amounts of iron with further formation of iron sludge that must be removed and properly treated at the end of the treatment, and (iii) the operation at acidic

pH, which usually results in the need for acidification and subsequent neutralization [76]. To overcome some of these drawbacks and increase the efficiency of pollutants removal, EAOPs based on Fenton's reaction have been developed. The EF process is the most known and popular EAOP based on Fenton's reaction chemistry and it was developed and extensively applied over the last 15 years by Brillas' and Oturan's groups [23, 77, 78]. It comprises: (i) the in situ and continuous electrogeneration of H_2O_2 at a carbonaceous cathode fed with pure oxygen or air via Eq. (16), (ii) the addition of Fe^{2+} catalyst to the solution, and (iii) the cathodically reduction of Fe^{3+} to Fe^{2+} by Eq. (26), with consequent continuous production of Fenton's reagent [23].



When an undivided cell is used, the EF process also counts on ROS produced at the anode, mainly $\text{M}(\bullet\text{OH})$. In this context, the use of the emergent BDD anode significantly enhances the EF oxidation power.

Several cathode materials such as carbon-PTFE gas (O_2 or air) diffusion electrodes [77, 79], carbon felt (CF) [78], carbon sponge [60], ACF [62] and RVC [67] have been applied for H_2O_2 electrogeneration in the EF process. Regarding the efficiencies, two major EF versions based on the nature of the cathode material can be distinguished, namely EF with carbon-PTFE air-diffusion electrode and EF with CF, which represent two extreme behaviors. In the former process, large amounts of H_2O_2 are accumulated in the medium with low Fe^{2+} regeneration from Eq. (26), whereas in the second one, all Fe^{3+} is continuously transformed into Fe^{2+} because of the low H_2O_2 electrogeneration at the CF cathode [177].

The EF process should not be confused with other variations like PC, Fered-Fenton and electrochemical peroxidation. The PC process, firstly proposed by Brillas' group [80], utilizes an individual cell that electrogenerates H_2O_2 at a carbonaceous cathode from Eq. (16) and simultaneously releases Fe^{2+} from a sacrificial iron anode according to Eq. (27). During this process, pollutants are oxidized by the attack of $\bullet\text{OH}$ in the bulk and their coagulation can also take place via $\text{Fe}(\text{OH})_3(\text{s})$ formation depending on pH.



The Fered-Fenton process involves the addition of both H_2O_2 and Fe^{2+} to the solution in an undivided cell along with the cathodic Fe^{3+} regeneration to Fe^{2+} by Eq. (26) [81]. In turn, the electrochemical peroxidation, firstly proposed by Lemley's group [82] and latter patented by

Chiarenzelli's group [83], generally involves an undivided cell composed of a sacrificial iron anode for Fe^{2+} electrogeneration according to Eq. (27) and an inert cathode where hydrogen is produced from water reduction. Fe^{2+} is cathodically regenerated by Eq. (26), simultaneously with the external addition of H_2O_2 to the solution. Pollutants can be removed both by the attack of $\bullet\text{OH}$ in the bulk and by coagulation with $\text{Fe}(\text{OH})_3$ precipitate. When a divided cell is applied this process is called anodic Fenton treatment and the cathodic Fe^{3+} regeneration to Fe^{2+} cannot take place [84]. Both electrochemical peroxidation and anodic Fenton treatment should be regarded as variants of the PC technology.

1.3.3 Photoelectro-Fenton and solar photoelectro-Fenton

The irradiation of a solution treated under EF conditions by artificial UV light or natural sunlight leads to the PEF or SPEF processes, respectively, both proposed and extensively studied by Brillas' group [23, 85-91]. In these photo-assisted treatments the degradation of pollutants is mainly accelerated by (i) the photoreduction of Fe(III)-hydroxy complexes, such as the most photoactive FeOH^{2+} at pH near 3 according to Eq. (28) [74], with consequent $\bullet\text{OH}$ production and Fe^{2+} regeneration, and (ii) the direct photolysis by ligand-to-metal charge transfer (LMCT) excitation of complexes formed between Fe^{3+} and some organics, namely carboxylic acids, according to the general Eq. (29) [92-94], allowing the regeneration of Fe^{2+} in parallel with the formation of weak oxidizing species such as superoxide anion radical, carbon dioxide anion radical and H_2O_2 .



Artificial lamps providing UVA (λ of 315-400 nm), UVB (λ of 280-315 nm) and UVC ($\lambda < 280$ nm) radiation can be employed in PEF treatments. Depending on the wavelength and intensity of the radiation source, the pollutants can be degraded by different mechanisms and with increasing degradation rates for higher radiation intensities up to a given value. The photoreduction of photoactive Fe(III)-hydroxy complexes by Eq. (28) and the photolysis of Fe^{3+} complexes with organics by Eq. (29) occur under UV-Vis radiation and direct photolysis of pollutants can take place when the light source emits radiation at the same wavelength range as the contaminants can absorb radiation efficiently. The application of UVC light in the presence of symmetrical peroxides such as H_2O_2 can lead to the generation of additional $\bullet\text{OH}$ through the homolytic cleavage of the

peroxide (–O–O–) bond via Eq. (30) [16, 95, 96]. Note that Eq. (30) only takes place under UVC radiation, a common confusion of many researchers that report that it occurs for any type of UV light.



Among artificial lamps, the UVA lamps have been the most widely employed [28, 97-99]. The use of artificial lamps in PEF technique is commonly responsible for high electrical costs, which can be minimized by the application of SPEF process, where the solution is directly irradiated with free and renewable natural sunlight. When comparing SPEF with PEF using low energy power artificial lamps, it is common to achieve higher pollutants degradation for SPEF due to a higher UV intensity of natural sunlight in simultaneous with an emission in the visible region ($\lambda > 400$ nm), thereby also leading to Fe(III)-carboxylate complexes direct photolysis according to Eq. (29).

Furthermore, the light irradiation of other species can lead to the production of other oxidation agents. For instance, persulfate can lead to the production of sulfate radical ($\text{SO}_4^{\bullet-}$) by Eq. (31) [100] and ClO^- can generate chlorine radical (Cl^\bullet) and $\bullet\text{OH}$ from Eqs. (32) and (33), respectively [101].



An acidic pH of 2.8-3.0 is usually used for PEF and SPEF, as for Fenton process, since for most of the aqueous solutions at this pH the dominant iron species in solution is FeOH^{2+} , the most photoactive Fe(III)-hydroxy complex, and, furthermore, precipitation does not take place yet [74].

1.4 Influence of operational parameters on EAOPs

The degradation of organic pollutants in aqueous solution by all mentioned EAOPs depends on various operational parameters such as initial organics concentration, background electrolyte composition, current density (j) or applied current (I) or applied electrode potential (E), stirring rate or liquid flow rate, temperature and pH. When carbonaceous cathodes are employed for H_2O_2 electrogeneration in AO- H_2O_2 , EF, PEF and SPEF processes, the oxygen or air feeding flow rate also influences the process efficiency. In addition, the initial total dissolved iron concentration ($[TDI]_0$) affects the efficiency of EAOPs based on Fenton's reaction. The effect of each parameter on EAOPs will be discussed in detail below and it is summarized in Table 1.2.

1.4.1 Initial organics concentration

For all EAOPs, the logical outcome is that solutions with higher initial organics concentration need longer treatment times to achieve a given degradation degree, as reported by many authors [102-106]. This outcome is often referred to as the attainment of lower percentages or efficiencies of pollutants removal for larger initial organics concentrations [88, 107-109]. Moreover, it is consensual that the employment of higher initial pollutants contents leads to the removal of higher amounts of pollutants per unit of time, i.e. higher pollutants removal rates [110-113]. This can be attributed to a faster oxidation of organics with $\bullet OH$, inhibiting parasitic reactions like Eqs. (24) and (25).

In terms of pseudo-first-order kinetic constants for pollutants removal and mineralization, it is theoretically expected that these values are independent of the substrate content. However, it has been experimentally observed lower pseudo-first-order kinetics constants for increasing pollutants concentrations [66, 105, 114, 115], which can be ascribed to: (i) some limitations of this kinetic model to describe precisely the decay profiles, considering that a comprehensive mechanistic kinetic model may include all chemical, photocatalytic and electrochemical reactions occurring for each contaminant in solution, especially involving its oxidation products, and/or (ii) lower diffusion and/or mass transport toward/from electrodes of H_2O_2 and Fe^{2+} species in the presence of higher organic matter content, simultaneously with possible formation of larger amounts of Fe^{3+} complexes with organic matter, thus diminishing the production of $\bullet OH$.

Contrary to what has been achieved for aromatic dyes, pesticides and pharmaceuticals, Oturan et al. [116] reached lower carboxylic acids removal rates when using rising organics content during the first treatment stages. The authors explained these results by the higher resistance to oxidation of carboxylic acids compared to aromatics, which can enhance parasitic reactions such as Eqs. (24) and (25) in detriment of the mineralization reaction.

1.4.2 Background electrolyte composition

Background electrolytes are employed in EAOPs used for the degradation of model compounds to allow the flow of electrical current. Furthermore, the efficiency of EAOPs for the remediation of real effluents can be enhanced by the addition of ions, not only to yield better electrical current flow but mainly to provide the electrogeneration of strong oxidizing agents like active chlorine species [46, 47, 117]. Note that the introduction of ions into solution can also be accomplished by the pH adjustment using an inorganic acid such as sulfuric or hydrochloric.

Sodium sulfate (Na_2SO_4), sodium chloride (NaCl), potassium chloride (KCl), sodium perchlorate (NaClO_4), sodium nitrate (NaNO_3) and sodium carbonate (Na_2CO_3) are common supporting electrolytes. The nature of the supporting electrolyte can highly affect the degradation kinetics since the presence of some ions in solution can lead to: (i) the formation of strong oxidants such as active chlorine species produced by direct oxidation of chloride at the anode according to Eqs. (5) and (6), (ii) the scavenging of $\bullet\text{OH}$ in the presence of sulfate and chloride via Eqs. (34) and (35), respectively [118, 119], (iii) the production of recalcitrant and toxic by-products like chloroderivatives that are only slowly degraded by $\bullet\text{OH}$ and active chlorine species, (iv) the consumption of H_2O_2 as it happens in the presence of $\text{SO}_4^{\bullet-}$ via Eqs. (36) and (37) and HClO at pH between 3 and 8 according to Eq. (38) [120], and (iv) the generation of complexes with iron like sulfato-iron and chloro-iron complexes [120], changing the amount of photoactive iron species like FeOH^{2+} and also promoting the loss of free Fe^{2+} to participate in Fenton's reaction (21).





For AO and AO-H₂O₂ processes, the removal of target compounds occurs more rapidly using NaCl when compared to Na₂SO₄ [33, 121]. This can be mainly attributed to the pollutants degradation in the bulk by active chlorine species in the presence of chloride and/or the scavenging of •OH by sulfate in higher extent than by chloride. For EF and PEF processes, the degradation of primary compounds by applying NaCl and Na₂SO₄ as background electrolytes has been attaining controversial results. While some studies achieved faster removal of target compounds using NaCl [33, 122, 123], others observed higher efficiency using Na₂SO₄ alone [66, 67]. In terms of mineralization ability (degradation of target compounds and their by-products), the superiority of Na₂SO₄ over NaCl is consensual [33, 123]. The faster target pollutants degradation by using NaCl instead of Na₂SO₄ was attributed to the attack of active chlorine species and the formation of sulfate-iron complexes in higher amount than chloro-iron complexes [120], leading to the loss of free Fe²⁺ to be used in Fenton's reaction. In contrast, the lower removal of primary compounds in chloride medium has been mainly related to the consumption of H₂O₂ by reaction with HClO via Eq. (38) and the slower mineralization has also been attributed to the generation of chloroderivatives that are hardly attacked by •OH and active chlorine species.

The efficiency of EF and PEF using NaClO₄ and NaCl electrolytes has reached divergent results. In the work presented by Daneshvar et al. [122], the use of NaClO₄ showed superiority over NaCl, whereas in Thiam et al. [123] the achievements were antagonistic. Since ClO₄⁻ ion does not form complexes with Fe²⁺ and Fe³⁺ and is not reactive toward •OH [120], the results attained by Daneshvar et al. [122] can seem more logical, but the action of Cl⁻ can be a function of its oxidation ability on the intermediates formed and this needs more research. Note that ClO₄⁻ ions are toxic and provoke damages in the environment and living organisms.

Under SPEF conditions, Thiam et al. [91] reported similar dye decays using Na₂SO₄, NaClO₄ and Na₂CO₃ background electrolytes and just a slightly lower mineralization using NaCl, which points to a low influence of the electrolyte nature in the presence of the beneficial effects of solar radiation.

Among all background electrolytes, the ones containing sulfate and chloride ions have been the most widely employed. In particular, the use of 7.0 g Na₂SO₄ L⁻¹ as supporting solution has been the most common alternative [98, 124-126].

1.4.3 Current density or applied current or potential

A constant j (in A m⁻² or mA cm⁻²) or I (in A or mA) is supplied to the cell when operating in galvanostatic mode, whereas a constant E (in V) is provided to the anode or the cathode of the cell vs. an electrode reference when working in potentiostatic mode. A constant potential can also be supplied to the electrochemical cell (E_{cell}), but this does not correspond to the operation in potentiostatic mode. Usually, EAOPs are operated in galvanostatic mode.

j (or I) is a key parameter in EAOPs since it regulates the amount of oxidizing species produced. For all EAOPs, j controls the amounts of M(\bullet OH) electrogenerated via Eq. (1) and indirect oxidation agents such as the active chlorine species generated from Eqs. (5) and (6). For EAOPs with H₂O₂ electrogeneration, it also regulates the quantity of electrogenerated H₂O₂ via Eq. (16). In the case of EAOPs based on Fenton's reaction, j sets the extent of cathodic Fe³⁺ regeneration to Fe²⁺ via Eq. (26), which, in parallel with the regulation of H₂O₂ electrogeneration, determines the amount of \bullet OH in the bulk produced from Fenton's reaction (21). In general, the rate of pollutants degradation increases with increasing j for all EAOPs since more oxidizing species are formed at a given time [90, 126-129]. However, this parameter cannot be increased indefinitely since the rate of parasitic reactions is also promoted, leading to the decrease of current efficiency and similar or even lower pollutants removal than at inferior j value. The parasitic reactions can involve: (i) the dimerization of M(\bullet OH) to H₂O₂ by Eq. (2), (ii) the anodic oxidation of M(\bullet OH) to oxygen through Eq. (39), (iii) the dimerization of \bullet OH to H₂O₂ via Eq. (40), (iv) the H₂O₂ electrochemical reduction (in a divided cell) via Eq. (17), (v) the H₂O₂ electrochemical oxidation (in an undivided cell) according to Eqs. (19) and (20), (vi) the H₂O₂ reaction with Fe³⁺ via Eq. (22), and (vii) the destruction of \bullet OH with H₂O₂ and Fe²⁺ via Eqs. (24) and (25), respectively [30, 35, 74].



Commonly, the degradation of wastewaters with high dissolved organic carbon (DOC) of 100-1000 mg L⁻¹ employ large cathodic j (j_{cat}) of 30-200 mA cm⁻² [47, 55, 102, 126, 130], whereas wastewaters with DOC values below 100 mg L⁻¹ apply j_{cat} values lower than 30 mA cm⁻² [116, 31-134]. Note that this thesis always employed the term DOC instead of total organic carbon (TOC), assuming always filtration of samples before analysis (required for most of the analytical equipments), although some studies have mentioned the term TOC, even when samples filtration was carried out.

To choose the best j , it is necessary to take into account not only the degradation decays but also the current efficiency, i.e. the feasibility of EAOPs in terms of consumed electrical charge and/or the energy consumption for electrochemical cell operation at large scale. The mineralization current efficiency (MCE, in %) is a widely employed current efficiency parameter and it can be determined by Eq. (41) for single pollutant solutions for which the mineralization reaction is known [135]:

$$\text{MCE} = \frac{n F V_s \Delta(\text{DOC})_{\text{exp}}}{4.32 \times 10^7 m I t} 100 \quad (41)$$

where n is the theoretical number of electrons exchanged in the mineralization process of the organic compound, F is the Faraday constant (96 487 C mol⁻¹), $\Delta(\text{DOC})_{\text{exp}}$ is the experimental DOC abatement (in mg L⁻¹), 4.32×10^7 is a conversion factor to homogenize the units (3600 s h⁻¹ × 12000 mg mol⁻¹), m is the number of carbon atoms of the molecule under study, I is the applied current (in A) and t is the electrolysis time (in h).

The specific energy consumption for electrochemical cell operation per unit DOC mass (EC_{DOC}, in kWh (kg DOC)⁻¹) and per unit volume (EC_V, in kWh m⁻³) can be calculated from Eqs. (42) and (43), respectively, when operating at constant j [87]:

$$\text{EC}_{\text{DOC}} = \frac{1000 E_{\text{cell}} I t}{V_s \Delta(\text{DOC})_{\text{exp}}} \quad (42)$$

$$\text{EC}_V = \frac{E_{\text{cell}} I t}{V_s} \quad (43)$$

where 1000 is a conversion factor (in mg g⁻¹), E_{cell} is the average cell potential (in V), I is the applied current (in A), t is the electrolysis time (in h), V_s is the solution volume (in L) and $\Delta(\text{DOC})_{\text{exp}}$ is the experimental DOC concentration decay (in mg L⁻¹).

1.4.4 Stirring rate or liquid flow rate

The solution stirring rate in tank reactors and liquid flow rate in flow cells must be regulated to obtain fast homogenization of treated solution, avoid deposition of solids and ensure proper mass transfer of pollutants towards electrodes, catalyst and, in case of light-assisted EAOPs, illuminated zone. Ideally, the turbulent flow along the reactor should be guaranteed to provide a good mixing and avoid any sedimentation.

1.4.5 Temperature

The influence of temperature on AO and AO-H₂O₂ processes is rather little as found by Tsantaki et al. [136] and Boye et al. [127], although higher temperature enhances the mass transfer of reactants toward/from the electrodes and kinetic constants (for •OH generation by Eqs. (1) and (21), H₂O₂ production via Eq. (16) and oxidation of organics by such species) are exponentially dependent on the temperature (Arrhenius law). In addition to these two effects, the EAOPs based on Fenton's reaction can also count on the faster Fe³⁺ regeneration to Fe²⁺ by thermal reactions (22), (23) and (44) for higher temperature, which has been reported as the main cause for the increase of degradation kinetics with temperature in these processes [76, 137]. To our knowledge, the influence of temperature on the distribution of iron species and the consequent effects on the degradation kinetics has never been assessed.



In all EAOPs, the implementation of temperatures above 35 °C should be taken with precaution since water evaporation and oxygen release can occur [127, 138]. Furthermore, the thermal decomposition of H₂O₂ into water and oxygen (inactive species) may occur in large extent for temperatures above 50 °C [139]. Note that thermal reactions (22), (23) and (44) can also lead to H₂O₂ decomposition, with formation of less reactive species.

The majority of EAOPs employ ambient temperature or a temperature of 35 °C.

1.4.6 pH

A literature review on the influence of pH on AO and AO-H₂O₂ processes reveals discrepant results. Some studies point to the independency of mineralization rate by changing pH in the 2.0-6.0 range [127, 140, 141]; others achieved greater process efficiency at pH of 3.0 compared to higher pH values [108, 134, 142], ascribing these results to the competitive electrogeneration of less powerful oxidizing species such as superoxide anion radical and, when chloride is available, to the formation of active chlorine species with higher oxidation ability at acidic pH [41]; and Hamza et al. [110] attained slightly faster mineralization at pH of 7.4 than at pH of 3.0. In contrast, the best pH value for EF, PEF and SPEF processes is in general close to 3.0 [89, 105, 127, 143-146], mainly due to: (i) higher amounts of photoactive Fe(III)-hydroxy complexes in solution [94, 147], (ii) absence of iron precipitation [94, 147], (iii) absence of carbonate and bicarbonate species, which reduce the process efficiency due to their •OH

scavenging effect [18], and (iv) null auto-decomposition rate of H_2O_2 to water and oxygen, typically for pH above 5 [148]. However, some authors reported maximal and similar mineralization rates for pH values from 2.0 to 4.0 [97, 132], 2.0 to 3.0 [88, 104] and 3.0 to 4.0 [86, 149].

To prevent or, at least, minimize the need for acidification to perform the EAOP and the necessity for subsequent neutralization to discharge the wastewater into the environment, the PEF process assisted by carboxylic acids, e.g. oxalic, citric, tartaric and malic, has been recently implemented [109, 150]. The presence of carboxylic acids can improve PEF efficiency because: (i) they promote the formation of more soluble complexes with Fe^{3+} , allowing maintaining the iron in solution at higher pH values [151], (ii) Fe(III)-carboxylate complexes can absorb radiation in the UV-Vis range, being photodecarboxylated according to the general Eq. (29) with higher quantum yields for Fe^{2+} generation than that of Fe(III)-hydroxy complexes [92-94, 152] and (iii) the establishment of Fe(III)-carboxylate complexes can avoid the formation of Fe(III)-sulfate, Fe(III)-chloride and Fe(III)-pollutants complexes in view of their greater formation constants in comparison with that of these species [153, 154].

1.4.7 Oxygen or air feeding flow rate

To electrogenerate H_2O_2 at carbonaceous cathodes according to Eq. (16), oxygen must be continuously provided during electrolysis either by means of expensive pure oxygen [127, 155] or easily obtainable air [89, 146]. In general, high flow rates of oxygen (pure or air) are employed for various types of carbonaceous cathodes in order to maintain oxygen-saturated solutions, thereby ensuring maximum H_2O_2 electrogeneration [62, 66, 69, 106, 146, 156]. The oxygen gas is often provided during some minutes prior to electrolysis to saturate the aqueous solution [69, 106, 157, 158]. For electrochemical cells with GDEs, it is necessary to establish a compromise between liquid and oxygen flow rates in order to apply similar pressures in both sides of the cathode and thus avoid cell flooding. Note that extremely high oxygen or air feeding flow rates are not recommended since they cause some operational problems such as: (i) the disruption of pumps used for liquid circulation, (ii) the fulfill of liquid compartments of filter-press cells with air, decreasing the contact between solution and electrodes and even obstructing ions transference, and (iii) the reduction of the irradiated volume in light-assisted EAOPs.

1.4.8 Initial total dissolved iron concentration

The $[TDI]_0$ (Fe^{2+} , Fe^{3+} or both species) is a crucial parameter for EAOPs based on Fenton's reaction chemistry since it determines the extent of Fenton's reaction (21) and, as a result, the pollutants degradation. For EF process, the best $[TDI]_0$ mainly depends on: (i) H_2O_2 concentration, (ii) system ability to regenerate Fe^{3+} to Fe^{2+} by means of cathodic reduction via Eq. (26) and thermal reactions (22), (23) and (44) and (iii) occurrence of parasitic reactions such as Eq. (25). For PEF and SPEF processes, it is also a function of: (i) Fe^{3+} regeneration to Fe^{2+} through photolysis of Fe(III)-hydroxy complexes by Eq. (28) and photolysis of complexes between Fe^{3+} and organics via Eq. (29), (ii) manifestation of inner filter effects, i.e. competitive absorption of photons between pollutants and Fe^{3+} photoactive species [76], and (iii) photoreactor geometry since the iron amount influences the light attenuation along the optical pathlength [76]. Note that the amount of iron added to the solution can diverge from $[TDI]_0$ since some precipitation can occur depending on pH and type and concentration of organic/inorganic compounds present in the solution.

For all wastewaters, it is expected the rise in process efficiency with increasing $[TDI]_0$ up to a value for which it is established an equilibrium between positive effects coming from the enhancement of Fenton's reaction (21) and negatives effects arising from the improvement of parasitic reactions and, for light-assisted EAOPs, inner filter effects and light attenuation along the photoreactor. In general, EF, PEF and SPEF treatments of wastewaters with DOC contents up to 50 mg L^{-1} use $[TDI]_0$ below than 30 mg L^{-1} as the best ones [66, 67, 114, 143], whereas wastewaters with DOC concentrations of $100\text{-}400\text{ mg L}^{-1}$ employ best $[TDI]_0$ of $30\text{-}120\text{ mg L}^{-1}$ [89, 144-146, 159, 160]. Wherever possible, effluents with low organic contents up to few mg L^{-1} should use a total iron concentration in agreement with regulatory limits for the discharge of effluents into the environment to avoid the need for iron removal.

Table 1.2. Main EAOPs operational parameters and influence on degradation effectiveness.

Parameter	Influence on degradation efficiency
Initial organics concentration	All EAOPs – Higher initial organics concentrations require longer treatment times, lead to higher pollutants removal rates due to faster oxidation of organics with $\bullet\text{OH}$ and inhibition of parasitic reactions and also result in unexpected lower pseudo-first-order kinetics constants, pointing to limitations of this kinetic model and/or lower diffusion and/or mass transport toward/from electrodes of oxidizing species.
Background electrolyte composition	AO and AO- H_2O_2 – NaCl vs. Na_2SO_4 – NaCl > Na_2SO_4 mainly due to pollutants degradation by active chlorine species in the presence of chloride and/or scavenge of $\bullet\text{OH}$ by sulfate in higher extent than by chloride. EF and PEF – NaCl vs. Na_2SO_4 – Controversial results in terms of degradation of target compounds: (i) NaCl > Na_2SO_4 mainly due to formation of sulfate-iron complexes or (ii) Na_2SO_4 > NaCl due to H_2O_2 consumption by reaction with HClO. Consensual results in terms of mineralization ability: Na_2SO_4 > NaCl due to H_2O_2 consumption by reaction with HClO and formation of recalcitrant chloroderivatives. EF and PEF – NaCl vs. NaClO_4 – Controversial results: (i) NaClO_4 > NaCl due to non-reactivity of ClO_4^- towards iron and $\bullet\text{OH}$ or (ii) NaCl > NaClO_4 . Production of hazardous compounds in the presence of NaClO_4 . SPEF – Low influence of the electrolyte nature.
Current density (or applied current or potential)	All EAOPs – Higher generation of oxidizing species, and consequent higher pollutants degradation, for larger j (or I or E) up to a value for which parasitic reactions occur in a such high extent that similar or even lower pollutants removal is attained for higher j .
Stirring rate or liquid flow rate	All EAOPs – High stirring rates or liquid flow rate lead to fast solution homogenization, prevention of solids deposition and assurance of proper mass transfer of pollutants towards electrodes, catalyst and, in case of light-assisted EAOPs, illuminated zone.
Temperature	AO and AO- H_2O_2 – Little influence. Increasing temperature enhances the mass transfer of reactants toward/from the electrodes and kinetic constants (both for $\bullet\text{OH}$ production and oxidation of organics by such species) are exponentially dependent on the temperature (Arrhenius law). EF, PEF and SPEF – In general, the increase of degradation kinetics with temperature is attributed to higher rates of thermal reactions (22), (23) and (44). The effect of temperature on the distribution of iron species has never been assessed. Water evaporation and release of oxygen can occur for temperatures above 35 °C. Thermal decomposition of H_2O_2 into water and oxygen occurs in large extent for temperatures above 50 °C.
pH	AO and AO- H_2O_2 – Controversial results: (i) independency of pollutants degradation on pH or (ii) higher pollutants degradation at pH of 3.0 or (iii) higher pollutants degradation at neutral pH. EF, PEF and SPEF: Commonly, maximum pollutants degradation at pH close to 3.0 due to predominance of Fenton's reaction, higher amounts of photoactive Fe(III)-hydroxy complexes, absence of iron precipitation, absence of scavenge of $\bullet\text{OH}$ by carbonate and bicarbonate species and null auto-decomposition of H_2O_2 . Even though, some studies found similar process efficiency at pH of 2.0-4.0. The addition of carboxylic acids can allow using higher pH values with high degradation efficiency.
O₂ or air feeding flow rate	AO- H_2O_2 , EF, PEF and SPEF – High flow rates of oxygen (pure or air) ensure maximum H_2O_2 electrogeneration. Electrochemical cells with GDEs need to establish a compromise between liquid and oxygen flow rates to avoid cell flooding.
Initial total dissolved iron concentration	EF, PEF and SPEF – Higher degradation efficiency for increasing $[\text{TDI}]_0$ up to a value for which it is established an equilibrium between positive effects coming from the enhancement of Fenton's reaction and negatives effects arising from the growth of parasitic reactions and, for light-assisted EAOPs, inner filter effects and light attenuation along the photoreactor.

1.5 Degradation of synthetic wastewaters by EAOPs

A review on an extensive number of studies from EAOPs origins up to now regarding the treatment of synthetic wastewaters containing dyes, pesticides, pharmaceuticals and other pollutants by these processes is presented. It comprises many features like wastewater composition, applied EAOPs, configuration of electrochemical reactor, anode and cathode characteristics and operational parameters such as applied j or E , liquid flow rate, temperature, pH and $[TDI]_0$.

1.5.1 Wastewaters containing dyes

Table 1.3 collects information regarding thirty-four studies on the degradation of synthetic wastewaters containing dyes by EAOPs. The following discussion on degradation of wastewaters containing dyes is based on those studies.

1.5.1.1 Dye content

The majority of works refers to the degradation of azo dyes. In general, the synthetic wastewaters were produced using just one dye. Among the few studies regarding comparative degradations between two or more dyes [88, 156, 161], highlight can be given to Garcia-Segura et al. [161] that determined noticeable lower initial decolorization rates and dye removals for dye molecules with increasing number of azo bonds.

Distinct initial dye contents from 1.4 to 3580 mg L⁻¹ have been employed. Half of the publications assessed the effect of initial dye concentration on the process efficiency, achieving results in agreement with Section 1.4.1.

Table 1.3. Examples on the treatment of synthetic wastewaters contaminated with dyes by EAOPs.

Pollutant	Wastewater characteristics	Process	Electrochemical reactor		Operational parameters (Maximal DOC decay ^a)	Ref.
			Configuration	V (L)		
4-amino-3-hydroxy-2-p-tolylazo-naphthalene-1-sulfonicacid (AHPS) azo dye	88-263 mg AHPS L ⁻¹ in 7.0 g Na ₂ SO ₄ L ⁻¹	EF catalyzed by pyrite	UC	0.2	Anode: BDD (6 cm ²) Cathode: CF (60 cm ²) j_{cat} : 1.7-7.5 mA cm ⁻² Q : MS T: 25 °C pH: 2.9-4.0 [TDI] ₀ (pyrite): 0.5-2 g L ⁻¹ (95%)	[106]

Table 1.3. Examples on the treatment of synthetic wastewaters contaminated with dyes by EAOPs.

Pollutant	Wastewater characteristics	Process	Electrochemical reactor		Operational parameters (Maximal DOC decay ^a)	Ref.
			Configuration	V (L)		
Acid Orange 7 azo dye	1.4-18 mg Acid Orange 7 L ⁻¹ in 7.0-14 g Na ₂ SO ₄ L ⁻¹ or 6.1-12 g NaClO ₄ L ⁻¹ or 2.9 g NaCl L ⁻¹	EF	UC	0.2	Anode: Pt (1 cm ²) Cathode: Graphite felt (3.8-7.6 cm ²) E: -0.5 to -1.0 V Q: MS T: Amb. pH: 3.0 [TDI] ₀ : 5.6 mg L ⁻¹ (75%)	[122]
Acid Orange 7 azo dye metabolites: sulphanilic acid (SA), 1-amino-2-naphthol (AN)	20-60 mg SA or AN L ⁻¹ in 5.0 g Na ₂ SO ₄ L ⁻¹ or 5.8 g NaCl L ⁻¹ 300 mg Acid Orange 7 L ⁻¹ in a simulated effluent	AO	UC or FP with plug-flow cell	0.2	Anode: UC: BDD (20 cm ²) FP: BDD (8 cm ²) Cathode: UC: SS (20 cm ²) FP: SS (8 cm ²) j _{cat} : 1.3-30 mA cm ⁻² Q (UC): MS Q (FP): MS T: 25 °C pH: Neutral (41%)	[121]
Acid Orange 7 monoazo dye Acid Red 151 diazo dye Direct Blue 71 triazo dye	6.3-350 mg Acid Orange 7 L ⁻¹ or 8.2-454 mg Acid Red 151 L ⁻¹ or 19-1030 mg Direct Blue 71 L ⁻¹ in 7.0 g Na ₂ SO ₄ L ⁻¹	AO-H ₂ O ₂ EF	UC	0.1	Anode: Pt or BDD (3 cm ²) Cathode: C-PTFE A-D or Graphite (3 cm ²) j _{cat} : 8.3-100 mA cm ⁻² Q: MS T: 35 °C pH: 3.0 [TDI] ₀ (EF): 28 mg L ⁻¹ (n.a.)	[161]
Acid Red 1 azo dye	236 mg Acid Red 1 L ⁻¹ in 7.0 g Na ₂ SO ₄ L ⁻¹	AO-H ₂ O ₂ EF PEF-UVA	UC	0.1	Anode: Pt or BDD (3 cm ²) Cathode: C-PTFE A-D (3 cm ²) j _{cat} : 17-100 mA cm ⁻² Q: MS T: 35 °C pH: 3.0 [TDI] ₀ (EF, PEF-UVA): 28 mg L ⁻¹ (≈100% – PEF-UVA)	[162]
Acid Red 29 azo dye	244 mg Acid Red 29 L ⁻¹ in 7.0 g Na ₂ SO ₄ L ⁻¹	EF PEF-UVA	UC	0.1	Anode: BDD (3 cm ²) Cathode: C-PTFE A-D (3 cm ²) j _{cat} : 17-100 mA cm ⁻² Q: MS T: 35 °C pH: 2.0-6.0 [TDI] ₀ : 11-279 mg L ⁻¹ (>92% – PEF-UVA)	[89]
Acid Red 88, Acid Yellow 9 azo dyes	119 mg Acid Red 88 L ⁻¹ or 127-508 mg Acid Yellow 9 L ⁻¹ in 7.0 or 14 g Na ₂ SO ₄ L ⁻¹	EF SPEF	FP with undivided FPC and planar photoreactor	2.5	Anode: BDD (20 cm ²) Cathode: C-PTFE A-D (20 cm ²) j _{cat} : 25-150 mA cm ⁻² Q: 3.3 L min ⁻¹ T: 35 °C pH: 3.0 [TDI] ₀ : 5.6-45 mg L ⁻¹ (93% – SPEF)	[163]
Acid Yellow 23 azo dye	278 mg Acid Yellow 23 L ⁻¹ in 7.0 g Na ₂ SO ₄ L ⁻¹ or 2.9 g NaCl L ⁻¹	EC + AO, AO-H ₂ O ₂ , EF or PEF-UVA	UC	0.13	Anode: Pt or BDD (3 cm ²) Cathode: AO: SS (3 cm ²) AO-H ₂ O ₂ , EF, PEF-UVA: C-PTFE A-D (3 cm ²) j _{cat} : 33-100 mA cm ⁻² Q: MS T: 25 °C pH: 3.0 [TDI] ₀ (EAOPs as a single stage): 28 mg L ⁻¹ [TDI] ₀ (EAOPs after EC): 34 mg L ⁻¹ (100% – EC + PEF-UVA)	[33]
Acid Yellow 36 azo dye	20 mg Acid Yellow 36 L ⁻¹ + 5 mg kaolin L ⁻¹ in 1.1 g KCl L ⁻¹	AO + MF	FP with tubular ceramic membrane with imbedded electrodes	2	Anode: BDD (9.4 cm ²) Cathode: SS tube j _{cat} : 30 mA cm ⁻² Q: n.s. T: Amb. pH: 3.0 (n.a.)	[164]

Table 1.3. Examples on the treatment of synthetic wastewaters contaminated with dyes by EAOPs.

Pollutant	Wastewater characteristics	Process	Electrochemical reactor		Operational parameters (Maximal DOC decay ^a)	Ref.
			Configuration	V (L)		
Allura Red AC azo dye	115-460 mg Allura Red AC L ⁻¹ in 3.5-43 g Na ₂ SO ₄ L ⁻¹ or 5.3 g LiClO ₄ L ⁻¹ or 4.2 g NaNO ₃ L ⁻¹ or 1.5-8.8 g NaCl L ⁻¹	AO-H ₂ O ₂ EF PEF-UVA	UC	0.13	Anode: Pt or BDD (3 cm ²) Cathode: C-PTFE A-D (3 cm ²) <i>j</i> _{cat} : 33-150 mA cm ⁻² <i>Q</i> : MS T: 25 °C pH: 3.0 [TDI] ₀ (EF, PEF-UVA): 28 mg L ⁻¹ (100% – PEF-UVA)	[123]
Azure B dye	31 mg Azure B L ⁻¹ in 7.0 g Na ₂ SO ₄ L ⁻¹	AO-H ₂ O ₂ EF	UC	0.2	Anode: Pt mesh or BDD (25 cm ²) Cathode: CF <i>I</i> : 50-500 mA <i>Q</i> : MS T: Amb. pH: 3.0 [TDI] ₀ (EF): 5.6 mg L ⁻¹ (90% – EF)	[165]
Basic Red 46 azo dye	2-20 mg Basic Red 46 L ⁻¹ in 7.0 g Na ₂ SO ₄ L ⁻¹	EF PEF-Vis PEF-Vis/oxalate	UC	0.8	Anode: Pt (1 cm ²) Cathode: Multi walled CNT-PTFE (5.4 cm ²) <i>j</i> _{cat} : 19 mA cm ⁻² <i>Q</i> : MS T: Amb. pH: 3.0 [TDI] ₀ : 5.6-28 mg L ⁻¹ (n.a.)	[150]
Basic Yellow 28 dye	10-40 mg Basic Yellow 28 L ⁻¹ in 7.0 g Na ₂ SO ₄ L ⁻¹	EF PEF-UVC PEF-UVA or PEF-UVB or PEF-UVC catalyzed by ZnO nanoparticles	UC	2	Anode: Pt (11.5 cm ²) Cathode: Multi walled CNT-PTFE (5.4 cm ²) <i>j</i> _{cat} : 9.2-93 mA cm ⁻² <i>Q</i> : MS T: Amb. pH: 2.0-6.0 [TDI] ₀ : 5.6 mg L ⁻¹ (95% – PEF-UVC-ZnO)	[107]
Cationic red X-GRL azo dye	38-150 mg Cationic red X-GRL L ⁻¹ in 7.0 g Na ₂ SO ₄ L ⁻¹	EF	UC	1	Anode: RuO ₂ (90 cm ²) Cathode: ACF or grafite (90 cm ²) <i>j</i> _{cat} : 2.2-13 mA cm ⁻² <i>Q</i> : MS T: 27-60 °C pH: 2.0-5.0 [TDI] ₀ : 56-558 mg L ⁻¹ or 64-635 mg Cu ²⁺ L ⁻¹ or 55-549 mg Mn ²⁺ L ⁻¹ (68%)	[62]
Cibacron Marine FG azo dye	30-70 mg Cibacron Marine FG L ⁻¹ in ultrapure water	AO	FP with undivided FPC	1	Anode: Sb-SnO ₂ (40 cm ²) Cathode: SS (40 cm ²) <i>j</i> _{cat} : 10-30 mA cm ⁻² <i>Q</i> : 0.36-0.67 T: 24 °C pH: 5.8 (n.s.)	[112]
Congo Red azo dye	45-362 mg Congo Red L ⁻¹ in 7.0 g Na ₂ SO ₄ L ⁻¹	AO-H ₂ O ₂ EF PEF-UVA SPEF	AO-H ₂ O ₂ , EF, PEF-UVA: UC SPEF: FP with undivided FPC and planar photoreactor	AO-H ₂ O ₂ , EF, PEF-UVA: 0.1 SPEF: 2.5	Anode: AO-H ₂ O ₂ , EF, PEF-UVA: BDD (3 cm ²) SPEF: BDD (20 cm ²) Cathode: AO-H ₂ O ₂ , EF, PEF-UVA: C-PTFE A-D (3 cm ²) SPEF: C-PTFE A-D (20 cm ²) <i>j</i> _{cat} : 50-150 mA cm ⁻² <i>Q</i> (SPEF): 3.3 L min ⁻¹ <i>Q</i> (others): MS T: 35 °C pH: 3.0 [TDI] ₀ (EF, PEF-UVA, SPEF): 14-112 mg L ⁻¹ (100% – SPEF)	[160]

Table 1.3. Examples on the treatment of synthetic wastewaters contaminated with dyes by EAOPs.

Pollutant	Wastewater characteristics	Process	Electrochemical reactor		Operational parameters (Maximal DOC decay ^a)	Ref.
			Configuration	V (L)		
Direct Orange 61 azo dye	44-175 mg Direct Orange 61 L ⁻¹ in 7.0 g Na ₂ SO ₄ L ⁻¹	EF	UC	-	Anode: Pt (5.5 cm ²) Cathode: CF (60 cm ²) <i>j</i> _{cat} : 0.5-1.7 mA cm ⁻² <i>Q</i> : MS T: Amb. pH: 3.0 [TDI] ₀ : 5.6-28 mg L ⁻¹ (98%)	[103]
Direct Red 23 azo dye	10-50 mg Direct Red 23 L ⁻¹ in 7.0 g Na ₂ SO ₄ L ⁻¹	EF PEF-Vis PEF-Vis/citrate	UC	2	Anode: Pt (11.5 cm ²) Cathode: Multi walled CNT-PTFE (5.4 cm ²) <i>j</i> _{cat} : 19-93 mA cm ⁻² <i>Q</i> : MS T: Amb. pH: 2.0-9.0 [TDI] ₀ : 5.6-45 mg L ⁻¹ (n.a.)	[109]
Direct Yellow 4 azo dye	50-200 mg Direct Yellow 4 L ⁻¹ in 7.0 g Na ₂ SO ₄ L ⁻¹	SPEF	FP with undivided FPC and photoreactor	10	Anode: Pt or BDD (90.2 cm ²) Cathode: C-PTFE A-D (90.2 cm ²) <i>j</i> _{cat} : 33-55 mA cm ⁻² <i>Q</i> : 3.3 L min ⁻¹ T: 35 °C pH: 3.0 [TDI] ₀ : 14-279 mg L ⁻¹ (≈100%)	[114]
Disperse Red 1, Disperse Yellow 3 azo dyes	82-327 mg Disperse Red 1 L ⁻¹ or 150 mg Disperse Yellow 3 L ⁻¹ in 14.0 g Na ₂ SO ₄ L ⁻¹	EF SPEF	FP with undivided FPC and planar photoreactor	2.5	Anode: BDD (20 cm ²) Cathode: C-PTFE A-D (20 cm ²) <i>j</i> _{cat} : 15-80 mA cm ⁻² <i>Q</i> : 3.3 L min ⁻¹ T: 35 °C pH: 2.0-6.0 [TDI] ₀ : 28 mg L ⁻¹ (>90% – SPEF)	[88]
E122 (Azorubine), E124 (Ponceau 4R), E129 (Allura Red AC) azo dyes	7.0 or 70 mg E122 L ⁻¹ , 8.5 or 85 mg E124 L ⁻¹ , 7.2 or 72 mg E129 L ⁻¹ (mixture) in 7.0 g Na ₂ SO ₄ L ⁻¹ or 5.3 g LiClO ₄ L ⁻¹ or 4.2 g NaNO ₃ L ⁻¹ or 2.9 g NaCl L ⁻¹ or simulated wastewater or real WWTP secondary effluent	EF PEF-UVA SPEF	EF, PEF-UVA: UC SPEF: FP with undivided FPC and photoreactor	EF, PEF-UVA: 0.13 SPEF: 2.5	Anode: EF, PEF-UVA: Pt or BDD (3 cm ²) SPEF: BDD (20 cm ²) Cathode: EF, PEF-UVA: Pt or BDD (3 cm ²) SPEF: BDD (20 cm ²) <i>j</i> _{cat} (EF, PEF-UVA): 33 mA cm ⁻² <i>j</i> _{cat} (SPEF): 50-150 mA cm ⁻² <i>Q</i> (SPEF): 3.3 L min ⁻¹ <i>Q</i> (others): MS T: 35 °C pH: 3.0 [TDI] ₀ : 28 mg L ⁻¹ (100% – SPEF)	[91]
Evans Blue azo dye	235 mg Evans Blue L ⁻¹ in 7.0 g Na ₂ SO ₄ L ⁻¹	EF PEF-UVA SPEF	LS: UC PS: FP with undivided FPC and photoreactor	LS: 0.1 PS: 10	Anode: LS: BDD (3 cm ²); PS: Pt (90.3 cm ²) Cathode: C-PTFE A-D LS: 3 cm ² ; PS: 90.3 cm ² <i>j</i> _{cat} : 17-100 mA cm ⁻² <i>Q</i> : LS: MS; PS: 3.3 L min ⁻¹ T: 35 °C pH: 3.0 [TDI] ₀ : 28 mg L ⁻¹ (88% – SPEF)	[126]
Indigo Carmine dye	112-881 mg Indigo Carmine L ⁻¹ in 7.0 g Na ₂ SO ₄ L ⁻¹	EF PEF-UVA PEF/UVA catalyzed by Cu ²⁺	UC	0.1	Anode: Pt or BDD (3 cm ²) Cathode: C-PTFE A-D (3 cm ²) <i>j</i> _{cat} : 33-150 mA cm ⁻² <i>Q</i> : MS T: 35 °C pH: 2.0-6.0 [TDI] ₀ : 11-279 mg L ⁻¹ (alone or + 16 mg Cu ²⁺ L ⁻¹) (≈100% – PEF-UVA-Cu²⁺)	[97]

Table 1.3. Examples on the treatment of synthetic wastewaters contaminated with dyes by EAOPs.

Pollutant	Wastewater characteristics	Process	Electrochemical reactor		Operational parameters (Maximal DOC decay ^a)	Ref.
			Configuration	V (L)		
Indigo dye	315 mg Indigo L ⁻¹ in 2.9 g NaCl L ⁻¹	AO	FP with undivided FPC	1	Anode: 2D (plate) BDD (64 cm ²) or 3D (mesh) BDD (444 cm ²) Cathode: Pt j_{cat} : 5.6 or 15 mA cm ⁻² Q : 0.10-1.1 L min ⁻¹ T: 25 °C pH: 6.3 (n.a.)	[166]
Lissamine Green B, Methyl Orange azo, Reactive Black 5 azo, Fuchsin Acid dyes	8.5 mg Lissamine Green B L ⁻¹ , 1.5 mg Methyl Orange L ⁻¹ , 70 mg Reactive Black 5 L ⁻¹ , 15 mg Fuchsin Acid L ⁻¹ in 1.4 g Na ₂ SO ₄ L ⁻¹ for solutions with one dye or in 5.7 g Na ₂ SO ₄ L ⁻¹ for a mixture of all dyes	EF	Flow bubble reactor with UC	0.675	Anode: Graphite (1.27 cm ²) Cathode: Graphite (1.27 cm ²) E_{cell} : 15 V Q : n.s. T: Amb. pH: 2.0-5.0 [TDI] ₀ (single solutions): 150 mg L ⁻¹ [TDI] ₀ (mixture): 600 mg L ⁻¹ (46%)	[156]
Lissamine Green B, Azure B dyes	8.5 mg Lissamine Green L ⁻¹ or 4.83 mg Azure B L ⁻¹ in 1.4 g Na ₂ SO ₄ L ⁻¹	EF catalyzed by Fe alginate gel beads	UC or flow bubble reactor with UC	UC: n.s. Flow bubble reactor with UC: 0.15	Anode: Graphite (1.27 cm ²) Cathode: Graphite (1.27 cm ²) E_{cell} : 14 V Q (UC): MS Q (Flow bubble reactor): n.s. T: Amb. pH: 2.0-8.0 [TDI] ₀ (Fe alginate gel beads): 58 g L ⁻¹ (93%)	[167]
Methyl Red, Orange II, Biebrich Scarlett azo dyes	100 mg L ⁻¹ in pure water for each dye solution	EF	DC	n.s.	Anode: Pt (31.4 cm ²) Cathode: CF (42 or 378 cm ²) E : -0.5 V Q : MS T: 30 °C pH: 1.0 or 3.0 [TDI] ₀ : 56 mg L ⁻¹ (11%)	[168]
Methyl Violet 2B dye	69-548 mg Methyl Violet 2B L ⁻¹ in 7.0 g Na ₂ SO ₄ L ⁻¹	AO	UC	0.1	Anode: BDD or Pt (3 cm ²) Cathode: SS (3 cm ²) j_{cat} : 33-150 mA cm ⁻² Q : MS T: 35 °C pH: 3.0 or 7.4 (≈100%)	[110]
Orange G azo dye	294-3580 mg Orange G L ⁻¹ in 7.0 g Na ₂ SO ₄ L ⁻¹	AO	UC or DC	0.1	Anode: BDD (3 cm ²) Cathode: SS (3 cm ²) j_{cat} : 33-150 mA cm ⁻² Q : MS T: 35 °C pH: 2.0-6.0 (100%)	[141]
Orange II azo dye	50 mg Orange II L ⁻¹ in 7.0 g Na ₂ SO ₄ L ⁻¹	AO-H ₂ O ₂ EF PEF-UVA	FP with concentric annular cell	0.4	Anode: Graphite cloth (200 cm ²) Cathode: Graphite cloth (164 cm ²) j_{cat} : 300 mA cm ⁻² Q : 0.1 L min ⁻¹ T: Amb. pH: 3.0 [TDI] ₀ (EF, PEF-UVA): 11-28 mg L ⁻¹ (80% – PEF-UVA)	[169]
Ponceau S azo dye	34-202 mg Ponceau S L ⁻¹ in 7.0-14 g Na ₂ SO ₄ L ⁻¹ or 5.8 g NaCl L ⁻¹ or 7.5 g KCl L ⁻¹	EF	UC	0.45	Anode: Pt (3.8 cm ²) Cathode: RVC (35 cm ²) E : -0.5 to 1.0 V Q : MS T: Amb. pH: 2.5-4.5 [TDI] ₀ : 2.8-56 mg L ⁻¹ (98%)	[66]

Table 1.3. Examples on the treatment of synthetic wastewaters contaminated with dyes by EAOPs.

Pollutant	Wastewater characteristics	Process	Electrochemical reactor		Operational parameters (Maximal DOC decay ^a)	Ref.
			Configuration	V (L)		
Reactive Blue 4 dye	100 mg Reactive Blue 4 L ⁻¹ in 7.0 g Na ₂ SO ₄ L ⁻¹	EF	UC	0.2	Anode: Pt (6 cm ²) Cathode: CF (50 cm ²) <i>j</i> _{cat} : 1.2-4 mA cm ⁻² <i>Q</i> : MS T: Amb. pH: 3.0 [TDI] ₀ : 11 mg L ⁻¹ (78%)	[157]
Rhodamine B azo dye	5 mg Rhodamine B L ⁻¹ in 7.0 g Na ₂ SO ₄ L ⁻¹ or 5.3 mg Na ₂ CO ₃ L ⁻¹ or 4.2 g NaNO ₃ L ⁻¹	EF	UC	n.s.	Anode: Pt (2 cm ²) Cathode: Sandwich film cathode: ACF + Fe ²⁺ -chitosan deposited on Ni (6 cm ²) <i>j</i> _{cat} : 0.08-3.3 mA cm ⁻² <i>Q</i> : MS T: Amb. pH: 2.5-9.8 Electrogenerated iron (n.a.)	[132]
Sunset Yellow FCF azo dye	90 mg Sunset Yellow FCF L ⁻¹ in 7.0 g Na ₂ SO ₄ L ⁻¹ or 5.8 g NaCl L ⁻¹ or 7.5 g KCl L ⁻¹	EF	UC	0.45	Anode: Pt (3.8 cm ²) Cathode: RVC (35 cm ²) <i>E</i> : -0.5 to 1.0 V <i>Q</i> : MS T: 25 °C pH: 3.0-5.0 [TDI] ₀ : 0.56-28 mg L ⁻¹ (n.a.)	[67]

^a Under the best experimental conditions, when applicable;

Amb. – Ambient;

C-PTFE A-D – Carbon-PTFE air-diffusion;

DC – Divided cell;

FP – Flow plant;

FPC – Filter-press cell;

LS – Lab-scale;

MS – Magnetic stirring;

n.s. – not specified;

PS – Pilot-scale;

Q – Liquid flow rate;

UC – Undivided cell.

1.5.1.2 Background electrolyte

More than a half of works used Na₂SO₄ as background electrolyte and half of them employed a concentration of 7.0 g Na₂SO₄ L⁻¹. Thiam et al. [123] assessed a concentration range of 3.5-43 g Na₂SO₄ L⁻¹ in the degradation of Allura Red AC azo dye by PEF process employing BDD anode under UVA radiation (PEF-UVA-BDD). The authors attained lower decolorization for Na₂SO₄ contents above 14 g L⁻¹ and similar mineralization for all electrolyte contents.

Some articles evaluated the influence of the nature of background electrolyte on processes ability for decolorization and dye removal. For all EAOPs, decreases in color and dye content were predominantly favored by employing NaCl instead of Na₂SO₄ due to the attack of dye molecules by active chlorine species formed in the presence of chloride via Eqs. (5)-(7) [33, 121-123]. Nonetheless, El-Desoky et al. [66] and Ghoneim et al. [67] reported the superiority of Na₂SO₄ over

both NaCl and KCl in terms of decolorization ability, and have attributed these results to the scavenging of $\bullet\text{OH}$ by chloride via Eq. (35) in higher extent than by sulfate through Eq. (34) and also to a higher conductivity of sulfate compared to chloride. The performance of a ClO_4^- based electrolyte to remove color was controversial. While Daneshvar et al. [122] reached better results applying NaClO_4 instead of NaCl and Na_2SO_4 and linked that to the formation of chloro and sulfato-complexes with free iron in the last two systems, Thiam et al. [123] attained slower decolorization using LiClO_4 compared to NaCl, Na_2SO_4 and NaNO_3 . In turn, Fan et al. [132] found decolorization ability in the order $\text{Na}_2\text{SO}_4 > \text{NaNO}_3 > \text{Na}_2\text{CO}_3$, which was ascribed to a higher ability of carbonate to scavenge $\bullet\text{OH}$.

Regarding the effect of electrolyte nature on the mineralization ability, it was consensual a superiority of Na_2SO_4 over NaCl for AO-BDD, AO- H_2O_2 -BDD, EF-BDD, PEF-UVA-BDD and PEF-UVA-Pt processes, mainly attributed to the occurrence of parasitic reactions between chloride and $\bullet\text{OH}$ and formation of refractory chloroderivatives. On the contrary, for AO, AO- H_2O_2 and EF methods employing a Pt anode, the use of NaCl electrolyte led to faster mineralization than Na_2SO_4 since the pollutants degradation by active chlorine species took a more important role due to the lower reactivity of $\text{Pt}(\bullet\text{OH})$ compared to $\text{BDD}(\bullet\text{OH})$ [33].

1.5.1.3 Process

Most of the studies presented in Table 1.3 refer to the application of EF process, although a lot of works regarding AO are not included in it. AO- H_2O_2 and SPEF were the less applied processes. In general, processes efficiency in terms of mineralization could be arranged in the order $\text{SPEF} > \text{PEF-UVA} > \text{EF} > \text{AO-H}_2\text{O}_2$. For example, Solano et al. [160] found DOC removals of 99%, 92% and 39% after 360 min of PEF-UVA, EF and AO- H_2O_2 processes, respectively, for the treatment of a 181 mg Congo Red L^{-1} solution in 7.0 g $\text{Na}_2\text{SO}_4 \text{L}^{-1}$ using an undivided cell, BDD anode, carbon-PTFE air-diffusion cathode, pH of 3.0, 25 °C, $[\text{TDI}]_0$ of 28 mg L^{-1} for EF and PEF-UVA and j_{cat} of 100 mA cm^{-2} . Antonin et al. [126] attained total mineralization after 150 and 300 min for SPEF and PEF-UVA processes, respectively, by degrading a 235 mg Evans Blue L^{-1} solution upon the same system and conditions as Solano et al. [160].

In terms of decolorization and dye removal, controversial results have been reported. Some studies proved superiority of SPEF and PEF-UVA over EF [88, 91, 169], but other investigations found quite similar efficiencies for these three EAOPs [123, 160, 162, 163]. The identical dye and color removals under EF and light-assisted EAOPs means that parent compounds and their colored

by-products can be efficiently destroyed by $M(\bullet\text{OH})$ and $\bullet\text{OH}$ produced in the bulk from Fenton's reaction (21), with little contribution of photoreduction reactions (28) and (29). Moreover, the dye removal is usually faster than solution decolorization, indicating that some colored by-products that react more hardly with generated $\bullet\text{OH}$ are generated during the degradation process. For example, Solano et al. [160] found total dye decay and total color removal after 60 and 150 min of SPEF, respectively.

Thiam et al. [33] presented the only research study comparing AO with other processes. Similar mineralization and decolorization were attained for AO and AO- H_2O_2 processes, which revealed a negligible role of H_2O_2 on the dye degradation.

Khataee et al. [65, 109] executed PEF processes using visible light, alone and in combination with Fe(III)-oxalate and Fe(III)-citrate complexes, and achieved processes decolorization ability in the following order: PEF-Vis/oxalate or citrate > PEF-Vis > EF. As abovementioned, the Fe(III)-carboxylate complexes are able to be photodecarboxylated under UV-Vis radiation via Eq. (29) with higher quantum yields for Fe^{2+} generation than that of Fe(III)-hydroxy complexes, among other advantages. The improvement of PEF process was also accomplished by Flox et al. [97] and Iranifam et al. [107] by adding Cu^{2+} and ZnO nanoparticles, respectively. Cu^{2+} can form complexes with carboxylic acids that are more rapidly destroyed than Fe(III)-carboxylate complexes and acids alone and, in addition, greater amounts of $\bullet\text{OH}$ can be produced in the medium from the $\text{Cu}^{2+}/\text{Cu}^+$ catalytic system. ZnO is a semiconductor that forms an electron-hole pair under UV radiation and the hole has a so high oxidative potential that allows the direct oxidation of organics and also the generation of $\bullet\text{OH}$ by water decomposition.

The combination of EAOPs with other technologies for dyes removal has been only slightly explored. Juang et al. [164] used a microfiltration (MF)/AO system to remove a mixture of an azo dye and kaolin particles. The MF was able to remove particles but the performance of AO alone was not discussed. Thiam et al. [33] proved the suitability of applying EC prior to a PEF-UVA process. In this study, EC was used as source of $\text{Fe}(\text{OH})_2$ or $\text{Fe}(\text{OH})_3$ coagulant to provide color removal and separation of a large fraction of organic matter and also as source of $\text{Fe}^{3+}/\text{Fe}^{2+}$ catalyst to the subsequent EAOP, in which the remaining persistent organic matter was degraded.

1.5.1.4 Electrochemical reactor

Most of the studies regarding the treatment of wastewaters containing dyes by EAOPs have been performed in undivided electrochemical reactors, typically employing solution volumes of 100-200 mL, although volumes of 1 and 2 L were occasionally used [62, 107, 109, 164]. Figure 1.2 shows a schematic representation of a thermostated undivided electrochemical reactor with around 100 mL capacity equipped with a carbon-PTFE O₂-diffusion cathode. This equipment can also be used upon direct injection of an air flow to the cathode. Divided cells use a separator between the anolyte and the catholyte that makes the treatment process more expensive and demanding by the penalty overvoltage of the separator and, consequently, their use was very sparse, with only two studies displayed in Table 1.3 [141, 168]. El-Ghenmy et al. [141] compared the application of both undivided and divided cells and revealed the need for a higher electrolyte concentration in the divided cell due to a large E_{cell} increase. The decolorization was faster in the divided cell, which can be attributed to the interaction of organics with an electric field of higher magnitude because of the higher E_{cell} . This is responsible for the enhancement of the mass transport towards the anode, thus promoting a quicker reaction between organics and M([•]OH).

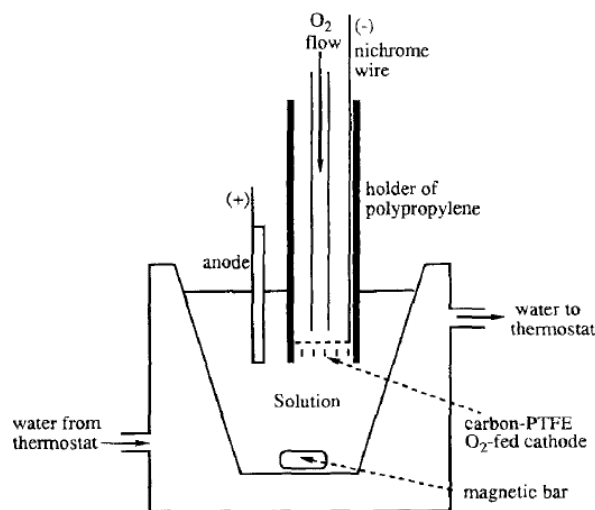


Figure 1.2. Sketch of a thermostated undivided cell of around 100 mL capacity equipped with a carbon-PTFE O₂-diffusion cathode. Reprinted (adapted) from Brillas et al. [55], Copyright © (1995), with permission from The Electrochemical Society.

Filter-press cells have shown quite popularity and they have been used in simple reactors by coupling to a pump and a reservoir (volume of solution of 1 L) [112, 166]. An example is presented in Figure 1.3. More complex flow plants with a structure for radiation capture have been described like a planar photoreactor with a mirror at the bottom and a volume of solution of

2.5 L [88, 91, 160, 163], schematized in Figure 1.4, or a photoreactor composed of borosilicate tubes mounted in an aluminum plane sheet with a solution volume of 10 L [114, 126], illustrated in Figure 1.5. Note that the photoreactor of Figure 1.5 was mentioned to be equipped with compound parabolic collectors (CPCs) in all studies regarding its application. However, this kind of collectors consists of two truncated parabolas, diverging from the applied aluminum plane sheet. Antonin et al. [126] reached total Evans Blue diazo dye removal after 60 and 5 min and 88% and more than 95 % mineralization after 300 min of SPEF reaction at the pilot-scale plant of Figure 1.5 and the 100 mL undivided cell of Figure 1.2, respectively. This difference was attributed to the distinct electrode area/solution volume ratio of both reactors, among other factors. Other kinds of flow plants equipped with a plug-flow cell [121], a tubular ceramic membrane with imbedded electrodes [164] or a concentric annular cell [169] were occasionally used.

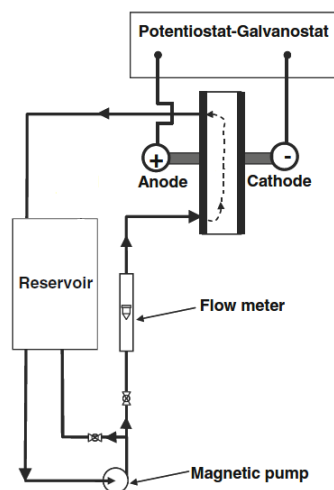


Figure 1.3. Sketch of a simple reactor equipped with an electrochemical cell, a pump and a reservoir. Reprinted (adapted) from Nava et al. [166], Copyright © (2014), with permission from Springer-Verlag Berlin Heidelberg.

EAOPs mainly used BDD or Pt as anode, with the exception of the employment of SnO₂ doped with antimony (Sb) in AO [112], graphite cloth in AO-H₂O₂, EF and PEF-UVA [169], RuO₂ in EF [62] and graphite bar in EF [156, 167]. Some studies performed a comparison between BDD and Pt anodes and, in general, BDD exhibited superiority over Pt, both in terms of decolorization and mineralization [33, 97, 110, 123, 162], since BDD shows a much higher potential for O₂ evolution, producing larger amounts of M([•]OH) to degrade organics. Surprisingly, in Garcia-Segura et al. [161] both AO-H₂O₂ and EF processes achieved quite similar decolorization by applying BDD or Pt anodes, pointing to very slow reaction of both BDD([•]OH) and Pt([•]OH) with the Acid Orange 7 monoazo dye. In turn, Thiam et al. [33] achieved similar mineralization

by applying Pt and BDD in a PEF-UVA process, contrasting to what was found for AO, AO-H₂O₂ and EF, which can be related to the improvement of Acid Yellow 23 removal by light-induced mechanisms. Nava et al. [166] determined superiority of 2D (plate) BDD anode over 3D (mesh) BDD in terms of chemical oxygen demand (COD) removal.

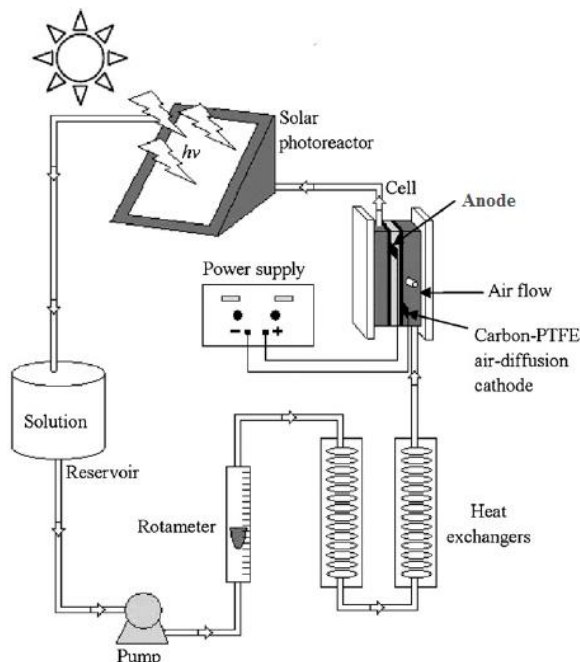


Figure 1.4. Sketch of a 2.5 L pre-pilot-scale flow plant equipped with a filter-press electrochemical cell, a planar photoreactor with a mirror at the bottom, a reservoir, a pump and heat exchangers. Reprinted (adapted) from Salazar et al. [88], Copyright © (2011), with permission from Elsevier.

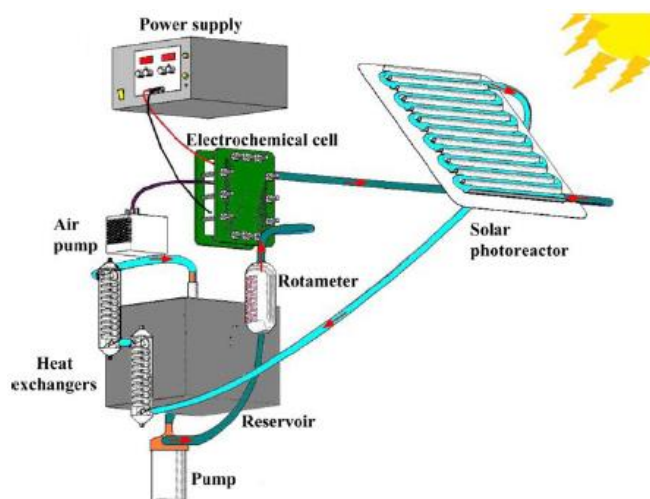


Figure 1.5. Sketch of a 10 L pilot-scale flow plant equipped with a filter-press electrochemical cell, a photoreactor with borosilicate tubes and an aluminum reflector, a reservoir, a pump and heat exchangers. Reprinted (adapted) from Garcia-Segura et al. [146], Copyright © (2011), with permission from Elsevier.

All AO processes in Table 1.3 used steel cathodes, apart from Nava et al. [166] in which a Pt cathode was applied. The most popular cathode for AO-H₂O₂, EF, PEF and SPEF techniques has been carbon-PTFE air-diffusion electrodes, widely used by Brillas' research team. Some EF applications, chiefly carried out by Oturan's group, employed CF as cathode. Few investigations have operated with other cathodes like RVC [66], ACF [62], CNT [107, 109, 150], graphite cloth [169] and graphite bar [156, 161, 167]. Garcia-Segura et al. [161] compared the decolorization ability of azo dyes by AO-H₂O₂ either using carbon-PTFE air-diffusion electrode or graphite bar as cathode. Results showed a superiority of graphite over carbon-PTFE air-diffusion, which was related to the parallel direct reduction of the azo dye on the graphite cathode. This did not take place on the GDE cathode as it mostly comprised the two-electron reduction of oxygen to H₂O₂ via Eq. (16).

Commonly, undivided cells with working volumes of 100-200 mL employed electrodes with active areas of 3 cm², although areas up to 20 cm² were used. Undivided cells with superior solution volumes up to 2 L and flow plants with a filter-press cell using 1 L of solution applied larger electrodes areas from 11.5 to 90 cm². The 2.5 L flow plant with planar photoreactor used electrodes of 20 cm² of active area (see Figure 1.4) and the 10 L flow plant equipped with borosilicate tubes used ca. 90 cm² electrodes (see Figure 1.5). While steel and carbon-PTFE air-diffusion cathodes usually presented the same active area as the anode, graphite felts were always much larger, thus favoring the reduction of Fe³⁺ to Fe²⁺.

1.5.1.5 Operational parameters

The operation in galvanostatic mode has been predominant for the degradation of wastewaters contaminated with dyes. The majority of studies assessed the influence of j on dyes degradation. In general, larger j always led to faster degradations in terms of decolorization, dye removal and mineralization for all EAOPs, as exemplified in Figure 1.6a for DOC removal of Acid Yellow 9. However, in some cases lower or null degradation improvement was achieved for the highest j tested due to the occurrence of parasitic reactions in larger extent.

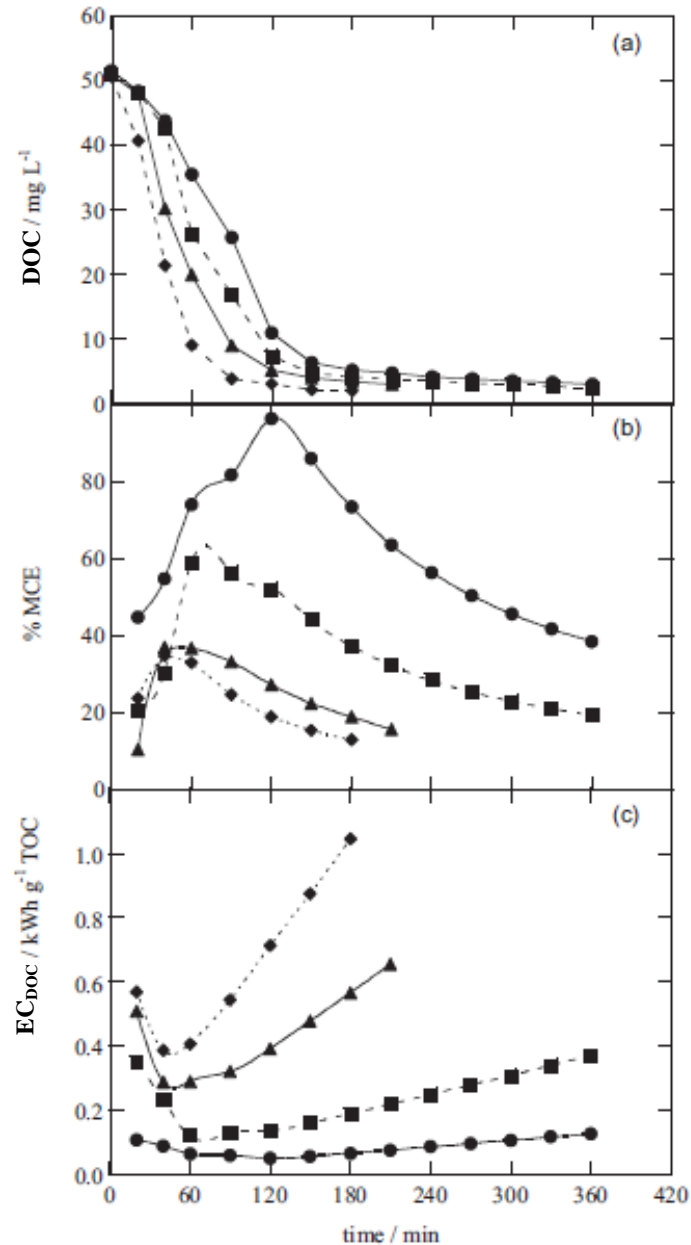


Figure 1.6. Effect of current density on (a) DOC removal, (b) mineralization current efficiency and (c) energy consumption per unit DOC mass as a function of time for the treatment of 127 mg Acid Yellow 9 L^{-1} in 14 g Na_2SO_4 L^{-1} by SPEF using the 2.5 L flow plant with a filter-press cell and a planar photoreactor of Figure 1.4 equipped with a BDD anode and a carbon-PTFE air-diffusion cathode, pH of 3.0, 35 °C and $[\text{TDI}]_0$ of 28 mg L^{-1} . Current density: (●) 25, (■) 50, (▲) 100 and (◆) 150 mA cm^{-2} . Reprinted (adapted) from Ruiz et al. [163], Copyright © (2011), with permission from Elsevier.

The rise in j came along with greater consumption of specific charge and energy and lower current efficiency. An example of the decrease of MCE and increase of EC_{DOC} with higher j can be seen in Figures 1.6b and c, respectively. For initial DOC contents of around 100 mg L^{-1} , j_{cat} of

30-150 mA cm⁻² were mostly employed, excluding when applying CF cathodes, for which j_{cat} below 10 mA cm⁻² were used due to the larger active areas of these electrodes.

Only Nava et al. [166] evaluated the effect of liquid flow rate on the process efficiency. It was found a very low influence of this parameter on COD decay using AO process in a flow plant with an undivided filter-press cell with continuous solution recirculation.

Lei et al. [62] attained increasing decolorization and mineralization with rising temperature from 27 to 60 °C for EF, whereas the other studies employed ambient temperature or a temperature of 35 °C to avoid water evaporation and H₂O₂ decomposition.

Both El-Ghenymy et al. [141] and Hamza et al. [110] assessed the influence of pH on AO process using Na₂SO₄ as background electrolyte and attained distinct results. The former achieved similar degradation for pH of 2.0-6.0, whereas the latter reached a slightly higher degradation at pH of 7.4 when compared to 3.0, suggesting that the neutral medium favored the production of structures more easily oxidizable by M([•]OH). A large part of remaining AO studies used neutral/close to neutral pH, although some AO and AO-H₂O₂ investigations employed pH of 3.0 for directly comparison with EAOPs based on Fenton's reaction chemistry. An optimum pH of 2.5-3.0 was pointed out by various studies of EF, PEF-UVA, PEF-UVC-ZnO and PEF-Vis/citrate [66, 67, 89, 107, 109]. Flox et al. [97] achieved similar and best degradations at pH of 2.0 and 3.0 for EF, such as Salazar et al. [88] also found for PEF-UVA and SPEF processes. Rosales et al. [156, 167] reported best operation at pH of 2.0 for EF.

Studies on the influence of [TDI]₀ revealed best results for contents of 5.6-28 mg L⁻¹ in EF, PEF-UVA, PEF-Vis/oxalate, PEF-Vis/citrate and SPEF treatments of wastewaters with DOC up to 50 mg L⁻¹ [67, 103, 109, 114, 150, 163, 169], except Lei et al. [62] who reported a best content of 279 mg L⁻¹ employing a RuO₂ anode and an ACF cathode. For dye wastewaters with DOC contents around 100 mg L⁻¹, larger [TDI]₀ of 28-56 mg L⁻¹ were needed for PEF-UVA and SPEF processes [89, 160], excluding the work of Flox et al. [97] where similar and best mineralization was attained for [TDI]₀ of 11-279 mg L⁻¹, indicating a very important role of BDD([•]OH) on the dye degradation.

Although most of the investigations have employed iron salts like FeSO₄·7H₂O and FeCl₃·6H₂O as iron source, some studies resorted to distinct sources. Rosales et al. [167] used Fe alginate gel beads in a concentration of 58 g L⁻¹ for EF process, which attained higher decolorization than the classical EF using [TDI]₀ of 150 mg L⁻¹. This heterogeneous catalyst can avoid iron precipitation

in virtue of the formation of ionic cross-links between the carboxyl group on alginate chains. In turn, Labiadh et al. [106] employed 0.5-2 g L⁻¹ of pyrite as iron source for EF treatment, which allowed to get [TDI] of 50-130 mg L⁻¹. Faster dye removals were reached at higher pyrite contents and the employment of 2 g pyrite L⁻¹ led to faster degradation than using [TDI]₀ of 25 mg L⁻¹. Moreover, the addition of pyrite drove to pH self-regulation from neutral to 2.9-4.0. On the other hand, a sandwich film cathode composed of an active carbon fiber and Fe²⁺-chitosan deposited on Ni was used by Fan et al. [132], allowing the release of iron into the solution and operation with similar efficiency at pH range of 2.5-6.2. The application of an EC step prior to EAOP stage in Thiam et al. [33] permitted to attain a [TDI] of 34 mg L⁻¹.

Surprisingly, Lei et al. [62] claimed superiority of Cu²⁺ and Mn²⁺ over Fe²⁺ to catalyze Cationic Red X-GRL dye removal. The two former ions can yield Fenton-like reactions with production of •OH, but more studies are needed to confirm this behavior, which could be due to the formation of more easily oxidizable complexes of such ionic metals with the dye and its products.

1.5.2 Wastewaters containing pesticides

The term pesticide refers to herbicides, insecticides, bactericides, fungicides, antimicrobials, rodenticides and various other substances used to control pests. Information of nineteen articles about decontamination of synthetic wastewaters with pesticides by EAOPs is summarized in Table 1.4. The following review on degradation of wastewaters polluted with pesticides is based on those studies.

1.5.2.1 Pesticide content

A look of Table 1.4 highlights that most of the articles refer to the treatment of herbicides, excluding the works of Skoumal et al. [135] and Vargas et al. [115], which regarded the degradation of antimicrobial and insecticide agents, respectively. Only a small number of investigations used mixtures of pesticides or compared the degradation of various pesticides [56, 131, 142], with almost all surveys using a single model compound. Abdessalem et al. [131, 142] found pesticides removal readiness in the order chlorotoluron > carbofuran > bentazon for AO-H₂O₂ and EF processes.

Initial pesticide contents from 4.0 to 634 mg L⁻¹ have been applied. Some publications assessed the influence of initial pesticide concentration on EAOPs efficiency, always attaining lower percentages of mineralization and/or pollutant removal for larger initial pesticide amounts, as pointed out above.

Table 1.4. Examples on the treatment of synthetic wastewaters contaminated with pesticides by EAOPs.

Pollutant	Wastewater characteristics	Process	Electrochemical reactor		Operational parameters (Maximal DOC decay ^a)	Ref.
			Configuration	V (L)		
2-(2,4-dichlorophenoxy)-propionic acid (2,4-D) pesticide	217 mg 2,4-D L ⁻¹ in 7.0 g Na ₂ SO ₄ L ⁻¹	AO EF PEF-UVA	UC	0.1	Anode: Pt (10 cm ²) or BDD (3 cm ²) Cathode: AO: Graphite (3 cm ²) EF, PEF-UVA: C-PTFE O-D (3 cm ²) <i>j</i> _{cat} : 33-150 mA cm ⁻² <i>Q</i> : MS T: 35 °C pH: 3.0 [TDI] ₀ (EF, PEF-UVA): 112 mg L ⁻¹ (83% – PEF-UVA)	[155]
2,4,5-trichlorophenoxyacetic acid (2,4,5-T) pesticide	53-266 mg 2,4,5-T L ⁻¹ in 7.0 g Na ₂ SO ₄ L ⁻¹	AO AO-H ₂ O ₂ EF PEF-UVA	UC	0.1	Anode: Pt (10 cm ²) Cathode: AO: Graphite (3 cm ²) AO-H ₂ O ₂ , EF, PEF-UVA: C-PTFE O-D (3.1 cm ²) <i>j</i> _{cat} : 32-145 mA cm ⁻² <i>Q</i> : MS T: 35 °C pH: 2.0-6.0 [TDI] ₀ (EF, PEF-UVA): 28-112 mg L ⁻¹ (100% – PEF-UVA)	[86]
2,4-dichlorophenoxyacetic acid (2,4-D) pesticide	60 mg 2,4-D L ⁻¹ in 7.0 g Na ₂ SO ₄ L ⁻¹	AO EF	FP with undivided FPC	3	Anode: BDD (64 cm ²) Cathode: BDD (64 cm ²) (with or without air bubbling for EF or AO, respectively) <i>j</i> _{cat} : 7.8-31 mA cm ⁻² <i>Q</i> : 4-10 L min ⁻¹ T: Amb. pH: 3.0 [TDI] ₀ (EF): 17 or 39 mg L ⁻¹ (83% – EF)	[69]
4-chloro-2-methylphenoxyacetic acid (MCPA) pesticide	186 mg MCPA L ⁻¹ in 7.0 g Na ₂ SO ₄ L ⁻¹	SPEF	FP with undivided FPC and photoreactor	10	Anode: Pt (90.3 cm ²) Cathode: C-PTFE A-D (90.3 cm ²) <i>j</i> _{cat} : 18-93 mA cm ⁻² <i>Q</i> : 3 L min ⁻¹ T: 35 °C pH: 3.0 [TDI] ₀ : 23-117 mg L ⁻¹ (75%)	[146]
4-chlorophenoxyacetic acid (4-CPA) pesticide	40-387 mg 4-CPA L ⁻¹ in 7.0 g Na ₂ SO ₄ L ⁻¹	AO AO-H ₂ O ₂ EF PEF-UVA	UC	0.1	Anode: Pt (10 cm ²) Cathode: AO: Graphite (3 cm ²) AO-H ₂ O ₂ , EF, PEF-UVA: C-PTFE O-D (3.1 cm ²) <i>j</i> _{cat} : 32-145 mA cm ⁻² <i>Q</i> : MS T: 25-45 °C pH: 2.0-6.0 [TDI] ₀ (EF, PEF-UVA): 28-112 mg L ⁻¹ (100% – PEF-UVA)	[127]
4-chlorophenoxyacetic acid (4-CPA), 4-chloro-2-methylphenoxyacetic acid (MCPA), 2,4-dichlorophenoxyacetic acid (2,4-D), 2,4,5-trichlorophenoxyacetic acid (2,4,5-T), 3,6-dichloro-2-methoxybenzoic acid (dicamba) pesticides	200 mg 4-CPC L ⁻¹ or 194 mg MCPA L ⁻¹ or 230 mg 2,4-D L ⁻¹ or 269 mg 2,4,5-T L ⁻¹ or 230 mg dicamba L ⁻¹ in 7.0 g Na ₂ SO ₄ L ⁻¹	PC EC EF	UC	0.1	Anode: PC, EC: Fe (10 cm ²) EF: Pt (10 cm ²) Cathode: PC, EF: C-PTFE O-D (3.1 cm ²) EC: Graphite (3 cm ²) <i>j</i> _{cat} : 33-150 mA cm ⁻² <i>Q</i> : MS T: 35 °C pH: 3.0 [TDI] ₀ (EF): 56 mg L ⁻¹ (94% – PC)	[56]

Table 1.4. Examples on the treatment of synthetic wastewaters contaminated with pesticides by EAOPs.

Pollutant	Wastewater characteristics	Process	Electrochemical reactor		Operational parameters (Maximal DOC decay ^a)	Ref.
			Configuration	V (L)		
Amitrole pesticide	350 mg amitrole L ⁻¹ in 7.0 g Na ₂ SO ₄ L ⁻¹	AO EF	UC	0.1	Anode: AO: Pt or BDD (3 cm ²) EF: Pt (3 cm ²) Cathode: AO: SS (3 cm ²) EF: C-PTFE O-D (3.1 cm ²) j_{cat} : 32-145 mA cm ⁻² Q: MS T: 35 °C pH: 3.0 [TDI] ₀ (EF): 56 mg L ⁻¹ (80% – EF)	[170]
Atrazine pesticide	20 mg atrazine L ⁻¹ in 7.0 g Na ₂ SO ₄ L ⁻¹	AO EF SPEF SPC SPEF-SPC	UC	0.2	Anode: BDD (7.5 cm ²) Cathode: AO: Pt mesh (7.5 cm ²) EF, SPEF, SPEF-SPC: BDD (7.5 cm ²) (with air bubbling) j_{cat} : 13 mA cm ⁻² Q: MS T: Amb. pH: 3.0 [TDI] ₀ (EF, SPEF, SPEF-SPC): 5.6 mg L ⁻¹ (80% – SPEF-SPC)	[171]
Atrazine pesticide	22 mg atrazine L ⁻¹ in 14 g Na ₂ SO ₄ L ⁻¹	AO-H ₂ O ₂ EF	UC	0.22	Anode: AO-H ₂ O ₂ EF: BDD (25 cm ²) EF: Pt mesh (4.5 cm ²) Cathode: CF (60 cm ²) j_{cat} : 0.83-17 mA cm ⁻² Q: MS T: Amb. pH (AO-H ₂ O ₂): 6.3 pH (EF): 3.0 [TDI] ₀ (EF): 5.6 mg L ⁻¹ (97% – EF)	[133]
Chloroxenol pesticide	100 mg chloroxenol L ⁻¹ in 7.0 g Na ₂ SO ₄ L ⁻¹	AO EF PEF-UVA	UC	0.1	Anode: Pt or BDD (3 cm ²) Cathode: AO: SS (3 cm ²) EF, PEF-UVA: C-PTFE O-D (3 cm ²) j_{cat} : 33-150 mA cm ⁻² Q: MS T: 25 °C pH: 3.0 [TDI] ₀ (EF, PEF-UVA): 11-279 mg L ⁻¹ (≈100% – PEF-UVA)	[135]
Chlortoluron, carbofuran, bentazon pesticides	27 mg chlortoluron L ⁻¹ , 28 mg carbofuran L ⁻¹ , 30 mg bentazon L ⁻¹ (mixture) in 7.0 g Na ₂ SO ₄ L ⁻¹	AO-H ₂ O ₂ EF	UC	0.25	Anode: BDD (14 cm ²) Cathode: CF (60 cm ²) j_{cat} : 5.0 mA cm ⁻² Q: MS T: 23 °C. pH (AO-H ₂ O ₂): 3.0-12 pH (EF): 3.0 [TDI] ₀ (EF): 5.6 mg L ⁻¹ (90% – EF)	[142]
Chlortoluron, carbofuran, bentazon pesticides	27 mg chlortoluron L ⁻¹ , 28 mg carbofuran L ⁻¹ , 30 mg bentazon L ⁻¹ (mixture) in 7.0 g Na ₂ SO ₄ L ⁻¹	EF PF-UVC	UC	0.25	Anode: Pt grid Cathode: CF (60 cm ²) j_{cat} : 5.0 mA cm ⁻² Q: MS T: Amb. pH: 3.0 [TDI] ₀ : 5.6 mg L ⁻¹ (82% – EF)	[131]
Cyanazine pesticide	55-145 mg cyanazine L ⁻¹ in 7.0 g Na ₂ SO ₄ L ⁻¹	AO-H ₂ O ₂ EF PEF-UVA	UC	0.1	Anode: BDD (3 cm ²) Cathode: C-PTFE A-D (3 cm ²) j_{cat} : 33-150 mA cm ⁻² Q: MS T: 35 °C pH: 3.0 [TDI] ₀ (EF, PEF-UVA): 28 mg L ⁻¹ (98% – PEF-UVA)	[98]

Table 1.4. Examples on the treatment of synthetic wastewaters contaminated with pesticides by EAOPs.

Pollutant	Wastewater characteristics	Process	Electrochemical reactor		Operational parameters (Maximal DOC decay ^a)	Ref.
			Configuration	V (L)		
Dichlorvos pesticide	4.0-87 mg dichlorvos L ⁻¹ in 14 g Na ₂ SO ₄ L ⁻¹	AO	DC	n.s.	Anode: SnO ₂ -Sb ₂ O ₅ (1 cm ²) Cathode: Pt gauze E: 1.8-2.7 V Q: MS T: Amb. pH: Neutral (n.a.)	[115]
Diuron pesticide	40 mg diuron L ⁻¹ in 7.0 g Na ₂ SO ₄ L ⁻¹	EF PF-UVC Fenton	EF: UC PF-UVC, Fenton: FP with an interior quartz tube that can allocate a lamp	0.25	Anode: n.s. Cathode: CF (40 cm ²) <i>j</i> _{cat} : 1.5-7.5 mA cm ⁻² Q: 3 L min ⁻¹ T: Amb. pH: 3.0 [TDI] ₀ (PEF-UVC): 14-140 mg L ⁻¹ [TDI] ₀ (Fenton): 11-56 mg L ⁻¹ [TDI] ₀ (EF): 11 mg L ⁻¹ (96% – EF)	[58]
Diuron pesticide	43 mg diuron L ⁻¹ in 7.0 g Na ₂ SO ₄ L ⁻¹	AO-H ₂ O ₂ EF PEF-UVA SPEF	LS: UC PS: FP with undivided FPC and planar photoreactor	LS: 0.1 PS: 2.5	Anode: LS: Pt or BDD (3 cm ²); PS: BDD (20 cm ²) Cathode: C-PTFE A-D LS: 3 cm ² ; PS: 20 cm ² <i>j</i> _{cat} : 33-150 mA cm ⁻² Q: LS: MS; PS: 3.3 L min ⁻¹ T: 25 °C pH: 3.0 [TDI] ₀ (EF, PEF-UVA, SPEF): 28 mg L ⁻¹ (70% – SPEF)	[172]
Mecoprop pesticide	100-634 mg mecoprop L ⁻¹ in 7.0 g Na ₂ SO ₄ L ⁻¹	AO-H ₂ O ₂ EF PEF-UVA SPEF	FP with undivided FPC and planar photoreactor	2.5	Anode: BDD (20 cm ²) Cathode: C-PTFE O-D (20 cm ²) <i>j</i> _{cat} : 25-150 mA cm ⁻² Q: 3 L min ⁻¹ T: 25 °C pH: 3.0 [TDI] ₀ (EF, PEF-UVA): 28 mg L ⁻¹ [TDI] ₀ (SPEF): 14-279 mg L ⁻¹ (>97% – SPEF)	[102]
Paraquat pesticide	10-50 mg paraquat L ⁻¹ in 7.0 g Na ₂ SO ₄ L ⁻¹	AO EF PEF-UVA PF-UVA	UC	0.1	Anode: Pt net (5 cm ²) Cathode: CF (15 cm ²) (with or without O ₂ bubbling for PEF-UVA/EF or AO, respectively) <i>j</i> _{cat} : 3.3-13 mA cm ⁻² Q: MS T: 25 °C pH: 3.0 [TDI] ₀ (EF): 5.6-112 mg L ⁻¹ or Co ²⁺ or Ag ⁺ [TDI] ₀ (PEF-UVA): 11 mg L ⁻¹ (97% – PEF-UVA)	[173]
Picloram pesticide	30-242 mg picloram L ⁻¹ in 7.0 g Na ₂ SO ₄ L ⁻¹	EF	UC	0.15	Anode: Pt gauze Cathode: CF (50 cm ²) <i>j</i> _{cat} : 0.6-10 mA cm ⁻² Q: MS T: Amb. pH: 3.0 [TDI] ₀ : 1.1-56 mg L ⁻¹ (≈100%)	[174]

^a Under the best experimental conditions, when applicable;

Amb. – Ambient;

C-PTFE A-D – Carbon-PTFE air-diffusion;

C-PTFE O-D – Carbon-PTFE O₂-diffusion;

DC – Divided cell;

FP – Flow plant;

FPC – Filter-press cell;

LS – Lab-scale;

MS – Magnetic stirring;

n.s. – not specified;

PS – Pilot-scale;

Q – Liquid flow rate;

UC – Undivided cell.

1.5.2.2 Background electrolyte

The main employed background electrolyte has been Na_2SO_4 , mostly in a concentration of 7.0 g L^{-1} , with the exception of Oturan et al. [133] and Vargas et al. [115] that doubled this concentration. This is in contrast with the vast number of studies about the effect of background electrolyte nature on the process efficiency reported for synthetic wastewaters polluted with dyes.

1.5.2.3 Process

Most of the works of Table 1.4 embraced EF technique. A lot of works regarding AO treatment were also reported, although some works regarding AO treatment are not included in it. Only few studies assessed the application of SPEF. Predominantly, the mineralization ability of EAOPs followed the order $\text{SPEF} > \text{PEF-UVA} > \text{EF} > \text{AO-H}_2\text{O}_2 \approx \text{AO}$. As can be seen in Figure 1.7, Boye et al. [127] achieved 98%, 60%, 28% and 25% of DOC removal after 180 min of treatment by PEF-UVA, EF, AO- H_2O_2 and AO processes, respectively, using 194 mg L^{-1} 4-chlorophenoxyacetic acid (4-CPA) pesticide. Flox et al. [102] found a mineralization of 80% and 67% after 100 min of SPEF and PEF-UVA methods, respectively, for the treatment of 2.5 L of 100 mg L^{-1} mecoprop pesticide using a BDD anode, a carbon-PTFE air-diffusion cathode, pH of 3.0, $25 \text{ }^\circ\text{C}$, $[\text{TDI}]_0$ of 28 mg L^{-1} and j_{cat} of 50 mA cm^{-2} . Only Brillas et al. [155] and Skoumal et al. [135] attained different mineralization abilities from what mentioned above. In the former study, similar DOC removals were reached for PEF-UVA and EF technologies, indicating a large participation of $\bullet\text{OH}$ in the bulk from Fenton's reaction (21) on the degradation of 2-(2,4-dichlorophenoxy)-propionic acid (2,4-D) pesticide and its by-products. In the second study, AO gained superiority over EF for longer reaction times, suggesting that BDD($\bullet\text{OH}$) were able to oxidize more quickly the final carboxylic acids than their Fe(III) complexes.

With respect to pesticide removal, SPEF, PEF-UVA and EF processes usually attained similar results and better than AO- H_2O_2 and AO, pointing to effective degradation of parent compound by $\bullet\text{OH}$ in the bulk. On opposite, Borràs et al. [98], Dhaouadi and Adhoum [173] and Garza-Campos et al. [171] observed superiority of light-assisted EAOPs over EF in terms of pesticide abatement, proposing contribution of photoreduction reactions (28) and (29) under the applied conditions. Regarding AO and AO- H_2O_2 efficiencies in terms of pesticide removal, tendencies are not clear since Boye et al. [127] determined superiority of AO- H_2O_2 over AO, but in Boye et al. [86] both processes yielded similar herbicide decay. This may be related to the

oxidation ability of H_2O_2 on the initial molecule, although more research is required for confirmation.

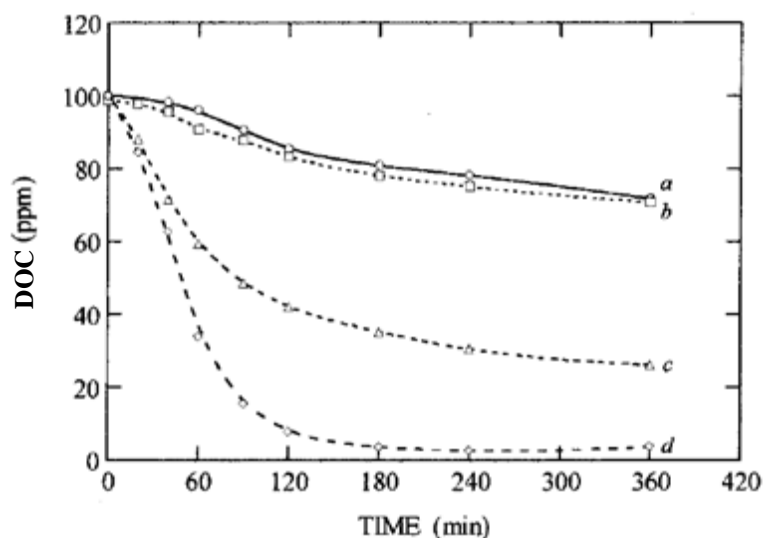


Figure 1.7. DOC removal as a function of time for the treatment of $194 \text{ mg } 4\text{-CPA L}^{-1}$ in $7.0 \text{ g Na}_2\text{SO}_4 \text{ L}^{-1}$ by various EAOPs using a 100 mL undivided cell equipped with a Pt anode and a carbon-PTFE air-diffusion cathode, pH of 3.0, $35 \text{ }^\circ\text{C}$, $[\text{TDI}]_0$ of 56 mg L^{-1} for EF, PEF-UVA and SPEF and j_{cat} of 32 mA cm^{-2} . EAOP: (a-○) AO, (b-□) AO- H_2O_2 , (c-△) EF and (d-◇) PEF-UVA. Reprinted (adapted) from Boye et al. [127], Copyright © (2002), with permission from American Chemical Society.

Abdessalem et al. [131] accomplished a direct comparison between EF and PF-UVC using an initial $[\text{H}_2\text{O}_2]$ of 340 mg L^{-1} . The PF-UVC process attained faster mineralization than EF, which was attributed to the initial addition of H_2O_2 and Fe^{3+} to form $\bullet\text{OH}$ in the bulk from Fenton's reaction (21) in the former in contrast with the gradual formation of $\bullet\text{OH}$ in the latter. Certainly, the generation of additional $\bullet\text{OH}$ in the presence of H_2O_2 and UVC radiation via Eq. (30) and photoreduction reactions (28) and (29) also had a large contribution to the faster mineralization by PF-UVC. Moreover, costs of reagents and electrical energy consumption were evaluated to be 4 times lower for EF, which then results clearly beneficial for application. In turn, Dhaouadi and Adhoum [173] observed superiority of PF-UVA over PEF-UVA in terms of COD and pesticide removals for the first times of reaction, followed by very poor decays with superiority of the electrochemical process over the chemical one. While the initial superiority of PF-UVA over PEF-UVA can be associated with the presence of higher contents of reactants at the beginning of the reaction, parasitic reactions such as Eqs. (24) and (25) probably occurred in large extent in both processes for longer reaction times.

Comparison between PC, EF and EC technologies for several chlorophenoxy and chlorobenzoic herbicides was performed by Brillas et al. [56]. The authors achieved the following mineralization ability: PC > EF >> EC. These results pointed to a small retention of pesticide into Fe(OH)₃ precipitate in EC method and a larger production of •OH in the bulk in PC technique due to the generation of Fe²⁺ at the anode via Eq. (27), simultaneously with the coagulation of oxidation by-products.

Garza-Campos et al. [171] performed an innovative SPEF process combined with solar heterogeneous photocatalysis (SPEF-SPC) using TiO₂ nanoparticles synthesized by sol-gel and supported on glass spheres by dip-coating as catalyst. This combined process attained higher degradation ability in terms of atrazine decay and DOC removal compared to traditional SPEF, with 10% larger mineralization after 300 min of reaction.

1.5.2.4 Electrochemical reactor

Undivided cells have been by far the most popular electrochemical reactors for wastewaters contaminated with pesticides, commonly applying volumes from 100 to 250 mL and electrodes with active areas up to 25 cm², except for CF cathode, which were larger. Few investigations used other reactors like a divided cell [115], a simple 3 L flow plant with a filter-press cell [69], the 2.5 L flow plant with a filter-press cell and a planar photoreactor with a mirror at the bottom of Figure 1.4 [102, 172] and the 10 L pilot-scale flow plant with a filter-press cell and a photoreactor made-up of borosilicate tubes of Figure 1.5 [146]. Papi et al. [172] reported faster pesticide degradation by SPEF using a 100 mL undivided cell than the above 2.5 L flow plant, which was mainly attributed to the distinct electrode area/solution volume ratio.

Pt and BDD have been mainly and equally used as anode. Only Vargas et al. [115] employed a different anode material like SnO₂-SbO₅. In general, the BDD anode showed superiority over Pt both in terms of mineralization and pesticide removal for all EAOPs due to its higher potential for O₂ evolution [133, 155, 170, 172, 175]. Exceptionally, Skoumal et al. [135] found similar pesticide abatement using BDD and Pt for EF and PEF-UVA processes, meaning that the main oxidant for chloroxylenol pesticide was •OH generated from Fenton's reaction (21). Da Pozzo et al. [170] found an unusual fast DOC removal of amitrole pesticide in aqueous solution using an AO-Pt system, which could be due to the release of volatile species that are not mineralized.

Various cathodes have been used in AO treatment, including graphite [86, 127, 155, 175], stainless steel (SS) [135, 170], Pt [115, 171], BDD without air bubbling [69] and CF without oxygen bubbling [173]. AO-H₂O₂, EF and PEF-UVA mostly applied carbon-PTFE air-diffusion electrodes and CF as cathodes, with the exception of García et al. [69], which employed BDD with air injection as cathode in EF process. SPEF mainly resorted to carbon-PTFE air-diffusion cathodes, apart from Garza-Campos et al. [171] that used BDD with air injection. None of the presented studies performed a comparison between cathodes efficiencies.

1.5.2.5 Operational parameters

With the exception of Vargas et al. [115], all the other works were performed in galvanostatic mode. Almost all studies assessed the effect of j on pesticides degradation, mainly in terms of DOC removal and, in less extent, in terms of pesticide decay. Typically, increasing j led to higher degradation for all EAOPs. However, Borràs et al. [98] found similar results for the two highest j values due to the occurrence of parasitic reactions and, moreover, Papi et al. [172] attained quite similar mineralization with the increment of j for PEF-UVA and SPEF systems at lab-scale and pilot-scale, respectively, pointing to mineralization control by photoreduction reactions (28) and (29). Lower current efficiencies and greater energy consumptions were observed in some studies with the rise in j . In general, pesticide solutions with DOC contents of 50-100 mg L⁻¹ were tested at j_{cat} of 25-150 mA cm⁻², apart from when employing CF as cathode, where j_{cat} below 17 mA cm⁻² were used. Brillas et al. [56] determined higher treatment efficiency for PC process using low j_{cat} and short electrolysis times. At low j_{cat} , mineralization and coagulation were in competition, whereas at high j_{cat} the coagulation process was predominant, impeding further mineralization.

García et al. [69] assessed the influence of liquid flow rate from 4 to 10 L min⁻¹ for 2,4-dichlorophenoxyacetic acid mineralization by AO using a flow plant with an undivided filter-press cell. A faster mineralization was reached for higher liquid flow rate due to the improvement of mass transfer of pesticide and its oxidation products to anode surface to react with BDD([•]OH).

The effect of temperature on pesticide degradation was checked by Boye et al. [127]. A temperature increase from 25 to 35 °C enhanced the mineralization ability mainly for PEF-UVA process, with very poor improvement for AO-H₂O₂ and EF processes. From 35 to 45 °C, the degradation improvement was null and it was related to a significant increase of water evaporation

and oxygen release with electrolysis time. Based on this study, most subsequent research used 35 °C as the best temperature, although many works preferred the use of ambient temperature.

Abdessalem et al. [142] found lower mineralization for higher pH from 3.0 to 12 for AO-H₂O₂ process applied to a mixture of chlortoluron, carbofuran and bentazon pesticides, whereas Boye et al. [127] achieved similar mineralization for pH values from 2.0 to 6.0 for AO and AO-H₂O₂ techniques applied to 4-chlorophenoxyacetic acid. EF reached fastest and similar oxidation ability at pH of 3.0 and 4.0 in Boye et al. [86] and PEF-UVA attained best mineralization at pH of 3.0 in the same study, which can be mainly attributed to the predominance of higher amounts of photoactive Fe(III)-hydroxy complexes and absence of iron precipitation at these pH values. Garcia-Segura et al. [146] optimized the degradation of the herbicide 4-chloro-2-methylphenoxyacetic acid by SPEF using response surface methodology (RSM), which allowed determining an optimum pH of 3.0.

Best results for the degradation of synthetic wastewaters contaminated with pesticides were achieved employing [TDI]₀ of 1-56 mg L⁻¹ for EF, PEF-UVA and SPEF processes using wastewaters with around 100 mg DOC L⁻¹ [86, 127, 146, 155, 175]. For EF applied to wastewaters up to 50 mg DOC L⁻¹, best [TDI]₀ of 11-39 mg L⁻¹ were found [69, 170, 173]. Flox et al. [102] and Skoumal et al. [135] observed a small influence of [TDI]₀ on DOC removal using a wide [TDI]₀ range of 14-279 and 28-112 mg L⁻¹ in SPEF and PEF-UVA processes, respectively, to degrade solutions with around 50 mg DOC L⁻¹. These results indicate that a small amount of this catalyst was sufficient to yield the maximum generation of oxidant •OH from Fenton's reaction (21) under the experimental conditions used. Other catalysts such as Ag⁺ and Co²⁺ were tested by Dhaouadi and Adhoum [173] in EF process, reaching a degradation ability in the order Ag⁺ > Fe²⁺ > Co²⁺. Despite these achievements, Fe²⁺ was selected as the best catalyst due to the higher cost and toxicity of Ag⁺.

1.5.3 Wastewaters containing pharmaceuticals

Pharmaceuticals include various compounds such as antibiotics, antipyretics, analgesics, anti-inflammatories, antimicrobials and hormones. Twenty-one studies regarding the treatment of synthetic wastewaters polluted with pharmaceuticals by the application of EAOPs are displayed in Table 1.5.

1.5.3.1 Pharmaceutical content

The decontamination of wastewaters with antibiotics or antimicrobial drugs was more expressive, although many other pharmaceuticals were considered such as anti-inflammatories, beta-blockers and endocrine disrupting agents. All investigations were performed with synthetic solutions of just one pharmaceutical.

A vast range of drug contents from 2.0 to 2390 mg L⁻¹ have been used. Approximately half of the studies evaluated the effect of initial drug content on the process efficiency, conquering greater DOC and/or pollutants removal rates with increasing initial drug contents for AO, AO-H₂O₂, EF, PEF-UVA, PEF-UVA/citrate and SPEF.

Table 1.5. Examples on the treatment of synthetic wastewaters contaminated with pharmaceuticals by EAOPs.

Pollutant	Wastewater characteristics	Process	Electrochemical reactor		Operational parameters (Maximal DOC decay ^a)	Ref.
			Configuration	V (L)		
Atenolol, metoprolol, propranolol beta-blockers	158 mg atenolol L ⁻¹ or 66 mg metoprolol L ⁻¹ or 135 mg propranolol L ⁻¹ in 14 g Na ₂ SO ₄ L ⁻¹	EF SPEF	FP with undivided FPC and photoreactor	10	Anode: Pt or BDD (90.3 cm ²) Cathode: C-PTFE A-D or CF (90.3 cm ²) j_{cat} (C-PTFE A-D): 17-55 mA cm ⁻² j_{cat} (CF): 4.4 mA cm ⁻² Q : 4.2 L min ⁻¹ T: 35 °C pH: 3.0 [TDI] ₀ : 28 mg L ⁻¹ (93% – SPEF)	[176]
Chloramphenicol antibiotic	25-245 mg chloramphenicol L ⁻¹ in 7.0 g Na ₂ SO ₄ L ⁻¹	AO-H ₂ O ₂ EF PEF-UVA SPEF	LS: UC PS: FP with undivided FPC and photoreactor	LS: 0.1 PS: 10	Anode: LS: Pt or BDD (3 cm ²); PS: Pt (90.2 cm ²) Cathode: C-PTFE A-D LS: 3 cm ² ; PS: 90.2 cm ² j_{cat} : 33-100 mA cm ⁻² Q : LS: MS; PS: 3.3 L min ⁻¹ T: 35 °C pH: 3.0 [TDI] ₀ : 28 mg L ⁻¹ (≈100% – SPEF)	[90]
Chlorophene antimicrobial drug	84 mg chlorophene L ⁻¹ in 7.0 g Na ₂ SO ₄ L ⁻¹	AO-H ₂ O ₂ EF	UC	0.2	Anode: Pt or BDD (3 cm ²) or Pt mesh (4.5 cm ²) Cathode: C-PTFE O-D (3 cm ²) or CF (70 cm ²) j_{cat} (C-PTFE A-D): 20-100 mA cm ⁻² j_{cat} (CF): 0.86-4.3 mA cm ⁻² Q : MS T: Amb. pH: 3.0 [TDI] ₀ (EF): 11-447 mg L ⁻¹ (≈100% – EF)	[177]
Clofibric acid	89-557 mg clofibric L ⁻¹ in 7.0 g Na ₂ SO ₄ L ⁻¹	AO-H ₂ O ₂ EF PEF-UVA	UC	0.1	Anode: BDD (3 cm ²) Cathode: C-PTFE O-D (3 cm ²) j_{cat} : 33-150 mA cm ⁻² Q : MS T: 35 °C pH: 3.0 [TDI] ₀ (EF, PEF-UVA): 56 mg L ⁻¹ (≈100% – PEF-UVA)	[178]
Diclofenac anti-inflammatory	175 mg diclofenac L ⁻¹ in 7.0 g Na ₂ SO ₄ L ⁻¹ or neutral buffer solution of 7.0 g Na ₂ SO ₄ L ⁻¹ + 20 g KH ₂ PO ₄ L ⁻¹ + NaOH	AO	UC	0.1	Anode: Pt or BDD (3 cm ²) Cathode: SS (3 cm ²) j_{cat} : 17-150 mA cm ⁻² Q : MS T: 35 °C pH: 6.5 (100%)	[179]

Table 1.5. Examples on the treatment of synthetic wastewaters contaminated with pharmaceuticals by EAOPs.

Pollutant	Wastewater characteristics	Process	Electrochemical reactor		Operational parameters (Maximal DOC decay ^a)	Ref.
			Configuration	V (L)		
Ibuprofen anti-inflammatory drug	41 mg ibuprofen L ⁻¹ in 7.0 g Na ₂ SO ₄ L ⁻¹	EF PEF-UVA SPEF	UC	0.1	Anode: Pt or BDD (3 cm ²) Cathode: C-PTFE O-D (3 cm ²) <i>j</i> _{cat} : 3.3-100 mA cm ⁻² <i>Q</i> : MS T: 25 °C pH: 2.0-6.0 [TDI] ₀ : 5.6-112 mg L ⁻¹ (92% – SPEF)	[143]
Ketoprofen endocrine disrupting drug	50 mg ketoprofen L ⁻¹ in 7.0-70 g Na ₂ SO ₄ L ⁻¹	AO	FP with undivided FPC	n.s.	Anode: BDD (12.5 cm ²) Cathode: BDD (12.5 cm ²) <i>j</i> _{cat} : 40-320 mA cm ⁻² <i>Q</i> : 0.00142-0.00834 L min ⁻¹ T: 25 °C pH: 3.0-11 (n.a.)	[68]
Omeprazole gastrointestinal drug	17-169 mg omeprazole L ⁻¹ in neutral buffer solution of 18 g NaH ₂ PO ₄ L ⁻¹ + 2.5 g H ₃ PO ₄ L ⁻¹	AO-H ₂ O ₂	UC	0.1	Anode: Pt or BDD (3 cm ²) Cathode: C-PTFE A-D (3 cm ²) <i>j</i> _{cat} : 33-150 mA cm ⁻² <i>Q</i> : MS T: 35 °C pH: 7.0 (78%)	[111]
Paracetamol analgesic, antipyretic	157 mg paracetamol L ⁻¹ in 7.0 g Na ₂ SO ₄ L ⁻¹	SPEF	FP with undivided FPC and photoreactor	10	Anode: Pt (90.2 cm ²) Cathode: C-PTFE A-D (90.2 cm ²) <i>j</i> _{cat} : 39-94 mA cm ⁻² <i>Q</i> : 3 L min ⁻¹ T: 35 °C pH: 1.4-4.4 [TDI] ₀ : 18-65 mg L ⁻¹ (75%)	[145]
Propranolol beta-blocker	77-616 mg propranolol L ⁻¹ in 7.0 g Na ₂ SO ₄ L ⁻¹	EF PEF-UVA	UC	0.1	Anode: Pt or BDD (3 cm ²) Cathode: C-PTFE A-D or CF (3 cm ²) <i>j</i> _{cat} (C-PTFE A-D): 10-80 mA cm ⁻² <i>j</i> _{cat} (CF): 4 mA cm ⁻² <i>Q</i> : MS T: 35 °C pH: 2.0-6.0 [TDI] ₀ : 5.6-279 mg L ⁻¹ (≈100% – PEF-UVA)	[104]
Ranitidine H ₂ receptor antagonist	34-113 mg ranitidine L ⁻¹ in 7.0 g Na ₂ SO ₄ L ⁻¹	EF SPEF	FP with undivided FPC and planar photoreactor	2.5	Anode: Pt (20 cm ²) Cathode: C-PTFE A-D (20 cm ²) <i>j</i> _{cat} : 25-100 mA cm ⁻² <i>Q</i> : 3.3 L min ⁻¹ T: 35 °C pH: 3.0 [TDI] ₀ : 11-112 mg L ⁻¹ (70% – SPEF)	[180]
Salicylic acid	164 mg salicylic acid L ⁻¹ in 7.0 g Na ₂ SO ₄ L ⁻¹	AO AO-H ₂ O ₂ EF PEF-UVA SPEF	UC	0.1	Anode: Pt or BDD (3 cm ²) Cathode: AO: Graphite (3 cm ²) Others: C-PTFE A-D (3 cm ²) <i>j</i> _{cat} : 33-150 mA cm ⁻² <i>Q</i> : MS T: 35 °C pH: 2.0-6.0 [TDI] ₀ : 11-112 mg L ⁻¹ (>82% – SPEF)	[149]
Sulfamethazine antimicrobial veterinary drug	193-1930 mg sulfamethazine L ⁻¹ in 7.0 g Na ₂ SO ₄ L ⁻¹	EF PEF-UVA	UC	0.1	Anode: BDD (3 cm ²) Cathode: C-PTFE A-D (3 cm ²) <i>j</i> _{cat} : 33-100 mA cm ⁻² <i>Q</i> : MS T: 35 °C pH: 2.0-6.0 [TDI] ₀ : 11-84 mg L ⁻¹ (≈100% – PEF-UVA)	[105]

Table 1.5. Examples on the treatment of synthetic wastewaters contaminated with pharmaceuticals by EAOPs.

Pollutant	Wastewater characteristics	Process	Electrochemical reactor		Operational parameters (Maximal DOC decay ^a)	Ref.
			Configuration	V (L)		
Sulfamethazine antimicrobial veterinary drug	25-198 mg sulfamethazine L ⁻¹ in 7.0 g Na ₂ SO ₄ L ⁻¹	AO-H ₂ O ₂ EF	FP with UC	1	Anode: Pt (38 cm ²) Cathode: CF (208 cm ²) <i>j</i> _{cat} : 0.24-2.9 mA cm ⁻² <i>Q</i> : 2 L min ⁻¹ T: 18-45 °C pH: 3.0 [TDI] ₀ (EF): 2.8-56 mg L ⁻¹ (n.a.)	[138]
Sulfamethoxazole antibiotic	21-329 mg sulfamethoxazole L ⁻¹ in 7.0 g Na ₂ SO ₄ L ⁻¹	AO-H ₂ O ₂ EF	UC	0.22	Anode: AO: Pt mesh EF: Pt mesh or BDD (25 cm ²) Cathode: CF (60 cm ²) <i>j</i> _{cat} : 1.0-7.5 mA cm ⁻² <i>Q</i> : MS T: Amb. pH: 3.0 [TDI] ₀ (EF): 11 mg L ⁻¹ (+/-or 13 mg Cu ²⁺ L ⁻¹) (96% – EF)	[124]
Sulfamethoxazole antibiotic	50-300 mg sulfamethoxazole L ⁻¹ in 7.0 g Na ₂ SO ₄ L ⁻¹	AO AO-H ₂ O ₂ EF PEF-UVA	UC	0.125	Anode: RuO ₂ mesh (16 cm ²) Cathode: AO: RuO ₂ mesh (16 cm ²) Others: ACF (16 cm ²) <i>j</i> _{cat} : 7.5-31 mA cm ⁻² <i>Q</i> : MS T: Amb. pH: 3.0 [TDI] ₀ (EF, PEF-UVA): 28-112 mg L ⁻¹ (80% – PEF-UVA)	[63]
Sulfanilamide antimicrobial drug	239-2390 mg sulfanilamide L ⁻¹ in 7.0 g Na ₂ SO ₄ L ⁻¹ in (UC) or 70 g Na ₂ SO ₄ L ⁻¹ (DC)	AO	UC or DC	0.1	Anode: BDD (3 cm ²) Cathode: SS (3 cm ²) <i>j</i> _{cat} : 33-150 mA cm ⁻² <i>Q</i> : MS T: 35 °C pH: 2.0-6.0 (≈100%)	[140]
Sulfanilamide antimicrobial drug	239-1195 mg sulfanilamide L ⁻¹ in 7.0 g Na ₂ SO ₄ L ⁻¹	EF SPEF	FP with undivided FPC and planar photoreactor	2.5	Anode: Pt (20 cm ²) Cathode: C-PTFE A-D (20 cm ²) <i>j</i> _{cat} : 50-150 mA cm ⁻² <i>Q</i> : 3.3 L min ⁻¹ T: 35 °C pH: 3.0 [TDI] ₀ : 14-279 mg L ⁻¹ (≈100% – SPEF)	[130]
Tetracycline antibiotic	25-150 mg tetracycline L ⁻¹ in 7.0 g Na ₂ SO ₄ L ⁻¹	EF + Biological treatment	UC	0.8	Anode: Pt (17 cm ²) Cathode: CF (78 cm ²) <i>j</i> _{cat} : 0.64-5.1 mA cm ⁻² <i>Q</i> : MS T: Amb. pH: 3.0 [TDI] ₀ : 2.8-11 mg L ⁻¹ (86%)	[181]
Tetracycline antibiotic	100-300 mg tetracycline L ⁻¹ in 14 g Na ₂ SO ₄ L ⁻¹	AO-H ₂ O ₂	UC	0.4	Anode: RuO ₂ -IrO ₂ Cathode: CF (240 cm ²) <i>j</i> _{cat} : 2.1-6.3 mA cm ⁻² <i>Q</i> : MS T: Amb. pH: 3.0-9.0 (n.a.)	[108]

Table 1.5. Examples on the treatment of synthetic wastewaters contaminated with pharmaceuticals by EAOPs.

Pollutant	Wastewater characteristics	Process	Electrochemical reactor		Operational parameters (Maximal DOC decay ^a)	Ref.
			Configuration	V (L)		
Trimethoprim antibiotic	50 mg trimethoprim L ⁻¹ in 0-70 g Na ₂ SO ₄ L ⁻¹	AO	FP with undivided FPC	n.s.	Anode: BDD (12.5 cm ²) Cathode: BDD (12.5 cm ²) j_{cat} : 0-320 mA cm ⁻² Q : 0.00125-0.0108 L min ⁻¹ T: 25 °C pH: 3.0-11 (51%)	[182]

^aUnder the best experimental conditions, when applicable;

Amb. – Ambient;

C-PTFE A-D – Carbon-PTFE air-diffusion;

C-PTFE O-D – Carbon-PTFE O₂-diffusion;

DC – Divided cell;

FP – Flow plant;

FPC – Filter-press cell;

LS – Lab-scale;

MS – Magnetic stirring;

n.s. – not specified;

PS – Pilot-scale;

Q – Liquid flow rate;

UC – Undivided cell.

1.5.3.2 Background electrolyte

Na₂SO₄ was again the most employed background electrolyte, mainly in a concentration of 7.0 g L⁻¹, although also in a content of 14 g L⁻¹ [108, 176] and 70 g L⁻¹ [68, 140, 182]. In El-Ghenymy et al. [140], the employing of the high Na₂SO₄ content of 70 g L⁻¹ was justified by the large E_{cell} increase verified in the divided cell used. Domínguez et al. [68] and González et al. [182] determined an optimum concentration of 70 g Na₂SO₄ L⁻¹ by applying RSM in AO treatments. On the other hand, Brillas et al. [179] and Cavalcanti et al. [111] used neutral buffer solutions as background electrolytes in AO and AO-H₂O₂ treatments of diclofenac and omeprazole drugs, respectively, in order to maintain constant pH along electrolysis since the former authors observed pH decreases up to 3.4 for AO-Pt and pH increases up to 9.7 for AO-BDD operating without pH regulation.

1.5.3.3 Process

The majority of works of Table 1.5 embraced EF process, however a large number of investigations on AO treatment are not included. Some studies on AO-H₂O₂, PEF-UVA and SPEF processes are also reported. In general, processes ability to remove drugs and oxidize their by-products could be arranged in the order SPEF > PEF-UVA > EF > AO-H₂O₂ ≈ AO. Figure 1.8 illustrates this tendency in terms of mineralization of 164 mg salicylic acid L⁻¹ in 7.0 g Na₂SO₄ L⁻¹,

and the corresponding MCE values of Figure 1.8b are given in Figure 1.9. Some studies reached similarity between EF and PEF-UVA [63, 143, 149, 178] and between EF and SPEF [90] in terms of drug decay, indicating that drug molecules were mainly degraded by $\bullet\text{OH}$ in the bulk. Furthermore, Wang et al. [63] attained superiority of AO-H₂O₂ over AO in terms of sulfamethoxazole antibiotic removal.

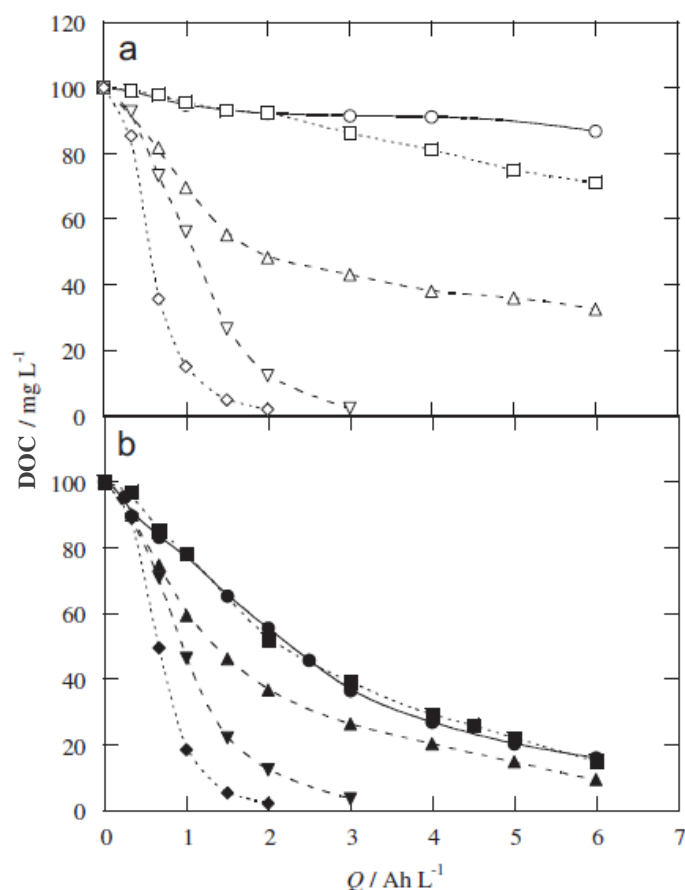


Figure 1.8. DOC removal as a function of consumed specific charge for the treatment of 164 mg salicylic acid L⁻¹ in 7.0 g Na₂SO₄ L⁻¹ by various EAOPs using a 100 mL undivided cell equipped with a (a) Pt or (b) BDD anode and a carbon-PTFE air-diffusion cathode, using pH of 3.0, 35 °C, [TDI]₀ of 28 mg L⁻¹ for EF, PEF-UVA and SPEF and j_{cat} of 33 mA cm⁻². EAOP: (○,●) AO, (□,■) AO-H₂O₂, (△,▲) EF, (▽,▼) PEF-UVA and (◇,◆) SPEF. Reprinted (adapted) from Guinea et al. [149], Copyright © (2008), with permission from Elsevier.

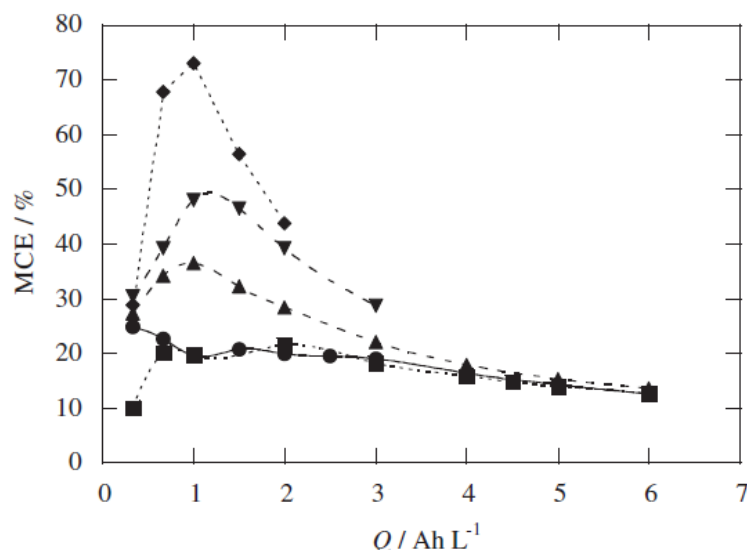


Figure 1.9. Mineralization current efficiency as a function of consumed specific charge for experiments reported in Figure 1.8b. Reprinted from Guinea et al. [149], Copyright © (2008), with permission from Elsevier.

Dirany et al. [124] tested the EF process catalyzed by Cu^{2+} instead of Fe^{2+} and simultaneously by Fe^{2+} and Cu^{2+} to degrade sulfamethoxazole antibiotic, noticing lower drug decay and mineralization using Cu^{2+} alone and in combination with Fe^{2+} compared to Fe^{2+} alone. The beneficial effect of Cu^{2+} has been mainly attributed to the formation of Cu(II)-carboxylate complexes that can be more quickly destroyed than Fe(III)-carboxylate complexes. Consequently, one can infer that carboxylic acids with the ability to form complexes with Cu^{2+} were not produced during the degradation of sulfamethoxazole.

Ferrag-Siagh et al. [181] degraded tetracycline antibiotic solutions by coupling an EF pre-treatment with a further biological process. The 5-day biochemical oxygen demand (BOD_5)/COD ratio increased from 0.02 to 0.56 after 6 h of EF and, as a result, tests using activated sludge reached mineralization enhancement from 28% for the non-pretreated solution to 68% and 86% after 2 and 4 h of EF, respectively.

1.5.3.4 Electrochemical reactor

The majority of studies presented in Table 1.5 used undivided cells with a wastewater volume of 100 mL and electrodes of 3 cm² of active area, although solution volumes up to 800 mL, anodes up to 25 cm² and CF cathodes up to 78 cm² were employed as well. The flow plants of Figures 1.4 and 1.5 used in dyes and pesticides degradations were also employed for the decontamination of

synthetic pharmaceutical wastewaters [90, 130, 145, 176, 180]. Beyond that, other reactors have been utilized such as a divided cell [140] and simple flow plants with a filter-press cell [68, 182]. El-Ghenymy et al. [140] achieved higher mineralization of sulfanilamide antimicrobial drug by AO using a divided cell instead of an undivided one, mainly because of the action of the BDD electrode over half of the volume in the divided cell compared to the undivided one. Garcia-Segura et al. [90] found faster mineralization under SPEF conditions using the 100 mL undivided cell of Figure 1.2 instead of the 10 L pilot-scale flow plant of Figure 1.5, along with greater persistence of Fe(III)-carboxylate complexes at the flow plant, probably mainly due to a low irradiated volume/total volume ratio.

Pt and BDD electrodes have been chiefly and similarly employed as anode in the degradation of synthetic pharmaceutical wastewaters. Wang et al. [63] and Wu et al. [108] used RuO₂ and RuO₂-IrO₂ anodes, respectively. Many surveys compared the performance of Pt and BDD anodes and, for the major part of them, BDD showed superiority over Pt in terms of oxidation ability and drug decay, independently on the EAOP checked. However, as attained by Thiam et al. [33] in a dye removal, Figure 1.8 shows almost null or even null superiority of BDD over Pt for PEF-UVA and SPEF processes, indicating an important role of light-induced mechanisms on salicylic acid removal. A similar behavior was also checked for ibuprofen and chloramphenicol by Skoumal et al. [143] and Garcia-Segura et al. [90], respectively. Surprisingly, Sirés et al. [177] attained higher rates for chlorophene antimicrobial drug decay and mineralization using Pt instead of BDD anode for EF systems employing either a carbon-PTFE O₂-diffusion electrode or a CF as cathode. This was ascribed to a quicker oxidation of Fe²⁺ to Fe³⁺ at the BDD anode together with Fe²⁺ destruction with persulfate ion to get Fe³⁺ and sulfate at this anode, diminishing the amount of Fe²⁺ to produce •OH by Fenton's reaction (21). Note that the superiority of Pt over BDD using CF in terms of mineralization was only verified for the first 2 h of EF. For longer reaction times, the BDD achieved larger mineralization due to the faster destruction of final recalcitrant by-products such as carboxylic acids by BDD(•OH) compared to Pt(•OH).

From Table 1.5, one can infer that AO process used various cathodes such as SS [140, 179], graphite [149], RuO₂ [63] and BDD [68, 182], whereas AO-H₂O₂, EF, PEF-UVA and SPEF processes have been mainly resorting to carbon-PTFE air-diffusion electrodes as cathode, followed by CF. Sirés et al. [177] compared the ability of carbon-PTFE air-diffusion and CF cathodes to electrogenerate H₂O₂ by Eq. (16), regenerate Fe³⁺ to Fe²⁺ via Eq. (26) and oxidize chlorophene antimicrobial drug and its by-products. The carbon-PTFE air-diffusion cathode showed higher ability for H₂O₂ electrogeneration, but the CF demonstrated larger ability to regenerate Fe³⁺ to

Fe^{2+} , leading to generation of more $\bullet\text{OH}$ from Fenton's reaction (21) and then faster mineralization. Isarain-Chávez et al. [104, 176] employed a novel electrochemical cell composed of two pairs of electrodes. One pair comprising a Pt or a BDD anode and a carbon-PTFE air-diffusion cathode and the other pair equipped with a Pt anode and a CF cathode. These systems were compared to Pt/Carbon-PTFE air-diffusion and BDD/Carbon-PTFE air-diffusion single systems. EF and PEF-UVA degradations of beta-blockers such as atenolol, metoprolol and propranolol revealed higher efficiency for combined systems in terms of drugs removal and mineralization in comparison to the single systems because of the larger production of $\bullet\text{OH}$ from Fenton's reaction (21) by the quicker Fe^{2+} regeneration from Fe^{3+} reduction via Eq. (26) at the CF cathode.

1.5.3.5 Operational parameters

All the surveys were developed under galvanostatic conditions. The majority of studies evaluated the influence of j on the degradation of pharmaceuticals both in terms of parent compound removal and mineralization. In general, the use of higher j led to faster pollutants degradation, although in some cases similar degradations were found from a given j value [63, 124, 143, 176, 181]. Some investigations determined lower current efficiencies and higher specific charge and energy consumptions with the increase of j . Typically and for treatments not using CF, pharmaceutical solutions with DOC around 100 mg L^{-1} were degraded with j_{cat} of $17\text{-}150 \text{ mA cm}^{-2}$, whereas solutions with lower DOC employed j_{cat} with a minimum value of 3.3 mA cm^{-2} . When using CF, j_{cat} values from 0.24 to 7.5 mA cm^{-2} were applied.

Domínguez et al. [68] and González et al. [182] applied RSM to determine the optimum liquid flow rate for AO treatments in a system composed of a flow plant with an undivided filter-press cell. The obtained efficiencies corresponds to a single-pass of the solution through the cell (continuous mode). Slightly larger drug removals were reached for the lowest liquid flow rate as long as this parameter was inversely proportional to the residence time of molecules inside the reactor, providing more contact between reactants and pollutant.

Mansour et al. [138] found higher drug removal in EF from 18 to $35 \text{ }^\circ\text{C}$ and a lower gain from 35 to $45 \text{ }^\circ\text{C}$. This slight efficiency enhancement in the latter range was attributed to lower concentration of dissolved oxygen and also to self-decomposition of H_2O_2 , although the last reaction may occur in large extent only for temperatures above $50 \text{ }^\circ\text{C}$ [139]. All remaining studies employed ambient temperatures or $35 \text{ }^\circ\text{C}$.

The application of RSM to AO and AO-H₂O₂ processes determined optimum pH values of 3.0 or 4.0, with decreasing drug removals for higher pH, although with low significance [68, 108, 182]. El-Ghenymy et al. [140] inclusively found quite similar mineralization for pH values from 2.0 to 6.0 for AO of sulfanilamide. Some studies attained a best pH of 3.0 for EF and PEF-UVA techniques [105, 130, 143]. Isarain-Chávez et al. [104] accomplished similar and highest mineralization at pH of 2.0 and 3.0 for PEF-UVA treatment of propranolol. Guinea et al. [149] achieved similar and best mineralization at pH of 3.0 and 4.0 for EF degradation of salicylic acid. An optimum pH value of 3.0 for SPEF treatment of paracetamol was assessed by Almeida et al. [145] by performing RSM.

The remediation of synthetic pharmaceutical wastewaters with 100 mg DOC L⁻¹ has been achieving better performance using [TDI]₀ contents of 11-56 mg L⁻¹ for EF, PEF-UVA and SPEF treatments [63, 104, 105, 130, 145, 149]. Solutions with DOC amounts below 60 mg L⁻¹ mainly used [TDI]₀ from 5.6 to 28 mg L⁻¹ for EF and PEF-UVA treatments [138, 143, 177, 180, 181]. Some reports attained similar and best degradations for a large range of [TDI]₀, namely for 11-56 mg L⁻¹ in Guinea et al. [149], 5.6-28 mg L⁻¹ in Isarain-Chávez et al. [104] and 5.6-56 mg L⁻¹ in Mansour et al. [138], suggesting the enhancement of Fenton's reaction (21) in similar extent than parasitic reactions and, for PEF-UVA, inner filter effects and light attenuation along the photoreactor.

1.5.4 Other synthetic wastewaters

Beyond the application of EAOPs to synthetic wastewaters containing dyes, pesticides and pharmaceuticals, many other wastewaters contaminated with pollutants such as anilines, phenols and low-molecular-weight carboxylic acids (LMCA) have been degraded by EAOPs. Examples of these studies are collected in Table 1.6.

Table 1.6. Examples on the treatment of synthetic effluents polluted with other contaminants by EAOPs.

Pollutant	Wastewater characteristics	Process	Electrochemical reactor		Operational parameters (Maximal DOC decay °)	Ref.
			Configuration	V (L)		
Aniline	100-550 mg aniline L ⁻¹ in 7.0 g Na ₂ SO ₄ L ⁻¹	AO-H ₂ O ₂ EF PEF-UVA	UC	0.1	Anode: Pt (10 cm ²) Cathode: C-PTFE O-D or graphite (3.1 cm ²) <i>j</i> _{cat} : 32.97 mA cm ⁻² <i>Q</i> : MS T: 25 °C pH: 3.0 [TDI] ₀ (EF): 56 mg L ⁻¹ [TDI] ₀ (PEF-UVA): 14-167 mg L ⁻¹ (92% – PEF-UVA)	[183]

Table 1.6. Examples on the treatment of synthetic effluents polluted with other contaminants by EAOPs.

Pollutant	Wastewater characteristics	Process	Electrochemical reactor		Operational parameters (Maximal DOC decay ^a)	Ref.
			Configuration	V (L)		
Aniline, 4-chloroaniline	100 mg aniline L ⁻¹ or 100 mg 4-chloroaniline L ⁻¹ in 2.0 g NaOH L ⁻¹ or 11 g Na ₂ CO ₃ L ⁻¹ or 11 g Na ₂ CO ₃ L ⁻¹ + 8.4 g NaHCO ₃ L ⁻¹	AO AO-H ₂ O ₂	UC	0.1	Anode: PbO ₂ (10 cm ²) Cathode: AO: Graphite (3.1 cm ²) AO-H ₂ O ₂ : C-PTFE O-D or graphite (3.1 cm ²) <i>j</i> _{cat} : 32-194 mA cm ⁻² <i>Q</i> : MS T: 25 °C pH: 10-13 (100% – AO-H₂O₂)	[55]
Phenol	31 or 99 mg phenol L ⁻¹ in 7.0 g Na ₂ SO ₄ L ⁻¹	EF	UC	0.15-0.4	Anode: Pt grid Cathode: CF (48 or 102 cm ²) <i>j</i> _{cat} (CF-48 cm ²): 2.1 mA cm ⁻² <i>j</i> _{cat} (CF-102 cm ²): 0.98 mA cm ⁻² <i>Q</i> : MS T: Amb. pH: 3.0 [TDI] ₀ : 2.8-56 mg L ⁻¹ or 2.9-59 Co ²⁺ or 5.5-55 mg Mn ²⁺ L ⁻¹ or 64-635 mg Cu ²⁺ L ⁻¹ (100%)	[184]
<i>o</i> -, <i>m</i> -, <i>p</i> -Cresols	541 mg <i>o</i> -, <i>m</i> - or <i>p</i> -cresol L ⁻¹ in 7.0 g Na ₂ SO ₄ L ⁻¹	AO	FP with undivided FPC	1	Anode: BDD or PbO ₂ (63 cm ²) Cathode: Zr (63 cm ²) <i>j</i> _{cat} : 40 mA cm ⁻² <i>Q</i> : 2.1 L min ⁻¹ T: 25 °C pH: 4.0 (100%)	[185]
Formic, glyoxylic, oxalic, acetic, glycolic, pyruvic, malonic, maleic, fumaric, succinic, malic acids	4.6-23 mg formic L ⁻¹ , 7.4-37 mg glyoxylic L ⁻¹ , 9.0-45 mg oxalic L ⁻¹ , 6.0-30 mg acetic L ⁻¹ , 7.6-38 mg glycolic L ⁻¹ , 8.8-44 mg pyruvic L ⁻¹ , 10-52 mg malonic L ⁻¹ , 12-58 mg maleic L ⁻¹ , 12-58 mg fumaric L ⁻¹ , 12-59 mg succinic L ⁻¹ or 13-67 mg malic L ⁻¹ in 5.6 g KCl L ⁻¹	EF	UC	0.2	Anode: Pt mesh (4.5 cm ²) Cathode: CF (56 or 112 cm ²) <i>j</i> _{cat} (CF-56 cm ²): 1.1-5.4 mA cm ⁻² <i>j</i> _{cat} (CF-112 cm ²): 1.8-2.7 mA cm ⁻² <i>Q</i> : MS T: Amb. pH: 3.0 [TDI] ₀ : 5.6 mg L ⁻¹ (100%)	[116]
Formic, oxalic, acetic, pyruvic or maleic acids	192 mg formic L ⁻¹ , 188 mg oxalic L ⁻¹ , 125 mg acetic L ⁻¹ , 122 mg pyruvic L ⁻¹ or 121 mg maleic L ⁻¹ in 14 g Na ₂ SO ₄ L ⁻¹	UVA-Vis H ₂ O ₂ H ₂ O ₂ -UVA-Vis Fenton (Fe ³⁺) SPF (Fe ³⁺) AO AO-UVA-Vis AO-Fe ³⁺ AO-Fe ³⁺ -UVA-Vis	FP with FPC and planar photoreactor	2.5	Anode: BDD (20 cm ²) Cathode: SS (20 cm ²) <i>j</i> _{cat} : 50 mA cm ⁻² <i>Q</i> : 3.3 L min ⁻¹ T: 35 °C pH: 3.0 [TDI] ₀ (Fenton, SPF, AO-Fe ³⁺ , AO-Fe ³⁺ -UVA-Vis): 56 mg L ⁻¹ (100%)	[186]

Table 1.6. Examples on the treatment of synthetic effluents polluted with other contaminants by EAOPs.

Pollutant	Wastewater characteristics	Process	Electrochemical reactor		Operational parameters (Maximal DOC decay ^a)	Ref.
			Configuration	V (L)		
Oxalic, oxamic acids	188 mg oxalic L ⁻¹ or 185 mg oxamic L ⁻¹ in 7.0 g Na ₂ SO ₄ L ⁻¹	UVA Fe ²⁺ -UVA Fe ³⁺ -UVA AO AO-Fe ²⁺ AO-Fe ²⁺ -UVA EF	UC	0.1	Anode: BDD (3 cm ²) Cathode: AO, AO-Fe ²⁺ , AO-Fe ²⁺ -UVA: SS (3 cm ²) EF: C-PTFE A-D (3 cm ²) <i>j</i> _{cat} : 33 mA cm ⁻² <i>Q</i> : MS T: 35 °C pH: 3.0 [TDI] ₀ (Fe ²⁺ -UVA, Fe ³⁺ -UVA, AO-Fe ²⁺ , AO-Fe ²⁺ -UVA, EF): 28 mg L ⁻¹ (100%)	[125]

^a Under the best experimental conditions, when applicable;

Amb. – Ambient;

C-PTFE A-D – Carbon-PTFE air-diffusion;

C-PTFE O-D – Carbon-PTFE O₂-diffusion;

FP – Flow plant;

FPC – Filter-press cell;

MS – Magnetic stirring;

Q – Liquid flow rate;

UC – Undivided cell.

Aniline and its derivatives are commonly produced as by-products of petroleum, pulp and paper, coal, perfume and rubber industries. These compounds are highly toxic because they react easily in the blood to convert hemoglobin into methahemoglobin, thereby preventing oxygen uptake [187]. Brillas et al. [55] degraded 100 mg L⁻¹ of aniline and 4-chloroaniline solutions by AO and AO-H₂O₂ techniques at alkaline pH in a 100 mL undivided cell using a PbO₂ anode and a graphite (for AO) or a carbon-PTFE O₂-diffusion (for AO-H₂O₂) cathode. Various background electrolytes were tested such as NaOH, Na₂CO₃ and Na₂CO₃ in combination with NaHCO₃, all leading to quite similar compounds removal. In turn, Brillas et al. [183] degraded 100 mg L⁻¹ of aniline in Na₂SO₄ aqueous solution by AO-H₂O₂, EF and PEF-UVA processes at pH of 3.0, resorting to a Pt anode and a carbon-PTFE O₂-diffusion cathode. The mineralization rates decreased with the increment of [TDI]₀ from 14 to 167 mg L⁻¹ in PEF-UVA process and a gradual increase in DOC removal rate was achieved for growing initial aniline concentration, but with decreasing percentage of DOC removal. Taking into consideration the achievements of both abovementioned frameworks, processes for anilines mineralization can be arranged in the order PEF-UVA > EF > AO-H₂O₂ > AO. Furthermore, faster degradations were achieved for higher *j* in AO-H₂O₂ and PEF-UVA. Brillas et al. [55] proposed two parallel decomposition pathways for aniline and 4-chloroaniline that occur via degradation of either the corresponding nitrobenzene derivative or benzoquinone imine. Benzoquinone, hydroquinone, nitrobenzene, phenol and 1,2,4-benzenetriol were detected as intermediates [183].

Phenols are present in wastewaters from pharmaceutical plants, oil refineries, coke plants, pulp and food-processing industries, constituting a serious hazardous for the environment since they are highly toxic for aquatic fauna and flora and also for human beings [188]. Pimentel et al. [184] assessed the degradation of 31 or 99 mg L⁻¹ of phenol solutions by EF process at pH of 3.0 in an undivided cell equipped with a Pt grid as anode and a CF as cathode. Distinct catalysts like Fe²⁺, Co²⁺, Mn²⁺ and Cu²⁺ were tested. While 5.6 mg Fe²⁺ L⁻¹ led to the best degradation in terms of pollutant removal and mineralization, 5.9 mg Co²⁺ L⁻¹ led to equal compound abatement but with lower mineralization. Mn²⁺ and Cu²⁺ induced to highly poorer degradation, which was mainly ascribed to changes in catalyst content due to the formation of metal deposits. Larger cathode surface area and smaller solution volumes managed higher oxidation ability. The main reaction intermediates were hydroquinone, *p*-benzoquinone and catechol.

Cresols are very popular phenols that have a methyl group linked to the ring of phenol. Flox et al. [185] appraised the degradation of the three *o*-, *m*- and *p*- cresol isomers by AO process at pH of 4.0 in a 1 L flow plant with an undivided filter-press cell composed of a BDD or a PbO₂ anode and a zirconium (Zr) cathode. While cresols mineralization was faster using BDD instead of PbO₂, their concentration decay was similar using both anodes. Aromatic intermediates such as 2-methylhydroquinone and 2-methyl-*p*-benzoquinone were identified.

LMCA have been detected as final and recalcitrant by-products of various aromatics, being hardly destroyed by •OH and largely prolonging the mineralization time with consequent efficiency loss and/or greater operation cost of the treatment. Although their intrinsic toxicity is low, they have a potential environmental impact due to their tendency to form complexes with heavy metals like Fe³⁺. Oxalic, oxamic, formic, acetic, pyruvic, maleic, malic, fumaric, glyoxylic, glycolic, malonic and succinic acids are some of the main LMCA identified during the degradation of aromatics by EAOPs and their removal was extensively studied by Oturan et al. [116], Guinea et al. [186] and Garcia-Segura and Brillas [125]. According to Oturan et al. [116], the ability of some acids to be degraded by EF process using a Pt mesh anode and a CF cathode decreased in the following order: fumaric ≈ maleic > glyoxylic > malic > glycolic > pyruvic > succinic > formic > malonic ≈ acetic. These results represent the ability of free acids and/or their Fe(III)-carboxylate complexes to be mainly degraded by •OH in the bulk and Pt(•OH). In Guinea et al. [186], the individual effect of •OH in the bulk, BDD(•OH), H₂O₂ and UVA-Vis radiation on the removal of either free carboxylic acids or their Fe(III)-carboxylate complexes was assessed by applying distinct processes such as UVA-Vis, Fenton, solar photo-Fenton (SPF), H₂O₂, H₂O₂-UVA-Vis and electrochemical AO, AO-UVA-Vis, AO-Fe³⁺ and AO-Fe³⁺-UVA-Vis processes using a BDD anode and a SS cathode.

Formic and maleic free acids as well as their Fe(III)-carboxylate complexes proved to be mainly degraded by $\bullet\text{OH}$ in the bulk and BDD($\bullet\text{OH}$). Acetic acid, either free or complexed with Fe^{3+} , was predominantly degraded by BDD($\bullet\text{OH}$), even though at a slow rate, showing a very high recalcitrant character. In turn, oxalic free acid was only degraded by BDD($\bullet\text{OH}$) and at very slow rate, whereas Fe(III)-oxalate complexes were highly photodecarboxylated and only slightly degraded by BDD($\bullet\text{OH}$). Pyruvic free acid was rapidly degraded by $\bullet\text{OH}$ in the bulk, BDD($\bullet\text{OH}$) and H_2O_2 , but with null abatement upon UVA-Vis radiation, whereas Fe(III)-pyruvate complexes were rapidly removed by all these agents. Moreover, cyclic voltammetry analyses carried out by Garcia-Segura and Brillas [125] indicated that the ultimate oxalic acid is not degraded by BDD($\bullet\text{OH}$) but rather by direct anodic oxidation at the BDD surface. These results were extended to the ultimate oxamic acid. On the other hand, cyclic voltammograms of Fe(III)-oxalate and Fe(III)-oxamate complexes suggested that these compounds react with BDD($\bullet\text{OH}$) at the anode surface. Further application of UVA, Fe^{2+} -UVA, Fe^{3+} -UVA and electrochemical AO, AO- Fe^{2+} , AO- Fe^{2+} -UVA and EF processes employing BDD as anode and SS (for AO and AO based processes) or carbon-PTFE air-diffusion electrode (for EF) as cathode allowed concluding about the participation of $\bullet\text{OH}$ in the bulk, BDD($\bullet\text{OH}$) and UVA radiation on the direct mineralization of oxalic and oxamic acids either free or complexed with Fe^{3+} . While both free acids showed null ability to be destroyed by UVA light, Fe(III)-oxamate complexes were slowly photolyzed and Fe(III)-oxalate complexes proved to be much more rapidly photodecarboxylated. Free acids and their Fe(III) complexes were poorly oxidized by $\bullet\text{OH}$ in the bulk. Furthermore, Fe(III)-oxamate complexes were oxidized more quickly with BDD($\bullet\text{OH}$) than Fe(III)-oxalate ones.

1.6 Degradation of real wastewaters by EAOPs

A review on many studies regarding the remediation of real textile effluents, pharmaceutical effluents, wastewaters from secondary treatment of wastewater treatment plants (WWTPs), landfill leachates, among others, by EAOPs is presented.

1.6.1 Textile wastewaters

Textile wastewaters result from several different activities involved in the dyeing process, such as pre-treatment, dyeing, printing and finishing of the textile material. They are composed by various dyes with a complex organic structure, surfactants, detergents and inorganic salts, which constitutes a risk for the environment and ecosystems when they are improperly released into the environment [189].

Three examples of textile wastewaters treatments by EAOPs are given in Table 1.7. While Wang et al. [144] treated the effluent as collected, both Tsantaki et al. [136] and Vaghela et al. [190] filtered the wastewater prior to treatment in order to remove any suspended particle. Furthermore, Tsantaki et al. [136] added perchloric acid (HClO_4) as supporting electrolyte, a popular practice to increase effluent conductivity and decrease the electrical consumption, although the conductivity of this effluent was already high ($7200 \mu\text{S cm}^{-1}$). In fact, the three effluents exhibited high conductivity, above $2900 \mu\text{S cm}^{-1}$. Vaghela et al. [190] performed trials not only using the original effluent after filtration but also subjecting it to dilutions of 25% and 50%. The organic load of the three raw effluents embraced distinct COD values from 470 to $5957 \text{ mg O}_2 \text{ L}^{-1}$. Only Wang et al. [144] determined the BOD_5 content, attaining a BOD_5/COD ratio of 0.26 that reveals a low biodegradability. Divergent pH values of 8.8, 7.3 and 4.8 were utilized by Tsantaki et al. [136], Vaghela et al. [190] and Wang et al. [144], respectively. The amount of some ions was only assessed by Wang et al. [144], pointing out a moderate chloride content of 234 mg L^{-1} and a low sulfate content of 38 mg L^{-1} .

Table 1.7. Examples on the treatment of real textile wastewaters by EAOPs.

Pollutant	Wastewater characteristics		Process	Electrochemical reactor		Operational parameters (Maximal DOC decay ^a)	Ref.	
				Configuration	V (L)			
Real or synthetic textile wastewater	DOC (mg L ⁻¹)	Real 120	Synthetic 82	AO	UC	0.12	Anode: BDD (15 cm ²) Cathode: Zr <i>j</i> _{cat} (synthetic): 4-50 mA cm ⁻² <i>j</i> _{cat} (real): 8 mA cm ⁻² <i>Q</i> : MS T (synthetic): 22-43 °C T (real): 22 °C pH (synthetic): 1.0-12 pH (real): 1 (70%)	[136]
	COD (mg O ₂ L ⁻¹)	470	300					
	C (μS cm ⁻¹)	7200	8400					
	TSS (mg L ⁻¹)	68	0					
	pH	8.8	11					
	[Total iron] (mg L ⁻¹)	0.1	0					
	in 10-50 g HClO ₄ L ⁻¹ (synthetic) or 25 g HClO ₄ L ⁻¹ (real)							
	Filtered before trials							
Textile wastewater	COD (mg O ₂ L ⁻¹)	Raw 5957	1:2 diluted 2978	AO	FP with undivided FPC	n.s.	Anode: DSA (50 cm ²) Cathode: SS (88 cm ²) <i>j</i> _{cat} : 10-100 mA cm ⁻² <i>Q</i> : 0.0005-0.015 L min ⁻¹ T: Amb. pH: 2.8-12 (n.a.)	[190]
	C (μS cm ⁻¹)	n.m.	135000					
	pH	7.3	8.1					
Textile wastewater	DOC (mg L ⁻¹) = 395			EF	UC	0.5	Anode: Pt wire Cathode: PAN based-ACF (63 cm ²) <i>j</i> _{cat} : 0.8-4.8 mA cm ⁻² <i>Q</i> : MS T: 20-40 °C pH: 2.0-5.0 [TDI] ₀ : 18-147 mg L ⁻¹ (n.a.)	[144]
	COD (mg O ₂ L ⁻¹) = 1224							
	BOD ₅ (mg O ₂ L ⁻¹) = 324							
	C (μS cm ⁻¹) = 2914							
	pH = 4.8							
	[SO ₄ ²⁻] (mg L ⁻¹) = 38							
	[Cl ⁻] (mg L ⁻¹) = 234							
	Filtered before trials							

^a Under the best experimental conditions, when applicable;

Amb. – Ambient;

FP – Flow plant;

FPC – Filter-press cell;

MS – Magnetic stirring;

n.m. – not measured;

n.s. – not specified;

Q – Liquid flow rate;

UC – Undivided cell.

Tsantaki et al. [136] and Vaghela et al. [190] applied AO treatments, the first using a BDD anode and a Zr cathode and the second employing a dimensionally stable anode (DSA) and a SS cathode. In turn, Wang et al. [144] assessed the effluent treatment by EF technique using a Pt anode and a polyacrylonitrile (PAN) based ACF. Undivided cells or simple flow plants with a filter-press cell were employed with volumes up to 0.5 L. Trials were performed under galvanostatic conditions, with low *j*_{cat} values of 8.0 and 3.2 mA cm⁻² indicated as the best ones by Tsantaki et al. [136] and Wang et al. [144], respectively. For AO process, the effect of temperature proved to be negligible [136], whereas higher COD decay was achieved for increasing temperature in EF [144]. Distinct best pH values for AO were pointed out. Tsantaki et al. [136] indicated pH of 1 as the best one, attributing this to a change in electrode surface properties under alkaline conditions, whereas Vaghela et al. [190] achieved highest and similar color removal at pH of 2.8 and 8.1 and highest COD removal at pH of 8.1. The best attained pH for EF was 3.0, along with a best [TDI]₀ of 112 mg L⁻¹.

70% of DOC removal and 53% of COD removal were achieved for AO treatments of raw filtered effluent with 25 g HClO₄ L⁻¹ or raw effluent by Tsantaki et al. [136] and Vaghela et al. [190], respectively, after 180 or 20 min of electrolysis using pH of 1 or 7.3, ambient temperature and j_{cat} of 8 or 100 mA cm⁻², respectively. The EF process reached 74% of COD removal after 240 min of reaction using pH of 3.0, 20 °C, [TDI]₀ of 112 mg L⁻¹ and j_{cat} of 3.2 mA cm⁻² [144].

Moreover, Tsantaki et al. [136] also employed a simulated textile effluent, reaching a quite similar DOC removal for simulated and real effluents and faster COD decay and lower energy consumption for the real one.

1.6.2 Pharmaceutical wastewaters and urban wastewaters after secondary treatment

The application of an AO process to the treatment of a wastewater from a pharmaceutical industry plant using a BDD anode and a SS cathode under galvanostatic conditions was carried out by Domínguez et al. [191] (see Table 1.8). The real effluent exhibited a high organic content, with DOC of 1600 mg L⁻¹ and COD of 12000 mg L⁻¹, composed of high amounts of pharmaceuticals (aromatic and aliphatic compounds) and also solvents such as methanol and ethanol. Its pH was alkaline and it exhibited a high conductivity of 7000 μS cm⁻¹. A RSM was performed to optimize j and liquid flow rate, using ambient temperature and original pH. Higher mineralization was achieved for greater j from 26 to 179 mA cm⁻². The reactor operated in continuous mode and, as a consequence, the increment of liquid flow rate led to shorter residence times in the filter-press cell, diminishing the mineralization.

Conventional WWTPs are not able to entirely remove micropollutants at ng L⁻¹ and μg L⁻¹ levels, such as pharmaceuticals, personal care products, pesticides, detergents and various industrial additives [192]. As a result, these undesirable compounds end up in the environment and may cause a multitude of risks to all living organisms. Table 1.8 collects some studies on the treatment of effluents collected after the secondary treatment in WWTPs, mostly municipal WWTPs (MWWTPs), by EAOPs. The treatment was directly applied to the secondary effluent [134] or a membrane separation process like MF, ultrafiltration (UF) and/or reverse osmosis (RO) was firstly employed to concentrate pollutants and treat only the concentrate by EAOPs [32, 193-195]. After membrane filtration processes, micropollutants concentrations from 0.005 to 24 μg L⁻¹ were reported [32, 194]. In some cases, the effluent was spiked with micropollutants contents of 7.8-100 μg L⁻¹ to allow their determination in the analytical equipment throughout EAOPs

[134, 195]. The total organic content of effluents was very low, mainly from 10-24 mg DOC L⁻¹ for both unchanged and concentrated effluents, but Radjenovic et al. [195] presented a higher DOC of 57 mg L⁻¹. The pH was near neutral for all wastewaters to comply with regulatory limits for the discharge of wastewaters from WWTPs into the environment. Chloride ions were available in moderate/high concentrations of 302-1500 mg L⁻¹ and the amounts of sulfate and ammonium were low (25-584 and 18-208 mg L⁻¹, respectively), which led a low/moderate conductivity of 1700-4800 $\mu\text{S cm}^{-1}$.

All studies referred to the treatment of secondary effluents by AO process at ambient temperature using 2-10 L flow plants equipped with an undivided or a divided filter-press cell. The most widely employed anode was BDD, with only Radjenovic et al. [195] using another anode, i.e. Ru_{0.7}Ir_{0.3}O₂. Both BDD and SS were used as cathodes.

Most of the degradations were performed in galvanostatic mode. Exceptionally, Dialynas et al. [193] mentioned the employment of two j , 51 and 254 mA cm⁻², by using the effluent after RO without changes and by adding sulfuric acid to increase its conductivity, respectively. Besides the use of a single j value along the experiment in batch mode, Radjenovic et al. [195] also applied AO with increasing j values from 0.1 to 25 mA cm⁻² in continuous mode, achieving higher micropollutants removal efficiency when operating in batch mode. DOC and COD removals were faster with increasing j in Garcia-Segura et al. [134] and Pérez et al. [194], but micropollutants removal was not significantly influenced by j in Pérez et al. [194]. This was ascribed to the control of removal kinetics of pollutants at trace contents by the mass transfer resistance given by the diffusion of pollutants from the bulk solution to the anode surface. The majority of micropollutants was completely removed after 1-2 h of AO using 2-20 mA cm⁻². Nevertheless, some recalcitrant micropollutants required longer times of 24 h to be totally degraded and few could not be removed even after long times of electrolysis [32, 134, 194, 195]. In addition, Pérez et al. [194] detected faster ammonium conversion to nitrate at larger j together with the production of increasing amounts of ClO₃⁻, free chlorine and trihalomethanes. Garcia-Segura et al. [134] detected the formation of active chlorine species, ClO₃⁻ and ClO₄⁻ ions and organochloride and organobromide derivatives.

Contrasting to all the other studies, which performed AO with the original neutral pH of the effluent, Garcia-Segura et al. [134] tested both pH of 7.0 and 3.0. Faster DOC and COD removals were attained at acidic pH, which was ascribed to the electrogeneration of higher amounts of active chlorine species with higher standard redox potential, predominantly HClO, in parallel with the

formation of lower amounts of BDD($\bullet\text{OH}$) and higher contents of less oxidizing species such as $\text{O}_2^{\bullet-}$ at the BDD anode at neutral and alkaline medium.

Van Hege et al. [196, 197] degraded RO concentrates from mixtures of secondary MWWTP effluents and textile wastewaters by AO using a 1 L flow plant with an undivided filter-press cell, 22 °C and alkaline pH. These mixtures were characterized by COD values of 151-218 mg $\text{O}_2 \text{L}^{-1}$, high conductivities of 3990-5290 $\mu\text{S cm}^{-1}$, alkaline pH and moderate chloride content of 592-804 mg L^{-1} . Ti was employed as cathode in both studies and Van Hege et al. [197] found that the ability of different anodes for COD removal could be arranged in the order $\text{BDD} > \text{SnO}_2 \approx \text{PbO}_2 > \text{RuO}_2$. For PbO_2 and SnO_2 , salts precipitation and electrode scaling were experienced due to pH increase, whereas j values in a range of 10-30 mA cm^{-2} proved to have a low influence on COD removal both using BDD and RuO_2 anodes. In addition, it was observed increasing accumulation of ClO_3^- using both anodes, with a greater accumulation for BDD. Active chlorine species were also accumulated, but only at the end of electrolysis and, once again, in larger extent for BDD.

Table 1.8. Examples on the treatment of real pharmaceutical and secondary WWTPs effluents by AO.

Pollutant	Wastewater characteristics			Electrochemical reactor		Operational parameters (Maximal DOC decay ^a)	Ref.	
				Configuration	V (L)			
Pharmaceutical wastewater	DOC (mg L^{-1}) = 1600 COD (mg $\text{O}_2 \text{L}^{-1}$) = 12000 C ($\mu\text{S cm}^{-1}$) = 7000 TSS (mg L^{-1}) = 5000 pH = 8.5			FP with undivided FPC	0.6	Anode: BDD (78 cm^2) Cathode: SS (78 cm^2) j_{cat} : 26-179 mA cm^{-2} Q : 0.10-0.56 L min^{-1} T: 20 °C pH: 8.5 (≈100%)	[191]	
Mixture of secondary MWWTP and textile wastewaters after RO	COD (mg $\text{O}_2 \text{L}^{-1}$) = 158 C ($\mu\text{S cm}^{-1}$) = 3990 pH = 8.2 [Cl^-] (mg L^{-1}) = 592			FP with undivided FPC	1	Anode: BDD (60 cm^2) Cathode: Ti (60 cm^2) j_{cat} : 17 mA cm^{-2} Q : 0.25 L min^{-1} T: 22 °C pH: 8.2 (n.a.)	[196]	
Mixture of secondary MWWTP and textile wastewaters after RO	COD (mg $\text{O}_2 \text{L}^{-1}$)	No. 1 151	No. 2 218	No. 3 171	FP with undivided FPC	1	Anode: PbO_2 , SnO_2 , RuO_2 or BDD (50 cm^2) Cathode: Ti (50 cm^2) j_{cat} : 10-30 mA cm^{-2} Q : 0.25 L min^{-1} T: 22 °C pH: 8.7/7.9/8.0 (n.a.)	[197]
Mixture of secondary WWTP wastewaters after MF + RO spiked with 28 micropollutants at 7.8-37 $\mu\text{g L}^{-1}$ each	DOC (mg L^{-1})	No. 1 57	No. 2 57		FP with divided FPC	10	Anode: $\text{Ru}_{0.7}\text{Ir}_{0.3}\text{O}_2$ (24 cm^2) Cathode: SS mesh (24 cm^2) j_{cat} (continuous mode): 0.1-25 mA cm^{-2} j_{cat} (batch mode): 25 mA cm^{-2} Q : 0.16 L min^{-1} T: Amb. pH: 7.5/7.7 [Fe^{2+}] ₀ : 0.22/0.35 mg L^{-1} (31%)	[195]
	C ($\mu\text{S cm}^{-1}$)	4250	3970					
	pH	7.5	7.7					
	[Fe^{2+}] (mg L^{-1})	0.22	0.35					
	[SO_4^{2-}] (mg L^{-1})	242	239					
	[Cl^-] (mg L^{-1})	1500	1200					

Table 1.8. Examples on the treatment of real pharmaceutical and secondary WWTPs effluents by AO.

Pollutant	Wastewater characteristics	Electrochemical reactor		Operational parameters (Maximal DOC decay ^a)	Ref.		
		Configuration	V (L)				
Primary MWWTP wastewater after MBR + RO	DOC (mg L ⁻¹) = 10	FP with undivided FPC	8	BDD-70 cm ² Anode: BDD (70 cm ²) Cathode: BDD (70 cm ²) Operated in potentiostatic mode <i>Q</i> : 20 L min ⁻¹ T: Amb. pH: 8.5 (36%)	[193]		
Secondary MWWTP wastewater spiked with 29 micropollutants at ≈ 100 µg L ⁻¹ each	DOC (mg L ⁻¹) = 23 COD (mg O ₂ L ⁻¹) = 21 pH = 7.0 [SO ₄ ²⁻] (mg L ⁻¹) = 25 [Cl ⁻] (mg L ⁻¹) = 309	FP with divided FPC	10	Anode: BDD (41 cm ²) Cathode: SS (41 cm ²) <i>j</i> _{cat} : 9.8 or 20 mA cm ⁻² <i>Q</i> : 0.16 L min ⁻¹ pH: 3.0 or 7.0 (100%)	[134]		
Secondary MWWTP wastewater after UF + RO	DOC (mg L ⁻¹) = 17 C (µS cm ⁻¹) = 2665 TSS (mg L ⁻¹) = 5.7 pH = 7.5 [SO ₄ ²⁻] (mg L ⁻¹) = 537 [Cl ⁻] (mg L ⁻¹) = 655 [NH ₄ ⁺] (mg L ⁻¹) = 120 [NO ₃ ⁻] (mg L ⁻¹) = 114 [PO ₄ ³⁻] (mg L ⁻¹) = n.d.	FP with undivided FPC	2	Anode: BDD (70 cm ²) Cathode: BDD (70 cm ²) <i>j</i> _{cat} : 10 mA cm ⁻² <i>Q</i> : 10 L min ⁻¹ T: 20 °C pH: 7.5 (n.a.)	[32]		
Secondary WWTP wastewater after UF + RO	No. 1	No. 2	FP with undivided FPC	2	Anode: BDD (70 cm ²) Cathode: BDD (70 cm ²) <i>j</i> _{cat} : 2-20 mA cm ⁻² <i>Q</i> : 10 L min ⁻¹ T: 20 °C pH: 7.6/7.9 (n.a.)	[194]	
	DOC (mg L ⁻¹)	20					27
	COD (mg O ₂ L ⁻¹)	n.m.					133
	C (µS cm ⁻¹)	1700					4800
	TSS (mg L ⁻¹)	0					0
	pH	7.6					7.9
	[SO ₄ ²⁻] (mg L ⁻¹)	302					584
	[Cl ⁻] (mg L ⁻¹)	328					630
[NH ₄ ⁺] (mg L ⁻¹)	18	208					
[NO ₂ ⁻] (mg L ⁻¹)	n.d.	n.d.					
[NO ₃ ⁻] (mg L ⁻¹)	n.d.	12					

^a Under the best experimental conditions, when applicable;

Amb. – Ambient;

FP – Flow plant;

FPC – Filter-press cell;

MBR – Membrane bioreactor;

n.d. – not detected;

n.m. – not measured;

Q – Liquid flow rate.

1.6.3 Landfill leachates

Characteristics of landfill leachates vary with the amount, composition and moisture of solid wastes, age of the landfill, hydrogeology and climate of the site, seasonal weather variations, among other factors [198]. Table 1.9 displays ten surveys regarding the treatment of municipal landfill leachates and one investigation on the remediation of an industrial landfill leachate by EAOPs.

Table 1.9. Examples on the treatment of real landfill leachates by AO.

Pollutant	Wastewater characteristics	Process	Electrochemical reactor		Operational parameters (Maximal DOC decay ^a)	Ref.
			Configuration	V (L)		
Municipal sanitary landfill leachate	Biologically pretreated COD (mg O ₂ L ⁻¹) = 920-1448 C (μS cm ⁻¹) = 10000-10900 pH = 8.1-9.4 [SO ₄ ²⁻] (mg L ⁻¹) = 140-199 [Cl ⁻] (mg L ⁻¹) = 1615-1819 [NH ₄ ⁺] (mg L ⁻¹) = 896-980 [NO ₂ ⁻] (mg L ⁻¹) = n.d.-163 [NO ₃ ⁻] (mg L ⁻¹) = 5-1207	AO	LS, PS: FP with undivided FPC	LS: 1 PS: 250	Anode: BDD LS: 70 cm ² ; 10500 cm ² Cathode: SS LS: 70 cm ² ; PS: 10500 cm ² <i>j</i> _{cat} : 45 mA cm ⁻² <i>Q</i> : LS: 3.8-12 L min ⁻¹ ; PS: 5.6-18.3 L min ⁻¹ T: LS: 20-40 °C; PS: 20 °C pH: 8.1-9.4 (n.a.)	[199]
Municipal sanitary landfill leachate	Raw COD (mg O ₂ L ⁻¹) = 3385 BOD ₅ (mg O ₂ L ⁻¹) = 500 C (μS cm ⁻¹) = 22600 pH = 8.4 [SO ₄ ²⁻] (mg L ⁻¹) = 11 [Cl ⁻] (mg L ⁻¹) = 2574 [NH ₄ ⁺] (mg L ⁻¹) = 1591 [NO ₂ ⁻] (mg L ⁻¹) = < 2 [NO ₃ ⁻] (mg L ⁻¹) = 1.9 [PO ₄ ³⁻] (mg L ⁻¹) = 31 in 0-3.1 g NaCl L ⁻¹ ([Cl ⁻] ₀ = 2574-4476 mg L ⁻¹)	AO	FP with undivided FPC	10	Anode: BDD (70 cm ²) Cathode: BDD (70 cm ²) <i>j</i> _{cat} : 90-257 mA cm ⁻² <i>Q</i> : 10 L min ⁻¹ pH: 5.0-8.3 (n.a.)	[47]
Municipal sanitary landfill leachate	Bio/ physicochemically pretreated Raw DOC (mg L ⁻¹) 2782 COD (mg O ₂ L ⁻¹) 4434 BOD ₅ (mg O ₂ L ⁻¹) 640 C (μS cm ⁻¹) 12770 TSS (mg L ⁻¹) 317 pH 8.4 [SO ₄ ²⁻] (mg L ⁻¹) 39 [Cl ⁻] (mg L ⁻¹) 3235 [NH ₄ ⁺] (mg L ⁻¹) 2492 [NO ₂ ⁻] (mg L ⁻¹) n.d. [NO ₃ ⁻] (mg L ⁻¹) n.d. [PO ₄ ³⁻] (mg L ⁻¹) 55 Raw: without dilution or 1:2 or 1:4 diluted with addition of NaCl to get [Cl ⁻] ₀ ≈ 3235 mg L ⁻¹ Pretreated: in 0-12 g NaCl L ⁻¹ ([Cl ⁻] ₀ = 1420-8570 mg L ⁻¹)	AO	FP with undivided FPC	n.s.	Anode: BDD (70 cm ²) Cathode: SS (70 cm ²) <i>j</i> _{cat} (raw): 15-90 mA cm ⁻² <i>j</i> _{cat} (pre-treated): 30 mA cm ⁻² T: 20 °C pH: 8.4/7.5 (n.a.)	[200]
Municipal sanitary landfill leachate	Raw COD (mg O ₂ L ⁻¹) = 4100-5000 BOD ₅ (mg O ₂ L ⁻¹) = < 1000 C (μS cm ⁻¹) = 25000 pH = 8 [Cl ⁻] (mg L ⁻¹) = 2500 [NH ₄ ⁺] (mg L ⁻¹) = 2100-3000 in 0-12 g NaCl L ⁻¹ ([Cl ⁻] ₀ = 2500-10000 mg L ⁻¹) without or with addition of 5.3 g Na ₂ SO ₄ L ⁻¹ (5000 mg SO ₄ ²⁻ L ⁻¹)	AO	UC	n.s.	Anode: Graphite, PbO ₂ , DSA or Sn-Pd-Ru (40 cm ²) Cathode: Steel (40 cm ²) <i>j</i> _{cat} : 25-100 mA cm ⁻² <i>Q</i> : MS pH: 4.0-10 (n.a.)	[46]
Municipal sanitary landfill leachate	Biologically pre-treated DOC (mg L ⁻¹) = 830 COD (mg O ₂ L ⁻¹) = 5800 C (μS cm ⁻¹) = 22100 TSS (mg L ⁻¹) = 1770 pH = 8.4 [Cl ⁻] (mg L ⁻¹) = 4400 [NH ₄ ⁺] (mg L ⁻¹) = 1210 without dilution or 1:2-1:16 diluted in 4.3 g Na ₂ SO ₄ L ⁻¹	AO	UC	0.2	Anode: BDD (10 cm ²) Cathode: SS (10 cm ²) <i>j</i> _{cat} : 5-70 mA cm ⁻² <i>Q</i> : MS T: 25 °C pH: 8.4 (37% – 1:1 dilution)	[129]

Table 1.9. Examples on the treatment of real landfill leachates by AO.

Pollutant	Wastewater characteristics	Process	Electrochemical reactor		Operational parameters (Maximal DOC decay ^a)	Ref.	
			Configuration	V (L)			
Municipal sanitary landfill leachate	Biologically pre-treated DOC (mg L ⁻¹) = 2060 COD (mg O ₂ L ⁻¹) = 6200 BOD ₅ (mg O ₂ L ⁻¹) = 800 C (μS cm ⁻¹) = 22000 pH = 9.0 [Cl ⁻] (mg L ⁻¹) = 4700 [NH ₄ ⁺] (mg L ⁻¹) = 480 [NO ₂ ⁻] (mg L ⁻¹) = 300 [NO ₃ ⁻] (mg L ⁻¹) = 80	AO	UC	0.2	Anode: Ti/Pt/PbO ₂ , Ti/Pt/SnO ₂ -Sb ₂ O ₄ or BDD (10 cm ²) Cathode: SS (10 cm ²) <i>j</i> _{cat} : 30 mA cm ⁻² <i>Q</i> : MS T: Amb. pH: 8.4 (32%)	[201]	
Municipal sanitary landfill leachate	Filtrated COD (mg O ₂ L ⁻¹) = 780 BOD ₅ (mg O ₂ L ⁻¹) = <78 C (μS cm ⁻¹) = 9770 pH = 8.2 [Cl ⁻] (mg L ⁻¹) = 1800 [NH ₄ ⁺] (mg L ⁻¹) = 343	AO	FP with UC	0.35	Anode: Ti-Ru-SnO ₂ , PbO ₂ or BDD (50 cm ²) Cathode: SS (50 cm ²) <i>j</i> _{cat} : 40 mA cm ⁻² <i>Q</i> : 7.0 L min ⁻¹ T: 25 °C pH: 8.2 (n.a.)	[202]	
Municipal sanitary landfill leachate	Raw DOC (mg L ⁻¹) = 2780 COD (mg O ₂ L ⁻¹) = 4430 BOD ₅ (mg O ₂ L ⁻¹) = 1196 C (μS cm ⁻¹) = 12770 pH = 8.4 [SO ₄ ²⁻] (mg L ⁻¹) = 438 [Cl ⁻] (mg L ⁻¹) = 2124 [NH ₄ ⁺] (mg L ⁻¹) = 1225 [NO ₂ ⁻] (mg L ⁻¹) = n.d. [NO ₃ ⁻] (mg L ⁻¹) = n.d.	Bio-treated 1300 After Fenton 200	Bio-treatment + Fenton + AO	FP with undivided FPC	LS: 1 PS: n.s.	Anode: BDD LS: 70 cm ² ; PS: 10500 cm ² Cathode: SS LS: 70 cm ² ; PS: 10500 cm ² <i>j</i> _{cat} : LS: 10-45 mA cm ⁻² ; PS: 45 mA cm ⁻² <i>Q</i> : LS: 11 L min ⁻¹ ; PS: n.s. T: 20 °C pH (Fenton): 3-3.5 pH (AO): 7.5 (n.a.)	[203]
Municipal sanitary landfill leachate	Raw COD (mg O ₂ L ⁻¹) = 3782 BOD ₅ (mg O ₂ L ⁻¹) = 560 pH = 8.4 [Cl ⁻] (mg L ⁻¹) = 3702 [NH ₄ ⁺] (mg L ⁻¹) = 3143	AO	FP with three-dimensional granular AC bed reactor	0.8	Anode: RuO ₂ -IrO ₂ (300 cm ²) Cathode: SS (300 cm ²) <i>j</i> _{cat} : 30-90 mA cm ⁻² <i>Q</i> : Air diffusion, recirculation at n.s. flow T: Amb. pH: 8.4 (n.a.)	[204]	
Industrial landfill leachate	Raw COD (mg O ₂ L ⁻¹) = 17100-18400 pH = 8.9 [Total iron] (mg L ⁻¹) = 20 [Cl ⁻] (mg L ⁻¹) = 52300-54280 [NH ₄ ⁺] (mg L ⁻¹) = 1200-1320	AO	UC with three-dimensional granular AC bed reactor	1.1	Anode: Carbon plate Cathode: 2 SS (140 cm ² × 2) <i>I</i> : 1-3 A <i>Q</i> : Air diffusion T: Amb. pH: 8.9 (83%)	[205]	

^a Under the best experimental conditions, when applicable;

Amb. – Ambient;
FP – Flow plant;
FPC – Filter-press cell;
LS – Lab-scale;
MS – Magnetic stirring;
n.d. – not detected;
n.s. – not specified;
PS – Pilot-scale;
Q – Liquid flow rate;
UC – Undivided cell.

1.6.3.1 Landfill leachate characteristics and pre-treatments

Raw municipal landfill leachates are characterized by: (i) high amounts of organic matter, with DOC of around 2780 mg L⁻¹ and COD of 3385-5000 mg O₂ L⁻¹, including recalcitrant compounds like humic and fulvic acids and xenobiotic organic compounds such as aromatic hydrocarbons, phenols, chlorinated aliphatics, pesticides, plastizers, among others; (ii) low amounts of biodegradable organic compounds (BOD₅/COD ratios of 0.13-0.27); (iii) high contents of inorganic ions like chloride (2124-3702 mg L⁻¹) and ammonium (1125-3143 mg L⁻¹), leading to very high conductivities of 12770-25000 µS cm⁻¹; (iv) alkaline pH; and (v) presence of heavy metals like cadmium, chromium, copper, lead, nickel and zinc [46, 47, 200, 203, 204]. The raw industrial landfill leachate displayed much larger COD and chloride contents of 17100-18400 mg O₂ L⁻¹ and 52300-54280 mg L⁻¹, respectively [205]. Some authors directly applied EAOPs to the remediation of raw landfill leachates [195, 200, 204, 205], whereas others subjected the raw municipal landfill leachate to the following treatments before EAOPs application: (i) biological treatment [129, 199, 201], (ii) biological treatment followed by physico-chemical treatment [200], (iii) biological treatment followed by Fenton process [203], or (iv) filtration [202]. Biological pre-treatments led to the removal of biodegradable organic matter, which culminated in only slightly lower DOC and COD values since it only represents a low fraction of organic compounds. For Urriaga et al. [203], a conversion of ammonium into nitrite and/or nitrate along with alkalinity consumption was observed. The biological/physico-chemical pre-treatment carried out by Cabeza et al. [200] was not specified but it led to high DOC, COD and BOD₅ abatements of 66%, 74% and 81%, respectively, simultaneously with the removal of 56% of ammonium and 52% of chloride. The application of a Fenton process to the bio-treated landfill leachate by Urriaga et al. [203] intended to degrade non-biodegradable organic matter, achieving 85% COD removal. Panizza and Martinez-Huitle [202] proceeded with the filtration of raw leachate in order to remove suspended solids that can influence the electrochemical process.

1.6.3.2 Process

All the studies presented in Table 1.9 refer to the application of AO process. This EAOP was performed with two purposes: (i) ammonium oxidation through indirect oxidation by active chlorine species, and (ii) organics oxidation via reaction at the anode surface with electrogenerated M([•]OH) and indirect oxidation. Cabeza et al. [200] and Chiang et al. [46] demonstrated that faster ammonium oxidation and COD removal were achieved by adding larger chloride contents from

around 1400 to 10000 mg L⁻¹ to the effluent, which was associated with the production of higher amounts of Cl₂/ClO⁻. To take advantage of high chloride content benefits, Anglada et al. [47] increased the concentration of chloride up to 4500 mg L⁻¹ by adding NaCl before starting AO.

Fernandes et al. [129] diluted the bio-treated landfill leachate to be subjected to AO and added Na₂SO₄ to compensate the greater ohmic drop attained by diluting samples. Slower organics removal in terms of absolute value and higher energy consumption were attained for higher dilutions. Moreover, the authors also established that electrolysis was controlled by *j* for small dilutions and by mass transport for high dilutions. Note that Chiang et al. [46] detected that the addition of Na₂SO₄ caused a negative effect on both ammonium oxidation and COD removal due to the suppression of Cl₂/ClO⁻ formation.

1.6.3.3 Electrochemical reactor

Reactors with different configurations have been used for landfill leachate treatments such as undivided cells with magnetic stirring [46, 129, 201], an undivided cell with flow circulation [202], undivided cells with three-dimensional granular activated carbon (AC) bed reactor [204, 205] and flow plants with an undivided filter-press cell [47, 199, 200, 203]. Most of the reactors treated solutions up to around 1 L, but much larger solution volumes up to 250 L were employed. The pilot-scale plant with capacity of 250 L achieved more than 90% of COD after 5 h of reaction and total ammonium oxidation to nitrate after 8 h for the remediation of a biologically treated municipal sanitary landfill leachate using a BDD anode and a SS cathode, effluent pH, 20 °C and *j*_{cat} of 45 mA cm⁻² [199].

When using three-dimensional electrodes, faster ammonium oxidation and COD removals were obtained for higher surface area of the granular AC [204, 205]. Zhang et al. [204] also found superiority of a three-dimensional electrochemical cell over a two-dimensional one when ammonia removal was concerned.

Although BDD has been the most popular anode utilized, other anodes have been used and some studies have compared the performance of various anodes. Panizza and Martinez-Huitle [202] reported that AO ability for both ammonium oxidation and COD removal decreased in the order BDD > PbO₂ > Ti-Ru-SnO₂. BDD also exhibited lower energy consumption and higher current efficiency. In contrast, Fernandes et al. [201] found higher propensity of PbO₂ and SnO₂-Sb₂O₄ (antimony tetroxide) anodes for ammonium oxidation than BDD. Furthermore, metal oxides

promoted ammonium oxidation to nitrogen gas, whereas BDD only oxidized ammonium to nitrate, maintaining a high nitrogen content. Quite similar COD removals were reached for the three anodes, although BDD was superior for DOC removal. In addition, metal oxide anodes led to lower energy consumption because of their higher conductivity. Chiang et al. [46] found increasing Cl_2/ClO^- production in AO for anodes in the following order: graphite < PbO_2 < DSA < Sn-Pd-Ru. These authors correlated the ability for Cl_2/ClO^- production with ammonium oxidation, COD removal and chloramines production. Since ammonium and COD removals occurred simultaneously by the indirect oxidation, it was proposed a competition between them.

SS has been the most widely employed cathode for landfill leachate remediation by AO, although BDD was also used.

1.6.3.4 Operational parameters

All AO processes for landfill leachate remediation outlined in Table 1.9 were conducted under galvanostatic conditions, commonly using j_{cat} from 5 to 100 mA cm^{-2} either for raw or pre-treated leachates. Faster organics degradation and ammonium oxidation were always attained for larger j and, beyond that, Chiang et al. [46] also found increasing Cl_2/ClO^- production.

The mass transfer was enhanced by applying higher liquid flow rates and temperatures from 20 to 40 °C in an AO process performed at a flow plant with an undivided filter-press cell with continuous solution recirculation [199].

The effect of pH on AO process was assessed by Anglada et al. [47], where increasing COD removal and decolorization were reported for pH values from 8.3 to 5.0, and also by Chiang et al. [46], in which the pH had a negligible effect from 4.0 to 10.

1.6.4 Other real wastewaters

Other real effluents arising from the production of wine, pulp, paper, dairy, tannery and other outputs have also been treated by EAOPs, as can be seen in Table 1.10.

The various activities carried out during processing and cleaning operations in wineries lead to the generation of high amounts of wastewaters mainly composed of organic compounds like organic acids (tartaric, lactic and acetic), sugars (glucose and fructose) and alcohols (ethanol and glycerol) and also recalcitrant high-molecular weight compounds like polyphenols and lignins [206]. The

release of this kind of effluent into natural aquatic environments without proper treatment can cause deficient oxygen balance, bad odors and decrease of natural photoactivity due to color and turbidity. The raw winery wastewater used by Orescanin et al. [117] was characterized by very high COD content of 10240 mg O₂ L⁻¹, acidic pH and low ions content, with consequent low/moderate conductivity of 1100 μS cm⁻¹. The authors firstly added NaCl to the raw winery wastewater in order to allow the formation of active chlorine species by indirect anodic oxidation. Afterwards, an innovative treatment system embracing three consecutive electrochemical methods was implemented, including AO with SS electrodes, EC with iron electrodes and EC with aluminum electrodes, the three with simultaneous sonication, followed by effluent recirculation through an electromagnet, clarification and ozonation in the presence of added H₂O₂ combined with UV radiation (O₃/H₂O₂/UV). AO aimed the degradation of organics and EC intended to remove suspended solids, heavy metals and phosphates. Sonication led to rapid formation, growth and collapse of cavitation bubbles that allowed additional pyrolytic organics degradation inside the bubbles. Along electrochemical treatments, pH increased from 3.7 to 7.6 probably due to the degradation of the polyphenols into phenols that exhibited an alkaline reaction. After electrochemical processes, 55% COD decay and more than 92% suspended solids, heavy metals and phosphate removal were attained. The further O₃/H₂O₂/UV treatment promoted higher degradation, with a removal of 77% at the end.

Most of the industrial cellulose bleaching processes are based on the use of ClO₂ (elementary chlorine free processes), with consequent production of toxic and poorly biodegradable organochlorinated by-products in bleaching effluents. Two kinds of bleaching effluents can be generated: (i) an acidic stream from the oxidation stages with ClO₂, and (ii) an alkaline one as a result of alkaline extraction enhanced with oxygen and H₂O₂ [207]. Both acidic and alkaline wastewaters were treated by Salazar et al. [207] utilizing a first filtration process like UF, nanofiltration (NF) or RO, followed by an AO-H₂O₂ method with a RuO₂ DSA or a BDD anode and a carbon-PTFE air-diffusion cathode. The main characteristics of wastewaters were pH of 2.5 and 10.5, DOC of 499 and 594 mg L⁻¹, BOD₅/COD ratio of 0.5 and 0.4, chloride concentration of 488 and 350 mg L⁻¹ and moderate/high conductivity of 5920 and 4410 μS cm⁻¹ for acidic and alkaline effluents, respectively. The best coupling in terms of mineralization was UF/AO-H₂O₂ for the acidic wastewater and NF/AO-H₂O₂ for the alkaline wastewater. Only the NF/H₂O₂ treatment for the alkaline wastewater entailed a real advantage compared to H₂O₂ alone in terms of mineralization. However, regarding energy consumption, the UF/AO-H₂O₂ coupling for the acidic effluent was advantageous as well. Mineralization was faster at low E_{cell} for the acidic wastewater

by the participation of active chlorine species and at high E_{cell} for alkaline wastewater since $\bullet\text{OH}$ production was favored. The DOC removal of both bleaching effluents by AO- H_2O_2 was faster using the BDD anode due to the higher oxidizing power of BDD($\bullet\text{OH}$) and fouling of RuO_2 DSA.

Dairy wastewaters are characterized by high contents of recalcitrant organic compounds such as refractory alcohols, carboxylic acids and indole derivatives, which can damage the natural waters in case of improper discharge [208]. Borbón et al. [209] focused on the treatment of a dairy wastewater with 1062 mg L^{-1} of DOC, a BOD_5/COD ratio of 0.4, alkaline pH, high suspended solids content and moderate ions amount, embracing $1131 \text{ mg chloride L}^{-1}$ and conveying in a moderate conductivity of $2360 \text{ }\mu\text{S cm}^{-1}$. A sequential two-step treatment was performed, involving (i) EC to remove solids, which employed an aluminum plate and a large surface iron mesh as monopolar anode and cathode, respectively, followed by (ii) AO to remove organics, in which an IrO_2 -tantalum pentoxide (Ta_2O_5) anode and a Pt wire cathode were used at j_{cat} of 30 mA cm^{-2} . A concentration of $0.5 \text{ g NaCl L}^{-1}$ was added to the wastewater before EC treatment in order to inhibit or slow down the anode passivation, typically observed for aluminum.

Tannery wastewaters are composed of high amounts of organics, which result from hides and skins and from the addition of reagents during the different operations made on these materials, and also by inorganic contaminants such as ammonia, sulfides and heavy metals [210]. Comparison of tannery wastewater treatment by EC, AO, EF, PEF-UVA and combination of EC followed by PEF-UVA was accomplished by Isarain-Chávez et al. [211]. EC employed iron electrodes, AO used a BDD/iron plate cell and EF and PEF-UVA resorted to a BDD/BDD one with air bubbling to produce H_2O_2 at the cathode. The tannery wastewater was characterized by average DOC of 1875 mg L^{-1} , BOD_5/COD ratio of only 0.05, acidic pH, moderate chloride content of 1239 mg L^{-1} and high conductivity of $7700 \text{ }\mu\text{S cm}^{-1}$. The mineralization ability of individual processes dropped in the order $\text{PEF-UVA} > \text{EF} \approx \text{EC} > \text{AO}$. DOC removal of 74% and 80% were achieved after 180 min of EC and PEF-UVA, respectively, whereas the combined process attained 90% DOC abatement after 180 min of each process.

Table 1.10. Examples on the treatment of other real wastewaters by EAOPs.

Pollutant	Wastewater characteristics	Process	Electrochemical reactor		Operational parameters (Maximal DOC decay ^a)	Ref.	
			Configuration	V (L)			
Winery wastewater	Raw COD (mg O ₂ L ⁻¹) = 10240 C (μS cm ⁻¹) = 1100 TSS (mg L ⁻¹) = 2860 pH = 3.7 [Total iron] (mg L ⁻¹) = 17 [SO ₄ ²⁻] (mg L ⁻¹) = 187 [NH ₄ ⁺] (mg L ⁻¹) = 5.4 [PO ₄ ³⁻] (mg L ⁻¹) = 7.5 in 2.0 g NaCl L ⁻¹	AO + EC (Fe, Al) (3 treatments in parallel with sonication) + Electromagnetization + Clarification + O ₃ /H ₂ O ₂ /UV	UC	8	Anode: SS Cathode: SS Operate in galvanostatic mode <i>Q</i> : Sonication pH: 3.7 (n.a.)	[117]	
		Cellulose bleaching wastewater	Acidic DOC (mg L ⁻¹) 499 COD (mg O ₂ L ⁻¹) 1250 BOD ₅ (mg O ₂ L ⁻¹) 563 C (μS cm ⁻¹) 5920 pH 2.5 [Cl ⁻] (mg L ⁻¹) 488	Alkaline 594 1500 595 4410 10.5 350	Filtration (UF, NF or RO) + AO-H ₂ O ₂	UC	0.2
Dairy wastewater or indole derivative	Raw DOC (mg L ⁻¹) 1062 COD (mg O ₂ L ⁻¹) 3859 BOD ₅ (mg O ₂ L ⁻¹) 1517 C (μS cm ⁻¹) 2360 TSS (mg L ⁻¹) >1988 pH 8.3 [Cl ⁻] (mg L ⁻¹) 1131 [NH ₄ ⁺] (mg L ⁻¹) 177 [NO ₂ ⁻] (mg L ⁻¹) 0.4 [NO ₃ ⁻] (mg L ⁻¹) 1.5 in 0.5 g NaCl L ⁻¹	Electrocoagulated 198 395 n.m. n.m. n.m. 890 n.m. n.m. n.m.	EC + AO	UC	0.1	Anode (dairy wastewater): DAS-IrO ₂ -Ta ₂ O ₅ (6.6 cm ²) Anode (indole solution): DSA-IrO ₂ -Ta ₂ O ₅ (2.5 cm ²) Cathode: Pt wire <i>j_{cat}</i> (dairy wastewater): 30 mA cm ⁻² <i>j_{cat}</i> (indole solution): 4-80 mA cm ⁻² <i>Q</i> : MS T: 25 °C pH (dairy wastewater): 8.3 pH (indole solution): 3.0 or 8.0 (85%)	[209]
		Tannery wastewater	DOC (mg L ⁻¹) = 1800-1950 COD (mg O ₂ L ⁻¹) = 9922-10180 BOD ₅ (mg O ₂ L ⁻¹) = 528 C (μS cm ⁻¹) = 6300-9100 TSS (mg L ⁻¹) = 445-530 pH = 3.7-4.3 [Total iron] (mg L ⁻¹) = 2.0-2.8 [Cl ⁻] (mg L ⁻¹) = 1239	EC AO EF PEF-UVA EC + PEF-UVA	UC	0.25	Anode: BDD (7.6 cm ²) Cathode (AO): Iron plate (7.6 cm ²) Cathode (EF, PEF-UVA): BDD with air bubbling (7.6 cm ²) <i>j_{cat}</i> : 65 or 111 mA cm ⁻² <i>Q</i> : MS T: Amb. pH (AO): ≈ 4.0 pH (EF, PEF-UVA): 3.0 [TDI] ₀ (AO): n.s. [TDI] ₀ (EF, PEF-UVA): 56 or 167 mg L ⁻¹ (90% – EC + PEF-UVA)

^a Under the best experimental conditions, when applicable;

Amb. – Ambient;

C-PTFE A-D – Carbon-PTFE air-diffusion;

MS – Magnetic stirring;

n.m. – not measured;

n.s. – not specified;

Q – Liquid flow rate;

UC – Undivided cell.

1.7 Objectives and outline of the thesis

The present thesis focuses on the technical feasibility of applying EAOPs to the degradation of recalcitrant compounds from various synthetic and real wastewaters. The following five EAOPs were considered: AO, AO-H₂O₂, EF, PEF and SPEF. Two synthetic solutions were employed, one polluted with Sunset Yellow FCF azo dye and the other with trimethoprim antibiotic. Both pollutants were diluted in an aqueous solution with 7.0 g Na₂SO₄ L⁻¹. The real effluents included a wastewater collected after secondary treatment of a MWWTP, a winery wastewater and a municipal sanitary landfill leachate. Due to the complexity of the winery wastewater and the landfill leachate, the feasibility of combining EAOPs with conventional technologies was assessed.

Two main objectives were addressed:

- (i) Assessment of the efficiency of the various EAOPs for recalcitrant compounds degradation, mainly in terms of mineralization and pollutants concentration decay;
- (ii) Assessment of the influence of various operational variables on EAOPs efficiency, including the nature of the anode, j , [TDI]₀, pH, use of Fe(III)-carboxylate complexes, initial pollutants concentration, temperature and radiation source.

Additionally, other objectives were covered:

- (iii) Design and construction of two experimental units for EAOPs application: a 2.2 L capacity lab-scale flow plant and a 35 L capacity pilot-scale flow plant;
- (iv) Comparison between EAOPs and the analogous chemical processes;
- (v) Appraisal of feasibility of scaling-up from lab- to pilot-scale;
- (vi) Determination of by-products generated during the degradation of pollutants.

The thesis is structured in 9 chapters:

Chapter 1 corresponds to the present introductory section, wherein the problem of water pollution by recalcitrant organic compounds and the current and potential decontamination methods are covered. Emphasis is given to EAOPs, for which fundamentals and effects of various operational parameters are described, complemented with an exhaustive literature survey on the treatment of various synthetic and real wastewaters by these processes.

Chapter 2 describes all chemicals, analytical determinations, modeling of degradation kinetics, experimental setups and respective experimental procedures used within this thesis.

The experimental results are given from Chapter 3 to 8.

Chapter 3 focuses on the degradation of 290 mg L⁻¹ of Sunset Yellow FCF azo dye in an aqueous solution with 7.0 g Na₂SO₄ L⁻¹ by AO-H₂O₂, EF, PEF-UVA and SPEF processes. The influence of j on the efficiency of the various processes was evaluated. The scale-up from lab- to pilot-scale as well as the nature of the anode were also assessed. Aromatic by-products and LMCA were identified during the dye degradation and a reaction sequence was proposed.

Chapter 4 reports the degradation of 20.0 mg L⁻¹ of trimethoprim antibiotic in an aqueous solution with 7.0 g Na₂SO₄ L⁻¹ by AO-H₂O₂, EF, PEF-UVA and SPEF processes, as well as by the classical Fenton and PF-UVA processes. The effect of the nature of the anode, [TDI]₀, j and pH on the oxidation ability of processes was assessed. The scale-up from lab- to pilot-scale was appraised and aromatic intermediates and LMCA generated during the degradation of the antibiotic were identified. Moreover, the efficiency of EAOPs using a real wastewater collected after secondary treatment in a MWWTP spiked with TMP at mg L⁻¹ levels or 19 pharmaceutical compounds at µg L⁻¹ levels was assessed.

Chapter 5 discloses the feasibility of using a PEF-UVA process assisted by Fe(III)-carboxylate complexes for the degradation of the pure trimethoprim solution used in Chapter 4. Various carboxylate ligands like oxalate, citrate, tartrate and malate were used and the effect of the initial Fe(III)-to-carboxylate molar ratio and pH on the process efficiency was also determined. Additionally, the effect of initial contaminant content and solution temperature as well as the role of the different reactive oxidizing species were clarified.

Chapter 6 reports the remediation of a winery wastewater by applying a biological oxidation to mineralize the biodegradable organic fraction followed by an EAOP to oxidize the refractory molecules or transform them into simpler ones that can be further biodegraded. The efficiency of AO-H₂O₂, EF, PEF-UVA and SPEF processes was assessed as well as the influence of [TDI]₀ and j on the degradation kinetics. Respirometry tests were applied to determine the biodegradability enhancement along the EAOP stage.

Chapter 7 focuses on the assessment of the technical feasibility of including EAOPs in a multistage strategy for the remediation of a sanitary landfill leachate that comprises the following steps: (i) initial biological process for removal of biodegradable organic compounds, nitrification/denitrification reactions and alkalinity reduction, (ii) coagulation with subsequent separation of the formed sludge for the removal of humic acids, suspended solids and other species filtering the radiation, and (iii) EAOP for recalcitrant compounds degradation and biodegradability enhancement so that a second biological process for removal of biodegradable organics and nitrogen content could be applied. EF, PEF-UVA and SPEF processes were tested as EAOP and their oxidation ability was compared with the analogous chemical processes. The influence of j on the degradation efficiency was also assessed. A Zahn-Wellens test was applied to determine the biodegradability enhancement during the EAOP stage and define the ideal organics oxidation state to stop it and apply the second biological treatment.

In Chapter 8, the influence of various parameters on the degradation of the landfill leachate used in Chapter 7 by EF, PEF and SPEF processes was assessed. The following parameters were studied: anode material, $[TDI]_0$, pH, use of Fe(III)-carboxylate complexes, temperature and radiation source.

Finally, Chapter 9 displays a discussion of the most pertinent results and conclusions of this thesis and a list of subsequent suggestions for future work.

1.8 References

- [1] Zollinger, H., 2003. *Color Chemistry: Syntheses, Properties, and Applications of Organic Dyes and Pigments*, 3rd, revised ed., VHCA and Wiley-VCH, Zurich, Switzerland/Weinheim, Germany.
- [2] Sharma, K.P., Sharma, S., Sharma, S., Singh, P.K., Kumar, S., Grover, R., Sharma, P.K., 2007. A comparative study on characterization of textile wastewaters (untreated and treated) toxicity by chemical and biological tests. *Chemosphere* 69(1), 48-54.
- [3] Kümmerer, K., 2009. The presence of pharmaceuticals in the environment due to human use – Present knowledge and future challenges. *Journal of Environmental Management* 90(8), 2354-2366.
- [4] Damalas, C.A., Eleftherohorinos, I.G., 2011. Pesticide exposure, safety issues, and risk assessment indicators. *International Journal of Environmental Research and Public Health* 8(5), 1402-1419.
- [5] Hunger, K. (ed) 2003. *Industrial Dyes, Chemistry, Properties, Applications*, Wiley-VCH, Weinheim, Germany.
- [6] Forgacs, E., Cserháti, T., Oros, G., 2004. Removal of synthetic dyes from wastewaters: A review. *Environment International* 30(7), 953-971.
- [7] Kümmerer, K., 2001. Drugs in the environment: Emission of drugs, diagnostic aids and disinfectants into wastewater by hospitals in relation to other sources – A review. *Chemosphere* 45(6-7), 957-969.
- [8] Tchobanoglous, G., Kreith, F., 2002. *Handbook of Solid Waste Management*, 2nd ed., McGraw-Hill, New York, United States.
- [9] Chan, Y.J., Chong, M.F., Law, C.L., Hassell, D.G., 2009. A review on anaerobic-aerobic treatment of industrial and municipal wastewater. *Chemical Engineering Journal* 155(1-2), 1-18.
- [10] Homem, V., Santos, L., 2011. Degradation and removal methods of antibiotics from aqueous matrices – A review. *Journal of Environmental Management* 92(10), 2304-2347.
- [11] Wiszniowski, J., Robert, D., Surmacz-Gorska, J., Miksch, K., Weber, J.V., 2006. Landfill leachate treatment methods: A review. *Environmental Chemistry Letters* 4(1), 51-61.
- [12] Dionysiou, D.D., Suidan, M.T., Baudin, I., Laîné, J.-M., 2004. Effect of hydrogen peroxide on the destruction of organic contaminants-synergism and inhibition in a continuous-mode photocatalytic reactor. *Applied Catalysis B: Environmental* 50(4), 259-269.
- [13] Vaid, R., Linton, R.H., Morgan, M.T., 2010. Comparison of inactivation of *Listeria monocytogenes* within a biofilm matrix using chlorine dioxide gas, aqueous chlorine dioxide and sodium hypochlorite treatments. *Food Microbiology* 27(8), 979-984.
- [14] Ivancev-Tumbas, I., Dalmacija, B., Tamas, Z., Karlovic, E., 1999. The effect of different drinking water treatment processes on the rate of chloroform formation in the reactions of natural organic matter with hypochlorite. *Water Research* 33(18), 3715-3722.

- [15] Oturan, M.A., Aaron, J.J., 2014. Advanced oxidation processes in water/wastewater treatment: Principles and applications. A review. *Critical Reviews in Environmental Science and Technology* 44(23), 2577-2641.
- [16] Glaze, W.H., Kang, J.-W., Chapin, D.H., 1987. The chemistry of water treatment processes involving ozone, hydrogen peroxide and ultraviolet radiation. *Ozone Science and Engineering* 9(4), 335-352.
- [17] Latimer, W.M., 1952. *Oxidation Potentials*, 2nd ed., Prentice-Hall, New York, United States.
- [18] Buxton, G.V., Greenstock, C.L., Helman, W.P., Ross, A.B., 1988. Critical review of rate constants for reactions of hydrated electrons, hydrogen atoms and hydroxyl radicals ($\cdot\text{OH}/\text{O}^-$) in aqueous solution. *Journal of Physical and Chemical Reference Data* 17(2), 513-886.
- [19] Janzen, E.G., Kotake, Y., Hinton, R.D., 1992. Stabilities of hydroxyl radical spin adducts of PBN-type spin traps. *Free Radical Biology & Medicine* 12(2), 169-173.
- [20] Suty, H., De Traversay, C., Cost, M., 2004. Applications of advanced oxidation processes: present and future. *Water Science & Technology* 49(4), 227-233.
- [21] Chong, M.N., Sharma, A.K., Burn, S., Saint, C.P., 2012. Feasibility study on the application of advanced oxidation technologies for decentralised wastewater treatment. *Journal of Cleaner Production* 35, 230-238.
- [22] Comninellis, C., Kapalka, A., Malato, S., Parsons, S.A., Poulios, I., Mantzavinos, D., 2008. Advanced oxidation processes for water treatment: Advances and trends for R&D. *Journal of Chemical Technology and Biotechnology* 83(6), 769-776.
- [23] Brillas, E., Sirés, I., Oturan, M.A., 2009. Electro-Fenton process and related electrochemical technologies based on Fenton's reaction chemistry. *Chemical Reviews* 109(12), 6570-6631.
- [24] Barrera-Díaz, C., Cañizares, P., Fernández, F.J., Natividad, R., Rodrigo, M.A., 2014. Electrochemical advanced oxidation processes: An overview of the current applications to actual industrial effluents. *Journal of the Mexican Chemical Society* 58(3), 256-275.
- [25] Chaplin, B.P., 2014. Critical review of electrochemical advanced oxidation processes for water treatment applications. *Environmental Sciences: Processes and Impacts* 16(6), 1182-1203.
- [26] Martínez-Huitle, C.A., Ferro, S., 2006. Electrochemical oxidation of organic pollutants for the wastewater treatment: Direct and indirect processes. *Chemical Society Reviews* 35, 1324-1340.
- [27] Panizza, M., Cerisola, G., 2009. Direct and mediated anodic oxidation of organic pollutants. *Chemical Reviews* 109(12), 6541-6569.
- [28] Brillas, E., Garrido, J.A., Rodríguez, R.M., Arias, C., Cabot, P.L., Centellas, F., 2008. Wastewaters by electrochemical advanced oxidation processes using a BDD anode and electrogenerated H_2O_2 with Fe(II) and UVA light as catalysts. *Portugaliae Electrochimica Acta* 26(1), 15-46.
- [29] Ganzenko, O., Huguenot, D., van Hullebusch, E.D., Esposito, G., Oturan, M.A., 2014. Electrochemical advanced oxidation and biological processes for wastewater treatment: A review of the combined approaches. *Environmental Science and Pollution Research* 21(14), 8493-8524.

- [30] Sirés, I., Brillas, E., Oturan, M., Rodrigo, M., Panizza, M., 2014. Electrochemical advanced oxidation processes: today and tomorrow. A review. *Environmental Science and Pollution Research* 21(14), 8336-8367.
- [31] Brillas, E., Martínez-Huitle, C.A., 2015. Decontamination of wastewaters containing synthetic organic dyes by electrochemical methods. An updated review. *Applied Catalysis B: Environmental* 166-167, 603-643.
- [32] Urtiaga, A.M., Pérez, G., Ibáñez, R., Ortiz, I., 2013. Removal of pharmaceuticals from a WWTP secondary effluent by ultrafiltration/reverse osmosis followed by electrochemical oxidation of the RO concentrate. *Desalination* 331, 26-34.
- [33] Thiam, A., Zhou, M., Brillas, E., Sirés, I., 2014. Two-step mineralization of Tartrazine solutions: Study of parameters and by-products during the coupling of electrocoagulation with electrochemical advanced oxidation processes. *Applied Catalysis B: Environmental* 150-151, 116-125.
- [34] Comninellis, C., 1994. Electrocatalysis in the electrochemical conversion/combustion of organic pollutants for waste water treatment. *Electrochimica Acta* 39(11), 1857-1862.
- [35] Marselli, B., Garcia-Gomez, J., Michaud, P.A., Rodrigo, M.A., Comninellis, C., 2003. Electrogeneration of hydroxyl radicals on boron-doped diamond electrodes. *Journal of the Electrochemical Society* 150, D79-D83.
- [36] Sopaj, F., Rodrigo, M.A., Oturan, N., Podvorica, F.I., Pinson, J., Oturan, M.A., 2015. Influence of the anode materials on the electrochemical oxidation efficiency. Application to oxidative degradation of the pharmaceutical amoxicillin. *Chemical Engineering Journal* 262, 286-294.
- [37] Brillas, E., Martínez-Huitle, C.A., 2011. *Synthetic Diamond Films: Preparation, Electrochemistry, Characterization, and Applications*, John Wiley & Sons, Inc., New Jersey, United States.
- [38] Panizza, M., Cerisola, G., 2006. *Advances in Chemistry Research*, Vol. 2. Zinger, D.V. (ed), Nova Science, New York, United States, pp. 1-38.
- [39] Harris, D.C., 2009. *Exploring Chemical Analysis*, 4th ed., W. H. Freeman and Company, New York, United States.
- [40] Boxall, C., Kelsall, G.H., 1992. Hypochlorite electrogeneration. 2. Thermodynamics and kinetic-model of the anode reaction layer, Institution of Chemical Engineers, Rugby, United Kingdom, pp. 59-70.
- [41] Martínez-Huitle, C.A., Brillas, E., 2009. Decontamination of wastewaters containing synthetic organic dyes by electrochemical methods: A general review. *Applied Catalysis B: Environmental* 87(3-4), 105-145.
- [42] Sánchez-Carretero, A., Sáez, C., Cañizares, P., Rodrigo, M.A., 2011. Electrochemical production of perchlorates using conductive diamond electrolyses. *Chemical Engineering Journal* 166(2), 710-714.
- [43] Brown, G.M., Gu, B., 2006. Perchlorate. *Environmental Occurrence, Interactions and Treatment*, Chapter 2. Gu, B. and Coates, J.B. (eds), Springer, New York, United States, pp. 17-47.
- [44] Zhang, C., Wang, J., Murakami, T., Fujishima, A., Fu, D., Gu, Z., 2010. Influence of cations during Orange-II degradation on boron-doped diamond electrode. *Journal of Electroanalytical Chemistry* 638(1), 91-99.

- [45] Gomes, L., Miwa, D.W., Malpass, G.R.P., Motheo, A.J., 2011. Electrochemical degradation of the dye Reactive Orange 16 using electrochemical flow-cell. *Journal of the Brazilian Chemical Society* 22, 1299-1306.
- [46] Chiang, L.-C., Chang, J.-E., Wen, T.-C., 1995. Indirect oxidation effect in electrochemical oxidation treatment of landfill leachate. *Water Research* 29(2), 671-678.
- [47] Anglada, A., Urtiaga, A., Ortiz, I., Mantzavinos, D., Diamadopoulos, E., 2011. Boron-doped diamond anodic treatment of landfill leachate: Evaluation of operating variables and formation of oxidation by-products. *Water Research* 45(2), 828-838.
- [48] Bagastyo, A.Y., Batstone, D.J., Kristiana, I., Gernjak, W., Joll, C., Radjenovic, J., 2012. Electrochemical oxidation of reverse osmosis concentrate on boron-doped diamond anodes at circumneutral and acidic pH. *Water Research* 46(18), 6104-6112.
- [49] Cañizares, P., Sáez, C., Lobato, J., Rodrigo, M.A., 2004. Electrochemical oxidation of polyhydroxybenzenes on boron-doped diamond anodes. *Industrial & Engineering Chemistry Research* 43(21), 6629-6637.
- [50] Cañizares, P., Gadri, A., Lobato, J., Nasr, B., Paz, R., Rodrigo, M.A., Saez, C., 2006. Electrochemical oxidation of azoic dyes with conductive-diamond anodes. *Industrial & Engineering Chemistry Research* 45(10), 3468-3473.
- [51] Foller, P.C., Bombard, R.T., 1995. Processes for the production of mixtures of caustic soda and hydrogen peroxide via the reduction of oxygen. *Journal of Applied Electrochemistry* 25(7), 613-627.
- [52] Brillas, E., Maestro, A., Moratalla, M., Casado, J., 1997. Electrochemical extraction of oxygen from air via hydroperoxide ion. *Journal of Applied Electrochemistry* 27(1), 83-92.
- [53] Drogui, P., Elmaleh, S., Rumeau, M., Bernard, C., Rambaud, A., 2001. Oxidising and disinfecting by hydrogen peroxide produced in a two-electrode cell. *Water Research* 35(13), 3235-3241.
- [54] Gallegos, A.A., García, Y.V., Zamudio, A., 2005. Solar hydrogen peroxide. *Solar Energy Materials and Solar Cells* 88(2), 157-167.
- [55] Brillas, E., Bastida, R.M., Llosa, E., Casado, J., 1995. Electrochemical destruction of aniline and 4-chloroaniline for wastewater treatment using a carbon-PTFE O₂-fed cathode. *Journal of the Electrochemical Society* 142(6), 1733-1741.
- [56] Brillas, E., Boye, B., Ángel Baños, M., Calpe, J.C., Garrido, J.A., 2003. Electrochemical degradation of chlorophenoxy and chlorobenzoic herbicides in acidic aqueous medium by the peroxi-coagulation method. *Chemosphere* 51(4), 227-235.
- [57] Garcia-Segura, S., Salazar, R., Brillas, E., 2013. Mineralization of phthalic acid by solar photoelectro-Fenton with a stirred boron-doped diamond/air-diffusion tank reactor: Influence of Fe³⁺ and Cu²⁺ catalysts and identification of oxidation products. *Electrochimica Acta* 113, 609-619.
- [58] Oturan, M.A., Oturan, N., Edelahe, M.C., Podvorica, F.I., Kacemi, K.E., 2011. Oxidative degradation of herbicide diuron in aqueous medium by Fenton's reaction based advanced oxidation processes. *Chemical Engineering Journal* 171(1), 127-135.
- [59] Zhou, M., Tan, Q., Wang, Q., Jiao, Y., Oturan, N., Oturan, M.A., 2012. Degradation of organics in reverse osmosis concentrate by electro-Fenton process. *Journal of Hazardous Materials* 215-216, 287-293.

- [60] Özcan, A., Şahin, Y., Savaş Koparal, A., Oturan, M.A., 2008. Carbon sponge as a new cathode material for the electro-Fenton process: Comparison with carbon felt cathode and application to degradation of synthetic dye Basic Blue 3 in aqueous medium. *Journal of Electroanalytical Chemistry* 616(1-2), 71-78.
- [61] Özcan, A., Şahin, Y., Koparal, A.S., Oturan, M.A., 2009. A comparative study on the efficiency of electro-Fenton process in the removal of prophan from water. *Applied Catalysis B: Environmental* 89(3-4), 620-626.
- [62] Lei, H., Li, H., Li, Z., Li, Z., Chen, K., Zhang, X., Wang, H., 2010. Electro-Fenton degradation of Cationic Red X-GRL using an activated carbon fiber cathode. *Process Safety and Environmental Protection* 88(6), 431-438.
- [63] Wang, A., Li, Y.-Y., Estrada, A.L., 2011. Mineralization of antibiotic sulfamethoxazole by photoelectro-Fenton treatment using activated carbon fiber cathode and under UVA irradiation. *Applied Catalysis B: Environmental* 102(3-4), 378-386.
- [64] Zarei, M., Niaei, A., Salari, D., Khataee, A., 2010. Application of response surface methodology for optimization of peroxi-coagulation of textile dye solution using carbon nanotube-PTFE cathode. *Journal of Hazardous Materials* 173(1-3), 544-551.
- [65] Khataee, A.R., Zarei, M., Khataee, A.R., 2011. Electrochemical treatment of dye solution by oxalate catalyzed photoelectro-Fenton process using a carbon nanotube-PTFE cathode: Optimization by central composite design. *Clean - Soil, Air, Water* 39(5), 482-490.
- [66] El-Desoky, H.S., Ghoneim, M.M., Zidan, N.M., 2010. Decolorization and degradation of Ponceau S azo-dye in aqueous solutions by the electrochemical advanced Fenton oxidation. *Desalination* 264(1-2), 143-150.
- [67] Ghoneim, M.M., El-Desoky, H.S., Zidan, N.M., 2011. Electro-Fenton oxidation of Sunset Yellow FCF azo-dye in aqueous solutions. *Desalination* 274(1-3), 22-30.
- [68] Domínguez, J.R., González, T., Palo, P., Sánchez-Martín, J., 2010. Anodic oxidation of ketoprofen on boron-doped diamond (BDD) electrodes. Role of operative parameters. *Chemical Engineering Journal* 162(3), 1012-1018.
- [69] García, O., Isarain-Chávez, E., Garcia-Segura, S., Brillas, E., Peralta-Hernández, J.M., 2013. Degradation of 2,4-dichlorophenoxyacetic acid by electro-oxidation and electro-Fenton/BDD processes using a pre-pilot plant. *Electrocatalysis* 4(4), 224-234.
- [70] Campos-Martin, J.M., Blanco-Brieva, G., Fierro, J.L.G., 2006. Hydrogen peroxide synthesis: An outlook beyond the anthraquinone process. *Angewandte Chemie International Edition* 45(42), 6962-6984.
- [71] Pletcher, D., 1999. Indirect oxidation using electrogenerated hydrogen peroxide. *Acta Chemica Scandinavica* 53, 745-750.
- [72] Fenton, H.J.H., 1894. LXXIII.-Oxidation of tartaric acid in presence of iron. *Journal of the Chemical Society, Transactions* 65, 899-910.
- [73] Haber, F., Weiss, J., 1934. The Catalytic Decomposition of Hydrogen Peroxide by Iron Salts. *Proceedings of the Royal Society of London. Series A, Mathematical and Physical Sciences* 147(861), 332-351.
- [74] Sun, Y., Pignatello, J.J., 1993. Photochemical reactions involved in the total mineralization of 2,4-D by $\text{Fe}^{3+}/\text{H}_2\text{O}_2/\text{UV}$. *Environmental Science & Technology* 27(2), 304-310.

- [75] Bouafia-Chergui, S., Oturan, N., Khalaf, H., Oturan, M.A., 2010. Parametric study on the effect of the ratios $[H_2O_2]/[Fe^{3+}]$ and $[H_2O_2]/[substrate]$ on the photo-Fenton degradation of cationic azo dye Basic Blue 41. *Journal of Environmental Science and Health - Part A Toxic/Hazardous Substances and Environmental Engineering* 45(5), 622-629.
- [76] Malato, S., Fernández-Ibáñez, P., Maldonado, M.I., Blanco, J., Gernjak, W., 2009. Decontamination and disinfection of water by solar photocatalysis: Recent overview and trends. *Catalysis Today* 147(1), 1-59.
- [77] Brillas, E., Calpe, J.C., Casado, J., 2000. Mineralization of 2,4-D by advanced electrochemical oxidation processes. *Water Research* 34(8), 2253-2262.
- [78] Oturan, M.A., 2000. An ecologically effective water treatment technique using electrochemically generated hydroxyl radicals for in situ destruction of organic pollutants: Application to herbicide 2,4-D. *Journal of Applied Electrochemistry* 30(4), 475-482.
- [79] Isarain-Chávez, E., Arias, C., Cabot, P.L., Centellas, F., Rodríguez, R.M., Garrido, J.A., Brillas, E., 2010. Mineralization of the drug beta-blocker atenolol by electro-Fenton and photoelectro-Fenton using an air-diffusion cathode for H_2O_2 electrogeneration combined with a carbon-felt cathode for Fe^{2+} regeneration. *Applied Catalysis B: Environmental* 96(3-4), 361-369.
- [80] Brillas, E., Sauleda, R., Casado, J., 1997. Peroxi-coagulation of aniline in acidic medium using an oxygen diffusion cathode. *Journal of the Electrochemical Society* 144(7), 2374-2379.
- [81] Huang, Y.-H., Huang, G.-H., Lee, S.-N., Lin, S.-M., inventors. Industrial Technology Research Institute, assignee. Method of wastewater treatment by electrolysis and oxidization. United States Patent 6126838 A. 2000 October 3.
- [82] Pratap, K., Lemley, A.T., 1994. Electrochemical peroxide treatment of aqueous herbicide solutions. *Journal of Agricultural and Food Chemistry* 42(1), 209-215.
- [83] Scudato, R.J., Chiarenzelli, J.R., inventors. The Research Foundation of State University of New York, assignee. Electrochemical peroxidation of contaminated liquids and slurries. United States Patent 6045707 A. 2000
- [84] Saltmiras, D.A., Lemley, A.T., 2000. Degradation of ethylene thiourea (ETU) with three Fenton treatment processes. *Journal of Agricultural and Food Chemistry* 48(12), 6149-6157.
- [85] Brillas, E., Sauleda, R., Casado, J., 1998. Degradation of 4-chlorophenol by anodic oxidation, electro-Fenton, photoelectro-Fenton, and peroxi-coagulation processes. *Journal of the Electrochemical Society* 145(3), 759-765.
- [86] Boye, B., Dieng, M.M., Brillas, E., 2003. Anodic oxidation, electro-Fenton and photoelectro-Fenton treatments of 2,4,5-trichlorophenoxyacetic acid. *Journal of Electroanalytical Chemistry* 557, 135-146.
- [87] Flox, C., Cabot, P.L., Centellas, F., Garrido, J.A., Rodríguez, R.M., Arias, C., Brillas, E., 2007. Solar photoelectro-Fenton degradation of cresols using a flow reactor with a boron-doped diamond anode. *Applied Catalysis B: Environmental* 75(1-2), 17-28.
- [88] Salazar, R., Garcia-Segura, S., Ureta-Zañartu, M.S., Brillas, E., 2011. Degradation of disperse azo dyes from waters by solar photoelectro-Fenton. *Electrochimica Acta* 56(18), 6371-6379.
- [89] Almeida, L.C., Garcia-Segura, S., Arias, C., Bocchi, N., Brillas, E., 2012. Electrochemical mineralization of the azo dye Acid Red 29 (Chromotrope 2R) by photoelectro-Fenton process. *Chemosphere* 89(6), 751-758.

- [90] Garcia-Segura, S., Cavalcanti, E.B., Brillas, E., 2014. Mineralization of the antibiotic chloramphenicol by solar photoelectro-Fenton. From stirred tank reactor to solar pre-pilot plant. *Applied Catalysis B: Environmental* 144, 588-598.
- [91] Thiam, A., Sirés, I., Brillas, E., 2015. Treatment of a mixture of food color additives (E122, E124 and E129) in different water matrices by UVA and solar photoelectro-Fenton. *Water Research* 81, 178-187.
- [92] Horváth, O., Stevenson, K.L., 1992. *Charge Transfer Photochemistry of Coordination Compounds*, VCH, New York, United States.
- [93] Zuo, Y., Hoigne, J., 1992. Formation of hydrogen peroxide and depletion of oxalic acid in atmospheric water by photolysis of iron(III)-oxalato complexes. *Environmental Science & Technology* 26(5), 1014-1022.
- [94] Faust, B.C., Zepp, R.G., 1993. Photochemistry of aqueous iron(III)-polycarboxylate complexes: Roles in the chemistry of atmospheric and surface waters. *Environmental Science & Technology* 27(12), 2517-2522.
- [95] Baxendale, J.H., Wilson, J.A., 1957. The photolysis of hydrogen peroxide at high light intensities. *Transactions of the Faraday Society* 53, 344-356.
- [96] Venkatadri, R., Peters, R.W., 1993. Chemical oxidation technologies: ultraviolet light/hydrogen peroxide, Fenton's reagent, and titanium dioxide-assisted photocatalysis. *Hazardous Waste and Hazardous Materials* 10(2), 107-149.
- [97] Flox, C., Ammar, S., Arias, C., Brillas, E., Vargas-Zavala, A.V., Abdelhedi, R., 2006. Electro-Fenton and photoelectro-Fenton degradation of Indigo Carmine in acidic aqueous medium. *Applied Catalysis B: Environmental* 67(1-2), 93-104.
- [98] Borràs, N., Arias, C., Oliver, R., Brillas, E., 2013. Anodic oxidation, electro-Fenton and photoelectro-Fenton degradation of cyanazine using a boron-doped diamond anode and an oxygen-diffusion cathode. *Journal of Electroanalytical Chemistry* 689, 158-167.
- [99] El-Ghenymy, A., Oturan, N., Oturan, M.A., Garrido, J.A., Cabot, P.L., Centellas, F., Rodríguez, R.M., Brillas, E., 2013. Comparative electro-Fenton and UVA photoelectro-Fenton degradation of the antibiotic sulfanilamide using a stirred BDD/air-diffusion tank reactor. *Chemical Engineering Journal* 234, 115-123.
- [100] Lin, Y.-T., Liang, C., Chen, J.-H., 2011. Feasibility study of ultraviolet activated persulfate oxidation of phenol. *Chemosphere* 82(8), 1168-1172.
- [101] Oliver, B.G., Carey, J.H., 1977. Photochemical production of chlorinated organics in aqueous solutions containing chlorine. *Environmental Science & Technology* 11(9), 893-895.
- [102] Flox, C., Garrido, J.A., Rodríguez, R.M., Cabot, P.L., Centellas, F., Arias, C., Brillas, E., 2007. Mineralization of herbicide mecoprop by photoelectro-Fenton with UVA and solar light. *Catalysis Today* 129(1-2 Spec. Iss.), 29-36.
- [103] Hammami, S., Oturan, N., Bellakhal, N., Dachraoui, M., Oturan, M.A., 2007. Oxidative degradation of Direct Orange 61 by electro-Fenton process using a carbon felt electrode: Application of the experimental design methodology. *Journal of Electroanalytical Chemistry* 610(1), 75-84.
- [104] Isarain-Chávez, E., Rodríguez, R.M., Garrido, J.A., Arias, C., Centellas, F., Cabot, P.L., Brillas, E., 2010. Degradation of the beta-blocker propranolol by electrochemical advanced

oxidation processes based on Fenton's reaction chemistry using a boron-doped diamond anode. *Electrochimica Acta* 56(1), 215-221.

[105] El-Ghenymy, A., Rodríguez, R.M., Arias, C., Centellas, F., Garrido, J.A., Cabot, P.L., Brillas, E., 2013. Electro-Fenton and photoelectro-Fenton degradation of the antimicrobial sulfamethazine using a boron-doped diamond anode and an air-diffusion cathode. *Journal of Electroanalytical Chemistry* 701, 7-13.

[106] Labiadh, L., Oturan, M.A., Panizza, M., Hamadi, N.B., Ammar, S., 2015. Complete removal of AHPS synthetic dye from water using new electro-Fenton oxidation catalyzed by natural pyrite as heterogeneous catalyst. *Journal of Hazardous Materials* 297, 34-41.

[107] Iranifam, M., Zarei, M., Khataee, A.R., 2011. Decolorization of C.I. Basic Yellow 28 solution using supported ZnO nanoparticles coupled with photoelectro-Fenton process. *Journal of Electroanalytical Chemistry* 659(1), 107-112.

[108] Wu, J., Zhang, H., Oturan, N., Wang, Y., Chen, L., Oturan, M.A., 2012. Application of response surface methodology to the removal of the antibiotic tetracycline by electrochemical process using carbon-felt cathode and DSA (Ti/RuO₂-IrO₂) anode. *Chemosphere* 87(6), 614-620.

[109] Khataee, A., Marandizadeh, H., Zarei, M., Aber, S., Vahid, B., Hanifehpour, Y., Joo, S.W., 2013. Treatment of an azo dye by citrate catalyzed photoelectro-Fenton process under visible light using carbon nanotube-polytetrafluoroethylene cathode. *Current Nanoscience* 9(3), 387-393.

[110] Hamza, M., Abdelhedi, R., Brillas, E., Sirés, I., 2009. Comparative electrochemical degradation of the triphenylmethane dye Methyl Violet with boron-doped diamond and Pt anodes. *Journal of Electroanalytical Chemistry* 627(1-2), 41-50.

[111] Cavalcanti, E.B., Segura, S.G., Centellas, F., Brillas, E., 2013. Electrochemical incineration of omeprazole in neutral aqueous medium using a platinum or boron-doped diamond anode: Degradation kinetics and oxidation products. *Water Research* 47(5), 1803-1815.

[112] Da Silva, L.M., Gonçalves, I.C., Teles, J.J.S., Franco, D.V., 2014. Application of oxide fine-mesh electrodes composed of Sb-SnO₂ for the electrochemical oxidation of Cibacron Marine FG using an SPE filter-press reactor. *Electrochimica Acta* 146, 714-732.

[113] Madsen, H.T., Søggaard, E.G., Muff, J., 2015. Reduction in energy consumption of electrochemical pesticide degradation through combination with membrane filtration. *Chemical Engineering Journal* 276, 358-364.

[114] Garcia-Segura, S., Brillas, E., 2014. Advances in solar photoelectro-Fenton: Decolorization and mineralization of the Direct Yellow 4 diazo dye using an autonomous solar pre-pilot plant. *Electrochimica Acta* 140, 384-395.

[115] Vargas, R., Díaz, S., Viele, L., Núñez, O., Borrás, C., Mostany, J., Scharifker, B.R., 2013. Electrochemical oxidation of dichlorvos on SnO₂-Sb₂O₅ electrodes. *Applied Catalysis B: Environmental* 144(1), 107-111.

[116] Oturan, M.A., Pimentel, M., Oturan, N., Sirés, I., 2008. Reaction sequence for the mineralization of the short-chain carboxylic acids usually formed upon cleavage of aromatics during electrochemical Fenton treatment. *Electrochimica Acta* 54(2), 173-182.

[117] Orescanin, V., Kollar, R., Nad, K., Mikelic, I.L., Gustek, S.F., 2013. Treatment of winery wastewater by electrochemical methods and advanced oxidation processes. *Journal of Environmental Science and Health - Part A Toxic/Hazardous Substances and Environmental Engineering* 48(12), 1543-1547.

- [118] Martell, A.E., Smith, R.M., 1974, 1975, 1976, 1977, 1982, 1989. *Critical Stability Constants*, Vols. 1-6, Plenum Press, New York, United States.
- [119] Neta, P., Huie, R.E., Ross, A.B., 1988. Rate constants for reactions for inorganic radicals in aqueous solution. *Journal of Physical and Chemical Reference Data Reprints* 17(3), 1027-1247.
- [120] De Laat, J., Truong Le, G., Legube, B., 2004. A comparative study of the effects of chloride, sulfate and nitrate ions on the rates of decomposition of H₂O₂ and organic compounds by Fe(II)/H₂O₂ and Fe(III)/H₂O₂. *Chemosphere* 55(5), 715-723.
- [121] Carvalho, C., Fernandes, A., Lopes, A., Pinheiro, H., Gonçalves, I., 2007. Electrochemical degradation applied to the metabolites of Acid Orange 7 anaerobic biotreatment. *Chemosphere* 67(7), 1316-1324.
- [122] Daneshvar, N., Aber, S., Vatanpour, V., Rasoulifard, M.H., 2008. Electro-Fenton treatment of dye solution containing Orange II: Influence of operational parameters. *Journal of Electroanalytical Chemistry* 615(2), 165-174.
- [123] Thiam, A., Sirés, I., Garrido, J.A., Rodríguez, R.M., Brillas, E., 2015. Decolorization and mineralization of Allura Red AC aqueous solutions by electrochemical advanced oxidation processes. *Journal of Hazardous Materials* 290, 34-42.
- [124] Dirany, A., Sirés, I., Oturan, N., Oturan, M.A., 2010. Electrochemical abatement of the antibiotic sulfamethoxazole from water. *Chemosphere* 81(5), 594-602.
- [125] Garcia-Segura, S., Brillas, E., 2011. Mineralization of the recalcitrant oxalic and oxamic acids by electrochemical advanced oxidation processes using a boron-doped diamond anode. *Water Research* 45(9), 2975-2984.
- [126] Antonin, V.S., Garcia-Segura, S., Santos, M.C., Brillas, E., 2015. Degradation of Evans Blue diazo dye by electrochemical processes based on Fenton's reaction chemistry. *Journal of Electroanalytical Chemistry* 747, 1-11.
- [127] Boye, B., Dieng, M.M., Brillas, E., 2002. Degradation of herbicide 4-chlorophenoxyacetic acid by advanced electrochemical oxidation methods. *Environmental Science & Technology* 36(13), 3030-3035.
- [128] Serra, A., Domènech, X., Arias, C., Brillas, E., Peral, J., 2009. Oxidation of α -methylphenylglycine under Fenton and electro-Fenton conditions in the dark and in the presence of solar light. *Applied Catalysis B: Environmental* 89(1-2), 12-21.
- [129] Fernandes, A., Pacheco, M.J., Ciríaco, L., Lopes, A., 2012. Anodic oxidation of a biologically treated leachate on a boron-doped diamond anode. *Journal of Hazardous Materials* 199-200, 82-87.
- [130] El-Ghenymy, A., Cabot, P.L., Centellas, F., Garrido, J.A., Rodríguez, R.M., Arias, C., Brillas, E., 2013. Mineralization of sulfanilamide by electro-Fenton and solar photoelectro-Fenton in a pre-pilot plant with a Pt/air-diffusion cell. *Chemosphere* 91(9), 1324-1331.
- [131] Abdessalem, A.K., Bellakhal, N., Oturan, N., Dachraoui, M., Oturan, M.A., 2010. Treatment of a mixture of three pesticides by photo- and electro-Fenton processes. *Desalination* 250(1), 450-455.
- [132] Fan, Y., Ai, Z., Zhang, L., 2010. Design of an electro-Fenton system with a novel sandwich film cathode for wastewater treatment. *Journal of Hazardous Materials* 176(1-3), 678-684.

- [133] Oturan, N., Brillas, E., Oturan, M., 2012. Unprecedented total mineralization of atrazine and cyanuric acid by anodic oxidation and electro-Fenton with a boron-doped diamond anode. *Environmental Chemistry Letters* 10(2), 165-170.
- [134] Garcia-Segura, S., Keller, J., Brillas, E., Radjenovic, J., 2015. Removal of organic contaminants from secondary effluent by anodic oxidation with a boron-doped diamond anode as tertiary treatment. *Journal of Hazardous Materials* 283, 551-557.
- [135] Skoumal, M., Arias, C., Cabot, P.L., Centellas, F., Garrido, J.A., Rodríguez, R.M., Brillas, E., 2008. Mineralization of the biocide chloroxylenol by electrochemical advanced oxidation processes. *Chemosphere* 71(9), 1718-1729.
- [136] Tsantaki, E., Velegraki, T., Katsaounis, A., Mantzavinos, D., 2012. Anodic oxidation of textile dyehouse effluents on boron-doped diamond electrode. *Journal of Hazardous Materials* 207-208, 91-96.
- [137] Sychev, A.Y., Isak, V.G., 1995. Iron compounds and the mechanisms of the homogeneous catalysis of the activation of O₂ and H₂O₂ and of the oxidation of organic substrates. *Russian Chemical Reviews* 64(12), 1105-1129.
- [138] Mansour, D., Fourcade, F., Bellakhal, N., Dachraoui, M., Hauchard, D., Amrane, A., 2012. Biodegradability improvement of sulfamethazine solutions by means of an electro-Fenton process. *Water, Air, & Soil Pollution* 223(5), 2023-2034.
- [139] Santos, A., Yustos, P., Rodriguez, S., Simon, E., Garcia-Ochoa, F., 2007. Abatement of phenolic mixtures by catalytic wet oxidation enhanced by Fenton's pretreatment: Effect of H₂O₂ dosage and temperature. *Journal of Hazardous Materials* 146(3), 595-601.
- [140] El-Ghenymy, A., Garrido, J.A., Rodríguez, R.M., Cabot, P.L., Centellas, F., Arias, C., Brillas, E., 2013. Degradation of sulfanilamide in acidic medium by anodic oxidation with a boron-doped diamond anode. *Journal of Electroanalytical Chemistry* 689, 149-157.
- [141] El-Ghenymy, A., Centellas, F., Garrido, J.A., Rodríguez, R.M., Sirés, I., Cabot, P.L., Brillas, E., 2014. Decolorization and mineralization of Orange G azo dye solutions by anodic oxidation with a boron-doped diamond anode in divided and undivided tank reactors. *Electrochimica Acta* 130, 568-576.
- [142] Abdessalem, A.K., Oturan, M.A., Oturan, N., Bellakhal, N., Dachraoui, M., 2010. Treatment of an aqueous pesticides mixture solution by direct and indirect electrochemical advanced oxidation processes. *International Journal of Environmental Analytical Chemistry* 90(3-6), 468-477.
- [143] Skoumal, M., Rodríguez, R.M., Cabot, P.L., Centellas, F., Garrido, J.A., Arias, C., Brillas, E., 2009. Electro-Fenton, UVA photoelectro-Fenton and solar photoelectro-Fenton degradation of the drug ibuprofen in acid aqueous medium using platinum and boron-doped diamond anodes. *Electrochimica Acta* 54(7), 2077-2085.
- [144] Wang, C.-T., Chou, W.-L., Chung, M.-H., Kuo, Y.-M., 2010. COD removal from real dyeing wastewater by electro-Fenton technology using an activated carbon fiber cathode. *Desalination* 253(1-3), 129-134.
- [145] Almeida, L.C., Garcia-Segura, S., Bocchi, N., Brillas, E., 2011. Solar photoelectro-Fenton degradation of paracetamol using a flow plant with a Pt/air-diffusion cell coupled with a compound parabolic collector: Process optimization by response surface methodology. *Applied Catalysis B: Environmental* 103(1-2), 21-30.

- [146] Garcia-Segura, S., Almeida, L.C., Bocchi, N., Brillas, E., 2011. Solar photoelectro-Fenton degradation of the herbicide 4-chloro-2-methylphenoxyacetic acid optimized by response surface methodology. *Journal of Hazardous Materials* 194, 109-118.
- [147] Pignatello, J.J., 1992. Dark and photoassisted Fe³⁺-catalyzed degradation of chlorophenoxy herbicides by hydrogen peroxide. *Environmental Science & Technology* 26(5), 944-951.
- [148] Meeker, R.E., inventors. Stabilization of hydrogen peroxide. United States Patent 3208825 A. 1965 September 28.
- [149] Guinea, E., Arias, C., Cabot, P.L., Garrido, J.A., Rodríguez, R.M., Centellas, F., Brillas, E., 2008. Mineralization of salicylic acid in acidic aqueous medium by electrochemical advanced oxidation processes using platinum and boron-doped diamond as anode and cathodically generated hydrogen peroxide. *Water Research* 42(1-2), 499-511.
- [150] Khataee, A.R., Zarei, M., Moradkhannejhad, L., 2010. Application of response surface methodology for optimization of azo dye removal by oxalate catalyzed photoelectro-Fenton process using carbon nanotube-PTFE cathode. *Desalination* 258(1-3), 112-119.
- [151] Sun, Y., Pignatello, J.J., 1992. Chemical treatment of pesticide wastes. Evaluation of iron(III) chelates for catalytic hydrogen peroxide oxidation of 2,4-D at circumneutral pH. *Journal of Agricultural and Food Chemistry* 40(2), 322-327.
- [152] Safarzadeh-Amiri, A., Bolton, J.R., Cater, S.R., 1997. Ferrioxalate-mediated photodegradation of organic pollutants in contaminated water. *Water Research* 31(4), 787-798.
- [153] Smith, R.M., Martell, A.E., 1987. Critical stability constants, enthalpies and entropies for the formation of metal complexes of aminopolycarboxylic acids and carboxylic acids. *Science of the Total Environment* 64(1-2), 125-147.
- [154] Batista, A.P.S., Nogueira, R.F.P., 2012. Parameters affecting sulfonamide photo-Fenton degradation-Iron complexation and substituent group. *Journal of Photochemistry and Photobiology A: Chemistry* 232, 8-13.
- [155] Brillas, E., Baños, M.A., Skoumal, M., Cabot, P.L., Garrido, J.A., Rodríguez, R.M., 2007. Degradation of the herbicide 2,4-DP by anodic oxidation, electro-Fenton and photoelectro-Fenton using platinum and boron-doped diamond anodes. *Chemosphere* 68(2), 199-209.
- [156] Rosales, E., Pazos, M., Longo, M.A., Sanromán, M.A., 2009. Electro-Fenton decoloration of dyes in a continuous reactor: A promising technology in colored wastewater treatment. *Chemical Engineering Journal* 155(1-2), 62-67.
- [157] Gözmen, B., Kayan, B., Gizir, A.M., Hesenov, A., 2009. Oxidative degradations of Reactive Blue 4 dye by different advanced oxidation methods. *Journal of Hazardous Materials* 168(1), 129-136.
- [158] Galbavy, E.S., Ram, K., Anastasio, C., 2010. 2-Nitrobenzaldehyde as a chemical actinometer for solution and ice photochemistry. *Journal of Photochemistry and Photobiology A: Chemistry* 209(2-3), 186-192.
- [159] Aaron, J.-J., Oturan, M.A., 2001. New photochemical and electrochemical methods for the degradation of pesticides in aqueous media. Environmental applications. *Turkish Journal of Chemistry* 25, 509-520.
- [160] Solano, A.M.S., Garcia-Segura, S., Martínez-Huitle, C.A., Brillas, E., 2015. Degradation of acidic aqueous solutions of the diazo dye Congo Red by photo-assisted electrochemical

processes based on Fenton's reaction chemistry. *Applied Catalysis B: Environmental* 168-169, 559-571.

[161] Garcia-Segura, S., Centellas, F., Arias, C., Garrido, J.A., Rodríguez, R.M., Cabot, P.L., Brillas, E., 2011. Comparative decolorization of monoazo, diazo and triazo dyes by electro-Fenton process. *Electrochimica Acta* 58(1), 303-311.

[162] Florenza, X., Solano, A.M.S., Centellas, F., Martínez-Huitle, C.A., Brillas, E., Garcia-Segura, S., 2014. Degradation of the azo dye Acid Red 1 by anodic oxidation and indirect electrochemical processes based on Fenton's reaction chemistry. Relationship between decolorization, mineralization and products. *Electrochimica Acta* 142, 276-288.

[163] Ruiz, E.J., Hernández-Ramírez, A., Peralta-Hernández, J.M., Arias, C., Brillas, E., 2011. Application of solar photoelectro-Fenton technology to azo dyes mineralization: Effect of current density, Fe^{2+} and dye concentrations. *Chemical Engineering Journal* 171(2), 385-392.

[164] Juang, Y., Nurhayati, E., Huang, C., Pan, J.R., Huang, S., 2013. A hybrid electrochemical advanced oxidation/microfiltration system using BDD/Ti anode for Acid Yellow 36 dye wastewater treatment. *Separation and Purification Technology* 120, 289-295.

[165] Olvera-Vargas, H., Oturan, N., Aravindakumar, C.T., Paul, M.M.S., Sharma, V.K., Oturan, M.A., 2014. Electro-oxidation of the dye Azure B: Kinetics, mechanism, and by-products. *Environmental Science and Pollution Research* 21(14), 8379-8386.

[166] Nava, J.L., Sirés, I., Brillas, E., 2014. Electrochemical incineration of Indigo. A comparative study between 2D (plate) and 3D (mesh) BDD anodes fitted into a filter-press reactor. *Environmental Science and Pollution Research* 21(14), 8485-8492.

[167] Rosales, E., Iglesias, O., Pazos, M., Sanromán, M.A., 2012. Decolourisation of dyes under electro-Fenton process using Fe alginate gel beads. *Journal of Hazardous Materials* 213-214, 369-377.

[168] Elias, B., Guihard, L., Nicolas, S., Fourcade, F., Amrane, A., 2011. Effect of electro-Fenton application on azo dyes biodegradability. *Environmental Progress & Sustainable Energy* 30(2), 160-167.

[169] Peralta-Hernández, J.M., Meas-Vong, Y., Rodríguez, F.J., Chapman, T.W., Maldonado, M.I., Godínez, L.A., 2008. Comparison of hydrogen peroxide-based processes for treating dye-containing wastewater: Decolorization and destruction of Orange II azo dye in dilute solution. *Dyes and Pigments* 76(3), 656-662.

[170] Da Pozzo, A., Merli, C., Sirés, I., Garrido, J.A., Rodríguez, R.M., Brillas, E., 2005. Removal of the herbicide amitrole from water by anodic oxidation and electro-Fenton. *Environmental Chemistry Letters* 3(1), 7-11.

[171] Garza-Campos, B.R., Guzmán-Mar, J.L., Reyes, L.H., Brillas, E., Hernández-Ramírez, A., Ruiz-Ruiz, E.J., 2014. Coupling of solar photoelectro-Fenton with a BDD anode and solar heterogeneous photocatalysis for the mineralization of the herbicide atrazine. *Chemosphere* 97, 26-33.

[172] Pipi, A.R.F., Sirés, I., De Andrade, A.R., Brillas, E., 2014. Application of electrochemical advanced oxidation processes to the mineralization of the herbicide diuron. *Chemosphere* 109, 49-55.

[173] Dhaouadi, A., Adhoum, N., 2009. Degradation of paraquat herbicide by electrochemical advanced oxidation methods. *Journal of Electroanalytical Chemistry* 637(1-2), 33-42.

- [174] Özcan, A., Şahin, Y., Koparal, A.S., Oturan, M.A., 2008. Degradation of picloram by the electro-Fenton process. *Journal of Hazardous Materials* 153(1-2), 718-727.
- [175] Babuponnusami, A., Muthukumar, K., 2012. Advanced oxidation of phenol: A comparison between Fenton, electro-Fenton, sono-electro-Fenton and photo-electro-Fenton processes. *Chemical Engineering Journal* 183, 1-9.
- [176] Isarain-Chávez, E., Rodríguez, R.M., Cabot, P.L., Centellas, F., Arias, C., Garrido, J.A., Brillas, E., 2011. Degradation of pharmaceutical beta-blockers by electrochemical advanced oxidation processes using a flow plant with a solar compound parabolic collector. *Water Research* 45(14), 4119-4130.
- [177] Sirés, I., Garrido, J.A., Rodríguez, R.M., Brillas, E., Oturan, N., Oturan, M.A., 2007. Catalytic behavior of the $\text{Fe}^{3+}/\text{Fe}^{2+}$ system in the electro-Fenton degradation of the antimicrobial chlorophene. *Applied Catalysis B: Environmental* 72(3-4), 382-394.
- [178] Sirés, I., Centellas, F., Garrido, J.A., Rodríguez, R.M., Arias, C., Cabot, P.L., Brillas, E., 2007. Mineralization of clofibric acid by electrochemical advanced oxidation processes using a boron-doped diamond anode and Fe^{2+} and UVA light as catalysts. *Applied Catalysis B: Environmental* 72(3-4), 373-381.
- [179] Brillas, E., Garcia-Segura, S., Skoumal, M., Arias, C., 2010. Electrochemical incineration of diclofenac in neutral aqueous medium by anodic oxidation using Pt and boron-doped diamond anodes. *Chemosphere* 79(6), 605-612.
- [180] Olvera-Vargas, H., Oturan, N., Oturan, M.A., Brillas, E., 2015. Electro-Fenton and solar photoelectro-Fenton treatments of the pharmaceutical ranitidine in pre-pilot flow plant scale. *Separation and Purification Technology* 146, 127-135.
- [181] Ferrag-Siagh, F., Fourcade, F., Soutrel, I., Aït-Amar, H., Djelal, H., Amrane, A., 2013. Tetracycline degradation and mineralization by the coupling of an electro-Fenton pretreatment and a biological process. *Journal of Chemical Technology & Biotechnology* 88(7), 1380-1386.
- [182] González, T., Domínguez, J.R., Palo, P., Sánchez-Martín, J., Cuerda-Correa, E.M., 2011. Development and optimization of the BDD-electrochemical oxidation of the antibiotic trimethoprim in aqueous solution. *Desalination* 280(1-3), 197-202.
- [183] Brillas, E., Mur, E., Sauleda, R., Sánchez, L., Peral, J., Domènech, X., Casado, J., 1998. Aniline mineralization by AOP's: Anodic oxidation, photocatalysis, electro-Fenton and photoelectro-Fenton processes. *Applied Catalysis B: Environmental* 16(1), 31-42.
- [184] Pimentel, M., Oturan, N., Dezotti, M., Oturan, M.A., 2008. Phenol degradation by advanced electrochemical oxidation process electro-Fenton using a carbon felt cathode. *Applied Catalysis B: Environmental* 83(1-2), 140-149.
- [185] Flox, C., Arias, C., Brillas, E., Savall, A., Groenen-Serrano, K., 2009. Electrochemical incineration of cresols: A comparative study between PbO_2 and boron-doped diamond anodes. *Chemosphere* 74(10), 1340-1347.
- [186] Guinea, E., Centellas, F., Garrido, J.A., Rodríguez, R.M., Arias, C., Cabot, P.-L., Brillas, E., 2009. Solar photoassisted anodic oxidation of carboxylic acids in presence of Fe^{3+} using a boron-doped diamond electrode. *Applied Catalysis B: Environmental* 89(3-4), 459-468.
- [187] Rajeshwar, K., Ibanez, J.G., 1997. *Environmental Electrochemistry: Fundamentals and Application in Pollution Abatement*, Academic Press, San Diego, United States.

- [188] Rappoport, Z., 2003. *The Chemistry of Phenols*, John Wiley & Sons Ltd., West Sussex, England.
- [189] Patel, H., Vashi, R.T., 2015. *Characterization and Treatment of Textile Wastewater*, 1st Ed., Elsevier, United States.
- [190] Vaghela, S.S., Jethva, A.D., Mehta, B.B., Dave, S.P., Adimurthy, S., Ramachandraiah, G., 2005. Laboratory studies of electrochemical treatment of industrial azo dye effluent. *Environmental Science & Technology* 39(8), 2848-2855.
- [191] Domínguez, J.R., González, T., Palo, P., Sánchez-Martín, J., Rodrigo, M.A., Sáez, C., 2012. Electrochemical degradation of a real pharmaceutical effluent. *Water, Air, & Soil Pollution* 223(5), 2685-2694.
- [192] Kasprzyk-Hordern, B., Dinsdale, R.M., Guwy, A.J., 2009. The removal of pharmaceuticals, personal care products, endocrine disruptors and illicit drugs during wastewater treatment and its impact on the quality of receiving waters. *Water Research* 43(2), 363-380.
- [193] Dialynas, E., Mantzavinos, D., Diamadopoulos, E., 2008. Advanced treatment of the reverse osmosis concentrate produced during reclamation of municipal wastewater. *Water Research* 42(18), 4603-4608.
- [194] Pérez, G., Fernández-Alba, A.R., Urriaga, A.M., Ortiz, I., 2010. Electro-oxidation of reverse osmosis concentrates generated in tertiary water treatment. *Water Research* 44(9), 2763-2772.
- [195] Radjenovic, J., Bagastyo, A., Rozendal, R.A., Mu, Y., Keller, J., Rabaey, K., 2011. Electrochemical oxidation of trace organic contaminants in reverse osmosis concentrate using RuO₂/IrO₂-coated titanium anodes. *Water Research* 45(4), 1579-1586.
- [196] Van Hege, K., Verhaege, M., Verstraete, W., 2002. Indirect electrochemical oxidation of reverse osmosis membrane concentrates at boron-doped diamond electrodes. *Electrochemistry Communications* 4(4), 296-300.
- [197] Van Hege, K., Verhaege, M., Verstraete, W., 2004. Electro-oxidative abatement of low-salinity reverse osmosis membrane concentrates. *Water Research* 38(6), 1550-1558.
- [198] Qasim, S.R., Chiang, W., 1994. *Sanitary Landfill Leachate - Generation, Control and Treatment*, CRC Press LLC, Boca Raton, United States.
- [199] Anglada, A., Urriaga, A.M., Ortiz, I., 2010. Laboratory and pilot plant scale study on the electrochemical oxidation of landfill leachate. *Journal of Hazardous Materials* 181(1-3), 729-735.
- [200] Cabeza, A., Urriaga, A., Rivero, M.-J., Ortiz, I., 2007. Ammonium removal from landfill leachate by anodic oxidation. *Journal of Hazardous Materials* 144(3), 715-719.
- [201] Fernandes, A., Santos, D., Pacheco, M.J., Ciríaco, L., Lopes, A., 2014. Nitrogen and organic load removal from sanitary landfill leachates by anodic oxidation at Ti/Pt/PbO₂, Ti/Pt/SnO₂-Sb₂O₄ and Si/BDD. *Applied Catalysis B: Environmental* 148-149, 288-294.
- [202] Panizza, M., Martinez-Huitle, C.A., 2013. Role of electrode materials for the anodic oxidation of a real landfill leachate - Comparison between Ti-Ru-Sn ternary oxide, PbO₂ and boron-doped diamond anode. *Chemosphere* 90(4), 1455-1460.
- [203] Urriaga, A., Rueda, A., Anglada, Á., Ortiz, I., 2009. Integrated treatment of landfill leachates including electrooxidation at pilot plant scale. *Journal of Hazardous Materials* 166(2-3), 1530-1534.

- [204] Zhang, H., Li, Y., Wu, X., Zhang, Y., Zhang, D., 2010. Application of response surface methodology to the treatment landfill leachate in a three-dimensional electrochemical reactor. *Waste Management* 30(11), 2096-2102.
- [205] Nageswara Rao, N., Rohit, M., Nitin, G., Parameswaran, P.N., Astik, J.K., 2009. Kinetics of electrooxidation of landfill leachate in a three-dimensional carbon bed electrochemical reactor. *Chemosphere* 76(9), 1206-1212.
- [206] Chapman, J., Baker, P., Wills, S., 2001. *Winery Wastewater Handbook: Production, Impacts and Management*, Winetitles, Adelaide, Australia.
- [207] Salazar, C., Sirés, I., Salazar, R., Mansilla, H.D., Zaror, C.A., 2015. Treatment of cellulose bleaching effluents and their filtration permeates by anodic oxidation with H₂O₂ production. *Journal of Chemical Technology & Biotechnology* 90(11), 2017-2026.
- [208] Laor, Y., Koziel, J.A., Cai, L., Ravid, U., 2008. Chemical-sensory characterization of dairy manure odor using headspace solid-phase microextraction and multidimensional gas chromatography mass spectrometry-olfactometry. *Journal of the Air & Waste Management Association* 58(9), 1187-1197.
- [209] Borbón, B., Oropeza-Guzman, M.T., Brillas, E., Sirés, I., 2014. Sequential electrochemical treatment of dairy wastewater using aluminum and DSA-type anodes. *Environmental Science and Pollution Research* 21(14), 8573-8584.
- [210] Saha, P.D., Banerjee, P.K., 2012. *Treatability Studies of Tannery Wastewater: Treatment of Tannery wastewater using Chemical and Bioremediation Techniques*, LAP Lambert Academic Publishing, Saarbrücken, Germany.
- [211] Isarain-Chávez, E., De La Rosa, C., Godínez, L.A., Brillas, E., Peralta-Hernández, J.M., 2014. Comparative study of electrochemical water treatment processes for a tannery wastewater effluent. *Journal of Electroanalytical Chemistry* 713, 62-69.

2 Materials and methods

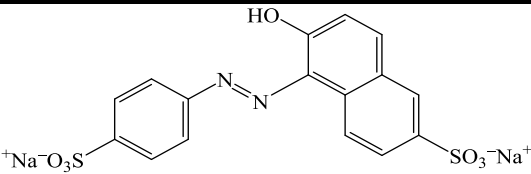
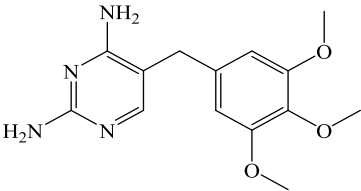
This chapter presents a detailed description of chemicals, analytical determinations, modeling of degradation kinetics, experimental units and respective procedures used within this thesis. Analytical determinations include tests for biodegradability assessment and actinometry measurements. Four experimental units were used for EAOPs implementation: (1) a 150 mL capacity lab-scale undivided reactor, (2) a 10 L capacity pilot-scale flow plant, (3) a 2.2 L capacity lab-scale flow plant and (4) a 35 L capacity pilot-scale flow plant. Systems (3) and (4) were built within this thesis and, as a consequence, are herein deeply described and characterized in terms of available radiation sources and photonic flux reaching the system, as well as with regard to H₂O₂ accumulation. Two biological systems and a coagulation/aeration process were also used for the treatment of real effluents.

The experimental work was mainly developed in the Laboratory of Separation and Reaction Engineering – Laboratory of Catalysis and Materials (LSRE-LCM), Department of Chemical Engineering, Faculty of Engineering, University of Porto, Portugal, where systems (3) and (4) are placed. A lower number of trials were carried out in the Laboratory for Materials Electrochemistry and the Environment, Chemical Physical Department, Faculty of Chemistry, University of Barcelona, Spain, where units (1) and (2) are located.

2.1 Chemicals

Table 2.1 presents a short summary of the physico-chemical properties of Sunset Yellow FCF (SY) azo dye and trimethoprim (TMP) antibiotic, used as model compounds in this thesis. Solutions of these two compounds were prepared daily by weighting the appropriate mass, taking into account their purity, and dissolving it into ultrapure water in the presence of sodium sulfate anhydrous, used as background electrolyte.

Table 2.1. Physico-chemical properties of Sunset Yellow FCF azo dye and trimethoprim antibiotic.

	Sunset Yellow FCF	Trimethoprim
Molecular structure		
Molecular formula	C ₁₆ H ₁₀ N ₂ Na ₂ O ₇ S ₂	C ₁₄ H ₁₈ N ₄ O ₃
Chemical name	Disodium 6-hydroxy-5-[(4-sulfophenyl)azo]-2-naphthalene-sulfonate	5-(3,4,5-trimethoxybenzyl)pyrimidine-2,4-diamine
Molecular weight (g mol ⁻¹)	452.37	290.32
Purity	81% (w/w)	≥ 99% (w/w)
Wavelength of maximum absorption - λ_{max} (nm)	482	270
Supplier	Sigma-Aldrich	Sigma-Aldrich

Chemicals employed in EAOPs, AOPs, biological treatments, coagulation and actinometry experiments are briefly described in Table 2.2.

Ultrapure and pure water were obtained by a Millipore[®] Direct-Q system (18.2 MΩ cm resistivity at 25 °C) and a reverse osmosis system (Panice), respectively.

All reagents employed in the analytical methods were of analytical grade, high performance liquid chromatography (HPLC) grade or ultragradient grade for liquid chromatography-mass spectrometry (LC-MS) supplied by Acros Organics, Chem-lab, Dionex, Fisher Scientific, Fluka, Izasa, Lancaster, Merck, Panreac, Pronalab, Quimitécnica.com, Scharlau, Sigma-Aldrich, VWR-Prolabo, Panreac, Merck, Fisher Scientific, Pronalab, LGC Standards and J.T. Baker.

Table 2.2. Physico-chemical properties of chemicals employed in EAOPs, AOPs, biological treatments and coagulation.

Chemical	Molecular formula	Molecular weight (g mol ⁻¹)	Purity	Density (g cm ⁻³)	Supplier	Purpose
Sodium sulfate anhydrous	Na ₂ SO ₄	142.04	≥ 99% (w/w)	2.70	Merck	Background electrolyte in EAOPs
Iron(II) sulfate heptahydrate	FeSO ₄ ·7H ₂ O	278.05	98% (w/w)	1.90	Panreac or Fluka	Catalyst in EF, PEF, SPEF, Fenton, PF and SPF
Iron(III) chloride hexahydrate	FeCl ₃ ·6H ₂ O	270.33	≥ 98% (w/w)	1.82	Merck	Catalyst in PEF assisted by Fe(III)-carboxylate complexes
Oxalic acid dihydrate	C ₂ H ₂ O ₄ ·2H ₂ O	126.07	≥ 99% (w/w)	1.65	VWR-Prolabo	Ligands in PEF assisted by Fe(III)-carboxylate complexes
Citric acid monohydrate	C ₆ H ₈ O ₇ ·H ₂ O	210.14	≥ 99% (w/w)	1.54	VWR-Prolabo	
DL-tartaric acid	C ₄ H ₆ O ₆	150.09	99% (w/w)	1.79	Sigma-Aldrich	
L(-)-malic acid	C ₄ H ₆ O ₅	134.09	99% (w/w)	1.61	Acros Organics	
D-mannitol	C ₆ H ₁₄ O ₆	182.17	≥ 99% (w/w)	1.49	Sigma-Aldrich	Scavenging agents
Sodium azide	NaN ₃	65.01	≥ 99% (w/w)	1.85	Panreac	
Hydrogen peroxide	H ₂ O ₂	34.02	30% (w/v)	1.10	Fisher Chemical	Oxidant in Fenton, PF and SPF
Sodium carbonate anhydrous	Na ₂ CO ₃	105.99	≥ 99% (w/w)	2.53	Merck	Source of alkalinity along the biological treatment of Chapter 7
Iron(III) chloride	FeCl ₃	162.20	40% (w/w)	1.44	Quimitécnica.com	Coagulant in Chapter 7
Sulfuric acid	H ₂ SO ₄	98.08	96% (w/w)	1.84	Pronalab or Acros Organics	pH adjustment (pure or diluted solutions)
Sodium hydroxide	NaOH	40.00	≥ 99% (w/w)	2.13	Merck or Panreac	
Hydrochloric acid	HCl	36.46	37% (w/w)	1.19	Sigma-Aldrich	
2-nitrobenzaldehyde	C ₇ H ₅ NO ₃	151.12	> 98% (w/w)	1.35	Alfa Aesar	Actinometry experiments
Ethanol	C ₂ H ₆ O	46.07	≥ 99.8% (w/w)	0.79	AGA-Álcool e Genéricos Alimentares S.A.	
Hydrogen peroxide	H ₂ O ₂	34.02	30% (w/v)	1.10	Fisher Chemical	Actinometry experiments
Iron(III) chloride hexahydrate	FeCl ₃ ·6H ₂ O	270.33	≥ 98% (w/w)	1.82	Merck	
Dipotassium oxalate monohydrate	C ₂ H ₂ K ₂ O ₅	184.23	≥ 99% (w/w)	2.13	VWR-Prolabo	Actinometry experiments
Oxalic acid dihydrate	C ₂ H ₂ O ₄ ·2H ₂ O	126.07	≥ 99% (w/w)	1.65	VWR-Prolabo	

2.2 Analytical determinations

2.2.1 Miscellaneous

Table 2.3 collects the description of the various analytical determinations used throughout the experimental work of this thesis.

Table 2.3. Analytical determinations.

Parameter	Methodology													
Sunset Yellow FCF azo dye ^a	<p>SY concentration was followed by reversed-phase HPLC by injecting 20 μL samples in a Waters 600 liquid chromatograph (LC) fitted with a photodiode array detector (PAD) set at $\lambda = 482 \text{ nm}$ and a Spherisorb ODS2 (5 μm) 150 mm \times 4.6 mm column at 35 $^{\circ}\text{C}$. The mobile phase was a 5:95 (v/v) acetonitrile/water (with 2.4 mM <i>n</i>-butylamine) mixture at a flow rate of 0.4 mL min^{-1}. The retention time (t_r) was 5.4 min.</p> <p>A calibration curve was constructed with 6 concentration levels ranging from 1.0 to 50.0 mg L^{-1}. The analytical parameters of working calibration curve are collected in Table 2.3.1.</p>													
	<p>Table 2.3.1. Analytical parameters of SY calibration curve.</p> <table border="1"> <thead> <tr> <th>Range (mg L^{-1})</th> <th>Slope ($a \pm s_a^a$)</th> <th>Interception ($b \pm s_b^b$)</th> <th>R^2 ^c</th> <th>s_a/a ^d (%)</th> <th>LOQ ^e (mg L^{-1})</th> <th>LOD ^f (mg L^{-1})</th> </tr> </thead> <tbody> <tr> <td>1.0-50.0</td> <td>$(885 \pm 9) \times 10^2$</td> <td>$(1 \pm 2) \times 10^4$</td> <td>1.000</td> <td>1.0</td> <td>2.7</td> <td>0.8</td> </tr> </tbody> </table> <p>^a Standard deviation of a; ^b Standard deviation of b; ^c Coefficient of determination; ^d Relative standard deviation of a; ^e Limit of quantification; ^f Limit of detection.</p>	Range (mg L^{-1})	Slope ($a \pm s_a^a$)	Interception ($b \pm s_b^b$)	R^2 ^c	s_a/a ^d (%)	LOQ ^e (mg L^{-1})	LOD ^f (mg L^{-1})	1.0-50.0	$(885 \pm 9) \times 10^2$	$(1 \pm 2) \times 10^4$	1.000	1.0	2.7
Range (mg L^{-1})	Slope ($a \pm s_a^a$)	Interception ($b \pm s_b^b$)	R^2 ^c	s_a/a ^d (%)	LOQ ^e (mg L^{-1})	LOD ^f (mg L^{-1})								
1.0-50.0	$(885 \pm 9) \times 10^2$	$(1 \pm 2) \times 10^4$	1.000	1.0	2.7	0.8								
Color removal ^a	<p>Null retention of SY in the 0.45 μm PTFE membrane filters was observed. Before analysis, samples were alkalized to stop the oxidation process.</p> <p>Decolorization was determined by the decrease of absorbance (A) at the λ_{max} (482 nm for SY), recorded on a Shimadzu 1800 UV-Vis spectrophotometer. Samples were always diluted 1:5 times in water. The percentage of color removal or decolorization efficiency was calculated as follows [2]:</p> $\% \text{ Color removal} = \frac{A_0 - A_t}{A_0} 100 \quad (45)$ <p>where A_0 and A_t are the absorbance at initial time and time t at λ_{max}, respectively.</p>													
TDC ^a DIC ^a DOC ^a	<p>Total dissolved carbon (TDC) and dissolved inorganic carbon (DIC) were separately determined by catalytic combustion at 680 $^{\circ}\text{C}$ and acidification, respectively, using a nondispersive infrared detector (NDIR) in a Shimadzu TOC-V_{CSN} analyzer. Dissolved organic carbon (DOC) was given by the difference between TDC and DIC (DOC = TDC - DIC).</p> <p>For samples with DOC contents below 20 mg L^{-1}, Na_2SO_3 in a Na_2SO_3-to-H_2O_2 molar ratio of 1:1 [3] was added to quench remaining H_2O_2 and stop the mineralization process.</p>													
Temperature	Temperature was measured by a WTW inoLab 730 laboratory meter.													
pH	pH was measured by a Crison pH 25 portable pH meter or a WTW inoLab 730 laboratory meter.													

Table 2.3. Analytical determinations.

Parameter	Methodology
Fe²⁺ ^{a, b} Fe³⁺ ^{a, b} TDI ^{a, b}	Concentrations of dissolved Fe ²⁺ and Fe ³⁺ and total dissolved iron (TDI), i.e. Fe ²⁺ + Fe ³⁺ , were obtained from the colorimetric 1,10-phenantroline standardized procedure ISO 6332 [4], determining the absorbance at 510 nm in a VWR UV-6300PC spectrophotometer.
H₂O₂ ^{a, b}	H ₂ O ₂ concentration was determined by the colorimetric metavanadate method [5], measuring the absorbance at 450 nm in a VWR UV-6300PC spectrophotometer.
LMCA ^a	<p>Chapter 3: Low-molecular-weight carboxylic acids (LMCA) like oxalic ($t_r = 7.0$ min), tartronic ($t_r = 7.9$ min), oxamic ($t_r = 9.3$ min) and formic ($t_r = 13.8$ min) acids were determined by ion-exclusion HPLC by injecting 20 μL samples into a Waters 600 LC fitted with a PAD set at $\lambda = 210$ nm and a Bio-Rad Aminex HPX-87H 300 mm \times 7.8 mm column at 35 °C. The mobile phase was 4 mM H₂SO₄ at a flow rate of 0.6 mL min⁻¹.</p> <p>Other chapters: LMCA like oxalic ($t_r = 8.5$ min), citric ($t_r = 11.0$ min), oxamic ($t_r = 11.5$ min), tartaric ($t_r = 11.7$ min), malic ($t_r = 13.2$ min) and formic ($t_r = 18.1$-18.5 min) acids were determined by ion-exclusion HPLC by injecting 10 μL samples into a VWR Hitachi ELITE LaChrom LC fitted with a DAD set at $\lambda = 210$ nm and a Phenomenex Rezex™ ROA-Organic Acid H+ (8%) 300 mm \times 7.8 mm column at ambient temperature (25 °C). The mobile phase was 2.5 mM H₂SO₄ at a flow rate of 0.5 mL min⁻¹.</p> <p>Before analysis, 1 M methanol, a well-known •OH scavenger ($k_{\text{OH}} = 9.7 \times 10^8 \text{ M}^{-1} \text{ s}^{-1}$ [1], was added to samples to stop the oxidation process.</p> <p>Besides the detection of oxalic, tartronic, oxamic, formic, citric, tartaric and malic acids, the two HPLC methods were able to detected other LMCA such as maleic, malonic, glycolic, succinic, shikimic, acetic, glutaric, fumaric, propionic, acrylic, adipic and phtalic. Limit of quantification (LOQ) and limit of detection (LOD) were in the range of 0.06-1.9 and 0.02-0.6 mg L⁻¹ for the various LMCA, respectively.</p>
Intermediates ^d	Intermediates were determined by LC-MS in the Laboratory for Materials Electrochemistry and the Environment (LMEE), University of Barcelona, Spain. Analyses were carried out by a Shimadzu SIL-20AC LC filled with a Teknokroma Mediterranea Sea C-18 (3 μ m) 15 mm \times 0.46 mm column at 30 °C and coupled to a Shimadzu LCMS-2020 MS. The MS operated in negative mode for SY intermediates determination (Chapter 3) and in negative and positive mode for TMP intermediates assessment (Chapter 4), both with electrospray source ionization, by applying an interface voltage of -4.5 kV and +4.5 kV, respectively, and 60 V Q-array radiofrequency voltage. The desolvation line temperature was 250 °C and pure N ₂ was used as nebulizing and dryer gas. Mass spectra were collected in the m/z range of 50-420 using both, total ion current and selected-ion acquisition. Samples volumes of 15 and 30 μ L were injected into the LC for SY and TMP intermediates detection, respectively, and the mobile phase was a 75:25 (v/v) acetonitrile/water (5 mM ammonium acetate) mixture for negative mode and 75:25 (v/v) acetonitrile/water (5 mM acetic acid) mixture for positive mode, both at a flow rate of 0.2 mL min ⁻¹ .
Inorganic anions ^a	<p>Chapter 3: Nitrite (NO₂⁻), nitrate (NO₃⁻) and sulfate (SO₄²⁻) ions were determined by ion chromatography by injecting 25 μL samples into a Shimadzu 10Avp LC equipped with a Shim-Pack IC-A1S 100 mm \times 4.6 mm column at 40 °C and applying a mobile phase of 2.6 mM phthalic acid and 2.4 mM tris(hydroxymethyl)aminomethane (pH = 4.0) at a flow rate of 1.5 mL min⁻¹.</p> <p>Other chapters: Chloride (Cl⁻), NO₂⁻, SO₄²⁻, NO₃⁻ and phosphate (PO₄³⁻) ions were determined by ion chromatography by injecting 10 μL samples into a Dionex ICS-2100 LC equipped with an IonPac® AS11-HC 250 mm \times 4 mm column at 30 °C and an anion self-regenerating suppressor (ASRS® 300, 4 mm) under isocratic elution of 30 mM NaOH at a flow rate of 1.5 mL min⁻¹.</p>

Table 2.3. Analytical determinations.

Parameter	Methodology
Inorganic cations ^a	Chapter 3: Ammonium (NH ₄ ⁺) ion was identified and quantified by ion chromatography by injecting 25 µL samples into a Shimadzu 10Avp LC equipped with a Shodex IC YK-421 125 mm × 4.6 mm column at 40 °C and applying a mobile phase of 24.2 mM boric acid, 5.0 mM tartaric acid, 2.0 mM 2,6-pyridinedicarboxylic acid and 1.5 mM 18-crown-6 at a flow rate of 1.0 mL min ⁻¹ . Chapter 4: NH ₄ ⁺ ion was determined by means of a Thermo Scientific Orion High-Performance 9512HPBNWP ammonia selective electrode connected to a Hanna Instruments HI 253 bench meter since the sulfate peak overlapped the NH ₄ ⁺ peak in ion chromatography analysis. Other chapters: Sodium (Na ⁺), NH ₄ ⁺ , potassium (K ⁺), magnesium (Mg ²⁺) and calcium (Ca ²⁺) were identified and quantified by ion chromatography by injecting 25 µL samples into a Dionex DX-120 LC equipped with an IonPac [®] CS12A 250 mm × 4 mm column at ambient temperature and a cation self-regenerating (CSRS [®] Ultra II, 4 mm) suppressor under isocratic elution of 20 mM methanesulfonic acid at a flow rate of 1.0 mL min ⁻¹ .
Total dissolved nitrogen ^a	Total dissolved nitrogen was determined by thermal decomposition and nitric oxide detection by chemiluminescence method in a Shimadzu TOC-VCSN analyzer coupled with a TNM-1 unit.
Total nitrogen	Total nitrogen was determined from the digestion with peroxodisulfate standardized procedure ISO 11905-1 [7] and further colorimetry based on reaction with 2,6-dimethylphenol, using Merck Spectroquant [®] kits Cat. No. 114763, a WTW CR4200 thermoreactor and a Merck Spectroquant [®] Pharo 100 spectrophotometer.
Total phosphorus	Total phosphorus was determined according to the Standard Methods for the Examination of Water and Wastewater [6], 4500-P E test, by colorimetry based on ascorbic acid, using Merck Spectroquant [®] kits Cat. No. 114543, a WTW CR4200 thermoreactor and a Merck Spectroquant [®] Pharo 100 spectrophotometer.
Aromatic compounds ^a	The presence of aromatic compounds was qualitatively assessed by means of the absorbance at 254 nm determined by UV spectrometry carried out in a VWR UV-6300PC spectrophotometer.
SUVA₂₅₄	The specific ultraviolet absorbance at 254 nm (SUVA ₂₅₄ , in L mg ⁻¹ m ⁻¹) was obtained by dividing the absorbance at 254 nm (in m ⁻¹) of filtered samples by their DOC concentration (in mg L ⁻¹).
COD	Chemical oxygen demand (COD) was determined photometrically according to the Standard Methods for the Examination of Water and Wastewater [6], 5220 D test, by oxidation with potassium dichromate, using Merck Spectroquant [®] kits Cat. No. 114541, a WTW CR4200 thermoreactor and a Merck Spectroquant [®] Pharo 100 spectrophotometer.
BOD₅ ^c	5-day biochemical oxygen demand (BOD ₅) was determined according to the Standard Methods for the Examination of Water and Wastewater [6], 5210 B test, using OxiTop [®] system (manometric respirometry).
Conductivity	Conductivity was determined with a HANNA Instruments HI 9828 Multiparameter analyzer.
Alkalinity	Alkalinity was determined according to the Standard Methods for the Examination of Water and Wastewater [6], 2320 B test, by titration.
Turbidity	Turbidity was measured according to the Standard Methods for the Examination of Water and Wastewater [6], 2130 B test, using a Merck Turbiquant [®] 3000 IR turbidimeter.
TSS	Total suspended solids (TSS) content was determined according to Standard Methods for the Examination of Water and Wastewater [6], 2540 D test, by filtration through a weighed standard glass-fiber filter and drying of the solid residue at 105 °C up to constant weight.

Table 2.3. Analytical determinations.

Parameter	Methodology
VSS	Volatile suspended solids (VSS) content was determined according to Standard Methods for the Examination of Water and Wastewater [6], 2540 E test, by ignition of the residue from TSS determination at 550 °C up to constant weight.
SVI	Sludge volume index (SVI) was determined according to Standard Methods for the Examination of Water and Wastewater [6], 2710 D test, which uses 30-min settled sludge volume (SSV ₃₀) and TSS values. The SSV ₃₀ value was measured according to the Standard Methods for the Examination of Water and Wastewater [6], 2710 C test.
Dissolved oxygen	Dissolved oxygen was determined in a HANNA Instruments HI 9828 Multiparameter analyzer.
Redox potential	Redox potential was determined in a HANNA Instruments HI 9828 Multiparameter analyzer.
	TMP concentration was followed by reversed-phase HPLC by injecting 50 µL samples in a VWR Hitachi ELITE LaChrom LC fitted with a diode array detector (DAD) set at $\lambda = 270$ nm and a Merck LiChrosorb® RP-18 (5 µm) LiChroCART® 125-4 125 mm × 4 mm column at 25 °C. The mobile phase was a 30:70 (v/v) methanol/0.014M oxalic acid mixture at a flow rate of 0.8 mL min ⁻¹ . The t_r was 3.2 min. Three calibration curves were constructed, each one with 6 or 7 concentration levels ranging from 0.01 to 1.0 mg L ⁻¹ , 0.4 to 10.0 mg L ⁻¹ and 1.0 to 30.0 mg L ⁻¹ . The analytical parameters of working calibration curves are shown in Table 2.3.2.

Table 2.3.2. Analytical parameters of TMP calibration curves.

Trimethoprim antibiotic at mg L ⁻¹ levels ^a	Range	Slope	Interception	R ² ^c	sa/la ^d	LOQ ^e	LOD ^f
	(mg L ⁻¹)	(a±s _a ^a)	(b±s _b ^b)		(%)	(mg L ⁻¹)	(mg L ⁻¹)
	0.01-1.0	(278±3)×10 ³	(-1±2)×10 ³	0.999	1.1	0.06	0.02
	0.4-10.0	(289±4)×10 ³	(-1±2)×10 ⁴	0.999	1.3	0.6	0.2
	1.0-30.0	(284±6)×10 ³	(1±1)×10 ⁵	0.998	2.0	3.3	1.0

^a Standard deviation of a; ^b Standard deviation of b; ^c Coefficient of determination;

^d Relative standard deviation of a; ^e Limit of quantification; ^f Limit of detection.

Null retention of TMP in the 0.45 µm Nylon membrane filters was observed.

The ability of this analytical method to detect the drug contained in Fe(III)-TMP complexes was checked by injecting solutions of 2.0 mg Fe³⁺ L⁻¹ and 20.0 mg TMP L⁻¹, with and without 7.0 g Na₂SO₄ L⁻¹, at pH of 2.0, 3.5, 5.0 and 9.0. No change on TMP concentration was observed.

Before analysis, 1 M methanol, a well-known ·OH scavenger ($k_{\text{OH}} = 9.7 \times 10^8 \text{ M}^{-1} \text{ s}^{-1}$ [1]), was added to samples to stop the oxidation process.

Table 2.3. Analytical determinations.

Parameter	Methodology
Pharmaceutical compounds at ng and $\mu\text{g L}^{-1}$ levels	<p>The quantitative analysis of pharmaceutical compounds at ng and $\mu\text{g L}^{-1}$ levels was performed by ultra performance liquid chromatography-tandem mass spectrometer (UPLC-MS/MS) by an external entity, the Water Institute of the Northern Region (IAREN), Porto, Portugal.</p> <p>Individual stock standard solutions were regularly prepared in methanol, at the approximate concentration of 1000 mg L^{-1} and stored at $-18 \text{ }^\circ\text{C}$ in the dark. A mixture of all pharmaceutical standards at 5 mg L^{-1} was prepared every 4 months. A working standard solution containing $500 \mu\text{g L}^{-1}$ of all pharmaceuticals prepared in methanol/water (25:75, v/v) was run daily before each sample batch.</p> <p>Before analysis, a solid phase extraction (SPE) was performed by using an automated device ASPEC XL from Gilson (Middleton, USA) fitted to accommodate 6 mL cartridges. The conditioning of the extraction cartridges, OASIS HLB (200 mg, 6 mL), was performed with 3 mL of methanol followed by 3 mL of acidified ultrapure water at pH of 2 with hydrochloric acid (HCl). 250 mL of standards and samples were percolated through the OASIS HLB cartridge at a flow rate of 10 mL min^{-1}. The adsorbent was allowed to dry under vacuum in an Analytichem International SPE manifold (Varian). The analytes were then eluted with 6 mL of methanol, the extract was evaporated to dryness under a gentle stream of nitrogen and redissolved in $500 \mu\text{L}$ of methanol/water (25:75, v/v).</p> <p>For UPLC-MS/MS analysis, samples were injected in the UPLC (Acquity, Ultra Performance LC) equipped with an analytical column Acquity (UPLC BEH C18 $1.7 \mu\text{m}$ $2.1 \times 100 \text{ mm}$) and a pre-column Acquity (UPLC BEH C18 $1.7 \mu\text{m}$ $2.1 \times 5 \text{ mm}$) coupled to a mass spectrometer (TQ detector). The mass detector was operated in multiple reaction monitoring mode, after thorough selection of the specific transitions for each pharmaceutical, according to the internal procedure by IAREN. The final optimized method allowed the concurrent detection of 27 pharmaceutical compounds, during 11 min chromatographic runs.</p>
Total dissolved polyphenols ^{a, b}	<p>Total dissolved polyphenols concentration, expressed in terms of caffeic acid equivalent concentration ($\text{mg caffeic acid equivalent L}^{-1}$), was determined by spectrophotometry using the Folin-Ciocalteu reagent [8], measuring the absorbance at 765 nm on a VWR UV-6300PC spectrophotometer.</p>
Sulfite ^a	<p>Sulfite (SO_3^{2-}) concentration was determined photometrically using Merck Spectroquant[®] kits Cat. No. 101746 and a Merck Spectroquant[®] Pharo 100 spectrophotometer. The analysis is based on the reaction of sulfite ions with 2,2'-dinitro-5,5'-dithiodibenzoic acid (Ellman's reagent) to form an organic thiosulfate along with the release of a thiol that is determined photometrically.</p>
Sulfide ^a	<p>Sulfide (S^{2-}) concentration was determined photometrically according to Standard Methods for the Examination of Water and Wastewater [6], 4500-S²⁻ D test, by reaction with dimethyl-<i>p</i>-phenylenediamine and iron(III) ions to form methylene blue, using Merck Spectroquant[®] kits Cat. No. 114779 and a Merck Spectroquant[®] Pharo 100 spectrophotometer.</p>
Total chlorine ^a	<p>Total free chlorine concentration was determined photometrically according to Standard Methods for the Examination of Water and Wastewater [6], 4500-Cl G test, by reaction with dipropyl-<i>p</i>-phenylenediamine, using Merck Spectroquant[®] kits Cat. No. 100602 and a Merck Spectroquant[®] Pharo 100 spectrophotometer.</p>
Spectral irradiance of UVA and UVA-Vis lamps	<p>The UVA lamp spectral irradiance was collected between 350 and 700 nm using a spectro-radiometer consisting of a mini spectrophotometer (USB2000 + UV-Vis, OceanOptics, USA) connected to an optical fiber (QP600-1-SR, OceanOptics, USA) with an irradiance probe on its tip (CC-UV-S cosine-corrected irradiance probe, OceanOptics, USA).</p>

Table 2.3. Analytical determinations.

Parameter	Methodology
2-nitrobenzaldehyde ^a	2-nitrobenzaldehyde (2-NB) concentration was followed by reversed-phase HPLC by injecting 5 µL samples into a VWR Hitachi ELITE LaChrom LC fitted with a DAD set at $\lambda = 258$ nm and a Merck LiChrosorb [®] RP-18 (5 µm) LiChroCART [®] 125-4 125 mm × 4 mm column at 25 °C. The mobile phase was a 40:60 (v/v) acetonitrile/0.014M oxalic acid mixture at a flow rate of 0.6 mL min ⁻¹ . The t_r was 6.9 min. A calibration curve was constructed with 6 concentration levels ranging from 5.0 to 50.0 mg L ⁻¹ . The analytical parameters of working calibration curve are given in Table 2.3.3.

Table 2.3.3. Analytical parameters of 2-NB calibration curve.

Range (mg L ⁻¹)	Slope ($a \pm s_a$ ^a)	Interception ($b \pm s_b$ ^b)	R^2 ^c	sa/a ^d (%)	LOQ ^e (mg L ⁻¹)	LOD ^f (mg L ⁻¹)
5.0-50.0	(68±2)×10 ³	(-23±6)×10 ⁴	0.996	3.1	9.4	2.8

^a Standard deviation of a ; ^b Standard deviation of b ; ^c Coefficient of determination;

^d Relative standard deviation of a ; ^e Limit of quantification; ^f Limit of detection.

^a Samples filtration through 0.45 µm Nylon or PTFE membrane filters before analysis;

^b For colored samples, the absorbance of a control sample was determined at the same wavelength as the analysis to correct the color interference;

^c The excess of H₂O₂ was previously removed using a small volume of 0.1 g L⁻¹ catalase solution (2500 U mg⁻¹ bovine liver) after adjusting the sample pH to 6.5-7.5 (the catalase contribution to BOD₅ was taken into account);

^d Samples filtration through 0.22 µm PTFE membrane filters before analysis.

2.2.2 Biodegradability assessment

Before biodegradability assessment, the excess of H₂O₂ was removed using a small volume of 0.1 g L⁻¹ catalase solution (2500 U mg⁻¹ bovine liver) after adjusting the sample pH to 6.5-7.5. The catalase contribution to DOC and COD, although minimal, was taken into account.

2.2.2.1 Respirometry

Respirometry tests were used to check the biodegradability enhancement along winery wastewater degradation by SPEF in Chapter 6.

These tests were carried out with a Surcis, S.L. BM-Advance analyzer. The reactor vessel was loaded with 1000 mL of activated sludge from an urban WWTP of Northern Portugal previously aerated for 24 h and with the addition of 2 mg *N*-allylthiourea per g of VSS to stop the nitrification process. The activated sludge was subjected to continuous agitation, aeration and recirculation by means of a peristaltic pump and the temperature and pH were maintained at 20 °C and 7.0±0.2, respectively, during all the trial. Firstly, the heterotrophic biomass yield coefficient (Y_H) was calculated via Eq. (46) by the addition of an acetate solution with known COD (COD_{acetate},

in mg O₂ L⁻¹) to the reactor vessel and performance of a *R* test to determine the total consumed oxygen (CO_T , in mg O₂ L⁻¹) to biodegrade the acetate solution. Afterwards, 34-50 mL of sample (winery wastewater) were added to the reactor vessel and other *R* test was accomplished to determine the CO_T to biodegrade the sample. Then, the biodegradable fraction of COD (bCOD, in mg O₂ L⁻¹) was calculated from Eq. (47) using this CO_T value and the previously determined Y_H . The ratio between bCOD and the COD measured according to the Standard Methods for the Examination of Water and Wastewater [6] gives information on the sample biodegradability: values below 0.05 indicate that the sample is not biodegradable; values between 0.05 and 0.1 correspond to low biodegradable samples; values higher than 0.1 up to 0.3 indicate that the sample is biodegradable; and values higher than 0.3 point to very biodegradable samples [9].

$$Y_H = 1 - CO_T / COD_{\text{acetate}} \quad (46)$$

$$\text{bCOD} = CO_T / (1 - Y_H) \quad (47)$$

2.2.2.2 Zahn-Wellens test

Raw winery wastewater biodegradability in Chapter 6 and landfill leachate biodegradability attained throughout degradation by SPEF in Chapter 7 were determined by a 28-day Zahn-Wellens test from the Test Guideline no. 302 B [10]. A mixture composed of (i) 240 mL of sample at neutral pH, (ii) activated sludge from an urban WWTP of Northern Portugal previously centrifuged, and (iii) mineral nutrients (KH₂PO₄, K₂HPO₄, Na₂HPO₄, NH₄Cl, CaCl₂, MgSO₄ and FeCl₃) was added to an open glass vessel magnetically stirred and kept in the dark at 25 °C. Control and blank experiments were prepared using the highly biodegradable glucose and pure water, respectively, instead of sample. The percentage of biodegradation (D_t) was calculated through Eq. (48) [10]:

$$D_t = \left[1 - \frac{C_T - C_B}{C_A - C_{BA}} \right] \times 100 \quad (48)$$

where C_T and C_B are the sample and blank DOC concentrations (in mg L⁻¹) determined at the sampling time t , respectively, and C_A and C_{BA} are the corresponding sample and blank DOC concentrations measured 3 h after beginning the test.

2.2.3 Actinometry measurements

Actinometry measurements were used to determine the photonic flux reaching the 2.2 L capacity lab-scale flow reactor when employing different radiation sources (see Section 2.4.3.2.2) and also reaching the 35 L pilot-scale flow plant when irradiated by natural sunlight (see Section 2.4.4.2).

2.2.3.1 2-Nitrobenzaldehyde concentration actinometry

2-NB can absorb UV radiation from 300 to 410 nm. This actinometry was accomplished by adapting the method proposed by Willett and Hites [11]. A 2.5×10^{-3} M 2-NB solution was prepared using 90:10 (v/v) water/ethanol as solvent and stored in the dark.

2.2 L capacity lab-scale flow plant

A volume of 1250 mL of 2-NB solution was added to the system and recirculated for 10 min in the dark. Afterwards, radiation was provided and samples were collected every 5 min for 30 min to follow 2-NB concentration. A zero-order kinetic model was fitted to irradiation time (s) vs. 2-NB concentration (M) data to get the zero-order kinetics constant ($d[2\text{-NB}]/dt$, in M s^{-1}).

35 L capacity pilot-scale flow plant

A volume of 24.7 L of 2-NB solution was added to the system and recirculated for 30 min in the dark. Afterwards, the photoreactor was uncovered and samples were collected every 5 min for 30 min to follow 2-NB concentration. A zero-order kinetic model was fitted to irradiation time (s) vs. 2-NB concentration (M) data to get the zero-order kinetics constant ($d[2\text{-NB}]/dt$, in M s^{-1}).

2.2.3.2 Hydrogen peroxide actinometry

H_2O_2 can absorb UVC radiation ($\lambda < 280$ nm). This actinometry was performed according to Nicole et al. [12], which employed a 50 mM H_2O_2 solution prepared with pure water at pH of 7.5. A volume of 1.250 L of this solution was added to the system and recirculated for 10 min in darkness. Afterwards, radiation was provided and samples were collected every 5 min for 60 min to determine H_2O_2 concentration. A zero-order kinetic model was fitted to irradiation time (s) vs. H_2O_2 concentration (M) data to get the zero-order kinetics constant ($d[\text{H}_2\text{O}_2]/dt$, in M s^{-1}).

2.2.3.3 Ferrioxalate actinometry

Two ferrioxalate actinometries were employed: one using crystals of $K_3[Fe(C_2O_4)_3] \cdot 3H_2O$ and the other using $[Fe(C_2O_4)_3]^{3-}$ ion prepared in situ. Ferrioxalate can absorb radiation from 250 to 500 nm.

The ferrioxalate actinometry using crystals of $K_3[Fe(C_2O_4)_3] \cdot 3H_2O$ was carried out by adapting the method described by Kuhn et al. [13]. Immediately before beginning the experiment, a 0.006 M $K_3[Fe(C_2O_4)_3] \cdot 3H_2O$ solution was prepared by dissolving 3.68 g of previously produced $K_3[Fe(C_2O_4)_3] \cdot 3H_2O$ crystals in 125 mL of 0.5 M H_2SO_4 and ultrapure water. A volume of 1250 mL of this solution was added to the glass vessel and recirculated during 10 min in darkness.

The ferrioxalate actinometry with $[Fe(C_2O_4)_3]^{3-}$ ion prepared in situ used a solution of 0.006 M of Fe^{3+} produced by dissolving $FeCl_3 \cdot 6H_2O$ at pH of 3 during 1 h, with addition of 0.03 M of oxalic acid under dark conditions just before beginning the trial. Subsequently, the solution was magnetically stirred for 15 min to form the iron complex. A volume of 1250 mL of this solution was added to the system and recirculated for 10 min in darkness.

In both ferrioxalate actinometries, radiation was provided and samples were collected every 5 min for 45 min to measure Fe^{2+} concentration. A zero-order kinetic model was fitted to irradiation time (s) vs. Fe^{2+} concentration (M) data to determine the zero-order kinetics constant ($d[Fe^{2+}]/dt$, in $M s^{-1}$).

2.2.3.4 Calculations

The determination of the photonic flux, called F_0 for calculation purposes, was similar for the three abovementioned actinometry analyses.

Firstly, Eq. (49) was applied to calculate F_0 in Einstein s^{-1} :

$$F_0 \text{ (Einstein } s^{-1}) = \frac{d[X]}{dt} \times \left(\frac{1}{\phi}\right) \times V \quad (49)$$

where $d[X]/dt$ corresponds to the zero-order kinetics constant ($d[2-NB]/dt$, $d[H_2O_2]/dt$ or $d[Fe^{2+}]/dt$, in $mol L^{-1} s^{-1}$), ϕ is the quantum yield of 2-NB, H_2O_2 or ferrioxalate at the radiation source wavelength (0.41 at 280-405 nm for 2-NB [14], 1.11 at 205-280 nm for H_2O_2 [15] and 1.26 at 360 nm for ferrioxalate [16]) and V is the solution volume (L).

Afterwards, F_0 was converted into J s^{-1} via Eq. (50):

$$F_0 (\text{J s}^{-1}) = F_0 (\text{Einstein s}^{-1}) \times E \times N_A \quad (50)$$

where E is the energy (J) calculated from Plank's equation for λ_{max} of the radiation source (360 nm for the UVA lamp, 531 nm for the UVA-Vis lamp (average value), 254 nm for the UVC lamp and 360 nm for the natural sunlight (average value)) and N_A is Avogadro's number ($6.022 \times 10^{23} \text{ mol}^{-1}$).

Note that the calculation of photonic flux depends on the fraction of light absorbed by the actinometer, although for high compound concentration and path length this parameter can be omitted since it is very close to unity.

2.3 Modeling of degradation kinetics

A pseudo-first-order kinetic model was fitted to the experimental data as a simple mathematical model from which properly kinetic constants could be calculated to quantitatively compare the various degradations under distinct conditions. This kinetic model was adjusted by a nonlinear regression method using the Fig.P software for Windows from Biosoft. The pseudo-first-order kinetic constants (k_X , dimensionless, in min^{-1} or in L kJ^{-1}) were calculated from the general Eq. (51):

$$X_t = X_0 \times e^{-k_X \times t} \quad (51)$$

where X_t and X_0 are the values of a given parameter after t time or accumulated UV radiation and at time or accumulated UV radiation of 0, respectively.

X can assume various parameters: (i) SY absorbance at $\lambda_{\text{max}} = 482$ nm, corresponding to the assessment of SY decolorization (k_{dec}) in Chapter 3, (ii) SY concentration, corresponding to the evaluation of SY content decay (k_{SY}) in Chapter 3, (iii) TMP concentration, corresponding to the appraisal of TMP content decay (k_{TMP}) in Chapters 4 and 5, and (iv) DOC concentration, corresponding to the assessment of DOC removal (k_{DOC}) in Chapters 3, 4, 5, 6, 7 and 8.

Initial removal rates ($r_{0(X)}$) were also calculated for the appraisal of TMP content decay ($r_{0(\text{TMP})}$) in Chapters 4 and 5 and DOC removal ($r_{0(\text{DOC})}$) in Chapter 5, both in $\text{mg L}^{-1} \text{min}^{-1}$, according to the general Eq. (52).

$$r_{0(X)} = k_X \times X_0 \quad (52)$$

The fitting was performed by minimizing the sum of the squared deviations between experimental and predicted values. The goodness of fitting was assessed by calculating the standard deviations, the coefficient of determination (R^2) and the residual variance (S^2_{R}).

2.4 Experimental units and procedures

Four experimental units were used within this thesis to evaluate the performance of EAOPs and two biological systems were used to treat the winery wastewater and the landfill leachate. Table 2.4 assigns each experimental setup to the respective chapter(s) where it was employed. Beyond that, a coagulation aeration process was employed in Chapter 7.

Table 2.4. Use of experimental units within the thesis.

Experimental unit	Chapter(s)
Lab-scale undivided reactor with 150 mL capacity	3
Pilot-scale flow plant with 10 L capacity	3
Lab-scale flow plant with 2.2 L capacity	4, 5, 6, 7, 8
Pilot-scale flow plant with 35 L capacity	4, 7
Biological system I	6
Biological system II	7

Since one of the objectives of this thesis was the design and construction of two EAOPs experimental units, namely the 2.2 L capacity lab-scale flow plant and the 35 L capacity pilot-scale flow plant, these two units are herein extensively described and characterized.

2.4.1 Lab-scale undivided reactor with 150 mL capacity

2.4.1.1 Description

The 150 mL lab-scale undivided reactor was placed at the Laboratory for Materials Electrochemistry and the Environment, Chemical Physical Department, Faculty of Chemistry, University of Barcelona, Spain.

Figure 2.1 displays a sketch of this reactor. It was an open, undivided and truncated conical glass cell with a total volume of 150 mL equipped with a cooling jacket connected to a temperature controller to ensure constant temperature. The anode was a BDD thin-film electrode from Adamant Technologies (La-Chaux-de-Fonds, Switzerland), synthesized by the hot filament chemical vapor deposition technique on single-crystal *p*-type Si(100) wafers (0.1 Ω cm, Siltronix). The cathode was a carbon-PTFE air-diffusion electrode from E-TEK (Somerset, NJ, USA), placed at the bottom

of a cylindrical holder of polyvinyl chloride (PVC). The inner face of the cathode was in contact with a nickel screen connected to a nichrome wire, which acted as electrical connector. A glass tube was placed inside the holder and compressed air at a flow rate of 300 mL min^{-1} was provided by an air pump. The outer face of the cathode was in contact with the solution. Both electrodes exhibited an active area of 3 cm^2 and the interelectrode gap was about 1 cm. The solution was under vigorous stirring provided by a magnetic stirrer at 700 rpm to ensure homogenization and transport of reactants towards/from the electrodes. Constant j was provided by an Amel 2051 potentiostat-galvanostat. The potential of the cell was directly measured with a Demestres 601BR digital multimeter.

In PEF-UVA experiments, the solution was irradiated by a Philips TL 6W/08 fluorescent blacklight blue lamp placed at the top of the glass cell. This lamp emits UVA light in the wavelength region between 350-410 nm with λ_{max} at 360 nm, yielding an average UVA photoionization energy of 5.0 W m^{-2} at solution surface as detected by a global UV radiometer (Kipp & Zonen B.V., model CUV5), which provided the incident UV intensity in W m^{-2} from 280 to 400 nm. In SPEF assays, the cell was directly exposed to solar radiation and a mirror was placed at its bottom to better collect the sun rays.

To remove impurities on the BDD surface and activate the cathode, both electrodes were polarized in $7.0 \text{ g Na}_2\text{SO}_4 \text{ L}^{-1}$ at 100 mA cm^{-2} for 180 min before trials.

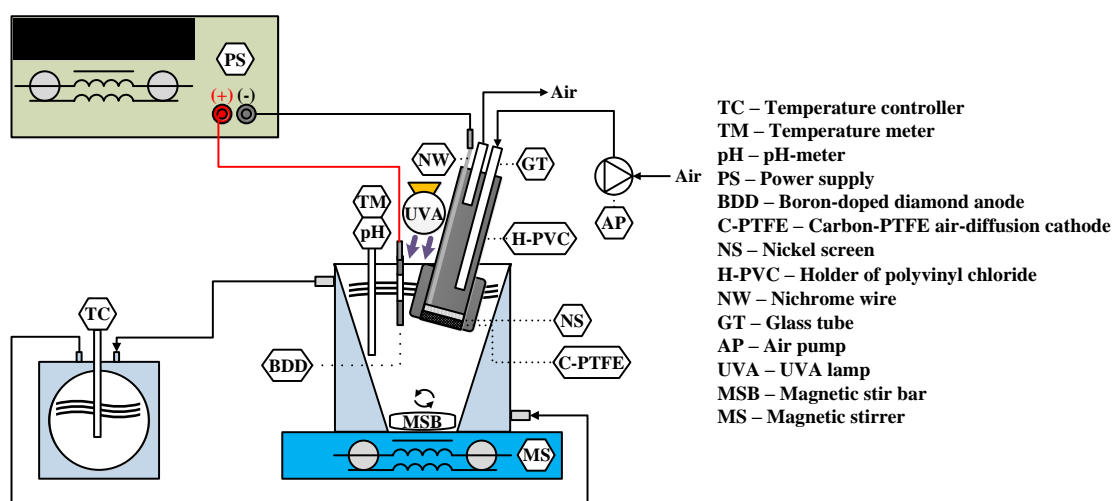


Figure 2.1. Sketch of the lab-scale undivided reactor with 150 mL capacity.

2.4.1.2 Hydrogen peroxide accumulation

To characterize the 150 mL capacity lab-scale undivided reactor equipped with a BDD anode and a carbon-PTFE air-diffusion cathode in terms of H_2O_2 accumulation, three electrolysis at different j were carried out, using 100 mL of a $7.0 \text{ g Na}_2\text{SO}_4 \text{ L}^{-1}$ solution at pH of 3.0 and $35 \text{ }^\circ\text{C}$. Figure 2.2 shows increasing H_2O_2 contents with electrolysis time for all j values. Nevertheless, for times longer than 120-180 min the H_2O_2 accumulation was decelerated, suggesting that the reaction rate of H_2O_2 decomposition via Eq. (19) is likely to become similar to that of its electrogeneration by Eq. (16) at high H_2O_2 contents. From Figure 2.2, one can also infer that higher j led to larger ability for H_2O_2 accumulation, with the achievement of accumulations of 748, 1381 and $3281 \text{ mg H}_2\text{O}_2 \text{ L}^{-1}$ after 360 min of electrolysis for j of 16.7, 33.3 and 100 mA cm^{-2} , respectively. These results point out to an almost linear relation between accumulated H_2O_2 and j due to the concomitant acceleration of H_2O_2 electrogeneration and decomposition reactions.

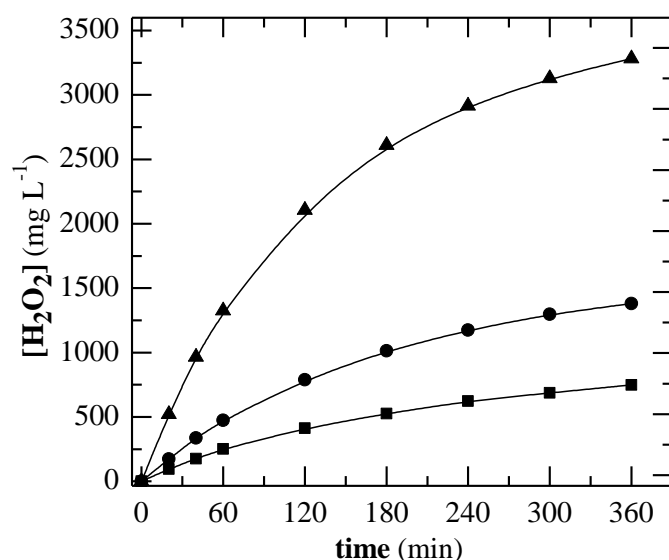


Figure 2.2. Variation of accumulated H_2O_2 concentration with time during the electrolysis of 100 mL of a $7.0 \text{ g Na}_2\text{SO}_4 \text{ L}^{-1}$ solution at pH of 3.0 and $35 \text{ }^\circ\text{C}$ in the 150 mL capacity lab-scale undivided reactor equipped with a BDD anode and a carbon-PTFE air-diffusion cathode. Current density: (■) 16.7, (●) 33.3 and (▲) 100 mA cm^{-2} .

2.4.1.3 Experimental procedure

The temperature controller was switched on at a temperature set-point that allowed preserving the inner solution at $35 \text{ }^\circ\text{C}$. A volume of 100 mL of 290 mg SY L^{-1} in $7.0 \text{ g Na}_2\text{SO}_4 \text{ L}^{-1}$ was added to the undivided reactor and the solution was homogenized by magnetic stirring for 5 min in the dark (a first control sample was taken). Afterwards, the pH was adjusted to 3.0 and the solution was

homogenized for 10 min in the dark (a second control sample was taken). For EF, PEF and SPEF trials, $\text{FeSO}_4 \cdot 7\text{H}_2\text{O}$ was added to obtain a $[\text{TDI}]_0$ of 28 mg L^{-1} , followed by further solution homogenization for another 10 min in the dark (a third control sample was taken). Finally, j was set at 16.7, 33.3 or 100 mA cm^{-2} and, in light-assisted EAOPs, the radiation was simultaneously provided (the artificial UVA lamp was switched on in PEF trials or the reactor was uncovered in SPEF trials). Samples of 1-2 mL were taken at different time intervals to evaluate the degradation process. Due to the very small capacity of the reactor, various similar processes were accomplished to determine the behavior of the different degradation parameters (color and concentration of DOC, SY, carboxylic acids and inorganic ions). Table 2.5 summarizes the operational variables used in this reactor.

Table 2.5. Operational characterization of EAOPs performed in the various plants.

Chapter	Wastewater	Process	V_{add}^a (mL)	V_0^b (mL)	V_{sample}^c (mL)	j (mA cm ⁻²)	T (°C)	pH	[TDI] ₀ (mg L ⁻¹)	
150 mL capacity lab-scale undivided reactor										
3	290 mg SY L ⁻¹ in 7.0 g Na ₂ SO ₄ L ⁻¹	AO-H ₂ O ₂ -BDD	100	≈99	1-2	16.7, 33.3, 100	35	3.0	-	
		EF-BDD	100	≈97	1-2	16.7, 33.3, 100	35	3.0	28	
		PEF-UVA-BDD	100	≈97	1-2	16.7, 33.3, 100	35	3.0	28	
		SPEF-BDD	100	≈97	1-2	16.7, 33.3, 100	35	3.0	28	
10 L capacity pilot-scale flow plant										
3	290 mg SY L ⁻¹ in 7.0 g Na ₂ SO ₄ L ⁻¹	SPEF-Pt	10000	9850	50	33.2, 55.4, 77.6	35	3.0	28	
2.2 L capacity lab-scale flow plant										
4	20.0 mg TMP L ⁻¹ in 7.0 g Na ₂ SO ₄ L ⁻¹	AO-H ₂ O ₂ -BDD	1280	1250	30	5.0	20	3.5	-	
		EF-BDD	1340	1250	30	5.0	20	3.5	2.0	
		PEF-UVA-BDD	1340	1250	30	2.5, 5.0, 10, 50, 100, 150	20	3.0, 3.5, 4.0, 4.5	2.0, 3.0, 4.0, 8.0	
		PEF-UVA-Pt	1340	1250	30	5.0	20	3.5	2.0	
		SPEF-BDD	1340	1250	30	5.0	20	3.5	2.0	
		SPEF-Pt	1340	1250	30	5.0	20	3.5	2.0	
		Fenton	1340	1250	30	-	20	3.5	2.0	
		PF-UVA	1340	1250	30	-	20	3.5	2.0	
		20.0 mg TMP L ⁻¹ in secondary MWWTP wastewater	SPEF-Pt	1340	1250	30	5.0	20	3.5	2.0
		5.0 mg TMP L ⁻¹ in secondary MWWTP wastewater	AO-BDD	1280	1250	30	5.0	20	6.8	-
	AO-H ₂ O ₂ -BDD	1280	1250	30	5.0	20	6.8	-		
	PEF-UVA-BDD	1340	1250	30	5.0	20	3.5	2.0		
	PEF-UVC-BDD	1340	1250	30	5.0	20	3.5	2.0		

Table 2.5. Operational characterization of EAOPs performed in the various plants.

Chapter	Wastewater	Process	V_{add}^a (mL)	V_0^b (mL)	V_{sample}^c (mL)	j (mA cm ⁻²)	T (°C)	pH	[TDI] ₀ (mg L ⁻¹)
4	Secondary MWWTP wastewater spiked with 19 pharmaceutical compounds in µg L ⁻¹ levels	AO-BDD	1250	1250	1000 ^d	5.0	20	6.8	-
		PEF-UVA-BDD	1250	1250	1000 ^d	5.0	20	3.5	-
		PEF-UVC-BDD	1250	1250	1000 ^d	5.0	20	3.5	-
5	20.0 mg TMP L ⁻¹ in 7.0 g Na ₂ SO ₄ L ⁻¹	PEF-UVA-BDD/oxalate	1340	1250	30	5.0	10, 20, 40	4.5, 5.0, 5.5	2.0
		PEF-UVA-BDD/tartrate	1340	1250	30	5.0	20	4.5	2.0
		PEF-UVA-BDD/malate	1340	1250	30	5.0	20	4.5	2.0
		PEF-UVA-BDD/citrate	1340	1250	30	5.0	20	4.5, 5.0	2.0
6	Winery wastewater (Bio-treatment + EAOP)	AO-H ₂ O ₂ -BDD	1265	1250	15 ^e	25	25	2.8	-
		EF-BDD	1295	1250	20 or	25	25	2.8	35
		PEF-UVA-BDD	1295	1250	25 ^f	10, 25, 100	25	2.8	20, 35, 70
		SPEF-BDD	1295	1250		25	25	2.8	35
7	Municipal sanitary landfill leachate (Bio-treatment + coagulation/aeration + EAOP/AOP)	EF-BDD	1160	1150	10	200	20	2.8	12 ^g
		EF-BDD	1180	1150	10	200	20	2.8	60
		PEF-UVA-BDD	1180	1150	10	25, 100, 200, 300	20	2.8	60
		SPEF-BDD	1180	1150	10	200	20	2.8	60
		Fenton	1180	1150	10	-	20	2.8	60
		PF-UVA	1180	1150	10	-	20	2.8	60
	SPF	1180	1150	10	-	20	2.8	60	

Table 2.5. Operational characterization of EAOPs performed in the various plants.

Chapter	Wastewater	Process	V_{add}^a (mL)	V_0^b (mL)	V_{sample}^c (mL)	j (mA cm ⁻²)	T (°C)	pH	[TDI] ₀ (mg L ⁻¹)
8	Municipal sanitary landfill leachate after bio-treatment and coagulation/aeration + EAOP	AO-BDD	1160	1150	10	200	20	2.8	12 ^g
		EF-BDD	1160	1150	10	200	20	2.8	12 ^g
		EF-Pt	1160	1150	10	200	20	2.8	12 ^g
		EF-BDD	1180	1150	10	200	20	2.8	60
		EF-Pt	1180	1150	10	200	20	2.8	60
		PEF-UVA-BDD	1180	1150	10	200	15, 20, 30, 40	2.8, 3.5, 4.0	20, 40, 60, 80
		PEF-UVA-Pt	1180	1150	10	200	20	2.8	60
		SPEF-BDD	1180	1150	10	200	20	2.8	60
		SPEF-Pt	1180	1150	10	200	20	2.8	60
		PEF-UVA-BDD/oxalate	1190	1150	10	200	20	2.8, 3.5, 4.0, 5.0	60
		PEF-UVA-Vis-BDD	1180	1150	10	200	20	2.8	60
		PEF-UVC-BDD	1180	1150	10	200	20	2.8	60
PEF-UVC-BDD	1180	1150	10	200	20	2.8	12 ^g		
PF-UVA	1180	1150	10	200	20, 30, 40	2.8	60		
35 L capacity pilot-scale flow plant									
4	20.0 mg TMP L ⁻¹ in 7.0 g Na ₂ SO ₄ L ⁻¹	SPEF-Pt	25000	24700	100	5.0	20	3.5	2.0
7	Municipal sanitary landfill leachate (Bio-treatment + coagulation/aeration + SPEF-Pt)	SPEF-Pt	25000	24400	50 ^h 500 ⁱ	200	20	2.8	60

^a V_{add} – Volume of solution initially added to the reactor;

^b V_0 – Volume of solution at time = 0 min inside the reactor;

^c V_{sample} – Volume of sample collected during the experiment;

^d It was carried out an individual experiment for each reaction time;

^e Volume of sample collected up to time = 0 min (inclusively);

^f Volume of sample collected during the experiment;

^g [TDI]₀ intrinsic to the landfill leachate;

^h Volume of sample collected up to time = 0 min (exclusively);

ⁱ Volume of sample collected at time = 0 min and during the experiment.

2.4.2 Pilot-scale flow plant with 10 L capacity

2.4.2.1 Description

The 10 L pilot-scale flow plant was placed at a terrace of the Chemical Physical Department, Faculty of Chemistry, University of Barcelona, Spain (latitude: 41° 23' 5.0'' N; longitude: 2° 7' 3.7'' E).

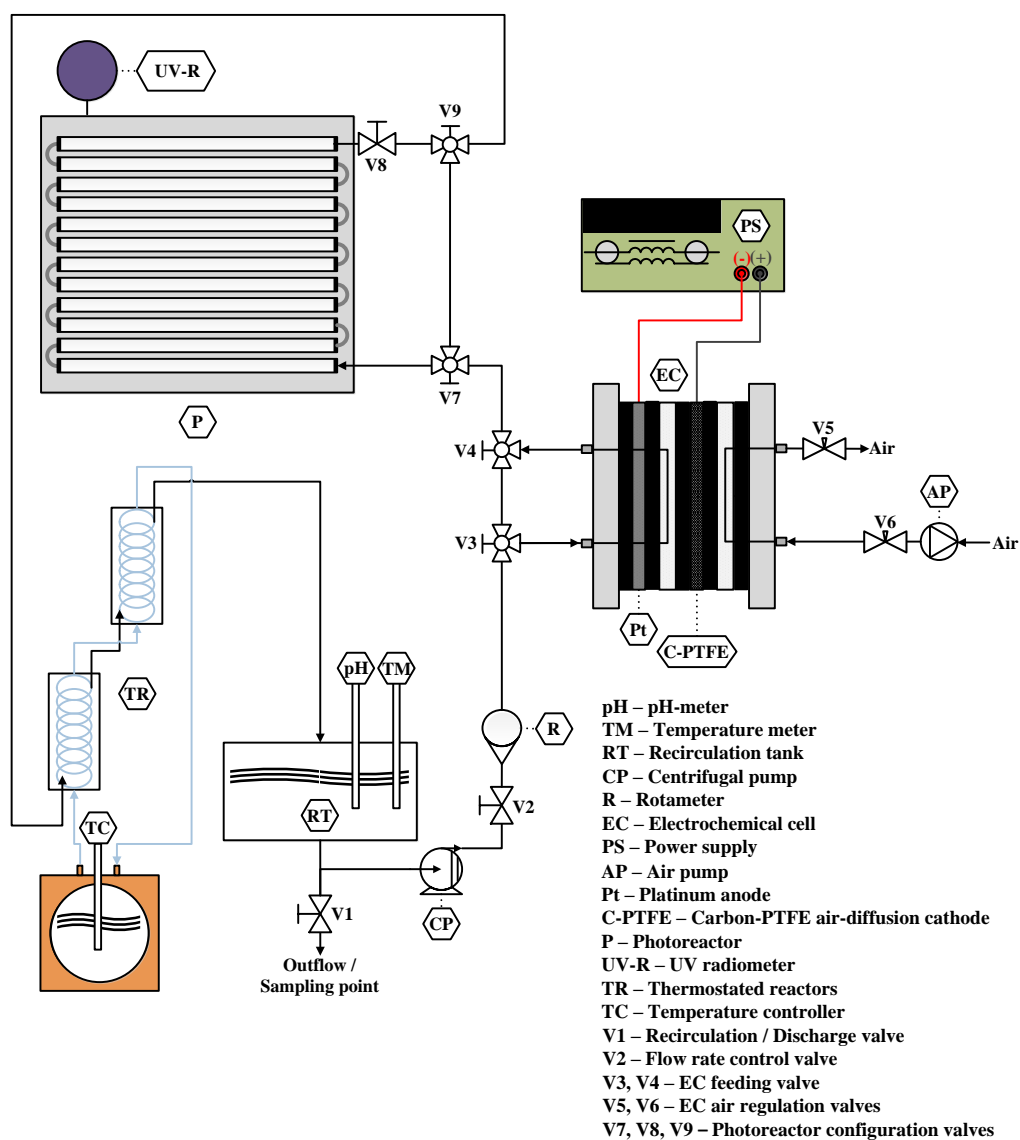
Figure 2.3a illustrates the experimental set-up of this plant. Its main components were: (i) a rectangular reservoir, (ii) two small thermostated glass cylindrical reactors, (iii) a solar photoreactor, and (iv) an electrochemical cell. The solution flowed continuously throughout the system at a flow rate of 3.0 L min⁻¹ regulated by a rotameter by means of a centrifugal pump (Iwaki).

The two thermostated glass cylindrical reactors were composed of an internal glass coil connected to a temperature controller to regulate temperature and ensure a constant temperature during the experiment.

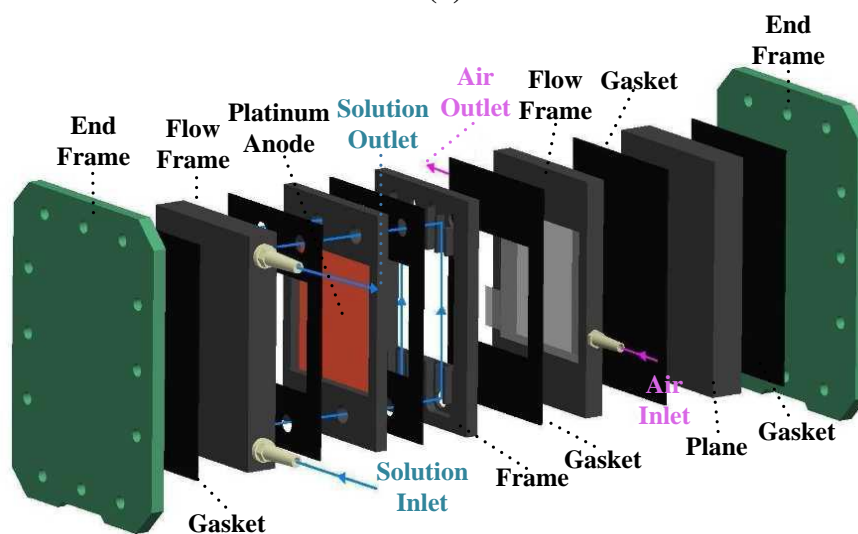
The solar photoreactor consisted of twelve borosilicate tubes (internal diameter 18.2 mm and length 505 mm), comprising an irradiated volume of 1.57 L, mounted in a 0.4 m² aluminum plane sheet tilted 41° (local latitude) with south-west orientation. The solar UV radiation was measured by a global UV radiometer (Kipp & Zonen B.V., model CUV5) placed at the same angle, which provided the incident UV intensity in W m⁻² from 280 to 400 nm.

The electrochemical cell was a one-compartment filter-press reactor equipped with a Pt sheet anode of 99.99% purity from SEMPSA (Barcelona, Spain) and a carbon-PTFE air-diffusion electrode from E-TEK (Somerset, United States), schematized in Figure 2.3b. The inner face of the cathode was pressed onto a Ni mesh as electrical connector and contacted with a PVC gas chamber fed by compressed air at a flow rate of 4.5 L min⁻¹ provided by an air pump and regulated with a back-pressure gauge. Both electrodes, separated 12 mm, had an active area of 90.2 cm². The components were divided by Viton gaskets to avoid leakages. Constant *j* was provided by a Grelco GDL3020 power supply, which directly displayed the potential of the cell.

To remove impurities of the Pt surface and activate the cathode, both electrodes were polarized in 7.0 g Na₂SO₄ L⁻¹ at 100 mA cm⁻² for 180 min before trials.



(a)



(b)

Figure 2.3. Sketches of (a) the pilot-scale flow plant with 10 L capacity and (b) the respective one-compartment filter-press reactor.

2.4.2.2 Experimental procedure

The temperature controller was switched on at a temperature set-point that allowed maintaining the inner solution at 35 °C. 10 L of 290 mg SY L⁻¹ in 7.0 g Na₂SO₄ L⁻¹ were added to the reservoir and the solution was homogenized by recirculation for 20 min in the dark (a first control sample was taken). Afterwards, the pH was adjusted to 3.0 and the solution was homogenized for more 20 min in the dark (a second control sample was taken). FeSO₄·7H₂O was added to obtain a [TDI]₀ of 28 mg L⁻¹, followed by further solution homogenization for 20 min in the dark (a third control sample was taken). Finally, *j* was set at 33.2, 55.4 or 100 mA cm⁻² and the solar photoreactor was simultaneously uncovered. 50 mL of sample were taken at different time intervals to evaluate the degradation process. Table 2.5 outcomes the operational variables used in this plant.

2.4.3 Lab-scale flow plant with 2.2 L capacity

2.4.3.1 Description

The 2.2 L lab-scale flow plant was placed at LSRE – Laboratory of Separation and Reaction Engineering, Department of Chemical Engineering, Faculty of Engineering, University of Porto, Portugal. When performing SPEF trials, the plant was moved to the roof of the Chemical Engineering Department, Faculty of Engineering, University of Porto, Portugal (latitude: 41° 10' 41.2'' N; longitude: 8° 35' 49.2'' E).

The experimental set-up of this plant is illustrated in Figures 2.4a and 2.5. It was mainly composed of: (i) a 1.5 L capacity cylindrical glass vessel, (ii) a photoreactor composed of CPCs, and (iii) an electrochemical cell. All the system units were connected by PTFE tube. The solution flowed continuously throughout the plant by means of a peristaltic pump (Ismatec, model Ecoline VC-380 II) at a flow rate of 40 L h⁻¹. This flow rate in combination with magnetic stirring into the glass vessel ensured proper mass transfer of pollutants towards electrodes, catalyst and illuminated zone.

The cylindrical glass vessel was equipped with a cooling jacket coupled to a refrigerated thermostatic bath (Julabo, model F12-EH) to regulate temperature during the experiment. Furthermore, it was under vigorous stirring at 400 rpm provided by a magnetic stirrer (Velp Scientifica, model T.ARE) to enhance the solution homogenization.

The photoreactor included a borosilicate tube (Schott-Duran type 3.3, Germany, cut-off at 280 nm, internal diameter 70 mm, length 200 mm and thickness 1.8 mm) connected to a concentric inner quartz tube with 22 mm external diameter that can be filled with a lamp (e.g. UVA, UVA-Vis or UVC lamp described below) in PEF experiments, bringing an irradiated volume of 694 mL. Two polypropylene caps with four equidistant inlets and outlets ensured a better distribution of the feed stream throughout the photoreactor. The borosilicate tube was allocated in the focus of two stainless steel reflectors, one at the bottom and another at the top (double CPC), each one consisting of two truncated parabolas and exhibiting a total dimension of 19.5 cm × 21.0 cm. These reflectors allowed the illumination along the total tubular reactor perimeter and the minimization of radiation losses. The top reflector was removed and the photoreactor was illuminated by natural sunlight in SPEF experiments. For this purpose, the photoreactor was tilted 41° (local latitude) with south orientation and the intensity of the solar UV radiation was measured by a global UV radiometer (Kipp & Zonen B.V., model CUV5) placed at the same angle, which provided the incident UV intensity in W m^{-2} from 280 to 400 nm.

The electrochemical cell was a MicroFlowCell from ElectroCell (Tarm, Denmark), illustrated in Figure 2.4b. It consisted of a one-compartment filter-press reactor that can be equipped with a common anode and a common or GDE cathode. The following three electrodes were available during the experimental work of this thesis: BDD, Pt and carbon-PTFE air-diffusion electrodes. All the electrodes had an active area of 10 cm² and were supplied by ElectroCell. The BDD electrode comprised a conductive 2 mm thickness Nb sheet coated with approximately 5 μm BDD thin film and the Pt electrode consisted of a conductive 2 mm thickness Ti sheet coated with 2.5 μm pure Pt layer. The carbon-PTFE air-diffusion electrode was compressed onto a 2 mm thickness Ti frame, which acted as electrical connector. A 2 mm thickness PTFE flow frame fitted with a central window filled with a polypropylene turbulence mesh was placed between both electrodes, separated 4 mm, for solution circulation. An identical frame was put in contact with the outer face of the cathode to be fed with compressed air at a flow rate of ca. 5 L min⁻¹ supplied by an air pump (Aqua Medic, model Mistral 2000). The electrochemical reactor components were divided by 1 mm thickness peroxide-cured ethylene propylene diene monomer (EPDM) gaskets in order to avoid leakages. An Agilent E3634A 200W power supply (7 A, 25 V or 4 A, 50 V) was responsible to provide constant j . The applied potential of the cell was directly displayed.

To remove impurities of the anodes surface and activate the cathode, all electrodes were polarized in 7.0 g Na₂SO₄ L⁻¹ at 100 mA cm⁻² for 180 min before experiments.

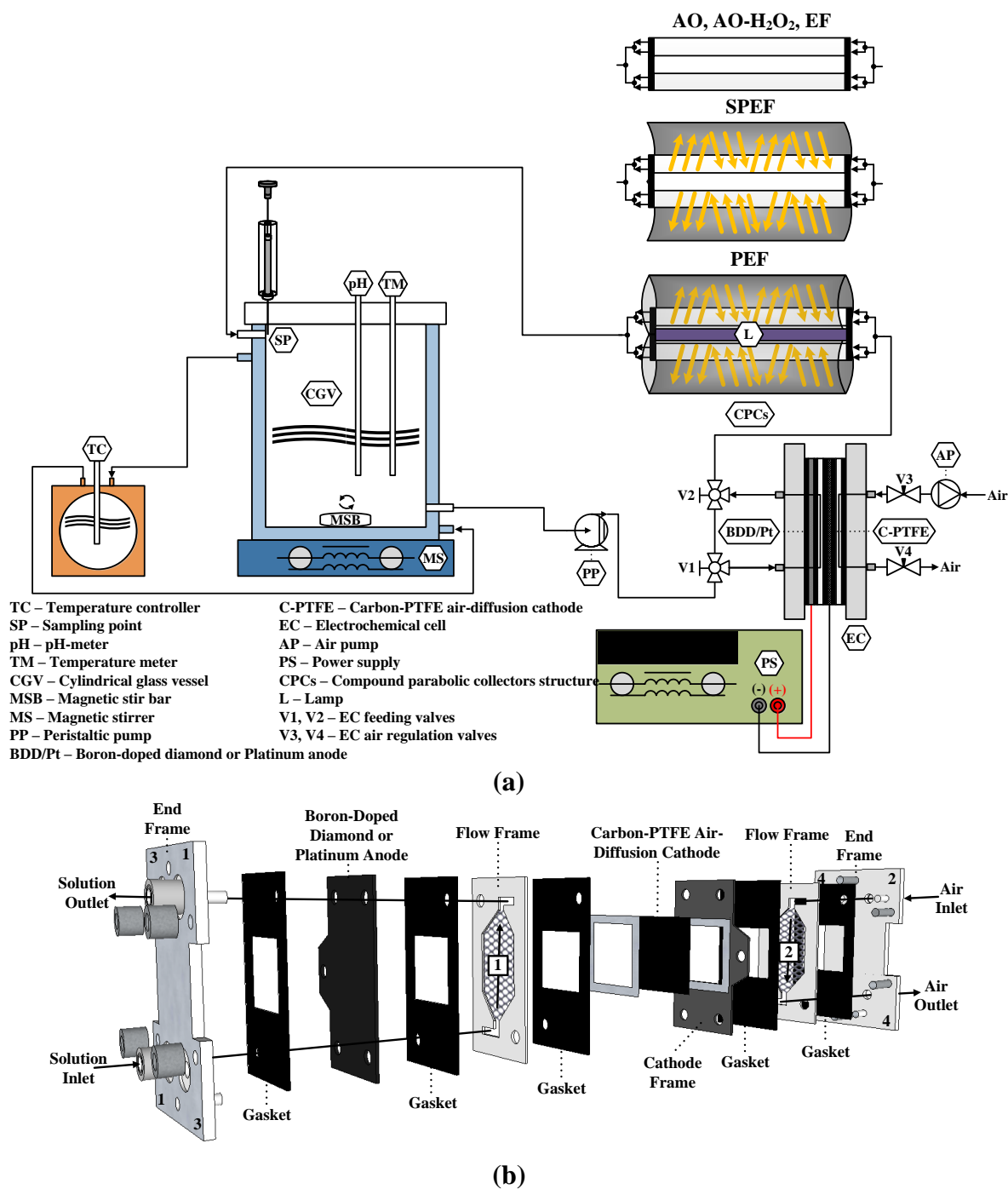


Figure 2.4. Sketches of (a) the lab-scale flow plant with 2.2 L capacity and (b) the one-compartment filter-press MicroFlowCell reactor.

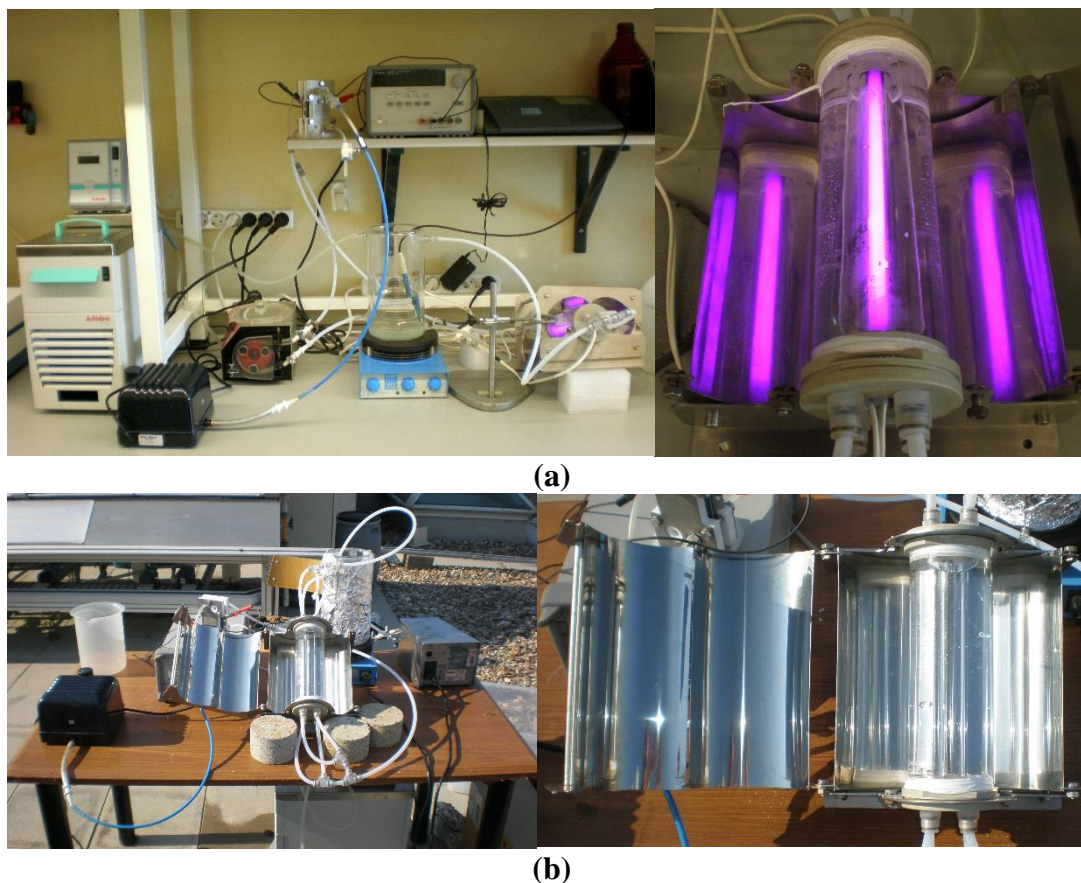


Figure 2.5. Pictures of the lab-scale flow plant with 2.2 L capacity under (a) PEF operation using an UVA artificial lamp and (b) SPEF operation.

2.4.3.2 Radiation sources and photonic flux

Three lamps were used within this thesis: UVA, UVA-Vis and UVC lamps. The UVA lamp was a Philips fluorescent blacklight blue lamp, 6 W energy power, model TL 6W/08; the UVA-Vis lamp corresponded to a Luxram[®] UVA-Vis lamp, 6 W energy power; and the UVC lamp was a Philips UVC low pressure mercury lamp, 6 W energy power, model TUV G6T5. SPEF trials were performed in sunny days.

2.4.3.2.1 Spectral irradiance

Figure 2.6 shows the spectral irradiance of all lamps as well as of natural sunlight. From this figure, one can conclude that both artificial UVA-Vis lamp and natural sunlight emit radiation in a 350-700 nm range, but while the UVA-Vis light exhibits various emission peaks, with emphasis for the larger peaks at 436, 546 and 611 nm, the solar radiation does not show severe fluctuations. In turn, the UVA lamp embraces a single and short UVA emission region from 350 to 410 nm,

with λ_{\max} of 360 nm, whereas the UVC lamp mainly emits at 254 nm, with very small emissions for higher wavelengths.

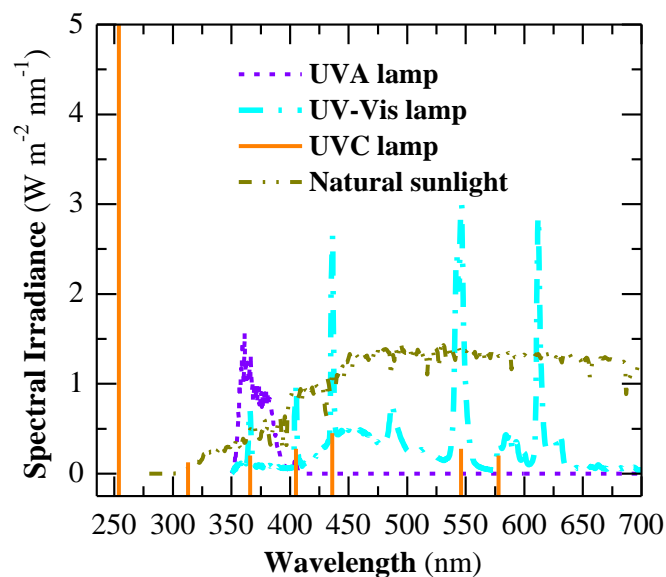


Figure 2.6. Spectral irradiance of UVA, UVA-Vis and UVC lamps and natural sunlight (UVA lamp: measured with the spectro-radiometer and confirmed by Philips; UVA-Vis lamp: measured with the spectro-radiometer – not calibrated – qualitative information; UVC lamp: supplied by Philips; natural sunlight: AM1.5G reference spectrum [17]).

2.4.3.2.2 UV intensity and photonic flux

Table 2.6 displays the average UV intensity at lamps surface and at borosilicate tube surface for natural sunlight as well as the photonic flux reaching the solution when applying the different radiation sources.

Natural sunlight commonly displays an incident UV intensity in the 280-400 nm range of 18.5-45.0 W m⁻², which corresponds to photonic fluxes from 0.44±0.02 to 0.76±0.08 J s⁻¹ in the 300-400 nm range (2-NB actinometry). These values are very similar to the ones observed using the UVA lamp, i.e. 30 W m⁻² and 0.65±0.04 J s⁻¹, although natural sunlight has showed to be able to emit at slightly higher UV intensity and, moreover, these measurements do not take into account the emission in the visible region, which would highly increment the values for the natural sunlight. The UVA-Vis lamp exhibits an almost null emission at 300-410 nm along with a very small emission at 250-500 nm (ferrioxalate actinometry), thereby suggesting a chiefly irradiation in the visible region. The UVC system exhibits a very similar photonic flux at 250-450 nm (H₂O₂ actinometry) to that of the UVA lamp at 300-410 nm.

Since UVA, UVA-Vis and UVC lamps have similar power energy (6 W) and dimensions, degradations under the same conditions using these three light sources can be directly compared in terms of time.

Table 2.6. Characteristics of UVA, UVA-Vis and UVC lamps and natural sunlight.

Light source	Average UV intensity (280-400 nm) ^a (W m ⁻²)	Photonic flux (300-410 nm) ^b (J s ⁻¹)	Photonic flux (< 280 nm) ^c (J s ⁻¹)	Photonic flux (250-500 nm) ^d (J s ⁻¹)	Photonic flux (250-500 nm) ^e (J s ⁻¹)
UVA lamp	30	0.65±0.04	-	1.06±0.05	1.02±0.03
UVA-Vis lamp	0.3	0.08±0.01	-	-	0.16±0.02
UVC lamp	0	-	0.72±0.01	-	-
Natural sunlight	18.5-45.0	0.44±0.02-0.76±0.08	-	-	-

^a At the lamp surface; Measured by a global UV radiometer (Kipp & Zonen B.V., model CUV5);

^b Determined by 2-NB concentration actinometry;

^c Determined by H₂O₂ actinometry;

^d Determined by ferrioxalate actinometry using K₃[Fe(C₂O₄)₃].3H₂O crystals;

^e Determined by ferrioxalate actinometry using [Fe(C₂O₄)₃]³⁻ ion prepared in situ.

Ferrioxalate actinometries using either crystals of K₃[Fe(C₂O₄)₃].3H₂O or [Fe(C₂O₄)₃]³⁻ ion prepared in situ attained similar photonic fluxes when employing the UVA lamp. However, these photonic fluxes differ from the one determined by 2-NB actinometry, using the same lamp. This can be attributed to the fact that 2-NB actinometry implicates a more reliable experimental procedure than ferrioxalate actinometry since the associated error of samples dilution is lower and the 2-NB concentration is more stable and accurate to assess than the Fe²⁺ concentration.

The following linear correlation between the incident UV intensity ($\overline{UV}_{G,n}$, in W m⁻²) in the range 18.5-45.0 W m⁻² and the photonic flux (F_0 , in J s⁻¹) reaching the SPEF system could be established: $F_0 = (0.0121 \pm 0.0001) \overline{UV}_{G,n} + (0.216 \pm 0.002)$ ($R^2 = 1.00$; $S^2_R = 1.27 \times 10^{-6} \text{ J}^2 \text{ s}^{-2}$).

From photonic flux values, the accumulated UV energy ($Q_{UV,n}$, in kJ L⁻¹) inside the reactor under PEF-UVA and SPEF conditions in a time interval Δt per unit of effluent volume was calculated according to Eqs. (53) and (54), respectively:

$$Q_{UV,n} = 0.65 \frac{t_n}{V_s \times 1000} \quad (53)$$

$$Q_{UV,n} = Q_{UV,n-1} + (0.0121 \overline{UV}_{G,n} + 0.216) \frac{\Delta t_n}{V_s \times 1000}; \quad \Delta t_n = t_n - t_{n-1} \quad (54)$$

where 0.65 is the photonic flux determined by 2-NB actinometry reaching the PEF-UVA system (in J s⁻¹), t_n is the time corresponding to the n sample (in s), V_s is the solution volume (in L), 1000

is a conversion factor (in J kJ^{-1}), $\overline{UV}_{G,n}$ is the average solar UV radiation (in W m^{-2}) measured during the period Δt_n (in s) and $(0.0121\overline{UV}_{G,n} + 0.2161)$ is the correlation between the solar UV intensity (in W m^{-2}) and the photonic flux (in J s^{-1}), valid for 18.5-45.0 W m^{-2} .

2.4.3.3 Hydrogen peroxide accumulation

The 2.2 L capacity lab-scale flow plant equipped with a BDD anode and a carbon-PTFE air-diffusion cathode was characterized in terms of H_2O_2 accumulation by performing electrolysis of 1250 mL of a 7.0 g $\text{Na}_2\text{SO}_4 \text{L}^{-1}$ solution at pH of 3.0, 20 °C and various j . Figures 2.7a,b show a gradual rise in H_2O_2 concentration with electrolysis time for all j values. However, for times longer than 180-240 min a gradual deceleration of H_2O_2 accumulation was always observed, suggesting that the reaction rate of H_2O_2 decomposition via Eq. (19) is likely to become similar to that of its electrogeneration by Eq. (16) at high H_2O_2 contents. Furthermore, Figures 2.7a,b also reveal a higher ability for H_2O_2 accumulation when applying larger j , with accumulations of 41, 86, 156, 760, 1420 and 2121 mg $\text{H}_2\text{O}_2 \text{L}^{-1}$ after 360 min of electrolysis for j of 2.5, 5, 10, 50, 100 and 150 mA cm^{-2} , respectively. This indicates a practically linear relation between accumulated H_2O_2 and j due to the concomitant acceleration of H_2O_2 electrogeneration and decomposition reactions.

Figure 2.7a also highlights the effect of Fe^{2+} addition (EF conditions) and presence of artificial UVA radiation (PEF-UVA conditions) and natural sunlight (SPEF conditions) on H_2O_2 accumulation at j of 5 mA cm^{-2} . Under EF conditions, less H_2O_2 was accumulated because of its additional destruction via Fenton's reaction (21). The loss of H_2O_2 was more significant in PEF-UVA conditions due to the quicker Fe^{2+} regeneration from Eq. (28), being even more pronounced under SPEF conditions since sunlight provided a greater UV intensity than the artificial UVA light.

Additionally, it was tested the H_2O_2 accumulation in the same system but equipped with a Pt anode instead of BDD, yielding similar results (see Figure 2.7a).

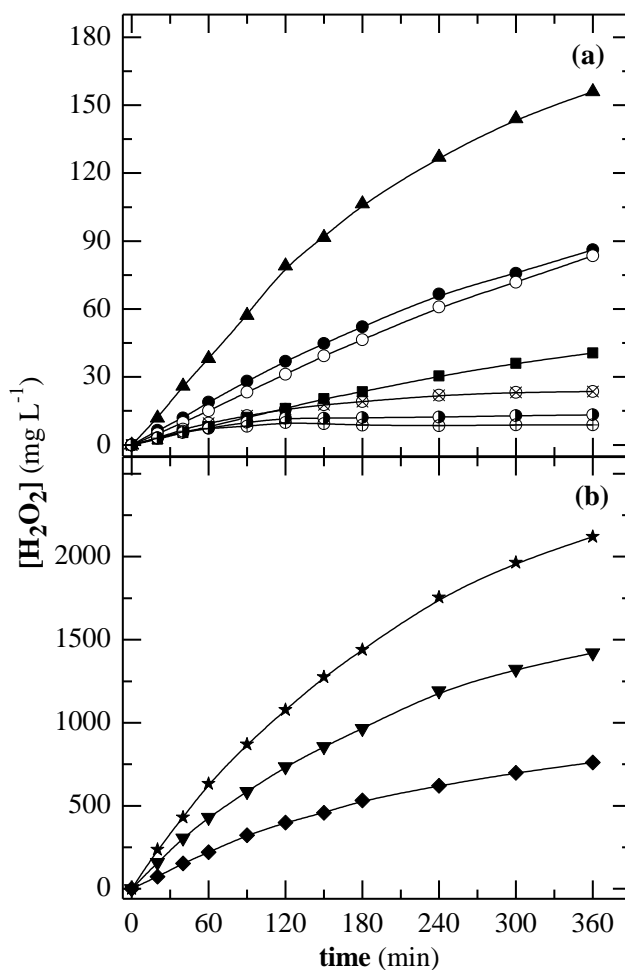


Figure 2.7. Variation of accumulated H_2O_2 concentration with time during the electrolysis of 1250 mL of a $7.0 \text{ g Na}_2\text{SO}_4 \text{ L}^{-1}$ solution at pH of 3.0 and $20 \text{ }^\circ\text{C}$ in the 2.2 L capacity lab-scale flow plant equipped with a BDD anode and a carbon-PTFE air-diffusion cathode. Current density: (a) (\blacksquare) 2.5, (\bullet) 5 and (\blacktriangle) 10 mA cm^{-2} and (b) (\blacklozenge) 50, (\blacktriangledown) 100 and (\star) 150 mA cm^{-2} . Plot (a) also presents the change of H_2O_2 concentration under (\otimes) EF, (\bullet) PEF and (\oplus) SPEF conditions with $[\text{TDI}]_0 = 2.0 \text{ mg L}^{-1}$ at 5 mA cm^{-2} and (\circ) using a Pt anode instead of BDD.

2.4.3.4 Experimental procedure

Table 2.5 shows all the variables values used in experiments performed in this plant for each chapter.

The temperature controller was switched on at a temperature set-point that allowed preserving the inner solution at a given temperature. A volume of solution was added to the glass vessel and it was homogenized by recirculation during 10 min in the dark (a first control sample was taken). Afterwards, the following procedures were carried out, according to the EAOP/AOP used.

AO and AO-H₂O₂ experiments

The pH was adjusted to the desired value and the solution was homogenized for 10 min in the dark (a second control sample was taken). j was set at a given value and a volume of sample was taken at different time intervals to evaluate the degradation process.

EF experiments

The pH was adjusted to a desired value and the solution was homogenized for 10 min in the dark (a second control sample was taken). FeSO₄·7H₂O was added (when applicable) to obtain a given [TDI]₀, taking into account the iron content of the solution. Afterwards, the solution was homogenized for another 10 min in the dark (a third control sample was taken). j was set at a given value and a volume of sample was taken at different time intervals to evaluate the degradation process.

PEF and SPEF experiments without addition of carboxylic acids

The pH was adjusted to a desired value and the solution was homogenized for 10 min in the dark (a second control sample was taken). FeSO₄·7H₂O was added (when applicable) to obtain a given [TDI]₀, taking into account the iron content of the solution. Afterwards, the solution was homogenized for another 10 min in the dark (a third control sample was taken). j was set at a given value and the radiation was simultaneously provided (the artificial UVA, UVA-Vis or UVC lamp was switched on in PEF trials or the CPCs structure was uncovered in SPEF trials). A volume of samples was taken at different time intervals to evaluate the degradation process.

PEF experiments with carboxylic acids addition in Chapter 5

The carboxylic acid (oxalic, citric, tartaric or malic acid) was added and the solution was homogenized for 10 min in the dark (a second control sample was taken). FeCl₃·6H₂O was added to reach a [TDI]₀ of 2.0 mg L⁻¹ and, after solution homogenization for more 10 min in the dark, the pH was adjusted to a desired value and a final mixing for another 10 min in the dark took place (a third control sample was taken). j was set at 5.0 mA cm⁻² and the UVA lamp was simultaneously switched on. Samples of 30 mL were taken at different time intervals to evaluate the degradation process.

Addition of scavenging agents was performed before pH adjustment and was followed by a 10 min homogenization in darkness.

PEF experiments with oxalic acid addition in Chapter 8

Oxalic acid was added and the solution was homogenized for 10 min in the dark (a second control sample was taken). Then, the pH was adjusted to a desired value and the solution was subjected to homogenization for another 10 min in the dark (a third control sample was taken). Lastly, $\text{FeCl}_3 \cdot 6\text{H}_2\text{O}$ was added to reach a $[\text{TDI}]_0$ of 60 mg L^{-1} , taking into account the iron content of the effluent, and the solution was homogenized for more 10 min in the dark (a fourth control sample was taken). j was set at 200 mA cm^{-2} and the radiation was simultaneously provided (the UVA, UVA-Vis or UVC lamp was switched on). Samples of 10 mL were taken at different time intervals to evaluate the degradation process.

Fenton, PF and SPF experiments

The pH was adjusted to a desired value and the solution was homogenized for 10 min in the dark (a second control sample was taken). $\text{FeSO}_4 \cdot 7\text{H}_2\text{O}$ was added to obtain a given $[\text{TDI}]_0$, taking into account the iron content of the solution. Afterwards, the solution was homogenized for another 10 min in the dark (a third control sample was taken). H_2O_2 was added and, in PF and SPF processes, the radiation was simultaneously provided (the UVA lamp was switched on in PF trials or the CPCs structure was uncovered in SPF trials). In Chapter 4, the stoichiometric amount of H_2O_2 needed for $20.0 \text{ mg TMP L}^{-1}$ mineralization (103 mg L^{-1}) was initially added. In Chapters 7 and 8, multiple additions of H_2O_2 were carried out to maintain the oxidant content between 200 and 400 mg L^{-1} since similar approaches have improved the oxidation rate, avoiding the absence of H_2O_2 and minimizing its consumption [18]. A volume of sample was taken at different time intervals to evaluate the degradation process.

2.4.4 Pilot-scale flow plant with 35 L capacity

2.4.4.1 Description

The 35 L pilot-scale flow plant was installed at the roof of the Chemical Engineering Department, Faculty of Engineering, University of Porto, Portugal (latitude: 41° 10' 41.2'' N; longitude: 8° 35' 49.2'' E).

A sketch and pictures of this novel plant are displayed in Figures 2.8a and 2.9, respectively. It can be operated under two distinct configurations, either using the electrochemical components to apply an EAOP or bypassing the electrochemical devices to execute an AOP. The main constituents of the EAOPs system were: (i) a 25 L capacity recirculation conical tank, (ii) a 5 L thermostated acrylic cylindrical reactor, (iii) a structure composed of CPCs, and (iv) an electrochemical cell. All the system units are connected by polypropylene (PP) tube. The solution flowed continuously throughout the system at a flow rate of 9.0 L min⁻¹ regulated by a rotameter by means of a centrifugal pump (Grundfos, model CM5-5 A-R-G-V-AQQV) connected to a frequency inverter. A turbulent flow was ensured.

The thermostated acrylic cylindrical reactor was equipped with an outer jacket and an internal glass coil, both connected to a temperature controller (Surcis S.L., model TCH5) to regulate temperature during the experiment.

The structure composed of CPCs was made-up of four borosilicate tubes (Schott-Duran type 3.3, Germany, cut-off at 280 nm, internal diameter 46.4 mm, length 1500 mm and thickness 1.8 mm), each one allocated in the focus of an anodized aluminum reflector consisting of two truncated parabolas. These collectors were mounted on a fixed platform tilted 41° (local latitude) with south orientation and the intensity of the solar UV radiation was measured by a global UV radiometer (Kipp & Zonen B.V., model CUV5) placed at the same angle, which provided the incident UV intensity in W m⁻² from 280 to 400 nm. The solution can flow throughout the four borosilicate tubes (0.91 m² of irradiated area and 9.6 L of irradiated volume) or throughout two borosilicate tubes (0.455 m² of irradiated area and 4.8 L of irradiated volume).

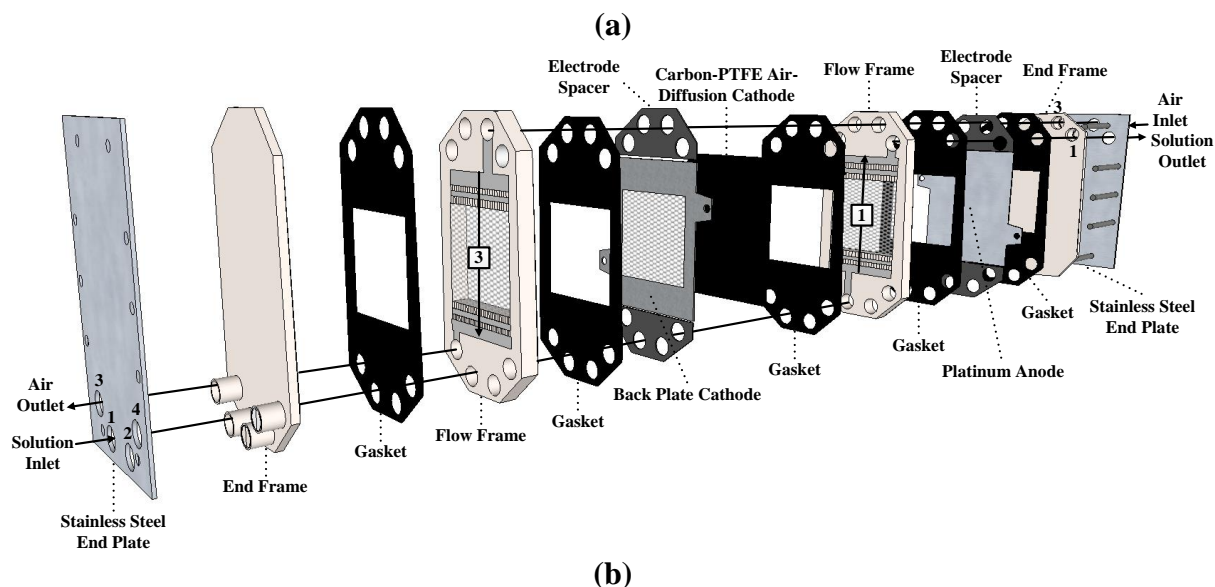
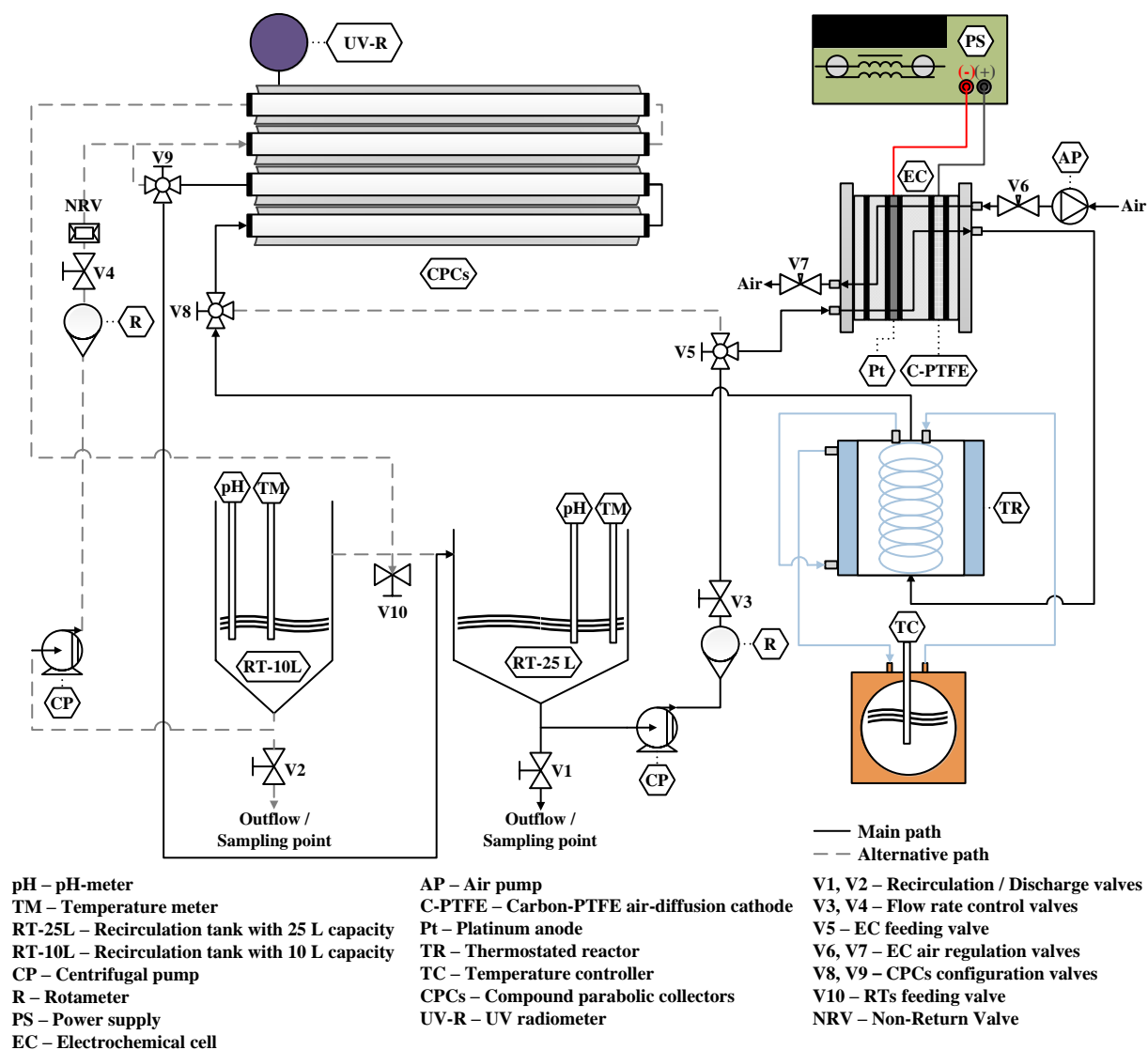


Figure 2.8. Sketches of (a) the pilot-scale flow plant with 35 L capacity and (b) the one-compartment filter-press ElectroMPCCell reactor.

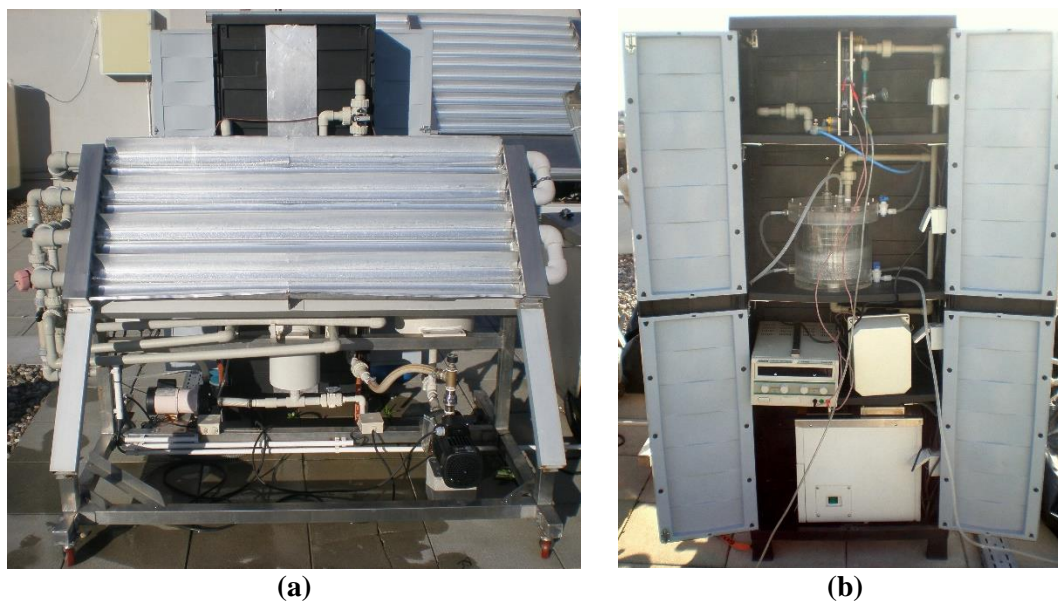


Figure 2.9. Pictures of the pilot-scale flow plant with 35 L capacity. (a) Front view and (b) back view.

The electrochemical cell was an ElectroMPCell from ElectroCell (Tarm, Denmark), schematized in Figure 2.8b. It consisted of a one-compartment filter-press reactor that can be equipped with a common anode and a common or GDE cathode. Two electrodes were available during the experimental work of this thesis: a conductive 2 mm thickness Ti sheet coated with 2.5 μm pure Pt layer used as anode and a carbon-PTFE air-diffusion electrode employed as cathode, which was compressed onto a 2 mm thickness Ti frame, acting as electrical connector. Both electrodes exhibited an active area of 100 cm^2 and were supplied by ElectroCell. A 8 mm thickness PP flow frame fitted with a central window filled with a PP turbulence mesh was placed between both electrodes, separated 10 mm, for solution circulation. An identical frame was put in contact with the outer face of the cathode to be fed with compressed air at a flow rate of ca. 60 L min^{-1} supplied by an air compressor (Cevik, model Pro 3 HP, 50 L, 340 L min^{-1} , 8 bar). The components were divided by 1 mm thickness peroxide-cured EPDM gaskets to avoid leakages. A Velleman PS3020 power supply (20 A, 30 V) was responsible to provide constant j . The applied potential of the cell was directly displayed.

To remove impurities of the Pt surface and activate the cathode, both electrodes were polarized in 7.0 g $\text{Na}_2\text{SO}_4 \text{L}^{-1}$ at 100 mA cm^{-2} for 180 min before trials.

2.4.4.2 Photonic flux

Photonic fluxes from 3.1 ± 0.1 to 5.1 ± 0.1 J s^{-1} were attained by 2-NB actinometry when applying an incident UV intensity in the 280-400 nm range of 20.0 - 45.0 W m^{-2} . These values of photonic flux are around 7 times higher than the ones found for the 2.2 L lab-scale flow reactor.

The following linear correlation between the incident UV intensity ($\overline{UV}_{G,n}$, in W m^{-2}) in the range 20.0 - 45.0 W m^{-2} and the photonic flux (F_0 , in J s^{-1}) reaching the SPEF system could be established: $F_0 = (0.0804 \pm 0.0003) \overline{UV}_{G,n} + (1.4 \pm 0.1)$ ($R^2 = 0.996$; $S^2_R = 0.01$ $\text{J}^2 \text{s}^{-2}$). From this correlation, the accumulated UV energy ($Q_{UV,n}$, in kJ L^{-1}) inside the pilot-scale plant under SPEF conditions in a time interval Δt per unit of effluent volume was calculated according to Eq. (55):

$$Q_{UV,n} = Q_{UV,n-1} + (0.0804 \overline{UV}_{G,n} + 1.4) \frac{\Delta t_n}{V_s \times 1000}; \quad \Delta t_n = t_n - t_{n-1} \quad (55)$$

where $(0.00416 \overline{UV}_{G,n} + 0.0753)$ is the correlation between the solar UV intensity (in W m^{-2}) and the photonic flux (in J s^{-1}), valid for 20.0 - 45.0 W m^{-2} , $\overline{UV}_{G,n}$ is the average solar UV radiation (in W m^{-2}) measured during the period Δt_n (in s), V_s is the solution volume (in L) and 1000 is a conversion factor (in J kJ^{-1}).

2.4.4.3 Hydrogen peroxide accumulation

To characterize the 35 L capacity pilot-scale flow plant equipped with the Pt anode and the carbon-PTFE air-diffusion cathode in terms of H_2O_2 accumulation, electrolysis at three different j values were performed, all using 25 L of a 7.0 g $\text{Na}_2\text{SO}_4 \text{L}^{-1}$ solution at pH of 3.0 and 20 °C. Figure 2.10 reveals that this unit presents similar ability for H_2O_2 accumulation to the 2.2 L capacity lab-scale flow plant. Note that to directly compare both units in terms of accumulation of H_2O_2 , the solution volume/electrodes area ratio needs to be taken into account. This ratio is the double for the 35 L capacity pilot-scale flow plant ($25000 \text{ mL}/100 \text{ cm}^2 = 250$) when compared to the 2.2 L capacity lab-scale flow plant ($1250 \text{ mL}/10 \text{ cm}^2 = 125$) and then it is expected half of H_2O_2 accumulation, as verified.

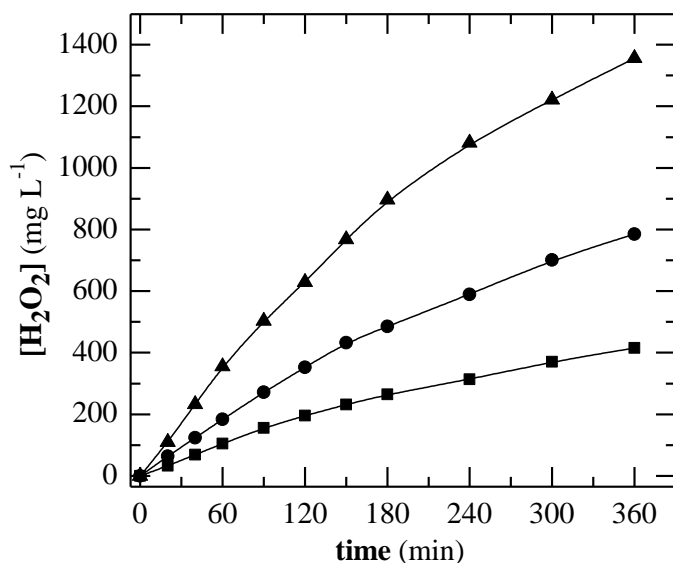


Figure 2.10. Variation of accumulated H₂O₂ concentration with time during the electrolysis of 25 L of a 7.0 g Na₂SO₄L⁻¹ solution at pH of 3.0 and 20 °C in the 35 L capacity pilot-scale flow plant equipped with a Pt anode and a carbon-PTFE air-diffusion cathode. Current density: (■) 50, (●) 100 and (▲) 200 mA cm⁻².

2.4.4.4 Experimental procedure

Table 2.5 collects the operational variables used in this plant for SPEF-Pt application in each chapter of this thesis.

The temperature controller was switched on at a temperature set-point that allowed maintaining the solution temperature at 20 °C. A volume of 25 L of solution was added to the recirculation tank and homogenized by recirculation during 30 min in the dark through the system using the EAOPs configuration and two borosilicate tubes with 4.8 L of irradiated volume (a first control sample was taken). Afterwards, the following procedures were carried out for Chapters 4 and 7.

SPEF-Pt experiment in Chapter 4

The pH was adjusted to 3.5 and the solution was homogenized for more 30 min in the dark (a second 100 mL control sample was taken). 247 mg of FeSO₄·7H₂O were added to obtain a 2.0 mg [TDI]₀ L⁻¹ concentration and the solution was homogenized for another 30 min in the dark (a 100 mL third control sample was taken). j was set at 5.0 mA cm⁻² simultaneously with the cover removal from the CPCs structure. Samples of 100 mL were taken at different time intervals to evaluate the degradation process.

SPEF-Pt experiment in Chapter 7

The pH was adjusted to 2.8 and the solution was homogenized for more 30 min in the dark (a second 50 mL control sample was taken). 5.84 g of $\text{FeSO}_4 \cdot 7\text{H}_2\text{O}$ were added to obtain a 60 mg $[\text{TDI}]_0 \text{ L}^{-1}$ concentration and the solution was homogenized for another 30 min in the dark (a 500 mL third control sample was taken - S_1). j was set at 200 mA cm^{-2} simultaneously with the cover removal from the CPCs structure. Samples of 500 mL were taken at different time intervals to evaluate the biodegradability enhancement.

2.4.5 Biological system I

2.4.5.1 Description

Figure 2.11 displays a sketch of the main components of the biological system I.

This biological system was equipped with an immobilized biomass reactor (IBR) of 45 L capacity and a conditioner tank of 50 L capacity. The IBR was a flat-bottom container packed with 62 units of propylene rings (nominal diameter of 50 mm) colonized by activated sludge from an urban WWTP of Northern Portugal and equipped with a Hailea V-20 air pump providing an air flow rate of 20 L min^{-1} through a ceramic air diffuser. The conditioner tank was a flat-bottom vessel equipped with a mechanical stirrer (Timsa) and control units for dissolved oxygen (Crison, electrode and OXI49P controller) and pH (Crison, electrode and PH27P controller) in order to keep these parameters in a selected range. H_2SO_4 or NaOH was added by means of two metering pumps (Dosapro Milton Roy, series GTM A) to control the effluent pH.

2.4.5.2 Experimental procedure

A volume of 40 L of raw winery wastewater was added to the aerobic biological system and recirculated in batch mode for 10 days at a flow rate of 6.6 L min^{-1} . The pH was maintained between 6.5 and 7.5, the dissolved oxygen in a $2\text{-}4 \text{ mg O}_2 \text{ L}^{-1}$ range and temperature values from 20 to 30 °C were registered.

2.4.6.2 Experimental procedure

Raw landfill leachate (8 L) and previously centrifuged activated sludge from the biological reactor of the MSW sanitary landfill located nearby Porto (1.5 L) were added to the reactor. The pH was maintained between 6.5 and 9.0 through the addition of Na_2CO_3 , which also provided alkalinity to be consumed in the nitrification process. Dissolved oxygen was maintained between 2 and 4 $\text{mg O}_2 \text{ L}^{-1}$ and temperature at 27 °C. Samples were taken throughout the biological treatment to assess TDC, DIC, DOC and inorganic ions. The biological oxidation was stopped when a residual content of ammonium was reached. After 3 h of sedimentation, the supernatant was carefully transferred to another container. Various biological oxidation batches were performed to obtain enough volume for all the trials.

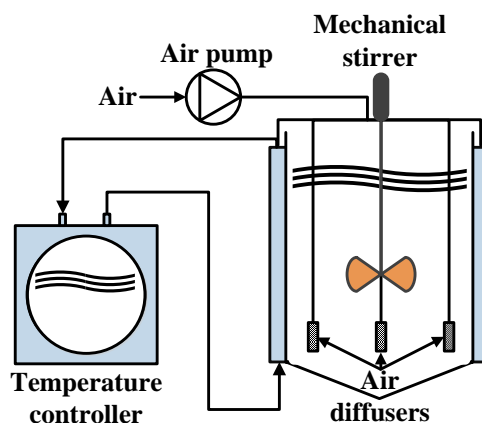


Figure 2.12. Sketch of the biological system II (reactor vessel).

2.4.7 Coagulation/aeration process

Mixtures of ca. 30 L of bio-treated landfill leachate were subjected to coagulation. To do this, FeCl_3 was added to the landfill leachate free of sludge as described by Saraiva et al. [19] ($240 \text{ mg Fe}^{3+} \text{ L}^{-1}$), followed by acidification to pH of 3.3 (using H_2SO_4 up to a concentration of around $2.0 \text{ g SO}_4^{2-} \text{ L}^{-1}$ and thereon HCl) and mechanical stirring for 15 min at 100 rpm. After sedimentation for 48 h, the clarified effluent was carefully transferred to a container where it was aerated with a 4000 L h^{-1} air pump (Aqua Medic, model Mistral 4000) for 3 h. After 24 h of sedimentation, the supernatant, i.e. the final pre-treated landfill leachate, was moved to another container to be used in EAOPs. Note that long sedimentation times were implemented to ensure complete settling and shorter times of 12 h or less can be used with the same efficiency [19].

2.5 References

- [1] Buxton, G.V., Greenstock, C.L., Helman, W.P., Ross, A.B., 1988. Critical review of rate constants for reactions of hydrated electrons, hydrogen atoms and hydroxyl radicals ($\cdot\text{OH}/\text{O}^-$) in aqueous solution. *Journal of Physical and Chemical Reference Data* 17(2), 513-886.
- [2] Raghu, S., Ahmed Basha, C., 2007. Chemical or electrochemical techniques, followed by ion exchange, for recycle of textile dye wastewater. *Journal of Hazardous Materials* 149(2), 324-330.
- [3] Liu, W., Andrews, S.A., Stefan, M.I., Bolton, J.R., 2003. Optimal methods for quenching H_2O_2 residuals prior to UFC testing. *Water Research* 37(15), 3697-3703.
- [4] 6332:1998, I., 1998. Water Quality - Determination of iron - Spectrometric Method Using 1,10-Phenanthroline.
- [5] Nogueira, R.F.P., Oliveira, M.C., Paterlini, W.C., 2005. Simple and fast spectrophotometric determination of H_2O_2 in photo-Fenton reactions using metavanadate. *Talanta* 66(1), 86-91.
- [6] Clesceri, L.S., Greenberg, A.E., Eaton, A.D., 2005. Standard methods for examination of water & wastewater, 21st ed., American Public Health Association (APHA), American Water Works Association (AWWA) & Water Environment Federation (WEF).
- [7] 11905-1:1997, I., 1997. Water quality - Determination of nitrogen - Part 1: Method using oxidative digestion with peroxodisulfate.
- [8] Folin, O., Ciocalteu, V., 1927. On tyrosine and tryptophane determinations in proteins. *Journal of Biological Chemistry* 73(2), 627-650.
- [9] Ballesteros Martín, M.M., Casas López, J.L., Oller, I., Malato, S., Sánchez Pérez, J.A., 2010. A comparative study of different tests for biodegradability enhancement determination during AOP treatment of recalcitrant toxic aqueous solutions. *Ecotoxicology and Environmental Safety* 73(6), 1189-1195.
- [10] OECD, 1992. Guideline for testing of chemicals 302 B, Inherent biodegradability: Zahn Wellens/EMPA test, Organization of Economic Cooperation and Development, Paris.
- [11] Willett, K.L., Hites, R.A., 2000. Chemical Actinometry: Using o-Nitrobenzaldehyde to Measure Lamp Intensity in Photochemical Experiments. *Journal of Chemical Education* 77(7), 900.
- [12] Nicole, I., De Laat, J., Dore, M., Duguet, J.P., Bonnel, C., 1990. Utilisation du rayonnement ultraviolet dans le traitement des eaux: mesure du flux photonique par actinometrie chimique au peroxyde d'hydrogene. *Water Research* 24(2), 157-168.
- [13] Kuhn, H.J., Braslavsky, S.E., Schmidt, R., 2004. Chemical Actinometry (IUPAC Technical Report). *Pure and Applied Chemistry* 76, 2105-2146.
- [14] Galbavy, E.S., Ram, K., Anastasio, C., 2010. 2-Nitrobenzaldehyde as a chemical actinometer for solution and ice photochemistry. *Journal of Photochemistry and Photobiology A: Chemistry* 209(2-3), 186-192.

- [15] Goldstein, S., Aschengrau, D., Diamant, Y., Rabani, J., 2007. Photolysis of aqueous H₂O₂: Quantum yield and applications for polychromatic UV actinometry in photoreactors. *Environmental Science & Technology* 41(21), 7486-7490.
- [16] Lee, J., Seliger, H.H., 1964. Quantum Yield of the Ferrioxalate Actinometer. *The Journal of Chemical Physics* 40(2), 519-523.
- [17] ASTM, 2003. Standard tables for reference solar spectral irradiances: direct normal and hemispherical on 37° tilted surface.
- [18] Bacardit, J., Oller, I., Maldonado, M.I., Chamarro, E., Malato, S., Esplugas, S., 2007. Simple models for the control of photo-Fenton by monitoring H₂O₂. *Journal of Advanced Oxidation Technologies* 10(2), 219-228.
- [19] Saraiva, I.M.A., Fonseca, M.A.F., Vilar, V.J.P., Silva, T.F.C.V., Boaventura, R.A.R., inventors. Efacec Engenharia e Sistemas, S.A., assignee. Method of treating leachate, phototreatment reactors and respective use. European Patent 2 784 031. 2014 October 1.

3 Degradation of Sunset Yellow FCF azo dye by electrochemical advanced oxidation processes

The degradation of 290 mg L⁻¹ of Sunset Yellow FCF (SY) azo dye (DOC of 100 mg L⁻¹) in an aqueous solution with 7.0 g Na₂SO₄ L⁻¹ at pH of 3.0 was studied by AO-H₂O₂, EF, PEF-UVA and SPEF processes. Trials were performed in a 150 mL capacity lab-scale undivided reactor equipped with a BDD anode and a carbon-PTFE air-diffusion cathode. The relative oxidation ability of EAOPs decreased in the order: SPEF-BDD > PEF-UVA-BDD > EF-BDD > AO-H₂O₂-BDD. In contrast, the processes ability to remove the SY parent compound and to decolorize the SY solution was quite similar for EF-BDD, PEF-UVA-BDD and SPEF-BDD processes and slower for AO-H₂O₂-BDD. This means that the azo dye was mainly destroyed by •OH produced from Fenton's reaction. It was more rapidly removed than decolorized, indicating the formation of colored aromatic by-products. The influence of j on the efficiency of all EAOPs was assessed. The SPEF treatment was scaled-up by degrading the same SY solution in a 10 L pilot-scale flow plant composed of a one-compartment filter-press cell equipped with a Pt anode and a carbon-PTFE air-diffusion cathode coupled to a solar photoreactor. The viability of SPEF at pilot-scale was demonstrated since it allowed the complete decolorization and almost total mineralization. The main oxidative difference perceived when using a Pt anode instead of BDD was the persistence of Fe(III) complexes of formic and oxamic acids since they were not removed by Pt(•OH). Furthermore, a total of 14 aromatic products and 34 hydroxylated derivatives, including benzenic, naphthalenic and phthalic acid compounds, were detected by LC-MS. Generated LMCA like tartronic, oxalic, formic and oxamic were identified by ion-exclusion HPLC. A plausible general reaction sequence for SY mineralization involving all oxidation by-products detected was finally proposed.

This Chapter is based on the following research article: “Moreira, F.C., Garcia-Segura, S., Vilar, V.J.P., Boaventura, R.A.R., Brillas, E., 2013. Decolorization and mineralization of Sunset Yellow FCF azo dye by anodic oxidation, electro-Fenton, UVA photoelectro-Fenton and solar photoelectro-Fenton processes. Applied Catalysis B: Environmental 142-143, 877-890”.

3.1 Introduction

Azo dyes account for over 70% of all commercial dyes. They are characterized by one or more azo groups ($-N=N-$) as chromophore, with each group attached to two radicals of which at least one is aromatic containing functional groups such as $-OH$ and $-SO_3H$, among others [1-3]. Large volumes of wastewaters with high azo dye contents are released by many industries into water bodies, causing not only aesthetic problems associated with wastewaters color, but also environmental damages and health risks on human beings due to toxicity, carcinogenicity, potential mutagenicity and resistance to biodegradation of these pollutants and their by-products [1, 4, 5]. Research efforts are then needed for the development of powerful oxidation processes to destroy azo dyes and their by-products from waters.

At the time of this study, some important aspects regarding the viability of PEF-UVA and SPEF processes had not been well clarified yet, namely their direct comparison with AO- H_2O_2 and EF in terms of oxidation ability, the use of different anodes, the reactions producing aromatic intermediates and the influence of generated oxidants and UVA light on final by-products. In this way, the degradation of Sunset Yellow FCF (SY) azo dye (see characteristics in Table 2.1) was carefully assessed by AO- H_2O_2 , EF, PEF-UVA and SPEF processes, using both BDD and Pt anodes and following the formation of aromatic by-products and LMCA by LC-MS and HPLC, respectively. SY is widely used as colorant in food, drugs and cosmetics [6]. Several papers have reported its removal by H_2O_2 [7], peroxodisulfate in the absence and presence of Ag(I) [8], photocatalysis with transition metal complexes and H_2O_2 [9] and SPF with copper loaded bentonite [10]. In all these studies the SY degradation was only spectrophotometrically monitored by absorbance measurements. Furthermore, Ghoneim et al. [11] evaluated the degradation of SY by EF process using a Pt anode and a RVC cathode in terms of decolorization, COD and dye concentration decay.

The present Chapter reports the results obtained for the comparative degradation of 290 mg L^{-1} of SY (DOC of 100 mg L^{-1}) in aqueous solutions with $7.0\text{ g Na}_2\text{SO}_4\text{ L}^{-1}$ at pH of 3.0 by AO- H_2O_2 , EF, PEF-UVA and SPEF processes. Experiments were carried out in a 150 mL capacity lab-scale undivided reactor equipped with a BDD anode and a carbon-PTFE air-diffusion cathode. To clarify the viability of scaling-up the SPEF treatment and also the effect of the nature of the anode, SY solutions were also degraded using the 10 L pilot-scale flow plant equipped with a

one-compartment filter-press cell with a Pt anode and a carbon-PTFE air-diffusion cathode coupled to a solar photoreactor. The influence of j on the decolorization rate and mineralization degree was examined for all processes. The SY content decay using the various processes was also assessed. A general reaction sequence for SY mineralization was proposed taking into consideration all by-products detected by LC-MS and generated LMCA followed by HPLC.

3.2 Materials and methods

All chemicals, analytical determinations, modeling of degradation kinetics and experimental units and procedures can be accessed in the Chapter 2. Table 2.5 summarizes the operational conditions of EAOPs performed in the current Chapter.

3.3 Results and discussion

3.3.1 Comparative decolorization and mineralization of SY by EAOPs at lab-scale

The decolorization and mineralization of SY by AO-H₂O₂-BDD, EF-BDD, PEF-UVA-BDD and SPEF-BDD processes in the 150 mL lab-scale undivided reactor were comparatively assessed by electrolyzing 100 mL of an aqueous solution composed of 290 mg L⁻¹ of the azo dye and 7.0 g Na₂SO₄ L⁻¹ at pH of 3.0, 35 °C, with addition of [TDI]₀ of 28 mg L⁻¹ for the three latter EAOPs and at *j* of 33.3 mA cm⁻². This pH value was chosen since maximal pollutants degradation at pH close to 3.0 has been reported for such processes [12-14] due to predominance of higher amounts of photoactive Fe(III)-hydroxy complexes, absence of iron precipitation, absence of scavenge of •OH by carbonate and bicarbonate species and null auto-decomposition of H₂O₂. A temperature of 35 °C was applied since water evaporation can occur for temperatures above it [15]. Optimum [TDI]₀ of 28 mg L⁻¹ has been found for Fenton's reaction based EAOPs of aromatics [12, 16]. During experiments, the solution pH decreased slowly to pH of 2.4-2.7, probably due to the formation of carboxylic acids [14, 17], and for this reason the pH was regularly adjusted to its initial value by adding small volumes of 0.5 M NaOH. As can be seen in the inset panel of Figure 3.1a, the UV-Vis spectrum of the initial solution (diluted 1:5) shows a strong visible band with λ_{\max} at 482 nm (characteristic of SY, see Table 2.1), along with a much weaker shoulder near 420 nm. According to the behavior of other similar azo dyes [18], these bands can be associated with two tautomeric forms in equilibrium, (i) the hydrazone form, where the hydroxyl group appears as carbonyl group and its hydrogen is linked to the azo group, and (ii) the azo form (presented in Table 2.1). The hydrazone form is expected to yield the stronger band at 482 nm [18] and then predominates over the azo form that gives the weak shoulder at 420 nm. In addition, the UV-Vis spectrum of Figure 3.1a exhibits a weak band in the UV region centered at 314 nm due to the naphthalene group of SY [18], but it does not display clearly the band related to the benzene group, expected at about 240 nm, because it overlaps with the band of high absorbance recorded up to λ of 280 nm. Based on this, the decolorization efficiency for SY by the EAOPs tested was determined from the absorbance decay at 482 nm.

Figure 3.1a highlights that the AO-H₂O₂-BDD process only allowed a slow decolorization, reaching 88% color removal in 360 min. The initial orange solution lost gradually intensity to

attain a light orange color at the end of this treatment. This means that SY and its conjugated colored aromatic products react very slowly with BDD($\bullet\text{OH}$) formed from Eq. (1) as well as with other weaker ROS (H_2O_2 , BDD($\text{HO}_2\bullet$)). In contrast, Figure 3.1b evidences a similar and much quicker color removal when EF-BDD, PEF-UVA-BDD and SPEF-BDD were tested. In these three treatments, the initial solution reached over 50% color removal during the first 5 min of electrolysis. At longer time, it acquired a brown color, probably due to the fast formation of great amounts of initial conjugated aromatic products, which were rapidly oxidized becoming the solution colorless in 40-45 min. This behavior indicates that in EF-BDD, PEF-UVA-BDD and SPEF-BDD, the azo dye and its conjugated colored aromatic products were mainly destroyed by $\bullet\text{OH}$ produced from Fenton's reaction (21), with a small participation of the photolytic reaction (28) induced by UVA light or sunlight.

Table 3.1 collects the k_{dec} values, along with the corresponding R^2 and S^2_{R} , obtained for the four EAOPs tested. Quite similar k_{dec} values can be observed for EF-BDD, PEF-UVA-BDD and SPEF-BDD processes. Those values are about 30 times higher than the k_{dec} attained for AO- H_2O_2 -BDD, as expected since in the former three methods much higher amounts of $\bullet\text{OH}$ were produced in the bulk than at the anode surface.

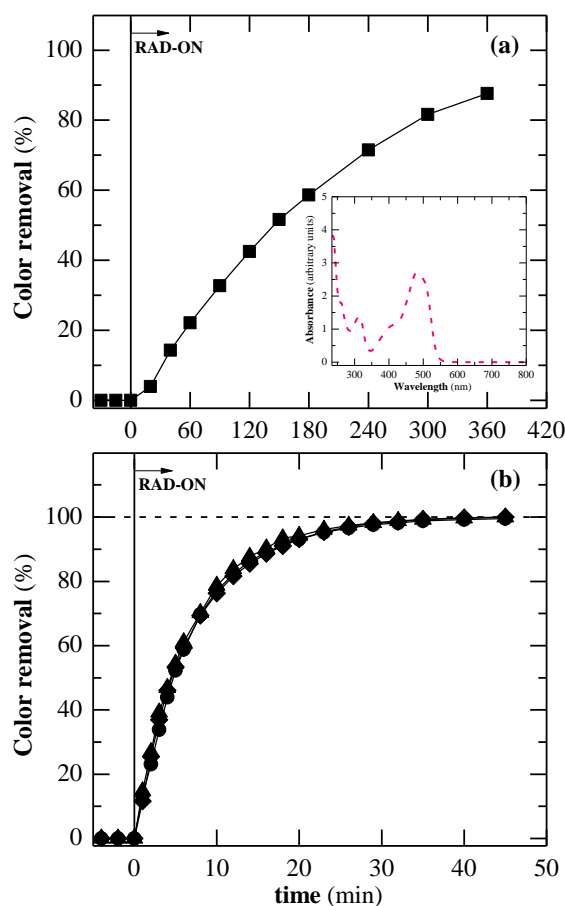


Figure 3.1. Evaluation of color removal as a function of time for the treatment of 290 mg SY L⁻¹ in 7.0 g Na₂SO₄ L⁻¹ by various EAOPs using pH of 3.0, 35 °C, [TDI]₀ of 28 mg L⁻¹ for EF-BDD, PEF-UVA-BDD and SPEF-BDD and j of 33.3 mA cm⁻². EAOP: (■) AO-H₂O₂-BDD, (●) EF-BDD, (▲) PEF-UVA-BDD and (◆) SPEF-BDD. The inset panel of Figure 3.1a shows the UV-Vis absorption spectrum of the initial SY solution diluted 1:5.

Table 3.1. Pseudo-first-order kinetic constants for SY decolorization (k_{dec}) and SY concentration decay (k_{SY}) along with the corresponding R^2 and S^2_R , obtained for the treatment of solutions of 290 mg SY L⁻¹ in 7.0 g Na₂SO₄ L⁻¹ under conditions of Figures 3.1, 3.4, 3.6a and 3.7a.

System	j (mA cm ⁻²)	k_{dec} (×10 ⁻² min ⁻¹)	R^2	S^2_R	k_{SY} (×10 ⁻² min ⁻¹)	R^2	S^2_R (mg ² L ⁻²)
150 mL lab-scale undivided reactor							
AO-H₂O₂-BDD	33.3	0.49±0.02	0.996	0.008	0.83±0.02	0.993	34
EF-BDD	33.3	14.3±0.1	0.999	0.001	14.9±0.3	0.998	32
PEF-UVA-BDD	33.3	15.5±0.1	1.000	0.0005	17.0±0.3	0.995	37
SPEF-BDD	33.3	14.6±0.2	0.999	0.001	21.0±0.2	0.995	61
10 L pilot-scale flow plant							
	33.2	5.5±0.3	0.994	0.007	n.a.	n.a.	n.a.
SPEF-Pt	55.4	6.9±0.5	0.993	0.004	n.a.	n.a.	n.a.
	77.6	10.0±0.4	0.993	0.005	19.1±0.2	0.999	13

n.a. – not assessed.

A very different behavior was found when DOC abatement was measured for the above trials. Figure 3.2 shows that the oxidation power of EAOPs increased in the sequence: AO-H₂O₂-BDD < EF-BDD < PEF-UVA-BDD < SPEF-BDD. The AO-H₂O₂-BDD method led to a very poor DOC removal, only attaining 65% mineralization at 360 min, attributed to the little oxidation action of BDD([•]OH) and other generated ROS, as stated above. In EF-BDD, the higher oxidation ability of additional [•]OH produced from Fenton's reaction (21) allowed a quicker DOC decay up to 82% mineralization. Note that for times longer than 120 min the EF-BDD process was progressively decelerated, probably due to the formation of Fe(III)-carboxylate complexes that are hardly oxidized by [•]OH [17, 19, 20]. This point was confirmed in the PEF-UVA-BDD process, where the fast photolysis of these complexes under UVA radiation via Eq. (29) in simultaneous with the additional action of [•]OH produced from photolytic reaction (28) can explain the almost total mineralization with 95% DOC removal reached at 240 min. Figure 3.2 also shows that the azo dye underwent even a quicker degradation using SPEF-BDD with 93% DOC decay reached in only 150 min, which can be ascribed to a higher rate of photoreactions (28) and (29) due to the emission of natural sunlight in the visible region and its ability to emit at slightly higher UV intensity compared to the UVA lamp here used. The slow mineralization achieved at long electrolysis times for PEF-UVA-BDD and SPEF-BDD suggests the presence of hardly oxidizable final by-products that can only react slowly with BDD([•]OH), but neither destroyed by [•]OH nor photodecomposed, as will be better discussed below.

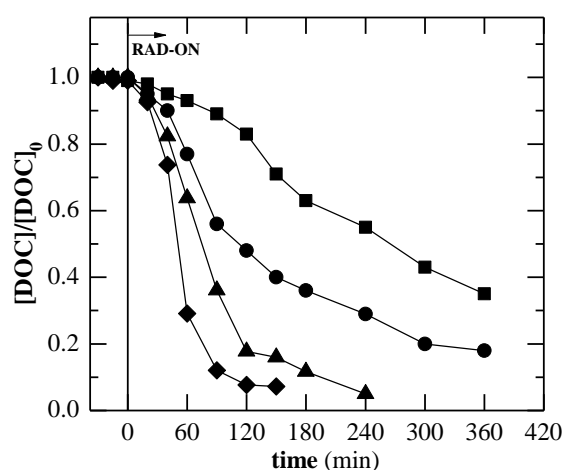


Figure 3.2. Evolution of normalized DOC removal as a function of time for the treatment of 290 mg SY L⁻¹ in 7.0 g Na₂SO₄ L⁻¹ by various EAOPs using pH of 3.0, 35 °C, [TDI]₀ of 28 mg L⁻¹ for EF-BDD, PEF-UVA-BDD and SPEF-BDD and *j* of 33.3 mA cm⁻². EAOP: (■) AO-H₂O₂-BDD, (●) EF-BDD, (▲) PEF-UVA-BDD and (◆) SPEF-BDD.

Table 3.2. Pseudo-first-order kinetic constants for DOC removal (k_{DOC}) along with the corresponding R^2 and S^2_{R} , obtained for the treatment of solutions of 290 mg SY L⁻¹ in 7.0 g Na₂SO₄ L⁻¹ under conditions of Figures 3.2, 3.3 and 3.6b.

System	j (mA cm ⁻²)	k_{DOC} (× 10 ⁻³ min ⁻¹)	R^2	S^2_{R} (mg ² L ⁻²)
150 mL lab-scale undivided reactor				
AO-H ₂ O ₂ -BDD	16.7	1.5±0.1	0.986	7
	33.3	2.4±0.2	0.974	24
	100	4.1±0.2	0.987	12
EF-BDD	16.7	3.1±0.2	0.988	17
	33.3	6.9±0.4	0.975	26
	100	10.9±0.8	0.976	25
PEF-UVA-BDD	16.7	11±1	0.968	72
	33.3	13±1	0.981	45
	100	18±1	0.985	28
SPEF-BDD	16.7	18±2	0.981	29
	33.3	24±4	0.950	92
	100	34±5	0.969	65
10 L pilot-scale flow plant				
SPEF-Pt	33.2	11±1	0.975	46
	55.4	18±0.2	0.984	44
	77.6	20±4	0.937	105

The applied j is a key factor in the oxidation ability of EAOPs because it regulates the amount of •OH acting as oxidizing agents. The effect of this experimental variable was checked by electrolyzing the above 290 mg SY L⁻¹ solution using j of 16.7, 33.3 and 100 mA cm⁻² for each EAOP. For all processes, higher mineralization rates were attained with the increment of j . Table 3.2 shows that k_{DOC} increased with raising j for each EAOP and SPEF-BDD was always the most powerful treatment. After 120 min of SPEF-BDD treatment, DOC decays of 76%, 92% and 97% were found for j values of 16.7, 33.3 and 100 mA cm⁻², respectively. The faster mineralization observed for all EAOPs at higher j can be simply related to the concomitant production of more •OH, due to the acceleration of Eq. (1) to yield larger quantities of BDD(•OH) and/or of Fenton's reaction (21) to give greater amounts of •OH in the bulk as a result of the faster cathodic generation of H₂O₂ [17]. However, the opposite tendency was found when DOC removal was plotted against the consumed specific charge (Q , in Ah L⁻¹). Figures 3.3a-d present the normalized DOC vs. Q for AO-H₂O₂-BDD, EF-BDD, PEF-UVA-BDD and SPEF-BDD trials. Higher specific charge values can be observed for higher j values, principally when j changes from 33.3 to 100 mA cm⁻². This loss in efficiency can be related to the generation of less relative amounts of •OH owing to the higher increase in rate of their non-oxidizing waste reactions (24), (25), (39) and (40).

The aforementioned results indicate that SPEF-BDD is the most powerful treatment for SY degradation, although EF-BDD and PEF-UVA-BDD yield similar decolorization efficiency. Greater j accelerates the mineralization process, but it is preferable the use of low j values to enhance the efficiency. The role of $\bullet\text{OH}$, UVA light and sunlight in the treatments tested was further examined from the SY concentration decay, as discussed in subsection below.

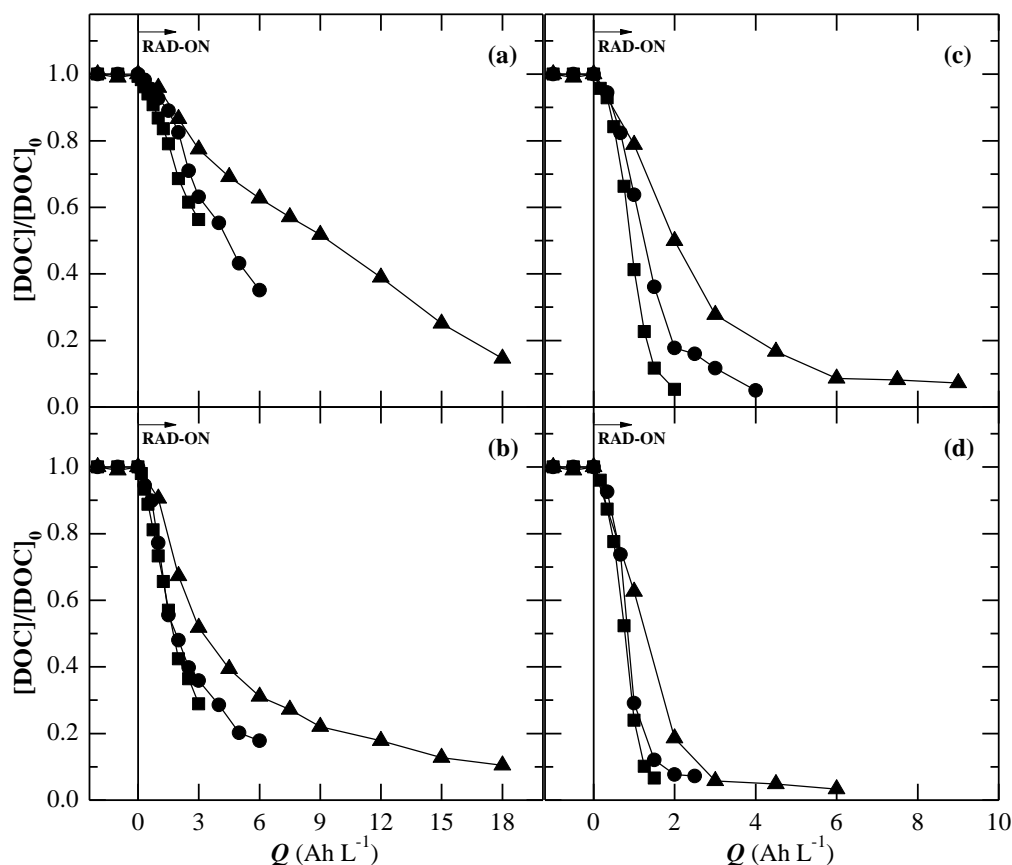


Figure 3.3. Effect of current density on normalized DOC removal as a function of consumed specific charge for the treatment of 290 mg SY L^{-1} in $7.0 \text{ g Na}_2\text{SO}_4 \text{ L}^{-1}$ by (a) AO- H_2O_2 -BDD, (b) EF-BDD, (c) PEF-UVA-BDD and (d) SPEF-BDD using pH of 3.0, $35 \text{ }^\circ\text{C}$ and $[\text{TDI}]_0$ of 28 mg L^{-1} for EF-BDD, PEF-UVA-BDD and SPEF-BDD. Current density: (■) 16.7 , (●) 33.3 and (▲) 100 mA cm^{-2} .

3.3.2 Comparative SY concentration decay by EAOPs at lab-scale

No significant removal of SY was found in blank experiments performed with a solution composed of 290 mg SY L^{-1} and $7.0 \text{ g Na}_2\text{SO}_4 \text{ L}^{-1}$ at pH of 3.0 and $35 \text{ }^\circ\text{C}$ with and without the initial addition of $700 \text{ mg H}_2\text{O}_2 \text{ L}^{-1}$ under UVA and solar radiation. This indicates that the SY molecule is mainly attacked by BDD($\bullet\text{OH}$) and/or $\bullet\text{OH}$ in the EAOPs tested. Figure 3.4 presents the decay of SY concentration in the treatment of 290 mg L^{-1} of dye solutions by all EAOPs at j of 33.3 mA cm^{-2} .

Its inset panel evidences that the azo dye underwent a slow removal by AO-H₂O₂-BDD until 95% disappearance at 360 min of reaction, as a result of its low reaction rate with BDD([•]OH). The use of EF-BDD strongly accelerated the SY removal, leading to its disappearance in 26 min, since this compound is much more rapidly attacked by the [•]OH formed from Fenton's reaction (21). For PEF-UVA-BDD and SPEF-BDD processes, the SY destruction became only slightly faster, with total removals in 20 min and 16 min, respectively. A pseudo-first-order kinetic model was able to fit well the above SY concentration decays, suggesting a constant production of BDD([•]OH) and/or [•]OH in each EAOP. The corresponding k_{SY} , along with their R^2 and S^2_R values, are listed in Table 3.1. As expected, k_{SY} rose in the order AO-H₂O₂-BDD \ll EF-BDD $<$ PEF-UVA-BDD $<$ SPEF-BDD, in agreement with the increasing generation of [•]OH in the bulk. Results of Table 3.1 also evidence that k_{SY} values are higher than k_{dec} values for all treatments. This means that decolorization involves the simultaneous destruction of the azo dye and some colored aromatic products that absorb at a wavelength similar to λ_{max} of 482 nm, being this process slower than SY removal alone. The fast SY removal compared with the slow DOC decay indicates the formation of more persistent oxidation products, which were identified by LC-MS and ion-exclusion HPLC, as described in subsection below.

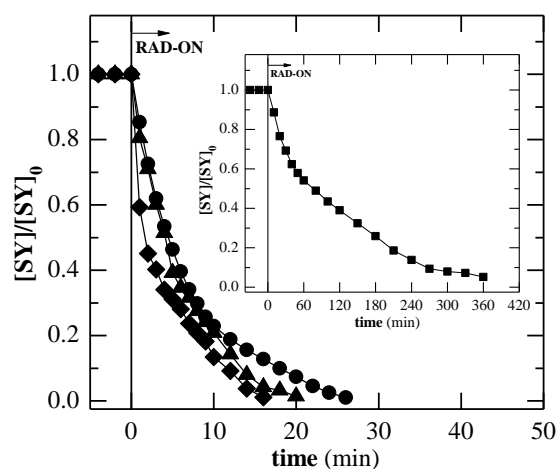


Figure 3.4. Evolution of normalized SY concentration decay as a function of time for the treatment of 290 mg SY L⁻¹ in 7.0 g Na₂SO₄ L⁻¹ by various EAOPs using pH of 3.0, 35 °C, [TDI]₀ of 28 mg L⁻¹ for EF-BDD, PEF-UVA-BDD and SPEF-BDD and j of 33.3 mA cm⁻². EAOP: (■) AO-H₂O₂-BDD, (●) EF-BDD, (▲) PEF-UVA-BDD and (◆) SPEF-BDD.

3.3.3 Identification and evolution of oxidation products at lab-scale

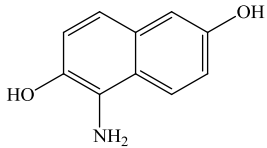
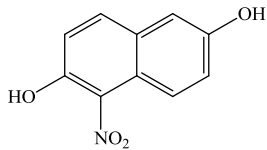
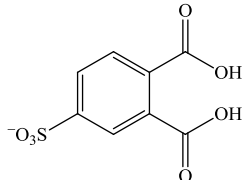
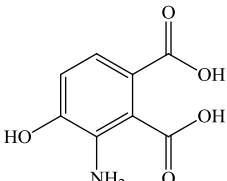
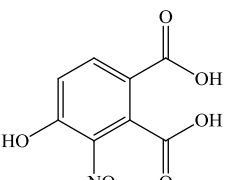
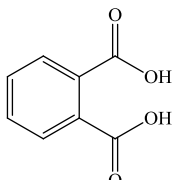
Since organics are mainly attacked by $\bullet\text{OH}$, the same kind of oxidation products are expected in all EAOPs tested. Table 3.3 collects 15 aromatic compounds, including the initial SY dianion (**1**), and 34 hydroxylated derivatives detected by LC-MS after 10-15 min of EF-BDD treatment at j of 33.3 mA cm^{-2} . As can be seen, the desulfonation of **1** yields the compounds **2** and **3**, whereas the cleavage of the $-\text{N}=\text{N}-$ bond of these three aromatics leads to: (i) benzenic derivatives (compounds **4-7**), and (ii) naphthalenic derivatives (compounds **8-11**), which are degraded to phthalic acid derivatives (compounds **12-15**). These reactions involve the oxidation of $-\text{NH}_2$ to $-\text{NO}_2$ group, deamination, denitration, hydroxylation, desulfonation and the breaking of the naphthalene moiety. Note that the hydroxylated compounds of **1**, as well as **2**, **3** and their hydroxylated compounds, are colored aromatics that are expected to absorb near λ_{max} of 482 nm, and hence, their accumulation in the medium due to their lower reaction rate with $\bullet\text{OH}$ than SY could justify the longer time needed for decolorization compared with the azo dye removal.

Ion-exclusion chromatograms of electrolyzed solutions at j of 33.3 mA cm^{-2} revealed the generation of LMCA like oxalic, tartronic, oxamic and formic acids. Tartronic acid can be formed from the cleavage of the benzene and naphthalene rings of aromatic products and its further oxidation, as well as the degradation of other unidentified carboxylic acids, yields formic and oxalic acids [13, 21-24]. Oxamic acid is expected to be formed from the destruction of *N*-intermediates with a $-\text{NH}_2$ group. Oxalic, formic and oxamic acids are ultimate acids since they are directly mineralized to CO_2 [19]. In EF-BDD, PEF-UVA-BDD and SPEF-BDD these LMCA should be primordially present in solution as Fe(III)-carboxylate complexes because Fe^{2+} ion is largely converted into Fe^{3+} ion [19, 22, 25].

Table 3.3. Aromatic products and hydroxylated derivatives identified by LC-MS in negative mode during the EF-BDD treatment of 290 mg SY L⁻¹ in 7.0 g Na₂SO₄ L⁻¹.

Compound	Molecular structure	Number of -OH added	<i>m/z</i>
Sunset Yellow FCF dianion (1)		-	407 ^a 203 ^b
		1	- 211 ^b
		2	- 219 ^b
		4	- 235 ^b
		5	- 243 ^b
		6	- 251 ^b
		7	- 259 ^b
6-Hydroxy-5-[(phenyl)azo]-2-naphthalenesulfonate ion (2)		-	327 ^a
		1	343 ^a
		2	359 ^a
		3	375 ^a
		4	391 ^a
		7	439 ^a
10	487 ^a		
2,6-Dihydroxy-5-[(phenyl)azo]-naphthalene (3)		-	263 ^a
		1	279 ^a
4-Aminobenzenesulfonate ion (4)		-	172 ^a
		1	188 ^a
4-Nitrobenzenesulfonate ion (5)		-	202 ^a
		1	218 ^a
4-Hydroxybenzenesulfonate ion (6)		-	173 ^a
		1	189 ^a
4-Nitrophenol (7)		-	138 ^a
		3	186 ^a
5-Nitro-6-hydroxy-2-naphthalenesulfonate ion (8)		-	268 ^a
		1	284 ^a
		2	300 ^a
		3	316 ^a
6-Hydroxy-2-naphthalenesulfonate ion (9)		-	223 ^a

Table 3.3. Aromatic products and hydroxylated derivatives identified by LC-MS in negative mode during the EF-BDD treatment of 290 mg SY L⁻¹ in 7.0 g Na₂SO₄ L⁻¹.

Compound	Molecular structure	Number of -OH added	<i>m/z</i>
		-	174 ^a
5-Amino-2,6-dihydroxy-naphtalene (10)		1	190 ^a
		2	206 ^a
		3	222 ^a
		4	238 ^a
		5	254 ^a
5-Nitro-2,6-dihydroxy-naphtalene (11)		-	204 ^a
		1	220 ^a
4-Sulfophthalic acid (12)		-	245 ^a
		1	261 ^a
3-Amino-4-hydroxyphthalic acid (13)		-	196 ^a
		1	212 ^a
		2	228 ^a
3-Nitro-4-hydroxyphthalic acid (14)		-	226 ^a
		1	242 ^a
		2	258 ^a
Phthalic acid (15)		-	165 ^a
		3	213 ^a
		4	229 ^a

^a Negative ions detected with $z = 1$;^b Negative ions detected with $z = 2$.

Figure 3.5a depicts that tartronic acid was poorly accumulated ($< 1.5 \text{ mg L}^{-1}$) and slowly removed by BDD($\bullet\text{OH}$) in AO-H₂O₂-BDD, whereas in EF-BDD it was much more largely accumulated up to ca. 7 mg L^{-1} after 135 min, disappearing at 360 min of reaction. The greater concentration achieved by this acid in the EF-BDD treatment can be related to the quicker degradation of

precedent products by $\bullet\text{OH}$ and its fast decay indicates a high reaction rate of Fe(III)-tartronate complexes with $\bullet\text{OH}$, mainly BDD($\bullet\text{OH}$) [19, 22]. The faster photodecomposition of these complexes under UVA light accounts for their quicker disappearance in PEF-UVA-BDD, which was accelerated in SPEF-BDD by the higher UV irradiance from sunlight. Figure 3.5b highlights that oxalic acid was only accumulated up to ca. 1.1 mg L^{-1} by AO- H_2O_2 -BDD, attaining a concentration as high as 85 mg L^{-1} at 150 min of EF-BDD, which only dropped to 60 mg L^{-1} at the end of reaction because of the low reaction rate of Fe(III)-oxalate complexes with BDD($\bullet\text{OH}$). In contrast, these species were totally photolyzed by UVA light after 180 min of PEF-UVA-BDD. The photolysis rate of Fe(III)-oxalate complexes became so fast under solar radiation that they were not detected during SPEF-BDD. Figure 3.5c shows a different trend for formic acid, which was very poorly accumulated and destroyed with BDD($\bullet\text{OH}$) in AO- H_2O_2 -BDD, but more largely accumulated and rapidly removed in a similar way by EF-BDD, PEF-UVA-BDD and SPEF-BDD, as expected if Fe(III)-formate complexes are oxidized with BDD($\bullet\text{OH}$) but poorly photolyzed. Figure 3.5d highlights the existence of a slow destruction of oxamic acid with BDD($\bullet\text{OH}$) in AO- H_2O_2 -BDD, but, in turn, Fe(III)-oxamate complexes were more rapidly removed with $\bullet\text{OH}$ in EF-BDD. In PEF-UVA-BDD, these complexes were slowly photolyzed and the sunlight slightly accelerated their photodecomposition in SPEF-BDD.

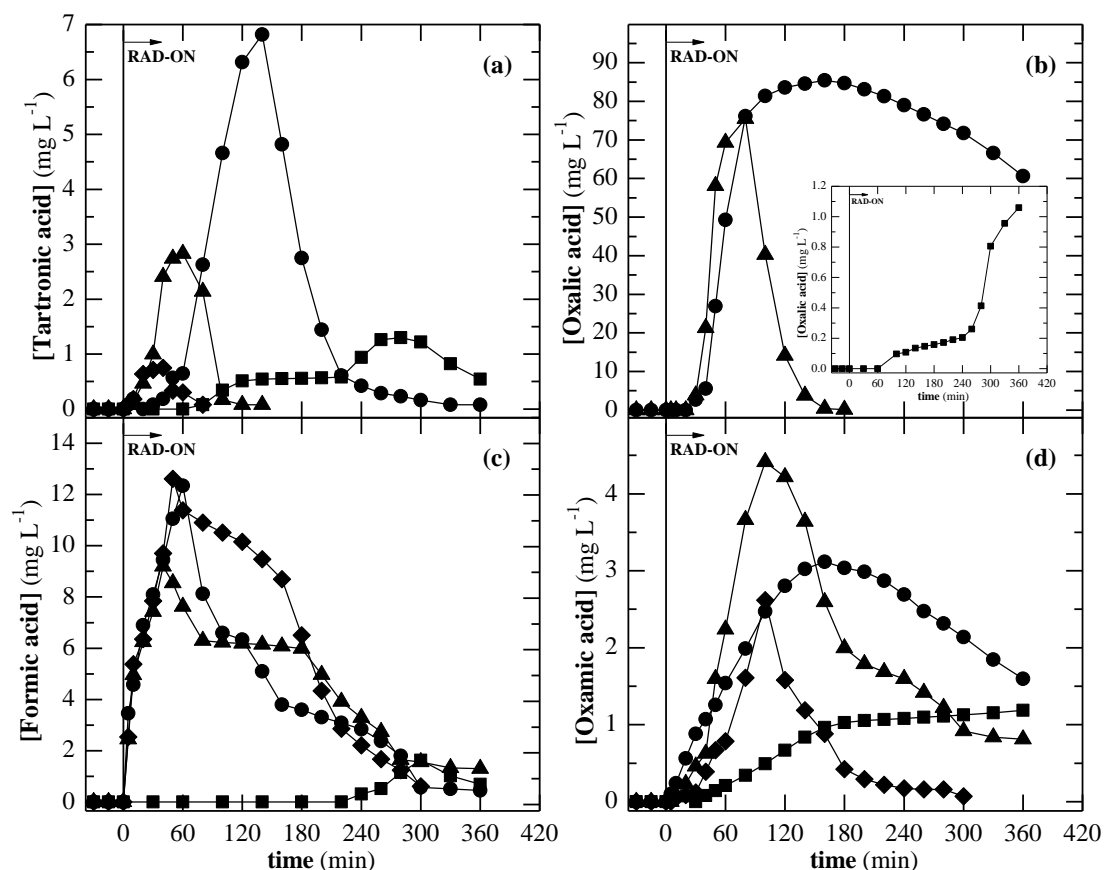


Figure 3.5. Evolution of the concentration of (a) tartronic, (b) oxalic, (c) formic and (d) oxamic acids during the treatment of 290 mg SY L⁻¹ in 7.0 g Na₂SO₄ L⁻¹ by (■) AO-H₂O₂-BDD, (●) EF-BDD, (▲) PEF-UVA-BDD and (◆) SPEF-BDD using pH of 3.0, 35 °C, [TDI]₀ of 28 mg L⁻¹ and *j* of 33.3 mA cm⁻².

From the aforementioned findings, one can infer that SPEF-BDD is the most powerful EAOP for SY mineralization because sunlight can rapidly photolyze oxidation products like Fe(III) complexes of tartronic and oxalic acids, owing to the incapacity of $\bullet\text{OH}$ to remove these recalcitrant compounds in AO-H₂O₂-BDD and EF-BDD. A simple mass balance of organic carbon at the end of all treatments (see Figures 3.2 and 3.5) reveals that at the final of AO-H₂O₂-BDD process 0.9 mg L⁻¹ of DOC was due to LMCA and 31.5 mg L⁻¹ of DOC corresponded to unidentified recalcitrant products. In contrast, the attack of $\bullet\text{OH}$ in the bulk during EF-BDD led to a final solution preferentially composed of oxalic acid (16.2 mg L⁻¹ of DOC), with low contents of other LMCA (0.6 mg L⁻¹ of DOC) and unidentified compounds (2.8 mg L⁻¹ of DOC) that can be hardly removed by BDD($\bullet\text{OH}$) but not by $\bullet\text{OH}$. The quick photodecarboxylation of Fe(III)-oxalate species by UVA light in PEF-UVA-BDD and sunlight in SPEF-BDD (see Figure 3.5b) contributed to the faster DOC abatement using both methods compared with EF-BDD. The final solutions from PEF-UVA-BDD and SPEF-BDD processes contained residual

contents of LMCA and an amount of unidentified by-products corresponding to 3.5 and 4.7 mg L⁻¹ of DOC, respectively, that were even more recalcitrant than LMCA since they could be very difficultly destroyed by •OH but not photolyzed.

The mineralization of azo dyes usually involves the release of their nitrogen and sulfur atoms in the form of inorganic ions such as ammonium, nitrate and sulfate [3, 20, 22, 25]. Quantification of inorganic nitrogen ions formed after electrolyzing 290 mg SY L⁻¹ by all EAOPs during 360 min at j of 33.3 mA cm⁻² was attempted by ion chromatography. However, this technique did not allow the detection of nitrate and nitrite ions, only being found very low concentrations of ammonium ion (< 1 mg L⁻¹). The total nitrogen analysis of such electrolyzed solutions confirmed that the initial nitrogen content of 14.6 mg L⁻¹ was drastically reduced to 3-4 mg L⁻¹ in all EAOPs. This suggests the release of the major part of the initial nitrogen (73-79%) from the solution during all mineralization processes, probably as N₂ and N_xO_y species, while the rest of nitrogen mainly formed recalcitrant unidentified *N*-derivatives that remained in the final solutions. On the other hand, to confirm the generation of sulfate ion, a 290 mg SY L⁻¹ solution (33.3 mg L⁻¹ of initial sulfur) in 5.3 g LiClO₄ L⁻¹ was degraded by SPEF-BDD using pH of 3.0 (adjusted with HClO₄), 35 °C, [TDI]₀ of 28 mg L⁻¹ and j of 33.3 mA cm⁻². Under these conditions, the DOC was reduced by 96% in 240 min and all the initial sulfur was released as sulfate ion (about 100 mg L⁻¹) in only 80 min, indicating that this ion was formed from all sulfonated derivatives at the first stages of the process.

3.3.4 Degradation of SY by SPEF at pilot-scale

The degradation of SY was scaled-up from lab- to pilot-scale for SPEF process, i.e. the most powerful EAOP tested. Experiments were made by electrolyzing 10 L of the 290 mg SY L⁻¹ solution in 7.0 g Na₂SO₄ L⁻¹ using pH of 3.0, 35 °C and [TDI]₀ of 28 mg L⁻¹ in a 10 L pilot-scale flow plant equipped with a one-compartment filter-press cell with a Pt anode and a carbon-PTFE air-diffusion cathode coupled to a solar photoreactor. Distinct j values of 33.2, 55.4 and 77.6 mA cm⁻² were employed. In all these trials, the solution pH dropped slowly to final values of 2.8-2.9 and it was regulated by adding 50% (w/v) NaOH.

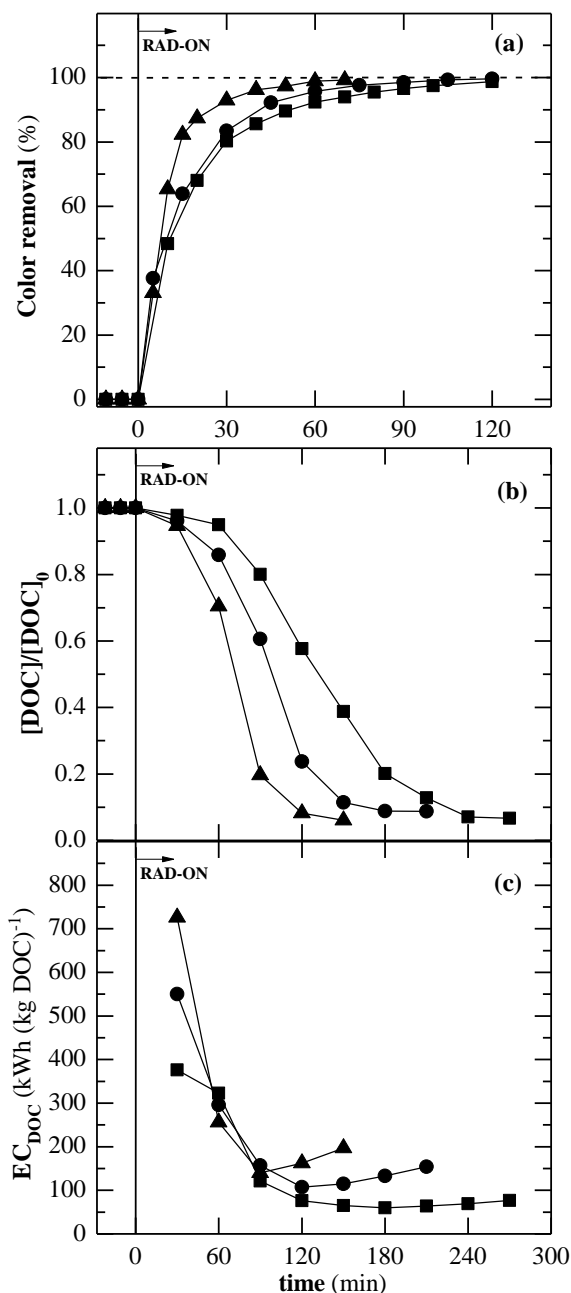


Figure 3.6. Effect of current density on (a) color removal, (b) normalized DOC removal and (c) energy consumption per unit DOC mass as a function of time for the treatment of 290 mg SY L⁻¹ in 7.0 g Na₂SO₄ L⁻¹ by SPEF-Pt at the 10 L pilot-scale flow plant using pH of 3.0, 35 °C and [TDI]₀ of 28 mg L⁻¹. Current density: (■) 33.2, (●) 55.4 and (▲) 77.6 mA cm⁻².

Figure 3.6a depicts the time course of the percentage of color removal for the above trials. As expected, this parameter rose with increasing j by the greater production of Pt(\bullet OH) and \bullet OH in the bulk. Total decolorization was thus achieved at shorter times of 120, 100 and 70 min for increasing j of 33.2, 55.4 and 77.6 mA cm⁻², respectively. The corresponding k_{dec} values are given in Table 3.1. Comparison of Figures 3.1b and 3.6a for SPEF as well as of k_{dec} values obtained for

the lab- and pilot-scale plants at j near 33 mA cm^{-2} indicates that SY decolorization was much faster in the former system. This is not surprising in view of the different experimental conditions used in both cases. Since the electrodes area/solution volume ratio was $30 \text{ cm}^2 \text{ L}^{-1}$ for the lab-scale reactor and $9 \text{ cm}^2 \text{ L}^{-1}$ for the pilot-scale plant, one may expect an acceleration of $30/9 = 3.33$ times for the decolorization rate of the former respect to the latter. This is in good agreement with the increase in 2.65-fold of k_{dec} found for the lab-scale reactor (see Table 3.1), corroborating that $\bullet\text{OH}$ is the main oxidant of SY and its colored aromatic products in the pilot-scale plant, with small participation of $\text{Pt}(\bullet\text{OH})$. Besides, other aspects related to solar radiation could influence the efficiency of the two tested systems such as: (i) the lab-scale reactor was totally irradiated by sunlight in contrast to the very low irradiated volume/total volume ratio of 16% in the pilot-scale plant, and (ii) while at the lab-scale reactor all solar wavelengths reached the solution in direct contact with the atmosphere, the borosilicate glass tubes of the solar photoreactor of the pilot-scale plant exhibits a cut-off of about 285 nm.

The normalized DOC decay shown in Figure 3.6b for the same trials also evidences an increase in degradation rate with increasing j , attaining an almost total mineralization of 91-94% after 270 min at 33.2 mA cm^{-2} , 210 min at 55.4 mA cm^{-2} and 150 min at 77.6 mA cm^{-2} . This was also reflected in the gradual rise of k_{DOC} from 11 ± 1 to $20 \pm 4 \text{ min}^{-1}$ in the j range tested (see Table 3.2). However, more Q was consumed when j rose, reaching final values from 1.35 to 1.75 Ah L^{-1} . This means that more $\bullet\text{OH}$ were formed at greater j , but their relative amounts diminished as a result of the increase in rate of their non-oxidizing reactions, as pointed out above in the behavior of the lab-scale cell. Moreover, Figure 3.6b also shows that at a given j the mineralization process was gradually accelerated up to about 80% of DOC removal, which can be related to the progressive formation of products that can be more rapidly photolyzed by sunlight. This behavior caused a dramatic drop in EC_{DOC} at the beginning of all trials up to minimum values between 90 and 120 min, as can be seen in Figure 3.6c. The increase in j caused higher EC_{DOC} values, as expected by the gradual rise in cell voltage. Thus, $77 \text{ kWh (kg DOC)}^{-1}$ (7.2 kWh m^{-3}) for 33.2 mA cm^{-2} , $154 \text{ kWh (kg DOC)}^{-1}$ (14.2 kWh m^{-3}) for 55.4 mA cm^{-2} and $197 \text{ kWh (kg DOC)}^{-1}$ (16.6 kWh m^{-3}) for 77.6 mA cm^{-2} were spent for achieving 91-94% mineralization. Note that for the lowest j tested, similar EC_{DOC} values between 60 and $77 \text{ kWh (kg DOC)}^{-1}$ were obtained from 120 min to the end of the treatment at 270 min (see Figure 3.6c), when a fast DOC abatement took place (see Figure 3.6b), while EC_v increased from 3.2 to 7.1 kWh m^{-3} . All these findings demonstrate the viability of using the SPEF process for SY degradation at pilot scale, where low j values proved

to be more useful since they yield a more efficient and economic process with lower EC_{DOC} , although longer times were needed for reaching almost total mineralization.

The decay on SY initial concentration by the action of $Pt(\bullet OH)$ formed from Eq. (1) and mainly $\bullet OH$ produced from Fenton's reaction (21) and photolytic reaction (28) was assessed. Figure 3.7a exemplifies the fast decay in the azo dye concentration at j of 77.6 mA cm^{-2} to disappear in 22 min. Nevertheless, the corresponding k_{SY} value, given in Table 3.1, was even lower than the one determined for the lab-scale plant at 33.3 mA cm^{-2} because of the different experimental conditions used. This pseudo-first-order kinetics suggests again the constant production of $\bullet OH$. An energy consumption of 2.3 kWh m^{-3} was found for total removal of SY. Moreover, the same generated LMCA were identified by ion-exclusion HPLC in both electrolytic systems. Figure 3.7b shows that at j of 77.6 mA cm^{-2} , both tartronic and oxalic acids were rapidly and completely removed in less than 150 min, as expected from the quick photolysis of their Fe(III) complexes under solar radiation. In contrast, formic and oxamic acids remained in solution, a different behavior to that found for the lab-scale cell with the BDD anode, where these compounds were almost totally degraded (see Figures 3.5c,d). After 150 min of reaction, these two acids contributed with 3.6 mg L^{-1} of DOC to the remaining solution, also containing 2.0 mg L^{-1} of DOC of unidentified by-products. This means that Fe(III)-formate and Fe(III)-oxamate complexes were not attacked by $Pt(\bullet OH)$ produced in the pilot-scale plant but reacted with BDD($\bullet OH$) generated in the lab-scale reactor. This effect on generated LMCA was the main oxidative difference found in SPEF when a Pt anode was used instead of a BDD one, since aromatics were mainly destroyed by $\bullet OH$ in the bulk.

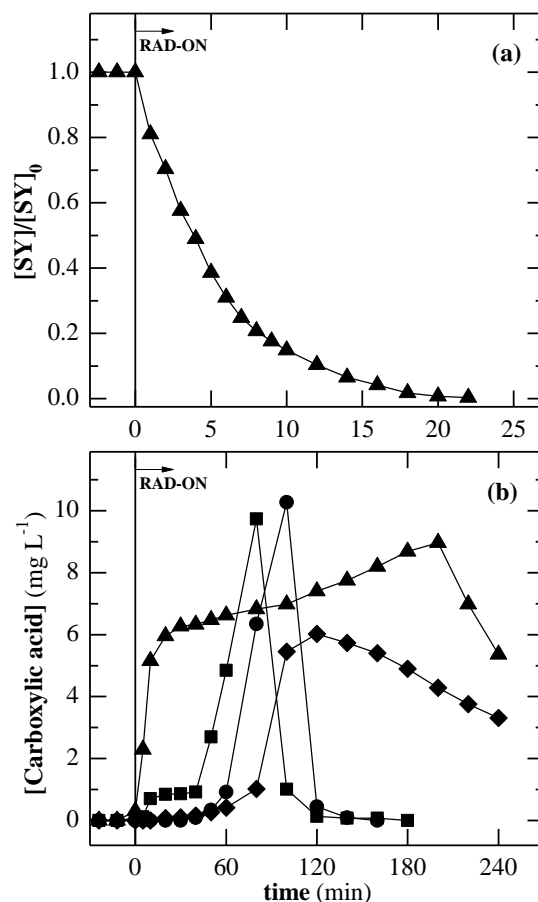


Figure 3.7. (a) Evolution of normalized SY concentration decay as a function of time for the treatment of 290 mg SY L⁻¹ in 7.0 g Na₂SO₄ L⁻¹ by SPEF-Pt at the 10 L pilot-scale flow plant using pH of 3.0, 35 °C, [TDI]₀ of 28 mg L⁻¹ and *j* of 77.6 mA cm⁻². (b) Evolution of the concentration of (■) tartronic, (●) oxalic, (▲) formic and (◆) oxamic acids during the abovementioned treatment.

3.3.5 Proposed reaction pathway for SY mineralization

Based on the oxidation products detected (see Table 3.3 and Figure 3.5), Figure 3.8 presents a general reaction sequence proposed for SY mineralization in acidic medium by the EAOPs tested. In this pathway, M(•OH) denotes BDD(•OH) or Pt(•OH), which attack aromatic products much more slowly than •OH in the bulk. Parallel and slower reaction of products with other ROS (H₂O₂, HO₂•) is also feasible. Formation of Fe(III) complexes in EF, PEF-UVA and SPEF is only highlighted for the ultimate LMCA for simplicity.

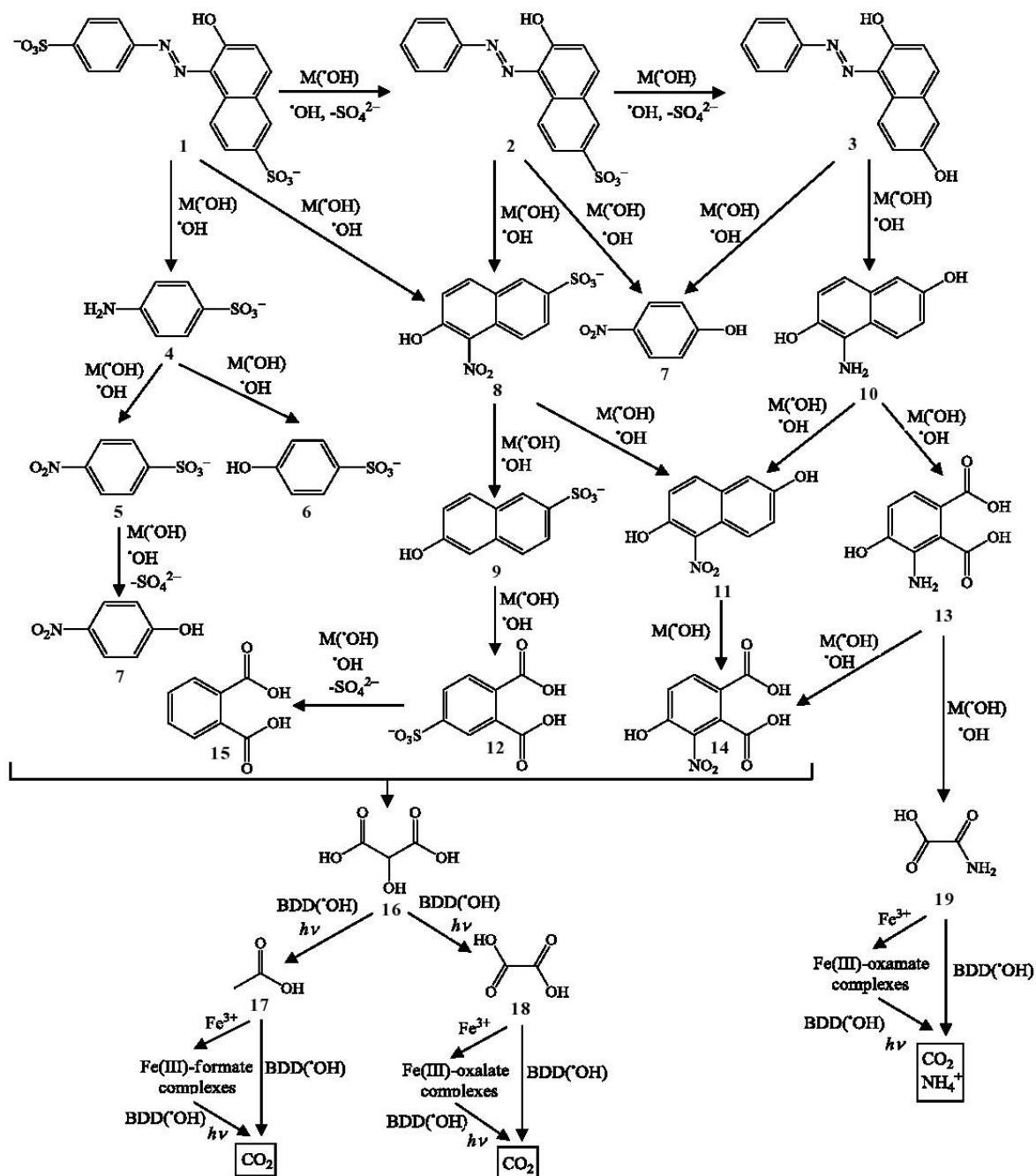


Figure 3.8. Proposed reaction sequence for the mineralization of Sunset Yellow FCF in acidic medium by EAOPs. M([•]OH) denotes the reactive [•]OH generated either at a Pt or BDD anode surface, whereas BDD([•]OH) represents this radical on a BDD anode surface.

The process is initiated either by the desulfonation of **1** to yield **2** or the cleavage of its –N=N– bond giving the benzenic compound **4** and the naphthalenic compound **8**. Further desulfonation of **2** leads to **3**. Compound **4** is subsequently either oxidized to **5**, which is desulfonated to **7**, or hydroxylated to **6**. The benzenic compound **7** can also be formed from the cleavage of the azo bond of **2** and **3**, which also produce the naphthalenic derivatives **8** and **10**, respectively. The degradation of **8** yields **15** via denitration to **9** followed by opening of its naphthalenic ring to **12**. Compound **10** is oxidized to **11** or **13**, which are then transformed into **14**. Compound **11** can also be formed from desulfonation and hydroxylation of **8**. Further oxidation of benzenic and phthalic acid derivatives with ring opening leads to shorter aliphatic products like LMCA. Thus, compounds without heteroatoms like **15** evolve to acids **16-18**, whereas *N*-derivatives with a –NH₂ group like **13** can produce the ultimate acid **19**. Acid **16** is oxidized to the ultimate acids **17** and **18**. All these ultimate acids can then be slowly mineralized with BDD(•OH) in AO-H₂O₂, but they form Fe(III) complexes in EF, PEF-UVA and SPEF that react with this radical and/or are photolyzed by UVA light or solar radiation. While Fe(III)-oxalate complexes are rapidly photodecomposed, Fe(III)-formate and Fe(III)-oxamate species are mainly destroyed by BDD(•OH).

3.4 Conclusions

A slow decolorization of the 290 mg SY L⁻¹ aqueous solution in 7.0 g Na₂SO₄ L⁻¹ at pH of 3.0 was achieved by AO-H₂O₂ process performed in the lab-scale undivided reactor equipped with a BDD anode and a carbon-PTFE air-diffusion cathode, which was associated with the low reaction rate of this azo dye with BDD([•]OH). EF-BDD, PEF-UVA-BDD and SPEF-BDD treatments led to a much faster and total decolorization at similar rate due to the quicker oxidation by [•]OH in the bulk. The relative ability of EAOPs to mineralize the dye solution increased in the sequence: AO-H₂O₂-BDD < EF-BDD < PEF-UVA-BDD < SPEF-BDD. The little oxidation action of BDD([•]OH) yielded the poor mineralization in AO-H₂O₂-BDD. By virtue of the attack of [•]OH produced in the bulk in EF-BDD, the mineralization was enhanced. However, almost total DOC removals were only attained for PEF-UVA-BDD and SPEF-BDD processes due to the occurrence of a quick photolysis of several Fe(III)-carboxylate complexes that cannot be removed by [•]OH. Because of the emission of sunlight in the visible region and its slightly higher UV intensity compared to the UVA lamp here used, the SPEF-BDD was the most powerful process, achieving almost total mineralization in 150 min of reaction. Greater *j* increased the mineralization rate of SY in all EAOPs, but with the spent of higher *Q* due to the acceleration of non-oxidizing reactions of BDD([•]OH) and [•]OH. The ability of EAOPs to degrade SY molecule was quite similar for EF-BDD, PEF-UVA-BDD and SPEF-BDD processes and slower for AO-H₂O₂-BDD. SY was more rapidly removed than decolorized, indicating that decolorization involves the destruction of colored aromatic products that absorb at the same λ_{max} of 482 nm as the azo dye.

Up to 14 aromatic products and 34 hydroxylated derivatives, including benzenic, naphthalenic and phthalic acid compounds, were detected by LC-MS. Ion-exclusion HPLC revealed a slow removal of generated LMCA with BDD([•]OH), a rapid photodecomposition of Fe(III)-tartronate and Fe(III)-oxalate complexes by UV light and a gradual destruction of Fe(III)-formate and Fe(III)-oxamate species with BDD([•]OH).

The use of a pilot-scale flow plant with a Pt/carbon-PTFE air-diffusion electrochemical cell coupled to a solar photoreactor demonstrated the viability of SPEF at large scale since it allowed the complete decolorization and almost total mineralization of 10 L of a 290 mg SY L⁻¹ solution in 7.0 g Na₂SO₄ L⁻¹ at pH of 3.0. The increase in *j* from 33.2 to 77.6 mA cm⁻² gave 91-94% mineralization at shorter times from 270 to 150 min, but with greater EC_v values from 7.3 to

17 kWh m⁻³. Fe(III) complexes of formic and oxamic acids remained in solution because they were not removed by Pt([•]OH), this being the main oxidative difference observed when a Pt anode was used instead of BDD in SPEF. Application of low *j* values proved to be more useful in SPEF-Pt since they provided a more efficient and economic process with lower energy consumption, although longer times were needed for reaching almost total mineralization.

3.5 References

- [1] Hunger, K. (ed) 2003. *Industrial Dyes, Chemistry, Properties, Applications*, Wiley-VCH, Weinheim, Germany.
- [2] Forgacs, E., Cserháti, T., Oros, G., 2004. Removal of synthetic dyes from wastewaters: A review. *Environment International* 30(7), 953-971.
- [3] Martínez-Huitle, C.A., Brillas, E., 2009. Decontamination of wastewaters containing synthetic organic dyes by electrochemical methods: A general review. *Applied Catalysis B: Environmental* 87(3-4), 105-145.
- [4] Zollinger, H., 2003. *Color Chemistry: Syntheses, Properties, and Applications of Organic Dyes and Pigments*, 3rd, revised ed., VCH and Wiley-VCH, Zurich, Switzerland/Weinheim, Germany.
- [5] Sharma, K.P., Sharma, S., Sharma, S., Singh, P.K., Kumar, S., Grover, R., Sharma, P.K., 2007. A comparative study on characterization of textile wastewaters (untreated and treated) toxicity by chemical and biological tests. *Chemosphere* 69(1), 48-54.
- [6] Marmion, D.M., 1991. *Handbook of U.S. Colorants: Foods, Drugs, Cosmetics, and Medical Devices*, 3rd ed., John Wiley and Sons, Inc., New York, United States.
- [7] Fragoso, C.T., Battisti, R., Miranda, C., de Jesus, P.C., 2009. Kinetic of the degradation of C.I. Food Yellow 3 and C.I. Food Yellow 4 azo dyes by the oxidation with hydrogen peroxide. *Journal of Molecular Catalysis A: Chemical* 301(1-2), 93-97.
- [8] Gemeay, A.H., Habib, A.-F.M., Borhan El-Din, M.A., 2007. Kinetics and mechanism of the uncatalyzed and Ag(I)-catalyzed oxidative decolorization of Sunset Yellow and Ponceau 4R with peroxydisulphate. *Dyes and Pigments* 74(2), 458-463.
- [9] Lodha, S., Jain, A., Sharma, V., Punjabi, P.B., 2008. Photocatalytic degradation of Sunset Yellow FCF in presence of some transition metal complexes and hydrogen peroxide. *Indian Journal of Chemistry Section A* 47A(03), 397-400.
- [10] Chanderia, K., Kumar, S., Sharma, J., Ameta, R., Punjabi, P.B., 2012. Degradation of Sunset Yellow FCF using copper loaded bentonite and H₂O₂ as photo-Fenton like reagent. *Arabian Journal of Chemistry* Article in press, DOI: 10.1016/j.arabjc.2012.07.023.
- [11] Ghoneim, M.M., El-Desoky, H.S., Zidan, N.M., 2011. Electro-Fenton oxidation of Sunset Yellow FCF azo-dye in aqueous solutions. *Desalination* 274(1-3), 22-30.
- [12] Skoumal, M., Rodríguez, R.M., Cabot, P.L., Centellas, F., Garrido, J.A., Arias, C., Brillas, E., 2009. Electro-Fenton, UVA photoelectro-Fenton and solar photoelectro-Fenton degradation of the drug ibuprofen in acid aqueous medium using platinum and boron-doped diamond anodes. *Electrochimica Acta* 54(7), 2077-2085.
- [13] Almeida, L.C., Garcia-Segura, S., Bocchi, N., Brillas, E., 2011. Solar photoelectro-Fenton degradation of paracetamol using a flow plant with a Pt/air-diffusion cell coupled with a compound parabolic collector: Process optimization by response surface methodology. *Applied Catalysis B: Environmental* 103(1-2), 21-30.

- [14] Garcia-Segura, S., Almeida, L.C., Bocchi, N., Brillas, E., 2011. Solar photoelectro-Fenton degradation of the herbicide 4-chloro-2-methylphenoxyacetic acid optimized by response surface methodology. *Journal of Hazardous Materials* 194, 109-118.
- [15] Boye, B., Dieng, M.M., Brillas, E., 2002. Degradation of herbicide 4-chlorophenoxyacetic acid by advanced electrochemical oxidation methods. *Environmental Science & Technology* 36(13), 3030-3035.
- [16] Garcia-Segura, S., Brillas, E., 2014. Advances in solar photoelectro-Fenton: Decolorization and mineralization of the Direct Yellow 4 diazo dye using an autonomous solar pre-pilot plant. *Electrochimica Acta* 140, 384-395.
- [17] Flox, C., Garrido, J.A., Rodríguez, R.M., Cabot, P.L., Centellas, F., Arias, C., Brillas, E., 2007. Mineralization of herbicide mecoprop by photoelectro-Fenton with UVA and solar light. *Catalysis Today* 129(1-2 Spec. Iss.), 29-36.
- [18] Styliidi, M., Kondarides, D.I., Verykios, X.E., 2003. Pathways of solar light-induced photocatalytic degradation of azo dyes in aqueous TiO₂ suspensions. *Applied Catalysis B: Environmental* 40(4), 271-286.
- [19] Garcia-Segura, S., Brillas, E., 2011. Mineralization of the recalcitrant oxalic and oxamic acids by electrochemical advanced oxidation processes using a boron-doped diamond anode. *Water Research* 45(9), 2975-2984.
- [20] Ruiz, E.J., Arias, C., Brillas, E., Hernández-Ramírez, A., Peralta-Hernández, J.M., 2011. Mineralization of Acid Yellow 36 azo dye by electro-Fenton and solar photoelectro-Fenton processes with a boron-doped diamond anode. *Chemosphere* 82(4), 495-501.
- [21] Hammami, S., Oturan, N., Bellakhal, N., Dachraoui, M., Oturan, M.A., 2007. Oxidative degradation of Direct Orange 61 by electro-Fenton process using a carbon felt electrode: Application of the experimental design methodology. *Journal of Electroanalytical Chemistry* 610(1), 75-84.
- [22] Brillas, E., Sirés, I., Oturan, M.A., 2009. Electro-Fenton process and related electrochemical technologies based on Fenton's reaction chemistry. *Chemical Reviews* 109(12), 6570-6631.
- [23] Sirés, I., Oturan, N., Oturan, M.A., 2010. Electrochemical degradation of β -blockers. Studies on single and multicomponent synthetic aqueous solutions. *Water Research* 44(10), 3109-3120.
- [24] Salazar, R., Brillas, E., Sirés, I., 2012. Finding the best Fe²⁺/Cu²⁺ combination for the solar photoelectro-Fenton treatment of simulated wastewater containing the industrial textile dye Disperse Blue 3. *Applied Catalysis B: Environmental* 115-116, 107-116.
- [25] Garcia-Segura, S., El-Ghenymy, A., Centellas, F., Rodríguez, R.M., Arias, C., Garrido, J.A., Cabot, P.L., Brillas, E., 2012. Comparative degradation of the diazo dye Direct Yellow 4 by electro-Fenton, photoelectro-Fenton and photo-assisted electro-Fenton. *Journal of Electroanalytical Chemistry* 681, 36-43.

4 Degradation of trimethoprim antibiotic by electrochemical advanced oxidation processes

The degradation of 20.0 mg L⁻¹ of trimethoprim (TMP) antibiotic (DOC of 11.6 mg L⁻¹) in an aqueous solution with 7.0 g Na₂SO₄ L⁻¹ was accomplished by various EAOPs such as AO-H₂O₂, EF, PEF-UVA and SPEF, as well as by the classical Fenton and PF-UVA processes. Experiments were performed in a 2.2 L lab-scale flow plant equipped with CPCs and an electrochemical filter-press cell with a BDD or Pt anode and a carbon-PTFE air-diffusion cathode. The effect of [TDI]₀, j and pH on the PEF-UVA-BDD method was firstly assessed by means of TMP and DOC decays, aiming to establish a treatment process using minimum iron concentration, adequate current density/H₂O₂ production and maximum pH. This treatment was efficiently performed using a low [TDI]₀ of 2.0 mg L⁻¹, a low j of 5.0 mA cm⁻² and pH of 3.5 without iron precipitation. The relative oxidation ability of EAOPs increased in the order: AO-H₂O₂-BDD < EF-BDD < PEF-UVA-BDD < SPEF-BDD. The EF-BDD and PEF-UVA-BDD processes were more effective than the comparable Fenton and PF-UVA ones. The PEF-UVA-BDD process led to a slightly faster TMP degradation than the PEF-UVA-Pt one, whereas in SPEF the influence of the nature of the anode was almost negligible. The scale-up to a 35 L capacity pilot-scale flow plant led to reproducible degradations taking into account the different experimental conditions of the systems. It was found a slow and partial TMP mineralization mainly attributed to the formation of a high content of hardly oxidizable N-derivatives, containing the major part of nitrogen. Up to 18 aromatic products and 19 hydroxylated derivatives were detected by LC-MS. Moreover, the efficiency of EAOPs using a real wastewater collected after secondary treatment in a MWWTP spiked with TMP at mg L⁻¹ levels or 19 pharmaceutical compounds at µg L⁻¹ levels was assessed. The use of this wastewater led to slower organics removal by SPEF-Pt compared to the 7.0 g Na₂SO₄ L⁻¹ solution. Furthermore, the oxidation ability of EAOPs increased in the order AO-H₂O₂ < AO < PEF-UVA < PEF-UVC. The decrease of pollutants content from mg L⁻¹ to µg L⁻¹ resulted in a lower degradation rate.

This Chapter is based on the following research article: “Moreira, F.C., Garcia-Segura, S., Boaventura, R.A.R., Brillas, E., Vilar, V.J.P., 2014. Degradation of the antibiotic trimethoprim by electrochemical advanced oxidation processes using a carbon-PTFE air-diffusion cathode and a boron-doped diamond or platinum anode. Applied Catalysis B: Environmental 160-161, 492-505”.

4.1 Introduction

Among pharmaceuticals, antibiotics have been recently classified as a priority risk group since they may cause resistance in bacterial populations, making them ineffective in the treatment of several diseases [1]. Trimethoprim (TMP) is an antibiotic commonly prescribed alone or in combination with a sulfonamide (e.g., sulfamethoxazole, sulfadiazine or sulfamoxole) for the treatment of specific bacterial infections, including gastro, respiratory and urinary infections in both human and veterinary medicine [2]. TMP has been detected in surface waters, WWTPs influents and effluents and hospital effluents at concentrations of 0.003-4.30 $\mu\text{g L}^{-1}$ [3, 4]. Since TMP cannot be degraded by conventional treatments, a promising approach to the remediation of wastewaters contaminated with high contents of this antibiotic is the application of AOPs and EAOPs, alone or in combination with technologies like nanofiltration and reverse osmosis to concentrate the pollutant before its treatment [5, 6].

While AOPs like ozonation [5, 7], photocatalysis with TiO_2 and in combination with H_2O_2 [8-10] and PF [10, 11] have been applied to the degradation of TMP, less is known about the use of EAOPs since only one paper has been published dealing with the AO treatment using a BDD anode [12]. Therefore, one can infer the importance of checking the viability of more powerful methods such as AO- H_2O_2 , EF, PEF and SPEF to remove TMP and its by-products from wastewaters.

The current Chapter reports a comparative study on the degradation of 20.0 mg TMP L^{-1} in an aqueous solution with 7.0 g $\text{Na}_2\text{SO}_4 \text{L}^{-1}$ by AO- H_2O_2 , EF, PEF-UVA and SPEF processes. Classical Fenton and PF-UVA processes were also comparatively examined. TMP and DOC decays were followed along reactions. The majority of trials was performed in a 2.2 L lab-scale flow plant containing CPCs and an electrochemical cell composed of a BDD or Pt anode and a carbon-PTFE air-diffusion cathode. In addition, a 35 L pilot-scale flow plant composed of CPCs and an electrochemical cell equipped with a Pt anode and a carbon-PTFE air-diffusion cathode was employed for comparison. The influence of $[\text{TDI}]_{0,j}$ and pH on the PEF-UVA-BDD process was assessed in a first approach, targeting to establish a treatment process using minimum iron concentration (below the Portuguese discharge limit), adequate current density/ H_2O_2 production and maximum pH. The effect of BDD and Pt anodes under PEF-UVA and SPEF conditions was examined. Generated LMCA and inorganic ions were followed by different techniques and aromatic products were detected by LC-MS. Moreover, the degradation of a real wastewater

collected after secondary treatment in a MWWTP spiked either with TMP at mg L⁻¹ levels or 19 pharmaceutical compounds at µg L⁻¹ levels was studied. The use of this real wastewater and the pure TMP solution was compared. The efficiency of AO, AO-H₂O₂, PEF-UVA and PEF-UVC processes employing this real wastewater was assessed and the concentration of 19 pharmaceutical micropollutants was followed during AO.

4.2 Materials and methods

All chemicals, analytical determinations, modeling of degradation kinetics and experimental units and procedures are depicted in the Chapter 2. Table 2.5 summarizes the operational conditions of EAOPs and AOPs performed in the current Chapter.

The real wastewater was collected after secondary treatment in an urban WWTP of Northern Portugal and its physicochemical characterization is presented in Table 4.1. Before submitting to treatment, this effluent was spiked with 5.0 mg TMP L⁻¹ or a mixture of 19 pharmaceutical compounds in concentrations of 16-34 µg L⁻¹.

The MCE was calculated from Eq. (41) considering that m is equal to 14, i.e. the number of carbon atoms of TMP molecule, and n is equal to 72, i.e. the number of electrons exchanged in the mineralization of TMP assuming the release of ammonium and nitrate ions, as will be discussed below, according to Eq. (56):

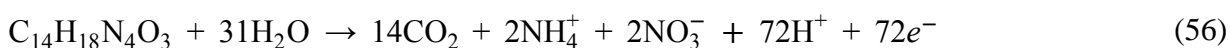


Table 4.1. Physicochemical characterization of the real wastewater collected after secondary treatment of a MWWTP.

Parameter (units)	MWWTP effluent
Color	Pale yellow
Odor	n.d. ^a
pH	6.8
Temperature (°C)	21.4
Conductivity ($\mu\text{S cm}^{-1}$)	890
Dissolved oxygen (mg L^{-1})	5.5
Redox potential (mV)	148
TDC (mg L^{-1})	36
DIC (mg L^{-1})	24
DOC (mg L^{-1})	12
COD ($\text{mg O}_2 \text{L}^{-1}$)	55
TDI (mg L^{-1})	<0.1 ^b
Absorbance at 254 nm (AU)	0.949
TSS (mg L^{-1})	11
VSS (mg L^{-1})	n.d. ^a
Total dissolved nitrogen (mg L^{-1})	18
Total organic nitrogen (mg L^{-1})	5.9
Ammonium – N-NH_4^+ (mg L^{-1})	4.3
Nitrite – N-NO_2^- (mg L^{-1})	1.0
Nitrate – N-NO_3^- (mg L^{-1})	6.8
Bromide – Br^- (mg L^{-1})	<0.008 ^b
Chloride – Cl^- (mg L^{-1})	110
Fluoride – F^- (mg L^{-1})	<0.1 ^c
Phosphate – PO_4^{3-} (mg L^{-1})	5.6
Sulfate – SO_4^{2-} (mg L^{-1})	60
Calcium – Ca^{2+} (mg L^{-1})	36
Lithium – Li^+ (mg L^{-1})	<0.004 ^b
Magnesium – Mg^{2+} (mg L^{-1})	7
Potassium – K^+ (mg L^{-1})	27
Sodium – Na^+ (mg L^{-1})	81
Total phosphorous – P (mg L^{-1})	5.7

^a n.d. – not detected;^b LOD;^c LOQ.

4.3 Results and discussion

4.3.1 Characteristics of the pure TMP solution

A pure solution with an initial TMP concentration of 20.0 mg L⁻¹ (DOC of 11.6 mg L⁻¹) in 7.0 g Na₂SO₄ L⁻¹ was used to achieve comprehensive TMP and DOC decay profiles, along with a good identification of intermediates formed.

The UV-Vis spectrum of TMP (see Figure 4.1) reveals that it absorbs radiation until ca. 310 nm with λ_{max} at 270 nm (characteristic of TMP, see Table 2.1). As a result, the drug cannot absorb the radiation of the UVA lamp and only a small fraction of the solar radiation can be absorbed (see spectral irradiance of these light sources in Figure 4.1). This corroborates the negligible TMP degradation found after 360 min of direct photolysis under UVA and solar radiation, alone or in combination with 103 mg L⁻¹ of H₂O₂, i.e. the stoichiometric amount necessary to completely mineralize 20.0 mg TMP L⁻¹ (data not shown). Sirtori et al. [9] have reported that TMP was highly stable to direct photolysis under simulated sunlight during 700 min and, afterwards, it dropped rapidly up to disappear at 1100 min. This severe drop on drug content was attributed to the formation of a photoreactive intermediate, a ketone derivative (2,4-diaminopyrimidin-5-yl)(3,4,5-trimethoxyphenyl)methanone), previously reported as a potential photosensitizer of its degradation [13]. This compound was also determined in the present study, as will be discussed below.

Figure 4.1 also shows that the presence of 2.0 mg L⁻¹ of Fe²⁺ did not change the TMP absorption spectrum. In contrast, a small increment of absorbance can be observed when 2.0 mg L⁻¹ of Fe³⁺ were added, which can be ascribed to the formation of Fe(III)-hydroxy complexes (see Fe³⁺ speciation diagrams vs. pH in Figure 4.1). Similar spectra were achieved for 2.0 mg Fe³⁺ L⁻¹ solutions in the presence and absence of 7.0 g Na₂SO₄ L⁻¹, indicating that the formation of Fe(III)-sulfate complexes, like FeSO₄⁺ and Fe(SO₄)₂⁻, showed a negligible influence on the absorption spectrum at pH of 3.5.

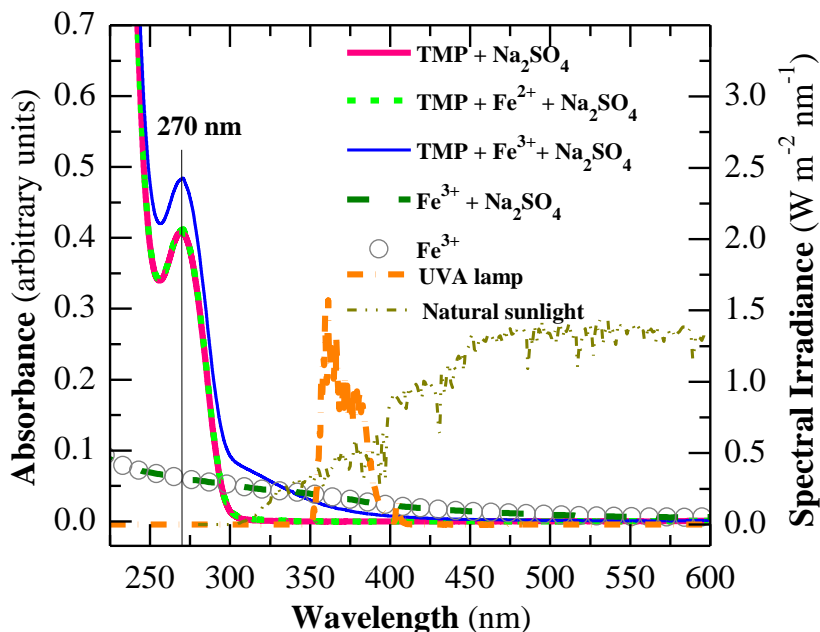


Figure 4.1. Absorption spectra of different solutions at pH = 3.5 (without dilution). [TMP] = 20.0 mg L⁻¹, [Na₂SO₄] = 7.0 g L⁻¹, [Fe²⁺] = 2.0 mg L⁻¹ and [Fe³⁺] = 2.0 mg L⁻¹. The spectral irradiances of UVA lamp and natural sunlight are also shown (UVA lamp: measured with the spectro-radiometer and confirmed by Philips; natural sunlight: AM1.5G reference spectrum [14]).

Table 4.2. Equilibrium reactions and respective equilibrium constants (log *K*) provided by the chemical equilibrium modeling system MINEQL+ [15] and used in the speciation diagrams calculation (T = 25 °C and ionic strength = 0 M).

Reaction	Log <i>K</i>
$\text{H}_2\text{O} \leftrightarrow \text{OH}^- + \text{H}^+$	-13.997
$\text{H}^+ + \text{SO}_4^{2-} \leftrightarrow \text{HSO}_4^-$	1.990
$\text{Na}^+ + \text{SO}_4^{2-} \leftrightarrow \text{NaSO}_4^-$	0.730
Fe(III)-hydroxy complexes	
$\text{Fe}^{3+} + \text{H}_2\text{O} \leftrightarrow \text{FeOH}^{2+} + \text{H}^+$	-2.187
$\text{Fe}^{3+} + 2\text{H}_2\text{O} \leftrightarrow \text{Fe}(\text{OH})_2^+ + 2\text{H}^+$	-4.594
$2\text{Fe}^{3+} + 2\text{H}_2\text{O} \leftrightarrow \text{Fe}_2(\text{OH})_2^{4+} + 2\text{H}^+$	-2.854
$\text{Fe}^{3+} + 3\text{H}_2\text{O} \leftrightarrow \text{Fe}(\text{OH})_3(\text{aq}) + 3\text{H}^+$	-12.560
$\text{Fe}^{3+} + 4\text{H}_2\text{O} \leftrightarrow \text{Fe}(\text{OH})_4^- + 4\text{H}^+$	-21.588
$3\text{Fe}^{3+} + 4\text{H}_2\text{O} \leftrightarrow \text{Fe}_3(\text{OH})_4^{5+} + 4\text{H}^+$	-6.288
Fe(III)-sulfate complexes	
$\text{Fe}^{3+} + \text{SO}_4^{2-} \leftrightarrow \text{FeSO}_4^+$	4.050
$\text{Fe}^{3+} + 2\text{SO}_4^{2-} \leftrightarrow \text{Fe}(\text{SO}_4)_2^-$	5.380

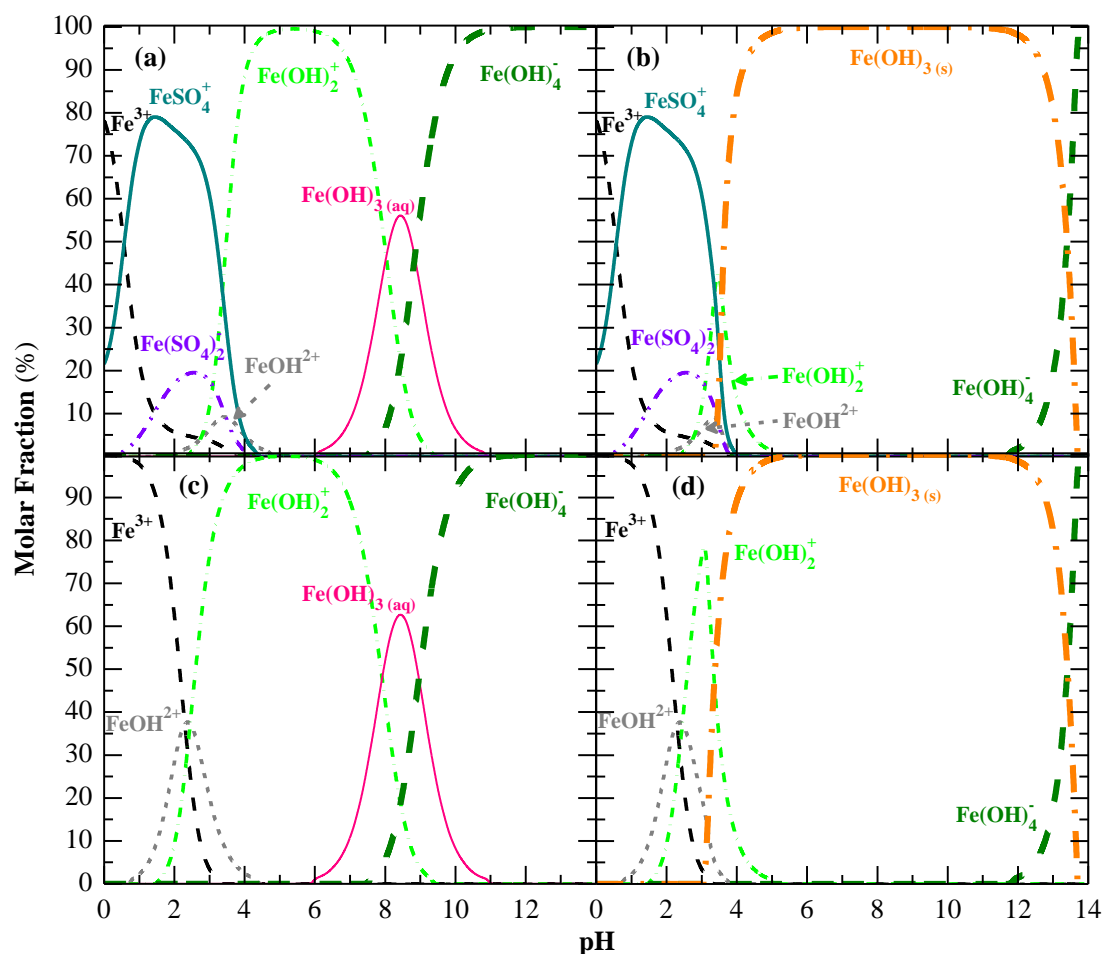


Figure 4.2. Fe^{3+} speciation diagrams as a function of solution pH in a calculated system containing: (a, b) 3.58×10^{-5} M of Fe^{3+} ($2.0 \text{ mg Fe}^{3+} \text{ L}^{-1}$), 4.93×10^{-2} M of SO_4^{2-} and 9.86×10^{-2} M of Na^+ ($7.0 \text{ g Na}_2\text{SO}_4 \text{ L}^{-1}$) (ionic strength = 0.148 M) or (c, d) 3.58×10^{-5} M of Fe^{3+} ($2.0 \text{ mg Fe}^{3+} \text{ L}^{-1}$) in absence of Na_2SO_4 (ionic strength ~ 0 M). Data were calculated by the chemical equilibrium modeling system MINEQL+ [15] using the equilibrium constants of Table 4.2. The formation of the solid iron phase $\text{Fe}(\text{OH})_3$ was (a, c) excluded and (b, d) included in the calculation.

4.3.2 Effect of operational parameters on the PEF-UVA-BDD process

4.3.2.1 Initial total dissolved iron concentration

The influence of $[\text{TDI}]_0$ on the performance of PEF-UVA-BDD was assessed by electrolyzing 1.250 L of 20.0 mg L^{-1} of TMP in $7.0 \text{ g Na}_2\text{SO}_4 \text{ L}^{-1}$ at pH of 3.0, 20°C , with addition of $[\text{TDI}]_0$ from 2.0 to 8.0 mg L^{-1} and at j of 10 mA cm^{-2} . This pH was chosen since it has been found as optimal for a vast number of aromatics degraded by PF, SPF, PEF and SPEF due to predominance of higher amounts of photoactive Fe(III)-hydroxy complexes, absence of iron precipitation,

absence of scavenge of $\bullet\text{OH}$ by carbonate and bicarbonate species and null auto-decomposition of H_2O_2 . [16-20]. 20 °C is an ambient temperature largely found in WWTPs final effluents [21]. Figure 4.3 depicts a progressively faster TMP concentration decay at higher $[\text{TDI}]_0$, with total removal after shorter times of 120, 90, 60 and 40 min for increasing $[\text{TDI}]_0$ of 2.0, 3.0, 4.0 and 8.0 mg L^{-1} , respectively. A pseudo-first-order kinetic model was fitted to the experimental data. The pseudo-first-order kinetic parameters both for TMP and DOC decays are displayed in Tables 4.3 and 4.4, respectively. Table 4.3 shows that the k_{TMP} values were 1.2, 2.3 and 4.9 times superior for 3.0, 4.0 and 8.0 mg L^{-1} compared with 2.0 mg L^{-1} , respectively. This trend can be related to the increasing amount of Fe^{2+} initially available and regenerated from: (i) photolysis of FeOH^{2+} through Eq. (28), and (ii) cathodic reduction of Fe^{3+} from Eq. (26), which improves the $\bullet\text{OH}$ production from Fenton's reaction (21). On the other hand, Figure 4.3 reveals the existence of a poor DOC abatement in the above trials, not higher than 61% after 180 min of electrolysis, with similar removal rate for $[\text{TDI}]_0$ higher than 4.0 mg L^{-1} . Moreover, slightly lower H_2O_2 accumulations were found for higher $[\text{TDI}]_0$ because of the existence of more Fe^{2+} available to react with H_2O_2 by Fenton's reaction (21), whereas $[\text{TDI}]$ remained constant and equal to the initial value during all the electrolysis time (data not displayed).

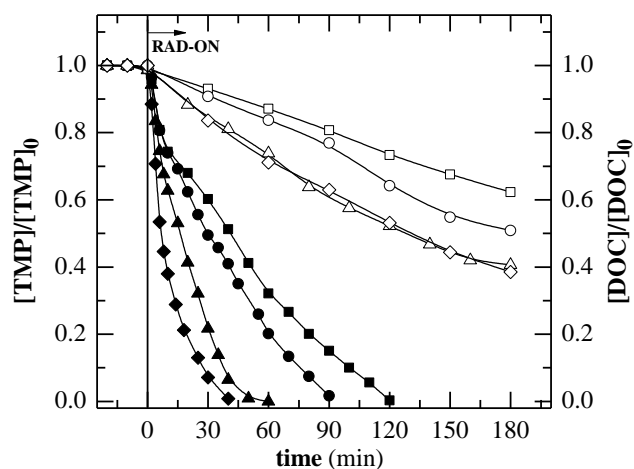


Figure 4.3. Effect of initial total dissolved iron concentration on (solid symbols) normalized TMP concentration decay and (open symbols) normalized DOC removal as a function of time for PEF-UVA-BDD treatment of a 20.0 mg TMP L^{-1} solution in 7.0 $\text{g Na}_2\text{SO}_4 \text{L}^{-1}$ using pH of 3.0, 20 °C and j of 10 mA cm^{-2} . $[\text{TDI}]_0$: (■, □) 2.0, (●, ○) 3.0, (▲, △) 4.0 and (◆, ◇) 8.0 mg L^{-1} .

Table 4.3. Pseudo-first-order kinetic constants for TMP concentration decay (k_{TMP}) along with the corresponding R^2 and S^2_{R} , obtained for the treatment of 20.0 mg TMP L⁻¹ in 7.0 g Na₂SO₄ L⁻¹ and real wastewater collected after secondary treatment of a MWWTP spiked with some pollutants under conditions of Figures 4.3, 4.4a, 4.5a, 4.6a, 4.7a, 4.8a, 4.9a, 4.11, 4.12a and 4.13.

System		k_{TMP} ($\times 10^{-3} \text{ min}^{-1}$)	R^2	S^2_{R} ($\text{mg}^2 \text{ L}^{-2}$)
Synthetic wastewater: 20.0 mg TMP L⁻¹ in 7.0 g Na₂SO₄ L⁻¹				
Effect of [TDI] ₀ (mg L ⁻¹) on PEF-UVA-BDD	2.0	19.1±0.6	0.994	0.21
	3.0	23.1±0.3	0.998	0.03
	4.0	44.1±0.8	0.997	0.06
	8.0	94±3	0.995	0.18
Effect of j (mA cm ⁻²) on PEF-UVA-BDD	2.5	16.8±0.6	0.993	0.37
	5	19.6±0.6	0.996	0.17
	10	19.1±0.6	0.994	0.21
	50	20.0±0.6	0.995	0.15
	100	33±2	0.978	0.47
	150	69±7	0.986	1.14
Effect of pH on PEF-UVA-BDD	3.0	19.6±0.6	0.996	0.17
	3.5	23.9±0.5	0.997	0.07
	4.0	22.3±0.3	0.998	0.05
	4.5	12.4±0.3	0.996	0.23
PF-UVA	With Na ₂ SO ₄ , initial H ₂ O ₂ addition	43±2	0.992	0.10
	Without Na ₂ SO ₄ , gradual H ₂ O ₂ addition	70±1	0.997	0.03
	With Na ₂ SO ₄ , gradual H ₂ O ₂ addition	38±2	0.992	0.13
Various processes	AO-H ₂ O ₂ -BDD	2.90±0.03	0.998	0.03
	EF-BDD	9.6±0.1	0.997	0.08
	PEF-UVA-BDD	23.9±0.5	0.997	0.07
	SPEF-BDD	50±1	0.998	0.08
	Fenton	11.2±0.2	0.996	0.09
	PF-UVA	43±2	0.992	0.10
	PEF-UVA-BDD with H ₂ O ₂ addition	55±1	0.994	0.05
		k_{TMP} (L kJ ⁻¹)	R^2	S^2_{R} ($\text{mg}^2 \text{ L}^{-2}$)
BDD vs. Pt anode	PEF-UVA-BDD	0.75±0.01	0.998	0.05
	PEF-UVA-Pt	0.50±0.01	0.997	0.08
	SPEF-BDD	1.98±0.07	0.991	0.41
	SPEF-Pt	2.0±0.1	0.974	1.07
SPEF-Pt at pilot-scale		1.00±0.07	0.946	1.84
Real wastewater: wastewater collected after secondary treatment of a MWWTP				
		k_{TMP} (L kJ ⁻¹)	R^2	S^2_{R} ($\text{mg}^2 \text{ L}^{-2}$)
SPEF-Pt using the real matrix spiked with 20.0 mg TMP L ⁻¹		0.72±0.04	0.974	0.63
		k_{TMP} ($\times 10^{-3} \text{ min}^{-1}$)	R^2	S^2_{R} ($\text{mg}^2 \text{ L}^{-2}$)
AO-BDD using the real matrix spiked with 5.0 mg TMP L ⁻¹		17±2	0.845	0.43
AO-H ₂ O ₂ -BDD using the real matrix spiked with 5.0 mg TMP L ⁻¹		6.8±0.3	0.978	0.03
PEF-UVA-BDD using the real matrix spiked with 5.0 mg TMP L ⁻¹		51±3	0.970	0.09
PEF-UVC-BDD using the real matrix spiked with 5.0 mg TMP L ⁻¹		138±5	0.991	0.03
AO-BDD using the real matrix spiked with 16-34 µg L ⁻¹ of 19 pharmaceutical compounds		43±7	0.906	0.00001

Table 4.4. Pseudo-first-order kinetic constants for DOC removal (k_{DOC}) along with the corresponding R^2 and S^2_{R} , obtained for the treatment of 20.0 mg TMP L⁻¹ in 7.0 g Na₂SO₄ L⁻¹ and real wastewater collected after secondary treatment of a MWWTP spiked with 20.0 mg TMP L⁻¹ under conditions of Figures 4.3, 4.4a, 4.5c, 4.6a, 4.7b, 4.8a,b, 4.9b and 4.11.

System		k_{DOC} ($\times 10^{-3} \text{ min}^{-1}$)	R^2	S^2_{R} ($\text{mg}^2 \text{ L}^{-2}$)
PF-UVA	With Na ₂ SO ₄ , initial H ₂ O ₂ addition	0.99±0.01	0.998	0.001
	Without Na ₂ SO ₄ , gradual H ₂ O ₂ addition	2.55±0.09	0.988	0.022
	With Na ₂ SO ₄ , gradual H ₂ O ₂ addition	1.76±0.04	0.996	0.003
Various processes	AO-H ₂ O ₂ -BDD	0.64±0.01	0.996	0.001
	EF-BDD	0.83±0.01	0.996	0.002
	PEF-UVA-BDD	2.11±0.05	0.995	0.010
	SPEF-BDD	6.17±0.08	0.999	0.014
	Fenton	0.76±0.02	0.994	0.003
	PF-UVA	0.99±0.01	0.998	0.001
	PEF-UVA-BDD with H ₂ O ₂ addition	4.15±0.10	0.995	0.027
		k_{DOC} ($\times 10^{-3} \text{ L kJ}^{-1}$)	R^2	S^2_{R} ($\text{mg}^2 \text{ L}^{-2}$)
BDD vs. Pt anode	PEF-UVA-BDD	62.1±0.8	0.998	0.003
	PEF-UVA-Pt	50±3	0.981	0.034
	SPEF-BDD	183±6	0.987	0.116
	SPEF-Pt	137±6	0.986	0.201
SPEF-Pt at pilot-scale		72±3	0.979	0.182
SPEF-Pt using real matrix spiked with 20.0 mg TMP L ⁻¹		57±1	0.996	0.065

Sirtori et al. [9] and Michael et al. [11] have also reported a slow and incomplete TMP mineralization by TiO₂ photocatalysis and SPF, respectively, and have correlated these results with the formation of very stable photo-transformation products, even more persistent than TMP, and the generation of carboxylic acids. These two contributions for the slow TMP mineralization will be analyzed below. Furthermore, it is well-known that the presence of sulfate and chloride ions in the medium can also inhibit the efficiency of the process [9, 11, 19, 22, 23]. In order to clarify the possible influence of the high sulfate content employed in the above mentioned PEF-UVA-BDD trials (4.7 g SO₄²⁻ L⁻¹ resulting from the employment of 7.0 g Na₂SO₄ L⁻¹ as background electrolyte) on TMP degradation kinetics, two PF-UVA trials were performed in the presence and absence of sulfate, using pH of 3.5 and [TDI]₀ of 2.0 mg L⁻¹. Figure 4.4a shows that both TMP and DOC removals for the PF-UVA trials were faster in the absence of sulfate ion, leading to k_{TMP} and k_{DOC} values 1.6 and 2.6 times superior, respectively, as can be seen in Tables 4.3 and 4.4, respectively. The lower efficiency of TMP degradation process in the presence of sulfate ions can be ascribed to four main causes: (i) the formation of complexes of sulfate with Fe³⁺ (FeSO₄⁺ and Fe(SO₄)₂⁻), thereby affecting the distribution and reactivity of the iron species since the establishment of these

complexes competes with the creation of much more photoactive Fe(III)-hydroxy complexes, yielding smaller amounts of FeOH^{2+} and thus decreasing the regeneration of Fe^{3+} to Fe^{2+} and $\bullet\text{OH}$ production [20, 22, 24] (see Fe^{3+} speciation diagrams in presence and absence of Na_2SO_4 in Figure 4.2); (ii) the scavenging of $\bullet\text{OH}$ by sulfate ion along with the formation of the weaker $\text{SO}_4^{\bullet-}$ oxidant when compared with $\bullet\text{OH}$ via Eq. (34) [25] (rate constants for reactions in aqueous solution are usually within the range of 10^6 - $10^9 \text{ M}^{-1} \text{ s}^{-1}$ for $\text{SO}_4^{\bullet-}$ and 10^7 - $10^{10} \text{ M}^{-1} \text{ s}^{-1}$ for $\bullet\text{OH}$ [22, 25, 26]); (iii) the decomposition of H_2O_2 through reaction with $\text{SO}_4^{\bullet-}$ by Eqs. (36) and (37) [25]; and (iv) the oxidation reactions involving $\text{SO}_4^{\bullet-}$ [22]. In addition, sulfate ions are considered a physical quencher of the ketone triplet state thereby leading to degradation mechanisms diverging from those taking place in the absence of sulfate [27].

Figure 4.4b depicts a gradual removal of [TDI] from the solution up to reach around 0.8 mg L^{-1} in the absence of sulfate ion since the introduction of this ion allows to work at higher pH values without iron precipitation as $\text{Fe}(\text{OH})_3 (s)$. Similar amounts of H_2O_2 were consumed in the presence and absence of sulfate (Figure 4.4b). Note that the presence of Fe^{2+} ion was omitted in the above considerations over the PF-UVA processes since it was rapidly converted into Fe^{3+} via Fenton's reaction (21).

Despite the aforementioned results, a $[\text{TDI}]_0$ of 2.0 mg L^{-1} was employed in the further trials because: (i) the Portuguese legislation imposes this value as emission limit for the discharge of treated effluents (Portuguese decree law n° 236/98), thus avoiding the removal of iron as a final step of the process; (ii) total iron values of 1.4 - 1.6 mg L^{-1} have been found in MWWTPs effluents after biological treatment and so there is no need for iron addition to oxidize organics in these effluents [28, 29]; and (iii) lower iron concentrations allows working at slightly higher pH values without $\text{Fe}(\text{OH})_3 (s)$ precipitation. For example, Fe^{3+} speciation diagrams allow predicting that $\text{Fe}(\text{OH})_3 (s)$ precipitates at increasing pH values of 3.2, 3.4, 3.4 and 3.5 for declining Fe^{3+} contents of 8.0, 4.0, 3.0 and 2.0 mg L^{-1} , respectively.

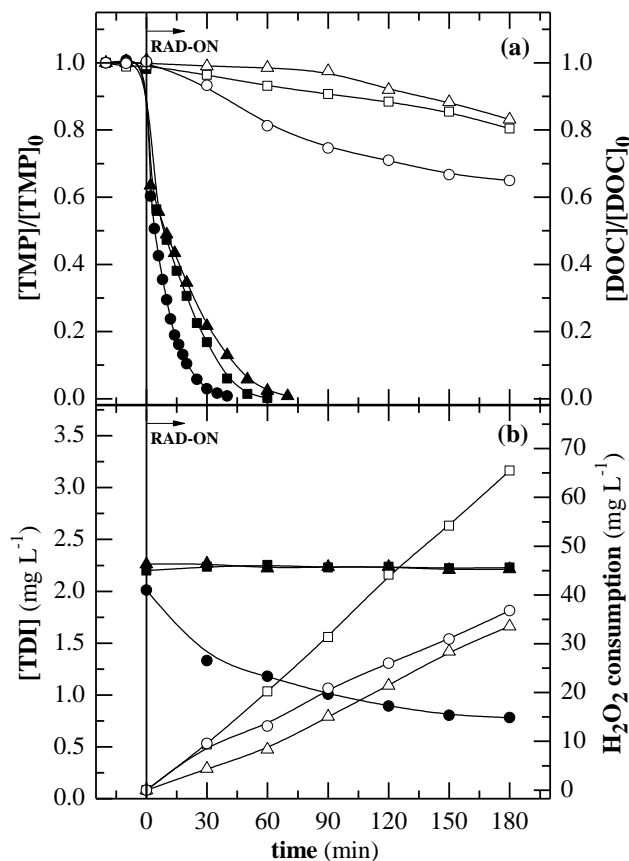


Figure 4.4. Evaluation of PF process in terms of: (a) (solid symbols) normalized TMP concentration decay and (open symbols) normalized DOC removal and (b) (solid symbols) total dissolved iron concentration and (open symbols) H_2O_2 consumption as a function of time for treatment of a $20.0 \text{ mg TMP L}^{-1}$ solution using pH of 3.5, $20 \text{ }^\circ\text{C}$ and $[TDI]_0$ of 2.0 mg L^{-1} . Conditions: (■, □) $7.0 \text{ g Na}_2\text{SO}_4 \text{ L}^{-1}$ and total addition of stoichiometric H_2O_2 at $t = 0 \text{ min}$, (●, ○) absence of Na_2SO_4 and gradual H_2O_2 addition and (▲, △) $7.0 \text{ g Na}_2\text{SO}_4 \text{ L}^{-1}$ and gradual H_2O_2 addition.

4.3.2.2 Current density

j is a key parameter in EAOPs since it regulates the amount of oxidizing species. The influence of this parameter on the PEF-UVA-BDD process for the degradation of 20.0 mg L^{-1} of TMP in $7.0 \text{ g Na}_2\text{SO}_4 \text{ L}^{-1}$ was tested using pH of 3.0, $20 \text{ }^\circ\text{C}$, $[TDI]_0$ of 2.0 mg L^{-1} and j from 2.5 to 150 mA cm^{-2} . Figure 4.5a shows a gradual enhancement of TMP concentration decay when j increased, excluding the values between 5.0 and 50 mA cm^{-2} which exhibited similar behavior. As can be seen in Table 4.3, the k_{TMP} value for j of 2.5 mA cm^{-2} increased up to 1.1-1.2, 1.9 and 4.1 times for j of 5-50, 100 and 150 mA cm^{-2} , respectively. These findings indicate that for j higher than 50 mA cm^{-2} the production of BDD($\bullet\text{OH}$) and $\bullet\text{OH}$ in the bulk was large enough to rapidly

degrade TMP. Nevertheless, the rise in j yielded higher energy consumption to destroy the drug, more evident for values higher than 10 mA cm^{-2} (Figure 4.5b).

Similarly, the DOC abatement rose when greater j was applied, but it was always inferior to 48% at the end of the process (Figure 4.5c). These achievements suggest the formation of by-products that are hardly oxidized by BDD($\bullet\text{OH}$), $\bullet\text{OH}$ and/or photodecomposed by UVA light. Since almost constant MCE values with time can be observed in Figure 4.5d for each applied j , one can infer that by-products were mineralized at similar rate during all the PEF-UVA-BDD processes. Moreover, lower MCE values were achieved for raising j from 2.5 to 50 mA cm^{-2} , being nearly equal between j of 50 and 150 mA cm^{-2} . This loss in current efficiency with raising j can be related to the formation of smaller relative amounts of oxidants BDD($\bullet\text{OH}$) and $\bullet\text{OH}$ because of the concomitant acceleration of their waste reactions (24), (25), (39) and (40).

On the other hand, Figure 4.5c shows that for j of 2.5 mA cm^{-2} , H_2O_2 was consumed at the same time it was produced. In contrast, higher j values led to the formation of H_2O_2 in excess from Eq. (16), which was accumulated during the process, thus ensuring that the system maintained the maximum production of $\bullet\text{OH}$ from Fenton's reaction (21).

From all the above findings, a j value of 5.0 mA cm^{-2} was taken for further trials because: (i) TMP concentration decay was almost similar to that obtained using 10 and 50 mA cm^{-2} ; (ii) DOC decay was within the values obtained for all the applied j but with higher MCE; and (iii) the production of $\bullet\text{OH}$ in the bulk was maximal since H_2O_2 was generated in excess.

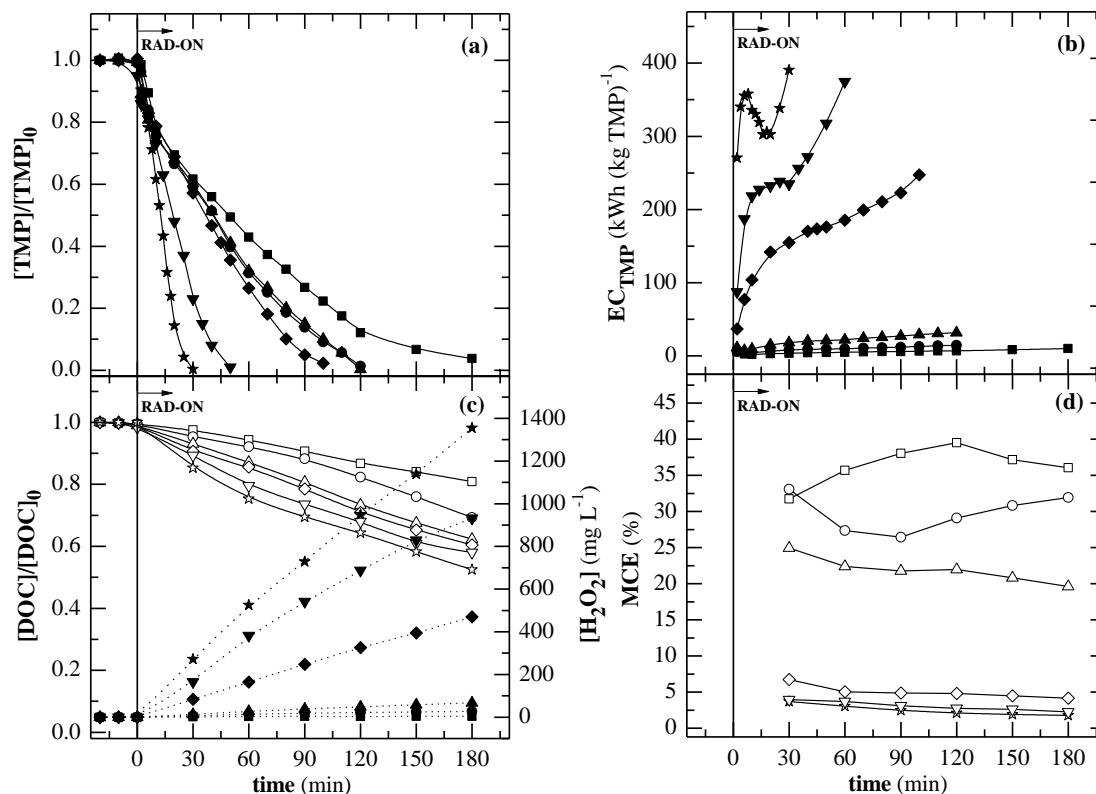


Figure 4.5. Effect of current density on (a) normalized TMP concentration decay, (b) energy consumption per unit TMP mass, (c) (open symbols) normalized DOC removal and (dot profile) H_2O_2 concentration and (d) mineralization current efficiency as a function of time for PEF-UVA-BDD treatment of a 20.0 mg TMP L $^{-1}$ solution in 7.0 g Na $_2$ SO $_4$ L $^{-1}$ using pH of 3.0, 20 °C and $[TDI]_0$ of 2.0 mg L $^{-1}$. Current density: (■, □) 2.5, (●, ○) 5.0, (▲, △) 10, (◆, ◇) 50, (▼, ▽) 100 and (★, ☆) 150 mA cm $^{-2}$.

4.3.2.3 pH

The effectiveness of the PEF-UVA-BDD process to degrade the 20.0 mg L $^{-1}$ of TMP in 7.0 g Na $_2$ SO $_4$ L $^{-1}$ was evaluated at pH values of 3.0, 3.5, 4.0 and 4.5, 20 °C, $[TDI]_0$ of 2.0 mg L $^{-1}$ and j of 5.0 mA cm $^{-2}$. The solutions with initial pH higher than 3.0 underwent a slight acidification during electrolysis and consequently their pH was continuously adjusted to the initial value by adding small volumes of 0.5 M NaOH. Although pH of 3.0 has been reported as optimal for many PEF and SPEF processes [16-18], Figure 4.6a reveals that pH values of 3.5 and 4.0 achieved similar and slightly faster TMP concentration decay. The corresponding k_{TMP} values (Table 4.3) were 1.2 and 1.1 times higher than the one reached at pH of 3.0, respectively, even with an iron precipitation to $[TDI]$ values ranging from 0.76 to 1.2 mg L $^{-1}$ during all the pH 4.0 experiment (Figure 4.6b), as predicted by Figure 4.2b. According to this diagram, lower molar fractions of $FeOH^{2+}$ and higher molar fractions of $FeSO_4^+$ and $Fe(SO_4)_2^-$ are available at pH of 3.0 when

compared with pH of 3.5, which can justify the lower oxidizing power of PEF-UVA-BDD at pH of 3.0 since Fe(III)-sulfate complexes are much less photoactive species than FeOH^{2+} , as mentioned above. At pH of 4.5, the slower TMP decay compared to that of pH of 3.5 can be ascribed to the almost total iron precipitation (Figure 4.6b). On the other hand, Figure 4.6a shows a similar and very low DOC decay for all pH values tested, corresponding to removals below 31%. Taking into account the above results, a pH of 3.5 can be set as the best one for the TMP degradation under PEF-UVA-BDD conditions since it allows the fastest TMP removal without iron precipitation.

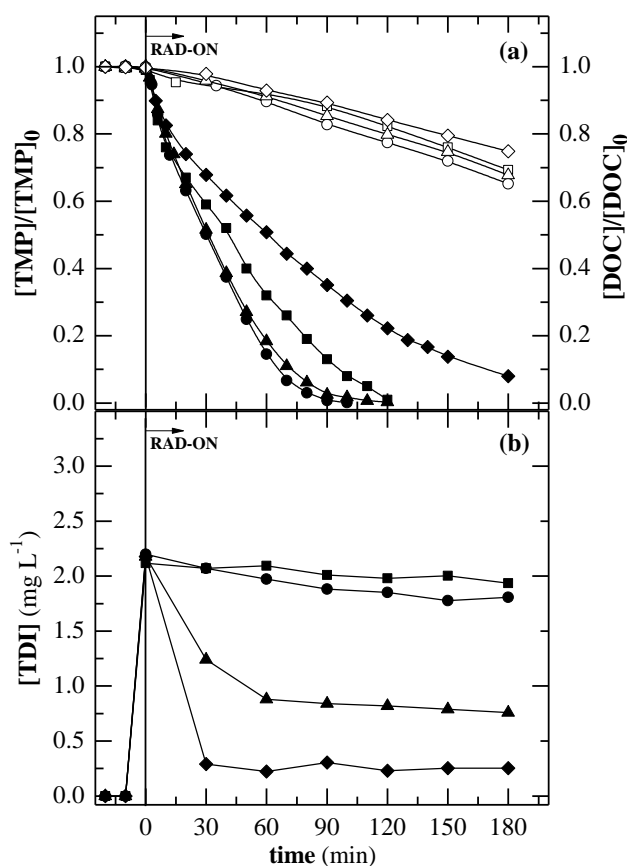


Figure 4.6. Effect of pH on (a) (solid symbols) normalized TMP concentration decay and (open symbols) normalized DOC removal and (b) total dissolved iron concentration as a function of time for PEF-UVA-BDD treatment of a 20.0 mg TMP L⁻¹ solution in 7.0 g Na₂SO₄ L⁻¹ using 20 °C, $[\text{TDI}]_0$ of 2.0 mg L⁻¹ and j of 5.0 mA cm⁻². Initial pH: (■, □) 3.0, (●, ○) 3.5, (▲, △) 4.0 and (◆, ◇) 4.5.

4.3.3 Comparison of AO-H₂O₂, EF, PEF-UVA, SPEF, Fenton and PF-UVA processes

The solution composed of 20.0 mg TMP L⁻¹ in 7.0 g Na₂SO₄ L⁻¹ was comparatively treated by EAOPs employing the BDD anode, i.e., AO-H₂O₂-BDD, EF-BDD, PEF-UVA-BDD and SPEF-BDD processes, under the best conditions above established, that is, [TDI]₀ of 2.0 mg L⁻¹, *j* of 5.0 mA cm⁻² and pH of 3.5. Fenton and PF-UVA comparative trials were also carried out using the stoichiometric amount of H₂O₂ needed for total antibiotic mineralization (103 mg L⁻¹). Results obtained are depicted in Figure 4.7. [TDI] remained almost constant and equal to 2.0 mg L⁻¹ for EF-BDD, PEF-UVA-BDD, SPEF-BDD, Fenton and PF-UVA processes (data not displayed).

The relative power of EAOPs to degrade the TMP solution increased in the sequence AO-H₂O₂-BDD < EF-BDD < PEF-UVA-BDD < SPEF-BDD (see Figure 4.7a), with relative *k*_{TMP} values of 1:3.3:8.3:17.2 (see Table 4.3). The poorer TMP removal by AO-H₂O₂-BDD can be related to the low reaction rate of TMP with the main oxidant BDD(•OH) generated according to Eq. (1). In EF-BDD, the high reaction rate between the drug and •OH generated from Fenton's reaction (21) improved its degradation. The faster TMP removal attained in PEF-UVA-BDD and SPEF-BDD evidences the additional •OH production induced by the UV photolysis of photoactive FeOH²⁺ as indicated by Eq. (28). The slightly higher UV intensity of sunlight compared to UVA light yielded a greater rate for the latter reaction, thus explaining that SPEF-BDD is the most powerful EAOP.

Figure 4.7b reveals the superiority of DOC removal by SPEF-BDD and, in turn, PEF-UVA-BDD exhibited dominance over AO-H₂O₂-BDD and EF-BDD, as can also be deduced from the *k*_{DOC} values given in Table 4.4. While the two latter processes only led to 11-14% mineralization after 180 min of reaction, the DOC was reduced by 35% and 66% in PEF-UVA-BDD and SPEF-BDD, respectively. Therefore, the supplementary •OH production under UV light from Eq. (28) along with the direct photolysis of Fe³⁺ complexes with some organic intermediates like generated carboxylic acids via Eq. (29), which occurred in larger extent under the powerful UV radiation provided by sunlight, revealed to play a crucial role on TMP and its intermediates degradation.

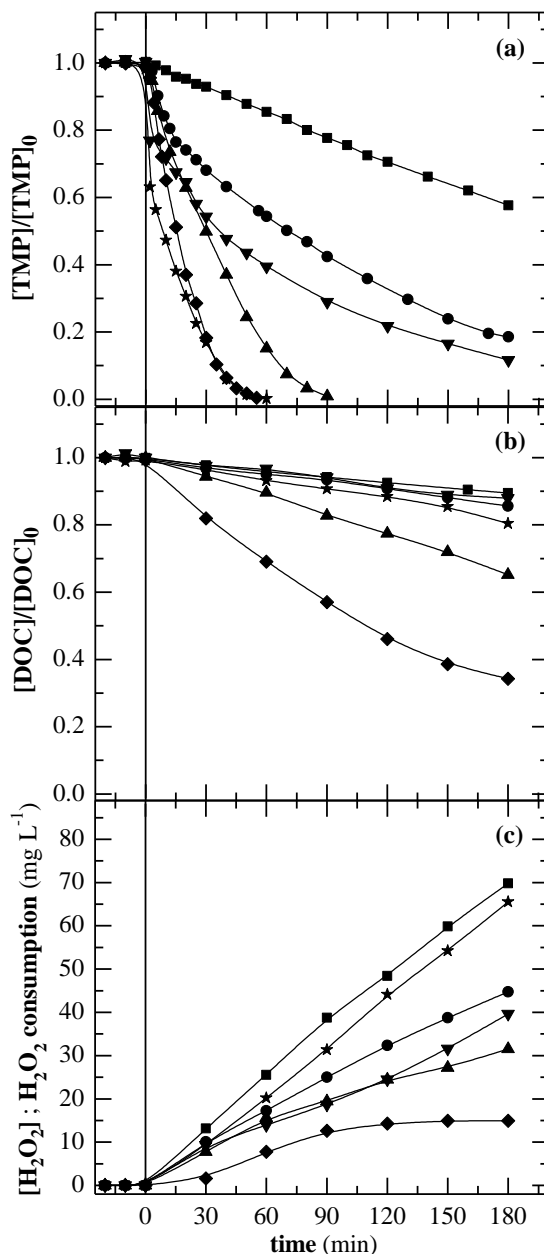


Figure 4.7. Evaluation of (a) normalized TMP concentration decay, (b) normalized DOC removal and (c) H₂O₂ concentration (for EAOPs) or H₂O₂ consumption (for AOPs) as a function of time for treatment of 20.0 mg TMP L⁻¹ solution in 7.0 g Na₂SO₄ L⁻¹ by various processes using pH of 3.5, 20 °C, [TDI]₀ of 2.0 mg L⁻¹ for Fenton's reaction based processes, *j* of 5.0 mA cm⁻² for EAOPs and initial H₂O₂ addition of 103 mg L⁻¹ for AOPs. Process: (■) AO-H₂O₂-BDD (●) EF-BDD, (▲) PEF-UVA-BDD, (◆) SPEF-BDD, (▼) Fenton and (★) PF-UVA.

On the other hand, Figure 4.7c shows that H₂O₂ was accumulated in smaller extent in the order: AO-H₂O₂-BDD > EF-BDD > PEF-UVA-BDD > SPEF-BDD, as expected by the increasing oxidation performance of these EAOPs, as stated above. Surprisingly, the comparison of these data with those reached for EF-BDD, PEF-UVA-BDD and SPEF-BDD in the absence of the antibiotic (see Figure 2.7) reveals that H₂O₂ attained higher concentrations in the presence of

20.0 mg TMP L⁻¹ (approximately the double at the end of reaction). This suggests that the oxidation of TMP and its by-products at the BDD anode competes with that of H₂O₂ by Eqs. (19) and (20), diminishing its decomposition rate. Therefore, the H₂O₂ consumed during EAOPs depends on the existing pollutants and so it is complex to estimate.

Considering that EF-BDD and PEF-UVA-BDD can count on (i) BDD(•OH) attack, (ii) Fe³⁺ regeneration to Fe²⁺ at the cathode from Eq. (26), and (iii) even the direct oxidation of TMP on BDD in addition to the reactions occurring in Fenton and PF-UVA treatments, one can expect, in a simple approach, that a faster antibiotic degradation will be obtained by EAOPs. However, some significant differences between both chemical and electrochemical treatments should be taken into account. In Fenton and PF-UVA, H₂O₂ is available in high concentrations at the first instant of reaction and known amounts of this oxidant are added to the solution, allowing the calculation of the H₂O₂ consumption. In contrast, in EF-BDD and PEF-UVA-BDD, H₂O₂ is not present when the reaction starts and it is continuously generated and consumed, depending on the presence of TMP and its intermediates, as stated above. Thus, when comparing these processes, the TMP and DOC decay profiles should be analyzed with precaution and no clear conclusions about efficiencies can be drawn in terms of H₂O₂ consumed from TMP or DOC removed. More effective comparisons can be performed by means of (i) economic analysis; (ii) environmental impact assessment due to the fact that H₂O₂ and electricity production are industrial activities that involve negative consequences to the environment; and (iii) implementation of new EF and PEF configurations that ensure H₂O₂ availability from the first instant of reaction.

Figure 4.7a shows that Fenton and PF-UVA processes led to much faster TMP decay than the analogous electrochemical during the first 2 min of reaction, where high removals of 23% and 37% were achieved, respectively. This behavior can be related to the larger amount of H₂O₂ present in solution at the start of the chemical processes with consequent maximum •OH production via Fenton's reaction (21) in contrast with the lower H₂O₂ concentration achieved in EF-BDD and PEF-UVA-BDD due to the H₂O₂ gradual generation along time (see Figure 4.7c). In order to confirm this hypothesis, a PEF-UVA-BDD trial with initial addition of the stoichiometric amount of H₂O₂ was performed and an identical initial TMP decay of 38% after 2 min was achieved, validating what was proposed. After this distinct initial phase in Fenton and PF-UVA processes, the TMP degradation became slower and, similarly to other processes, followed pseudo-first-order kinetics commonly correlated to the competition between initial degradation by-products and parent compound for oxidizing species and available radiation (see k_{TMP} values in Table 4.3). However, these slow reactions can also be related to the formation of strong and stable

Fe(III)-TMP complexes thereby limiting the regeneration of Fe^{3+} to Fe^{2+} and consequently the overall efficiency of the process. Demirezen et al. [30] described that Fe(III)-TMP complexes are characterized by two medium metal-*N* stretching bands and assumed that the two NH_2 groups on the pyrimidine rings act as monodentate ligands of ferric ions. Tella and Obaleye [31] reported the formation of Fe(III)-TMP complexes with a Fe(III)-to-TMP molar ratio of 1:2 and a stability constant ($\log K$) of 10.99 (ionic strength = 0.1 M).

As concerns DOC abatement, Figure 4.7b reveals an almost negligible mineralization by the Fenton process, slightly enhanced by EF-BDD, whereas PEF-UVA-BDD displayed a clear superiority over PF-UVA, yielding a final mineralization of 35% against 17% after 180 min, with a k_{DOC} value 2.1 times higher (see Table 4.4). This reveals that some intermediates need UVA light to be mineralized and are faster degraded under electrochemical conditions, as expected.

An extra PF-UVA trial with gradual H_2O_2 addition achieved TMP and DOC removals similar to those obtained when all the H_2O_2 was initially added, but the H_2O_2 consumption was inferior in the former approach (less than 32 mg L^{-1} after 180 min) as a consequence of undesirable waste reactions as Eq. (24) when H_2O_2 is available in high amounts (see Figures 4.4a,b and Tables 4.3 and 4.4).

4.3.4 BDD vs. Pt anodes in PEF-UVA and SPEF processes

The influence of BDD and Pt anodes on the degradation 20.0 mg L^{-1} of TMP in $7.0 \text{ g Na}_2\text{SO}_4 \text{ L}^{-1}$ was verified under PEF-UVA and SPEF conditions using pH of 3.5, $20 \text{ }^\circ\text{C}$, $[\text{TDI}]_0$ of 2.0 mg L^{-1} and j of 5.0 mA cm^{-2} . Figure 4.8a shows that PEF-UVA-BDD exhibited slightly faster TMP and DOC removals than PEF-UVA-Pt, being the corresponding k_{TMP} and k_{DOC} values about 1.5 and 1.2 times superior, respectively (see Tables 4.3 and 4.4, respectively). In turn, SPEF-BDD and SPEF-Pt treatments yielded a less variation regarding both TMP and DOC decays (see Figures 4.8a,b and Tables 4.3 and 4.4). Since it is well-known that BDD($\bullet\text{OH}$) are produced in more extent than Pt($\bullet\text{OH}$) from Eq. (1) [32], the minor discrepancies achieved using the both anodes confirm the minor role previously attributed to M($\bullet\text{OH}$) on the degradation of TMP and its intermediates under PEF-UVA and SPEF conditions due to the strong photocatalytic action of the UV radiation, especially under the action of the sun. Furthermore, as can be seen in Figure 4.8b, a quasi-steady DOC removal was achieved in SPEF-BDD and SPEF-Pt for accumulated radiations higher than ca. 10 kJ L^{-1} and incomplete DOC abatements of 73-77% were obtained after ca. 17 kJ L^{-1} at 420 min, thereby suggesting the formation of recalcitrant intermediates that are

hardly destroyed either by BDD($\bullet\text{OH}$) or Pt($\bullet\text{OH}$), $\bullet\text{OH}$ in the bulk and UV radiation provided by sunlight. The nature of these compounds will be discussed below. At the end of these trials (420 min of reaction and ca. 17 kJ L^{-1} of solar energy consumption), MCE values of 30% and 26% and energy consumptions of 123 and $99 \text{ kWh (kg DOC)}^{-1}$ or 1.2 and 0.9 kWh m^{-3} were found for SPEF-BDD and SPEF-Pt, respectively. Regarding the total removal of TMP, attained after around 55 min of reaction and 1.6 kJ L^{-1} of sunlight irradiation, energy consumptions of 6.3 and $4.4 \text{ kWh (kg TMP)}^{-1}$ or 0.14 and 0.10 kWh m^{-3} were found for SPEF-BDD and SPEF-Pt, respectively. This brings to consider that the use of Pt coated anode is preferable for SPEF since it yields similar current efficiency with lower energy consumption than a BDD one and, furthermore, this anode is much more inexpensive.

Ion-exclusion chromatograms of electrolyzed solutions revealed the formation of LMCA such as oxalic, oxamic and formic acids during 420 min of SPEF-BDD and SPEF-Pt. All these acids are ultimate acids and thus they are directly mineralized to CO_2 . Oxamic acid was detected in very low concentrations ($< 0.06 \text{ mg L}^{-1}$). In contrast, oxalic and formic acid were accumulated in a larger content up to 4.3 mg L^{-1} , as shown in Figure 4.8c. While the Fe(III)-formate complexes were accumulated and removed completely at similar rate for both anodes, the Fe(III)-oxalate species were more rapidly mineralized using BDD than Pt, because they can be oxidized by BDD($\bullet\text{OH}$) but not by Pt($\bullet\text{OH}$) [33, 34]. At 420 min (ca. 17 kJ L^{-1}), practically no LMCA were detected in both SPEF-BDD and SPEF-Pt treatments, indicating that the remaining DOC in their final solutions (23-27%) was due to the presence of other undetected and more stable by-products.

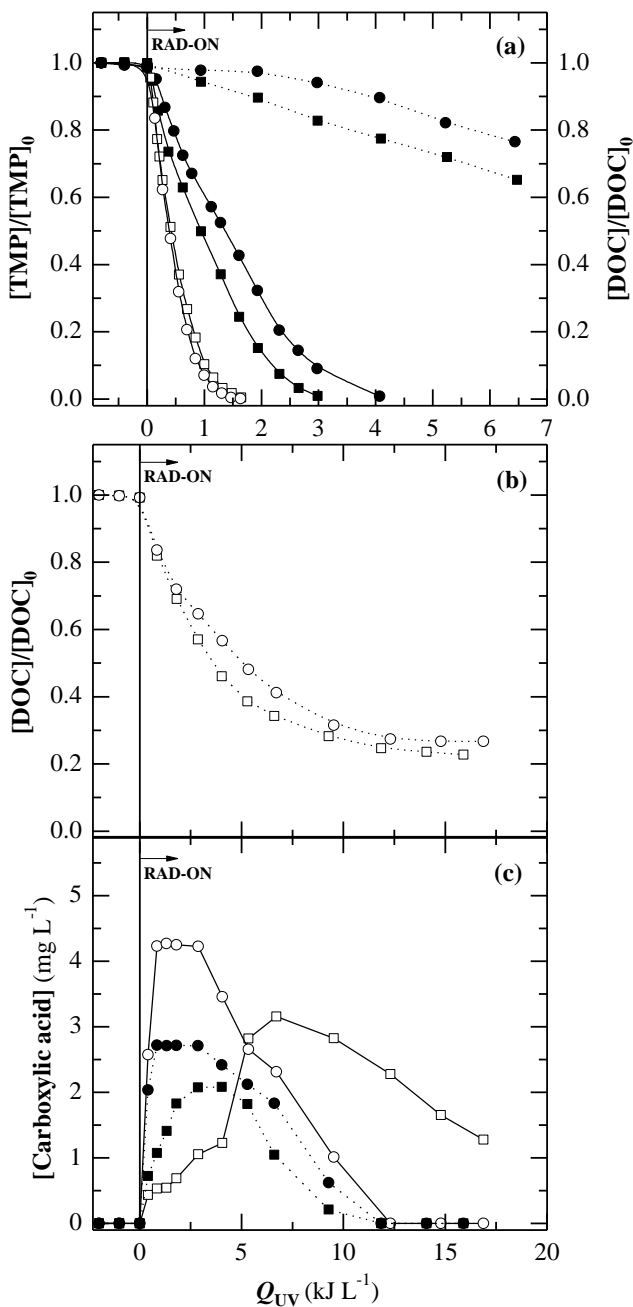


Figure 4.8. (a,b) Effect of (■,□) BDD and (●,○) Pt anodes on treatment by (solid symbols) PEF-UVA and (open symbols) SPEF processes of a 20.0 mg TMP L⁻¹ solution in 7.0 g Na₂SO₄ L⁻¹ using pH of 3.5, 20 °C, [TDI]₀ of 2.0 mg L⁻¹ and *j* of 5.0 mA cm⁻². (a) (Solid profile) normalized TMP concentration decay and (dot profile) normalized DOC removal for PEF-UVA and (b) normalized DOC removal for SPEF as a function of accumulated UV energy per L of solution. In plot (c), evolution of the concentration of (■,□) oxalic and (●,○) formic acids during (solid symbols) SPEF-BDD and (open symbols) SPEF-Pt.

4.3.5 TMP degradation at pilot-scale

The scale-up from a lab-scale system with 2.2 L capacity to a pilot-scale system with 35 L capacity, both composed of a filter-press electrochemical cell and CPCs, was assessed by employing a SPEF-Pt process to a 20.0 mg TMP L⁻¹ solution in 7.0 g Na₂SO₄ L⁻¹ using pH of 3.5, 20 °C, [TDI]₀ of 2.0 mg L⁻¹ and *j* of 5.0 mA cm⁻². Figure 4.9 reveals slower TMP and DOC removals for the pilot-scale plant, presenting *k*_{TMP} and *k*_{DOC} values 2.0 and 1.9 times lower (see Tables 4.3 and 4.4). This degradation deceleration at pilot-scale is in good agreement with the 2.0 times lower electrodes area/solution volume ratio observed for the pilot-scale system (4 against 8 cm² L⁻¹ for the pilot- and lab-scale systems, respectively). Furthermore, other experimental conditions influencing the degradation efficiency can be found in both systems such as (i) an irradiated volume/total volume ratio of around 3 times higher for the lab-scale system (56% against 19% for the pilot- and lab-scale systems, respectively), and (ii) distinct flow rates of 0.67 and 9.0 L min⁻¹ for lab- and pilot-scale systems, respectively. For the total removal of TMP (at 90 min of reaction and 2.1 kJ L⁻¹ of accumulated UV energy), an energy consumption of 0.08 kWh m⁻³ was found at pilot-scale. An energy of 0.31 kWh m⁻³ was consumed at the end of reaction (360 min; 17 kJ L⁻¹ of accumulated UV energy; 64% DOC removal).

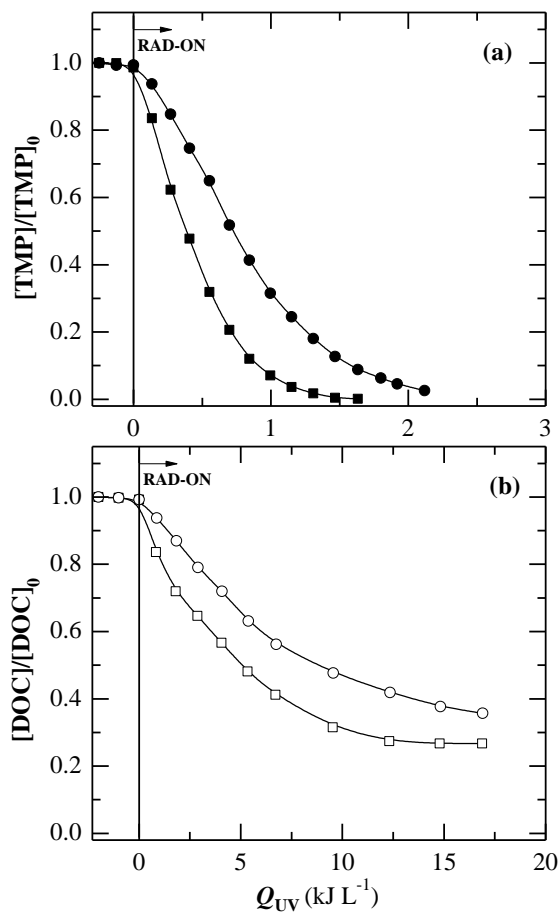


Figure 4.9. (a) Normalized TMP concentration decay and (b) normalized DOC removal as a function of accumulated UV energy per L of solution for SPEF-Pt treatment of a 20.0 mg TMP L⁻¹ solution in 7.0 g Na₂SO₄ L⁻¹ using pH of 3.5, 20 °C, [TDI]₀ of 2.0 mg L⁻¹ and *j* of 5.0 mA cm⁻² at (■, □) lab-scale, i.e. using the 2.2 L lab-scale flow plant, and at (●, ○) pilot-scale, i.e. using the 35 L pilot-scale flow plant.

4.3.6 Nitrogen mass balance

The mineralization of TMP is expected to be accompanied by the loss of its nitrogen atoms in the form of inorganic ions such as ammonium, nitrate and nitrite. To confirm this, the evolution of these ions was followed during the SPEF-Pt process applied to 20.0 mg L⁻¹ of TMP in 7.0 g Na₂SO₄ L⁻¹ using pH of 3.5, 20 °C, [TDI]₀ of 2.0 mg L⁻¹ and *j* of 5.0 mA cm⁻², where the initial total nitrogen content was of 3.86 mg L⁻¹. No nitrite ion was detected under these conditions as expected by its instability in strong oxidant media. Figure 4.10 shows the accumulation of both ammonium and nitrate ions up to 0.56 and 0.77 mg L⁻¹ of nitrogen at the end of electrolysis, respectively, without change in the total dissolved nitrogen concentration in solution. One can then infer that an equivalent proportion of both ions are released to the medium, as proposed in Eq. (56), and that a high amount of recalcitrant *N*-derivatives related to about 65% of total dissolved nitrogen remains

in the final treated solution, which also contains 27% of the initial DOC. Similarly to these results, Sirtori et al. [9] have described the generation of low concentrations of ammonium and nitrate ions during the TMP degradation by TiO₂ photocatalysis, corresponding only to 20% of initial nitrogen, and correlated this result to the persistence of high-molecular-weight *N*-intermediates. Michael et al. [11] have also reported the presence of *N*-generated intermediates until the end of the degradation by SPF of the same antibiotic.

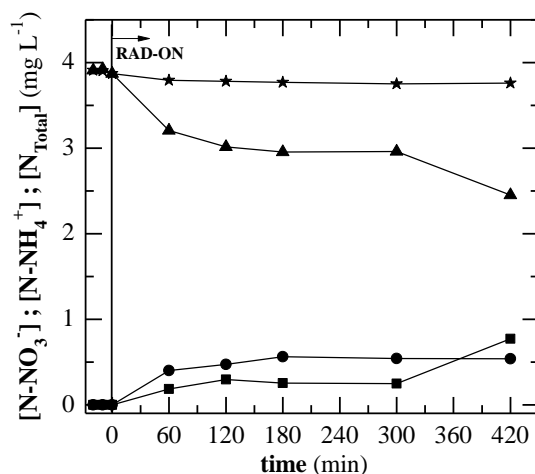


Figure 4.10. Evolution of (■) nitrate ion, (●) ammonium ion, (▲) total organic nitrogen and (★) total dissolved nitrogen as a function of time during SPEF-Pt process using pH of 3.5, 20 °C, [TDI]₀ of 2.0 mg L⁻¹ and *j* of 5.0 mA cm⁻².

4.3.7 Generated aromatic products

The SUVA₂₅₄ has been strongly correlated with the aromatic content of a solution [35]. From this measurement, the aromatic content of the TMP solution treated by the above SPEF-Pt process underwent a severe drop in its initial stages up to reach an almost constant value close to 43% of the initial SUVA₂₅₄ content (3.2 L mg⁻¹ m⁻¹). This finding in parallel with (i) the slow TMP mineralization attained along all the treatments, (ii) the incomplete mineralization attained by SPEF processes even after the accumulation of high UV light doses, and (iii) the high residual nitrogen content, suggests the formation of high amounts of recalcitrant *N*-heteroaromatic products.

To elucidate the nature of the oxidation products, and then to check the formation of recalcitrant nitrogen products, several samples withdrawn up to 60 min of the PEF-UVA-Pt degradation of a 20.0 mg TMP L⁻¹ solution in 7.0 g Na₂SO₄ L⁻¹ using pH of 3.5, 20 °C, [TDI]₀ of 2.0 mg L⁻¹ and *j* of 5.0 mA cm⁻² were analyzed by LC-MS. The aromatic products are mainly formed and oxidized

by $\bullet\text{OH}$ in the bulk and a significant photocatalytic action of UV light takes place in light-assisted processes, especially in SPEF due to the potent solar irradiation. Therefore, the same kind of intermediates is expected in all light-assisted Fenton's reaction based AOPs/EAOPs. Table 4.5 collects the 18 aromatic compounds identified, including the initial TMP (1), and 19 hydroxylated derivatives.

Table 4.5. Aromatic products and hydroxylated derivatives identified by LC-MS in positive and negative mode during the PEF-UVA-Pt treatment of 20.0 mg TMP L⁻¹ in 7.0 g Na₂SO₄ L⁻¹.

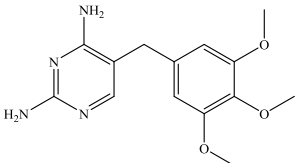
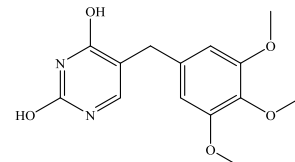
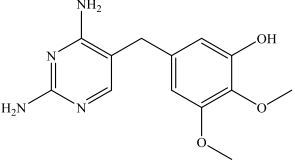
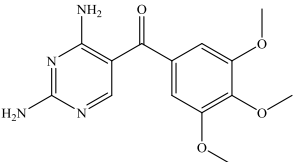
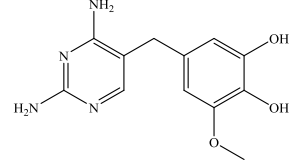
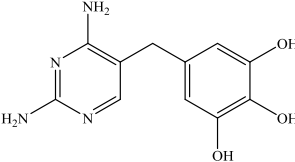
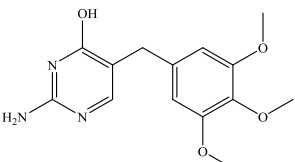
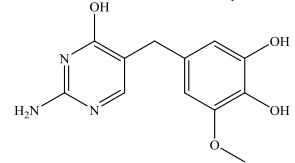
Compound	Molecular structure	Number of -OH added	<i>m/z</i>
Trimethoprim (1)		-	291 ^a
		1	307 ^a
		3	339 ^a
		4	355 ^a
(2,4-diaminopyrimidin-5-yl)(3,4,5-trimethoxyphenyl)methanone (2)		-	305 ^a 303 ^b
5-(3,4,5-trimethoxybenzyl)pyrimidine-2,4-diol (3)		-	-
		1	305 ^b
5-((2,4-diaminopyrimidin-5-yl)methyl)-2,3-dimethoxyphenol (4)		3	337 ^b
		1	277 ^a
		3	293 ^a
5-((2,4-diaminopyrimidin-5-yl)methyl)-3-methoxybenzene-1,2-diol (5)		4	325 ^a
		1	341 ^a
		2	295 ^a
5-((2,4-diaminopyrimidin-5-yl)methyl)benzene-1,2,3-triol (6)		-	-
		2	281 ^a
2-amino-5-(3,4,5-trimethoxybenzyl)pyrimidin-4-ol (7)		4	313 ^a
		1	289 ^b
5-((2-amino-4-hydroxypyrimidin-5-yl)methyl)-3-methoxybenzene-1,2-diol (8)		3	305 ^b
		-	337 ^b
		-	261 ^b

Table 4.5. Aromatic products and hydroxylated derivatives identified by LC-MS in positive and negative mode during the PEF-UVA-Pt treatment of 20.0 mg TMP L⁻¹ in 7.0 g Na₂SO₄ L⁻¹.

Compound	Molecular structure	Number of -OH added	<i>m/z</i>
5-((2-amino-4-hydroxypyrimidin-5-yl)methyl)benzene-1,2,3-triol (9)		-	247 ^b
5-(pyrimidin-5-ylmethyl)benzene-1,2,3-triol (10)		- 2 6	215 ^b 247 ^b 311 ^b
4,5-dimethoxybenzene-1,3-diol (11)		- 2	169 ^b 201 ^b
6-methoxybenzene-1,2,4-triol (12)		- 1 2	- 171 ^b 187 ^b
3,4,5-trimethoxybenzoic acid (13)		- 1	211 ^b 227 ^b
2,6-diaminopyrimidine-4,5-diol (14)		-	143 ^a
2-nitropyrimidin-4-amine (15)		-	141 ^a
methanol compound with pyrimidine-2,4-diol (1:1) (16)		-	127 ^b
2,4-diaminopyrimidine-5-carboxylic acid (17)		-	138 ^b
4-amino-6-hydroxy-2-nitropyrimidine-5-carboxylic acid (18)		-	202 ^a

^a Positive ionization;^b Negative ionization.

The primary ketone product **2** has been previously described as a photoreactive intermediate causing an autocatalytic effect on TMP degradation [13]. Deamination, demethylation and/or hydroxylation of **1** lead to compounds **3-10**, which maintain the two-ring TMP structure. The subsequent cleavage of **1-10** results in the benzenic derivatives **11-13** and *N*-heteroaromatics **14-18**. The products **11-18** with one aromatic moiety can be more rapidly mineralized under UV radiation. The cleavage of their ring produces Fe(III)-oxamate, Fe(III)-oxalate and Fe(III)-formate complexes, which can be completely photolyzed or destroyed by BDD(\bullet OH), as shown in Figure 4.8c. It is worth mentioning that the oxidation products detected from photolysis and TiO₂ photocatalysis only maintained the two-ring TMP structure and major changes occurred in the trimethoxybenzyl moiety [9].

4.3.8 Efficiency of EAOPs using a real wastewater matrix

4.3.8.1 Comparison of synthetic and real wastewaters

From the characteristics of the wastewater collected after secondary treatment in a MWWTP presented in Table 4.1, one can highlight: (i) neutral pH, (ii) low organic content (DOC of 12 mg L⁻¹), (iii) low nitrogen content (18 mg L⁻¹ of total dissolved nitrogen, 4.3 mg N-NH₄⁺ L⁻¹, 1.0 mg N-NO₂⁻ L⁻¹, 6.8 mg N-NO₃⁻ L⁻¹), (iv) chloride content of 110 mg L⁻¹, (v) low conductivity of 890 μS cm⁻¹, (vi) absence of dissolved iron, and (vii) a phosphate content of 5.6 mg L⁻¹. This conductivity value was ca. 10 times inferior to the 8600 μS cm⁻¹ values exhibited by the 7.0 g Na₂SO₄ L⁻¹ solution. The DOC of wastewaters from secondary treatment in WWTPs has been mainly attributed to the presence of humic and fulvic acids, LMCA and polysaccharides [36].

It is well-known that Fe³⁺ strongly precipitates with phosphates [37, 38]. To avoid fluctuations on the iron content and the need for iron control during Fenton's reaction based EAOPs, phosphates were previously removed by precipitation with Fe³⁺ to form strengite (FePO₄·2H₂O). DOC and [TDI] remained unchanged after this removal.

The effect of using the secondary MWWTP effluent instead of the Na₂SO₄ solution as background electrolyte was assessed by spiking both solutions with 20.0 mg TMP L⁻¹ and applying a SPEF-Pt method under the best conditions, i.e., pH of 3.5, 20 °C, [TDI]₀ of 2.0 mg L⁻¹ and *j* of 5.0 mA cm⁻². Figure 4.11 highlights the existence of slower TMP and DOC decays using the real wastewater, with *k*_{TMP} and *k*_{DOC} values 2.8 and 2.4 times lower, respectively (see Tables 4.3 and 4.4). After ca. 15 kJ L⁻¹ of accumulated UV energy, a partial mineralization of 62% and 73% was obtained

for the real wastewater and the Na_2SO_4 solution, respectively, with an energy consumption of 1.5 and 0.8 kWh m^{-3} , respectively. The higher energy consumption achieved for the real wastewater can be related to the lower conductivity of this effluent. The obtained results suggest the consumption of $\bullet\text{OH}$ to oxidize the additional dissolved organic compounds of the real wastewater, which can be more recalcitrant than TMP, and/or the filtration of photochemically active light by these dissolved organics, with consequent attenuation of photoreduction reactions (28) and (29) [39]. Nonetheless, it should be mentioned that in some situations the presence of dissolved organic matter can contribute to positive phenomena: (i) production of reactive species like $\bullet\text{OH}$ and excited triplet states by indirect photolysis; (ii) photolysis by LMCT excitation of Fe(III) complexes with dissolved organics via the general Eq. (29), leading to Fe^{2+} and $\bullet\text{OH}$ formation; and (iii) possibility of working at higher pH values without iron precipitation by the formation of Fe(III) complexes, attenuating or even avoiding acidification and neutralization steps [40].

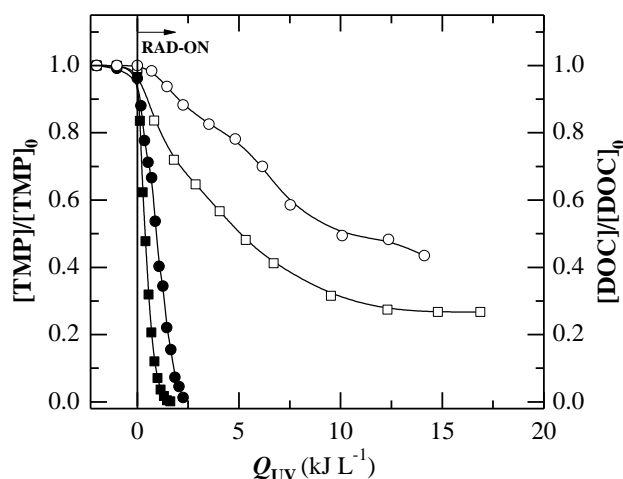


Figure 4.11. (Solid symbols) Normalized TMP concentration decay and (open symbols) normalized DOC removal as a function of accumulated UV energy per L of solution for SPEF-Pt treatment at pH of 3.5, 20 °C, $[\text{TDI}]_0$ of 2.0 mg L^{-1} and j of 5.0 mA cm^{-2} of two distinct matrices spiked with 20.0 mg TMP L^{-1} : (■, □) ultrapure water with 7.0 $\text{g Na}_2\text{SO}_4 \text{L}^{-1}$ and (●, ○) real wastewater collected after secondary treatment of a MWWTP.

4.3.8.2 Comparison of AO, AO-H₂O₂, PEF-UVA and PEF-UVC processes for the degradation of TMP in a real wastewater matrix

To elucidate the degradative behavior of TMP in the real wastewater, AO-BDD, AO-H₂O₂-BDD, PEF-UVA-BDD and PEF-UVC-BDD processes were applied to the degradation of this wastewater spiked with 5.0 mg TMP L⁻¹ using the pH of the effluent (6.8) for AO-BDD and AO-H₂O₂-BDD processes and pH of 3.5 for PEF processes, 20 °C, [TDI]₀ of 2.0 mg L⁻¹ for PEF processes and j of 5.0 mA cm⁻². In AO and AO-H₂O₂ processes, the acidification step was omitted to make these processes easier to apply. Additional experiments revealed that the use of the effluent pH on PEF-UVA-BDD and PEF-UVC-BDD processes led to k_{TMP} values 12 and 5.1 times lower compared to pH of 3.5 (data not showed).

Figure 4.12 shows that processes ability to degrade both TMP and DOC can be arranged in the following order: PEF-UVC-BDD > PEF-UVA-BDD > AO-BDD > AO-H₂O₂-BDD. The superiority of PEF-UVC-BDD over PEF-UVA-BDD can be attributed to the additional •OH production from the H₂O₂ photolysis according to Eq. (30). The chloride ions presented in the secondary WWTP effluent can be directly oxidized at the anode to yield Cl₂ via Eq. (5), which further evolves to HClO/ClO⁻ species by Eqs. (6) and (7). The latter species can react with H₂O₂ and, consequently, it is highly likely that the amounts of active chlorine species and H₂O₂ strongly decreased in AO-H₂O₂-BDD, in contrast to AO-BDD, yielding the slower organics removal with k_{TMP} 2.5 times lower (see Table 4.3). Furthermore, the •OH can be consumed by H₂O₂ via Eq. (24) in AO-H₂O₂-BDD.

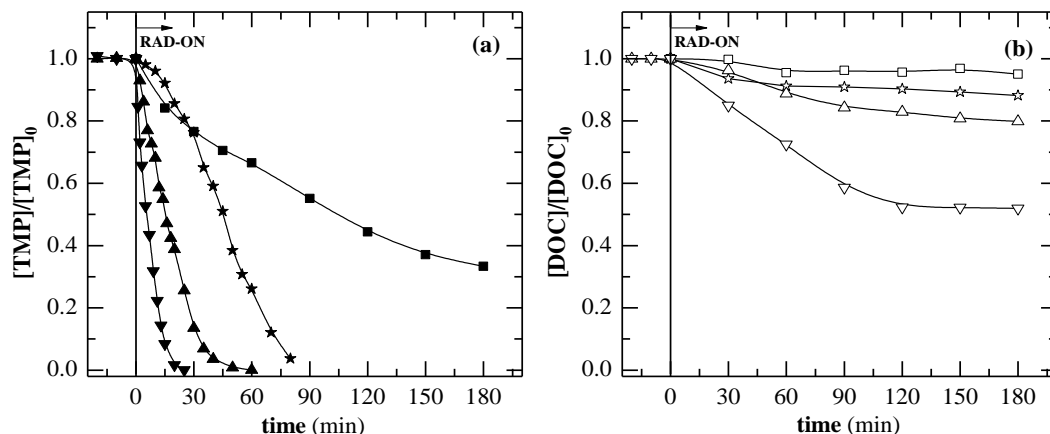


Figure 4.12. Evaluation of (a) normalized TMP concentration decay and (b) normalized DOC removal as a function of time for treatment of the real wastewater spiked with 5.0 mg TMP L⁻¹ by various EAOPs using the pH of the effluent (6.8) for AO and AO-H₂O₂ and pH of 3.5 for PEF, 20 °C, [TDI]₀ of 2.0 mg L⁻¹ for PEF and *j* of 5.0 mA cm⁻². EAOP: (★, ☆) AO-BDD, (■, □) AO-H₂O₂-BDD, (▲, △) PEF-UVA-BDD and (▼, ▽) PEF-UVC-BDD.

4.3.8.3 Degradation of pharmaceutical compounds in a real wastewater matrix at mg L⁻¹ and µg L⁻¹ levels

Effluents from secondary treatment of WWTPs display micropollutants levels in the order of ng L⁻¹ and µg L⁻¹ and the application of membrane filtration processes usually does not rise their content above µg L⁻¹ [41, 42]. Since the degradation rate is affected by the initial content of organics as elucidated in Chapter 1, the remediation of the real matrix with these low amounts of organics was assessed. The original real effluent exhibited amounts of pharmaceutical compounds below 2.7 µg L⁻¹. To achieve comprehensive pollutants decay profiles, the real wastewater was spiked with 19 pharmaceutical compounds in concentrations from 16 to 34 µg L⁻¹. An AO-BDD process using the pH of the effluent (6.8), 20 °C and *j* of 5.0 mA cm⁻² was then applied and the micropollutants were followed along the reaction time by UPLC-MS/MS.

Figure 4.13 compares the TMP decay using initial antibiotic contents of 5.0 mg L⁻¹ and 34 µg L⁻¹. It was observed the removal of higher amounts of TMP per unit of time, i.e. a higher TMP removal rate, for the real effluent spiked with 5.0 mg TMP L⁻¹, with $r_{0(\text{TMP})}$ values of $(1.5 \pm 0.2) \times 10^{-3}$ and $(75 \pm 8) \times 10^{-3}$ mg L⁻¹ min⁻¹ for initial TMP contents of 34 µg L⁻¹ and 5.0 mg L⁻¹, respectively. In view of the pseudo-first-order kinetic constants, it was perceived a large drop on k_{TMP} from 34 µg L⁻¹ to 5.0 mg L⁻¹ of initial TMP content (see Table 4.3). Theoretically, it should be expected an independence of k_{TMP} on the organic content, which is in disagreement with the obtained results.

Hence, the pseudo-first-order kinetic model may comprise some limitations to precisely describe the TMP decay profiles, as predictable since a comprehensive mechanistic kinetic model may include all reactions that each contaminant undergoes during the treatment.

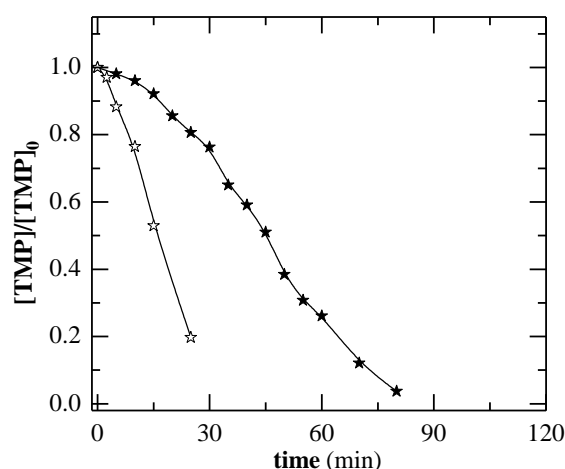


Figure 4.13. Normalized TMP concentration decay as a function of time for AO-BDD treatment of the real wastewater spiked with (★) 5.0 mg TMP L⁻¹ and (☆) mixture of 19 pharmaceutical compounds in 16-34 µg L⁻¹ levels using the pH of the effluent (6.8), 20 °C and *j* of 5.0 mA cm⁻².

After 25 min of AO-BDD treatment, it was achieved an average removal of 87% for the 19 pharmaceutical compounds. Urtiaga et al. [42] found removals above 95% for 12 micropollutants at 0.005-24 µg L⁻¹ by applying an AO-BDD process at *j* of 10 mA cm⁻² and neutral pH during 1 h to a secondary MWWTP effluent after UF and RO. Pérez et al. [41] attained an average micropollutants abatement of 93% for 10 micropollutants in the 0.80-20 µg L⁻¹ range after 2 h of AO-BDD treatment at *j* of 2-10 mA cm⁻² and neutral pH applied to a secondary WWTP effluent previously subjected to UF and RO.

Figure 4.14 shows that only 8 of the 19 micropollutants followed by UPLC-MS/MS during AO-BDD treatment were removed below 2.0 µg L⁻¹ after 25 min of reaction and some of them such as TMP, bisoprolol, diclofenac and paracetamol revealed a more recalcitrant character, displaying concentrations from 6.7 to 11 µg L⁻¹ at the end.

The ability of AO-BDD, PEF-UVA-BDD and PEF-UVC-BDD treatments to degrade the 19 pollutants at µg L⁻¹ levels was compared by applying these processes during 2.5 min. An average micropollutants removal of 80% and 88% was achieved for PEF-UVA-BDD and PEF-UVC-BDD processes, respectively, contrasting with the lower removal of 17% reached for AO-BDD.

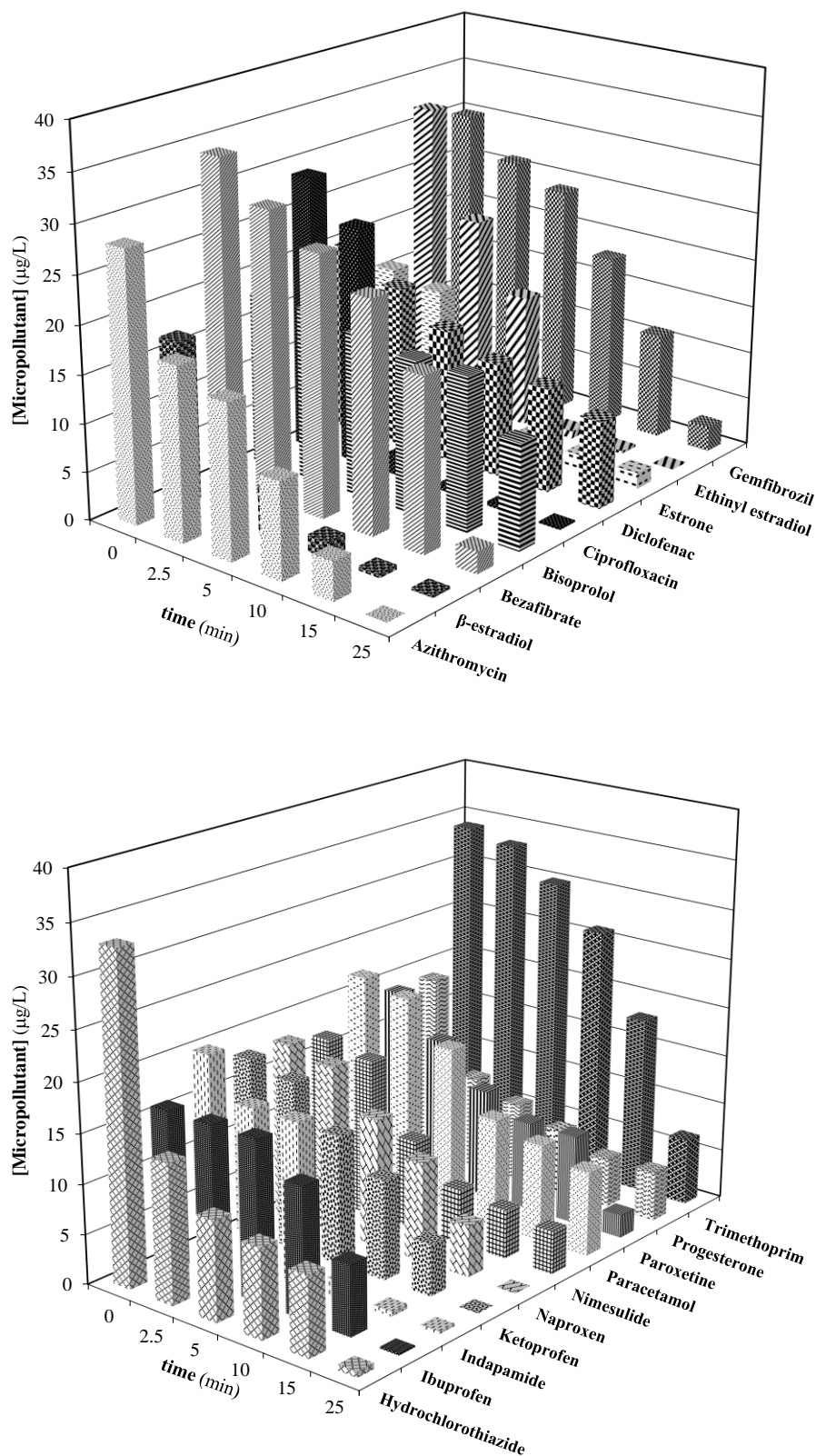


Figure 4.14. Decay profiles of 19 pharmaceutical compounds in 16-34 $\mu\text{g L}^{-1}$ levels as a function of time for AO-BDD treatment of Figure 4.13.

4.4 Conclusions

The degradation of a 20.0 mg TMP L⁻¹ solution in 7.0 g Na₂SO₄ L⁻¹ could be efficiently performed in a 2.2 L lab-scale flow plant equipped with a BDD/air-diffusion electrochemical cell by PEF-UVA-BDD at 20 °C using a low [TDI]₀ of 2.0 mg L⁻¹, which is the Portuguese total iron discharge limit for WWTP final effluents, a current density of 5.0 mA cm⁻² and a maximum pH of 3.5 without iron precipitation. Under these conditions, H₂O₂ was always accumulated in the medium, thus ensuring the maximum production of •OH by Fenton's reaction. The relative oxidation ability of EAOPs using the above conditions increased in the order: AO-H₂O₂-BDD < EF-BDD < PEF-UVA-BDD < SPEF-BDD. The slow removal of the antibiotic under AO-H₂O₂-BDD conditions was due to its low reaction with BDD(•OH) formed at the anode. The faster removal by EF-BDD, PEF-UVA-BDD and SPEF-BDD can be related to its high reaction rate with •OH produced in the bulk. In PEF-UVA-BDD, TMP was more rapidly degraded than in EF-BDD as a result of the additional •OH production induced by UVA irradiation. The most potent EAOP was SPEF-BDD since the slightly more potent UV intensity supplied by sunlight in comparison with the UVA lamp led to more •OH production yielding higher TMP and DOC removals and, furthermore, sunlight can provide the occurrence in larger extent of the photolysis of generated Fe(III)-carboxylate complexes. A total drug removal and a mineralization of 66% were attained after 55 or 180 min of SPEF-BDD, respectively, consuming 1.6 or 6.7 kJ L⁻¹ of UV energy and 0.09 or 0.44 kWh m⁻³ of electrical energy, respectively. Comparison of classical Fenton and PF-UVA processes with EF-BDD and PEF-BDD ones, respectively, demonstrated that electrochemical contributions like BDD(•OH) attack and Fe³⁺ regeneration to Fe²⁺ from cathodic reduction of Fe³⁺ played an important role in the mineralization enhancement of intermediates. The TMP decay underwent a greater drop at the beginning of the chemical processes due to the higher initial availability of H₂O₂.

The PEF-UVA process led to a slightly faster antibiotic degradation using a BDD anode instead of a Pt one, but for SPEF the influence of the anode was insignificant. After 420 min of SPEF-BDD and SPEF-Pt consuming ca. 17 kJ L⁻¹ UV energy, a partial mineralization of 77% and 73% with 30% and 26% current efficiency and 1.2 and 0.9 kWh m⁻³ energy consumption were obtained, respectively. The Pt coated anode, less expensive than the BDD one, seems then preferable to be used in SPEF. The scale-up from a 2.2 L capacity lab-scale flow plant to a 35 L capacity pilot-scale flow plant led to reproducible degradations taking into account the different experimental

conditions of both systems. A total TMP removal and a mineralization of 44% were achieved after 90 and 180 min of SPEF-Pt at pilot-scale, respectively, consuming 2.1 or 6.7 kJ L⁻¹ of UV energy and 0.08 or 0.15 kWh m⁻³ of electrical energy, respectively.

In all the methods tested, a slow and partial TMP mineralization was found, which can be linked to two main causes: (i) the formation of a high content of hardly oxidizable *N*-derivatives that remained in solution up to the end of the treatment, containing the major part of starting nitrogen, and (ii) the presence of sulfate ion in the background electrolyte, leading to the formation of Fe(III)-sulfate complexes instead of more potent photoactive species like FeOH²⁺ and favoring the •OH scavenging to yield the less reactive SO₄^{•-}. Low amounts of ultimate LMCA were generated and completely removed from the solution by SPEF. Up to 18 aromatic products and 19 hydroxylated derivatives were detected by LC-MS over the PEF-UVA-Pt process.

Regarding the assessment of EAOPs efficiency using a real wastewater collected after secondary treatment in a MWWTP, it was attained a slowly organics removal by SPEF-Pt using the real wastewater matrix compared to the 7.0 g Na₂SO₄ L⁻¹ solution, probably due to the use of •OH to oxidize the highly recalcitrant dissolved organic content of the real effluent and/or the filtration of photochemically active light by these dissolved organics. The efficiency of EAOPs to degrade both TMP and DOC using the real matrix can be arranged in the order PEF-UVC-BDD > PEF-UVA-BDD > AO-BDD > AO-H₂O₂-BDD. The superiority of PEF-UVC-BDD over PEF-UVA-BDD can be attributed to the additional •OH production from the H₂O₂ photolysis, whereas the superiority of AO-BDD over AO-H₂O₂-BDD can be related to the unavailability of active chlorine species to degrade organics in AO-H₂O₂-BDD due to the reaction of these species with the electrogenerated H₂O₂. The use of a TMP content in the order of µg L⁻¹ instead of mg L⁻¹ resulted in a lower TMP removal rate. After 25 min of AO-BDD treatment, an average removal of 87% was achieved for 19 pharmaceutical compounds at µg L⁻¹ levels. After 2.5 min, PEF-UVA-BDD and PEF-UVC-BDD processes led to an average micropollutants removal of 80% and 88%, respectively.

4.5 References

- [1] Hernando, M.D., Mezcua, M., Fernández-Alba, A.R., Barceló, D., 2006. Environmental risk assessment of pharmaceutical residues in wastewater effluents, surface waters and sediments. *Talanta* 69(2), 334-342.
- [2] Burchall, J.J., 1975. Mechanism of Action of Antimicrobial and Antitumor Agents. Corcoran, J.W., Hahn, F.E., Snell, J.F. and Arora, K.L. (eds), Springer-Verlag Berlin Heidelberg, New York, United States, pp. 304-320.
- [3] Watkinson, A.J., Murby, E.J., Kolpin, D.W., Costanzo, S.D., 2009. The occurrence of antibiotics in an urban watershed: from wastewater to drinking water. *The Science of the total environment* 407(8), 2711-2723.
- [4] Li, B., Zhang, T., 2011. Mass flows and removal of antibiotics in two municipal wastewater treatment plants. *Chemosphere* 83(9), 1284-1289.
- [5] Miralles-Cuevas, S., Arqués, A., Maldonado, M.I., Sánchez-Pérez, J.A., Malato Rodríguez, S., 2013. Combined nanofiltration and photo-Fenton treatment of water containing micropollutants. *Chemical Engineering Journal* 224, 89-95.
- [6] Pérez-González, A., Urtiaga, A.M., Ibáñez, R., Ortiz, I., 2012. State of the art and review on the treatment technologies of water reverse osmosis concentrates. *Water Research* 46(2), 267-283.
- [7] Ternes, T.A., Stüber, J., Herrmann, N., McDowell, D., Ried, A., Kampmann, M., Teiser, B., 2003. Ozonation: A tool for removal of pharmaceuticals, contrast media and musk fragrances from wastewater? *Water Research* 37(8), 1976-1982.
- [8] Abellán, M.N., Giménez, J., Esplugas, S., 2009. Photocatalytic degradation of antibiotics: The case of sulfamethoxazole and trimethoprim. *Catalysis Today* 144(1-2), 131-136.
- [9] Sirtori, C., Agüera, A., Gernjak, W., Malato, S., 2010. Effect of water-matrix composition on trimethoprim solar photodegradation kinetics and pathways. *Water Research* 44(9), 2735-2744.
- [10] Dias, I.N., Souza, B.S., Pereira, J.H.O.S., Moreira, F.C., Dezotti, M., Boaventura, R.A.R., Vilar, V.J.P., 2014. Enhancement of the photo-Fenton reaction at near neutral pH through the use of ferrioxalate complexes: A case study on trimethoprim and sulfamethoxazole antibiotics removal from aqueous solutions. *Chemical Engineering Journal* 247, 302-313.
- [11] Michael, I., Hapeshi, E., Osorio, V., Perez, S., Petrovic, M., Zapata, A., Malato, S., Barceló, D., Fatta-Kassinos, D., 2012. Solar photocatalytic treatment of trimethoprim in four environmental matrices at a pilot scale: Transformation products and ecotoxicity evaluation. *Science of the Total Environment* 430, 167-173.
- [12] González, T., Domínguez, J.R., Palo, P., Sánchez-Martín, J., Cuerda-Correa, E.M., 2011. Development and optimization of the BDD-electrochemical oxidation of the antibiotic trimethoprim in aqueous solution. *Desalination* 280(1-3), 197-202.
- [13] Canonica, S., Jans, U., Stemmler, K., Hoigne, J., 1995. Transformation kinetics of phenols in water: Photosensitization by dissolved natural organic material and aromatic ketones. *Environmental Science & Technology* 29(7), 1822-1831.

- [14] ASTM, 2003. Standard tables for reference solar spectral irradiances: direct normal and hemispherical on 37° tilted surface.
- [15] Schecher, W.D., McAvoy, D.C., 2007. MINEQL+: A Chemical Equilibrium Modeling System, Version 4.6 for Windows, Environmental Research Software, Hallowell, United States.
- [16] Almeida, L.C., Garcia-Segura, S., Arias, C., Bocchi, N., Brillas, E., 2012. Electrochemical mineralization of the azo dye Acid Red 29 (Chromotrope 2R) by photoelectro-Fenton process. *Chemosphere* 89(6), 751-758.
- [17] Flox, C., Cabot, P.L., Centellas, F., Garrido, J.A., Rodríguez, R.M., Arias, C., Brillas, E., 2007. Solar photoelectro-Fenton degradation of cresols using a flow reactor with a boron-doped diamond anode. *Applied Catalysis B: Environmental* 75(1-2), 17-28.
- [18] Garcia-Segura, S., Almeida, L.C., Bocchi, N., Brillas, E., 2011. Solar photoelectro-Fenton degradation of the herbicide 4-chloro-2-methylphenoxyacetic acid optimized by response surface methodology. *Journal of Hazardous Materials* 194, 109-118.
- [19] Pignatello, J.J., 1992. Dark and photoassisted Fe³⁺-catalyzed degradation of chlorophenoxy herbicides by hydrogen peroxide. *Environmental Science & Technology* 26(5), 944-951.
- [20] Safarzadeh-Amiri, A., Bolton, J.R., Cater, S.R., 1996. Ferrioxalate-mediated solar degradation of organic contaminants in water. *Solar Energy* 56(5), 439-443.
- [21] Sousa, M.A., Gonçalves, C., Vilar, V.J.P., Boaventura, R.A.R., Alpendurada, M.F., 2012. Suspended TiO₂-assisted photocatalytic degradation of emerging contaminants in a municipal WWTP effluent using a solar pilot plant with CPCs. *Chemical Engineering Journal* 198-199, 301-309.
- [22] De Laat, J., Truong Le, G., Legube, B., 2004. A comparative study of the effects of chloride, sulfate and nitrate ions on the rates of decomposition of H₂O₂ and organic compounds by Fe(II)/H₂O₂ and Fe(III)/H₂O₂. *Chemosphere* 55(5), 715-723.
- [23] Lu, M.-C., Chen, J.-N., Chang, C.-P., 1997. Effect of inorganic ions on the oxidation of dichlorvos insecticide with Fenton's reagent. *Chemosphere* 35(10), 2285-2293.
- [24] Benkelberg, H.-J., Warneck, P., 1995. Photodecomposition of iron(III) hydroxo and sulfato complexes in aqueous solution: Wavelength dependence of OH and SO₄⁻ quantum yields. *The Journal of Physical Chemistry* 99(14), 5214-5221.
- [25] Neta, P., Huie, R.E., Ross, A.B., 1988. Rate constants for reactions for inorganic radicals in aqueous solution. *Journal of Physical and Chemical Reference Data Reprints* 17(3), 1027-1247.
- [26] Buxton, G.V., Greenstock, C.L., Helman, W.P., Ross, A.B., 1988. Critical review of rate constants for reactions of hydrated electrons, hydrogen atoms and hydroxyl radicals (•OH/•O⁻) in aqueous solution. *Journal of Physical and Chemical Reference Data* 17(2), 513-886.
- [27] Gan, D., Jia, M., Vaughan, P.P., Falvey, D.E., Blough, N.V., 2008. Aqueous photochemistry of methyl-benzoquinone. *The Journal of Physical Chemistry A* 112(13), 2803-2812.
- [28] De la Cruz, N., Esquius, L., Grandjean, D., Magnet, A., Tungler, A., de Alencastro, L.F., Pulgarín, C., 2013. Degradation of emergent contaminants by UV, UV/H₂O₂ and neutral photo-Fenton at pilot scale in a domestic wastewater treatment plant. *Water Research* 47(15), 5836-5845.

- [29] De la Cruz, N., Giménez, J., Esplugas, S., Grandjean, D., De Alencastro, L.F., Pulgarín, C., 2012. Degradation of 32 emergent contaminants by UV and neutral photo-fenton in domestic wastewater effluent previously treated by activated sludge. *Water Research* 46(6), 1947-1957.
- [30] Demirezen, N., Tarınc, D., Polat, D., Çeşme, M., Gölcü, A., Tümer, M., 2012. Synthesis of trimethoprim metal complexes: Spectral, electrochemical, thermal, DNA-binding and surface morphology studies. *Spectrochimica Acta Part A: Molecular and Biomolecular Spectroscopy* 94, 243-255.
- [31] Tella, A.C., Obaleye, J.A., 2010. Metal-chelator therapy: Stability constants of transition metal complexes of pyrimidine and sulphonamide drugs. *International Journal of Chemical Sciences* 8(3), 1675-1683.
- [32] Kapałka, A., Fóti, G., Comninellis, C., 2008. Kinetic modelling of the electrochemical mineralization of organic pollutants for wastewater treatment. *Journal of Applied Electrochemistry* 38(1), 7-16.
- [33] Brillas, E., Baños, M.A., Skoumal, M., Cabot, P.L., Garrido, J.A., Rodríguez, R.M., 2007. Degradation of the herbicide 2,4-DP by anodic oxidation, electro-Fenton and photoelectro-Fenton using platinum and boron-doped diamond anodes. *Chemosphere* 68(2), 199-209.
- [34] Skoumal, M., Rodríguez, R.M., Cabot, P.L., Centellas, F., Garrido, J.A., Arias, C., Brillas, E., 2009. Electro-Fenton, UVA photoelectro-Fenton and solar photoelectro-Fenton degradation of the drug ibuprofen in acid aqueous medium using platinum and boron-doped diamond anodes. *Electrochimica Acta* 54(7), 2077-2085.
- [35] Weishaar, J.L., Aiken, G.R., Bergamaschi, B.A., Fram, M.S., Fujii, R., Mopper, K., 2003. Evaluation of specific ultraviolet absorbance as an indicator of the chemical composition and reactivity of dissolved organic carbon. *Environmental Science & Technology* 37(20), 4702-4708.
- [36] González, O., Justo, A., Bacardit, J., Ferrero, E., Malfeito, J.J., Sans, C., 2013. Characterization and fate of effluent organic matter treated with UV/H₂O₂ and ozonation. *Chemical Engineering Journal* 226, 402-408.
- [37] Sedlak, R.I., 1991. Phosphorous and Nitrogen Removal from Municipal Wastewater: Principles and Practice, 2nd ed., CRC Press LLC, Boca Raton, United States.
- [38] Pa Ho, H., 1976. Comparison of iron(III) and aluminum in precipitation of phosphate from solution. *Water Research* 10(10), 903-907.
- [39] Wenk, J., von Gunten, U., Canonica, S., 2011. Effect of dissolved organic matter on the transformation of contaminants induced by excited triplet states and the hydroxyl radical. *Environmental Science & Technology* 45(4), 1334-1340.
- [40] Sun, Y., Pignatello, J.J., 1992. Chemical treatment of pesticide wastes. Evaluation of iron(III) chelates for catalytic hydrogen peroxide oxidation of 2,4-D at circumneutral pH. *Journal of Agricultural and Food Chemistry* 40(2), 322-327.
- [41] Pérez, G., Fernández-Alba, A.R., Urtiaga, A.M., Ortiz, I., 2010. Electro-oxidation of reverse osmosis concentrates generated in tertiary water treatment. *Water Research* 44(9), 2763-2772.
- [42] Urtiaga, A.M., Pérez, G., Ibáñez, R., Ortiz, I., 2013. Removal of pharmaceuticals from a WWTP secondary effluent by ultrafiltration/reverse osmosis followed by electrochemical oxidation of the RO concentrate. *Desalination* 331, 26-34.

5 Degradation of trimethoprim antibiotic by UVA photoelectro-Fenton process assisted by Fe(III)-carboxylate complexes

A PEF-UVA process assisted by Fe(III)-carboxylate complexes was applied to the removal of TMP in an aqueous solution with 7.0 g Na₂SO₄ L⁻¹ using a 2.2 L lab-scale flow plant equipped with CPCs and an electrochemical cell equipped with a BDD anode and a carbon-PTFE air-diffusion cathode. The presence of Fe(III)-carboxylate complexes enhances the regeneration of Fe³⁺ to Fe²⁺, allows maintaining iron in solution at higher pH values and can decrease the formation of Fe(III)-sulfate, Fe(III)-chloride and some Fe(III)-pollutants complexes. Firstly, the efficiency of different carboxylate ligands like oxalate, citrate, tartrate and malate was assessed, followed by the application of various initial Fe(III)-to-carboxylate molar ratios and pH values. The PEF-UVA-BDD process with Fe(III)-oxalate, Fe(III)-citrate and Fe(III)-tartrate complexes revealed similar ability to degrade the antibiotic solution with the employment of 1:3, 1:1 and 1:1 Fe(III)-to-carboxylate molar ratios, respectively, and using pH of 4.5, [TDI]₀ of 2.0 mg L⁻¹, 20 °C and j of 5.0 mA cm⁻². The PEF-UVA-BDD process assisted by Fe(III)-malate complexes was much less effective. 1:6 and 1:9 Fe(III)-to-oxalate molar ratios were required to yield similar TMP removal kinetics at pH of 5.0 and 5.5 compared to pH of 4.5, respectively. Additionally, the influence of initial TMP content and solution temperature on the PEF-UVA-BDD process with Fe(III)-carboxylate complexes was assessed and the role of the different reactive oxidizing species was clarified by the addition of scavenging agents. Generated LMCA were monitored by ion-exclusion HPLC.

This Chapter is based on the following research article: “Moreira, F.C., Boaventura, R.A.R., Brillas, E., Vilar, V.J.P., 2015. Degradation of trimethoprim antibiotic by UVA photoelectron-Fenton process mediated by Fe(III)-carboxylate complexes. Applied Catalysis B: Environmental 162, 34-44”.

5.1 Introduction

The efficiency of PEF and SPEF systems may be improved by an initial input of some LMCA. The generated Fe(III)-carboxylate complexes can absorb radiation in the UV-Vis range, being photodecarboxylated according to the general Eq. (29) with higher quantum yields for Fe²⁺ generation than that of Fe(III)-hydroxy complexes [1-4]. The quantum yield for Fe²⁺ formation in Eq. (29) depends on various parameters such as the nature of the carboxylate ligand, Fe(III)-to-ligand ratio, wavelength of the light source and pH [5]. Fe(III)-oxalate, Fe(III)-citrate, Fe(III)-tartrate and Fe(III)-malate complexes have been pointed out as some of the main Fe(III)-carboxylate complexes with the highest quantum yields for Fe²⁺ generation, exhibiting much higher quantum yields for Fe²⁺ formation than FeOH²⁺ complex [2, 5, 6]. Furthermore, it could be expected that the use of Fe(III)-carboxylate complexes may solve two of the main limitations of PEF and SPEF since: (i) their presence maintains iron in solution at higher pH, thus extending the reaction optimal pH range from acid to neutral values and enabling the treatment of real waters and wastewaters without acidification and neutralization steps with consequent minimization of costs [7]; and (ii) Fe(III)-sulfate and Fe(III)-chloride complexes [8] and some Fe(III)-pollutants complexes [8-11] exhibit lower formation constants than Fe(III)-carboxylate complexes and then the formation of these undesirable species can be avoided with simultaneous increase of Fe³⁺ regeneration to Fe²⁺.

This Chapter presents a study on the degradation of a 20.0 mg TMP L⁻¹ solution in 7.0 g Na₂SO₄ L⁻¹ using a PEF-UVA process assisted by Fe(III)-carboxylate complexes. The experiments were performed in a 2.2 L lab-scale flow plant equipped with CPCs and an electrochemical reactor containing a BDD anode and a carbon-PTFE air-diffusion cathode. The aim was to check the feasibility of operating at circumneutral pH (5.5-7.4) with the employment of low amounts of carboxylate ligand and iron. To the best of our knowledge, this is the first time that a PEF process assisted by Fe(III)-carboxylate complexes is studied and its efficiency is assessed considering the different iron complexes present in solution and the photoactivity of each ferric species. Carboxylate ligands like oxalate, citrate, tartrate and malate were investigated and the influence of Fe(III)-to-carboxylate molar ratio and pH was also assessed. In addition, the effect of initial TMP concentration and temperature was considered and the role of the different reactive oxidizing species on the degradation processes was clarified by adding scavenging agents. Generated LMCA were followed throughout reactions by ion-exclusion HPLC.

5.2 Materials and methods

All chemicals, analytical determinations, modeling of degradation kinetics and the experimental unit and respective procedure are depicted in the Chapter 2. Table 2.5 summarizes the operational conditions of PEF-UVA-BDD process performed in the current Chapter.

5.3 Results and discussion

5.3.1 UV-Vis spectra of different solutions

Figure 5.1 illustrates the absorption spectra of various solutions at pH of 3.5. Note that this pH was selected to minimize iron precipitation, as can be seen in Figures 4.2b,d and 5.2. The Fe^{3+} solution absorbed radiation in the range of 200-500 nm that can be attributed to the formation of Fe(III)-hydroxy complexes such as FeOH^{2+} and mainly $\text{Fe}(\text{OH})_2^+$, which are the predominant species in this system according to the calculated Fe^{3+} speciation diagrams (see Figures 4.2c,d). The addition of Na_2SO_4 to this solution did not affect its ability to absorb radiation due to the presence of quite similar amounts of FeOH^{2+} and $\text{Fe}(\text{OH})_2^+$, despite the formation of Fe(III)-sulfate complexes like FeSO_4^+ and $\text{Fe}(\text{SO}_4)_2^-$ (see Figure 4.2). The TMP antibiotic solution exhibited a maximum absorption at 270 nm and after the addition of Fe^{3+} the absorbance raised in all the wavelength range, principally for values above 300 nm, which can be associated with the formation of Fe(III)-hydroxy complexes. No evidence of Fe(III)-TMP complexes [12, 13] formation was found by spectra analysis. In the presence of Fe^{2+} at pH of 3.5, the formation of Fe(II)-hydroxy complexes is not expected from the Fe^{2+} speciation diagram (data not displayed) and there is no evidence of Fe(II)-TMP species formation. The establishment of FeSO_4 , i.e. the only Fe(II)-sulfate complex that is expected to be present under the current conditions, revealed to have a negligible influence on the solution absorbance. On the other hand, the absorbance of solutions containing Fe(III)/TMP/oxalate, Fe(III)/TMP/citrate and Fe(III)/TMP/tartrate was higher than that of the Fe(III)/TMP solutions for wavelengths between 240 and 325 nm, especially in the former case. In contrast, the presence of Fe(III)-malate complexes did not increase the absorbance.

5.3.2 Preliminary results for TMP degradation

The TMP concentration of 20.0 mg L^{-1} was much higher than that found in aquatic systems (ng L^{-1} or $\mu\text{g L}^{-1}$ levels) in order to attain comprehensive TMP and DOC decay profiles to explain the degradation behavior. This antibiotic content corresponds to a DOC of 11.6 mg L^{-1} .

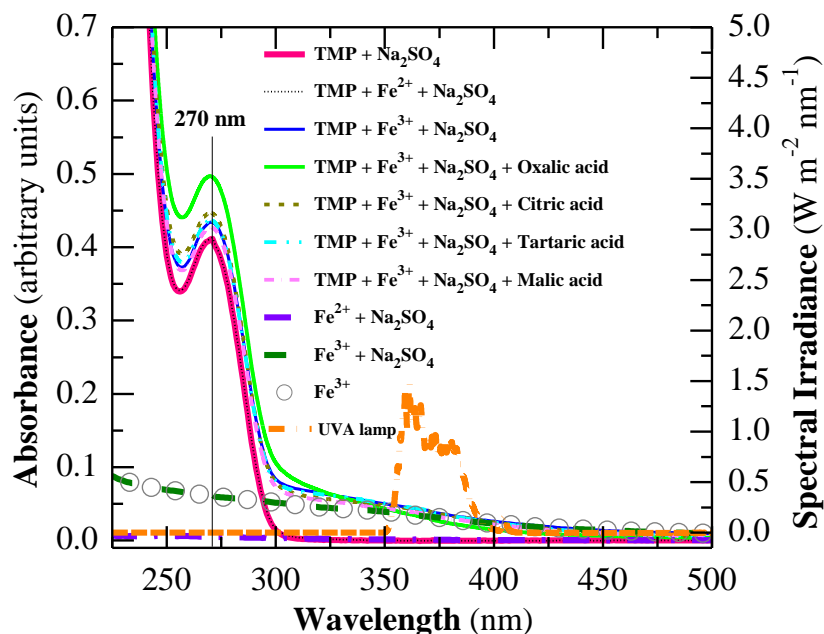


Figure 5.1. Absorption spectra of different solutions at pH = 3.5 (without dilution). [TMP] = 20.0 mg L⁻¹, [Na₂SO₄] = 7.0 g L⁻¹, [Fe²⁺] = 2.0 mg L⁻¹, [Fe³⁺] = 2.0 mg L⁻¹, 1:3 Fe(III)-to-oxalate molar ratio, 1:1 Fe(III)-to-citrate molar ratio, 1:1 Fe(III)-to-tartrate molar ratio and 1:1 Fe(III)-to-malate molar ratio. The spectral irradiance of UVA lamp is also shown, measured with the spectro-radiometer and confirmed by Philips.

In Chapter 4, the application of a PEF-UVA-BDD process to a 20.0 mg TMP L⁻¹ solution in 7.0 g Na₂SO₄ L⁻¹ revealed effectiveness using a low [TDI]₀ of 2.0 mg L⁻¹, which is the Portuguese total iron discharge limit for WWTPs final effluents (Portuguese decree law n° 236/98), a maximum pH of 3.5 without iron precipitation and *j* of 5.0 mA cm⁻², suggesting the need for the use of Fe(III)-carboxylate complexes to rise the working pH to circumneutral values.

In a first approach, a PEF-UVA-BDD experiment of the above antibiotic solution was performed under the reported conditions but using pH of 5.0 in the presence of 1:3 Fe(III)-to-oxalate molar ratio without pH regulation. A continuous rise in pH was observed up to reach a value of 6.4 after 180 min of electrolysis, which can be attributed to oxalic acid degradation. This behavior compromises data interpretation and, consequently, further trials were accomplished with pH adjustment to the initial value during the entire electrolysis time by adding small amounts of 0.5 M H₂SO₄. Note that in all the PEF-UVA-BDD trials performed, the H₂O₂ generated from Eq. (16) was continuously accumulated in the solution from 3.5-6.0 mg L⁻¹ to 30-47 mg L⁻¹ after 30 and 180 min, respectively (data not shown). This excess in H₂O₂ generation ensured maximum •OH production in the solution bulk from Fenton's reaction (21).

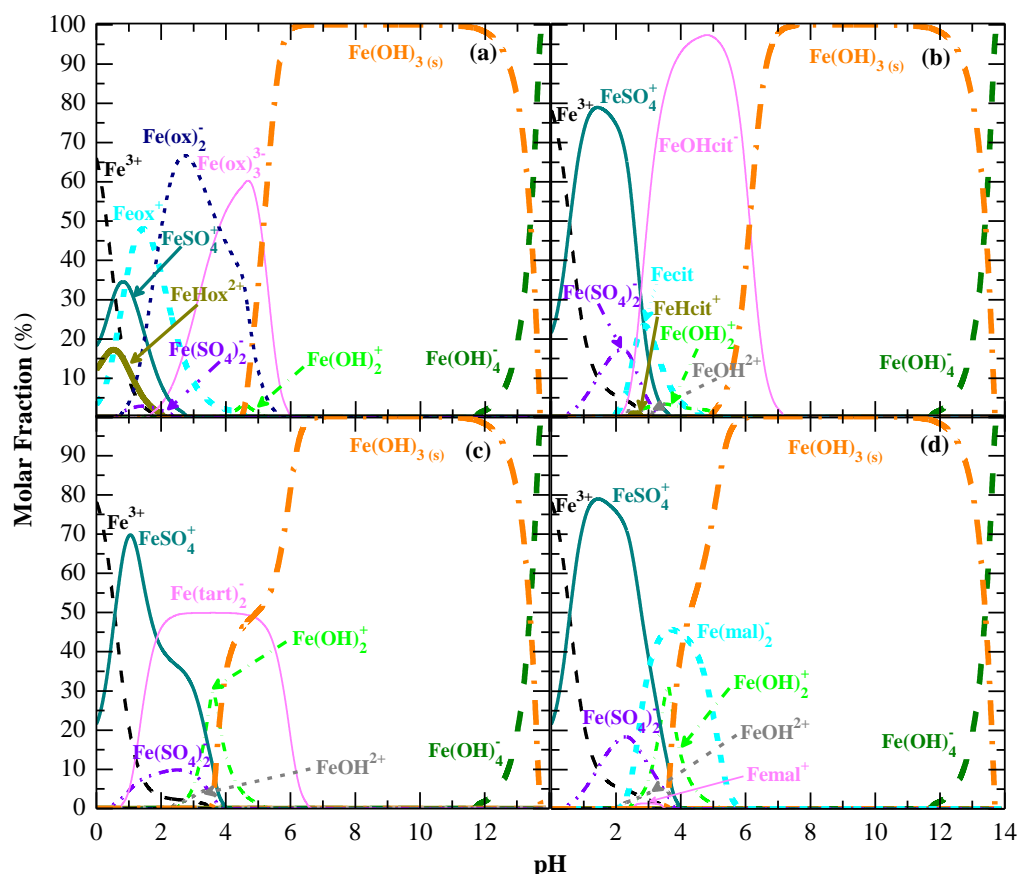


Figure 5.2. Fe³⁺ speciation diagrams as a function of solution pH in a calculated system containing: (a) 1.07×10^{-4} M of oxalate ion (1:3 Fe(III)-to-oxalate molar ratio), (b) 3.58×10^{-5} M of citrate ion (1:1 Fe(III)-to-citrate molar ratio), (c) 3.58×10^{-5} M of tartrate ion (1:1 Fe(III)-to-tartrate molar ratio) or (d) 3.58×10^{-5} M of malate ion (1:1 Fe(III)-to-malate molar ratio), with 3.58×10^{-5} M of Fe³⁺ (2.0 mg L^{-1}), 1.07×10^{-4} M of Cl⁻ ($9.7 \text{ mg FeCl}_3 \cdot 6\text{H}_2\text{O L}^{-1}$), 4.93×10^{-2} M of SO₄²⁻ and 9.86×10^{-2} M of Na⁺ ($7.0 \text{ g Na}_2\text{SO}_4 \text{ L}^{-1}$) (ionic strength = 0.148 M). Data were calculated from the chemical equilibrium modeling system MINEQL+ [14] using the equilibrium constants of Table 5.1. The formation of the solid iron phase Fe(OH)₃ was included in the calculation despite the slow formation of solid phases on the time scale of the experiments.

Table 5.1. Equilibrium reactions and respective equilibrium constants ($\log K^a$) and enthalpies (ΔH) used in the chemical equilibrium modeling system MINEQL+ [14] for speciation diagrams calculation ($T = 25\text{ }^\circ\text{C}$ and ionic strength = 0 M^a).

Reaction	$\log K^*$	Reference	ΔH (kcal mol ⁻¹)	Reference
$\text{H}_2\text{O} \leftrightarrow \text{OH}^- + \text{H}^+$	-13.997	[14]	13.339	[14]
$\text{H}^+ + \text{SO}_4^{2-} \leftrightarrow \text{HSO}_4^-$	1.990	[14]	5.258	[14]
$\text{Na}^+ + \text{SO}_4^{2-} \leftrightarrow \text{NaSO}_4^-$	0.730	[14]	0.239	[14]
Fe(III)-hydroxy complexes				
$\text{Fe}^{3+} + \text{H}_2\text{O} \leftrightarrow \text{FeOH}^{2+} + \text{H}^+$	-2.187	[14]	9.993	[14]
$\text{Fe}^{3+} + 2\text{H}_2\text{O} \leftrightarrow \text{Fe}(\text{OH})_2^+ + 2\text{H}^+$	-4.594	[14]	-	
$2\text{Fe}^{3+} + 2\text{H}_2\text{O} \leftrightarrow \text{Fe}_2(\text{OH})_2^{4+} + 2\text{H}^+$	-2.854	[14]	13.771	[14]
$\text{Fe}^{3+} + 3\text{H}_2\text{O} \leftrightarrow \text{Fe}(\text{OH})_3(\text{aq}) + 3\text{H}^+$	-12.560	[14]	24.809	[14]
$\text{Fe}^{3+} + 4\text{H}_2\text{O} \leftrightarrow \text{Fe}(\text{OH})_4^- + 4\text{H}^+$	-21.588	[14]	-	
$3\text{Fe}^{3+} + 4\text{H}_2\text{O} \leftrightarrow \text{Fe}_3(\text{OH})_4^{5+} + 4\text{H}^+$	-6.288	[14]	15.593	[14]
Fe(III)-sulfate complexes				
$\text{Fe}^{3+} + \text{SO}_4^{2-} \leftrightarrow \text{FeSO}_4^+$	4.050	[14]	5.975	[14]
$\text{Fe}^{3+} + 2\text{SO}_4^{2-} \leftrightarrow \text{Fe}(\text{SO}_4)_2^-$	5.380	[14]	4.589	[14]
Fe(III)-chloride complexes				
$\text{Fe}^{3+} + \text{Cl}^- \leftrightarrow \text{FeCl}^{2+}$	1.480	[14]	5.497	[14]
$\text{Fe}^{3+} + 2\text{Cl}^- \leftrightarrow \text{FeCl}_2^+$	2.130	[14]	-	
$\text{Fe}^{3+} + 3\text{Cl}^- \leftrightarrow \text{FeCl}_3(\text{aq})$	1.130	[14]	-	
Oxalic acid protonation/deprotonation equilibria				
$\text{ox}^{2-} + \text{H}^+ \leftrightarrow \text{Hox}^-$	4.266	[8]	1.58	[8]
$\text{ox}^{2-} + 2\text{H}^+ \leftrightarrow \text{H}_2\text{ox}$	5.516	[8]	2.38	[8]
Fe(III)-oxalate complexes				
$\text{Fe}^{3+} + \text{H}^+ + \text{ox}^{2-} \leftrightarrow \text{FeHox}^{2+}$	9.53	[15]	-	
$\text{Fe}^{3+} + \text{ox}^{2-} \leftrightarrow \text{Feox}^+$	9.40	[15]	1.30	[8]
$\text{Fe}^{3+} + 2\text{ox}^{2-} \leftrightarrow \text{Fe}(\text{ox})_2^-$	16.20	[15]	0.70	[8]
$\text{Fe}^{3+} + 3\text{ox}^{2-} \leftrightarrow \text{Fe}(\text{ox})_3^{3-}$	20.78	[15]	0.10	[8]
Citric acid protonation/deprotonation equilibria				
$\text{cit}^{3-} + \text{H}^+ \leftrightarrow \text{Hcit}^{2-}$	6.396	[14]	0.80	[14]
$\text{cit}^{3-} + 2\text{H}^+ \leftrightarrow \text{H}_2\text{cit}^-$	11.157	[14]	0.31	[14]
$\text{cit}^{3-} + 3\text{H}^+ \leftrightarrow \text{H}_3\text{cit}$	14.285	[14]	-0.66	[14]
Fe(III)-citrate complexes				
$\text{Fe}^{3+} + \text{cit}^{3-} \leftrightarrow \text{Fecit}$	13.10	[14]	-	
$\text{Fe}^{3+} + \text{H}^+ + \text{cit}^{3-} \leftrightarrow \text{FeHcit}^+$	14.40	[14]	-	
$\text{Fe}^{3+} + \text{cit}^{3-} \leftrightarrow \text{FeOHcit}^- + \text{H}^+$	10.33	[16]	-	
Tartaric acid protonation/deprotonation equilibria				
$\text{tart}^{2-} + \text{H}^+ \leftrightarrow \text{Htart}^-$	4.366	[14]	-0.18	[14]
$\text{tart}^{2-} + 2\text{H}^+ \leftrightarrow \text{H}_2\text{tart}$	7.402	[14]	-0.88	[14]
Fe(III)-tartrate complexes				
$\text{Fe}^{3+} + \text{tart}^{2-} \leftrightarrow \text{Fetart}^+$	7.78	[14]	-	
$\text{Fe}^{3+} + 2\text{tart}^{2-} \leftrightarrow \text{Fe}(\text{tart})_2^-$	20.08	[8]	-	
Malic acid protonation/deprotonation equilibria				
$\text{mal}^{2-} + \text{H}^+ \leftrightarrow \text{Hmal}^-$	5.097	[8]	-	
$\text{mal}^{2-} + 2\text{H}^+ \leftrightarrow \text{H}_2\text{mal}$	8.556	[8]	-	
Fe(III)-malate complexes				
$\text{Fe}^{3+} + \text{mal}^{2-} \leftrightarrow \text{Femal}^+$	8.43	[17]	-	
$\text{Fe}^{3+} + 2\text{mal}^{2-} \leftrightarrow \text{Fe}(\text{mal})_2^-$	17.51	[18]	-	

^a $\log K$ values found in the literature at ionic strengths differing from zero were corrected to zero ionic strength using Davies equation [19]; some reactions were manipulated in order to be established in function of particular species, as MINEQL+ requires, and consequently $\log K$ values were also converted.

5.3.3 PEF-UVA-BDD degradation in the presence of various Fe(III)-carboxylate complexes

The influence of the nature of the carboxylate ligand on TMP degradation by PEF-UVA-BDD was assessed by degrading 1.250 L of a 20.0 mg TMP L⁻¹ solution in 7.0 g Na₂SO₄ L⁻¹ using pH of 4.5, [TDI]₀ of 2.0 mg L⁻¹, 20 °C and *j* of 5.0 mA cm⁻². The stoichiometry of Fe(III)-to-carboxylate complexes was 1:3 for Fe(III)-oxalate and 1:1 for Fe(III)-citrate, Fe(III)-tartrate and Fe(III)-malate complexes, which has been reported as optimal by several authors [3, 17, 19-21]. Figures 5.3a,b depict quite similar TMP and DOC decays for the PEF-UVA-BDD treatments with the three first Fe(III)-carboxylate complexes, contrasting with the treatment with the Fe(III)-malate system, which displayed inferior ability to remove both TMP and DOC contents, with *k*_{TMP} and *k*_{DOC} values 1.4-2.3 and 2.2-2.6 times smaller, respectively (see Tables 5.2 and 5.3). Similarly to Chapter 4, all the systems led to a low DOC abatement that can be mainly attributed to the formation of high amounts of nitrogenated by-products, even more recalcitrant than the TMP parent compound [22, 23]. The presence of high amounts of sulfate ions from the background electrolyte probably did not contribute to the low ability of PEF-UVA-BDD assisted by Fe(III)-carboxylate complexes to degrade intermediates since theoretical Fe³⁺ speciation diagrams at pH of 4.5 demonstrated that the formation of Fe(III)-sulfate complexes has almost negligible effects on the distribution of Fe(III)-carboxylate and Fe(III)-hydroxy complexes either in the presence of oxalic, citric, tartaric and malic acids (see Figure 5.2 (with sulfate) and Figure 5.4 (without sulfate)) and in their absence (see Figure 4.2 (with and without sulfate)).

Figures 5.3a,b also revealed that PEF-UVA-BDD processes assisted by Fe(III)-carboxylate complexes at pH of 4.5 yielded faster TMP and DOC abatements than the classical PEF-UVA-BDD one (absence of the initial supply of a carboxylic acid) at pH of 3.5, with *k*_{TMP} and *k*_{DOC} values 1.1-2.5 and 1.7-2.0 times higher (see Tables 5.2 and 5.3), respectively, except for the DOC decay of the Fe(III)-malate system. The greater oxidation ability of PEF-UVA-BDD in the presence of Fe(III)-carboxylate complexes can be mainly associated with: (i) the superiority of quantum yields of Fe²⁺ formation from the Fe(III)-carboxylate complexes over Fe(III)-hydroxy complexes [2, 5, 6], because of the greater absorption of UVA light as confirmed from absorption spectra of Figure 5.1; and (ii) a possible prevention of the formation of Fe(III)-TMP complexes [8-11] or other Fe(III)-organic complexes with low photoactivity, with the consequent improvement of Fe³⁺ regeneration to Fe²⁺ and hence the overall efficiency of the PEF-UVA-BDD process.

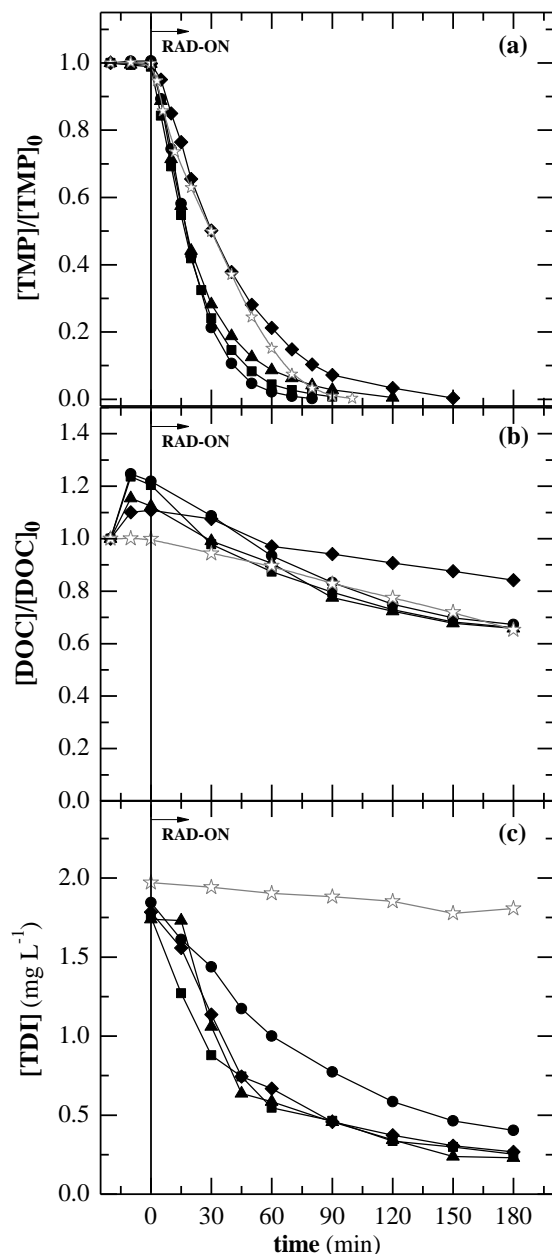


Figure 5.3. Effect of Fe(III)-carboxylate complexes on (a) normalized TMP concentration decay, (b) normalized DOC removal and (c) total dissolved iron concentration as a function of time for PEF-UVA-BDD treatment of a 20.0 mg TMP L⁻¹ solution in 7.0 g Na₂SO₄ L⁻¹ using pH of 4.5, [TDI]₀ of 2.0 mg L⁻¹, 20 °C and *j* of 5.0 mA cm⁻². Fe(III)-carboxylate complex (Fe(III)-to-carboxylate molar ratio): (■) Fe(III)-oxalate (1:3), (●) Fe(III)-citrate (1:1), (▲) Fe(III)-tartrate (1:1) and (◆) Fe(III)-malate (1:1). (☆) Classical PEF-UVA-BDD process (without carboxylic acids addition) at pH of 3.5.

Table 5.2. Pseudo-first-order kinetic constants for TMP concentration decay (k_{TMP}) and initial TMP removal rates ($r_{0(\text{TMP})}$) along with the corresponding R^2 and S^2_{R} , obtained for the PEF-UVA-BDD treatment of TMP solutions in 7.0 g Na₂SO₄ L⁻¹ under conditions of Figures 5.3a, 5.6a, 5.8a, 5.9a and 5.11.

System	pH	Fe(III):L	k_{TMP} ($\times 10^{-2}$ min ⁻¹)	$r_{0(\text{TMP})}$ ($\times 10^{-2}$ mg L ⁻¹ min ⁻¹)	R^2	S^2_{R} (mg ² L ⁻²)
PEF-UVA-BDD	3.5	-	2.4±0.1	47±1	0.997	0.072
PEF-UVA-BDD with Fe(III)-oxalate	4.5	1:3	4.8±0.1	96±2	0.999	0.087
PEF-UVA-BDD with Fe(III)-citrate	4.5	1:1	6.1±0.2	90±3	0.998	0.098
PEF-UVA-BDD with Fe(III)-tartrate	4.5	1:1	3.9±0.1	78±2	0.996	0.193
PEF-UVA-BDD with Fe(III)-malate	4.5	1:1	2.7±0.1	54±1	0.998	0.112
PEF-UVA-BDD with Fe(III)-oxalate	4.5	1:3	4.8±0.1	96±2	0.999	0.087
	5.0	1:3	2.28±0.04	45±1	0.998	0.122
	5.0	1:6	4.6±0.2	91±3	0.996	0.355
	5.0	1:9	7.4±0.2	148±4	0.999	0.025
	5.5	1:9	4.1±0.1	82±2	0.998	0.198
PEF-UVA-BDD with Fe(III)-citrate	5.0	1:1	2.8±0.1	57±1	0.996	0.116
Parameter						
Effect of [TMP] ₀ (mg L ⁻¹) on PEF-UVA-BDD	2.0		18.9±0.8	33±1	0.995	0.004
	5.0		11.4±0.8	47±3	0.987	0.036
	10.0		8.0±0.4	66±3	0.996	0.059
	20.0		6.1±0.2	105±6	0.998	0.098
Effect of temperature (°C) on PEF-UVA-BDD	10		4.4±0.3	81±5	0.992	0.739
	20		4.8±0.1	96±2	0.999	0.087
	40		8.1±0.2	132±3	0.998	0.074
Effect of scavenging agents on PEF-UVA-BDD	Absence		6.1±0.2	105±6	0.998	0.098
	D-mannitol		0.64±0.01	12.5±0.2	0.998	0.054
	Sodium azide		0.37±0.01	7.0±0.2	0.984	0.127

Table 5.3. Pseudo-first-order kinetic constants for DOC removal (k_{DOC}) and initial DOC removal rates ($r_{0(\text{DOC})}$) along with the corresponding R^2 and S^2_{R} , obtained for the PEF-UVA-BDD treatment of TMP solutions in 7.0 g Na₂SO₄ L⁻¹ under conditions of Figures 5.3b, 5.6c, 5.8b, and 5.9b.

System	pH	Fe(III):L	Period	k_{DOC} ($\times 10^{-3}$ min ⁻¹)	$r_{0(\text{DOC})}$ ($\times 10^{-3}$ mg L ⁻¹ min ⁻¹)	R^2	S^2_{R} (mg ² L ⁻²)
PEF	3.5	-	-	2.1±0.1	24.5±0.6	0.995	0.010
PEF-UVA-BDD with Fe(III)-oxalate	4.5	1:3	-	3.5±0.2	39±2	0.978	0.066
PEF-UVA-BDD with Fe(III)-citrate	4.5	1:1	-	4.2±0.1	58±1	0.997	0.015
PEF-UVA-BDD with Fe(III)-tartrate	4.5	1:1	-	3.8±0.1	52±2	0.992	0.033
PEF-UVA-BDD with Fe(III)-malate	4.5	1:1	-	1.6±0.1	22±1	0.966	0.052
PEF-UVA-BDD with Fe(III)-oxalate	4.5	1:3	-	3.5±0.2	39±2	0.978	0.066
	5.0	1:3	-	3.5±0.1	50±2	0.993	0.027
	5.0	1:6	1 st	7.5±0.4	131±8	0.989	0.120
			2 nd	0.5±0.1	5±2	0.943	0.104
	5.0	1:9	1 st	9.0±0.2	180±4	0.998	0.057
			2 nd	0.6±0.2	6±2	0.997	0.205
	5.5	1:9	1 st	7.5±0.2	156±4	0.997	0.066
			2 nd	0.6±0.1	6±2	0.995	0.168
PEF-UVA-BDD with Fe(III)-citrate	5.0	1:1	-	2.73±0.04	38.2±0.6	0.996	0.014
Parameter							
Effect of [TMP] ₀ (mg L ⁻¹) on PEF-UVA-BDD	2.0		-	6.2±0.1	15.2±0.1	1.000	0.0001
	5.0		-	6.2±0.1	21.4±0.3	0.999	0.001
	10.0		-	6.3±0.1	56±1	0.998	0.006
	20.0		-	4.2±0.1	58±1	0.997	0.015
Effect of temperature (°C) on PEF-UVA-BDD	10		-	3.9±0.3	46±3	0.971	0.115
	20		-	3.5±0.2	39±2	0.978	0.066
	40		1 st	8.8±0.8	127±9	0.972	0.257
			2 nd	2.6±0.1	22.8±0.9	0.989	0.008

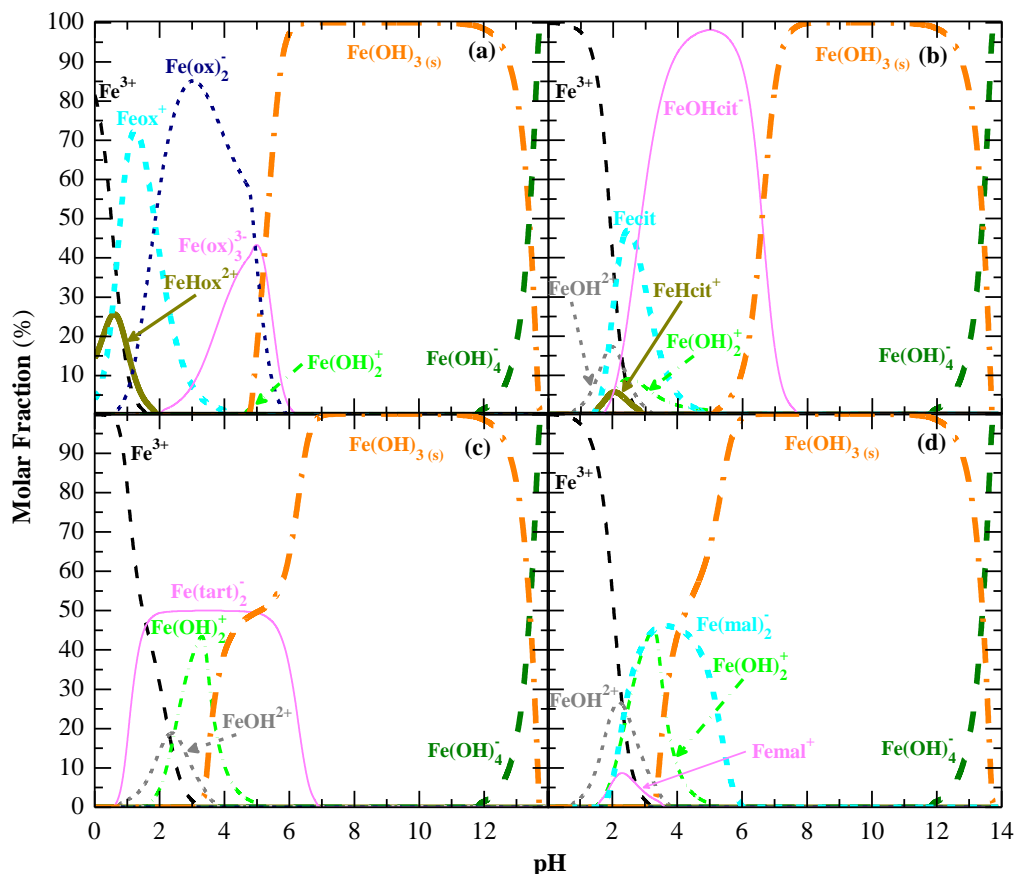


Figure 5.4. Fe^{3+} speciation diagrams as a function of solution pH in a calculated system containing: (a) 1.07×10^{-4} M of oxalate ion (1:3 Fe(III)-to-oxalate molar ratio), (b) 3.58×10^{-5} M of citrate ion (1:1 Fe(III)-to-citrate molar ratio), (c) 3.58×10^{-5} M of tartrate ion (1:1 Fe(III)-to-tartrate molar ratio) or (d) 3.58×10^{-5} M of malate ion (1:1 Fe(III)-to-malate molar ratio), with 3.58×10^{-5} M of Fe^{3+} (2.0 mg L^{-1}) and 1.07×10^{-4} M of Cl^- ($9.7 \text{ mg FeCl}_3 \cdot 6\text{H}_2\text{O L}^{-1}$ in the absence of Na_2SO_4 (ionic strength ~ 0 M)). Data were calculated from the chemical equilibrium modeling system MINEQL+ [14] using the equilibrium constants of Table 5.1. The formation of the solid iron phase $\text{Fe}(\text{OH})_3$ was included in the calculation despite the slow formation of solid phases on the time scale of the experiments.

Rodríguez et al. [6] determined the efficiencies of Fe(III)-carboxylate complexes to degrade 7.1 mg L^{-1} of muconic acid solutions using pH of 3.0, $20 \text{ }^\circ\text{C}$, $[\text{TDI}]_0$ of 2.8 mg L^{-1} , Fe(III)-to-carboxylate molar ratios of 1:2 and 15W black light lamps emitting between 350 and 400 nm with λ_{max} at 365 nm. They found the following performance: Fe(III)-oxalate > Fe(III)-tartrate \approx Fe(III)-citrate > Fe(III)-malate, with decreasing quantum yields of 1.102, 0.993, 0.589, 0.510 and 0.062 mol per photon, in terms of Fe^{2+} formation, respectively. Abrahamson et al. [5] reported decreasing quantum yields in the order Fe(III)-tartrate (0.58) > Fe(III)-citrate (0.45) > Fe(III)-oxalate (0.30) > Fe(III)-malate (0.29) at pH of 4.0 and Fe(III)-oxalate (0.65) > Fe(III)-tartrate (0.40) > Fe(III)-citrate (0.28) > Fe(III)-malate (0.21) at pH of 2.7, both using $[\text{TDI}]_0$ of 17 mg L^{-1} , Fe(III)-to-carboxylate molar ratio of 1:5 and a broad-band UV irradiation. The

superiority of Fe(III)-oxalate, Fe(III)-citrate and Fe(III)-tartrate over Fe(III)-malate complexes was always patent in both reported works, in agreement with the results obtained in this study. However, the above quantum yield values were determined under different experimental conditions like initial Fe(III)-to-carboxylate ratio, wavelength of the light source and pH and thus they should be taken carefully since these variables can affect them in different extent.

To clarify in detail the type of Fe(III)-carboxylate species acting in each PEF-UVA-BDD system and their proportion, Fe³⁺ speciation diagrams were calculated by the chemical equilibrium modeling system MINEQL+ [14] as a function of the solution pH considering the initial experimental conditions, as can be seen in Figure 5.2. The Fe³⁺ speciation diagram of the Fe(III)-oxalate system in Figure 5.2a shows the presence of four Fe(III)-oxalate complexes, FeHox²⁺, Feox⁺, Fe(ox)₂⁻ and Fe(ox)₃³⁻. FeHox²⁺ species acts at pH values below 2.1 in molar fractions lower than 18%, whereas Feox⁺ is available at a maximum molar fraction of 48% at pH of 1.4 and from this point its amount decreased up to disappear at pH of 4.5. From pH of 2.0 to 5.1, the predominant Fe(III)-oxalate complexes are the most photoactive Fe(ox)₂⁻ and Fe(ox)₃³⁻ species [3], which account for a total molar fraction of 95-97% at pH of 3.4-4.5, thereby covering the pH of 4.5 used in the PEF-UVA-BDD treatment. As a result, the high TMP degradation by this process shown in Figure 5.3a confirms the high photoactivity of Fe(ox)₂⁻ and Fe(ox)₃³⁻. The Fe(III)-citrate speciation diagram (Figure 5.2b) reveals the existence of three Fe(III)-citrate species, FeOHcit⁻, Fecit and FeHcit⁺, within the pH range from 2.0 to 7.1. FeOHcit⁻ is the dominant species at a pH range of 3.0-6.1 with maximum molar fractions of 95-97% at pH of 4.2-5.2. The great TMP degradation reached using the PEF-UVA-BDD system with Fe(III)-citrate complexes (see Figure 5.3a) suggests a high quantum yield of the FeOHcit⁻ species for Fe²⁺ formation. In turn, the equilibrium speciation of Fe(III)-tartrate system given in Figure 5.2c indicates the occurrence of a single Fe(tart)₂⁻ species available from pH of 0.8 to 6.5, with a highest molar fraction of 47-50% at pH of 2.1-5.2. Since PEF-UVA-BDD with Fe(III)-tartrate complexes also underwent a high TMP degradation (Figure 5.3a), it is highly likely that Fe(tart)₂⁻ species owns high photoactivity. Finally, Figure 5.2d displays the attendance of two Fe(III)-malate complexes, Femal⁺ and Fe(mal)₂⁻, although the former presents very low molar fractions (< 1.5%) and the maximum Fe(mal)₂⁻ molar fraction of 43-46% occurs from pH of 3.3 to 4.2, whereas at pH of 4.5 this species is available in 40%. Note that in PEF-UVA-BDD systems with Fe(III)-citrate, Fe(III)-tartrate and Fe(III)-malate complexes, the FeOH²⁺ species is also available but in amounts lower than 5.2% at pH values lesser than 4.0, not affecting the oxidation ability of the PEF-UVA-BDD processes performed at pH of 4.5.

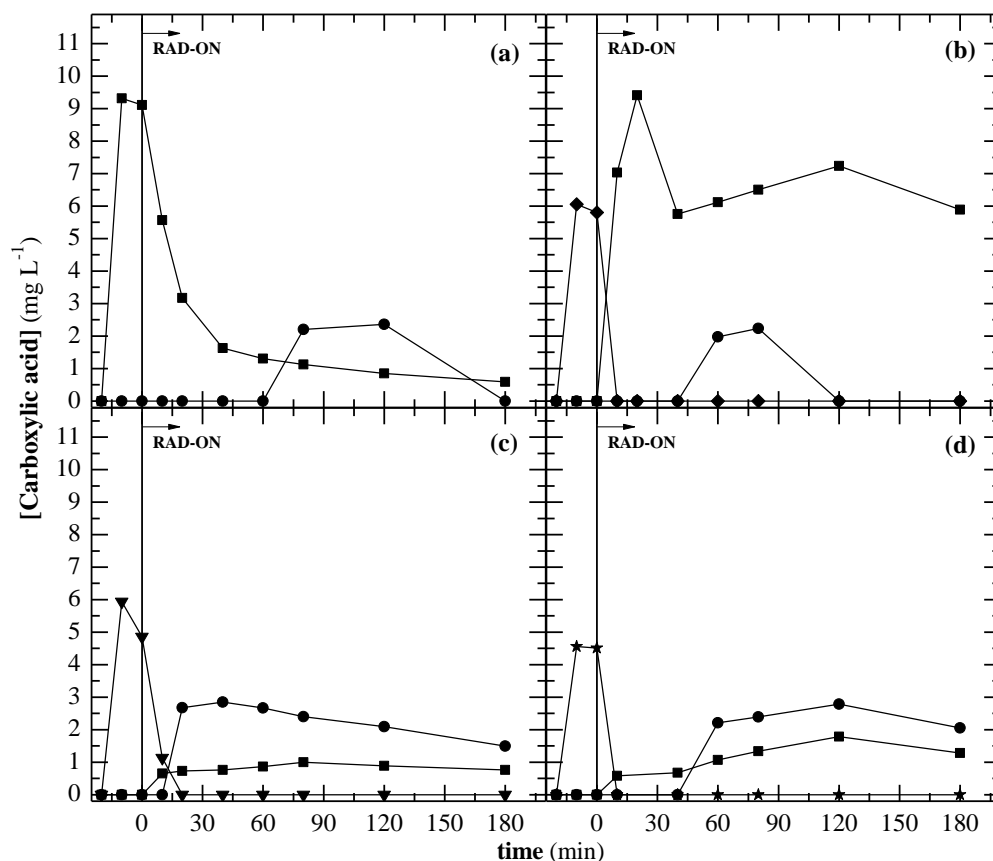


Figure 5.5. Evolution of the concentration of (■) oxalic, (●) formic, (◆) citric, (▼) tartaric and (★) malic acids during PEF-UVA-BDD treatment under conditions of Figure 5.3. System: (a) Fe(III)-oxalate, (b) Fe(III)-citrate, (c) Fe(III)-tartrate and (d) Fe(III)-malate.

Beyond the influence of quantum yields for Fe^{2+} formation on TMP degradation efficiency, the rate of photodecarboxylation of Fe(III)-carboxylate complexes can also affect the process since their presence allows preserving dissolved iron in solution with the consequent enhancement of TMP removal. Several authors have reported half-life of few minutes for Fe(III)-carboxylate complexes under UVA radiation [2, 3, 24]. This was confirmed by analyzing the treated TMP solutions by ion-exclusion HPLC. Figures 5.5b-d reveal a rapid and total degradation of citric, tartaric and malic acids after less than 10-15 min of electrolysis. In contrast, Figure 5.5a shows that oxalic acid sharply declined during the first 40 min, further remaining in solution at concentrations around 1.0 mg L^{-1} , due to the continuous formation of this acid as by-product of TMP degradation. Since Fe(III)-carboxylate complexes are quickly photodecarboxylated, their Fe^{3+} speciation diagrams in the initial conditions are inappropriate to describe properly their photocatalytic action during the entire reaction time. However, the construction of Fe^{3+} speciation diagrams with different doses of carboxylic acids showed that their degradation yielded lower

amounts of Fe(III)-carboxylate species along with the precipitation of iron as Fe(OH)_{3 (s)} at progressively inferior pH values (data not shown).

The theoretical ability of Fe³⁺ to precipitate at initial conditions was checked by including the Fe(OH)_{3 (s)} formation in the calculation of speciation diagrams. At pH of 4.5, the corresponding diagrams of Figure 5.2 predict null Fe³⁺ precipitation in Fe(III)-oxalate and Fe(III)-citrate systems, whereas molar fractions of 46% and 56% for Fe(OH)_{3 (s)} were formed in the Fe(III)-tartrate and Fe(III)-malate systems, respectively. However, the fast photodecarboxylation of all carboxylic acids led to the achievement of quite similar profiles of [TDI] using Fe(III)-oxalate, Fe(III)-tartrate and Fe(III)-malate systems, decreasing to values below 1.0 mg L⁻¹ after approximately 30 min of reaction, as can be seen in Figure 5.3c. The Fe(III)-citrate system exhibited higher [TDI] along all the electrolysis time, above 1.0 mg L⁻¹ until ca. 60 min. Regarding the generated LMCA acids in Figure 5.5, oxalic acid was found in 5.8-9.4 mg L⁻¹ in the Fe(III)-citrate system whereas lower amounts, below 1.9 mg L⁻¹, were accumulated in the other systems. Consequently, a greater Fe³⁺ content can be available in the form of Fe(III)-oxalate complexes using the Fe(III)-citrate system in PEF-UVA-BDD, thereby justifying the inferior iron precipitation attained in it. Note that the Fe(OH)_{3 (s)} phase was formed very slowly, which can explain its absence at the starting time in Fe(III)-tartrate and Fe(III)-malate systems despite their prevision from their speciation diagrams. A [TDI] of around 1.0 mg L⁻¹ then proved that can be efficiently used for the degradation of TMP using PEF-UVA-BDD process. In the presence of lower amounts of iron or in its absence, TMP and its intermediates may be pre-eminently degraded by BDD(*OH), thus explaining the slow TMP and DOC removal found for the PEF-UVA-BDD processes at long electrolysis times.

Oxamic and formic acids were also detected during all PEF-UVA-BDD processes with Fe(III)-carboxylate complexes. Oxamic acid was always found at contents lower than 0.06 mg L⁻¹. Formic acid exhibited higher contents up to 3.0 mg L⁻¹. After 180 min of PEF-UVA-BDD treatment, only 2-15% of remaining DOC was due to LMCA.

5.3.4 Effect of pH and initial Fe(III)-to-carboxylate molar ratio on PEF-UVA-BDD process

The effects of pH and initial Fe(III)-to-carboxylate molar ratio were evaluated in the PEF-UVA-BDD treatments assisted by Fe(III)-oxalate and Fe(III)-citrate complexes using pH values from 4.5 to 5.5 and Fe(III)-to-carboxylate molar ratios of 1:3, 1:6 and 1:9 in the former system and pH values of 4.5 and 5.0 and a 1:1 molar ratio in the latter one.

Figure 5.6a discloses similar TMP decay profiles at pH of 4.5, 5.0 and 5.5 for Fe(III)-to-oxalate molar ratios of 1:3, 1:6 and 1:9, with complete disappearance of TMP in 90 min in all cases. This advises for the need of applying double and triple oxalate ligand molar concentration to obtain similar results at pH of 5.0 and 5.5, respectively, when compared to pH of 4.5. Fe³⁺ speciation diagrams of 1:3 (see Figure 5.2a), 1:6 (see Figure 5.7a) and 1:9 (see Figure 5.7b) Fe(III)-to-oxalate molar ratios showed similar molar fractions of 95-100% for the sum of Fe(ox)₂⁻ and Fe(ox)₃³⁻ species and no iron precipitation, supporting the achieved findings. The use at pH of 5.0 of a Fe(III)-to-oxalate molar ratio of 1:3 against 1:6 led to a slower TMP removal with a k_{TMP} value 2.0 times inferior (see Table 5.2 and complete disappearance after only 180 min, which can be mainly attributed to (i) a higher iron precipitation since the use of a 1:3 Fe(III)-to-oxalate molar ratio estimates the presence of a Fe(OH)₃ (s) molar fraction of 34% at initial conditions (see Figure 5.2a), and (ii) the availability of lower amounts of Fe(III)-oxalate complexes, disappearing from the solution at shorter reaction times. In fact, the [TDI] attained a value below 1.0 mg L⁻¹ after ca. 25 min of treatment (see Figure 5.6b) when only 47% of TMP had been removed. On the other hand, the use at pH of 5.0 of a Fe(III)-to-oxalate molar ratio of 1:9 in contrast to 1:6 had an increase on TMP degradation with k_{TMP} 1.6 times higher (see Table 5.2), because iron remained in solution in much higher concentrations during longer times of ca. 90 min.

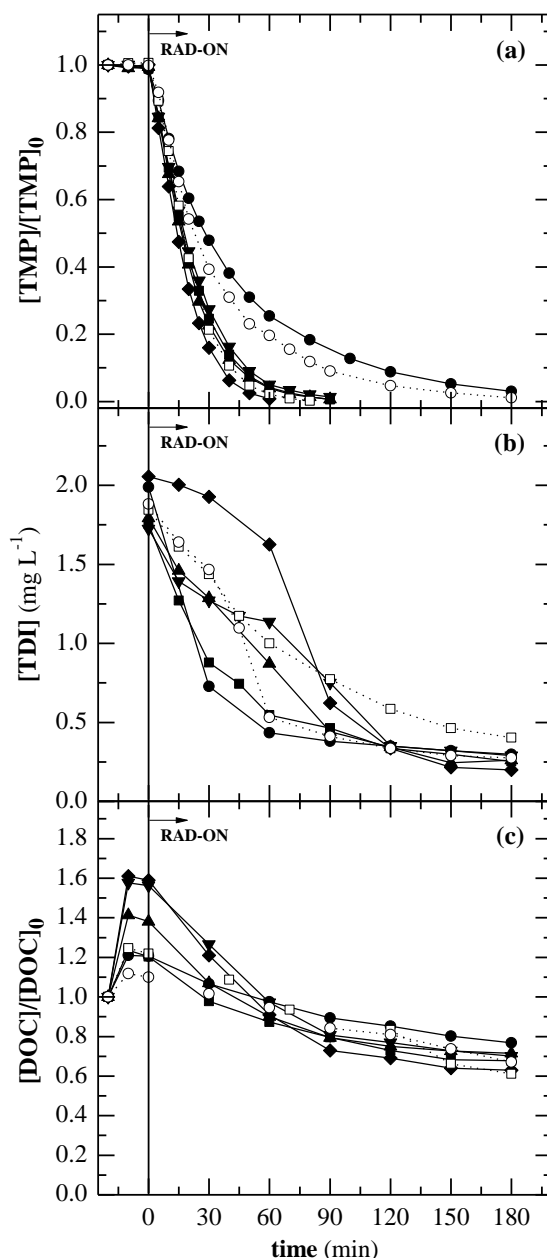


Figure 5.6. Effect of pH and initial Fe(III)-to-carboxylate molar ratio on (a) normalized TMP concentration decay, (b) total dissolved iron concentration and (c) normalized DOC removal as a function of time for PEF-UVA-BDD treatment of a 20.0 mg TMP L⁻¹ solution in 7.0 g Na₂SO₄ L⁻¹ using [TDI]₀ of 2.0 mg L⁻¹, 20 °C and *j* of 5.0 mA cm⁻². Conditions: (■) pH of 4.5 and 1:3 Fe(III)-to-oxalate molar ratio, (●) pH of 5.0 and 1:3 Fe(III)-to-oxalate molar ratio, (▲) pH of 5.0 and 1:6 Fe(III)-to-oxalate molar ratio, (◆) pH of 5.0 and 1:9 Fe(III)-to-oxalate molar ratio, (▼) pH of 5.5 and 1:9 Fe(III)-to-oxalate molar ratio, (□) pH of 4.5 and 1:1 Fe(III)-to-citrate molar ratio and (○) pH of 5.0 and 1:1 Fe(III)-to-citrate molar ratio.

When 1:6 and 1:9 Fe(III)-to-oxalate molar ratios were employed, the DOC decay profiles of Figure 5.6c were characterized by an initial period with sharp declines and a second period with a very slowly decay, probably due to the formation of nitrogenated organic oxidation products

hardly oxidized by BDD($\bullet\text{OH}$), $\bullet\text{OH}$ in the bulk and/or photodecomposed by UVA light, as stated above. A Fe(III)-to-oxalate molar ratio of 1:9 compared to 1:6 led to a larger initial period of 90 against 60 min with more pronounced DOC removal, giving slightly higher $r_{0(\text{DOC})}$ values (see Table 5.3). In contrast, the DOC profiles of the systems employing a 1:3 Fe(III)-to-oxalate molar ratio, as well as the aforementioned systems with a 1:1 Fe(III)-to-carboxylate molar ratio, did not experienced an initial quicker DOC abatement. These findings suggest that during this initial phase occurred the mineralization of oxalic acid since when changing from Fe(III)-to-oxalate molar fraction of 1:9 to 1:3 this acid gradually contributes less to DOC content (addition of 7.7, 5.2 and 2.6 mg C L⁻¹ for molar ratios of 1:9, 1:6 and 1:3, respectively).

The increment of pH value from 4.5 to 5.0 in the Fe(III)-citrate system led to slower TMP and DOC decays (see Figures 5.6a,c), with k_{TMP} and k_{DOC} values 2.1 and 1.5 times inferior, respectively (see Tables 5.2 and 5.3), along with faster decrease of [TDI] (see Figure 5.6b). The analysis of the evolution of LMCA showed a fast citric acid degradation in both systems and the formation of 0.8-1.9 mg L⁻¹ of oxalic acid at pH of 5.0 (data not displayed), values inferior to the 5.8-9.4 mg L⁻¹ accumulated in the system at pH of 4.5. The presence of smaller amounts of Fe(III)-oxalate complexes in the Fe(III)-citrate system at pH of 5.0 then corroborates the faster decay of [TDI], leading to a low process efficiency.

Despite the better results achieved when higher Fe(III)-to-carboxylate molar fractions were applied, the use of high amounts of carboxylic acids should be taken with precaution not only because of the presence of an excess of carboxylate ions that cannot be complexed with the Fe³⁺ ions in solution and can act as extra carbon source, but also due to a decrease of light penetration throughout the solution and the necessity to support higher reagent costs.

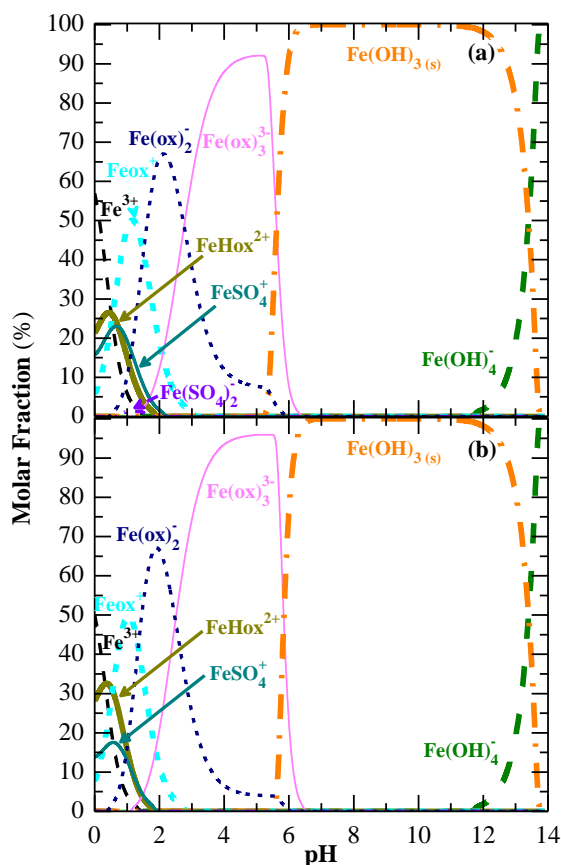


Figure 5.7. Fe^{3+} speciation diagrams as a function of solution pH in a calculated system containing: (a) 2.15×10^{-4} M of oxalate ion (1:6 Fe(III)-to-oxalate molar ratio) or (b) 3.22×10^{-4} M of oxalate ion (1:9 Fe(III)-to-oxalate molar ratio), with 3.58×10^{-5} M of Fe^{3+} (2.0 mg L^{-1}), 1.07×10^{-4} M of Cl^- ($9.7 \text{ mg FeCl}_3 \cdot 6\text{H}_2\text{O L}^{-1}$), 4.93×10^{-2} M of SO_4^{2-} and 9.86×10^{-2} M of Na^+ ($7.0 \text{ g Na}_2\text{SO}_4 \text{ L}^{-1}$) (ionic strength = 0.148 M). Data were calculated from the chemical equilibrium modeling system MINEQL+ [14] using the equilibrium constants of Table 5.1. The formation of the solid iron phase $\text{Fe}(\text{OH})_3$ was included in the calculation despite the slow formation of solid phases on the time scale of the experiments.

5.3.5 Effect of initial TMP concentration on PEF-UVA-BDD process

The influence of initial TMP concentration of 2.0, 5.0, 10.0 and 20.0 mg L^{-1} on the PEF-UVA-BDD process was assessed at pH of 4.5 in the presence of 1:1 Fe(III)-to-citrate molar ratio under the abovementioned conditions. Figure 5.8a reveals the removal of higher amounts of TMP per unit of time, i.e. higher TMP removal rates, for larger initial TMP contents, with $r_{0(\text{TMP})}$ values 1.4, 2.0 and 2.3 times higher for 5.0, 10.0 and 20.0 mg L^{-1} compared to 2.0 mg L^{-1} , respectively (see Table 5.2). Regarding the pseudo-first-order kinetic model, it should be theoretically expected an independence of k_{TMP} on the organic content, which is in disagreement with the large drop on k_{TMP} detected for higher initial amounts of TMP (see Table 5.2). These

results are similar to that found in Chapter 4 the degradation of a secondary WWTP effluent using two distinct TMP initial contents. They can be related to limitations of the pseudo-first-order kinetic model to precisely describe the TMP decay profiles, as indicated in Chapter 4, and, furthermore, lower diffusion and/or mass transport toward/from electrodes of H_2O_2 and Fe^{2+} species can be achieved in the presence of higher substrate concentration, simultaneously with possible formation of larger amounts of Fe(III) complexes with organics, thus varying the ability of $\cdot\text{OH}$ to react with the parent molecule and its by-products.

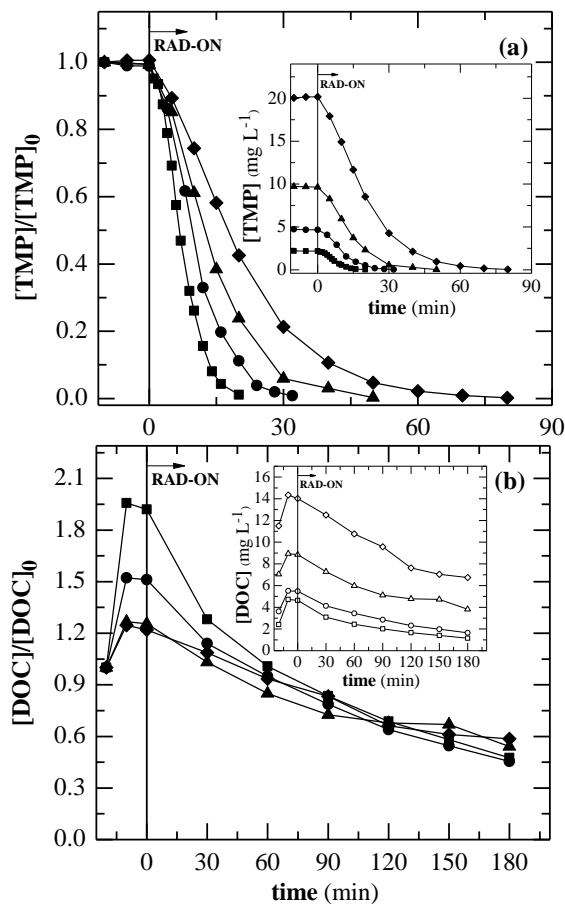


Figure 5.8. Effect of initial TMP concentration on (a) normalized TMP concentration decay and (b) normalized DOC removal for PEF-UVA-BDD treatment of a TMP solution in $7.0 \text{ g Na}_2\text{SO}_4 \text{ L}^{-1}$ using pH of 4.5, $[\text{TDI}]_0$ of 2.0 mg L^{-1} , 1:1 Fe(III)-to-citrate molar ratio, 20°C and j of 5.0 mA cm^{-2} . Initial TMP concentration: (■) 2.0, (●) 5.0, (▲) 10.0 and (◆) 20.0 mg L^{-1} . The inset panels depict the corresponding decays in mg L^{-1} .

Conversely, Figure 5.8b shows similar kinetics for DOC removal, with quite analogous k_{DOC} values for all tested antibiotic contents (see Table 5.3). The normalized DOC abatement profiles of the two lowest TMP solutions (2.0 and $5.0 \text{ mg TMP L}^{-1}$) layout an initial phase characterized by a more pronounced decay and a subsequent period with slow decline. The initial fast period can be related to the degradation of Fe(III)-citrate complexes since lower TMP contents resulted in a

higher ratio between the DOC of citric acid (2.6 mg C L⁻¹ in all the trials) and the antibiotic (11.6, 5.8, 2.9 and 1.2 mg C L⁻¹ for 2.0, 5.0, 10.0 and 20 mg TMP L⁻¹, respectively).

5.3.6 Effect of temperature on PEF-UVA-BDD process

The influence of temperature on TMP degradation was assessed by degrading 20.0 mg TMP L⁻¹ solution in 7.0 g Na₂SO₄ L⁻¹ at pH of 4.5 in the presence of 1:3 Fe(III)-to-oxalate molar ratio under the abovementioned conditions. Figure 5.9 shows that the use of temperatures of 10 and 20 °C led to quite similar TMP and DOC decays and, in turn, the use of a greater temperature of 40 °C caused slightly faster TMP and DOC removals, with k_{TMP} and k_{DOC} values 1.7-1.8 and 2.2-2.5 times higher, respectively (see Tables 5.2 and 5.3). The beneficial effect of high temperatures on reaction kinetics in Fenton's based processes has been largely attributed to a higher Fe³⁺ regeneration to Fe²⁺ through thermal reactions as Eqs. (22), (23) and (44) [25, 26], besides the enhancement of the mass transfer of reactants toward/from the electrodes with temperature and the exponential dependence of kinetic constants (for •OH and H₂O₂ production and oxidation of organics by such species) on the temperature (Arrhenius law).

The current study wanted to go further and examined the influence of temperature on the amount of the photoactive species in solution. To do this, the molar fractions of the most photoactive species, in terms of Fe³⁺ total concentration, were calculated by the chemical equilibrium modeling system MINEQL+ [14] under the initial conditions in the presence of oxalate, Fe³⁺, Na₂SO₄ and Cl⁻ (see Figure 5.10a) and under the same settings but in the absence of oxalate ion (see Figure 5.10b), which corresponds to the system after total photodecarboxylation of Fe(III)-oxalate complexes. As can be seen, at the starting conditions quite similar molar fractions of Fe(ox)₂⁻ and Fe(ox)₃³⁻ were obtained for all the temperatures in the overall pH range and, after Fe(III)-oxalate complexes photodecarboxylation, none photoactive species was available at pH of 4.5. The slightly reaction enhancement at 40 °C can then be mainly associated with higher Fe³⁺ regeneration to Fe²⁺ through the thermal reactions (22), (23) and (44), and in minor proportion to the rise in rate of electrode reactions (1), (16) and (26) due to the faster mass transport toward/from the electrodes.

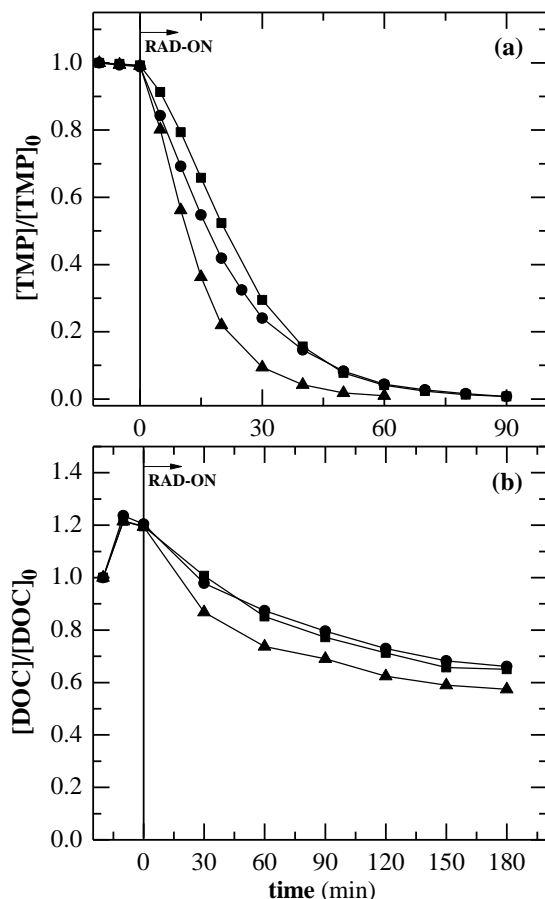


Figure 5.9. Effect of temperature on (a) normalized TMP concentration decay and (b) normalized DOC removal for PEF-UVA-BDD treatment of a 20.0 mg TMP L⁻¹ solution in 7.0 g Na₂SO₄ L⁻¹ using pH of 4.5, [TDI]₀ of 2.0 mg L⁻¹, 1:3 Fe(III)-to-oxalate molar ratio, 20 °C and *j* of 5.0 mA cm⁻². Temperature: (■) 10, (●) 20 and (▲) 40 °C.

Moreover, an analysis at pH of 2.8 (i.e. the pH value commonly assumed as optimal in light-assisted Fenton's based processes) revealed increasing FeOH²⁺ molar fractions together with temperature rise for the system in the absence of oxalate ion (see Figure 5.10b) and in the absence of both oxalate ion and Na₂SO₄ (see Figure 5.10c). Nevertheless, while the growth of the FeOH²⁺ molar fraction in the former system was very poor (FeOH²⁺ molar fractions of 2.7%, 3.8% and 6.9% for 10, 20 and 40 °C, respectively), in the latter one, common for PF processes without electrolyte, the rise of the FeOH²⁺ molar fraction was very accentuated (FeOH²⁺ molar fractions of 14%, 22% and 40% for 10, 20 and 40 °C, respectively). Hence, the influence of temperature in light-assisted Fenton's based processes at pH near 2.8 in the absence of high amounts of sulfate and carboxylic acids can be associated with the presence of different amounts of photoactive species besides of the occurrence of thermal reactions.

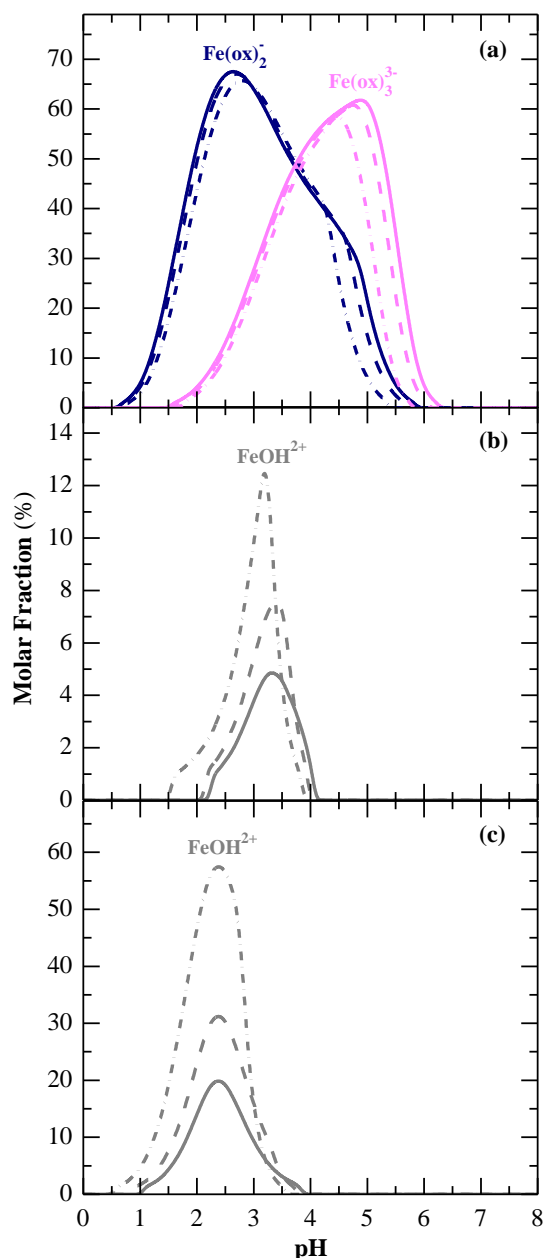


Figure 5.10. Theoretical molar fraction of (a) Fe(ox)_2^- and Fe(ox)_3^{3-} and (b, c) FeOH^{2+} species, regarding the total Fe^{3+} concentration, as a function of the solution pH at: (solid profile) 10 °C, (dash profile) 20 °C and (dash dot profile) 40 °C. Systems: (a) 1.07×10^{-4} M of oxalate ion (1:3 Fe(III)-to-oxalate molar ratio), 3.58×10^{-5} M of Fe^{3+} (2.0 mg L^{-1}), 1.07×10^{-4} M of Cl^- ($9.7 \text{ mg FeCl}_3 \cdot 6\text{H}_2\text{O L}^{-1}$), 4.93×10^{-2} M of SO_4^{2-} and 9.86×10^{-2} M of Na^+ ($7.0 \text{ g Na}_2\text{SO}_4 \text{ L}^{-1}$), (b) absence of oxalate ion and (c) absence of oxalate ion and Na_2SO_4 . Ionic strength of 0.148 or ~ 0 M in the presence and absence of Na_2SO_4 , respectively. Data were calculated from the chemical equilibrium modeling system MINEQL+ [14] using the equilibrium constants of Table 5.1. The formation of the solid iron phase Fe(OH)_3 was included in the calculation despite the slow formation of solid phases on the time scale of the experiments.

Despite the better results found at high temperatures, their use should be taken carefully mainly due to the occurrence of: (i) thermal decomposition of H_2O_2 into H_2O and O_2 (inactive species) for temperatures above $50\text{ }^\circ\text{C}$ [27], (ii) inefficient H_2O_2 decomposition through thermal reactions (22), (23) and (44) involved in the Fe^{3+} reduction, with formation of less reactive species, and (iii) significant water evaporation and O_2 release [28].

5.3.7 Role of different oxidizing species

As previously stated, $\bullet\text{OH}$ can be mainly produced by (i) electrochemical oxidation according to Eq. (1), (ii) Fenton's reaction (21), and (iii) photolysis of Fe(III)-hydroxy complexes through Eq. (28). In turn, the generation of other oxidizing species like the singlet oxygen ($^1\text{O}_2$) can occur from the excitation of the ground-state O_2 molecules in the presence of a sensitizer as is the case of TMP molecule and sub-structural moieties of TMP, 1,2,3-trimethoxybenzene and 2,4-diaminopyrimidine, in pure water [29, 30]. The role of $\bullet\text{OH}$ and $^1\text{O}_2$ was checked from the addition of selective scavenging agents like D-mannitol and sodium azide, respectively [31, 32]. Each scavenger in 2 mM content was added to a $20.0\text{ mg TMP L}^{-1}$ solution in $7.0\text{ g Na}_2\text{SO}_4\text{ L}^{-1}$ using $[\text{TDI}]_0$ of 2.0 mg L^{-1} and 1:1 Fe(III)-to-citrate molar ratio at pH of 4.5 and $20\text{ }^\circ\text{C}$ to be further treated by PEF-UVA-BDD at j of 5.0 mA cm^{-2} . Figure 5.11 confirms the important role of $\bullet\text{OH}$ on the degradation of TMP since the absence of this radical induced an inhibition of ca. 9.5 times in the k_{TMP} value (see Table 5.2). Surprisingly, the use of sodium azide led to an even slightly higher inhibition of TMP decay compared with D-mannitol, with k_{TMP} 0.6 times inferior, pointing to a strong participation of $^1\text{O}_2$ in the degradation process. Although sodium azide has been mainly described as a high selective $^1\text{O}_2$ scavenger, some authors reported its non-selectivity since it can also react with $\bullet\text{OH}$ [33], which could better justify the results reported in Figure 5.11.

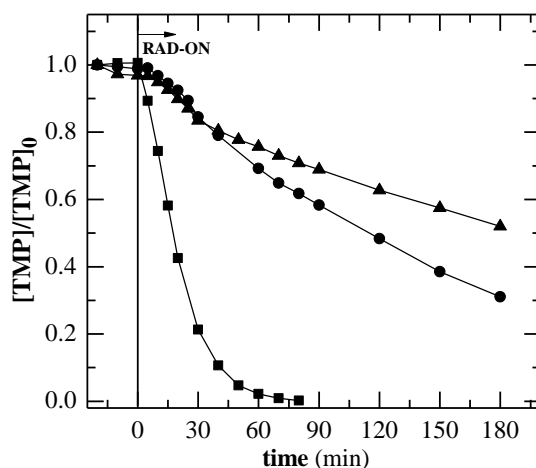


Figure 5.11. Effect of (●) D-mannitol and (▲) sodium azide on normalized TMP concentration decay for PEF-UVA-BDD treatment of a 20.0 mg TMP L⁻¹ solution in 7.0 g Na₂SO₄ L⁻¹ using pH of 4.5, [TDI]₀ of 2.0 mg L⁻¹, 1:1 Fe(III)-to-citrate molar ratio, 20 °C and *j* of 5.0 mA cm⁻². (■) Absence of scavenging agents.

5.3.8 Costs on carboxylate ligands

The selection of a carboxylate ligand should contemplate its price in order to minimize the global cost of the degradation process. Despite the similar reaction kinetics found for PEF-UVA-BDD processes with 1:3 Fe(III)-to-oxalate, 1:1 Fe(III)-to-citrate and 1:1 Fe(III)-to-tartrate molar ratios at pH of 4.5, the prices of carboxylic acids were ca. 28, 14 and 64 € per 1000 m³ of solution for Fe(III)-oxalate, Fe(III)-citrate and Fe(III)-tartrate systems, respectively, considering the information supplied by *Quimitécnica.com – Comércio e Indústria Química, SA* (Portugal) in January 2014. Therefore, the use of citrate can be economically advantageous for the PEF-UVA-BDD treatment.

5.4 Conclusions

The PEF-UVA-BDD process with 1:3 Fe(III)-to-oxalate, 1:1 Fe(III)-to-citrate and 1:1 Fe(III)-to-tartrate molar ratios showed similar ability, both in terms of TMP and DOC decays, to degrade a 20.0 mg TMP L⁻¹ solution in 7.0 g Na₂SO₄ L⁻¹ using pH of 4.5, [TDI]₀ of 2.0 mg L⁻¹, 20 °C and *j* of 5.0 mA cm⁻². In contrast, the PEF-UVA-BDD method with 1:1 Fe(III)-to-malate molar ratio showed inferior capacity to degrade TMP and its intermediates under similar conditions. 1:6 and 1:9 Fe(III)-to-oxalate molar ratios were required to work at pH of 5.0 and 5.5 with similar efficiencies to pH of 4.5, respectively. Lower TMP removal rates were achieved when using smaller antibiotic concentrations. The use of various temperatures proved that the regeneration of Fe³⁺ to Fe²⁺ through thermal reactions plays a poor role in PEF processes assisted by Fe(III)-oxalate complexes. On the other hand, the beneficial effect of temperature in light-assisted Fenton's based processes at pH near 2.8 in the absence of high amounts of Fe(III)-carboxylate complexes and sulfate ion can be strongly related to the presence of increasing amounts of FeOH²⁺ species. The use of scavengers confirmed that the TMP degradation in the PEF-UVA-BDD process can be mainly attributed to the action of •OH. Low amounts of oxalic, oxamic and formic acids were generated during all the PEF-UVA-BDD processes with Fe(III)-carboxylate complexes, being almost completely removed at the end of the TMP treatments. Ferric speciation diagrams demonstrated to be a good tool to elucidate the behavior of the PEF-UVA-BDD process assisted by Fe(III)-carboxylate complexes.

5.5 References

- [1] Horváth, O., Stevenson, K.L., 1992. Charge Transfer Photochemistry of Coordination Compounds, VCH, New York, United States.
- [2] Zuo, Y., Hoigne, J., 1992. Formation of hydrogen peroxide and depletion of oxalic acid in atmospheric water by photolysis of iron(III)-oxalato complexes. *Environmental Science & Technology* 26(5), 1014-1022.
- [3] Faust, B.C., Zepp, R.G., 1993. Photochemistry of aqueous iron(III)-polycarboxylate complexes: Roles in the chemistry of atmospheric and surface waters. *Environmental Science & Technology* 27(12), 2517-2522.
- [4] Safarzadeh-Amiri, A., Bolton, J.R., Cater, S.R., 1997. Ferrioxalate-mediated photodegradation of organic pollutants in contaminated water. *Water Research* 31(4), 787-798.
- [5] Abrahamson, H.B., Rezvani, A.B., Brushmiller, J.G., 1994. Photochemical and spectroscopic studies of complexes, of iron(III) with citric acid and other carboxylic acids. *Inorganica Chimica Acta* 226(1-2), 117-127.
- [6] Rodríguez, E.M., Núñez, B., Fernández, G., Beltrán, F.J., 2009. Effects of some carboxylic acids on the Fe(III)/UVA photocatalytic oxidation of muconic acid in water. *Applied Catalysis B: Environmental* 89(1-2), 214-222.
- [7] Sun, Y., Pignatello, J.J., 1992. Chemical treatment of pesticide wastes. Evaluation of iron(III) chelates for catalytic hydrogen peroxide oxidation of 2,4-D at circumneutral pH. *Journal of Agricultural and Food Chemistry* 40(2), 322-327.
- [8] Smith, R.M., Martell, A.E., 2004. NIST Critically Selected Stability Constants of Metal Complexes Database, Version 8.0 for Windows, Texas A&M University, United States.
- [9] Silva, M.R.A., Vilegas, W., Zanoni, M.V.B., Pupo Nogueira, R.F., 2010. Photo-Fenton degradation of the herbicide tebuthiuron under solar irradiation: Iron complexation and initial intermediates. *Water Research* 44(12), 3745-3753.
- [10] Batista, A.P.S., Nogueira, R.F.P., 2012. Parameters affecting sulfonamide photo-Fenton degradation-Iron complexation and substituent group. *Journal of Photochemistry and Photobiology A: Chemistry* 232, 8-13.
- [11] Dias, I.N., Souza, B.S., Pereira, J.H.O.S., Moreira, F.C., Dezotti, M., Boaventura, R.A.R., Vilar, V.J.P., 2014. Enhancement of the photo-Fenton reaction at near neutral pH through the use of ferrioxalate complexes: A case study on trimethoprim and sulfamethoxazole antibiotics removal from aqueous solutions. *Chemical Engineering Journal* 247, 302-313.
- [12] Demirezen, N., Tarınc, D., Polat, D., Çeşme, M., Gölcü, A., Tümer, M., 2012. Synthesis of trimethoprim metal complexes: Spectral, electrochemical, thermal, DNA-binding and surface morphology studies. *Spectrochimica Acta Part A: Molecular and Biomolecular Spectroscopy* 94, 243-255.
- [13] Tella, A.C., Obaleye, J.A., 2010. Metal-chelator therapy: Stability constants of transition metal complexes of pyrimidine and sulphonamide drugs. *International Journal of Chemical Sciences* 8(3), 1675-1683.

- [14] Schecher, W.D., McAvoy, D.C., 2007. MINEQL+: A Chemical Equilibrium Modeling System, Version 4.6 for Windows, Environmental Research Software, Hallowell, United States.
- [15] Vincze, L., Papp, S., 1987. Individual quantum yields of $\text{Fe}^{3+}\text{OX}_n^{2-}\text{H}_m^+$ complexes in aqueous acidic solutions ($\text{OX}^{2-} \equiv \text{C}_2\text{O}_4^{2-}$, $n = 1 - 3$, $m = 0,1$). *Journal of Photochemistry* 36(3), 289-296.
- [16] Field, T.B., McCourt, J.L., McBryde, W.A.E., 1974. Composition and stability of iron and copper citrate complexes in aqueous solution. *Canadian Journal of Chemistry* 52(17), 3119-3124.
- [17] Timberlake, C.F., 1964. 975. Iron-malate and iron-citrate complexes. *Journal of the Chemical Society (Resumed)*, 5078-5085.
- [18] Vukosav, P., Tomišić, V., Mlakar, M., 2010. Iron(III)-complexes engaged in the biochemical processes in seawater. II. Voltammetry of Fe(III)-malate complexes in model aqueous solution. *Electroanalysis* 22(19), 2179-2186.
- [19] Glebov, E.M., Pozdnyakov, I.P., Grivin, V.P., Plyusnin, V.F., Zhang, X., Wu, F., Deng, N., 2011. Intermediates in photochemistry of Fe(III) complexes with carboxylic acids in aqueous solutions. *Photochemical & Photobiological Sciences* 10(3), 425-430.
- [20] Huang, Y.-H., Tsai, S.-T., Huang, Y.-F., Chen, C.-Y., 2007. Degradation of commercial azo dye reactive Black B in photo/ferrioxalate system. *Journal of Hazardous Materials* 140(1-2), 382-388.
- [21] Zuo, Y., Hoigné, J., 1994. Photochemical decomposition of oxalic, glyoxalic and pyruvic acid catalysed by iron in atmospheric waters. *Atmospheric Environment* 28(7), 1231-1239.
- [22] Sirtori, C., Agüera, A., Gernjak, W., Malato, S., 2010. Effect of water-matrix composition on trimethoprim solar photodegradation kinetics and pathways. *Water Research* 44(9), 2735-2744.
- [23] Michael, I., Hapeshi, E., Osorio, V., Perez, S., Petrovic, M., Zapata, A., Malato, S., Barceló, D., Fatta-Kassinos, D., 2012. Solar photocatalytic treatment of trimethoprim in four environmental matrices at a pilot scale: Transformation products and ecotoxicity evaluation. *Science of the Total Environment* 430, 167-173.
- [24] Faust, B.C., Hoigné, J., 1990. Photolysis of Fe(III)-hydroxy complexes as sources of OH radicals in clouds, fog and rain. *Atmospheric Environment. Part A. General Topics* 24(1), 79-89.
- [25] Malato, S., Fernández-Ibáñez, P., Maldonado, M.I., Blanco, J., Gernjak, W., 2009. Decontamination and disinfection of water by solar photocatalysis: Recent overview and trends. *Catalysis Today* 147(1), 1-59.
- [26] Sychev, A.Y., Isak, V.G., 1995. Iron compounds and the mechanisms of the homogeneous catalysis of the activation of O_2 and H_2O_2 and of the oxidation of organic substrates. *Russian Chemical Reviews* 64(12), 1105-1129.
- [27] Santos, A., Yustos, P., Rodriguez, S., Simon, E., Garcia-Ochoa, F., 2007. Abatement of phenolic mixtures by catalytic wet oxidation enhanced by Fenton's pretreatment: Effect of H_2O_2 dosage and temperature. *Journal of Hazardous Materials* 146(3), 595-601.
- [28] Boye, B., Dieng, M.M., Brillas, E., 2002. Degradation of herbicide 4-chlorophenoxyacetic acid by advanced electrochemical oxidation methods. *Environmental Science & Technology* 36(13), 3030-3035.

- [29] Luo, X., Zheng, Z., Greaves, J., Cooper, W.J., Song, W., 2012. Trimethoprim: Kinetic and mechanistic considerations in photochemical environmental fate and AOP treatment. *Water Research* 46(4), 1327-1336.
- [30] Ryan, C.C., Tan, D.T., Arnold, W.A., 2011. Direct and indirect photolysis of sulfamethoxazole and trimethoprim in wastewater treatment plant effluent. *Water Research* 45(3), 1280-1286.
- [31] Bandara, J., Kiwi, J., 1999. Fast kinetic spectroscopy, decoloration and production of H₂O₂ induced by visible light in oxygenated solutions of the azo dye Orange II. *New Journal of Chemistry* 23(7), 717-724.
- [32] Monteagudo, J.M., Durán, A., San Martín, I., Carnicer, A., 2011. Roles of different intermediate active species in the mineralization reactions of phenolic pollutants under a UV-A/C photo-Fenton process. *Applied Catalysis B: Environmental* 106(1-2), 242-249.
- [33] Zhang, X., Rosenstein, B.S., Wang, Y., Lebowitz, M., Wei, H., 1997. Identification of possible reactive oxygen species involved in ultraviolet radiation-induced oxidative DNA damage. *Free Radical Biology and Medicine* 23(7), 980-985.

6 Remediation of a winery wastewater combining aerobic biological oxidation and electrochemical advanced oxidation processes

Apart from a high biodegradable organic fraction consisting of organic acids, sugars and alcohols, winery wastewaters exhibit a recalcitrant organic fraction containing high-molecular-weight compounds as polyphenols and lignins. In this context, a winery wastewater was firstly subjected to a biological oxidation to mineralize the biodegradable organic fraction and afterwards an EAOP was applied in order to mineralize the refractory molecules or transform them into simpler ones that can be further biodegraded. The biological oxidation led to removals above 97% of DOC, COD and BOD₅, but was inefficient on the degradation of a bioresistant fraction corresponding to 130 mg L⁻¹ of DOC, 380 mg O₂ L⁻¹ of COD and 8.2 mg caffeic acid equivalent L⁻¹ of total dissolved polyphenols. Various EAOPs such as AO-H₂O₂, EF, PEF-UVA and SPEF were then applied to the recalcitrant effluent fraction using a 2.2 L lab-scale flow plant coupled to a photoreactor with CPCs and an electrochemical cell equipped with a BDD anode and a carbon-PTFE air-diffusion cathode. The influence of [TDI]₀ and j on the PEF-UVA-BDD process was evaluated. The relative oxidative ability of EAOPs increased in the order AO-H₂O₂-BDD < EF-BDD < PEF-UVA-BDD ≤ SPEF-BDD. The SPEF-BDD process using pH of 2.8, 25 °C, [TDI]₀ of 35 mg L⁻¹ and j of 25 mA cm⁻² reached removals of 86% of DOC and 68% of COD after 240 min, regarding the biologically treated effluent, along with energy consumptions of 45 kWh (kg DOC)⁻¹ and 5.1 kWh m⁻³. After this coupled treatment, color, odor, COD, BOD₅, ammonium, nitrate and sulfate parameters complied with the legislation targets and, in addition, a total dissolved polyphenols content of 0.35 mg caffeic acid equivalent L⁻¹ was found. Respirometry tests revealed low biodegradability enhancement along the SPEF-BDD process.

This Chapter is based on the following research article: “Moreira, F.C., Boaventura, R.A.R., Brillas, E., Vilar, V.J.P., 2015. Remediation of a winery wastewater combining aerobic biological oxidation and electrochemical advanced oxidation processes. *Water Research* 75, 95-108”.

6.1 Introduction

Winery wastewaters are generated by the different activities carried out during processing and cleaning operations in wineries. The production of this kind of effluent is seasonal, which leads to significant variations in volume and organic load produced throughout the year, according to the type of wine (red, white, rosé, sparkling, etc.), the phase of production (grape harvesting, crushing, fermentation, aging, filtration, bottling, etc.), the processing operations and the cleaning practices. Typically, winery wastewaters are characterized by pH values from 2.5 to 6.0 and COD values of 0.8-70 g O₂ L⁻¹ [1-5]. The major constituents of such effluents are organic contaminants like organic acids (tartaric, lactic and acetic), sugars (glucose and fructose) and alcohols (ethanol and glycerol) and also recalcitrant high-molecular weight compounds like polyphenols and lignins [6]. The release of winery wastewaters into natural aquatic environments without adequate treatment can cause negative effects on the oxygen balance, bad odors and decrease of natural photoactivity due to color and turbidity.

The high biodegradability of this kind of effluent can often justifies their treatment by biological processes [3, 5]. However, such treatments may not be able to degrade the bioresistant fraction of these wastewaters and hence alternative treatment strategies have been investigated. Among them, the application of AOPs as a single stage treatment acquired significance. The main applied AOPs have been (i) ozone and ozone based processes (O₃, O₃/UV, O₃/UV/H₂O₂) [7], (ii) catalysis with TiO₂, TiO₂/H₂O₂ and TiO₂/S₂O₈²⁻ [8], and (iii) Fenton's reaction based processes like PF [9], SPF [8] and ferrioxalate-assisted SPF [10]. The AOPs have been used both as pretreatment and post-treatment steps, although the recommended treatment strategy for high biodegradable wastewaters, like winery effluents, combines (i) a biological pretreatment to remove the biodegradable organic compounds, (ii) a further AOP to convert the bioresistant molecules into simpler ones that are able to be further biodegraded and (iii) a final biological polishing step [11]. This integrated system may lead to the total mineralization of organics along with the minimization of the total treatment cost.

To the best of our knowledge, no reports on EAOPs, alone or in combination with other processes, to the remediation of winery wastewaters have been disclosed to date that the study was conducted. The aim of the current work was to evaluate the performance of a winery wastewater treatment comprising (i) an initial biological oxidation accomplished in an IBR to remove the biodegradable

fraction of the effluent, and (ii) a further EAOP such as AO-H₂O₂-BDD, EF-BDD, PEF-UVA-BDD or SPEF-BDD to degrade the refractory compounds. The biodegradability enhancement along the SPEF-BDD process was assessed to appraise the suitability of the application of a final biological oxidation. Moreover, the influence of [TDI]₀ and *j* on the PEF-UVA-BDD process was assessed.

6.2 Materials and methods

All chemicals, analytical determinations, modeling of degradation kinetics and the experimental unit and respective procedure can be accessed in the Chapter 2. Table 2.5 summarizes the operational conditions of EAOPs performed in the current Chapter.

The winery wastewater was collected in May 2013 at a Port wine company located in the northeast of Portugal. This company includes only bottling activities and the wastewater resulted from the washing of a container of ruby Port wine, which was produced from different grape varieties grown in the Douro Demarcated Region. The main physicochemical characteristics of the raw winery wastewater are summarized in Table 6.1.

6.3 Results and discussion

6.3.1 Characteristics of the raw winery wastewater

From Table 6.1, one can highlight the following main characteristics of the raw winery wastewater: (i) dark violet color; (ii) strong odor; (iii) acid pH of 3.7; (iv) high organic content; (v) high biodegradability; (vi) low nitrogen content; (vii) moderate total dissolved polyphenols content of 41 mg caffeic acid equivalent L⁻¹; (viii) moderate alkalinity of 545 mg CaCO₃ L⁻¹; (ix) moderate conductivity of 3178 μS cm⁻¹ and moderate ionic content corresponding to a calculated ionic strength of 8.5 × 10⁻³ M; (x) absence of phosphate; (xi) low total phosphorous concentration; and (xii) absence of dissolved iron.

6.3.2 Aerobic biological oxidation

Figure 6.1 depicts a removal of an organic load corresponding to 96% of DOC after 7 days of aerobic biological oxidation and afterwards the mineralization rate remained almost unchanged, achieving a value of 97% after 10 days. This DOC decay came along with 97 % of COD and 98% of BOD₅ abatements after 10 days of biological oxidation (see complete wastewater characterization after the biological treatment in Table 6.1). The high biodegradability here attained is in agreement with the 99% biodegradability determined by the Zahn-Wellens test. Compounds easily biodegradable like organic acids, sugars and alcohols might be mineralized throughout the treatment [6] and, in addition, the air stripping of ethanol might occur [12]. Nevertheless, the biological oxidation was inefficient to mineralize an organic fraction comprising 130 mg L⁻¹ of DOC, 380 mg O₂ L⁻¹ of COD and a total dissolved polyphenols content of 8.2 mg caffeic acid equivalent L⁻¹. A BOD₅ value of 150 mg O₂ L⁻¹ was registered at the end of the biological oxidation, which can be associated with the excretion of metabolites and/or release of products from cell lysis of the IBR microorganisms. The abovementioned results advise the application of a further oxidation process like an EAOP to degrade the remaining non-biodegradable compounds and hence allow to discharge this wastewater into the environment as a final effluent from a WWTP according to the Portuguese legislation (Decree-Law no. 236/98) and the European Directive no. 91/271/CEE.

Table 6.1. Physicochemical characterization of winery wastewater along the various stages of treatment: raw, after 10 days of biological oxidation and after 240 min of SPEF-BDD process. The discharge limits for WWTPs final effluents according to Portuguese legislation (Decree-Law no. 236/98) and European Directive no. 91/271/CEE are also displayed.

Parameter (units)	Winery wastewater			ELV ^d for Decree-Law no. 236/98 or Directive no. 91/271/CEE
	Raw	After biological oxidation (Removal ^a)	After SPEF-BDD ^b (Removal ^c)	
Color	Dark violet	Light brown	Very light yellow	-
Color (diluted 1:20)	d. ^e	n.d. ^f	n.d. ^f	n.d. ^f or -
Odor	Strong	Weak	Very weak	-
Odor (diluted 1:20)	d. ^e	n.d. ^f	n.d. ^f	n.d. ^f or -
pH	3.7	8.3	2.8	6.0 - 9.0
Temperature (°C)	20	20	20	3 °C increase ^g or -
Conductivity (µS cm ⁻¹)	3178	2998	4614	-
Alkalinity (mg CaCO ₃ L ⁻¹)	545	1561	n.d. ^f	-
Turbidity (NTU)	38	30	54	-
TDC (mg L ⁻¹)	4425	480	18	-
DIC (mg L ⁻¹)	128	350	0.2	-
DOC (mg L ⁻¹)	4298	130 (97%)	18 (86%)	-
COD (mg O ₂ L ⁻¹)	12000	380 (97%)	120 (68%)	150 or 125
BOD ₅ (mg O ₂ L ⁻¹)	7950	150 (98%)	16 (89%)	40 or 25
BOD ₅ /COD	0.7	0.4	0.1	-
Biodegradability – Zahn Wellens test (%)	99	n.a. ^h	n.a. ^h	-
TDI (mg L ⁻¹)	<0.1 ⁱ	<0.1 ⁱ	12/<0.1 ^{i,j}	2.0 or -
Absorbance at 254 nm (AU) (diluted 1:5)	0.25	0.21	0.08	-
TSS (mg L ⁻¹)	81	72	158/55 ^j	60 or 35 ^k
VSS (mg L ⁻¹)	70	68	80	-
Total nitrogen (mg L ⁻¹)	62	59	27/27 ^j	15 or 10
Total dissolved nitrogen (mg L ⁻¹)	18	18	18	-
Dissolved organic nitrogen (mg L ⁻¹)	6.0	6.8	9.5	-
Ammonium – N-NH ₄ ⁺ (mg L ⁻¹)	7.7	7.6	8.5	7.8 or -
Nitrite – N-NO ₂ ⁻ (mg L ⁻¹)	4.1	3.6	<0.01 ⁱ	-
Nitrate – N-NO ₃ ⁻ (mg L ⁻¹)	0.2	<0.01 ⁱ	<0.01 ⁱ	11 or -
Bromide – Br ⁻ (mg L ⁻¹)	<0.008 ⁱ	<0.008 ⁱ	<0.008 ⁱ	-
Chloride – Cl ⁻ (mg L ⁻¹)	20	19	17	-
Fluoride – F ⁻ (mg L ⁻¹)	<0.04 ⁱ	<0.04 ⁱ	<0.04 ⁱ	-
Sulfate – SO ₄ ²⁻ (mg L ⁻¹)	30	46	1729	2000 or -
Calcium – Ca ²⁺ (mg L ⁻¹)	20	20	15	-
Lithium – Li ⁺ (mg L ⁻¹)	<0.004 ⁱ	<0.004 ⁱ	<0.004 ⁱ	-
Magnesium – Mg ²⁺ (mg L ⁻¹)	5.2	5.4	4.2	-
Potassium – K ⁺ (mg L ⁻¹)	365	370	347	-
Sodium – Na ⁺ (mg L ⁻¹)	52	413	396	-
Total phosphorous (mg L ⁻¹)	8.2	10	10/0.35 ^j	10 or 1
Phosphate – PO ₄ ³⁻ (mg L ⁻¹)	<0.02 ⁱ	<0.02 ⁱ	<0.02 ⁱ	-
Total dissolved polyphenols (mg caffeic acid equivalent L ⁻¹)	41	8.2 (80%)	0.35 (96%)	-

^a From raw to after biological oxidation;

^b SPEF-BDD process using pH of 2.8, 25 °C, [TDI]₀ of 35 mg L⁻¹ and *j* of 25 mA cm⁻²;

^c From after biological oxidation to after SPEF-BDD;

^d ELV – Emission limit value;

^e d. – detected;

^f n.d. – not detected;

^g Comparatively to the receptor medium;

^h n.a. – not assessed;

ⁱ LOD;

^j Clarified effluent after neutralization;

^k Facultative.

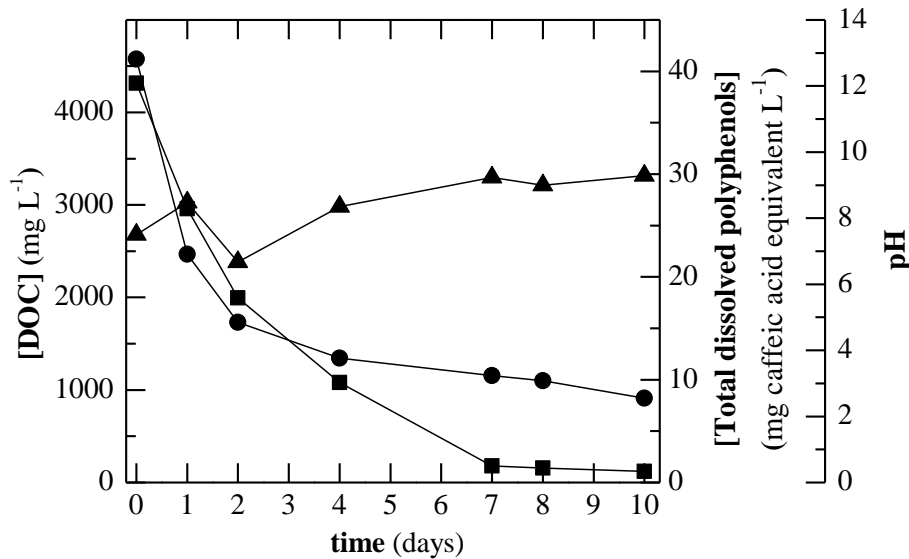


Figure 6.1. Assessment of the efficiency of biological oxidation in the treatment of the raw winery wastewater in terms of (■) DOC removal, (●) total dissolved polyphenols concentration decay and (▲) pH.

While some investigations have achieved very much alike DOC, COD and BOD₅ values after biological treatment [5, 13], other studies have handled with more biodegradable winery wastewaters. For example, Souza et al. [4] achieved DOC and COD values of 30 mg L⁻¹ and 84 mg O₂ L⁻¹, respectively, after 7 days of treatment also in an IBR; and Ioannou et al. [14] and Ioannou and Fatta-Kassinos [1] operated with winery wastewaters treated in a membrane bioreactor (MBR) displaying final DOC, COD and BOD₅ values of 30-60 mg L⁻¹, 120-210 mg O₂ L⁻¹ and < 5 mg O₂ L⁻¹, respectively. Consequently, the variable composition of the winery effluents may allow to occasionally omitting the application of a further oxidation process in order to comply with the legislation targets, though the removal of the bioresistant fraction of the effluent should always be taken into account due to its environmentally friendly character.

Color and odor were also reduced along the biological oxidation, reaching standards in agreement with the Portuguese discharge limits for final effluents from WWTPs. Due to the addition of high amounts of NaOH to increase the pH from acidic to neutral values, an increment on Na⁺ of ca. 360 mg L⁻¹ took place at the end of the biological treatment whereas the concentrations of the other ions remained practically constant.

Neither nitrification nor denitrification occurred throughout the biological treatment (see Table 6.1). As a result, the conditions of the biological oxidation treatment must be adjusted and

optimized to provide the nitrogen removal. In particular, the sludge age should be increased to ensure the development of nitrifying/denitrifying microorganisms [15].

6.3.3 EAOPs

6.3.3.1 General

To apply an EAOP to a wastewater, it has to possess conductivity large enough to transport the electric charge and minimize the power consumption. In some cases, it is necessary to add a salt like Na_2SO_4 , NaCl or HClO_4 to increase the conductivity. The biologically treated winery wastewater exhibited a moderate conductivity of 3.0 mS cm^{-1} (see Table 6.1) that increased to ca. 4.6 mS cm^{-1} after acidification to pH of 2.8, which allowed to directly apply an EAOP. However, this conductivity value was lower than the 8.6 mS cm^{-1} value exhibited by the $7.0 \text{ g Na}_2\text{SO}_4 \text{ L}^{-1}$ solution commonly applied as background electrolyte in EAOPs.

All trials were performed at $25 \text{ }^\circ\text{C}$ (ambient temperature) and pH of 2.8 since this pH value is often assumed as optimal because iron precipitation does not take place yet and the dominant iron species in solution is FeOH^{2+} , which is the most photoactive ferric iron–water complex [16]. For all the assays, the pH adjustment from 8.3 to 2.8 consumed high amounts of H_2SO_4 due to the high alkalinity of the biologically treated wastewater ($1561 \text{ mg CaCO}_3 \text{ L}^{-1}$) and induced (i) the reduction of 93-99% of DIC; (ii) the decrease of 16-28% of DOC; (iii) the formation of high amounts of foam and slight amounts of precipitate; and (v) no modification on TSS and turbidity values along with a color change to only a slightly lighter brown. From these results, one can suggest the following occurrences during the acidification step: (i) conversion of carbonates and/or bicarbonates into CO_2 ; (ii) retention of dissolved organic compounds (and perhaps some inorganic dissolved matter) into the foam; and (iii) precipitation in low extent of dissolved and/or suspended organic and/or inorganic compounds.

Furthermore, the addition of H_2SO_4 came along with a large increase of sulfate concentration from $46 \text{ mg SO}_4^{2-} \text{ L}^{-1}$ to $1.6 \text{ g SO}_4^{2-} \text{ L}^{-1}$. Although this sulfate content was below the discharge limit for WWTPs final effluents according to the Portuguese legislation ($2.0 \text{ g SO}_4^{2-} \text{ L}^{-1}$), the disadvantages arising from the presence of high sulfate contents are well-known: (i) the establishment of complexes of sulfate with Fe^{3+} (FeSO_4^+ and $\text{Fe}(\text{SO}_4)_2^-$), thus affecting the distribution and reactivity of the iron species [17-19]; (ii) the scavenging of $\bullet\text{OH}$ by sulfate ion along with the formation of the weaker $\text{SO}_4^{\bullet-}$ from Eq. (34) [20], and (iii) the decomposition of H_2O_2 by its

reaction with $\text{SO}_4^{\bullet-}$ by Eqs. (36) and (37) [20]. Table 6.2 shows the calculated concentrations of FeOH^{2+} and $\text{Fe}(\text{OH})_3$ (s) in the current systems calculated by the chemical equilibrium modeling system MINEQL+ [21]. For larger sulfate contents, it was theoretically predicted the formation of lower amounts of FeOH^{2+} (exception for $70 \text{ mg Fe}^{3+} \text{ L}^{-1}$) along with the prevention or, at least, reduction of iron precipitation as $\text{Fe}(\text{OH})_3$ (s), which can be interpreted as a benefit arising from sulfate addition. Nevertheless, the presence of more ions in solution increased the wastewater conductivity as abovementioned, reducing the power consumption.

No active chlorine species may be generated at the anode because of the low chloride concentration in the winery wastewater, ca. 20 mg L^{-1} . In a first glance this can be regarded as a drawback, but the formation of undesirable toxic chloro-organic derivatives and chlorine-oxygen by-products with a high health-risk in living beings might be avoided [22].

Table 6.2. Concentration of FeOH^{2+} and $\text{Fe}(\text{OH})_3$ (s) in various systems containing 46 or 1600 mg L^{-1} of SO_4^{2-} and 20, 35 or 70 mg L^{-1} of Fe^{3+} (ionic strength = $1.84\text{-}5.49 \times 10^{-2} \text{ M}$). Data were calculated by the chemical equilibrium modeling system MINEQL+ [21] using its equilibrium constants and considering the amounts of NH_4^+ , Cl^- , Ca^{2+} , Mg^{2+} , K^+ and Na^+ determined by ion chromatography after biological oxidation (Table 6.1).

System	Species concentration at pH of 2.8 (mg L^{-1})	
	FeOH^{2+}	$\text{Fe}(\text{OH})_3$ (s)
$[\text{SO}_4^{2-}]$ of 46 mg L^{-1} and $[\text{Fe}^{3+}]$ of $20/35/70 \text{ mg L}^{-1}$	4.6/4.6/4.6	15/44/111
$[\text{SO}_4^{2-}]$ of 1.6 g L^{-1} and $[\text{Fe}^{3+}]$ of $20/35/70 \text{ mg L}^{-1}$	1.6/2.9/5.7	0/0/1.7

6.3.3.2 Influence of initial total dissolved iron concentration on PEF-UVA-BDD process

$[\text{TDI}]_0$ from 20 to 70 mg L^{-1} were tested for PEF-UVA-BDD process using pH of 2.8, $25 \text{ }^\circ\text{C}$ and j of 100 mA cm^{-2} . This range of $[\text{TDI}]_0$ was selected considering other studies on PF processes applied to wastewaters with similar DOC values [23, 24]. Figure 6.2a shows a progressively faster DOC removal for higher $[\text{TDI}]_0$ that can be related to the increasing amount of Fe^{2+} initially available and regenerated both from (i) the photolysis of FeOH^{2+} through Eq. (28), and (ii) cathodic reduction of Fe^{3+} to Fe^{2+} from Eq. (26), which enhances the $\bullet\text{OH}$ production from Fenton's reaction (21) and subsequently its reaction with the organic compounds of the winery wastewater. Nevertheless, the difference between the two highest $[\text{TDI}]_0$ was not very emphasized, with a k_{DOC} value only 1.2 times higher for $[\text{TDI}]_0$ of 70 mg L^{-1} in comparison with 35 mg L^{-1} (see Table 6.3). Taking the aforementioned results into consideration, a $[\text{TDI}]_0$ of 35 mg L^{-1} can be chosen as the best one in this study.

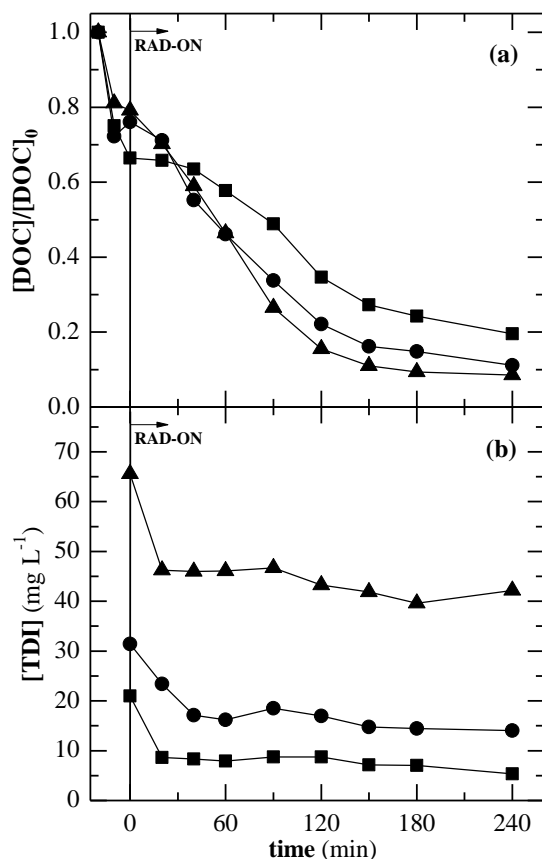


Figure 6.2. Influence of initial total dissolved iron concentration on (a) normalized DOC removal and (b) total dissolved iron concentration as a function of time for PEF-UVA-BDD treatment of the winery wastewater after biological oxidation using pH of 2.8, 25 °C and j of 100 mA cm^{-2} . $[\text{TDI}]_0$: (■) 20, (●) 35 and (▲) 70 mg L^{-1} .

Figure 6.2b displays a drop on the $[\text{TDI}]$ during the first 20-40 min of reaction in an extent of 55-75%, 34-60% and 33-50% for $[\text{TDI}]_0$ of 20, 35 and 70 mg L^{-1} , respectively. These results came along with a visible formation of iron sludge and TSS increase from 72 to 110-172 mg L^{-1} . The iron precipitation was not associated with sharp decays on the DOC content and, moreover, a blank test with the addition of 70 mg L^{-1} of Fe^{3+} to the biologically treated effluent revealed an iron precipitation of ca. 50% and null DOC abatement. From these results, one can suggest the formation Fe^{3+} complexes exclusively with non-dissolved inorganic and/or organic compounds. Note that null/almost null $\text{Fe}(\text{OH})_3 \text{ (s)}$ formation is predicted from a theoretical point of view (see Table 6.2).

Table 6.3. Pseudo-first-order kinetic constants for DOC removal (k_{DOC}) along with the corresponding R^2 and S^2_R , obtained for the treatment of the winery wastewater after biological oxidation under conditions of Figures 6.2a, 6.3a and 6.4a.

System		$k_{\text{DOC}} (\times 10^{-3} \text{ min}^{-1})$	R^2	$S^2_R (\text{mg}^2 \text{ L}^{-2})$
Effect of $[\text{TDI}]_0$ (mg L^{-1}) on PEF-UVA-BDD	20	7.0±0.6	0.976	9.0
	35	11.2±0.2	0.997	1.9
	70	13.0±1.0	0.985	21.8
Effect of j (mA cm^{-2}) on PEF-UVA-BDD	10	5.0±0.2	0.994	1.8
	25	8.3±0.5	0.984	7.9
	100	11.2±0.2	0.997	1.9
EAOPs	AO-H ₂ O ₂ -BDD	- ^a	- ^a	- ^a
	EF-BDD	- ^a	- ^a	- ^a
	PEF-UVA-BDD	8.3±0.5	0.984	7.9
	SPEF-BDD	8.9±0.5	0.990	10.4

^a No fitting of a pseudo-first-order kinetic model to experimental data.

6.3.3.3 Influence of current density on PEF-UVA-BDD process

A j range from 10 to 100 mA cm^{-2} was employed to assess the oxidation ability of PEF-UVA-BDD treatment using pH of 2.8, 20 °C and $[\text{TDI}]_0$ of 35 mg L^{-1} . These j values were chosen based on other EAOPs applied to wastewaters with similar DOC values [25, 26]. Figure 6.3a shows increasing DOC decays for raising j values with DOC removals of 73%, 84% and 89% after 240 min of electrolysis for j of 10, 25 and 100 mA cm^{-2} , respectively. The corresponding k_{DOC} values reported in Table 6.3 were 1.4 and 2.2 times higher for j of 100 mA cm^{-2} in comparison with j of 25 and 10 mA cm^{-2} , respectively. The quasi-steady DOC removal for times higher than 150 min at j of 100 mA cm^{-2} suggests the presence of compounds hardly oxidized by BDD($\bullet\text{OH}$), $\bullet\text{OH}$ in the bulk and/or photodecomposed by UVA radiation.

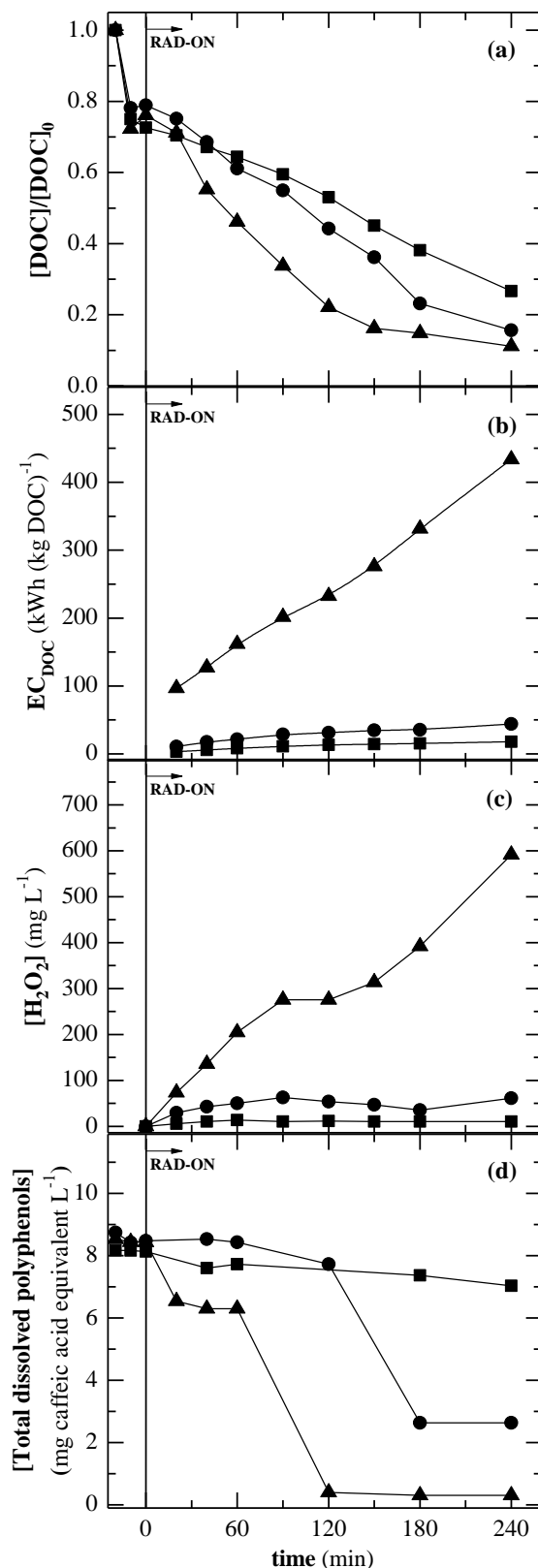


Figure 6.3. Effect of current density on (a) normalized DOC removal, (b) energy consumption per unit DOC mass, (c) H_2O_2 concentration and (d) total dissolved polyphenols concentration decay as a function of time for PEF-UVA-BDD treatment of the winery wastewater after biological oxidation using pH of 2.8, 25 °C and $[\text{TDI}]_0$ of 35 mg L⁻¹. Current density: (■) 10, (●) 25 and (▲) 100 mA cm⁻².

Despite the faster DOC decays with the rise in j , very high energy consumptions of 97-434 kWh (kg DOC)⁻¹ for j of 100 mA cm⁻² were obtained, which were 30-61 and 5-13 times superior to the ones found at j of 10 and 25 mA cm⁻², respectively (see Figure 6.3b). In terms of energy consumptions per unit volume, values of 1.4, 4.9 and 48 kWh m⁻³ were attained after 240 min of PEF-UVA-BDD process for j of 10, 25 and 100 mA cm⁻², respectively.

H₂O₂ was accumulated in excess during all reaction time for all systems, thus guaranteeing the maximum production of •OH from Fenton's reaction (21). Large concentrations of 73-591 mg L⁻¹ were available in the PEF-UVA-BDD system at j of 100 mA cm⁻², whereas much lower contents of 5-13 and 30-61 mg L⁻¹ were accumulated at j 10 and 25 mA cm⁻², respectively (see Figure 6.3c).

Figure 6.3d reveals that a j of 10 mA cm⁻² was not able to degrade the total dissolved polyphenols, whereas these compounds attained concentrations up to 2.6 and 0.31 mg caffeic acid equivalent L⁻¹ for j 25 and 100 mA cm⁻² after 180 and 120 min of reaction, respectively.

Taking into account the above outcomes, 25 mA cm⁻² can be selected as a pertinent j value for the degradation of the winery wastewater since (i) a high DOC removal of 84% was achieved at 240 min of PEF-UVA-BDD treatment; (ii) moderate energy consumptions of 61 kWh (kg DOC)⁻¹ and 4.9 kWh m⁻³ were spent at 240 min; (iii) the moderate content of accumulated H₂O₂ may ensure the presence of this species under SPEF-BDD conditions since Fe³⁺ regeneration to Fe²⁺ is favored accordingly to Eqs. (28) and (29) and hence the H₂O₂ consumption is expected to be greater compared to that of PEF-UVA-BDD; and (iv) the total dissolved polyphenols can reach almost null values.

6.3.3.4 Comparison of AO-H₂O₂, EF, PEF-UVA and SPEF processes

AO-H₂O₂-BDD, EF-BDD, PEF-UVA-BDD and SPEF-BDD treatments were applied to the degradation of the biologically treated winery wastewater using pH of 2.8, 25 °C, [TDI]₀ of 35 mg L⁻¹ in EAOPs based on Fenton's reaction chemistry, and *j* of 25 mA cm⁻². Figure 6.4a shows that the relative oxidation ability to remove DOC increased in the sequence AO-H₂O₂-BDD < EF-BDD < PEF-UVA-BDD ≤ SPEF-BDD. As can be seen in Table 6.3, quite similar *k*_{DOC} values for SPEF-BDD and PEF-UVA-BDD were obtained and the much slower degradations for EF-BDD and AO-H₂O₂-BDD were not able to be described by a pseudo-first order kinetic model. The low DOC abatement achieved in AO-H₂O₂-BDD can be mainly related to a small reaction rate of the organic matter with BDD(•OH) generated through Eq. (1). In EF-BDD, the presence of •OH in the bulk formed from Fenton's reaction (21) and their high potential to destroy organic compounds improved DOC removal. The faster DOC decay in PEF-UVA-BDD suggests a crucial effect of the extra •OH production under UVA light from the photolysis of FeOH²⁺ via Eq. (28) along with the possible direct photolysis of complexes formed between Fe³⁺ and some organic intermediates, according to the general Eq. (29). Surprisingly, the slightly more potent UV intensity supplied by sunlight compared to the UVA radiation here provided and the ability of this radiation source to emit in the visible region only had a little improvement on DOC removal, both in terms of time and accumulated UV energy (see inset panel of Figure 6.4a), in contrast to what happened in Chapters 3 and 4. This points to the formation of persistent organic intermediates hardly degraded by BDD(•OH), •OH in the bulk and/or photodecomposed even under sunlight.

On the other hand, H₂O₂ was always available in all EAOPs and was accumulated in smaller extent in the order AO-H₂O₂-BDD > EF-BDD > PEF-UVA-BDD > SPEF-BDD (see Figure 6.4b), as predicted by the increasing rate of Fe³⁺ regeneration to Fe²⁺ of these EAOPs. During the SPEF-BDD process, the H₂O₂ concentration diminished to very low values, 4-9 mg L⁻¹, when more pronounced DOC abatement was patent, 60-120 min, which confirms the operation at *j* of 25 mA cm⁻² as a good option since lower *j* might not ensure the H₂O₂ occurrence during all the SPEF-BDD process.

Figure 6.4c outlines that the AO-H₂O₂-BDD and EF-BDD processes were ineffective on the total dissolved polyphenols degradation. In contrast, the SPEF-BDD treatment was able to reduce these compounds to values as low as 0.4 mg caffeic acid equivalent L⁻¹ after a short time of 120 min, whereas the PEF-UVA-BDD process reduced polyphenols concentration up to 2.6 mg caffeic acid equivalent L⁻¹ at 180 min.

The SPEF-BDD process under the best conditions considered in the current study reached DOC and COD removals of 86% and 68%, respectively, in relation to the biologically treated effluent after 240 min of treatment (accumulated UV energy of 8.6 kJ L^{-1}), with energy consumptions of $45 \text{ kWh (kg DOC)}^{-1}$ and 5.1 kWh m^{-3} . Figure 6.4d reveals that the COD decay was similar (for times below 90 min) or lower (for times above 90 min) than the DOC abatement, thereby suggesting a contribution of the particulate organic compounds to the COD value. A decrease of 54% in the total nitrogen content was observed during the SPEF-BDD process (see Table 6.1), which can be linked with the retention of some non-dissolved *N*-compounds into the precipitate during the EAOP since the total dissolved nitrogen remained unaffected. Table 6.1 also shows that at 240 min of SPEF-BDD, COD and BOD_5 complied with the Portuguese and the European legislation limits for discharge of WWTPs final effluents (Decree-Law no. 236/98 and Directive no. 91/271/CEE, respectively), in contrast with TSS, total nitrogen and total phosphorous parameters (total phosphorous only exceeded the European limit). Moreover, color, odor, ammonium, nitrate and sulfate parameters were in agreement with the Portuguese targets, but pH and [TDI] surpassed the limits. In this context, the final SPEF-BDD solution was neutralized to pH of 6.2 with subsequent sedimentation for 30 min with a resultant supernatant effluent displaying a [TDI] below the LOD (0.13 mg L^{-1}), a total phosphorous concentration of 0.35 mg L^{-1} and 55 mg TSS L^{-1} but without change on total nitrogen. Therefore, besides the application of a further step comprising the effluent neutralization and subsequent precipitation of the settleable compounds, the initial biological oxidation should be enhanced and include nitrifying and denitrifying bacteria to promote total nitrogen release as nitrogen gas. The neutralization/precipitation step led to the formation of 26 mL of sludge per L of treated winery wastewater that require further adequate treatment.

Regarding the combination of the biological oxidation and SPEF-BDD processes, very high abatements on DOC, COD and BOD_5 parameters of ca. 99% were attained, which is in agreement with the great COD removals of 95% and above 99% accomplished by Anastasiou et al. [23] and Lucas et al. [27] for the combination of a biological oxidation and a further PF or Fenton process, respectively.

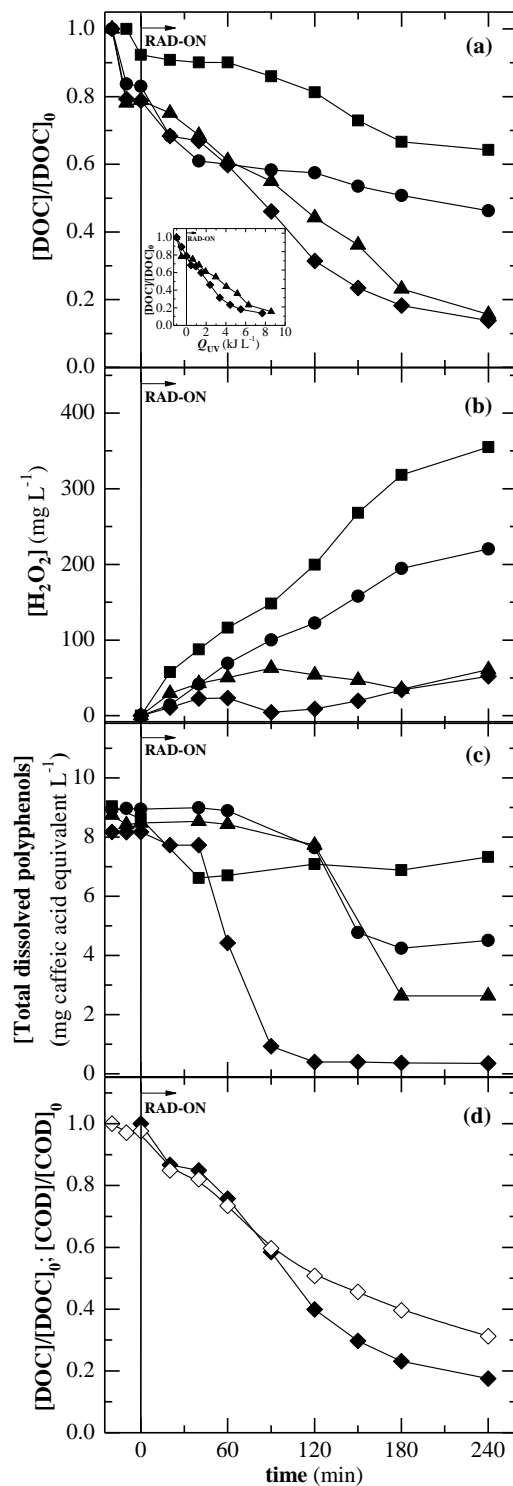


Figure 6.4. Evaluation of (a) normalized DOC removal, (b) H₂O₂ concentration and (c) total dissolved polyphenols concentration decay as a function of time for treatment of the winery wastewater after biological oxidation by various EAOPs using pH of 2.8, 25 °C, [TDI]₀ of 35 mg L⁻¹ in EF-BDD, PEF-UVA-BDD and SPEF-BDD, and *j* of 25 mA cm⁻². EAOP: (■) AO-H₂O₂-BDD, (●) EF-BDD, (▲) PEF-UVA-BDD and (◆) SPEF-BDD. The inset panel of Figure 6.4a depicts the normalized DOC removal in PEF-UVA-BDD and SPEF-BDD systems as a function of accumulated UV energy per L of solution. (d) SPEF-BDD process assessment in terms of (◆) normalized DOC removal and (◇) normalized COD removal.

6.3.3.5 Evolution of generated carboxylic acids and inorganic ions during EAOPs

The ion-exclusion HPLC analysis of LMCA revealed the formation of oxalic and malic acids during AO-H₂O₂-BDD, EF-BDD, PEF-UVA-BDD and SPEF-BDD treatments using pH of 2.8, 20 °C, [TDI]₀ of 35 mg L⁻¹ in EAOPs based on Fenton's reaction chemistry, and *j* of 25 mA cm⁻². These acids are expected to be formed from the oxidative cleavage of the benzenic ring of aromatic intermediates [28]. Malic acid can be subsequently transformed into oxalic acid, which is an ultimate acid that can be directly mineralized to CO₂ [29-31]. Malic and oxalic acids may be primordially present in solution as Fe(III)-carboxylate complexes because the iron is mainly available as Fe³⁺ during the processes. Figure 6.5a illustrates that in the AO-H₂O₂-BDD process the LMCA were accumulated in very low amounts with a contribution never higher than 1.2% for DOC, suggesting inefficiency of this process to convert high-molecular aromatic compounds into the simple LMCA, in corroboration with the low mineralization attained. In contrast, in EF-BDD both acids were accumulated in larger extent with maximum concentrations of ca. 10 mg C L⁻¹ for oxalic acid (see Figure 6.5b) and ca. 5 mg C L⁻¹ for malic acid (see Figure 6.5c), corresponding to 24% of DOC the end of the process (see Figure 6.5a). In PEF-UVA-BDD and SPEF-BDD, both oxalic and malic acids were accumulated in low extent, below 3.0 mg C L⁻¹ (Figures 6.5b,c), which might be related to a fast photolysis rate both of Fe(III)-oxalate and Fe(III)-malate complexes.

The mineralization of organic compounds is expected to be followed by the loss of their nitrogen and sulfur atoms in the form of inorganic ions such as ammonium, nitrate, nitrite and sulfate. In the SPEF-BDD process under the best conditions, nitrite was not found as expected due to their instability in strong oxidant media. Ammonium, nitrate and total dissolved nitrogen concentrations remained almost unaffected, suggesting the inability of SPEF-BDD to degrade dissolved recalcitrant organic *N*-compounds. As aforementioned, total nitrogen decreased in an extent of 54%, pointing to the retention of non-dissolved *N*-compounds into the precipitate. On the other hand, sulfate was gradually released into the solution up to ca. 150 mg L⁻¹ at 240 min, which can be mainly attributed to the dissolution of sulfate retained in the foam and also to a possible degradation of organic compounds containing sulfur in their structure.

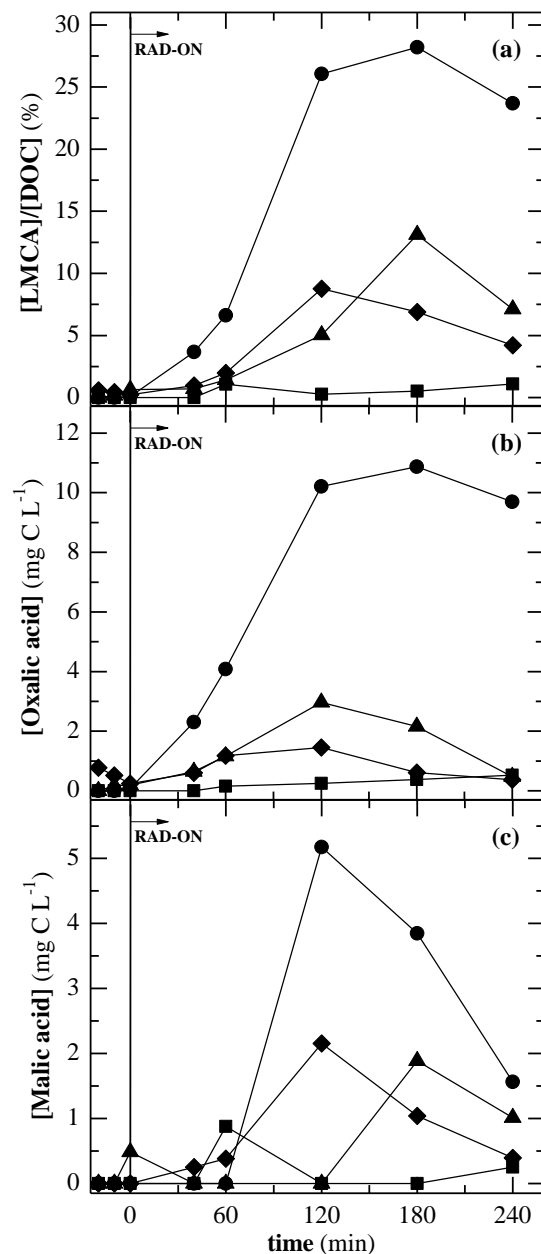


Figure 6.5. Time course of (a) percentage of [LMCA]/[DOC] ratio and concentration of (b) oxalic and (c) malic acids during the (■) AO-H₂O₂-BDD, (●) EF-BDD, (▲) PEF-UVA-BDD and (◆) SPEF-BDD processes of Figure 6.4.

6.3.4 Biodegradability during SPEF-BDD process

As abovementioned, alternatively to the application of a SPEF-BDD process to achieve organic loads in agreement with the discharge limits, the electrochemical process can be applied as a pre-treatment to transform recalcitrant compounds into simpler ones that can be subsequently biodegraded, thereby reducing the overall cost of the treatment. In this context, the biodegradability of the winery wastewater was assessed throughout the SPEF-BDD process using

pH of 2.8, 20 °C, $[TDI]_0$ of 35 mg L⁻¹ and j of 25 mA cm⁻² by means of respirometry assays. Figure 6.6 reveals the bCOD/[COD] ratios attained throughout the treatment. Maximum bCOD/[COD] of 0.1 were achieved for times of 40 and 90 min, corresponding to low biodegradable samples according to Ballesteros Martín et al. [32]. However, the short times employed in the respiration tests, ca. 30 min, could be insufficient to degrade the total content of slowly biodegradable organic matter [33], and, furthermore, the applied biomass was not adapted to degrade the organic matrix of the winery wastewater, probably reaching lower efficiencies than an adapted biomass test as Zahn-Wellens.

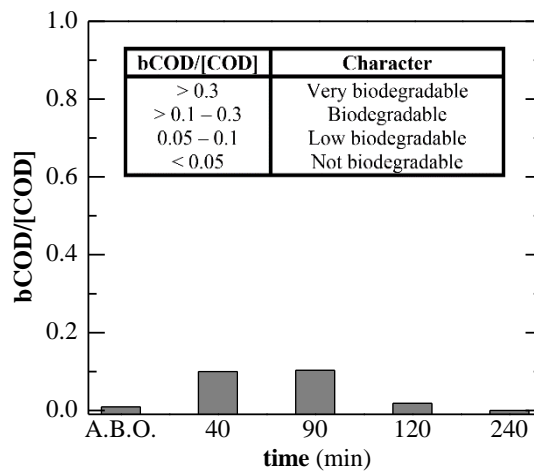


Figure 6.6. Biodegradability of samples collected at different times of a SPEF-BDD treatment under conditions of Figure 6.4 assessed by respirometry. The inset panel depicts the biodegradable character of a sample according to its bCOD/[COD] ratio. A.B.O.: Winery wastewater after biological oxidation.

6.4 Conclusions

The raw winery wastewater exhibited a high biodegradability and, as a consequence, the biological oxidation treatment attained high DOC, COD and BOD₅ removals as high as above 97%. However, the biologically treated effluent was composed of a bioresistant organic fraction comprising 130 mg L⁻¹ of DOC, 380 mg O₂ L⁻¹ of COD and 8.2 mg caffeic acid equivalent L⁻¹ of total dissolved polyphenols and a subsequent EAOP was then employed to mineralize the recalcitrant compounds or transform them into simpler ones. A [TDI]₀ of 35 mg L⁻¹ and *j* of 25 mA cm⁻² were chosen as the best values for the degradation of the bio-treated winery wastewater by PEF-UVA-BDD at pH of 2.8 and 25 °C. Under these conditions, the relative oxidative capability of EAOPs increased in the order AO-H₂O₂-BDD < EF-BDD < PEF-UVA-BDD ≤ SPEF-BDD, with DOC removals on the biologically treated effluent of 36%, 54%, 84% and 86%, respectively, after 240 min of reaction. The poor DOC removal attained in AO-H₂O₂-BDD revealed a small ability of BDD(•OH) generated at the anode surface to react with recalcitrant winery wastewater compounds. In EF-BDD, the production of •OH in the bulk increased the mineralization process. In PEF-UVA-BDD and SPEF-BDD processes, the additional •OH production induced by UVA or solar radiation, respectively, along with the possible direct photolysis of complexes formed between Fe³⁺ and some organic intermediates, led to the fastest reaction rates. The SPEF-BDD process under the best conditions chosen in the present study attained removals of 86% for DOC and 68% for COD regarding the biologically treated effluent after 240 min of treatment, with energy consumptions of 45 kWh (kg DOC)⁻¹ and 5.1 kWh m⁻³ and UV energy consumption of 7.7 kJ L⁻¹. At this time of SPEF-BDD, a total dissolved polyphenols content of 0.35 mg caffeic acid equivalent L⁻¹ was found and color, odor, COD, BOD₅, ammonium, nitrate and sulfate parameters complied with the European and/or Portuguese legislation limits for discharge of WWTPs final effluents. However, to achieve total nitrogen, total phosphorous, pH, [TDI] and TSS targets to discharge the winery wastewater into the environment, the biological oxidation treatment must be optimized to provide the removal of nitrogen and additional neutralization and precipitation steps should succeed the SPEF-BDD process. The respirometry assays revealed low biodegradability enhancement along the SPEF-BDD process.

6.5 References

- [1] Ioannou, L.A., Fatta-Kassinos, D., 2013. Solar photo-Fenton oxidation against the bioresistant fractions of winery wastewater. *Journal of Environmental Chemical Engineering* 1(4), 703-712.
- [2] Orescanin, V., Kollar, R., Nad, K., Mikelic, I.L., Gustek, S.F., 2013. Treatment of winery wastewater by electrochemical methods and advanced oxidation processes. *Journal of Environmental Science and Health - Part A Toxic/Hazardous Substances and Environmental Engineering* 48(12), 1543-1547.
- [3] Silva, F., Pirra, A., Sousa, J., Arroja, L., Capela, I., 2011. Biodegradation kinetics of winery wastewater from port wine production. *Chemical and Biochemical Engineering Quarterly* 25(4), 493-499.
- [4] Souza, B.S., Moreira, F.C., Dezotti, M.W.C., Vilar, V.J.P., Boaventura, R.A.R., 2013. Application of biological oxidation and solar driven advanced oxidation processes to remediation of winery wastewater. *Catalysis Today* 209, 201-208.
- [5] Petruccioli, M., Cardoso Duarte, J., Eusebio, A., Federici, F., 2002. Aerobic treatment of winery wastewater using a jet-loop activated sludge reactor. *Process Biochemistry* 37(8), 821-829.
- [6] Chapman, J., Baker, P., Wills, S., 2001. *Winery Wastewater Handbook: Production, Impacts and Management*, Winetitles, Adelaide, Australia.
- [7] Lucas, M.S., Peres, J.A., Li Puma, G., 2010. Treatment of winery wastewater by ozone-based advanced oxidation processes (O_3 , O_3/UV and $O_3/UV/H_2O_2$) in a pilot-scale bubble column reactor and process economics. *Separation and Purification Technology* 72(3), 235-241.
- [8] Lucas, M.S., Mosteo, R., Maldonado, M.I., Malato, S., Peres, J.A., 2009. Solar photochemical treatment of winery wastewater in a CPC reactor. *Journal of Agricultural and Food Chemistry* 57(23), 11242-11248.
- [9] Mosteo, R., Ormad, P., Mozas, E., Sarasa, J., Ovelleiro, J.L., 2006. Factorial experimental design of winery wastewaters treatment by heterogeneous photo-Fenton process. *Water Research* 40(8), 1561-1568.
- [10] Monteagudo, J.M., Durán, A., Corral, J.M., Carnicer, A., Frades, J.M., Alonso, M.A., 2012. Ferrioxalate-induced solar photo-Fenton system for the treatment of winery wastewaters. *Chemical Engineering Journal* 181-182, 281-288.
- [11] Oller, I., Malato, S., Sánchez-Pérez, J.A., 2011. Combination of advanced oxidation processes and biological treatments for wastewater decontamination-A review. *Science of the Total Environment* 409(20), 4141-4166.
- [12] Colin, T., Bories, A., Sire, Y., Perrin, R., 2005. Treatment and valorisation of winery wastewater by a new biophysical process (ECCF). *Water Science & Technology* 51(1), 99-106.
- [13] Ioannou, L., Velegraki, T., Michael, C., Mantzavinos, D., Fatta-Kassinos, D., 2013. Sunlight, iron and radicals to tackle the resistant leftovers of biotreated winery wastewater. *Photochemical & Photobiological Sciences* 12(4), 664-670.

- [14] Ioannou, L., Michael, C., Kyriakou, S., Fatta-Kassinos, D., 2014. Solar Fenton: From pilot to industrial scale application for polishing winery wastewater pretreated by MBR. *Journal of Chemical Technology & Biotechnology* 89(7), 1067-1076.
- [15] Wang, L.K., Shammas, N.K., Hung, Y.-T.E., 2009. *Advanced Biological Treatment Processes, Handbook of Environmental Engineering, Vol. 9*, Humana Press, New York, United States.
- [16] Pignatello, J.J., 1992. Dark and photoassisted Fe³⁺-catalyzed degradation of chlorophenoxy herbicides by hydrogen peroxide. *Environmental Science & Technology* 26(5), 944-951.
- [17] De Laat, J., Truong Le, G., Legube, B., 2004. A comparative study of the effects of chloride, sulfate and nitrate ions on the rates of decomposition of H₂O₂ and organic compounds by Fe(II)/H₂O₂ and Fe(III)/H₂O₂. *Chemosphere* 55(5), 715-723.
- [18] Safarzadeh-Amiri, A., Bolton, J.R., Cater, S.R., 1996. Ferrioxalate-mediated solar degradation of organic contaminants in water. *Solar Energy* 56(5), 439-443.
- [19] Benkelberg, H.-J., Warneck, P., 1995. Photodecomposition of iron(III) hydroxo and sulfato complexes in aqueous solution: Wavelength dependence of OH and SO₄⁻ quantum yields. *The Journal of Physical Chemistry* 99(14), 5214-5221.
- [20] Neta, P., Huie, R.E., Ross, A.B., 1988. Rate constants for reactions for inorganic radicals in aqueous solution. *Journal of Physical and Chemical Reference Data Reprints* 17(3), 1027-1247.
- [21] Schecher, W.D., McAvoy, D.C., 2007. *MINEQL+: A Chemical Equilibrium Modeling System, Version 4.6 for Windows*, Environmental Research Software, Hallowell, United States.
- [22] Martínez-Huitle, C.A., Ferro, S., 2006. Electrochemical oxidation of organic pollutants for the wastewater treatment: Direct and indirect processes. *Chemical Society Reviews* 35, 1324-1340.
- [23] Anastasiou, N., Monou, M., Mantzavinos, D., Kassinos, D., 2009. Monitoring of the quality of winery influents/effluents and polishing of partially treated winery flows by homogeneous Fe(II) photo-oxidation. *Desalination* 248(1-3), 836-842.
- [24] Soares, P., Silva, T.C.V., Manenti, D., Souza, S.A.G.U., Boaventura, R.R., Vilar, V.P., 2014. Insights into real cotton-textile dyeing wastewater treatment using solar advanced oxidation processes. *Environmental Science and Pollution Research* 21(2), 932-945.
- [25] Garcia-Segura, S., Almeida, L.C., Bocchi, N., Brillas, E., 2011. Solar photoelectro-Fenton degradation of the herbicide 4-chloro-2-methylphenoxyacetic acid optimized by response surface methodology. *Journal of Hazardous Materials* 194, 109-118.
- [26] Salazar, R., Garcia-Segura, S., Ureta-Zañartu, M.S., Brillas, E., 2011. Degradation of disperse azo dyes from waters by solar photoelectro-Fenton. *Electrochimica Acta* 56(18), 6371-6379.
- [27] Lucas, M.S., Mouta, M., Pirra, A., Peres, J.A., 2009. Winery wastewater treatment by a combined process: Long term aerated storage and Fenton's reagent. *Water Science and Technology* 60(4), 1089-1095.
- [28] Brillas, E., Sirés, I., Oturan, M.A., 2009. Electro-Fenton process and related electrochemical technologies based on Fenton's reaction chemistry. *Chemical Reviews* 109(12), 6570-6631.

- [29] Oturan, M.A., Pimentel, M., Oturan, N., Sirés, I., 2008. Reaction sequence for the mineralization of the short-chain carboxylic acids usually formed upon cleavage of aromatics during electrochemical Fenton treatment. *Electrochimica Acta* 54(2), 173-182.
- [30] Vel Leitner, N.K., Doré, M., 1997. Mécanisme d'action des radicaux OH· sur les acides glycolique, glyoxylique, acétique et oxalique en solution aqueuse: Incidence sur la consommation de peroxyde d'hydrogène dans les systèmes H₂O₂/UV et O₃/H₂O₂. *Water Research* 31(6), 1383-1397.
- [31] Garcia-Segura, S., Brillas, E., 2011. Mineralization of the recalcitrant oxalic and oxamic acids by electrochemical advanced oxidation processes using a boron-doped diamond anode. *Water Research* 45(9), 2975-2984.
- [32] Ballesteros Martín, M.M., Casas López, J.L., Oller, I., Malato, S., Sánchez Pérez, J.A., 2010. A comparative study of different tests for biodegradability enhancement determination during AOP treatment of recalcitrant toxic aqueous solutions. *Ecotoxicology and Environmental Safety* 73(6), 1189-1195.
- [33] Kümmerer, K., Alexy, R., Hüttig, J., Schöll, A., 2004. Standardized tests fail to assess the effects of antibiotics on environmental bacteria. *Water Research* 38(8), 2111-2116.

7 Incorporation of electrochemical advanced oxidation processes in a multistage strategy for sanitary landfill leachate remediation

The technical feasibility of including EAOPs in a multistage strategy for remediation of a sanitary landfill leachate was assessed. This treatment approach embraced: (i) a first biological treatment to remove the biodegradable organic fraction, oxidize ammonium and reduce alkalinity, (ii) a coagulation of the bio-treated leachate to precipitate humic acids and suspended solids, followed by separation of the clarified effluent, and (iii) the oxidation of the resulting effluent by an EAOP to degrade the recalcitrant organic matter and increase its biodegradability so that a second biological process for removal of biodegradable organics and nitrogen content could be applied. The influence of j on PEF-UVA-BDD process was firstly assessed. The oxidation ability of various EAOPs such EF-BDD with two distinct $[TDI]_0$, PEF-UVA-BDD and SPEF-BDD was further evaluated and these processes were compared with the analogous chemical ones. A detailed assessment of the two first treatment stages was made and the biodegradability enhancement during the SPEF process was determined by a Zahn-Wellens test to define the ideal organics oxidation state to stop the EAOP and apply the second biological treatment. The relative oxidation ability of EAOPs increased in the order EF-BDD- $[TDI]_0$ of 12 mg L⁻¹ < EF-BDD- $[TDI]_0$ of 60 mg L⁻¹ < PEF-UVA-BDD- $[TDI]_0$ of 60 mg L⁻¹ ≤ SPEF-BDD- $[TDI]_0$ of 60 mg L⁻¹, using pH of 2.8, 20 °C and j of 200 mA cm⁻². While EF-BDD process was much superior to the Fenton one, the superiority of PEF-UVA over PF-UVA was less evident and SPEF-BDD attained similar degradation to SPF. To provide a final DOC of 163 mg L⁻¹ to fulfill the discharge limits into the environment after a second biological process, 6.2 kJ L⁻¹ UV energy and 36 kWh m⁻³ electrical energy were consumed using SPEF-BDD.

This Chapter is based on the following research article: “Moreira, F.C., Soler, J., Fonseca, A., Saraiva, I., Boaventura, R.A.R., Brillas, E., Vilar, V.J.P., 2015. Incorporation of electrochemical advanced oxidation processes in a multistage treatment system for sanitary landfill leachate. Water Research 81, 375-387”.

7.1 Introduction

Municipal solid waste is predominantly disposed of into sanitary landfills, where the percolation of rainfall in combination with the decomposition of the solid wastes by simultaneous and interrelated biological, chemical and physical changes leads to the generation of a highly contaminated liquid called “leachate” [1]. The landfill leachate can reach the adjacent surface and groundwater, thus causing potentially serious hazards on the surrounding environment and public health [2]. The characteristics of the landfill leachate depend on diverse factors such as the amount, composition and moisture of the municipal solid waste, age of the landfill, hydrogeology and climate of the site and seasonal weather variations [3]. Four main groups of pollutants are present in this effluent: (i) dissolved organic matter, including volatile fatty acids and more recalcitrant compounds such as humic and fulvic acids, (ii) inorganic ions like chloride and ammonium, (iii) heavy metals like cadmium, chromium, copper, lead, nickel and zinc, and (iv) xenobiotic organic compounds originated from household or industrial chemicals (aromatic hydrocarbons, phenols, chlorinated aliphatics, pesticides and plastizers), available in low contents below 1 mg L^{-1} [4].

In recent years, several technologies have been applied to landfill leachate remediation such as: (i) biological treatments (aerobic and anaerobic) [5-7], (ii) physical/chemical methods (flotation, coagulation/flocculation, AC, air stripping, ion exchange and membrane separation processes such as MF, NF, UF and RO) [5-8], (iii) AOPs such as ozone and ozone based processes (O_3 , O_3/UV , $\text{O}_3/\text{UV}/\text{H}_2\text{O}_2$), TiO_2/UV photocatalysis, Fenton, PF and SPF [5-7], and (iv) AO process [9]. To the best of our knowledge, the degradation of sanitary landfill leachates by EF, PEF and SPEF has not been reported yet.

Due to the complexity and recalcitrant nature of the landfill leachate matrix and in order to reduce the total cost of the treatment, strategies based on integrated biological-physical-chemical techniques have been under focus [10-14]. Recently, Vilar and co-workers in cooperation with *Efacec Engenharia e Sistemas, S.A.* company have published an European Patent (EP 2 784 031) [15] concerning an innovative integrated treatment strategy for raw sanitary landfill leachate including the following treatment steps: (i) initial biological process for removal of biodegradable organic compounds, nitrification/denitrification reactions and alkalinity reduction; (ii) coagulation with subsequent separation of the formed sludge for the

removal of humic acids, suspended solids and other species filtering the radiation; (iii) PF and/or SPF processes for recalcitrant compounds degradation and biodegradability enhancement; and (iv) final biological polishing step to reduce organic matter and nitrogen to values in agreement with the discharge limits into the environment. One of the main drawbacks of the PF/SPF processes is related with the high H₂O₂ consumption, turning these technologies too costly and originating H₂O₂ delivery constraints in isolated areas [16]. In this context, the alternative use of quite similar processes based on H₂O₂ electrogeneration can be a very interesting solution.

The current Chapter is focused on the integration of EAOPs like EF, PEF and SPEF in the third step of the multistage strategy based on the aforementioned patented technology for the remediation of raw sanitary landfill leachates. The influence of j on PEF-UVA-BDD process was firstly assessed and at the best attained conditions the comparative efficiency of EF-BDD with two distinct [TDI]₀, PEF-UVA-BDD and SPEF-BDD treatments was evaluated. Further comparison of EAOPs with the analogous chemical processes was examined. Moreover, the biological oxidation and coagulation treatment steps preceding the EAOP were assessed in detail and the biodegradability enhancement along the SPEF process was determined by means of a Zahn-Wellens test to define the ideal organics oxidation state for further application of the second biological treatment.

7.2 Materials and methods

All chemicals, analytical determinations, modeling of degradation kinetics and experimental units and procedures can be accessed in the Chapter 2. Table 2.5 summarizes the operational conditions of EAOPs and AOPs performed in the current Chapter.

The leachate was collected in March and April 2014 from a municipal solid waste sanitary landfill located nearby Porto, Portugal, in operation since 1999 and enlarged in 2010. Before collection, the landfill leachate underwent a pre-treatment in an aerated lagoon situated onsite through an activated sludge biological process under both aerobic and anoxic conditions, promoting partial elimination of BOD₅, COD and DOC together with partial ammonium oxidation and nitrogen removal. For simplicity purposes, this effluent will be nominated as raw landfill leachate. Table 7.1 displays its main physicochemical characteristics.

Table 7.1. Physicochemical characterization of sanitary landfill leachate along the various stages of treatment: raw, after 6-7 days of biological process, after coagulation, after aeration, after SPEF-BDD/neutralization/clarification and after 28 days of Zahn-Wellens test. The discharge limits for WWTPs final effluents according to Portuguese legislation (Decree-Law no. 236/98) and European Directive no. 91/271/CEE are also displayed.

Parameter (units)	Sanitary landfill leachate						ELV ^d for Decree-Law no. 236/98 or Directive no. 91/271/CEE
	Raw	After biological process ^a	After coagulation ^b	After aeration ^b	After SPEF-BDD, neutralization and clarification ^c	After 28 days of Zahn-Wellens	
Color	Very dark brown	Very dark brown	Moderate yellowish brown	Moderate yellowish brown	Very light yellow	Very light yellow	-
Color (diluted 1:20)	d. ^e	d. ^e	d. ^e	d. ^e	n.d. ^f	n.d. ^f	n.d. ^f or -
Odor	Very strong	Weak	Very weak	Very weak	Very weak	n.d. ^f	-
Odor (diluted 1:20)	d. ^e	d. ^e	n.d. ^f	n.d. ^f	n.d. ^f	n.d. ^f	n.d. ^f or -
pH	8.2-9.0	7.0-8.0	2.7-3.4	2.2-2.9	6.2	7.5	6.0-9.0 or -3 °C
Temperature (°C)	20	20	20	20	20	20	increase ^g or -
Conductivity (mS cm ⁻¹)	21.0-23.3	18.8-22.0	18.0-21.0	18.9-20.3	19.6	-	-
Alkalinity (mg CaCO ₃ L ⁻¹)	7623-10593	419-772	n.d. ^f	n.d. ^f	n.d. ^f	-	-
Redox potential (mV)	-396 to -377	176-191	477-505	532-576	636	-	-
Turbidity (NTU)	43-64	5-8	5-8	5-6	1.7	-	-
TDC (mg L ⁻¹)	3172-4124	967-1081	337-403	337-403	164	70	-
DIC (mg L ⁻¹)	1950-2664	11-20	0.0-1.1	0.0-2.6	0.8	0.9	-
DOC (mg L ⁻¹)	1222-1460	956-1062	335-386	337-430	163	69	-
COD (mg O ₂ L ⁻¹)	3106-4057	2870-3201	1135-1690	1030-1505	290	102	150 or 125
BOD ₅ (mg O ₂ L ⁻¹)	180-300	16-18	2-14	1-10	60	15	40 or 25
BOD ₅ /COD	0.04-0.1	0.005-0.01	0.002-0.008	0.001-0.007	0.2	-	-
TDI (mg L ⁻¹)	2.2-3.0	2.5-3.0	3.4-18	11-21	<0.13 ^h	<0.13 ^h	2.0 or -
SUVA ₂₅₄ (L mg ⁻¹ m ⁻¹)	2.2-2.8	2.4-2.8	1.5-2.0	1.5-2.8	3.3	-	-
TSS (mg L ⁻¹)	525-630	441-580	145-250	140-230	33	31	60 or 35
VSS (mg L ⁻¹)	390-490	176-280	80-167	72-138	14	13	-
Total nitrogen (mg L ⁻¹)	2275-2550	2250-2675	1575-2050	1450-2050	1289	1146	15 or 10
Total dissolved nitrogen (mg L ⁻¹)	1833-1966	1833-2181	1362-1376	1138-1256	1160	1090	-
Total dissolved organic nitrogen (mg L ⁻¹)	391-600	286-557	165-327	46-64	20	19	-
Ammonium – N-NH ₄ ⁺ (mg L ⁻¹)	1300-1355	<0.04 ^h -20	<0.04 ^h -9	<0.04 ^h -9	<0.04 ^h	<0.04 ^h	7.8 or -
Nitrite – N-NO ₂ ⁻ (mg L ⁻¹)	49-84	1515-1527	546-694	3-18	1.3	1.6	-
Nitrate – N-NO ₃ ⁻ (mg L ⁻¹)	2-17	23-32	495-503	1035-1192	1139	1069	11 or -
Sulfate – SO ₄ ²⁻ (mg L ⁻¹)	46-120	44-83	1632-1974	1749-1917	1940	1936	2000 or -
Sulfite – SO ₃ ²⁻ (mg L ⁻¹)	98	28-29	2.5-4.7	3.0-4.9	<0.1 ^h	<0.1 ^h	1.0 or -
Sulfide – S ²⁻ (mg L ⁻¹)	1.7-6.5	0.58-0.78	<0.1 ^h	<0.1 ^h	<0.1 ^h	<0.1 ^h	1.0 or -
Chloride – Cl ⁻ (mg L ⁻¹)	2220-2780	2211-2906	2989-3823	3046-3822	3577	3605	-
Total phosphorous (mg L ⁻¹)	15	19-22	0.3-1.3	0.7-1.9	0.6	0.7	10 or 1
Phosphate – PO ₄ ³⁻ (mg L ⁻¹)	<0.02 ^h	<0.02 ^h	<0.02 ^h	<0.02 ^h	<0.02 ^h	<0.02 ^h	-
Bromide – Br ⁻ (mg L ⁻¹)	<0.008 ^h	<0.008 ^h	<0.008 ^h	<0.008 ^h	<0.008 ^h	<0.008 ^h	-
Fluoride – F ⁻ (mg L ⁻¹)	<0.04 ^h	<0.04 ^h	<0.04 ^h	<0.04 ^h	<0.04 ^h	<0.04 ^h	-
Calcium – Ca ²⁺ (mg L ⁻¹)	405-410	350-400	204-321	183-271	178	160	-
Lithium – Li ⁺ (mg L ⁻¹)	<0.004 ^h	<0.004 ^h	<0.004 ^h	<0.004 ^h	<0.004 ^h	<0.004 ^h	-
Magnesium – Mg ²⁺ (mg L ⁻¹)	253-347	142-190	125-152	120-136	130	128	-
Potassium – K ⁺ (mg L ⁻¹)	1948-2281	1901-2336	2152-2347	1948-2402	2387	2379	-
Sodium – Na ⁺ (mg L ⁻¹)	1885-2403	3140-3294	3284-3553	3010-3672	3701	3669	-

^a Without activated sludge;

^b Without coagulation sludge;

^c SPEF-BDD using pH of 2.8, 20 °C, [TDI]₀ of 60 mg L⁻¹ and *j* of 200 mA cm⁻² up to reach 163 mg L⁻¹ of DOC (147 min) and after sludge removal by neutralization to pH of 7.5 and sedimentation for 3 h;

^d ELV – Emission limit value;

^e d. – detected;

^f n.d. – not detected;

^g Comparatively to the receptor medium;

^h LOD.

7.3 Results and discussion

7.3.1 Characteristics of the raw sanitary landfill leachate

As can be seen in Table 7.1, the raw sanitary landfill leachate presented the following main characteristics: (i) very dark brown color that can be associated with the presence of humic acids [17]; (ii) very strong odor; (iii) slight alkaline pH; (iv) high DOC and COD contents with a low biodegradable organic fraction (BOD_5/COD ratio of 0.04-0.1); (v) high nitrogen content mainly due to ammonium (66-74%); (vi) high alkalinity; (vii) very high conductivity of 21.0-23.3 $mS\ cm^{-1}$ and high ionic content corresponding to a high calculated ionic strength of 0.206 M; (viii) absence of phosphate; (ix) low total phosphorous concentration; and (x) very low [TDI] of 2.2-3.0 $mg\ L^{-1}$. While ammonium, total nitrogen, alkalinity, conductivity and total phosphorous values are typically found for landfill leachates from sites within 3-6 years, BOD_5 and COD values are commonly attributed to older landfill leachates [1, 4, 18]. However, in the present study they may be related to the partial removal of biodegradable organic compounds in the aerated lagoon pre-treatment. In fact, the landfill leachate before biological lagooning from the same municipal solid waste sanitary landfill was previously characterized by greater BOD_5 of 1325 $mg\ O_2\ L^{-1}$ and COD of 7426 $mg\ O_2\ L^{-1}$ [13].

7.3.2 Biological treatment

The main goals of the aerobic biological process were to remove biodegradable organic matter, oxidize ammonium ions and consume alkalinity. The biological system was under well-operation as pointed out by: (i) an average SVI for the various batches of 55 $mL\ g^{-1}$, indicative of excellent sludge settling and compaction characteristics, typically between 50 and 100 $mL\ g^{-1}$ [19], and (ii) an average food to microorganism (F/M) ratio based on BOD_5 and VSS of 0.035 g substrate per g biomass per day, which corresponds to an extended aeration process [20]. The totality of data regarding the characteristics of the landfill leachate throughout the various biological treatment batches is not herein displayed. Nevertheless, Figure 7.1 exemplifies one biological treatment batch in terms of DOC and nitrogen content and Table 7.1 shows the characteristics of the landfill leachate at the end of the biological treatment.

The biodegradable organic carbon fraction was almost totally removed after 42-47 h of biological treatment, reaching abatements of 90-95% of BOD₅, 13-33% of DOC and 9-31% of COD. The low removals of DOC and COD suggest that the major organic fraction of the raw landfill leachate, corresponding to 956-1062 mg L⁻¹ of DOC and 2870-3201 mg O₂ L⁻¹ of COD, was composed of bioresistant compounds, probably humic substances [13]. In general, the treatment of landfill leachates by applying activated sludge reactors attains higher COD removals from 29% to 69% [13, 21, 22]. The lower organic removal here achieved can be attributed to the partial removal of biodegradable organic compounds in the upstream biological lagooning, since the applied landfill leachate showed a lower BOD₅ content of 180-300 mg O₂ L⁻¹ in contrast with BOD₅ contents greater than 1000 mg O₂ L⁻¹ for the cited studies. In all cases, the biological process was inefficient for the removal of refractory compounds.

Typically, the biological nitrification process comprises the oxidation of ammonium to nitrite by Eq. (57) and the subsequent oxidation of nitrite to nitrate via Eq. (58) [23].



Metcalf & Eddy [23] and Gerardi [24] stated the following considerations for nitrification: (i) optimum temperature range from 28 to 32 °C; (ii) optimum dissolved oxygen around 3.0 mg L⁻¹; (iii) optimum pH from 6.7 to 8.0; and (iv) alkalinity used as a carbon source by nitrifying bacteria in a ratio of 7.14 mg CaCO₃ per mg N-NH₄⁺ oxidized. Consequently, the conditions employed in the current activated sludge reactor, i.e. temperature of 27 °C, dissolved oxygen of 2-4 mg L⁻¹, pH of 6.5-9.0 and permanent availability of alkalinity, might maximize the nitrification process.

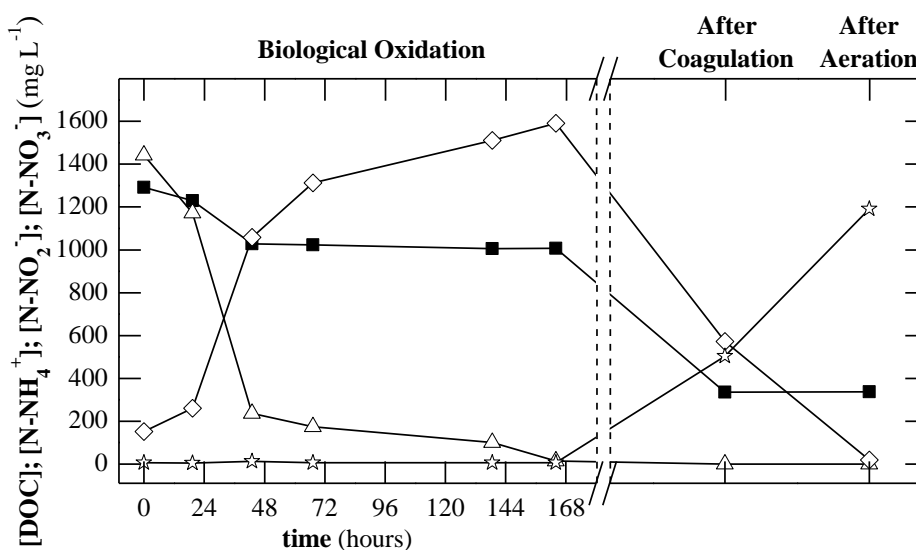


Figure 7.1. Change of (■) DOC, (△) ammonium (N-NH₄⁺), (◇) nitrite (N-NO₂⁻) and (☆) nitrate (N-NO₃⁻) concentrations in a biological process batch of the raw landfill leachate and after coagulation and aeration steps.

The ammonium ion was almost completely oxidized after 42-47 h of biological treatment, with an average specific nitrification rate of 13.6 mg N-NH₄⁺ per h per g VSS, and afterwards it was much more slowly converted since low amounts of Na₂CO₃ were provided for minimal alkalinity at the end of the treatment. This nitrification rate was very acceptable considering values reported in literature of 4.9-12.6 mg N per h per g VSS at 20 °C for a landfill leachate with 1199 mg N-NH₄⁺ L⁻¹ [25], 20.4 mg N-NH₄⁺ per h per g VSS at 24-27 °C for a landfill leachate with 1452 mg N-NH₄⁺ L⁻¹ [26] and 8.2 mg N-NH₄⁺ per h per g VSS at 26.9 °C for a landfill leachate with 3864 mg N-NH₄⁺ L⁻¹ [13]. After 138-164 h, ammonium removals of 98-100% were attained and high amounts of nitrite (1515-1862 mg N-NO₂⁻ L⁻¹) were formed but with almost null oxidation to nitrate (23-32 mg N-NO₃⁻ L⁻¹). The negligible nitrite oxidation might be due to the accumulation of free ammonia and free nitrous acid, which are known inhibitors of nitrite-oxidizing bacteria [27-29]. The overall nitrification process consumed in average 9.3 g CaCO₃ per L of raw leachate or 8.5 mg CaCO₃ per mg N-NH₄⁺, which was only slightly superior to the stoichiometric ratio (7.14 mg CaCO₃ per mg N-NH₄⁺). At the end of the treatment, alkalinity residual values of 419-772 mg CaCO₃ L⁻¹ and very low DIC values of 11-20 mg L⁻¹ were achieved. The total nitrogen was maintained unchanged, indicating null nitrogen gas stripping. Moreover, the biological treatment led to (i) substantial odor minimization, (ii) 70-72% of sulfite oxidation, and (iii) addition of 737-1409 mg Na⁺ L⁻¹ by Na₂CO₃ used to provide alkalinity.

7.3.3 Coagulation/aeration process

The purpose of the coagulation process was to remove humic acids, suspended solids and colloidal particles that are able to act as photons absorbers in the subsequent photo-assisted electrochemical treatments and also to provoke the electrochemical cell clogging. In a first approach, the bio-treated landfill leachate was subjected to coagulation using FeCl_3 at pH of 4.2, according to Saraiva et al. [15]. However, the subsequent EAOP step performed at pH of 2.8 revealed very fast pH decrease up to pH of 2.0 and total oxidation of nitrite to nitrate before reaction start under effluent recirculation in the EAOPs system, together with very low H_2O_2 accumulation during reaction. The pH drop can be attributed to the oxidation of nitrous acid by oxygen via Eq. (59) [30] since the use of the carbon-PTFE air-diffusion cathode introduces high amounts of air in the EAOPs system. Eq. (59) occurs preferentially at pH of 1.0-2.0, whereupon it is decelerated up to attain a very low rate at pH of 4.5, where the equilibrium speciation dictates a higher amount of nitrite ion to that of nitrous acid [30, 31]. On the other hand, the oxidation of nitrite to nitrate can occur in the presence of H_2O_2 by the formation of peroxynitrite (ONOO^-) in acid medium via Eqs. (60) and (61) [32, 33], explaining the low H_2O_2 accumulation.



To avoid the pH decay and the extra consumption of H_2O_2 during the EAOP step, all nitrite ions were previously oxidized to nitrate by performing the coagulation at pH of 3.3 and subjecting the clarified effluent to aeration for 3 h. This pH value was chosen since preliminary tests revealed an almost null nitrite oxidation by aeration at higher pH values and, in addition, a final pH value of 2.2-2.9 was reached, allowing applying the further EAOP with null/almost null pH correction. Note that an alternative strategy for nitrite oxidation by aeration could be to perform coagulation at pH of 4.2 and afterwards decrease the pH to 3.3 to proceed with aeration. However, a previous study on the best pH for coagulation has determined a slight enhancement on coagulation efficiency for pH values below 4.2 (data not shown). Traditional PF processes applied to a landfill leachate with and without nitrite revealed a reduction of 58% on the H_2O_2 consumption for the free-nitrite effluent.

The coagulation of the bio-treated landfill leachate with subsequent clarification achieved: (i) high organics removal of 63-65% of DOC and 44-51% of COD, (ii) TSS and VSS reductions of 57-67% and 40-54%, respectively, (iii) color changing from very dark brown to moderate yellowish brown, and (iv) SUVA₂₅₄ decrease of 27-40% (see Figure 7.1 and Table 7.1). The color changing can be ascribed to the presence of fulvic acids and absence of humic acids [17] and the SUVA₂₅₄ decay can be strongly correlated to the precipitation of humic substances [34]. Saraiva et al. [15] have reported similar organic fraction removal and color minimization, whereas Silva et al. [13] have determined an abatement on humic substances of 37% when a bio-treated landfill leachate was acidified from pH of 8.4 to 3.0. Note that the acidification of the current bio-treated effluent to pH of around 3 only led to 32% of DOC abatement along with color changing to a lighter brown, suggesting the inability of this procedure to precipitate humic acids with the same efficiency as the coagulation step. In addition, nitrogen compounds corresponding to 22-30% of total nitrogen and 26-37% of total dissolved nitrogen were removed during this step. The abatement on the dissolved nitrogen was composed of 19-23% of nitrite and 7-11% of organic nitrogen compounds. Apart from nitrite decay (23-33% of total nitrite), some nitrite ions were oxidized to nitrate ions at an extent of 31-33%.

The subsequent aeration of the coagulated landfill leachate led to total oxidation of nitrite to nitrate, along with a pH decrease to 2.2-2.9 (see Figure 7.1 and Table 7.1). Besides that, the total dissolved organic nitrogen was reduced by 72-80% due to an extra clarification of the effluent.

Moreover, the overall coagulation/aeration step induced to: (i) total/almost total inorganic carbon fraction removal as well as alkalinity; (ii) almost total phosphorous removal likely due to the precipitation of phosphorous compounds; (iii) introduction of high amounts of sulfate ions from 44-83 to 1749-1917 mg L⁻¹; (iv) increase of chloride content from 2211-2906 to 3046-3822 mg L⁻¹; and (vi) presence of a [TDI] of 11-21 mg L⁻¹ from the addition of FeCl₃ that can be applied as catalyst in the subsequent EAOP step based on Fenton's reaction chemistry. A volume of ca. 280 mL of sludge per L of effluent that require proper treatment for further storage in a specific site was also produced.

7.3.4 EAOPs

7.3.4.1 General

The solution conductivity is a key parameter for the treatment of wastewaters by EAOPs as long as high conductivity values allow minimizing the power consumption. The landfill leachate showed a very high conductivity of 18.0-23.3 mS cm⁻¹ along all treatment steps (see Table 7.1), being suitable for EAOPs application. This conductivity was even much higher than 8.6 mS cm⁻¹ of the 7.0 g Na₂SO₄ L⁻¹ solution commonly applied as background electrolyte in EAOPs.

A [TDI]₀ of 60 mg L⁻¹ was used in Fenton's reaction based processes since this iron content was applied by Saraiva et al. [15]. Figure 7.2 shows the Fe³⁺ speciation diagram calculated by the chemical equilibrium modeling system MINEQL+ [35] based on landfill leachate ions average concentration before the EAOP step for a total Fe³⁺ concentration of 60 mg L⁻¹. From this diagram, one can infer that the highest proportion of the most photoactive ferric iron-water complex, i.e. FeOH²⁺ species, occurs at pH of 2.8 (11% of Fe³⁺ molar fraction), together with no iron precipitation as Fe(OH)₃ (s). All trials were then performed at pH of 2.8. A temperature of 20 °C was selected since this is an average ambient temperature commonly found for landfill leachates in Portuguese WWTPs facilities [12].

Extra theoretical calculations using MINEQL+ [35] (data not shown) advised both negative and positive effects from the large sulfate content of the pre-treated landfill leachate compared to the low sulfate content of the raw landfill leachate. On the one hand, lower FeOH²⁺ concentration is expected (7.1 against 10 mg L⁻¹, respectively) and, on the other hand, iron precipitation is avoided (null iron precipitation against 33% of iron precipitation as Fe(OH)₃ (s), respectively). Additional calculations on the chloride content (data not shown) revealed a negligible influence of this species on FeOH²⁺ fraction and iron precipitation. However, chloride ion can be oxidized at the anode surface to form active chlorine species (HClO, ClO⁻ and Cl₂) via Eqs. (5)-(7) that contribute to organics removal [36], although these species can react with organics leading to harmful chlorinated organic by-products. While the high chloride concentration of the landfill leachate favors the electrogeneration of active chlorine species, the H₂O₂ produced at the cathode is a known dechlorination agent for free chlorine, avoiding their accumulation [37]. In fact, free chlorine was detected along reactions in low concentrations below 5.0 mg Cl₂ L⁻¹.

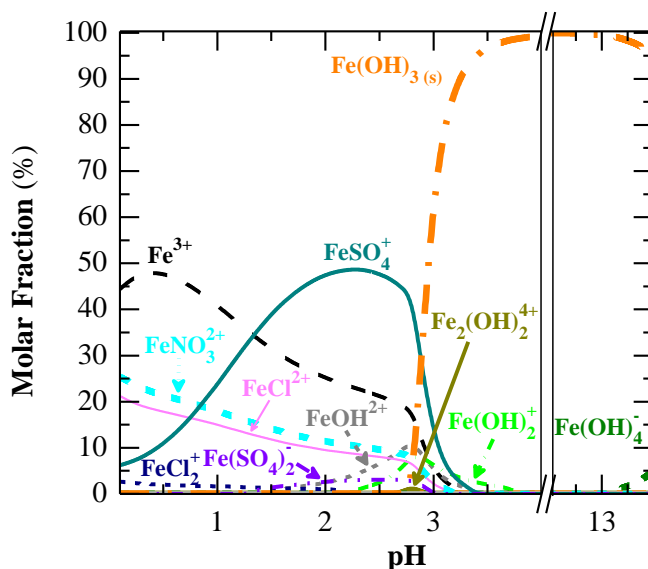


Figure 7.2. Fe^{3+} speciation diagrams as a function of solution pH in a calculated system containing the average amounts of NO_3^- , SO_4^{2-} , Cl^- , Ca^{2+} , Mg^{2+} , K^+ and Na^+ ions of the landfill leachate after aeration (Table 7.1) and 60 mg L^{-1} of Fe^{3+} (ionic strength = 0.390 M). Data were calculated from the chemical equilibrium modeling system MINEQL+ [35] using the equilibrium constants of Table 5.1. The formation of the solid iron phase $\text{Fe}(\text{OH})_3$ was included in the calculation despite the slow formation of solid phases on the time scale of the experiments.

7.3.4.2 Influence of current density on PEF-UVA-BDD process

The pre-treated landfill leachate was subjected to a PEF-UVA-BDD process using pH of 2.8, 20°C , $[\text{TDI}]_0$ of 60 mg L^{-1} and j values from 25 to 300 mA cm^{-2} . The high organic content of the effluent justifies the high j used. Figure 7.3a shows that the rise in j yielded higher DOC removal but this increment was almost negligible from 200 to 300 mA cm^{-2} . The corresponding k_{DOC} values, displayed in Table 7.2, were 1.7 and 2.6/2.7 times higher for j of 100 and 200/300 mA cm^{-2} , respectively, when compared to j of 25 mA cm^{-2} . DOC dropped more sharply in the first 30 min of reaction (2.1 kJ L^{-1} of accumulated radiation), at an extent of 14-33% for all j , whereupon its decay turned slighter. In the same period, Figure 7.3b shows small [TDI] decays near 9-13%. These results suggest that in a first stage more easily degradable compounds were mineralized and some complexes between Fe^{3+} and primary by-products were precipitated. Note that Fe^{3+} did not precipitate in the initial matrix of the pre-treated landfill leachate, in agreement with Figure 7.2 where the precipitation of Fe^{3+} as $\text{Fe}(\text{OH})_3$ (s) is not expected up to pH of 2.9.

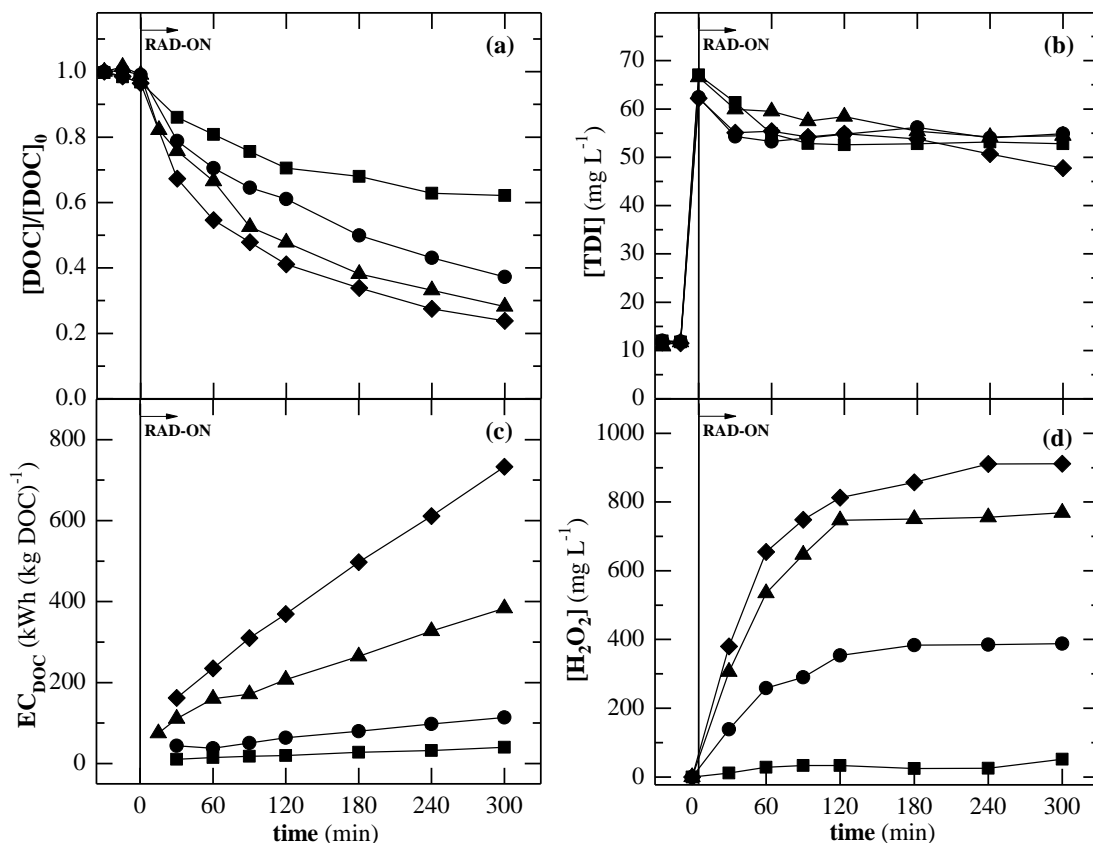


Figure 7.3. Effect of current density on (a) normalized DOC removal, (b) total dissolved iron concentration, (c) specific energy consumption per unit DOC mass and (d) H_2O_2 concentration as a function of time for PEF-UVA-BDD treatment of the pre-treated landfill leachate using pH of 2.8, 20 °C and $[\text{TDI}]_0$ of 60 mg L^{-1} . Current density: (■) 25, (●) 100, (▲) 200 and (◆) 300 mA cm^{-2} .

Table 7.2. Pseudo-first-order kinetic constants for DOC removal (k_{DOC}) along with the corresponding R^2 and S^2_R , obtained for the treatment of the pre-treated landfill leachate under conditions of Figures 7.3a and 7.4a1,b1.

System		$k_{\text{DOC}} (\times 10^{-3} \text{ min}^{-1})$	R^2	$S^2_R (\text{mg}^2 \text{ L}^{-2})$
Effect of j (mA cm^{-2}) on PEF-UVA-BDD	25	1.7 ± 0.1	0.955	50
	100	2.9 ± 0.1	0.996	15
	200	4.3 ± 0.3	0.970	144
	300	4.6 ± 0.3	0.980	99
EAOPs	EF-BDD- $[\text{TDI}]_0$ of 12 mg L^{-1}	1.67 ± 0.04	0.993	19
	EF-BDD- $[\text{TDI}]_0$ of 60 mg L^{-1}	2.3 ± 0.1	0.994	12
	PEF-UVA-BDD- $[\text{TDI}]_0$ of 60 mg L^{-1}	4.3 ± 0.3	0.970	144
	SPEF-BDD- $[\text{TDI}]_0$ of 60 mg L^{-1}	6.0 ± 0.2	0.991	129
AOPs	Fenton	- ^a	- ^a	- ^a
	PF-UVA	3.7 ± 0.1	0.991	53
	SPF	4.6 ± 0.2	0.985	125
PEF-UVA-BDD- $[\text{TDI}]_0$ of 60 mg L^{-1} with initial H_2O_2 addition of 700 mg L^{-1}		3.7 ± 0.2	0.985	109
Photolysis with initial H_2O_2 addition of 700 mg L^{-1}		- ^a	- ^a	- ^a

^aNo fitting of a pseudo-first-order kinetic model to experimental data.

On the other hand, the application of greater j values gave superior energy consumptions, as can be seen in Figure 7.3c. Despite the similar DOC decays at j of 200 and 300 mA cm⁻², an average EC_{DOC} value 1.7 times higher was reached for the higher j . Moreover, Figure 7.3d shows quite similar and very high H₂O₂ accumulations of 535-911 mg L⁻¹ for times above 60 min at j of 200 and 300 mA cm⁻². This suggests the occurrence of parasitic reactions like Eqs. (24), (25), (39) and (40), for j above 200 mA cm⁻² that lead to the formation of smaller relative amounts of BDD(•OH) and •OH in the bulk.

Hence, j of 200 mA cm⁻² can be chosen as the best j value for the PEF-UVA-BDD treatment of the pre-treated landfill leachate in the present study. Note that all tested j values ensured the presence of H₂O₂ during the reaction time, which in turn guaranteed the maximum production of •OH from Fenton's reaction (21).

7.3.4.3 Comparison of EF, PEF-UVA, SPEF, Fenton, PF-UVA and SPF processes

Various EAOPs such as EF-BDD with effluent dissolved iron content, i.e. [TDI]₀ of 12 mg L⁻¹, and EF-BDD, PEF-UVA-BDD and SPEF-BDD with [TDI]₀ of 60 mg L⁻¹ were applied to the degradation of the pre-treated landfill leachate using pH of 2.8, 20 °C and j 200 mA cm⁻². The comparative mineralization ability for these EAOPs is illustrated in Figure 7.4a1 and raised in the sequence EF-BDD-[TDI]₀ of 12 mg L⁻¹ < EF-BDD-[TDI]₀ of 60 mg L⁻¹ < PEF-UVA-BDD-[TDI]₀ of 60 mg L⁻¹ ≤ SPEF-BDD-[TDI]₀ of 60 mg L⁻¹, presenting DOC removals of 34%, 42%, 72% and 78%, respectively, after 300 min of reaction. Table 7.2 shows k_{DOC} values 1.4, 2.6 and 3.6 times higher for EF-BDD-[TDI]₀ of 60 mg L⁻¹, PEF-UVA-BDD and SPEF-BDD, respectively, in comparison with EF-BDD-[TDI]₀ of 12 mg L⁻¹. The DOC abatements attained for PEF-UVA-BDD and SPEF-BDD were very similar either in terms of time (Figure 7.4a1) or accumulated UV energy (Figure 7.4a1.1). These results allow assuming that: (i) the BDD(•OH) radicals formed via Eq. (1) had a large participation on the mineralization process, but they were only able to partially reduce the DOC; (ii) the additional •OH formed from Fenton's reaction (21) in the EF-BDD-[TDI]₀ of 60 mg L⁻¹ only slightly improved the effluent mineralization; (iii) the radiation provided in PEF-UVA-BDD and SPEF-BDD processes had a crucial role on the effluent mineralization (30-36% higher mineralization for PEF-UVA-BDD and SPEF-BDD compared to EF-BDD-[TDI]₀ of 60 mg L⁻¹ after 300 min of reaction) because of the additional •OH production from Eq. (28) and the possible direct photolysis of Fe(III)-carboxylate complexes via Eq. (29); and (iv) persistent organic intermediates were generated. Since sunlight and artificial radiation (even the one supplied

by low energy power artificial lamps) can be successfully applied for the landfill leachate mineralization, their combination can be contemplated. When deciding on EAOPs system configuration, one must consider that solar radiation is free and renewable.

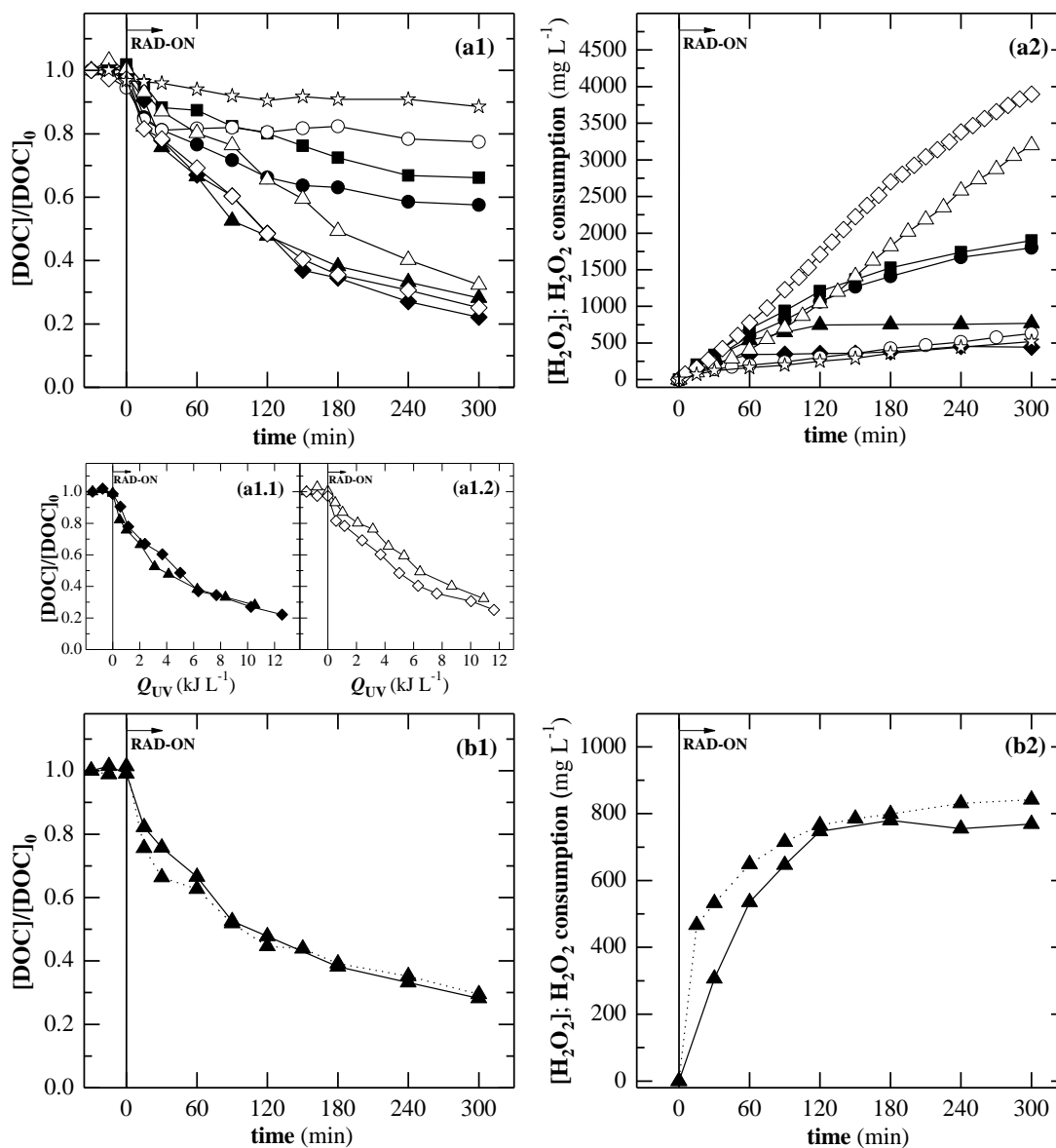


Figure 7.4. Evolution of normalized DOC removal (a1, b1) as a function of time and (a1.1 and a1.2) as a function of accumulated UV energy per L of solution; (a2, b2) time-course of H_2O_2 concentration (for EAOPs) or H_2O_2 consumption (for AOPs) during the treatment of the pre-treated landfill leachate by various processes using pH of 2.8, 20 °C, j of 200 mA cm⁻² for EAOPs and $[\text{H}_2\text{O}_2]$ of 200-400 mg L⁻¹ for AOPs. EAOPs: (■) EF-BDD- $[\text{TDI}]_0$ of 12 mg L⁻¹, (●) EF-BDD- $[\text{TDI}]_0$ of 60 mg L⁻¹, (▲) PEF-UVA-BDD- $[\text{TDI}]_0$ of 60 mg L⁻¹ and (◆) SPEF-BDD- $[\text{TDI}]_0$ of 60 mg L⁻¹. AOPs: (○) Fenton, (△) PF-UVA and (◇) SPF, all using $[\text{TDI}]_0$ of 60 mg L⁻¹. Extra processes: (☆) UVA photolysis with initial H_2O_2 addition of 700 mg L⁻¹ and (▲) (dot profile) PEF-UVA-BDD- $[\text{TDI}]_0$ of 60 mg L⁻¹ with initial H_2O_2 addition of 700 mg L⁻¹.

In addition, Figure 7.4a2 reveals the availability of H_2O_2 during all EAOPs treatments and a decreasing H_2O_2 accumulation in the order EF-BDD-[TDI]₀ of $12 \text{ mg L}^{-1} > \text{EF-BDD-[TDI]}_0$ of $60 \text{ mg L}^{-1} > \text{PEF-UVA-BDD-[TDI]}_0$ of $60 \text{ mg L}^{-1} > \text{SPEF-BDD-[TDI]}_0$ of 60 mg L^{-1} , in accordance with the increasing oxidation ability of these processes.

On the other hand, chemical Fenton, PF-UVA and SPF processes were applied to the degradation of the pre-treated landfill leachate for comparison with the analogous EF-BDD, PEF-UVA-BDD and SPEF-BDD processes, respectively. In all the AOPs, the H_2O_2 was supplied in multiple small additions between 200 and 400 mg L^{-1} since similar approaches have improved the oxidation rate, avoiding the absence of H_2O_2 and minimizing its consumption [38]. pH of 2.8, $20 \text{ }^\circ\text{C}$ and [TDI]₀ of 60 mg L^{-1} were used. The DOC decay profiles for AOPs are displayed in Figure 7.4a1 and, as expected, their mineralization ability raised in the sequence Fenton < PF-UVA < SPF. The faster DOC decay attained in SPF when compared with PF-UVA was slightly less pronounced in terms of accumulated UV energy (see Figure 7.4a1.2) and came along with a slightly higher H_2O_2 consumption (see Figure 7.4a2). The Fenton process induced a DOC removal of only 19% after 30 min of reaction that remained almost constant up to the end of the process. This removal was 1.8 times lower than that of EF-BDD (see Table 7.2) because in the latter also occurred: (i) the BDD($\bullet\text{OH}$) generation from Eq. (1), (ii) the cathodic Fe^{3+} regeneration to Fe^{2+} via Eq. (26), and (iii) even the direct oxidation of organic compounds on BDD surface. The superiority of PEF-UVA-BDD and SPEF-BDD over PF-UVA and SPF, respectively, was less pronounced than that of EF-BDD over Fenton, although the DOC decay was much less evident in the first 30 min of PF-UVA reaction compared with PEF-UVA-BDD. These findings suggest that the presence of radiation, mostly sunlight, reduces the oxidative role of electrochemically generated oxidants because of the efficient action of photolytic reactions (28) and (29).

The UVA photolysis with addition of 700 mg L^{-1} of H_2O_2 at the beginning of the reaction yielded a very slow DOC removal, only reaching 11% abatement in 300 min (see Figure 7.4a1). This indicates a very small participation of UVA radiation, H_2O_2 and PF reactions in the presence of [TDI]₀ of 12 mg L^{-1} in the effluent matrix on the degradation of the landfill leachate.

In Chapter 4, it was pointed out that the availability of H_2O_2 from the first instant of reaction in the AOPs in contrast with the gradual accumulation in EAOPs can increase some organics degradation during the first times of reaction. In this context, a PEF-UVA-BDD process with initial addition of 700 mg L^{-1} of H_2O_2 was performed to be compared with the regular PEF-UVA-BDD process. However, only a very slight increment of 4% on DOC removal was accomplished after

the first 15 min of reaction, followed by a very similar DOC decay profile (see Figure 7.4a3) with a very alike k_{DOC} value (see Table 7.2). This suggests that the high applied j of 200 mA cm^{-2} provides a sufficient H_2O_2 accumulation from the beginning of the process to maximize the Fenton's reaction (21) (see Figure 7.4b2). Furthermore, the H_2O_2 initial concentration can influence differently the degradation of distinct compounds.

7.3.5 Biodegradability enhancement during SPEF process

The assessment of the biodegradability enhancement during the EAOP treatment step was performed by means of a Zahn-Wellens test applied to various samples taken during a SPEF process in the pilot plant using a Pt anode, pH of 2.8, $20 \text{ }^\circ\text{C}$, $[\text{TDI}]_0$ of 60 mg L^{-1} and j of 200 mA cm^{-2} . Figure 7.5 exhibits the D_t evolution for various samples at different treatment stages during the Zahn-Wellens test and Table 7.3 displays the characteristics of each sample in terms of DOC, COD and BOD_5 at day 0 and day 28. As long as organics were degraded, more biodegradable samples were found, with exception of samples S_8 and S_9 , suggesting the presence of more recalcitrant intermediates when DOC was reduced up to ca. 85 mg L^{-1} . The treatment stage corresponding to sample S_6 with DOC of 163 mg L^{-1} and D_t of 61% can be selected as the best endpoint for the SPEF treatment since at this oxidation degree COD could be reduced up to $102 \text{ mg O}_2 \text{ L}^{-1}$ by means of a biological process, thereby comprising with Portuguese (Decree-Law no. 236/98) and European (Directive no. 91/271/CEE) discharge limits for WWTPs effluents, i.e. COD values of 150 and $125 \text{ mg O}_2 \text{ L}^{-1}$, respectively. As a result, the above SPEF-BDD process should be performed up to reach an accumulated UV energy of 6.2 kJ L^{-1} (ca. 147 min under an average solar UV radiation intensity of 46 W m^{-2}), consuming $137 \text{ kWh (kg DOC)}^{-1}$, i.e. 36 kWh m^{-3} , of electrical energy.

The pre-treated landfill leachate oxidized up to 163 mg L^{-1} of DOC and subjected to subsequent neutralization to pH of 7.5 and sludge removal by clarification for 3 h achieved COD, BOD_5 , total nitrogen and nitrate values above the Portuguese and European regulations for WWTPs release into the environment (see Table 7.1). These two latter steps led to a $[\text{TDI}]$ from 50 mg L^{-1} to below its LOD (0.13 mg L^{-1}) and the production of 53 mL of sludge per L of effluent that require further adequate treatment. The Zahn-Wellens biological process was able to reduce COD and BOD_5 to values in agreement with regulations, but a subsequent biological denitrification step must be performed to convert nitrates into nitrogen gas and hence comply with nitrate and total nitrogen legislation limits (see Table 7.1).

Ion-exclusion HPLC analysis on LMCA only revealed the formation of formic acid in the SPEF-Pt treatment at the pilot plant, with a maximum concentration of 14 mg C L⁻¹ and a contribution to DOC always below 4.5%. No significant changes in the content of inorganic ions of the leachate matrix were determined by ion chromatography.

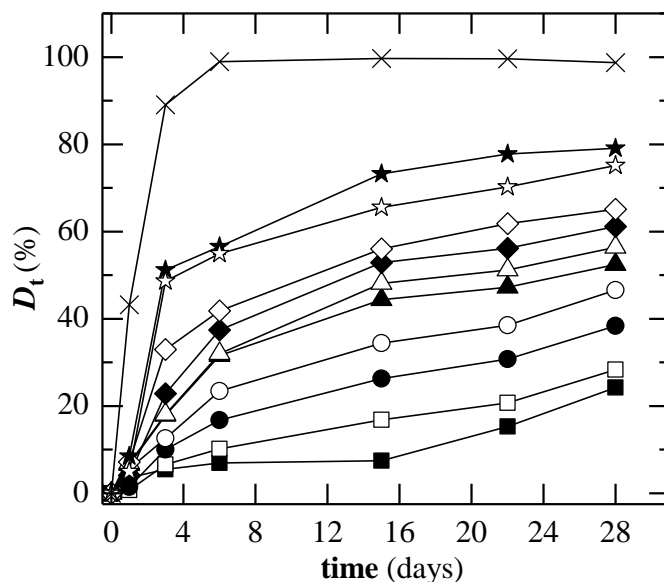


Figure 7.5. Zahn-Wellens test for samples collected during SPEF-Pt process at pilot-scale using pH of 2.8, 20 °C, [TDI]₀ of 60 mg L⁻¹ and *j* of 200 mA cm⁻². Samples were characterized in Table 7.3. (■) - S₀, (□) - S₁, (●) - S₂, (○) - S₃, (▲) - S₄, (△) - S₅, (◆) - S₆, (◇) - S₇, (★) - S₈, (☆) - S₉ and (×) - Reference (DOC at day 0 = 218 mg L⁻¹).

Table 7.3. Characterization of Zahn-Wellens test samples in terms of DOC and COD at day 0 and day 28, BOD₅ at day 0 and *D_t* at day 28.

Parameter (units)	S ₀	S ₁	S ₂	S ₃	S ₄	S ₅	S ₆	S ₇	S ₈	S ₉
DOC (day 0) (mg L ⁻¹)	347	314	267	250	211	186	163	140	110	85
DOC (day 28) (mg L ⁻¹)	266	232	168	138	105	86	69	55	30	28
COD (day 0) (mg O ₂ L ⁻¹)	950	925	720	690	445	370	290	268	206	160
COD (day 28) (mg O ₂ L ⁻¹)	904	602	442	332	228	158	102	85	50	47
BOD ₅ (day 0) (mg O ₂ L ⁻¹)	24	24	32	44	64	64	68	72	72	55
<i>D_t</i> (day 28) (%)	24	27	38	47	52	56	61	65	79	75

7.4 Conclusions

The raw sanitary landfill leachate exhibited very dark brown color, high alkalinity and high amounts of recalcitrant organic compounds and ammonium. The first biological treatment led to the removal of the biodegradable organic fraction corresponding to 13-33% of DOC, total ammonium oxidation predominantly to nitrite and almost total alkalinity removal. The subsequent coagulation process brought a large decolorization due to the removal of humic acids, TSS and VSS and came along with 63-65% DOC abatement. The presence of nitrite ion proved to have a negative effect on the EAOP step as long as it caused an extra H_2O_2 consumption and a high pH decrease and then a subsequent aeration stage at pH of 3.3 was applied to totally convert nitrite into nitrate.

The use of a j of 200 mA cm^{-2} was chosen as the best value for PEF-UVA-BDD process using pH of 2.8, $20 \text{ }^\circ\text{C}$ and $[\text{TDI}]_0$ of 60 mg L^{-1} . Under these conditions, the EAOPs relative oxidative capability of EAOPs increased in the order EF-BDD- $[\text{TDI}]_0$ of $12 \text{ mg L}^{-1} < \text{EF-BDD-}[\text{TDI}]_0$ of $60 \text{ mg L}^{-1} < \text{PEF-UVA-BDD-}[\text{TDI}]_0$ of $60 \text{ mg L}^{-1} \leq \text{SPEF-BDD-}[\text{TDI}]_0$ of 60 mg L^{-1} . The comparison between EAOPs and the analogous AOPs revealed a large superiority of EF-BDD over Fenton, less pronounced superiority of PEF-UVA-BDD over PF-UVA and similarity between SPEF-BDD and SPF in terms of oxidation ability.

The assessment of the biodegradability enhancement during the SPEF process revealed the need to perform the electrochemical treatment up to reach a DOC value around 163 mg L^{-1} to couple a further biological process that allows achieving a final wastewater quality in agreement with Portuguese and European regulations for the discharge of effluents from a WWTP in terms of organic content. Consumptions of 6.2 kJ L^{-1} of accumulated UV energy and 36 kWh m^{-3} of electrical energy were attained when using a BDD anode, pH of 2.8, $20 \text{ }^\circ\text{C}$, $[\text{TDI}]_0$ of 60 mg L^{-1} and j of 200 mA cm^{-2} . The subsequent biological treatment should also include a denitrification step to convert nitrates into nitrogen gas and thus comply with the limits imposed by regulations.

7.5 References

- [1] Tchobanoglous, G., Kreith, F., 2002. Handbook of Solid Waste Management, 2nd ed., McGraw-Hill, New York, United States.
- [2] Fatta, D., Papadopoulos, A., Loizidou, M., 1999. A study on the landfill leachate and its impact on the groundwater quality of the greater area. *Environmental Geochemistry and Health* 21(2), 175-190.
- [3] Qasim, S.R., Chiang, W., 1994. Sanitary Landfill Leachate - Generation, Control and Treatment, CRC Press LLC, Boca Raton, United States.
- [4] Kjeldsen, P., Barlaz, M.A., Rooker, A.P., Baun, A., Ledin, A., Christensen, T.H., 2002. Present and long-term composition of MSW Landfill leachate: A review. *Critical Reviews in Environmental Science and Technology* 32(4), 297-336.
- [5] Abbas, A.A., Jingsong, G., Ping, L.Z., Ya, P.Y., Al-Rekabi, W.S., 2009. Review on landfill leachate treatments. *American Journal of Applied Sciences* 6, 672-684.
- [6] Renou, S., Givaudan, J.G., Poulain, S., Dirassouyan, F., Moulin, P., 2008. Landfill leachate treatment: Review and opportunity. *Journal of Hazardous Materials* 150(3), 468-493.
- [7] Wiszniowski, J., Robert, D., Surmacz-Gorska, J., Miksch, K., Weber, J.V., 2006. Landfill leachate treatment methods: A review. *Environmental Chemistry Letters* 4(1), 51-61.
- [8] Kurniawan, T.A., Lo, W.-h., Chan, G.Y.S., 2006. Physico-chemical treatments for removal of recalcitrant contaminants from landfill leachate. *Journal of Hazardous Materials* 129(1-3), 80-100.
- [9] Deng, Y., Englehardt, J.D., 2007. Electrochemical oxidation for landfill leachate treatment. *Waste Management* 27(3), 380-388.
- [10] Anfruns, A., Gabarró, J., González-Olmos, R., Puig, S., Balaguer, M.D., Colprim, J., 2013. Coupling anammox and advanced oxidation-based technologies for mature landfill leachate treatment. *Journal of Hazardous Materials* 258-259, 27-34.
- [11] Guo, J.-S., Abbas, A.A., Chen, Y.-P., Liu, Z.-P., Fang, F., Chen, P., 2010. Treatment of landfill leachate using a combined stripping, Fenton, SBR, and coagulation process. *Journal of Hazardous Materials* 178(1-3), 699-705.
- [12] Silva, T.F.C.V., Silva, M.E.F., Cunha-Queda, A.C., Fonseca, A., Saraiva, I., Boaventura, R.A.R., Vilar, V.J.P., 2013. Sanitary landfill leachate treatment using combined solar photo-Fenton and biological oxidation processes at pre-industrial scale. *Chemical Engineering Journal* 228, 850-866.
- [13] Silva, T.F.C.V., Silva, M.E.F., Cunha-Queda, A.C., Fonseca, A., Saraiva, I., Sousa, M.A., Gonçalves, C., Alpendurada, M.F., Boaventura, R.A.R., Vilar, V.J.P., 2013. Multistage treatment system for raw leachate from sanitary landfill combining biological nitrification-denitrification/solar photo-Fenton/biological processes, at a scale close to industrial - Biodegradability enhancement and evolution profile of trace pollutants. *Water Research* 47(16), 6167-6186.

- [14] De Torres-Socías, E., Prieto-Rodríguez, L., Zapata, A., Fernández-Calderero, I., Oller, I., Malato, S., 2015. Detailed treatment line for a specific landfill leachate remediation. Brief economic assessment. *Chemical Engineering Journal* 261, 60-66.
- [15] Saraiva, I.M.A., Fonseca, M.A.F., Vilar, V.J.P., Silva, T.F.C.V., Boaventura, R.A.R., inventors. Efacec Engenharia e Sistemas, S.A., assignee. Method of treating leachate, phototreatment reactors and respective use. European Patent 2 784 031. 2014 October 1.
- [16] Brillas, E., Sirés, I., Oturan, M.A., 2009. Electro-Fenton process and related electrochemical technologies based on Fenton's reaction chemistry. *Chemical Reviews* 109(12), 6570-6631.
- [17] Nieder, R., Benbi, D.K., 2008. *Carbon and Nitrogen in the Terrestrial Environment*, Springer Science + Business Media B.V.
- [18] Ziyang, L., Youcai, Z., Tao, Y., Yu, S., Huili, C., Nanwen, Z., Renhua, H., 2009. Natural attenuation and characterization of contaminants composition in landfill leachate under different disposing ages. *Science of the Total Environment* 407(10), 3385-3391.
- [19] Cheremisinoff, N.P., 1994. *Handbook of Water and Wastewater Treatment Technology*, Marcel Dekker, Inc., New York, United States.
- [20] Spellman, F.R., 2004. *Mathematics manual for water and wastewater treatment plant operators*, CRC Press LLC, Boca Raton, United States.
- [21] Bae, B.-U., Jung, E.-S., Kim, Y.-R., Shin, H.-S., 1999. Treatment of landfill leachate using activated sludge process and electron-beam radiation. *Water Research* 33(11), 2669-2673.
- [22] Baumgarten, G., Seyfried, C.F., 1996. Experiences and new developments in biological pretreatment and physical posttreatment of landfill leachate. *Water Science and Technology* 34(7-8), 445-453.
- [23] Metcalf & Eddy, I., 2004. *Wastewater Engineering, Treatment and Reuse*, 4th ed., McGraw-Hill, New York, United States.
- [24] Gerardi, M.H., 2002. *Nitrification and Denitrification in the Activated Sludge Process*, John Wiley & Sons, Inc., New York, United States.
- [25] Spagni, A., Marsili-Libelli, S., 2009. Nitrogen removal via nitrite in a sequencing batch reactor treating sanitary landfill leachate. *Bioresource Technology* 100(2), 609-614.
- [26] Yusof, N., Hassan, M.A., Phang, L.Y., Tabatabaei, M., Othman, M.R., Mori, M., Wakisaka, M., Sakai, K., Shirai, Y., 2010. Nitrification of ammonium-rich sanitary landfill leachate. *Waste Management* 30(1), 100-109.
- [27] Canziani, R., Emondi, V., Garavaglia, M., Malpei, F., Pasinetti, E., Buttiglieri, G., 2006. Effect of oxygen concentration on biological nitrification and microbial kinetics in a cross-flow membrane bioreactor (MBR) and moving-bed biofilm reactor (MBBR) treating old landfill leachate. *Journal of Membrane Science* 286(1-2), 202-212.
- [28] Villaverde, S., Fernández, M.T., Urueña, M.A., Fdz-Polanco, F., 1997. Influence of substrate concentration on the growth and activity of a nitrifying biofilm in a submerged biofilter. *Environmental Technology* 18(9), 921-928.
- [29] Park, S., Chung, J., Rittmann, B.E., Bae, W., 2015. Nitrite accumulation from simultaneous free-ammonia and free-nitrous-acid inhibition and oxygen limitation in a continuous-flow biofilm reactor. *Biotechnology and Bioengineering* 112(1), 43-52.

- [30] Mudgal, P.K., Bansal, S.P., Gupta, K.S., 2007. Kinetics of atmospheric oxidation of nitrous acid by oxygen in aqueous medium. *Atmospheric Environment* 41(19), 4097-4105.
- [31] Braida, W., Ong, S., 2000. Decomposition of nitrite under various pH and aeration conditions. *Water, Air, and Soil Pollution* 118(1-2), 13-26.
- [32] Edwards, J.O., Plumb, R.C., 2007. The Chemistry of Peroxonitrites, In: Karlin K.D. (Ed), *Progress in Inorganic Chemistry*, Vol. 41, pp. 599-635, John Wiley & Sons, Inc., Hoboken, United States.
- [33] Goldstein, S., Squadrito, G.L., Pryor, W.A., Czapski, G., 1996. Direct and indirect oxidations by peroxyxynitrite, neither involving the hydroxyl radical. *Free Radical Biology and Medicine* 21(7), 965-974.
- [34] Letterman, R.D., Amirtharajah, A., O'Melia, C.R., 1999. Coagulation and Flocculation, In: Letterman R.D. (Ed), *Water Quality and Treatment*, 5th ed., McGraw-Hill, Inc., New York, United States.
- [35] Schecher, W.D., McAvoy, D.C., 2007. MINEQL+: A Chemical Equilibrium Modeling System, Version 4.6 for Windows, Environmental Research Software, Hallowell, United States.
- [36] Chiang, L.-C., Chang, J.-E., Wen, T.-C., 1995. Indirect oxidation effect in electrochemical oxidation treatment of landfill leachate. *Water Research* 29(2), 671-678.
- [37] Goldstein, S., Aschengrau, D., Diamant, Y., Rabani, J., 2007. Photolysis of aqueous H₂O₂: Quantum yield and applications for polychromatic UV actinometry in photoreactors. *Environmental Science & Technology* 41(21), 7486-7490.
- [38] Bacardit, J., Oller, I., Maldonado, M.I., Chamarro, E., Malato, S., Esplugas, S., 2007. Simple models for the control of photo-Fenton by monitoring H₂O₂. *Journal of Advanced Oxidation Technologies* 10(2), 219-228.

8 Electrochemical advanced oxidation processes for sanitary landfill leachate remediation: Evaluation of operational variables

The effect of various parameters on the performance of various EAOPs like EF, PEF and SPEF was assessed for the treatment of a sanitary landfill leachate previously subjected to biological and coagulation/aeration processes, also employed in Chapter 7. The tested operational variables included: (i) anode material (BDD vs. Pt), (ii) $[TDI]_0$ (20-80 mg L⁻¹), (iii) pH (2.8-4.0), (iv) initial addition of 1:3 Fe(III)-to-oxalate molar ratio at various pH values (2.8-5.0), (v) temperature (15-40 °C), and (vi) radiation source (UVA, UVA-Vis and UVC lamps and natural sunlight). The BDD anode showed high superiority over the Pt one for EF, PEF-UVA and SPEF processes, thereby advising an important role of the physisorbed •OH at the anode surface on landfill leachate oxidation even under irradiation. A $[TDI]_0$ of 60 mg L⁻¹ was chosen as the best dose for the PEF-UVA-BDD process. While PEF-UVA-BDD without external addition of oxalic acid yielded the best results at pH of 2.8, the initial addition of 1:3 Fe(III)-to-oxalate molar ratio allowed operating at pH of 3.5 with even higher efficiency and at pH of 4.0 with only slightly lower efficiency. Effluent temperatures from 20 to 40 °C led to similar mineralization rates for the PEF-UVA-BDD technique. The use of UVA and UVC lamps and natural sunlight as radiation sources in PEF-BDD and SPEF-BDD systems led to similar mineralization profiles as a function of time. The UVA-Vis lamp induced lower effluent mineralization mainly for longer reaction times.

This Chapter is based on the following research article: “Moreira, F.C., Soler, J., Fonseca, A., Saraiva, I., Boaventura, R.A.R., Brillas, E., Vilar, V.J.P., 2016. Electrochemical advanced oxidation processes for sanitary landfill leachate remediation: Evaluation of operational variables. Applied Catalysis B: Environmental 182, 161-171”.

8.1 Introduction

In Chapter 7, it was assessed the technical feasibility of integrating EAOPs in a multistage strategy for sanitary landfill leachate remediation. Despite all the work, there is a lack of knowledge on the best operational conditions for sanitary landfill leachate treatment by EAOPs. In this context, the current Chapter presents an unprecedented study on the influence of various key variables on the performance of EF, PEF and SPEF for the remediation of a sanitary landfill leachate previously subjected to biological and coagulation/aeration processes. The effect of anode material (BDD *vs.* Pt) was assessed for EF with two distinct $[TDI]_0$, PEF-UVA and SPEF methods. The influence of $[TDI]_0$ (20-80 mg L⁻¹), pH (2.8-4.0), addition of Fe(III)-oxalate complexes at various pH values (2.8-5.0) and temperature (15-40 °C) was evaluated for PEF-UVA-BDD. Beyond that, the effect of radiation source (UVA, UVA-Vis and UVC artificial lights and natural sunlight) was verified for PEF/SPEF-BDD.

8.2 Materials and methods

All chemicals, analytical determinations, modeling of degradation kinetics and experimental units and procedures are depicted in the Chapter 2. Table 2.5 summarizes the operational conditions of EAOPs and AOPs performed in the current Chapter.

It was employed the same pre-treated sanitary landfill leachate as in EAOPs/AOPs of Chapter 7, i.e. a sanitary landfill leachate previously subjected to biological treatment and coagulation and aeration processes. Its main characteristics are collected in Table 7.1.

8.3 Results and discussion

8.3.1 Influence of anode material on EF, PEF-UVA and SPEF processes

BDD thin-film anodes are usually preferred for wastewater remediation since they exhibit a higher O_2 -overpotential than classical anode materials such as Pt, RuO_2 , IrO_2 , PbO_2 and SnO_2 , generating larger amounts of $M(\cdot OH)$ from Eq. (1) to react with organics [1, 2]. Nevertheless, some waters contaminated with model pollutants achieved only a slight superiority of BDD over Pt anode or even similar degradations for PEF-UVA and SPEF treatments, as shown in Chapter 4 and by Thiam et al. [3] and Skoumal et al. [4]. This behavior has been attributed to the improvement of contaminants removal by light-induced mechanisms, advising the use of Pt coated anode due to its lower price.

The effect of BDD and Pt anodes on the mineralization of a pre-treated landfill leachate was checked for EF with $[TDI]_0$ of 12 mg L^{-1} and EF, PEF-UVA and SPEF with $[TDI]_0$ of 60 mg L^{-1} using pH of 2.8, $20 \text{ }^\circ\text{C}$ and j of 200 mA cm^{-2} . These conditions were chosen because: (i) Saraiva et al. [5] applied a $[TDI]_0$ of 60 mg L^{-1} ; (ii) a pH of 2.8 is often assumed as optimal for Fenton-based processes [6, 7]; (iii) $20 \text{ }^\circ\text{C}$ is an average leachate temperature commonly found in Portuguese sanitary landfill treatment plants [8]; and (iv) j of 200 mA cm^{-2} is the best value for the pre-treated landfill leachate remediation by EAOPs as discussed in Chapter 7.

Figure 8.1 and Table 8.1 reveal higher DOC removals for all EAOPs using BDD compared to the analogous methods using Pt, either in terms of time or accumulated UV energy per L of effluent (see inset panel of Figure 8.1). This suggests an important role of BDD($\cdot OH$) formed via Eq. (1) on the mineralization of the pre-treated landfill leachate even when light-induced reactions like Eqs. (28) and (29) enhance organics removal. These results contrast with some of the abovementioned achievements for waters spiked with model contaminants.

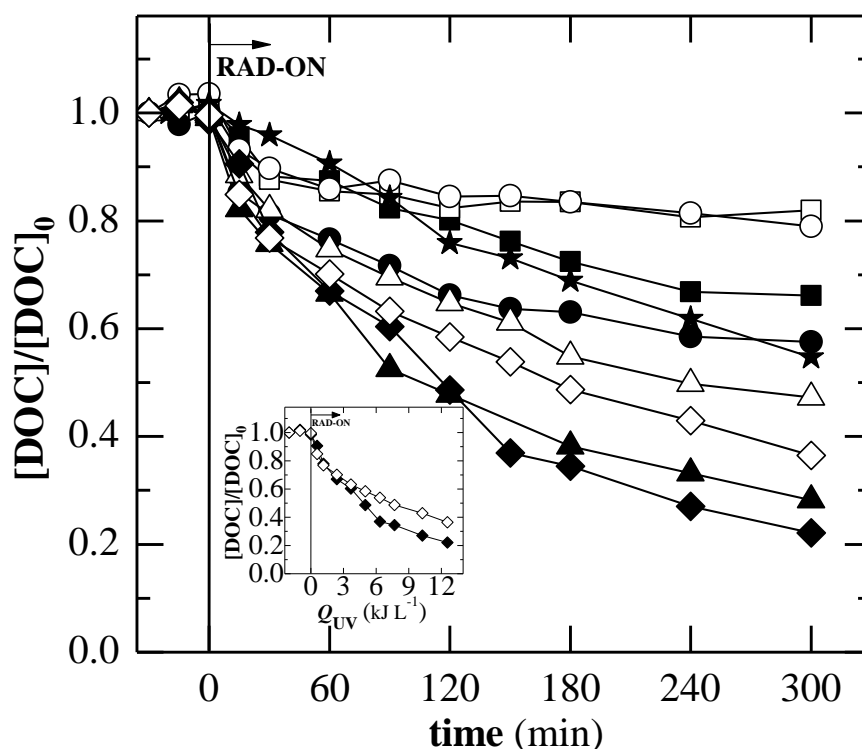


Figure 8.1. Influence of anode material, (solid symbols) BDD and (open symbols) Pt, on normalized DOC removal as a function of time for treatment of the pre-treated landfill leachate by (■, □) EF-[TDI]₀ of 12 mg L⁻¹, (●, ○) EF-[TDI]₀ of 60 mg L⁻¹, (▲, △) PEF-UVA-[TDI]₀ of 60 mg L⁻¹ and (◆, ◇) SPEF-[TDI]₀ of 60 mg L⁻¹ using pH of 2.8, 20 °C and *j* of 200 mA cm⁻². The inset panel depicts the normalized DOC removal in SPEF systems as a function of accumulated UV energy per L of solution. Extra process: (★) AO-[TDI]₀ of 12 mg L⁻¹ using a BDD anode, a Pt cathode, pH of 2.8, 20 °C and *j* of 200 mA cm⁻².

In Chapter 7, it was stated that the EAOP must provide a final landfill leachate with a DOC around 163 mg L⁻¹ to fulfill the discharge limits into the environment after a subsequent biological treatment. For the best EAOP, i.e. SPEF, energy consumptions for electrochemical cell operation of 137 or 277 kWh (kg DOC)⁻¹ (36 or 71 kWh m⁻³) were required to reach this DOC value when applying BDD or Pt anode, respectively, with correspondent UV energy consumptions of 6.2 or 12 kJ L⁻¹, respectively. Considering an average electricity cost of 0.10 € kWh⁻¹, the electrochemical cell operation under SPEF conditions demanded the following electric energy costs to fulfill the discharge limits: around 14 € (kg DOC)⁻¹ and 3.6 € m⁻³ using the BDD anode and 28 € (kg DOC)⁻¹ and 7.1 € m⁻³ using the Pt anode. Note that the use of Pt anode led to a slightly lower cell voltage of 8.2 V compared to 8.5 V for BDD, but it was insufficient to promote lower energy consumptions due to the deeply lower mineralization ability of Pt(•OH).

Table 8.1. Pseudo-first-order kinetic constants for DOC removal (k_{DOC}) along with the corresponding R^2 and S^2_R , obtained for the treatment of the pre-treated landfill leachate under conditions of Figures 8.1, 8.2a, 8.3a, 8.6a and 8.7.

System	k_{DOC} ($\times 10^{-3} \text{ min}^{-1}$)	R^2	S^2_R ($\text{mg}^2 \text{ L}^{-2}$)	
Effect of BDD vs. Pt anode on various EAOPs	EF-BDD-[TDI] ₀ of 12 mg L ⁻¹	1.67±0.04	0.993	19
	EF-Pt-[TDI] ₀ of 12 mg L ⁻¹	- ^a	- ^a	- ^a
	EF-BDD-[TDI] ₀ of 60 mg L ⁻¹	2.3±0.1	0.994	12
	EF-Pt-[TDI] ₀ of 60 mg L ⁻¹	- ^a	- ^a	- ^a
	PEF-UVA-BDD-[TDI] ₀ of 60 mg L ⁻¹	4.3±0.3	0.970	144
	PEF-UVA-Pt-[TDI] ₀ of 60 mg L ⁻¹	2.3±0.1	0.986	45
	SPEF-BDD-[TDI] ₀ of 60 mg L ⁻¹	6.0±0.2	0.991	129
	SPEF-Pt-[TDI] ₀ of 60 mg L ⁻¹	2.9±0.1	0.997	17
		k_{DOC} (kJ L ⁻¹)	R^2	S^2_R ($\text{mg}^2 \text{ L}^{-2}$)
	SPEF-BDD-[TDI] ₀ of 60 mg L ⁻¹	0.14±0.01	0.991	171
SPEF-Pt-[TDI] ₀ of 60 mg L ⁻¹	0.069±0.002	0.994	35	
	k_{DOC} ($\times 10^{-3} \text{ min}^{-1}$)	R^2	S^2_R ($\text{mg}^2 \text{ L}^{-2}$)	
AO-BDD-[TDI] ₀ of 12 mg L ⁻¹	2.13±0.04	0.995	18	
Effect of [TDI] ₀ (mg L ⁻¹) on PEF-UVA-BDD	20	2.5±0.1	0.995	14
	40	3.4±0.1	0.993	37
	60	4.3±0.3	0.970	144
	80	4.5±0.2	0.991	62
Effect of pH on PEF-UVA-BDD	2.8	4.3±0.3	0.970	144
	3.5	2.18±0.04	0.996	3
	4.0	1.6±0.1	0.986	14
Effect of 1:3 Fe(III)-to-oxalic molar ratio addition at various pH on PEF-UVA-BDD	2.8	5.8±0.5	0.992	264
	3.5	9.5±0.4	0.992	199
	4.0	4.4±0.1	0.998	25
	5.0	1.7±0.1	0.980	48
Effect of temperature (°C) on PEF-UVA-BDD	15	0.73±0.03	0.981	9
	20	4.3±0.3	0.970	144
	30	4.5±0.2	0.987	48
	40	6.1±0.2	0.988	59
Effect of temperature (°C) on PF-UVA	20	3.7±0.1	0.991	53
	30	5.4±0.2	0.986	67
	40	7.3±0.3	0.988	111
Effect of light source on PEF-BDD and SPEF-BDD	UVA	4.3±0.3	0.970	144
	UVA-Vis	3.6±0.3	0.979	125
	UVC	4.0±0.2	0.993	75
	Solar	6.0±0.2	0.991	129
PEF-UVC-BDD-[TDI] ₀ of 12 mg L ⁻¹	3.47±0.05	0.998	16	

^a No fitting of a pseudo-first-order kinetic model to experimental data.

Additionally, it was performed an assay under the same conditions as EF-BDD-[TDI]₀ of 12 mg L⁻¹ but using Pt as cathode in the absence of air supply to neglect the H₂O₂ electrogeneration, thereby establishing an AO-BDD process. Figure 8.1 shows a slower DOC removal for AO-BDD in comparison to EF-BDD during the first 90 min of reaction, which can be related to the generation of •OH from Fenton's reaction (21) in the latter. However, for longer times the mineralization was

slightly faster for AO-BDD, which can be mainly attributed to the inability of active chlorine species formed via Eqs. (5)-(7) to degrade organics in EF-BDD due to their reaction with the electrogenerated H_2O_2 and, besides that, it can be related to the scavenging of $\bullet\text{OH}$ by their reaction with H_2O_2 via Eq. (24) in EF-BDD.

8.3.2 Influence of initial total dissolved iron concentration on PEF-UVA-BDD process

The [TDI] in solution is a crucial parameter for Fenton-based processes as it determines the Fenton's reaction (21) extent and thus the pollutants degradation. As displayed in Chapter 1, the best [TDI] in light-assisted Fenton-based EAOPs depends on various factors such as: (i) H_2O_2 concentration, (ii) system ability to regenerate Fe^{3+} to Fe^{2+} , which can occur through photolysis of Fe(III)-hydroxy complexes by Eq. (28), photolysis of complexes between Fe(III) and organics via Eq. (29), cathodic reduction according to Eq. (26) and thermal reactions (22), (23) and (44), (iii) manifestation of inner filter effects, i.e. competitive absorption of photons between pollutants and Fe(III) photoactive species, and (iv) photoreactor geometry since the iron amount influences the light attenuation along the optical pathlength.

Landfill leachate remediation by the conventional PF process has been employing iron contents in a wide range of $10\text{-}2000\text{ mg L}^{-1}$, with highlighting on $60\text{-}80\text{ mg L}^{-1}$ [5, 9-12]. Because of the cathodic Fe^{3+} regeneration to Fe^{2+} through Eq. (26), PEF and SPEF processes may allow to work at minor iron doses than in the analogous chemical processes.

[TDI]₀ of 20, 40, 60 and 80 mg L^{-1} were tested for the degradation of pre-treated landfill leachate by PEF-UVA-BDD using pH of 2.8, $20\text{ }^\circ\text{C}$ and j of 200 mA cm^{-2} . Figure 8.2a depicts rising DOC abatements with the increment of iron content up to [TDI]₀ of 60 mg L^{-1} , with similar DOC decays for [TDI]₀ of 60 and 80 mg L^{-1} . Table 8.1 displays k_{DOC} values around 1.8 and 1.3 times superior for [TDI]₀ of 60/80 mg L^{-1} when compared to [TDI]₀ of 20 and 40 mg L^{-1} , respectively. These findings indicate that a [TDI]₀ of 60 mg L^{-1} ensured a maximum rate for Fenton's reaction (21), probably due to a maximum Fe^{3+} regeneration to Fe^{2+} together with minimum inner filter effects and light attenuation along the current photoreactor optical pathlength. For all the trials, the DOC dropped more sharply in the first 15-30 min of reaction (13-29%) (see Figure 8.2a) simultaneously with [TDI] decays of 8-18% (see Figure 8.2b). This can be related to the precipitation of Fe(III) complexes with primary by-products probably formed through the attack of $\bullet\text{OH}$ provided by Fenton's reaction (21) since in Chapter 7 it was found a DOC decrease of around 20% together

with a [TDI] decay of around 10% for a Fenton process using [TDI]₀ of 60 mg L⁻¹, [H₂O₂] of 200-400 mg L⁻¹, pH of 2.8 and 20 °C. Note that Fe³⁺ did not precipitate in the initial matrix of the pre-treated landfill leachate.

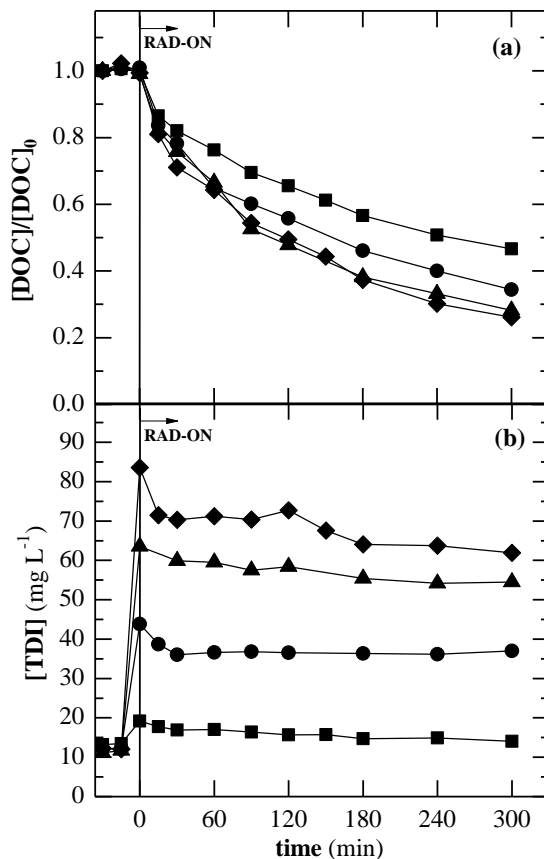


Figure 8.2. Effect of initial total dissolved iron concentration on (a) normalized DOC removal and (b) total dissolved iron concentration as a function of time for PEF-UVA-BDD treatment of the pre-treated landfill leachate using pH of 2.8, 20 °C and j of 200 mA cm⁻². [TDI]₀: (■) 20, (●) 40, (▲) 60 and (◆) 80 mg L⁻¹.

8.3.3 Influence of pH on PEF-UVA-BDD process and use of Fe(III)-oxalate complexes

Although the use of neutral pH in Fenton-based EAOPs could lead to acidification and neutralization prevention/minimization, it is well-known that higher pH values contribute to (i) lower amounts of photoactive Fe(III)-hydroxy complexes in solution [6, 13], (ii) iron precipitation [6, 13], (iii) presence of carbonate and bicarbonate species, which reduce the process efficiency due to their •OH scavenging effect [14], and (v) rise of the auto-decomposition rate of H₂O₂ to water and oxygen, typically for pH above 5 [15].

In general, the application of conventional PF processes for the treatment of raw or pre-treated landfill leachate employ pH values between 2.5 and 3.5 as optimal [5, 12, 16-19]. Kim et al. [17] reported a decrease of 8% on the efficiency of a PF process for a raw landfill leachate remediation when operating at pH of 4.0 in comparison to pH of 3.0. Kim et al. [17] and Lau et al. [18] stated efficiency reductions of more than 30% for pH equal or above 5.0 when compared to pH around 3 for a raw landfill leachate remediation by PF.

The influence of pH on the mineralization of the current pre-treated landfill leachate was tested at pH values of 2.8, 3.5 and 4.0 for a PEF-UVA-BDD process using 20 °C, [TDI]₀ of 60 mg L⁻¹ and *j* of 200 mA cm⁻². Figure 8.3a illustrates lower DOC decays for rising pH values and Table 8.1 reveals *k*_{DOC} values 2.0 and 2.7 times inferior for pH of 3.5 and 4.0, respectively, in comparison to pH of 2.8. The poorer mineralization at pH of 3.5 and 4.0 came along with [TDI] decrease from 60 to 16 and 10 mg L⁻¹, respectively, after 15-60 min of reaction, contrasting with the almost null iron precipitation achieved at pH of 2.8 (see Figure 8.3b). The theoretical Fe³⁺ speciation diagram shown in Figure 7.2 outlines the presence of a maximum FeOH²⁺ molar ratio at pH of 2.8, the absence of this species for pH values above 3.4 and iron precipitation as Fe(OH)₃ (s) for pH values above 2.8, which agrees with the experimental results. Note that the possible formation of Fe(III)-carboxylate complexes generated from organics degradation was excluded in the speciation diagrams calculation since ion-exclusion HPLC analysis only detected formic acid in low contents below 14 mg C L⁻¹. The reduction in efficiency of 63% in terms of *k*_{DOC} attained in the current study from pH of 3.0 to 4.0 contrasts with the drop in efficiency of 8% reached for the PF treatment of a raw landfill leachate in Kim et al. [17]. This is probably associated with the overall lower efficiency of this AOP due to the precipitation of Fe(III) complexes with humic acids because their removal was not performed in a preliminary treatment.

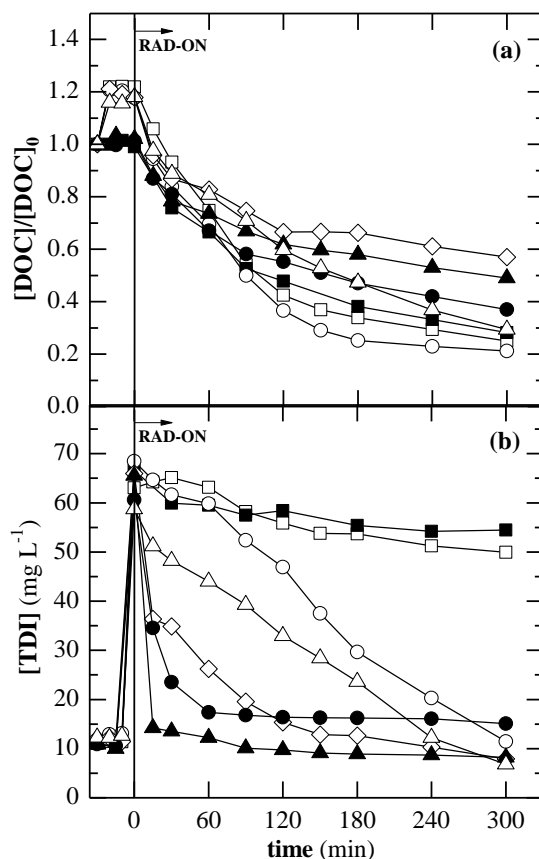


Figure 8.3. Effect of pH and initial addition of 1:3 Fe(III)-to-oxalate molar ratio on (a) normalized DOC removal and (b) total dissolved iron concentration as a function of time for PEF-UVA-BDD treatment of the pre-treated landfill leachate using 20 °C, $[TDI]_0$ of 60 mg L^{-1} and j of 200 mA cm^{-2} . pH values for trials without oxalic acid addition: (■) 2.8, (●) 3.5 and (▲) 4.0. pH values for trials with oxalic acid addition: (□) 2.8, (○) 3.5, (△) 4.0 and (◇) 5.0.

As mentioned in Chapters 1 and 5, the addition of carboxylic acids to Fenton-based processes can improve their efficiency because: (i) they promote the formation of more soluble complexes with Fe(III), allowing to maintain the iron in solution at higher pH values [20]; (ii) Fe(III)-carboxylate complexes can absorb radiation in the UV-Vis range, being photodecarboxylated according to the general Eq. (28) with higher quantum yields for Fe^{2+} generation than that of Fe(III)-hydroxy complexes [13, 21-23]; and (iii) the presence of Fe(III)-carboxylate complexes can avoid the formation of Fe(III)-sulfate, Fe(III)-chloride and Fe(III)-pollutants complexes in view of their higher formation constants in comparison with that of these species [24, 25]. In this context, PF and PEF processes assisted by Fe(III)-carboxylate complexes have been applied to synthetic and real wastewaters [26-29]. Among these species, Fe(III)-oxalate complexes have gained larger attention due to their high quantum yield for Fe^{2+} formation, with major application in a 1:3 Fe(III)-to-oxalate molar ratio [23, 30, 31].

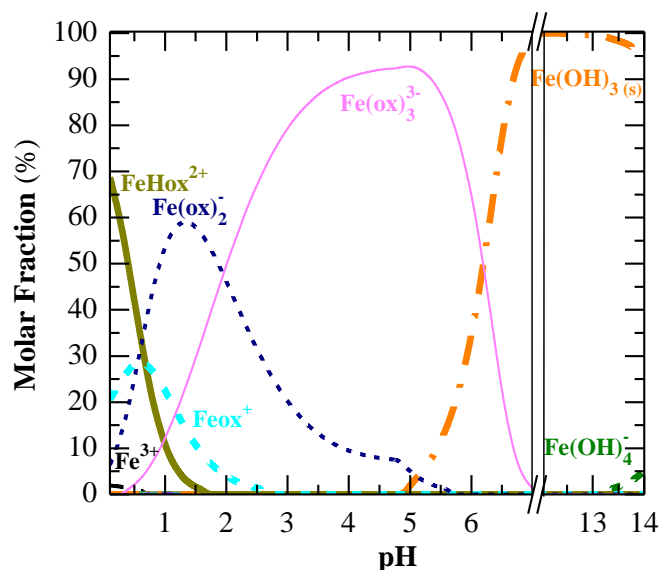


Figure 8.4. Fe^{3+} speciation diagrams as a function of the solution pH in a calculated system containing the average amounts of NO_3^- , SO_4^{2-} , Cl^- , Ca^{2+} , Mg^{2+} , K^+ and Na^+ of the landfill leachate after aeration (Table 7.1), 60 mg L^{-1} of Fe^{3+} and 1:3 Fe(III)-to-oxalate molar ratio (ionic strength = 0.396 M). Data were calculated by the chemical equilibrium modeling system MINEQL+ [32] using the equilibrium constants of Table 5.1. The formation of the solid iron phase $\text{Fe}(\text{OH})_3$ was included in the calculation despite the slow formation of solid phases on the time scale of the experiments.

The effect of an initial 1:3 Fe(III)-to-oxalate molar ratio in the PEF-UVA-BDD process was verified for pH of 2.8, 3.5, 4.0 and 5.0. For all these systems, the theoretical calculations point to the presence of 98-100% of total Fe^{3+} content in the form of $\text{Fe}(\text{ox})_2^-$ and $\text{Fe}(\text{ox})_3^{3-}$ species, which are the most photoactive Fe(III)-oxalate complexes, and null/almost null iron precipitation as $\text{Fe}(\text{OH})_3 (\text{s})$ at the beginning of the process (see Figure 8.4). At pH of 2.8, an initial 1:3 Fe(III)-to-oxalate molar ratio only led to slightly superior DOC decay in relation to the classical PEF-UVA-BDD method at the same pH (see Figure 8.3a), with a k_{DOC} value only 1.3 times higher (see Table 8.1), and similar and almost null iron precipitation (see Figure 8.3b). In contrast, at pH of 3.5 and 4.0 much higher mineralization rates upon addition of oxalic acid were found, with k_{DOC} values 4.4 and 2.8 times higher than the analogous processes without acid addition (see Table 8.1), respectively. This can be related to the gradual instead of abrupt iron precipitation (see Figure 8.3b) and the greater absorption of UVA light highlighted in the absorption spectra of Figure 8.5a. The addition of oxalic acid at pH of 3.5 and 4.0 led to even higher or only slightly lower efficiencies than that obtained at pH of 2.8 in the absence of oxalic acid addition, respectively. At pH of 5.0, the PEF-UVA-BDD with oxalic acid addition reached the lowest DOC decay due to iron precipitation to values below 20 mg L^{-1} from 60 min of reaction (see Figure 8.3b). Note that oxalic

acid highly contributed to DOC content (76 mg C L^{-1}) and Fe(III)-oxalate complexes were rapidly photodecarboxylated, in only some minutes.

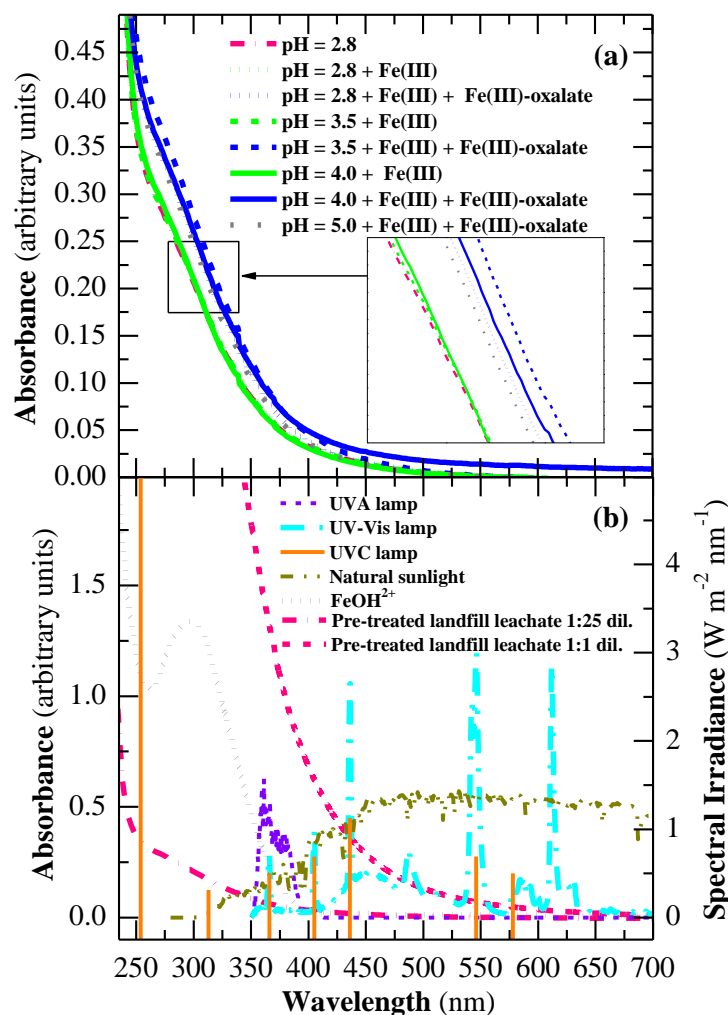


Figure 8.5. (a) Absorption spectra of the pre-treated sanitary landfill leachate at various pH values, without and with $[\text{Fe}^{3+}] = 60 \text{ mg L}^{-1}$ and 1:3 Fe(III)-to-oxalate molar ratio (diluted 1:25). (b) Absorption spectrum of FeOH^{2+} at pH of 2.9 [33]; absorption spectra of the pre-treated sanitary landfill leachate at pH of 2.8 (diluted 1:25 and without dilution); and spectral irradiances of UVA, UVA-Vis and UVC lamps and natural sunlight (UVA lamp: measured with the spectro-radiometer and confirmed by Philips; UVA-Vis lamp: measured with the spectro-radiometer – not calibrated – qualitative information; UVC lamp: supplied by Philips; natural sunlight: AM1.5G reference spectrum [34]).

8.3.4 Influence of temperature on PEF-UVA-BDD process

The mass transfer of reactants toward/from the electrodes is likely to increase with higher temperature and kinetic constants (for $\bullet\text{OH}$ and H_2O_2 and oxidation of organics by such species) are exponentially dependent on the temperature (Arrhenius law). The Fenton-based processes can also count on the faster Fe^{3+} regeneration to Fe^{2+} thermal reactions (22), (23) and (44) for higher

temperature, which has been described as the main cause for the growth of degradation kinetics with temperature in these processes [35, 36]. In Chapter 5, the change of organics degradation kinetics with temperature was also attributed to distinct distribution of molar fractions of photoactive iron species and $\text{Fe}(\text{OH})_{3(s)}$ with change of temperature.

The influence of temperature on the mineralization of the pre-treated landfill leachate was assessed by applying temperatures of 15, 20, 30 and 40 °C for a PEF-UVA-BDD process using pH of 2.8, $[\text{TDI}]_0$ of 60 mg L⁻¹ and j of 200 mA cm⁻². Figure 8.6a outlines quite similar DOC removals at 20, 30 and 40 °C together with a poorer mineralization at 15 °C, awarding a k_{DOC} value 5.9-8.4 times inferior (see Table 8.1). As can be seen in Figure 8.6b, at 30 and 40 °C the $[\text{TDI}]$ underwent decays of 31% and 68% after 300 min, respectively, whereas at 15 and 20 °C lower abatements below 18% were achieved. Taking into account all these results and the theoretical calculations on FeOH^{2+} and $\text{Fe}(\text{OH})_{3(s)}$ amounts given in Table 8.2, the following considerations can be carried out: (i) from 15 to 20 °C the increase on DOC removal can be attributed to higher rate of thermal reactions (22), (23) and (44) and a slightly higher content of FeOH^{2+} ; (ii) from 20 to 30 °C the theoretically predicted and experimentally observed iron precipitation as $\text{Fe}(\text{OH})_{3(s)}$ might compensate the increase of the rate of thermal reactions (22), (23) and (44) and the slightly larger theoretical amount of FeOH^{2+} ; and (iii) at 40 °C the highest iron precipitation along with the lower theoretical formation of FeOH^{2+} when compared to 20 and 30 °C might diminish the positive effect of thermal reactions (22), (23) and (44) rates.

Figure 8.6c shows decreasing H_2O_2 accumulations with increasing temperature that can be related to the scavenging of this oxidant by Eqs. (36), (37), (22), (23) and (44). Note that the thermal decomposition of H_2O_2 into H_2O and O_2 may occur in large extent only for temperatures above 50 °C, being almost negligible in the temperature range tested [37].

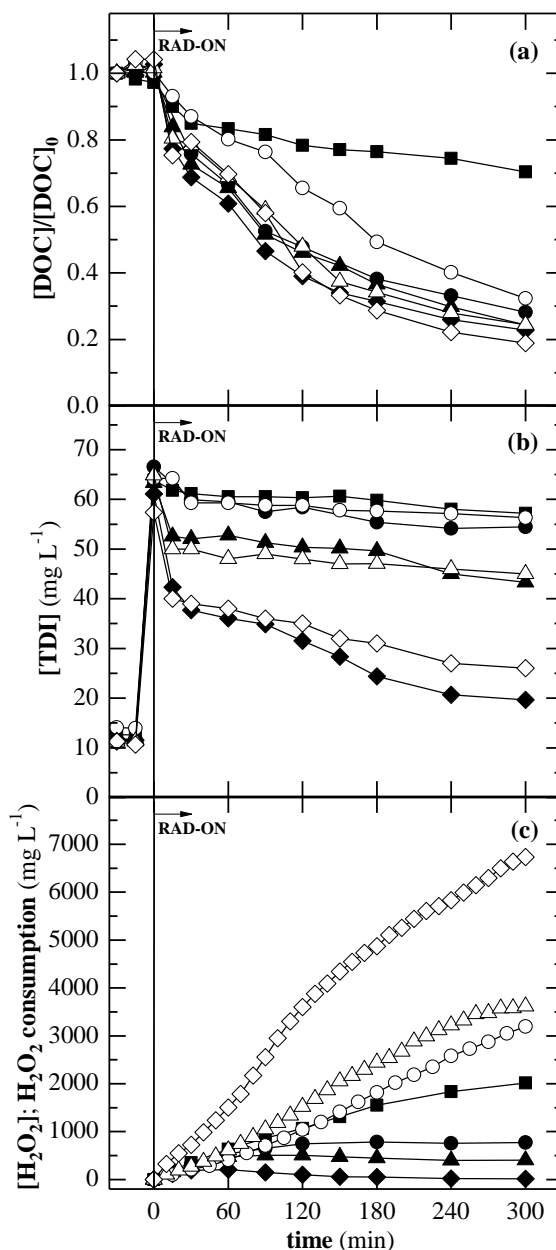


Figure 8.6. Effect of temperature on (a) normalized DOC removal, (b) total dissolved iron concentration and (c) H_2O_2 concentration (for PEF-UVA-BDD) or H_2O_2 consumption (for PF-UVA) as a function of time for (solid symbols) PEF-UVA-BDD and (open symbols) PF-UVA treatment of the pre-treated landfill leachate using pH of 2.8, $[\text{TDI}]_0$ of 60 mg L^{-1} , j of 200 mA cm^{-2} for PEF-UVA-BDD and $[\text{H}_2\text{O}_2]$ of $200\text{-}400 \text{ mg L}^{-1}$ for PF-UVA. Temperature: (■) 15, (●, ○) 20, (▲, △) 30 and (◆, ◇) 40 °C.

Conventional PF-UVA tests at 20, 30 and 40 °C were also performed using the same conditions than PEF-UVA-BDD but supplying H_2O_2 in multiple additions between 200 and 400 mg L^{-1} [38]. Besides the lower oxidation ability of PF-UVA comparatively to PEF-UVA-BDD at 20 °C already reported in Chapter 7, Figure 8.6a shows a large mineralization enhancement in PF-UVA from 20 to 30 °C, with a k_{DOC} value 1.5 times larger (see Table 8.1), contrasting with the almost null

improvement attained for PEF-UVA-BDD. On the other hand, at 30 and 40 °C the mineralization ability of PF-UVA was quite similar, as occurred for PEF-UVA-BDD. These results suggest a larger participation of electrochemical reactions, i.e. BDD(\bullet OH) generation from Eq. (1), cathodic Fe^{3+} regeneration to Fe^{2+} via Eq. (26) and even the direct oxidation of organic compounds on BDD surface, on the effluent mineralization at 20 °C than at 30 and 40 °C, probably due to the increase in rate of thermal reactions (22), (23) and (44). Silva et al. [8] determined an increase in rate of more than 3 times from 21 to 37 °C for the SPF treatment of a raw landfill leachate, higher than the enhancement achieved in this study, eventually mainly because of the composition of the effluent. Furthermore, Figure 8.6b depicts quite alike iron decays for chemical and electrochemical processes and Figure 8.6c shows a H_2O_2 consumption of more than double for PF-UVA at 40 °C compared to 20 and 30 °C due to the oxidant waste by Eqs. (36), (37), (22), (23) and (44).

Table 8.2. Concentration of FeOH^{2+} and $\text{Fe}(\text{OH})_3(\text{s})$ at temperatures of 15, 20, 30 and 40 °C in a system containing the average amounts of NO_3^- , SO_4^{2-} , Cl^- , Ca^{2+} , Mg^{2+} , K^+ and Na^+ of the landfill leachate after aeration (Table 7.1) and 60 mg L^{-1} of Fe^{3+} (ionic strength = 0.390 M). Data were calculated by the chemical equilibrium modeling system MINEQL+ [32] using the equilibrium constants of Table 5.1.

Temperature (°C)	Species concentration at pH of 2.8 (mg L^{-1})	
	FeOH^{2+}	$\text{Fe}(\text{OH})_3(\text{s})$
15	5.6	0
20	7.1	0
30	8.6	20
40	5.9	67

8.3.5 Influence of radiation source on PEF-BDD and SPEF-BDD processes

Depending on the radiation source, different wavelengths and radiations intensities will reach the solution, influencing: (i) the direct photolysis of pollutants, which takes place when the light source emits radiation at the same wavelength range as the contaminants can absorb radiation efficiently; (ii) the photoreduction of photoactive Fe(III)-hydroxy complexes and Fe(III) complexes with organics, especially those acting as ligands, that occurs under UV-Vis radiation according to Eqs. (28) and (29), respectively; and (iii) the generation of \bullet OH in the presence of symmetrical peroxides such as H_2O_2 through the homolytic cleavage of the peroxide ($-\text{O}-\text{O}-$) bond that happens at 200-280 nm (UVC radiation) via Eq. (30). The most photoactive Fe(III)-hydroxy complex, i.e. FeOH^{2+} , has been reported to absorb radiation from 200 to 400 nm at pH of 2.6-4.0 [33, 39, 40], following the behavior of Figure 8.5b, with decreasing quantum yields for Eq. (28) from 280 to 370 nm ($\Phi = 0.29$ to 0.08) [41]. In turn, photoactive Fe(III)-carboxylate

complexes like Fe(III)-oxalate ones are able to absorb the visible light up to 500 nm with higher quantum yields for Fe^{2+} generation than FeOH^{2+} [23, 42].

Studies on PF for landfill leachate remediation employed various light sources such as UVA lamps [17, 18], natural sunlight [11, 43] and UVC lamps [44] but no comparison between them has been performed. Regarding the PEF-BDD process, in Chapter 7 it was only directly compared the efficiency between UVA artificial light and natural sunlight.

The effect of radiation source on the pre-treated landfill leachate treatment was assessed by employing UVA, UVA-Vis and UVC lamps and also natural solar radiation in PEF-BDD and SPEF-BDD processes using pH of 2.8, 20°C, $[\text{TDI}]_0$ of 60 mg L⁻¹ and j of 200 mA cm⁻². Figure 2.6 and Table 2.6 summarize the main characteristics of the employed radiation sources.

Preliminary trials on 300 min of photolysis of the pre-treated landfill leachate upon UVA, UVA-Vis and UVC artificial radiation and natural sunlight with $\overline{UV}_{G,n}$ of 45 W m⁻² depicted very low mineralization decays near 4-8% (data not shown). This suggests the presence of very recalcitrant compounds in the landfill leachate that are not easily photoreduced, despite the ability of this effluent to absorb light up to near 700 nm (see Figure 8.5b). The high effluent absorbance may yield inner filter effects during PEF, resulting in a loss of photons efficiency since the photolysis of pollutants usually has a low quantum yield [36].

Figure 8.7 shows only a slightly higher mineralization for the SPEF-BDD process in terms of time compared to the PEF-UVA-BDD one, with a k_{DOC} value 1.4 times higher (see Table 8.1), notwithstanding the superior photonic flux provided by the solar radiation compared to the one supplied by the UVA lamp here used and the ability of sunlight to emit in the visible region. This suggests that the photonic flux in the PEF-UVA-BDD process was able to induce almost maximum photoreduction of FeOH^{2+} and/or Fe(III) complexes with organics by Eqs. (28) and (29), respectively. For the PEF-UVA-Vis-BDD, Figure 8.7 displays a similar and fast DOC abatement for times up to 90 min in comparison to all the other processes, followed by a poor mineralization up to the end of reaction. The sharply DOC decay of 21% attained during the first 15 min of reaction was accompanied by a [TDI] decay of 20% (data not shown) and so it can be related to the abovementioned precipitation of Fe(III) complexes with primary by-products generated mainly by the attack of $\bullet\text{OH}$ formed from Fenton's reaction (21). For longer times up to 90 min, direct and/or indirect photolysis of some by-products might occur. The indirect photolysis corresponds to the formation of reactive species like $\bullet\text{OH}$, peroxy radicals ($\text{ROO}\bullet$), $^1\text{O}_2$, carbon-centered

radicals and excited triplet states from reactions involving the irradiation of, for example, fulvic acids [45-47]. For times above 90 min, the slow mineralization achieved suggests a small occurrence of FeOH^{2+} photoreduction by UVA-Vis irradiation as expected in virtue of its poor light emission below 400 nm.

Figure 8.7 also exhibits similar DOC decays for PEF-UVC-BDD and PEF-UVA-BDD treatments. These results contrast with the superiority of PEF-UVC-BDD over PEF-UVA-BDD found for the treatment of the secondary WWTP effluent in Chapter 4. Since the PEF-BDD-UVC process could count on the additional $\bullet\text{OH}$ production from the H_2O_2 photolysis according to Eq. (30), it is highly likely that the FeOH^{2+} photoreduction occurred in lesser extent than for PEF-UVA-BDD, PEF-UVA-Vis-BDD and SPEF-BDD systems. An extra PEF-BDD-UVC process without iron addition, i.e. $[\text{TDI}]_0$ of 12 mg L^{-1} (see Figure 8.7 and Table 8.1, revealed a participation of 13% of the added 48 mg L^{-1} iron amount in the k_{DOC} value, which contrasts with the higher increment of 42% in k_{DOC} found for the PEF-UVA-BDD process when $[\text{TDI}]_0$ rose from 20 to 60 mg L^{-1} , confirming the small role of FeOH^{2+} photoreduction in PEF-BDD-UVC. Note that the H_2O_2 concentration was always higher than 300 mg L^{-1} for all the trials, thus ensuring the occurrence of Eqs. (21) and (30) (data not shown).

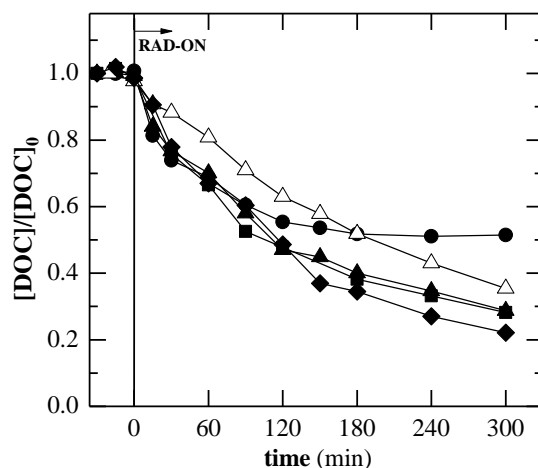


Figure 8.7. Effect of radiation source on normalized DOC removal as a function of time for PEF-BDD and SPEF-BDD treatment of the pre-treated landfill leachate using pH of 2.8, 20°C , $[\text{TDI}]_0$ of 60 mg L^{-1} and j of 200 mA cm^{-2} . Radiation: (■) UVA, (●) UVA-Vis and (▲) UVC artificial light and (◆) natural sunlight with $\overline{UV}_{G,n} = 46 \text{ W m}^{-2}$. (△) PEF-BDD-UVC process using $[\text{TDI}]_0$ of 12 mg L^{-1} (effluent content), pH of 2.8, 20°C and j of 200 mA cm^{-2} .

8.4 Conclusions

The mineralization of the pre-treated landfill leachate was faster for EF, PEF-UVA and SPEF processes using the BDD anode when compared to the analogous processes using the Pt anode, suggesting an important role of BDD(\bullet OH) on organics degradation even under irradiation. The use of a $[\text{TDI}]_0$ of 60 mg L^{-1} was chosen as the best one for a PEF-UVA-BDD process, reaching similar effluent mineralization as $[\text{TDI}]_0$ of 80 mg L^{-1} . A pH of 2.8 yielded the highest pre-treated landfill leachate mineralization by PEF-UVA-BDD process together with almost null iron precipitation. For higher pH values, iron precipitated progressively, thereby decreasing the mineralization rate. The initial addition of 1:3 Fe(III)-to-oxalate molar ratio to the system at pH of 3.5 and 4.0 highly enhanced the DOC removal since it maintained iron dissolved in solution for longer reaction times, resulting in higher or only slightly lower efficiencies than at pH of 2.8 in the absence of oxalic acid addition. The use of temperatures from 20 to 40 °C was affordable for the remediation of the pre-treated landfill leachate by PEF-UVA-BDD, presenting quite similar DOC decays, although temperatures above 20 °C led to iron precipitation. The application of UVA and UVC lamps and natural sunlight as radiation sources proved to be suitable for the current effluent remediation by PEF-BDD and SPEF-BDD since quite alike mineralization rates were achieved. The use of a UVA-Vis lamp led to lower effluent mineralization mainly for longer reaction times.

8.5 References

- [1] Brillas, E., Sirés, I., Oturan, M.A., 2009. Electro-Fenton process and related electrochemical technologies based on Fenton's reaction chemistry. *Chemical Reviews* 109(12), 6570-6631.
- [2] Kapałka, A., Fóti, G., Comninellis, C., 2008. Kinetic modelling of the electrochemical mineralization of organic pollutants for wastewater treatment. *Journal of Applied Electrochemistry* 38(1), 7-16.
- [3] Thiam, A., Zhou, M., Brillas, E., Sirés, I., 2014. Two-step mineralization of Tartrazine solutions: Study of parameters and by-products during the coupling of electrocoagulation with electrochemical advanced oxidation processes. *Applied Catalysis B: Environmental* 150-151, 116-125.
- [4] Skoumal, M., Rodríguez, R.M., Cabot, P.L., Centellas, F., Garrido, J.A., Arias, C., Brillas, E., 2009. Electro-Fenton, UVA photoelectro-Fenton and solar photoelectro-Fenton degradation of the drug ibuprofen in acid aqueous medium using platinum and boron-doped diamond anodes. *Electrochimica Acta* 54(7), 2077-2085.
- [5] Saraiva, I.M.A., Fonseca, M.A.F., Vilar, V.J.P., Silva, T.F.C.V., Boaventura, R.A.R., inventors. Efacec Engenharia e Sistemas, S.A., assignee. Method of treating leachate, phototreatment reactors and respective use. European Patent 2 784 031. 2014 October 1.
- [6] Pignatello, J.J., 1992. Dark and photoassisted Fe³⁺-catalyzed degradation of chlorophenoxy herbicides by hydrogen peroxide. *Environmental Science & Technology* 26(5), 944-951.
- [7] Safarzadeh-Amiri, A., Bolton, J.R., Cater, S.R., 1996. Ferrioxalate-mediated solar degradation of organic contaminants in water. *Solar Energy* 56(5), 439-443.
- [8] Silva, T.F.C.V., Silva, M.E.F., Cunha-Queda, A.C., Fonseca, A., Saraiva, I., Boaventura, R.A.R., Vilar, V.J.P., 2013. Sanitary landfill leachate treatment using combined solar photo-Fenton and biological oxidation processes at pre-industrial scale. *Chemical Engineering Journal* 228, 850-866.
- [9] de Moraes, J.L., Zamora, P.P., 2005. Use of advanced oxidation processes to improve the biodegradability of mature landfill leachates. *Journal of Hazardous Materials* 123(1-3), 181-186.
- [10] Primo, O., Rivero, M.J., Ortiz, I., 2008. Photo-Fenton process as an efficient alternative to the treatment of landfill leachates. *Journal of Hazardous Materials* 153(1-2), 834-842.
- [11] Silva, T.F.C.V., Fonseca, A., Saraiva, I., Vilar, V.J.P., Boaventura, R.A.R., 2013. Biodegradability enhancement of a leachate after biological lagooning using a solar driven photo-Fenton reaction, and further combination with an activated sludge biological process, at pre-industrial scale. *Water Research* 47(10), 3543-3557.
- [12] Silva, T.F.C.V., Silva, M.E.F., Cunha-Queda, A.C., Fonseca, A., Saraiva, I., Sousa, M.A., Gonçalves, C., Alpendurada, M.F., Boaventura, R.A.R., Vilar, V.J.P., 2013. Multistage treatment system for raw leachate from sanitary landfill combining biological nitrification-denitrification/solar photo-Fenton/biological processes, at a scale close to industrial - Biodegradability enhancement and evolution profile of trace pollutants. *Water Research* 47(16), 6167-6186.

- [13] Faust, B.C., Zepp, R.G., 1993. Photochemistry of aqueous iron(III)-polycarboxylate complexes: Roles in the chemistry of atmospheric and surface waters. *Environmental Science & Technology* 27(12), 2517-2522.
- [14] Buxton, G.V., Greenstock, C.L., Helman, W.P., Ross, A.B., 1988. Critical review of rate constants for reactions of hydrated electrons, hydrogen atoms and hydroxyl radicals ($\cdot\text{OH}/\text{O}^-$) in aqueous solution. *Journal of Physical and Chemical Reference Data* 17(2), 513-886.
- [15] Meeker, R.E., inventors. Stabilization of hydrogen peroxide. United States Patent 3208825 A. 1965 September 28.
- [16] Hermosilla, D., Cortijo, M., Huang, C.P., 2009. Optimizing the treatment of landfill leachate by conventional Fenton and photo-Fenton processes. *Science of the Total Environment* 407(11), 3473-3481.
- [17] Kim, S.-M., Geissen, S.-U., Vogelpohl, A., 1997. Landfill leachate treatment by a photoassisted Fenton reaction. *Water Science and Technology* 35(4), 239-248.
- [18] Lau, I.W.C., Wang, P., Chiu, S.S.T., Fang, H.H.P., 2002. Photoassisted Fenton oxidation of refractory organics in UASB-pretreated leachate. *Journal of Environmental Sciences* 14(3), 388-392.
- [19] Vilar, V.J.P., Rocha, E.M.R., Mota, F.S., Fonseca, A., Saraiva, I., Boaventura, R.A.R., 2011. Treatment of a sanitary landfill leachate using combined solar photo-Fenton and biological immobilized biomass reactor at a pilot scale. *Water Research* 45(8), 2647-2658.
- [20] Sun, Y., Pignatello, J.J., 1992. Chemical treatment of pesticide wastes. Evaluation of iron(III) chelates for catalytic hydrogen peroxide oxidation of 2,4-D at circumneutral pH. *Journal of Agricultural and Food Chemistry* 40(2), 322-327.
- [21] Horváth, O., Stevenson, K.L., 1992. *Charge Transfer Photochemistry of Coordination Compounds*, VCH, New York, United States.
- [22] Safarzadeh-Amiri, A., Bolton, J.R., Cater, S.R., 1997. Ferrioxalate-mediated photodegradation of organic pollutants in contaminated water. *Water Research* 31(4), 787-798.
- [23] Zuo, Y., Hoigne, J., 1992. Formation of hydrogen peroxide and depletion of oxalic acid in atmospheric water by photolysis of iron(III)-oxalato complexes. *Environmental Science & Technology* 26(5), 1014-1022.
- [24] Smith, R.M., Martell, A.E., 1987. Critical stability constants, enthalpies and entropies for the formation of metal complexes of aminopolycarboxylic acids and carboxylic acids. *Science of the Total Environment* 64(1-2), 125-147.
- [25] Batista, A.P.S., Nogueira, R.F.P., 2012. Parameters affecting sulfonamide photo-Fenton degradation-Iron complexation and substituent group. *Journal of Photochemistry and Photobiology A: Chemistry* 232, 8-13.
- [26] Monteagudo, J.M., Durán, A., Corral, J.M., Carnicer, A., Frades, J.M., Alonso, M.A., 2012. Ferrioxalate-induced solar photo-Fenton system for the treatment of winery wastewaters. *Chemical Engineering Journal* 181-182, 281-288.
- [27] Dias, I.N., Souza, B.S., Pereira, J.H.O.S., Moreira, F.C., Dezotti, M., Boaventura, R.A.R., Vilar, V.J.P., 2014. Enhancement of the photo-Fenton reaction at near neutral pH through the use of ferrioxalate complexes: A case study on trimethoprim and sulfamethoxazole antibiotics removal from aqueous solutions. *Chemical Engineering Journal* 247, 302-313.

- [28] Manenti, D.R., Soares, P.A., Módenes, A.N., Espinoza-Quiñones, F.R., Boaventura, R.A.R., Bergamasco, R., Vilar, V.J.P., 2015. Insights into solar photo-Fenton process using iron(III)-organic ligand complexes applied to real textile wastewater treatment. *Chemical Engineering Journal* 266, 203-212.
- [29] Soares, P.A., Batalha, M., Souza, S.M.A.G.U., Boaventura, R.A.R., Vilar, V.J.P., 2015. Enhancement of a solar photo-Fenton reaction with ferric-organic ligands for the treatment of acrylic-textile dyeing wastewater. *Journal of Environmental Management* 152, 120-131.
- [30] Huang, Y.-H., Tsai, S.-T., Huang, Y.-F., Chen, C.-Y., 2007. Degradation of commercial azo dye reactive Black B in photo/ferrioxalate system. *Journal of Hazardous Materials* 140(1-2), 382-388.
- [31] Rodríguez, E.M., Núñez, B., Fernández, G., Beltrán, F.J., 2009. Effects of some carboxylic acids on the Fe(III)/UVA photocatalytic oxidation of muconic acid in water. *Applied Catalysis B: Environmental* 89(1-2), 214-222.
- [32] Schecher, W.D., McAvoy, D.C., 2007. MINEQL+: A Chemical Equilibrium Modeling System, Version 4.6 for Windows, Environmental Research Software, Hallowell, United States.
- [33] Nadtochenko, V.A., Kiwi, J., 1998. Photolysis of FeOH^{2+} and FeCl^{2+} in aqueous solution. Photodissociation kinetics and quantum yields. *Inorganic Chemistry* 37(20), 5233-5238.
- [34] ASTM, 2003. Standard tables for reference solar spectral irradiances: direct normal and hemispherical on 37° tilted surface.
- [35] Sychev, A.Y., Isak, V.G., 1995. Iron compounds and the mechanisms of the homogeneous catalysis of the activation of O_2 and H_2O_2 and of the oxidation of organic substrates. *Russian Chemical Reviews* 64(12), 1105-1129.
- [36] Malato, S., Fernández-Ibáñez, P., Maldonado, M.I., Blanco, J., Gernjak, W., 2009. Decontamination and disinfection of water by solar photocatalysis: Recent overview and trends. *Catalysis Today* 147(1), 1-59.
- [37] Santos, A., Yustos, P., Rodriguez, S., Simon, E., Garcia-Ochoa, F., 2007. Abatement of phenolic mixtures by catalytic wet oxidation enhanced by Fenton's pretreatment: Effect of H_2O_2 dosage and temperature. *Journal of Hazardous Materials* 146(3), 595-601.
- [38] Bacardit, J., Oller, I., Maldonado, M.I., Chamarro, E., Malato, S., Esplugas, S., 2007. Simple models for the control of photo-Fenton by monitoring H_2O_2 . *Journal of Advanced Oxidation Technologies* 10(2), 219-228.
- [39] Turner, R.C., Miles, K.E., 1957. The ultraviolet absorption spectra of the ferric ion and its first hydrolysis product in aqueous solutions. *Canadian Journal of Chemistry* 35(9), 1002-1009.
- [40] Faust, B.C., Hoigné, J., 1990. Photolysis of Fe(III)-hydroxy complexes as sources of OH radicals in clouds, fog and rain. *Atmospheric Environment. Part A. General Topics* 24(1), 79-89.
- [41] Benkelberg, H.-J., Warneck, P., 1995. Photodecomposition of iron(III) hydroxo and sulfato complexes in aqueous solution: Wavelength dependence of OH and SO_4^- quantum yields. *The Journal of Physical Chemistry* 99(14), 5214-5221.
- [42] Pozdnyakov, I.P., Kolomeets, A.V., Plyusnin, V.F., Melnikov, A.A., Kompanets, V.O., Chekalin, S.V., Tkachenko, N., Lemmetyinen, H., 2012. Photophysics of Fe(III)-tartrate and Fe(III)-citrate complexes in aqueous solutions. *Chemical Physics Letters* 530, 45-48.

- [43] Amor, C., Torres-Sociás, E.D., Peres, J.A., Maldonado, M.I., Oller, I., Malato, S., Lucas, M.S., 2015. Mature landfill leachate treatment by coagulation/flocculation combined with Fenton and solar photo-Fenton processes. *Journal of Hazardous Materials* 286, 261-268.
- [44] Anfruns, A., Gabarró, J., González-Olmos, R., Puig, S., Balaguer, M.D., Colprim, J., 2013. Coupling anammox and advanced oxidation-based technologies for mature landfill leachate treatment. *Journal of Hazardous Materials* 258-259, 27-34.
- [45] Haag, W.R., Hoigné, J., 1986. Singlet oxygen in surface waters. 3. Photochemical formation and steady-state concentrations in various types of waters. *Environmental Science & Technology* 20(4), 341-348.
- [46] Faust, B.C., Hoigné, J., 1987. Sensitized photooxidation of phenols by fulvic acid and in natural waters. *Environmental Science & Technology* 21(10), 957-964.
- [47] Brezonik, P.L., Fulkerson-Brekken, J., 1998. Nitrate-induced photolysis in natural waters: Controls on concentrations of hydroxyl radical photo-intermediates by natural scavenging agents. *Environmental Science & Technology* 32(19), 3004-3010.

9 Conclusions and future work

This final chapter presents a recollection of the most relevant results and conclusions stated in the previous chapters, complemented with some suggestions for future work.

9.1 Conclusions

This thesis aimed to check the technical feasibility of using AO, AO-H₂O₂, EF, PEF and SPEF processes for the degradation of recalcitrant organic compounds of five solutions: (i) a 290 mg L⁻¹ SY azo dye solution in 7.0 g Na₂SO₄ L⁻¹, (ii) a 20.0 mg L⁻¹ TMP antibiotic solution in 7.0 g Na₂SO₄ L⁻¹, (iii) a wastewater collected after secondary treatment of a MWWTP spiked with TMP at mg L⁻¹ levels or 19 pharmaceutical compounds at µg L⁻¹ levels, (iv) a winery wastewater, and (v) a municipal sanitary landfill leachate. EAOPs were directly applied to the pure solutions and the secondary MWWTP effluent, but for the winery wastewater and the landfill leachate these processes were combined with other treatment technologies. The raw winery wastewater exhibited a high fraction of biodegradable organic matter and to restrict the application of EAOPs to the degradation of refractory compounds a biological oxidation was firstly carried out. Removals of 97% on organics were achieved and a remaining recalcitrant fraction was subjected to EAOPs. The raw sanitary landfill leachate presented high amounts of recalcitrant organic compounds, including humic and fulvic acids, high contents of ammonium and particles and also high alkalinity. Since EAOPs with H₂O₂ electrogeneration cannot oxidize ammonium to comprise with regulatory discharge limits and alkalinity must be removed to minimize the amount of acid used to adjust pH from alkaline to acidic, a first biological treatment was applied. This treatment led to total ammonium oxidation mainly to nitrite and almost total alkalinity removal and, in addition, a low mineralization of 13-33% was achieved. Considering that humic acids and particles are able to act as photons absorbers in light-assisted EAOPs and also can provoke the electrochemical cell clogging, their removal was accomplished by applying a coagulation process. It came along with 63-65% of mineralization. An additional aeration was carried to oxidize nitrite ions because their presence proved to have a negative effect on EAOPs as it caused an extra H₂O₂ consumption and a high pH decrease. This step can be omitted if the initial biological treatment is able to efficiently oxidize nitrite.

The results showed that the use of EAOPs for the degradation of various recalcitrant compounds is an interesting and feasible option.

9.1.1 Efficiency of EAOPs

The efficiency of the different EAOPs for the remediation of the pure SY solution and the winery wastewater was assessed under quite similar conditions: $[TDI]_0$ of 28 and 35 mg L⁻¹ and j of 33 and 25 mA cm⁻², respectively. This can be associated with the quite similar organic content of both solutions, i.e. DOC around 100 mg L⁻¹. For the remediation of the synthetic TMP solution and the secondary WWTP effluent, a low $[TDI]_0$ of 2.0 mg L⁻¹ was used to not exceed the Portuguese total iron discharge limit for WWTP final effluents and a low j of 5.0 mA cm⁻² was employed regarding the small DOC content of 12-24 mg L⁻¹. The higher organic concentration of the landfill leachate, i.e. DOC of 337-430 mg L⁻¹, and its very recalcitrant character pointed to the application of larger $[TDI]_0$ and j of 60 mg L⁻¹ and 200 mA cm⁻², respectively. pH values of 2.8-3.5 were always used, with exception of AO and AO-H₂O₂ treatments for the remediation of the secondary MWWTP effluent, where a neutral pH was employed (pH of the effluent). Temperatures from ambient to 35 °C were used for all solutions.

The effectiveness and efficiency of EAOPs was assessed in terms of mineralization, target pollutants decay and, for the synthetic dye solution, color removal.

9.1.1.1 Efficiency of EAOPs in terms of mineralization

Table 9.1 collects the main results on the efficiency of EAOPs in terms of wastewaters mineralization under the abovementioned experimental conditions. The oxidation ability of EAOPs could be arranged in the following order: AO-H₂O₂ < AO < EF < PEF-UVA < SPEF. The little oxidation action of BDD([•]OH) or Pt([•]OH) and H₂O₂ yielded the poor mineralization in AO-H₂O₂. The AO process was applied to wastewaters showing chloride ions in their composition, i.e. the secondary MWWTP effluent and the landfill leachate, and then the superiority of AO over AO-H₂O₂ can be mainly attributed to the unavailability of active chlorine species to degrade organics in the latter process due to the reaction of these species with the electrogenerated H₂O₂. By virtue of the attack of [•]OH produced in the bulk from Fenton's reaction in EF, the mineralization was enhanced. The superiority of PEF-UVA over EF was a result of the additional [•]OH production from the photoreduction of Fe(III)-hydroxy complexes and the possible direct photolysis of generated Fe(III)-carboxylate complexes. Because of the slightly higher UV intensity of natural sunlight compared to the UVA radiation here employed and its emission in the visible region, SPEF was the most powerful process. Nonetheless, the SPEF process only provided a

slightly mineralization improvement compared to PEF-UVA for the remediation of the winery wastewater and the landfill leachate. This suggests the suitability of using UVA artificial lamps, even with low energy power, for the degradation of some wastewaters.

Table 9.1. Main results on the efficiency of the EAOPs for the mineralization of the solutions under study.

Wastewater / Operational conditions	System	EAOP	Time (min)	Q_{UV} (kJ L ⁻¹)	DOC removal (%)	EC _v (kWh m ⁻³)
290 mg Sunset Yellow FCF L⁻¹ in 7.0 g Na₂SO₄ L⁻¹ (DOC of 100 mg L ⁻¹) pH of 3.0; 35 °C; <i>j</i> of 33 mA cm ⁻² ; ([TDI] ₀ of 28 mg L ⁻¹)	150 mL	AO-H ₂ O ₂ -BDD	360	-	65	n.a. ^a
	lab-scale	EF-BDD	360	-	82	n.a. ^a
	undivided	PEF-UVA-BDD	240	n.a. ^a	95	n.a. ^a
	reactor	SPEF-BDD	150	n.a. ^a	93	n.a. ^a
	10 L	SPEF-Pt	270	n.a. ^a	92	7.2
20.0 mg trimethoprim L⁻¹ in 7.0 g Na₂SO₄ L⁻¹ (DOC of 12 mg L ⁻¹) pH of 3.5; 20 °C; <i>j</i> of 5.0 mA cm ⁻² ; ([TDI] ₀ of 2.0 mg L ⁻¹)	2.2 L	AO-H ₂ O ₂ -BDD	180	-	11	0.44
	lab-scale	EF-BDD	180	-	14	0.44
	flow plant	PEF-UVA-BDD	180	6.5	35	0.44
		SPEF-BDD	180	6.7	66	0.44
		SPEF-Pt	180	6.7	59	0.34
35 L	SPEF-Pt	180	6.7	44	0.15	
20.0 mg trimethoprim L⁻¹ in secondary MWWTP wastewater (DOC of 24 mg L ⁻¹) pH of 3.5; 20 °C; <i>j</i> of 5.0 mA cm ⁻² ; ([TDI] ₀ of 2.0 mg L ⁻¹)	2.2 L	SPEF-Pt	180	7.5	41	0.83
	lab-scale flow plant					
5.0 mg trimethoprim L⁻¹ in secondary MWWTP wastewater (DOC of 15 mg L ⁻¹) pH of 3.5 or 6.8; 20 °C; <i>j</i> of 5.0 mA cm ⁻² ; ([TDI] ₀ of 2.0 mg L ⁻¹)	2.2 L	AO-BDD	180	-	12	0.83
	lab-scale	AO-H ₂ O ₂ -BDD	180	-	4.9	0.83
	flow plant	PEF-UVA-BDD	180	6.5	20	0.83
		SPEF-BDD	240	-	36	5.1
Winery wastewater (DOC of 130 mg L ⁻¹) pH of 2.8; 25 °C; <i>j</i> of 25 mA cm ⁻² ; ([TDI] ₀ of 35 mg L ⁻¹)	2.2 L	AO-H ₂ O ₂ -BDD	240	-	54	5.1
	lab-scale	EF-BDD	240	-	84	5.1
	flow plant	PEF-UVA-BDD	240	8.6	86	5.1
		SPEF-BDD	240	7.7	86	5.1
Sanitary landfill leachate (DOC of 337-430 mg L ⁻¹) pH of 2.8; 20 °C; <i>j</i> of 200 mA cm ⁻²	2.2 L	AO-BDD-[TDI] ₀ of 12 mg L ⁻¹	300	-	45	80
	lab-scale	EF-BDD-[TDI] ₀ of 12 mg L ⁻¹	300	-	34	85
	flow plant	EF-BDD-[TDI] ₀ of 60 mg L ⁻¹	300	-	42	85
		PEF-UVA-BDD-[TDI] ₀ of 60 mg L ⁻¹	300	10	72	85
		SPEF-BDD-[TDI] ₀ of 60 mg L ⁻¹	300	12	78	85

^a n.a. – not assessed.

Under the best conditions, high degradation rates were attained for all solutions by using light-assisted EAOPs, although with distinct consumptions of electrical energy for cell operation and UV radiation. To reach a mineralization of 50%, increasing electrical energy consumptions of 0.26, 1.1, 2.0, 3.5 and 30 kWh m⁻³ were needed for the 20.0 mg TMP L⁻¹ pure solution, the secondary MWWTP effluent spiked with 20.0 TMP L⁻¹, the winery wastewater, the pure SY solution and the landfill leachate, respectively, when applying SPEF-BDD or SPEF-Pt processes at the 2.2 L lab-scale flow plant, with exception for the degradation of SY solution, where the 35 L pilot-scale flow plant was employed. These electrical energy consumptions were attained after 109, 236, 104, 132 and 117 min of reaction, respectively. Corresponding UV energy consumptions of 3.6, 9.9, 2.8 and 4.9 kJ L⁻¹ were required for the synthetic TMP solution, the secondary

MWWTP effluent, the winery wastewater and the landfill leachate, respectively (the accumulated UV energy was not assessed for the degradation of the SY solution).

The slower mineralization achieved for the secondary MWWTP effluent spiked with 20.0 mg TMP L⁻¹ compared to the analogous synthetic solution can be attributed to the consumption of •OH to oxidize the additional dissolved organic compounds of the real wastewater, which can be more recalcitrant than TMP, and/or to the filtration of the photochemically active light by these dissolved organics, thereby attenuating the photoreduction reactions.

9.1.1.2 Efficiency of EAOPs in terms of target pollutants decay

EF, PEF-UVA and SPEF processes led to quite similar SY decays and superior to AO-H₂O₂. In contrast, EAOPs ability to remove TMP antibiotic was enhanced in the order AO-H₂O₂ < AO < EF < PEF-UVA < SPEF, as achieved in terms of mineralization. This means that the azo dye was mainly destroyed by •OH produced from Fenton's reaction, with a small participation of the photoreduction of Fe(III)-hydroxy complexes induced by UVA light or sunlight, whereas TMP degradation, both using synthetic and real matrices, is highly dependent on light-induced mechanisms.

SY was totally removed from the synthetic solution in 16 min by SPEF-BDD using the 150 mL undivided cell at j of 33 mA cm⁻² and in 22 min by SPEF-Pt using the 10 L pilot-scale flow plant at j of 78 mA cm⁻², consuming 2.3 kWh m⁻³ of electrical energy. At j of 78 mA cm⁻², the energy consumption to reach an almost total mineralization by SPEF-Pt at pilot-scale was 17 kWh m⁻³, a value around 7 times higher than that required for the dye removal.

For the synthetic TMP solution, a content of 20.0 mg L⁻¹ of TMP was completely degraded in 55 and 90 min, consuming 0.09 and 0.08 kWh m⁻³ of electrical energy and 1.6 and 2.1 kJ L⁻¹ of UV energy by SPEF-BDD process at the 2.2 L lab-scale flow plant or SPEF-Pt at the 35 L pilot-scale flow plant, respectively. For the real TMP wastewater, the total removal of 20.0 mg TMP L⁻¹ was achieved after 60 min of SPEF-Pt at the 2.2 L unit, consuming 0.10 kWh m⁻³ of electrical energy and 2.3 kJ L⁻¹ of UV energy. These consumptions for total TMP removal were 2-8 times lower than those needed to achieve 41-66% of mineralization. AO-BDD, PEF-UVA-BDD and PEF-UVC-BDD processes for the remediation of the real MWWTP wastewater spiked with 19 pharmaceutical compounds at µg L⁻¹ levels achieved average micropollutants removals of 17%, 80% and 88% after 2.5 min of treatment, respectively.

9.1.1.3 Efficiency of EAOPs in terms of decolorization

The ability of EAOPs to promote decolorization was assessed for the pure SY solution. EF, PEF-UVA and SPEF processes reached similar and much quicker color removals than AO-H₂O₂, suggesting that the azo dye and its conjugated colored aromatic products were mainly destroyed by •OH produced from Fenton's reaction, similarly to what was observed for the dye decay.

The pure SY solution was totally decolorized in 45 min by SPEF-BDD using the 150 mL undivided cell and in 120 or 70 min by SPEF-Pt using the 10 L pilot-scale flow plant at j of 33 or 78 mA cm⁻², consuming 3.2 or 7.8 kWh m⁻³ of electrical energy, respectively. The azo dye was more rapidly removed than decolorized, with an energy consumption around 4 times lower, indicating that decolorization involves the destruction of colored aromatic products that absorb at the same wavelength as the dye. When totally decolorized, the solution presented 37-47% of DOC removal.

9.1.2 Influence of operational variables on EAOPs efficiency

For the pure dye solution, the influence of j was evaluated. The effect of the nature of the anode, j , [TDI]₀, pH, use of Fe(III)-carboxylate complexes, initial pollutant concentration and temperature was assessed for the synthetic TMP solution. For the secondary MWWTP effluent, it was evaluated the influence of initial pollutant concentration and the use of UVA and UVC artificial lamps. For the winery wastewater, the effect of j and [TDI]₀ was appraised. The study on the remediation of the landfill leachate covered the assessment of the influence of a large number of operational parameters, namely the nature of the anode, j , [TDI]₀, pH, use of Fe(III)-carboxylate complexes, temperature and various radiation sources.

9.1.2.1 Nature of the anode

The use of a BDD anode for the treatment of the synthetic TMP solution by PEF-UVA and SPEF processes revealed only slightly superiority over a Pt anode, both in terms of antibiotic removal and mineralization. This can be attributed to a minor role of M(•OH) on the degradation of TMP and its intermediates under light-assisted EAOPs. Conversely, the BDD anode revealed superiority over the Pt one for the mineralization of the landfill leachate by EF, PEF-UVA and SPEF processes, suggesting an important role of BDD(•OH) on the mineralization of this effluent even under light-induced reactions. Hence, the effect of the anode nature proved to be dependent on the

wastewater composition. The Pt anode is much more inexpensive and its use induces a lower cell potential, which can make this anode a more appealing alternative for processes where $M(\bullet\text{OH})$ plays a minor role.

9.1.2.2 Current density

In the treatment of the dye solution, the influence of j was studied for AO-H₂O₂, EF, PEF-UVA and SPEF processes, whereas for the other solutions only the PEF-UVA process was regarded, with exception of the MWWTP effluent for which the influence of j was not assessed. In general, the use of higher j values led to increasing rates of mineralization, target pollutants removal and decolorization. However, almost negligible or only slightly mineralization improvement was achieved for the highest j tested in the degradation of the winery wastewater and the landfill leachate. Furthermore, higher consumptions of energy and specific charge and lower current efficiencies were achieved for higher j . This can be attributed to the rise in rate of parasitic reactions as j increases that lead to the formation of smaller relative amounts of oxidizing species. Therefore, the choice of a j value must contemplate a compromise between the pollutants degradation and the energy requirements. Distinct j values were selected as the best for the various solutions: 33, 5.0, 25 and 200 mA cm⁻² for the SY solution, the synthetic TMP solution, the winery wastewater and landfill leachate, respectively.

9.1.2.3 Initial total dissolved iron concentration

The TMP content decay was progressively faster for higher $[\text{TDI}]_0$ when applying a PEF-UVA process. For the winery wastewater and the landfill leachate, the efficiency of PEF-UVA process in terms of mineralization increased with $[\text{TDI}]_0$ up to a value for which it was detected an attenuation or ending of the improvement. This suggests an equilibrium between positive effects coming from the enhancement of Fenton's reaction and negative effects arising from the growth of parasitic reactions, inner filter effects and light attenuation along the photoreactor. Best $[\text{TDI}]_0$ of 2.0, 35 and 60 mg L⁻¹ were employed for the synthetic TMP solution, the winery effluent and the landfill leachate, respectively. An iron content of 2.0 mg L⁻¹ is the Portuguese legislation emission limit for the discharge of treated effluents (Portuguese decree law n° 236/98) and its use avoids the need for iron removal at the end of the treatment.

9.1.2.4 pH

Typically, a pH close to 2.8 leads to maximum degradation efficiencies for EAOPs based on Fenton's reaction chemistry mainly due to higher amounts of photoactive Fe(III)-hydroxy complexes and absence of iron precipitation. This was observed for the remediation of the sanitary landfill leachate by PEF-UVA, achieving lower DOC removals for rising pH values from 2.8 to 4.0, along with iron precipitation for pH values higher than 2.8. However, the TMP removal from the pure antibiotic solution by PEF-UVA method was similar and slightly faster at pH values of 3.5 and 4.0 than at pH of 3.0, pointing to the influence of the wastewater composition on the selection of a best pH.

9.1.2.5 Use of Fe(III)-carboxylate complexes

The addition of Fe(III)-carboxylate complexes to the synthetic TMP solution and the landfill leachate allowed working at higher pH values with even higher degradation rates. For the TMP solution, similar drug removals were reached by using a PEF-UVA process assisted by 1:3, 1:6 and 1:9 Fe(III)-to-oxalate molar ratios at pH values of 4.5, 5.0 and 5.5, respectively, which were around 2 times higher than that found for the classical PEF-UVA process at pH of 3.5. Furthermore, the PEF-UVA process assisted by 1:3 Fe(III)-to-oxalate, 1:1 Fe(III)-to-citrate and 1:1 Fe(III)-to-tartrate molar ratios at pH of 4.5 led to similar degradation efficiency in terms of antibiotic removal and mineralization, whereas the use of 1:1 Fe(III)-to-malate molar ratio showed inferior ability. For the sanitary landfill leachate, the use of 1:3 Fe(III)-to-oxalate molar ratio in a PEF-UVA system at pH values of 3.5 and 4.0 highly enhanced the mineralization since it maintained iron dissolved in solution for longer reaction times, resulting in higher or only slightly lower efficiencies than at pH of 2.8 in the absence of oxalic acid addition.

9.1.2.6 Initial pollutants concentration

The use of higher TMP contents led to the removal of greater amounts of pollutant per unit of time, i.e. higher pollutant removal rates, either for the degradation of the 7.0 g Na₂SO₄ L⁻¹ solution by PEF-UVA/citrate process or for the remediation of the secondary MWWTP effluent by AO.

9.1.2.7 Temperature

The application of PEF-UVA/oxalate process to the degradation of TMP revealed similar drug and DOC removals at 20 and 30 °C and only slightly higher degradation at 40 °C. For the remediation of the landfill leachate by PEF-UVA, the use of temperatures from 20 to 40 °C led to quite similar DOC decays, although iron precipitation occurred for temperatures above 20 °C. Besides that, theoretical calculations indicated that temperature can affect the amounts of Fe(OH)₃ precipitate, and, for light-assisted EAOPs, photoactive species. Therefore, the influence of temperature on the efficiency of EAOPs based on Fenton's reaction chemistry proved to be dependent on pH and wastewater composition, with higher temperatures not always providing faster removals.

9.1.2.8 Radiation source

For the secondary MWWTP effluent spiked with TMP, the use of UVC artificial radiation led to faster TMP and DOC removals than using UVA light. On the other hand, quite alike DOC removals were accomplished by PEF process employing either UVA or UVC artificial radiation for the landfill leachate. The use of an UVA-Vis lamp led to lower landfill leachate mineralization mainly for longer reaction times.

9.1.3 Comparison between EAOPs and the analogous AOPs

The mineralization was faster for EF, PEF-UVA and SPEF processes than for the analogous chemical processes when degrading the pure TMP solution and the landfill leachate, suggesting that electrochemical contributions like BDD(\bullet OH) attack and Fe³⁺ regeneration to Fe²⁺ via cathodic reduction played an important role. This superiority was less pronounced for light-assisted EAOPs, indicating that the presence of radiation, mostly sunlight, reduces the role of electrochemical reactions. Moreover, the TMP decay underwent a greater drop at the beginning of the chemical processes due to a higher initial availability of H₂O₂.

9.1.4 Scale-up from lab- to pilot-scale

The SPEF scale-up from the 150 mL undivided reactor to the 10 L pilot-scale flow plant to degrade the synthetic SY solution and the SPEF scale-up from the 2.2 L to the 35 L flow plant to the remediation of the landfill leachate led to reproducible degradations taking into account the different experimental conditions of both systems, thereby demonstrating the viability of SPEF at large scale. Note that the two later systems were successfully constructed within this thesis.

9.1.5 By-products generated during the degradation of pollutants

Up to 14 aromatic products and 34 hydroxylated derivatives, including benzenic, naphthalenic and phthalic acid compounds, were detected by LC-MS during the degradation of SY azo dye and, based on these compounds, a plausible general reaction sequence for the dye mineralization was proposed. 18 aromatic products and 19 hydroxylated derivatives were detected by LC-MS during the degradation of TMP antibiotic. Several LMCA like oxalic, oxamic and formic were detected along the degradation of the various wastewaters.

9.2 Suggestions for future work

Since the efficiency of EAOPs was proved within this thesis, showing even higher degradation rates than the analogous AOPs, a very interesting but complex approach would be the assessment of the economic feasibility of these electrochemical processes. To do it, the investment costs, mainly related to electrochemical cells and, for light-assisted EAOPs, UV lamps or photoreactors for natural sunlight capture, and also the operational costs, including electrical energy for electrochemical cell and plant operation, reagents and maintenance, should be considered.

The application of the various EAOPs to the degradation of a real textile wastewater can be also an interesting approach due to the lack of information on this topic. To the best of our knowledge, the viability of PEF and SPEF processes to degrade this kind of effluent has not been clarified yet, neither the comparison between the various EAOPs nor the comparison of EAOPs with their chemical analogous processes.

Due to the divergent achievements regarding the influence of background electrolyte composition on the efficiency of the various EAOPs and the effect of pH on the efficiency of AO and AO-H₂O₂ processes, additional research should be developed.

Efforts at developing new and optimized photoreactors for the application of PEF and SPEF processes (or PF and SPF processes) can be also made. Computational fluid dynamics (CFD) tools can be used for this purpose. The optical system for radiation capture and transference, both in terms of photon and thermal fluxes, can be optimized and the possibility of combining natural and natural radiation can also be investigated.

The development of an efficient immobilized catalyst for Fenton's reaction based processes would overcome the need for working at acidic pH values and employment of a final polishing step to remove the catalyst from solution up to the legal discharge limits.

Biological treatment applied as a first stage for the remediation of landfill leachate must be optimized to include nitrification and denitrification steps and, consequently, be able to promote total nitrogen release as nitrogen gas to comply with regulatory limits. The nitrification-denitrification process should take into account the alkalinity balance (consumed during nitrification and produced along denitrification) to ensure that sulfate content does not exceed the limit imposed by legislation.

